DNA REPLICATION STRESS AND CELL FATE

EDITED BY: Lin Deng, Chunlong Chen, Yunzhou Dong, Huiqiang Lou and Yuanliang Zhai

PUBLISHED IN: Frontiers in Cell and Developmental Biology

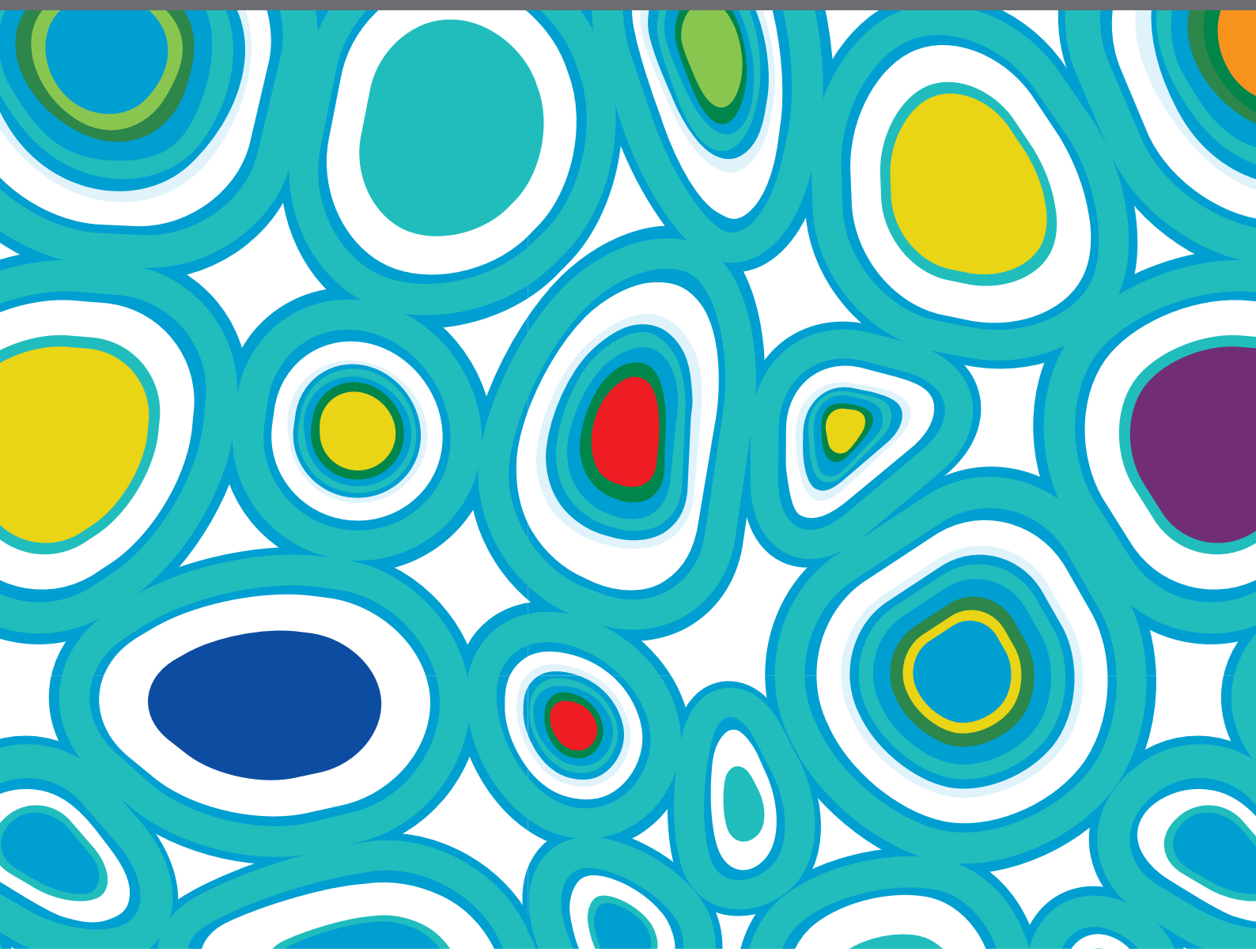

frontiers Research Topics

frontiers

ISSN 1664-8714
ISBN 978-2-88971-879-5
DOI 10.3389/978-2-88971-879-5

About Frontiers

Frontiers is more than just an open-access publisher of scholarly articles: it is a pioneering approach to the world of academia, radically improving the way scholarly research is managed. The grand vision of Frontiers is a world where all people have an equal opportunity to seek, share and generate knowledge. Frontiers provides immediate and permanent online open access to all its publications, but this alone is not enough to realize our grand goals.

Frontiers Journal Series

The Frontiers Journal Series is a multi-tier and interdisciplinary set of open-access, online journals, promising a paradigm shift from the current review, selection and dissemination processes in academic publishing. All Frontiers journals are driven by researchers for researchers; therefore, they constitute a service to the scholarly community. At the same time, the Frontiers Journal Series operates on a revolutionary invention, the tiered publishing system, initially addressing specific communities of scholars, and gradually climbing up to broader public understanding, thus serving the interests of the lay society, too.

Dedication to Quality

Each Frontiers article is a landmark of the highest quality, thanks to genuinely collaborative interactions between authors and review editors, who include some of the world's best academicians. Research must be certified by peers before entering a stream of knowledge that may eventually reach the public - and shape society; therefore, Frontiers only applies the most rigorous and unbiased reviews.
Frontiers revolutionizes research publishing by freely delivering the most outstanding research, evaluated with no bias from both the academic and social point of view. By applying the most advanced information technologies, Frontiers is catapulting scholarly publishing into a new generation.

What are Frontiers Research Topics?

Frontiers Research Topics are very popular trademarks of the Frontiers Journals Series: they are collections of at least ten articles, all centered on a particular subject. With their unique mix of varied contributions from Original Research to Review Articles, Frontiers Research Topics unify the most influential researchers, the latest key findings and historical advances in a hot research area! Find out more on how to host your own Frontiers Research Topic or contribute to one as an author by contacting the Frontiers Editorial Office: frontiersin.org/about/contact

DNA REPLICATION STRESS AND CELL FATE

Topic Editors:
Lin Deng, Shenzhen Bay Laboratory, China
Chunlong Chen, Institut Curie, France
Yunzhou Dong, Harvard Medical School, United States
Huiqiang Lou, China Agricultural University, China
Yuanliang Zhai, The University of Hong Kong, SAR China

Citation: Deng, L., Chen, C., Dong, Y., Lou, H., Zhai, Y., eds. (2021). DNA Replication Stress and Cell Fate. Lausanne: Frontiers Media SA.
doi: 10.3389/978-2-88971-879-5

Table of Contents

frontiers in Cell and Developmental Biology

EDITORIAL
published: 25 October 2021
doi: 10.3389/fcell.2021.778486

Editorial: DNA Replication Stress and Cell Fate

Lin Deng[1], Chun-Long Chen[2], Yuanliang Zhai[3], Yunzhou Dong[4] and Huiqiang Lou[5]**

[1] Shenzhen Bay Laboratory, Shenzhen, China, [2] Institut Curie, PSL Research University, CNRS UMR3244, Dynamics of Genetic Information, Sorbonne Université, Paris, France, [3] School of Biological Sciences, The University of Hong Kong, Hong Kong, Hong Kong, SAR China, [4] Boston Children's Hospital, Harvard Medical School, Boston, MA, United States, [5] State Key Laboratory of Agrobiotechnology, College of Biological Sciences, China Agricultural University, Beijing, China

Keywords: DNA replication, replication stress, fork reversal, DNA damage repair, genome instability, cell fate, diseases

Editorial on the Research Topic

DNA Replication Stress and Cell Fate

Faithful genome duplication through DNA replication is pivotal for genome maintenance. A variety of stresses could challenge this fundamental process and therefore endanger the genome integrity and change the cell fate. These stresses include misincorporation of ribonucleotides, unusual DNA structures, common fragile sites, replication-transcription conflicts, oncogene activation, treatment of pharmacological drugs, and so forth. Replication stress, if not dealt with timely and properly, may result in replication fork collapse, DNA double-strand breaks, and genome instability. Moreover, mutations in replication machinery or factors that combat replication stress can lead to numerous diseases such as developmental defects, microcephaly, anemia, aging, and cancer. Despite intensive studies, how cells deal with replication stress remains poorly understood. Thus, it is of importance to obtain mechanistic insights into DNA replication process and how DNA replication stresses manipulate and determine the cell fate. In this Research Topic, investigators have provided insightful points from their original research or review articles on the source, cellular response, and consequence of replication stress.

OPEN ACCESS

Edited and reviewed by:
Philipp Kaldis,
Lund University, Sweden

****Correspondence:***
Lin Deng
denglin@szbl.ac.cn
Huiqiang Lou
lou@cau.edu.cn

Specialty section:
This article was submitted to Cell Growth and Division, a section of the journal Frontiers in Cell and Developmental Biology

Received: *17 September 2021*
Accepted: *05 October 2021*
Published: *25 October 2021*

Citation:
Deng L, Chen C-L, Zhai Y, Dong Y and Lou H (2021) Editorial: DNA Replication Stress and Cell Fate. Front. Cell Dev. Biol. 9:778486. doi: 10.3389/fcell.2021.778486

CHAPTER 1: DNA REPLICATION AND REPLICATION STRESS

The core of the replisome at a replication fork is the replicative helicase known as CMG (Cdc45-MCM-GINS), which unwinds the double-strand DNA to allow replication. The CMG needs to be unloaded from DNA upon the completion of DNA replication. Xia summarized the recent progress in the field of DNA replication termination, focusing on the mechanisms of CMG disassembly, particularly the ubiquitination factors in yeast and metazoans (Xia). Replication forks often encounter endogenous and exogenous stresses that impede their progression. Tremblay et al. investigated the mechanism of how bacterial virulence factor cytolethal distending toxin (CDT) leads to genetic instability in human cell lines and colorectal organoids from healthy patients' biopsies. They demonstrated that CDT holotoxin induces replicative stress and results in the expression of fragile sites and genome instability. Because some CDT-carrying bacteria were detected in patients with colorectal cancer, the authors proposed that these bacteria could be important therapeutic targets (Tremblay et al.). Next, Lin et al. reported that administration of high doses of eCG (equine chorionic gonadotropin) for *in vitro* fertilization in mice causes

ROS (reactive oxygen species), DNA damage and mitotic catastrophe. Lastly, Luo et al. reported that Stattic, a STAT3 inhibitor, induces apoptosis and inhibits proliferation of MV4-11 leukemia cells. Interestingly, the DNA damage repair (DDR) related mRNAs are altered by Sattic treatment, underlying the importance of blocking DNA damage repair (Luo et al.).

CHAPTER 2: FORK PROCESSING AND REMODELING UNDER REPLICATION STRESS

If stalled forks are not properly processed and restarted, these unstable structures tend to collapse and rearrange. Técher and Pasero reviewed the mechanisms such as fork resection, fork reversal, and mitotic cleavage that ensure the completion of DNA replication under endogenous or exogenous stresses. For the pathological consequences, the processing of stalled forks may release small DNA fragments into the cytoplasm, activating the cGAS-STING pathway and inflammatory response that has both positive and negative impacts on the fate of stressed cells (Técher and Pasero). Moreover, replication fork reversal is a critical protective mechanism in higher eukaryotic cells in response to replication stress. Qiu et al. summarized the key factors and mechanisms required to remodel and protect stalled replication forks. Li et al. provided insights on how, in parallel with the Fanconi anemia pathway, PCNA interactions, and its ubiquitination induced by ICL (inter-strand crosslinks) regulate the recruitment, substrate specificity, activity, and coordinated action of certain nucleases and TLS (translesion DNA synthesis) polymerases during ICL repair and bypass. In addition, increasing numbers of evidence show that protein cofactors are needed for DNA metabolism. Shi et al. outlined the synthesis of mitochondrial, cytosolic and nuclear Iron–sulfur (Fe/S) clusters (ISCs) and discussed the role of ISCs in regulating DNA replication, damage repair and genome integrity.

CHAPTER 3: REPLICATION STRESS AND DISEASES

Replication stress and genome instability are hallmarks of cancers and many other diseases. Replication stress is generally considered to be the driving force behind cancer progression. Zhang et al. reported that RECQ1, a DNA helicase critical for fork restart after replication stress, acts at replication forks, binds PCNA, inhibits single-strand DNA formation and nascent strand degradation in glioblastoma cells. In parallel, the structure-specific endonuclease MUS81 plays a vital role in processing the stalled replication forks, and has a close relationship with cancers. Chen et al. reviewed the current understanding of how MUS81 functions in tumors with distinct genetic backgrounds and discussed the potential therapeutic strategies targeting MUS81 in cancer. In addition, HER2-enriched breast carcinomas display evidence of elevated levels of DNA damage associated with replication stress. Liang et al. reported that MiR-92b-3p suppresses proliferation of HER2-positive breast cancer cells by targeting the circular RNA circCDYL. Both circCDYL and miR-92b-3p might be biomarkers in predicting clinical outcomes of HER2-positive breast cancer patients (Liang et al.). Next, DDR and apoptosis are reported to be involved in the pathogenesis of many neurodegenerative diseases such as Spinocerebellar ataxia type 3 (SCA3) and Huntington's disease (HD). The polyQ expansion in ATX3 seems to affect its physiological functions in these distinct pathways. Tu et al. gave a comprehensive overview of the current studies about the physiological roles of ATX3 in DDR and related apoptosis, highlighting the association between these pathways and the pathogenesis of SCA3. Last, high Polθ-mediated end joining (TMEJ, also known as alternative end-joining) activity was observed in the breast cancer subgroup deficient of HR (homologous recombination). Prodhomme et al. discussed their recent finding that EMT (epithelial-to-mesenchymal transition) transcription factor ZEB1 modulates TMEJ activity by direct transcriptional suppression, providing insights into the relationship between replication stress and TMEJ or EMT features, and how these processes contribute to genomic stability.

Taken together, the articles in this issue could help researchers better understand the sources of replication stress and their cellular consequences, especially their impact on genome integrity, cell viability, and human diseases.

AUTHOR CONTRIBUTIONS

LD wrote the manuscript. HL edited the manuscript. All authors provided intellectual input to the editorial.

FUNDING

LD was supported by the Guangdong Basic and Applied Basic Research Foundation (2020A1515110542). C-LC was supported by the YPI program of I. Curie, the ATIP-Avenir program from Center national de la recherche scientifique (CNRS) and Plan Cancer from INSERM, the CNRS 80|Prime interdisciplinary program, the Agence Nationale pour la Recherche (ANR) and Institut National du Cancer (INCa). YZ was supported by the University of Hong Kong and the Research Grants Council (RGC) of Hong Kong (GRF16104617, GRF16103918, and C7009-20GF). YD was supported by American Heart Association (AHA) Grant (12SDG8760002). HL was supported by the National Key R&D Program of China (2019YFA0903900); National Natural Science Foundation of China Grants (31630005 and 31770084).

ACKNOWLEDGMENTS

We would like to thank all the authors contributing in this issue for their outstanding work and all the reviewers for their time, efforts, and critical comments in refining these manuscripts.

Conflict of Interest: The authors declare that the research was conducted in the absence of any commercial or financial relationships that could be construed as a potential conflict of interest.

Publisher's Note: All claims expressed in this article are solely those of the authors and do not necessarily represent those of their affiliated organizations, or those of the publisher, the editors and the reviewers. Any product that may be evaluated in this article, or claim that may be made by its manufacturer, is not guaranteed or endorsed by the publisher.

frontiers in Cell and Developmental Biology

REVIEW
published: 23 December 2020
doi: 10.3389/fcell.2020.619911

Determining the Fate of Neurons in SCA3: ATX3, a Rising Decision Maker in Response to DNA Stresses and Beyond

Yingfeng Tu[1†], Xiaoling Li[2†], Xuefei Zhu[3†], Xiaokang Liu[2], Caixia Guo[4], Da Jia[1] and Tie-Shan Tang[5,6*]*

[1] Key Laboratory of Birth Defects and Related Diseases of Women and Children, Department of Paediatrics, West China Second University Hospital, State Key Laboratory of Biotherapy and Collaborative Innovation Center of Biotherapy, Sichuan University, Chengdu, China, [2] Hebei Key Laboratory of Applied Chemistry, School of Environmental and Chemical Engineering, Yanshan University, Qinhuangdao, China, [3] Guangdong Key Laboratory for Genome Stability & Disease Prevention, Shenzhen University Health Science Center, Shenzhen, China, [4] Beijing Institute of Genomics (China National Center for Bioinformation), University of Chinese Academy of Sciences, Chinese Academy of Sciences, Beijing, China, [5] State Key Laboratory of Membrane Biology, Institute of Zoology, University of Chinese Academy of Sciences, Chinese Academy of Sciences, Beijing, China, [6] Institute for Stem Cell and Regeneration, Chinese Academy of Sciences, Beijing, China

OPEN ACCESS

Edited by:
Huiqiang Lou,
China Agricultural University, China

Reviewed by:
Ilya Bezprozvanny,
University of Texas Southwestern Medical Center, United States
Zhefan Stephen Chen,
University of Oxford, United Kingdom
Hayley S. McLoughlin,
University of Michigan, United States

***Correspondence:**
Da Jia
JiaDa@scu.edu.cn
Tie-Shan Tang
tangtsh@ioz.ac.cn

[†]These authors have contributed equally to this work

Specialty section:
This article was submitted to Cell Growth and Division, a section of the journal Frontiers in Cell and Developmental Biology

Received: *21 October 2020*
Accepted: *01 December 2020*
Published: *23 December 2020*

Citation:
Tu Y, Li X, Zhu X, Liu X, Guo C, Jia D and Tang T-S (2020) Determining the Fate of Neurons in SCA3: ATX3, a Rising Decision Maker in Response to DNA Stresses and Beyond. Front. Cell Dev. Biol. 8:619911. doi: 10.3389/fcell.2020.619911

DNA damage response (DDR) and apoptosis are reported to be involved in the pathogenesis of many neurodegenerative diseases including polyglutamine (polyQ) disorders, such as Spinocerebellar ataxia type 3 (SCA3) and Huntington's disease (HD). Consistently, an increasing body of studies provide compelling evidence for the crucial roles of ATX3, whose polyQ expansion is defined as the cause of SCA3, in the maintenance of genome integrity and regulation of apoptosis. The polyQ expansion in ATX3 seems to affect its physiological functions in these distinct pathways. These advances have expanded our understanding of the relationship between ATX3's cellular functions and the underlying molecular mechanism of SCA3. Interestingly, dysregulated DDR pathways also contribute to the pathogenesis of other neurodegenerative disorder such as HD, which presents a common molecular mechanism yet distinct in detail among different diseases. In this review, we provide a comprehensive overview of the current studies about the physiological roles of ATX3 in DDR and related apoptosis, highlighting the crosslinks between these impaired pathways and the pathogenesis of SCA3. Moreover, whether these mechanisms are shared in other neurodegenerative diseases are analyzed. Finally, the preclinical studies targeting DDR and related apoptosis for treatment of polyQ disorders including SCA3 and HD are also summarized and discussed.

Keywords: neurodegenerative diseases, spinocerebellar ataxia type 3, ataxin-3, DNA damage response, apoptosis

INTRODUCTION

Dominant inheritance of mutant Ataxin-3 (ATX3) leads to neurodegenerative disorder Machado-Joseph disease (MJD1, also known as spinocerebellar ataxia type 3/SCA3), with abnormal expansion of its C terminal polyglutamine (polyQ) repeats up to 55–87 in comparison to 10–51 in healthy individuals. The polyQ expansion length correlates positively with the disease severity

and inversely with the age of disease onset (Kawaguchi et al., 1994; Riess et al., 2008; Matos et al., 2011; Lee et al., 2015). SCA3 is the most common form of spinocerebellar ataxia worldwide (Schols et al., 2004; Paulson, 2012), characterized by progressive ataxia, spasticity, and ocular movement abnormalities (Matos et al., 2011). The cytologic abnormalities of SCA3 is typically neuronal loss, to date as reported. Although the pathogenic ATX3 is expressed ubiquitously in various tissues and cell types, the mutation of this protein seems only to induce neuronal dysfunction. Especially, the neuronal loss selectively occurs in specific brain domains including cerebellum, substantia nigra, and striatum, suggesting a region-specific toxic mechanism. The wealth of information has provided deep insights into the physiological functions of ATX3 and the etiology of SCA3. Although the precise molecular mechanism underlying SCA3 pathogenesis remains enigmatic, a better understanding might be developed when we take recently-established functions of ATX3 in DNA damage response (DDR) and apoptosis into account.

The evolutionally conserved DDR network guarantees genome integrity upon various kinds of damage insults, which can be spontaneous, such as reactive oxygen species (ROS) derived from normal metabolism, or be exogenous such as ultraviolet (UV) from sunlight (Hoeijmakers, 2009; Ciccia and Elledge, 2010). DDR involves sophisticated signaling networks, with the ability to sense DNA damage, to transduce the signal and in the end to evoke cellular responses including DNA repair, DNA damage checkpoint, chromatin remodeling and apoptosis, contributing to both parental survival and faithful transmission of genetic information to offsprings (Friedberg, 2003; Harper and Elledge, 2007; Jackson and Bartek, 2009). DDR defects are reported to associate with various genetic diseases accompanied by neurodegeneration, such as AT (ataxia telangiectasia), Xeroderma pigmentosum, Trichothiodystrophy, and Cockayne syndrome (Friedberg et al., 1995; Ciccia and Elledge, 2010). Recently, ATX3 has been reported to exert crucial roles in DDR via interacting with various DDR proteins such as polynucleotide kinase 3'-phosphatase (PNKP), mediator of DNA damage checkpoint protein 1 (MDC1), checkpoint kinase 1 (Chk1), Huntingtin (HTT), Ku70, DNA-PKcs, 53BP1 and p97 (Chatterjee et al., 2015; Gao et al., 2015, 2019; Pfeiffer et al., 2017; Tu et al., 2017; Singh et al., 2019; Chakraborty et al., 2020). Aberrant polyQ expansion in ATX3 results in accumulation of DNA damage, activation of pro-apoptotic signaling pathway, and neurodegeneration in SCA3. In addition, abnormal polyQ expansion abrogates the expression of superoxide dismutase 2 (SOD2) (Araujo et al., 2011), which is involved in the clearance of ROS. Given the high level of oxygen consumption in nervous system, the ROS-induced cytotoxicity and oxidative DNA damage are believed to contribute to SCA3 pathogenesis. Similar to SCA3, Huntington's disease (HD), an autosomal dominant neurodegenerative disease, is also caused by polyQ expansion in the HTT protein (Ross et al., 2014). Consistently, many studies indicate the involvement of HTT in DDR and apoptosis (Zeitlin et al., 1995; Dragatsis et al., 2000; Kegel et al., 2000; Rigamonti et al., 2000; Leavitt et al., 2001; Anne et al., 2007; Maiuri et al., 2017), and there is accumulated DNA damage in HD patient samples and HD models (Browne et al., 1997; Bogdanov et al., 2001; Chen et al., 2007; Acevedo-Torres et al., 2008; Illuzzi et al., 2009; Enokido et al., 2010; Stack et al., 2010; Ferlazzo et al., 2014), indicating that abnormal DDR may play a general role in the pathogenesis of polyQ-related neurodegenerative diseases.

Apoptosis plays essential roles in organism development as well as in tumor-suppression, whose dysfunction closely relates to disease pathogenesis. As a well-established apoptosis regulator, p53 is involved in the pathogenesis of neurodegenerative diseases such as Alzheimer's diseases (AD), Parkinson's disease (PD), and HD (Chang et al., 2012). The important roles of p53 in the development of neurodegenerative diseases are associated with its interaction with various factors which are capable of promoting the progression of these diseases. A recent work has identified ATX3 as a novel deubiquitinating enzyme of p53. Normal ATX3 regulates the stabilization and pro-apoptotic function of p53, while polyQ expansion impedes the dissociation between ATX3 and p53, therefore enhances the stability and pro-apoptotic function of p53, supporting the involvement of p53 in SCA3 pathology (Liu et al., 2016). The antiapoptotic role of HTT and the observation that mutant HTT induces apoptosis (Zeitlin et al., 1995; Cooper et al., 1998; Hackam et al., 1998; Lunkes and Mandel, 1998; Reddy et al., 1998; Hodgson et al., 1999; Dragatsis et al., 2000; Rigamonti et al., 2000; Leavitt et al., 2001) suggest that apoptosis may also be another common pathway shared in polyQ-related neurodegenerative diseases.

In this review, we will summarize the recent advances concerning the roles of ATX3 in DDR and apoptosis, and emphasize the potential link of abnormal DDR and apoptosis to pathogenesis of SCA3 and other neurodegenerative diseases including HD. Finally, we describe preclinical studies targeting these essential pathways for treatment of neurodegenerative diseases including SCA3 and HD.

THE DEUBIQUITINASE ACTIVITY OF ATX3

ATXN3 gene was first identified in 1993 and mapped to chromosome 14q24.3-q32.45 by Takiyama and coworkers. It encodes a deubiquitinase (DUB) called MJD1 or ATX3 which contains an unstable CAG repeat (Takiyama et al., 1993; Kawaguchi et al., 1994). The Josephin domain in ATX3, which is highly conserved from yeast to human, confers the deubiquitinase activity, with cysteine14 being the key catalytic residue. Correspondingly, both ATX3 knockout and ATX3 catalytic activity inhibition by mutating Cys14 lead to an obvious increase of polyubiquitinated proteins (Berke et al., 2005; Schmitt et al., 2007), verifying the DUB function of ATX3 *in vivo*. ATX3 also contains 2 to 3 ubiquitin interacting motif (UIM) domains, with the most common isoform found in human brain having 3 UIM domains (Schmidt et al., 1998). UIM domains play an essential role in regulating the DUB activity of ATX3 through their binding to polyubquitinated proteins (Donaldson et al., 2003), determining the cleavage preference to linkage of ubiquitin chain and regulating the ubiquitination state in Josephin domain (Lysine 117 being the primary ubiquitination site) (Berke et al., 2005; Todi et al., 2009, 2010). Collectively, the Josephin domain and UIMs make ATX3 a multifunctional

protein that plays vital roles in protein homeostasis, DDR and apoptosis through its interaction with key factors in above-mentioned pathways (**Figure 1**), and notably, its deubiquitinase activity is indispensable in many cases.

FUNCTIONS OF ATX3 IN DDR

Recent studies unraveled ATX3 to be an essential participant of DDR, including DNA strand break repair, cell cycle arrest, and oxidative stress response. Here, we summarize the key functions of ATX3 in genome integrity maintenance.

Roles of ATX3 in DNA Strand Break Repair

DNA stand breaks occur as double-strand breaks (DSBs) or single-strand breaks (SSBs). Except in routine cellular processes such as DNA replication, meiosis, and V(D)J recombination, DSBs are generally highly deleterious lesions arising from exposure to ionizing radiation (IR). DSBs can induce chromosomal rearrangement such as deletion, translocation, or amplification. DSBs are repaired primarily by homologous recombination (HR) and non-homologous end joining (NHEJ). The error-free HR repair operates in S and G2 phase, with sister chromatids available as repair templates, while error-prone NHEJ is active throughout the cell cycle. Failure to repair DSBs can trigger permanent growth arrest and finally cell death (Bennett et al., 1993; Sandell and Zakian, 1993). Compared to DSBs, SSBs can be induced by IR and ROS, and repaired by single-strand break repair (SSBR) (Caldecott, 2003; Katyal and McKinnon, 2008).

ATX3 Preserves Genome Integrity by Regulating PNKP Phosphatase/Kinase Activity

PNKP is a bi-functional enzyme with 3′-phophotase and 5′-kinase activities, capable of removing 3′-P and phosphorylating 5′-OH, facilitating DNA ligation (Jilani et al., 1999; Weinfeld et al., 2011). The roles of PNKP in DNA strand break repair and BER are particularly important for genome stability of neural cells. Mutations in PNKP (L176F, E326K, T424Gfs48X, and exon15Δfs4X) result in autosomal recessive neurological disorder characterized by microcephaly, seizures and developmental delay (MCSZ) (Shen et al., 2010), and the related cell lines exhibit compromised SSBR following γ-radiation (Ward et al., 1987). Importantly, a lot of evidence suggest that PNKP is also implicated in DSB repair (Chappell et al., 2002; Koch et al., 2004; Karimi-Busheri et al., 2007; Segal-Raz et al., 2011). Although it remains unclear whether the downregulation of kinase activity or phosphatase activity contribute to MCSZ, PNKP mutations cause a significant decrease of PNKP level in MCSZ patients (Shen et al., 2010; Reynolds et al., 2012), indicating the relevance of PNKP abundance.

Accordant with its role in the DDR, PNKP knockdown sensitizes cells to H_2O_2 and IR (Rasouli-Nia et al., 2004). PNKP can be phosphorylated at S114 and S126 by ATM (Segal-Raz et al., 2011; Zolner et al., 2011), which prevents its proteasomal degradation by Cul4A-DDB1-STRAP ubiquitin ligase complex and promotes effective DNA repair (Parsons et al., 2012). Moreover, lymphoblast of MCSZ patients displayed a remarkably compromised repair of oxidative DNA damage (Shen et al., 2010).

Gao et al. identified that ATX3 co-localizes with PNKP in cells and human brain sections, suggesting an association between ATX3 and PNKP. Accordantly, Chatterjee et al. substantiated the interaction by endogenous immunoprecipitation assays and proximity ligation assay (PLA) (Chatterjee et al., 2015; Gao et al., 2015), and found that this interaction is mediated by both kinase domain and phosphatase domain of PNKP. The association between ATX3 and PNKP is of biological significance to PNKP, as exemplified by the enhanced phosphatase activity of PNKP in an ATX3 dose-dependent manner, although the underlying mechanism remains unclear. Coincidently, ATX3 ablation results in decreased PNKP activity, and sequentially DNA strand breaks accumulation and delayed repair of DNA strand breaks induced by oxidative stress (Chatterjee et al., 2015). All these data demonstrate a role of ATX3 in genome integrity maintenance by promoting phosphatase/kinase activity of PNKP (**Figure 2**).

ATX3 in Classical NHEJ Repair of Transcribed Genes

PNKP was reported to participate in classical NHEJ-mediated error-free repair of DSBs in transcribed genes (Chakraborty et al., 2016). Later, ATX3 was identified to be a component of transcription-coupled DNA repair complex composed of ATX3, HTT, RNA polymerase II subunit A, PNKP, and cyclic AMP-response element-binding (CREB) protein (CBP). This complex senses DNA lesions and promotes their repair during transcriptional elongation (Gao et al., 2019). Given the role of ATX3 in promoting PNKP activity, it raises the possibility that ATX3 might be involved in the PNKP-mediated error-free DSB repair of the transcribed genome. Indeed, ATX3 was recently found to be essential for classical NHEJ repair of DSBs in transcribed genes (Chakraborty et al., 2020). ATX3 interacts with classical NHEJ components (such as Ku70, DNA PKcs, 53BP1, PNKP, and Lig IV), nascent transcripts and RNA polymerase II (RNAP II) under physiological conditions. Analogous to classical NHEJ proteins, ATX3 also exhibits preferential association with transcribed genes, indicating the potential role of ATX3 in classical NHEJ repair. Consistently, ATX3 depletion results in a compromised error-free repair of transcribed genes via classical NHEJ. In addition, ATX3 depletion causes a significant reduction in RNAP II level, probably caused by an enhanced ubiquitination of the stalled elongating RNAP II, which adversely impacts classical NHEJ repair and transcription (Chakraborty et al., 2020). Thus, ATX3 plays an important role in classical NHEJ repair of strand breaks in transcribed genes.

ATX3 Reinforces DSB Repair by Promoting the Retention of MDC1

MDC1, best known for its role in cellular response to DSBs, is recruited to the sites of DNA damage by phosphorylated histone variant H2AX (γH2AX), and further facilitates the loading of other DNA damage repair proteins, to promote DNA repair and checkpoint signaling. Previous studies revealed that DNA damage-induced SUMOylation, an ubiquitin-like modifier, recruits the SUMO-targeted ubiquitin ligase (STUBL) RNF4

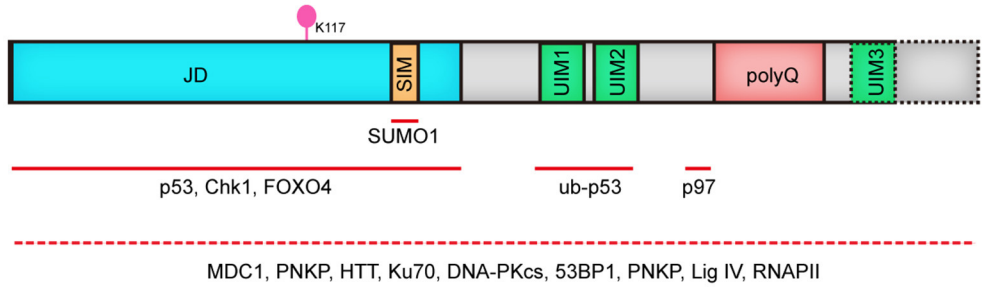

FIGURE 1 | Human ATX3 domain structure. ATX3 is comprised of the catalytic JD, followed by two or three UIMs, (depending on the types of protein isoforms, dashed line illustrates 3UIMs-containing isoform), and the polyQ stretch. JD, josephin domain; SIM, SUMO-interacting motif; UIM, ubiquitin interacting motif; polyQ, polyglutamine; Red lines indicate interacting regions with other proteins. Since the domain mediating the binding of ATX3 to MDC1, PNKP, HTT, Ku70, DNA PKcs, 53BP1, PNKP, Lig IV and RNAPII remains to be elucidated, we used dashed line covering its full length.

to the sites of DNA lesions, which promotes the ubiquitin-dependent extraction of MDC1 and RPA, and thus facilitates DSB repair via NHEJ and HR, respectively (Galanty et al., 2012; Luo et al., 2012; Yin et al., 2012). However, RNF4 is recruited to DSBs very quickly at a time when MDC1 removal would be unfavorable for the execution of DNA damage signaling (Vyas et al., 2013; Pfeiffer et al., 2017). Thus, MDC1 must be retained at the sites of DNA lesions to ensure efficient initiation of DNA repair (i.e., the RNF4 activity must be inhibited) at the early stage of DSBs response, and how this could be achieved?

It has been reported that ATX3 can be recruited to DNA damage sites induced by laser microirradiation (Nishi et al., 2014). Recent studies further demonstrated that ATX3 is recruited to DSBs in a SUMOylation-dependent manner. The interaction between ATX3 and SUMO1, mediated by N-terminal Josephin domain and further stimulated by DNA damage, is indispensable for the localization of ATX3 to DSBs (Pfeiffer et al., 2017). The similar spatial-temporal accumulation of ATX3 and RNF4 raises the possibility that they share the same SUMOylated substrates. ATX3 was demonstrated to be responsible for the stable retention of MDC1 at DSBs by repressing the RNF4-dependent ubiquitination of MDC1 (Pfeiffer et al., 2017). The deubiquitinase activity of ATX3 is indispensable for its role in facilitating MDC1 anchoring at DSB sites, which further promotes recruitment of RNF8 and RNF168 and subsequent accumulation of ubiquitination-dependent BRCA1 and 53BP1. Consequently, ATX3 depletion results in impaired DSB repair, as indicated by reduced RPA and RAD51 recruitment, and increased sensitivity to PARP inhibitor. Thus, the deubiquitinase ATX3 prevents premature MDC1 eviction by antagonizing RNF4 to reinforce effective DSB response (**Figure 2**).

The constitutive interaction between ATX3 and MDC1 is neither stimulated by DNA damage assault nor dependent on the major SUMOylation site of MDC1 (K1840) (Luo et al., 2012), As a SUMO-activated deubiquitinase, ATX3 antagonizes RNF4-mediated MDC1 ubiquitination and its subsequent extraction. Meanwhile, ATX3 depletion also results in compromised recruitment of RPA, which can be SUMOylated and regulated by RNF4 in response to DNA damage (Dou et al., 2010; Galanty et al., 2012; Yin et al., 2012). Whether ATX3 acts on other RNF4 substrates during DDR warrants further investigation.

ATX3 Promotes DSB Repair by Stimulating the Extraction of RNF8

RNF8 is an E3 ligase with crucial roles in the ubiquitination of histone H2A and H2AX, and subsequent recruitment of DNA repair factors including BRCA1 and 53BP1 (Huen et al., 2007). Although RNF8 is indispensable for both efficient DNA repair in response to genotoxic stimulus and genome integrity under physiological conditions, the homeostasis of RNF8 was reported to be tightly regulated very recently. Under physiological conditions, RNF8 catalyzes its own K48-linked ubiquitination, which is antagonized by the p97-ATX3 complex, contributing to preservation of RNF8 abundance. Expression of catalytically inactive ATX3-C14A or ubiquitin-binding defective ATX3-UIM* mutants result in accelerated degradation of RNF8, which can be rescued by wild-type ATX3 but not ATX3-VBM (VCP/p97-binding motif) mutant (Boeddrich et al., 2006; Singh et al., 2019), indicating the importance of p97-ATX3 complex in RNF8 stability. Under genotoxic attack, p97-ATX3 complex extracts RNF8 from DNA lesion sites (Singh et al., 2019). Consistently, ablation of either component led to aberrant accumulation of RNF8, defective DNA repair and sensitivity to IR. However, hyperaccumulation of RNF8 observed here is inconsistent with previous finding that RNF8 recruitment is reduced in ATX3 deficient cells. Furthermore, the authors failed to detect the interaction between MDC1 and ATX3 observed by Pfeiffer et al. (2017). Whether this contradiction is caused by different experimental conditions needs further investigation. The homologs of p97 and ATX3 in *C. elegans* was also reported to regulate DSB repair (Ackermann et al., 2016).

Functions of ATX3 in Cell Cycle Checkpoint

When confronted with DNA damage insults, appropriate cell cycle checkpoint can prevent cells from proceeding to the next cell cycle phase and provide enough time for DNA repair. After completion of DNA repair, the termination of checkpoint signaling allows the resumption of normal cell cycle progression.

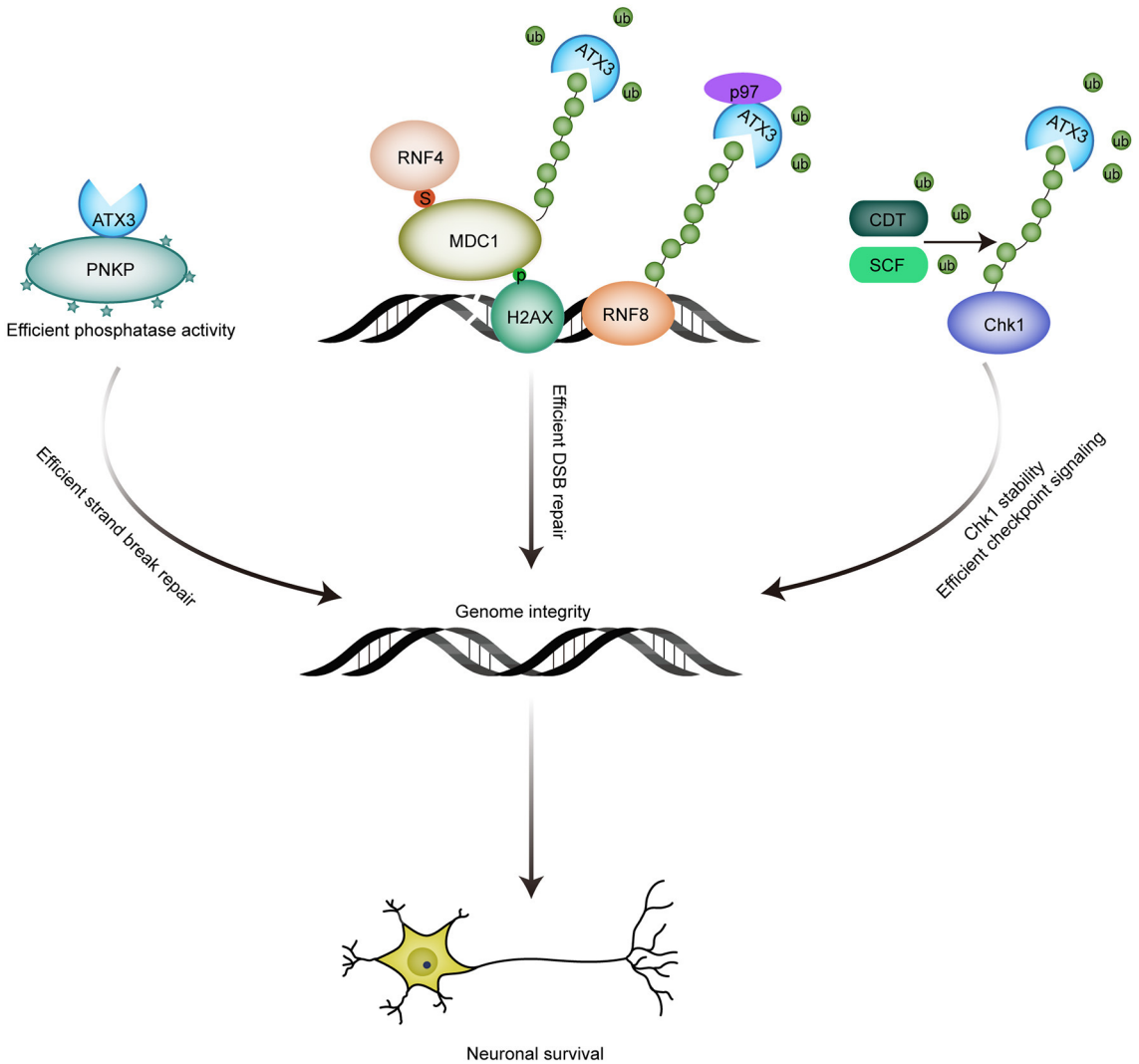

FIGURE 2 | Roles of ATX3 in genome integrity maintenance. (1) The association between ATX3 and PNKP promotes the phosphatase activity of PNKP, and consequent efficient strand break repair; (2) ATX3 antagonizes RNF4-induced polyubiquitination and subsequent chromatin eviction of MDC1, and thus ensures the residence of MDC1 at DSBs sites and efficient DSB repair; p97-ATX3 complex promotes RNF8 stability by antagonizing proteasome-dependent degradation under physiological conditions, while p97-ATX3 complex stimulates RNF8 extraction and ensures proper DSB repair in response to genotoxic stimulus. (3) ATX3 counteracts SCF- and CDT-induced polyubiquitination and degradation of Chk1. By promoting Chk1 stability, ATX3 ensures that checkpoint signaling is accurately activated.

Failure to repair DNA lesions can lead to permanent cell cycle arrest and apoptosis to the end.

Chk1, activated by various kinds of DNA damage insults including replication stress, interstrand cross-link (ICL) and DSBs, is essential for genome integrity maintenance and cell survival in eukaryotic cells. Chk1 can phosphorylate its downstream effectors to regulate various cellular pathways such as cell cycle checkpoint, DNA repair or cell death if the damage is too severe to be repaired (Takai et al., 2000; Feijoo et al., 2001). Post-translational modifications including phosphorylation and ubiquitination play important roles in modulating Chk1 activity. Recently, chaperone-mediated autophagy (CMA) is also described to play a crucial role in regulating Chk1 activity through degradation of activated Chk1 after genotoxic exposure, promoting checkpoint termination (Park et al., 2015).

After prolonged replication stress, Chk1 can also be targeted for proteasomal degradation by CUL1- and CUL4-containing E3 ligase complexes to terminate checkpoint signaling after completion of DNA repair. However, protecting Chk1 from degradation is absolutely necessary to maintain a steady-state level of Chk1 under unperturbed conditions to ensure proper activation of DNA damage checkpoint and DNA repair signaling in response to DNA damage. Although deubiquitinase USP1 and USP7 are reported to promote Chk1 stability (Guervilly et al., 2011; Alonso-de Vega et al., 2014; Zhang et al., 2014), whether SCF(SKP1-Cul1-FBXO6)-

or CDT(Cul4A-DDB1-CDT2)-mediated polyubiquitination of Chk1 can be restrained by deubquitinase(s) remains to be elucidated. Recently, we reported that ATX3 can stabilize Chk1 by antagonizing SCF- and CDT-mediated polyubiquitination and degradation, and ATX3 shows a dynamic regulation on Chk1 stability before and after prolonged replication stress. Under unperturbed conditions and upon DNA damage, ATX3 interacts with Chk1 and protects it from CDT- and SCF-mediated polyubiquitination and degradation, promoting DNA repair and checkpoint signaling. Under prolonged replication stress, ATX3 dissociates from Chk1, concomitant with a stronger association between Chk1 and its E3 ligase, leading to Chk1 degradation and checkpoint termination. Consequently, ATX3 deficiency results in reduced abundance of Chk1, abortive G2/M checkpoint and decreased cell survival after replication stress (Tu et al., 2017). Hence, ATX3 exerts its function in genome integrity partly through stabilizing Chk1 (**Figure 2**).

Roles of ATX3 in Oxidative Stress Response

ROS, produced in normal cellular metabolic processes, results in DNA base oxidation and DNA breaks. Due to substantial oxygen consumption of the central nervous system, efficient response to oxidative stress is particularly indispensable for neurons.

The forkhead box O (FOXO) transcription factors are reported to be associated with the regulation of cell cycle arrest, and protection against cell death induced by oxidative stress (Kops et al., 2002; van der Horst and Burgering, 2007). *SOD2* gene, encoding the antioxidant enzyme SOD2 with essential role in removal of ROS, is a well-known target of FOXO family (Kops et al., 2002; van der Horst and Burgering, 2007). ATX3 was reported to interact with the FOXO transcription factor FOXO4 through its Josephine domain and co-activate the FOXO4-dependent transcription of SOD2. Under oxidative stress, nuclear translocation and concomitantly increased binding of ATX3 and FOXO4 to SOD2 promoter can upregulate SOD2. Consistently, ATX3 knockdown leads to a reduced expression of SOD2 (Araujo et al., 2011). Although ATX3 fails to downregulate the ubiquitination level of FOXO4, the increased protein level of FOXO4 by co-expression of ATX3 indicates that ATX3 may participate in the stabilization of FOXO4. It is possible that nuclear localization of ATX3 induced by oxidative stress promotes the stabilization of transcriptionally active FOXO4 and thus cellular response to oxidative stress (Araujo et al., 2011).

ATX3 was also shown to be protective against oxidative stress in a Bcl-xL-dependent manner. ATX3 directly binds to Bcl-xL and promotes the interaction between Bcl-xL and Bax, which cooperate in modulating mitochondrial oxidative stress-induced apoptosis by preventing the activation of Bax (Cheng et al., 1996; Youle and Strasser, 2008; Zhou et al., 2013). Moreover, ATX3 can interact with HHR23 proteins (HHR23A and HHR23B), human homolog of yeast RAD23, which are required for NER (Sugasawa et al., 1997). Thus, it is plausible that ATX3 also participates in NER (Wang et al., 2000).

Above all, ATX3 plays multiple roles in DDR and genome stability. Being post-mitotic cells, neurons must overcome endogenous and exogenous DNA damage sources usually on a lifetime basis. Therefore, the efficient DDR signaling pathway promoted by ATX3 is expected to be crucial for the maintenance of healthy neurons.

ROLES OF ATX3 IN APOPTOSIS

Tumor suppressor protein p53 plays a crucial role in modulating cell fate under stress and suppressing the propagation of damaged cells (Muller and Vousden, 2013). As a transcription factor, p53 is involved in various cellular pathways such as DNA repair, cell differentiation, cell cycle progression and apoptosis. To maintain its normal cellular functions, p53 activity must be finely-tuned, and posttranslational modifications, including phosphorylation, acetylation and ubiquitination, play a dominant role in this aspect (Olsson et al., 2007). It is known that E3 ubiquitin ligase MDM2 mediates the ubiquitination of p53 and thus regulating its subcellular localization and degradation. Additionally, E3 ligases such COP1, Pirh2 and ARF-BP1 were also reported to modulate p53 stability or localization (Leng et al., 2003; Dornan et al., 2004; Chen et al., 2005). On the other side, deubiquitination mediated by deubiquitinases provides a parallel important control to p53. OTUB1 from otubain (OTU) family and several deubiquitinases such as USP7 and USP10 from ubiquitin-specific protease (USP) family were suggested to regulate p53 stability and function (Li et al., 2004; Yuan et al., 2010; Sun et al., 2012). Lately, we found that p53 is a substrate of ATX3. Under physiological conditions, Josephin domain of ATX3, DNA-binding domain and the C-terminal regulatory domain of p53 are required for their interaction. During deubiquitination process, ATX3 mainly associates with ubiquitinated p53 through its UIMs domain. ATX3-mediated deubiquitination of p53 promotes the stability of p53, and thus regulates its function in transcription, cell cycle progression and apoptosis. Consistently, ATX3 deletion results in decreased p53 stability, activity and function. Ectopic expression of ATX3 promotes p53-dependent apoptosis in cells and zebrafish (Liu et al., 2016). Therefore, ATX3 functions to facilitate the stability and apoptotic function of p53.

HOW PolyQ EXPANSION AFFECTS THE PHYSIOLOGICAL FUNCTIONS OF ATX3 IN DDR AND APOPTOSIS?

SCA3 is considered to be caused by abnormal polyQ expansion in ATX3, although the underlying mechanism remains enigmatic. The age at onset of the disease decreases with increasing polyQ repeats, and there is a positive correlation between the severity of the disease and the length of polyQ tracts (Lee et al., 2015). These facts indicate the relevance of expanded polyQ repeats in SCA3 pathogenesis. One hypothesis is that abnormal polyQ expansion in ATX3 results in protein aggregation, sequestering essential proteins involved in protein quality control and transcription, ultimately provoking cytotoxicity and cell death (Matos et al., 2011). Recent evidences propose the possibility that polyQ expansion of ATX3 might abrogate its functions in DDR and

apoptosis, which provides an explanation for the involvement of abnormal DDR and apoptosis in SCA3 pathogenesis.

The PolyQ Expansion of ATX3 Attenuates DNA Strand Break Repair

Unlike wild-type ATX3, which promotes PNKP phosphatase activity, the pathological form of ATX3 significantly inhibits PNKP's phosphatase activity *in vitro*. Results from cells and SCA3 mouse also confirm that the expanded ATX3 compromises the activity of PNKP, and that the decreased PNKP activity results in a decreased SSB repair and thus increased DNA damage (**Figure 3**; Chatterjee et al., 2015).

In accordant with its essential roles in both dividing and postmitotic neurons, PNKP is expressed in both neuronal precursors and differentiated neurons, and PNKP knockdown results in increased apoptosis of neuronal precursors and postmitotic neurons (Shen et al., 2010). Therefore, abnormal polyQ expansion-induced loss of PNKP function is implicated in SCA3 pathogenesis (Gao et al., 2015). PNKP was found to colocalize with both ATX3 and polyQ aggregates in SCA3 brain sections. Additionally, the ectopic expression of expanded-ATX3 promotes the foci formation of 53BP1 and γH2AX, indicating the accumulation of DNA damage. Accumulated DNA damage then promotes p53- and PKC-dependent apoptosis, which triggers neuron death in SCA3 (Shen et al., 2010; Gao et al., 2015). Given that PNKP is recruited to polyQ aggregates, as evidenced by co-localization of PNKP and polyQ aggregates, it is supposed that polyQ-expansion results in sequestration of PNKP, thus abrogating its function in DDR. Recently, it was also reported that phosphatase activity of PNKP is significantly abrogated in affected brain regions of SCA3 mice and SCA3 patients. Consistently, accumulation of DNA damage is observed in SCA3 mice and patients, as revealed by increased level of γH2AX and phosphorylated 53BP1. Furthermore, affected brain regions of SCA3 mice and patients exhibit higher level of strand breaks in transcribed genes. Given the essential role of PNKP in error-free repair of transcribed genes in postmitotic neurons, compromised PNKP activity induced by mutant ATX3 with polyQ expansion might be involved in the pathogenesis of SCA3. In support of that, PNKP overexpression partially rescues SCA3 phenotype in *Drosophila* model of SCA3 (Chakraborty et al., 2020).

The role of ATX3 in counteracting RNF4-induced chromatin removal of MDC1 to consolidate MDC1-dependent DSB response relies on the deubiquitinase activity of ATX3. However, whether the polyQ-expansion affects its deubiquitinase activity is controversial. Some studies support the idea that polyQ expansion has no significant influence on the protease activity of ATX3 (Burnett et al., 2003; Berke et al., 2004), while Winborn and coworkers observed that the expanded ATX3 was less effective in reducing general cellular protein ubiquitination than wild-type ATX3 (Winborn et al., 2008). Whether polyQ expansion of ATX3 affects its deubiquitinase activity toward MDC1 remains to be answered. In addition, expanded ATX3 was reported to retain enhanced interaction with p97 (Zhong and Pittman, 2006). How this enhanced association between p97 and ATX3 affects the DUB activity of ATX3 toward RNF8 and DDR remains elusive.

Mutant ATX3 Augments Apoptosis

It is thought that polyQ-expanded ATX3 undergoes conformational change and acquires some toxic properties, therefore resulting in altered interactions of ATX3. Liu et al. found that the pathological ATX3 binds to p53 with a stronger affinity compared to wild-type ATX3. Coincidently, mutant ATX3 exhibits stronger deubiquitinase activity toward p53 both *in vitro* and *in vivo*, leading to higher abundance and stability of p53 in mutant ATX3-expressing cells. The activity of p53 is also enhanced by polyQ-expanded ATX3, as evidenced by elevated expression of p53-responsive genes. Further, polyQ expansion of ATX3 causes more severe neurodegeneration in zebrafish and mice in a p53-dependent manner, providing a novel explanation for the pathogenesis of SCA3 (**Figure 3**; Liu et al., 2016). Interestingly, p53 level is also increased in brains affected by neurodegenerative diseases such as AD, PD and HD (Chang et al., 2012).

Mutant ATX3 expression in primary neuronal cultures derived from cerebellum, striatum, and substantia nigra, which are susceptible to neurotoxicity induced by expanded ATX3 *in vivo*, induces mitochondrial apoptotic death (Chou et al., 2006). More specifically, mutant ATX3 results in upregulation of pro-apoptotic Bax and downregulation of anti-apoptotic Bcl-xL, which leads to mitochondrial release of cytochrome c and Smac followed by activation of caspase-9, an essential initiator of mitochondrial apoptosis (Danial and Korsmeyer, 2004; Green and Kroemer, 2004). Notably, polyQ-expanded HTT also causes similar effects. Thus, polyQ-expanded protein-mediated mitochondrial apoptotic death of affected neurons might be a common mechanism for polyQ diseases (Wang et al., 2003; Choo et al., 2004).

Compromised Capacity to Activate FOXO4-Mediated SOD2 Expression

Compared with wild-type, polyQ-expanded ATX3 displays impaired ability to activate FOXO-dependent transcription of SOD2. This might result from an increased association of mutant ATX3 to *SOD2* promoter region, the very same region bound by FOXO4, and thus inhibit the FOXO4-mediated SOD2 expression. Accordantly, both mRNA and protein levels of SOD2 are decreased in lymphoblastoid cell (LC) lines and pons tissue from SCA3 patients (Araujo et al., 2011), and SCA3-LCs fails to increase the SOD2 expression in response to oxidative stress. Given the important role of SOD2 in scavenging ROS, impaired SOD2 expression would contribute to increased ROS accumulation in response to oxidative stress. Indeed, ROS level in SCA3 LCs exposed to H_2O_2 is obviously increased. Moreover, compared with LCs from unaffected controls, H_2O_2 exposure results in significantly decreased cell viability of LCs from SCA3 patients. Considering the rate of oxygen metabolism is relatively high in nervous system, impaired removal of ROS can be particularly detrimental to nervous system. Therefore, reduced expression of SOD2 in SCA3 patients may result in constant accumulation of ROS and cytotoxicity, contributing to neurodegeneration.

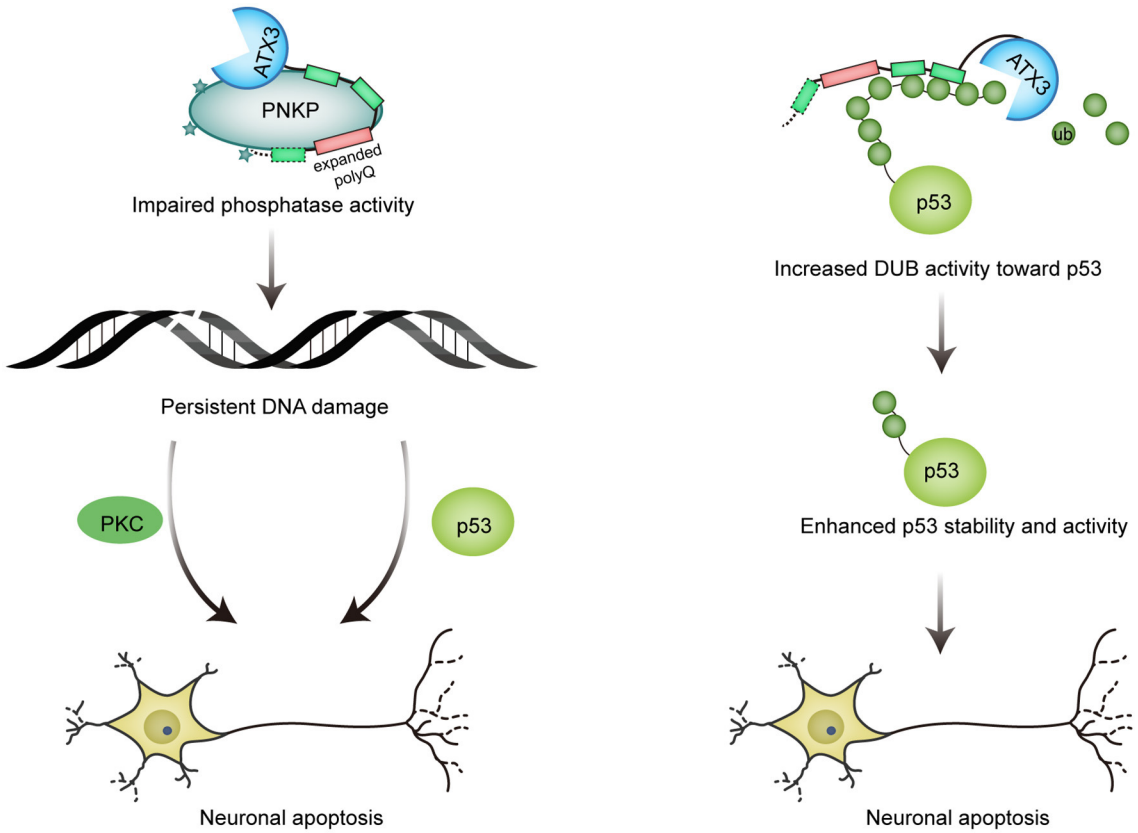

FIGURE 3 | Mutant ATX3 triggers neuronal death. (1) Expanded ATX3 inhibits the phosphatase activity of PNKP, leading to persistent accumulation of DNA damage and prolonged activation of p53 and PKC proapoptotic pathway, which are responsible for neuron loss in SCA3; (2) PolyQ-expanded ATX3 also obtains augmented deubiquitinase activity toward p53, resulting in enhanced stability and activity of p53 and consequent p53-mediated neuronal cell death.

Consistently, SOD2 knockout mice manifest neurodegeneration and progressive motor disturbance (Lebovitz et al., 1996; Williams et al., 1998).

Besides, a recent work suggests the toxicity of expanded ATX3 in abrogating transcriptional activity of FOXO. The coiled-coil structures of polyQ domain mediate the binding to transcription factor FOXO, and this interaction increases the nuclear localization of FOXO and impairs its transcriptional activity. Consequently, the mRNA levels of its representative target genes which are involved in dendrite morphogenesis or neurogenesis are significantly decreased. Moreover, the coiled-coil structures of expanded ATX3 cause dendrite defects in *Drosophila* dendritic arborization neurons as well as behavior abnormalities (Kwon et al., 2018).

Selective Tissue Vulnerability in SCA3

Selective neuronal loss and DNA damage accumulation are key features of many neurodegenerative disorders including SCA3 and HD, although the underlying mechanism remains unclear. High level of oxygen consumption in brain results in significantly increased oxidative stress, and postmitotic neurons rely on limited repair pathway such as NHEJ to counteract DNA damage assaults, which contribute to higher sensitivity of the nervous system. Mutant ATX3-mediated compromised DNA repair and increased ROS might be responsible for selective tissue vulnerability. Both WT and mutant ATX3 are shown to express in pontine nuclei, substantia nigra and dentate nuclei, regions mostly affected in SCA3 patients. In contrast, expression level in unaffected regions such as striatum, cortex and hippocampus is much lower (Chen et al., 2008). This differential expression pattern in brain might partially explain the selective tissue vulnerability in SCA3. Additionally, brain extracts from affected cerebellum region in SCA3 patients or affected brainstem (but not unaffected forebrain) in SCA3 mice model, specifically inhibit PNKP activity (Chakraborty et al., 2020). Consistent with the essential role of PNKP-mediated classical NHEJ repair in postmitotic neurons (Chatterjee et al., 2015; Chakraborty et al., 2016), higher level of DNA damage accumulates in affected brain regions of SCA3 patients and mice model (Gao et al., 2019; Chakraborty et al., 2020). Thus, selective PNKP activity impairment, DNA damage accumulation, and neuronal loss might represent potential biomarkers for SCA3 and HD.

PROSPECTS FOR THERAPY OF SCA3 AND OTHER NEURODEGENERATIVE DISEASES

Age-related neurodegenerative disorders including SCA3 and HD show elevated DNA damage (Illuzzi et al., 2009; Chatterjee et al., 2015), and significant advances have been achieved about the relevant molecular pathways. The role of aberrant apoptosis in the pathogenesis of these diseases are also reported (Ghavami et al., 2014; Liu et al., 2016). These studies might provide novel guideline for development of effective therapy of these neurodegenerative disorders. Here, we summarized preclinical studies targeting DDR and related apoptosis for treatment of neurodegenerative diseases, focusing on polyQ disorders including SCA3 and HD.

DNA Damage Response Pathways as Potential Therapeutic Targets

Decades of research in genetics and molecular biology have established the connection between inherited DNA repair defects and progressive neurodegenerative diseases, such as xeroderma pigmentosum, Cockayne syndrome, ataxia telangiectasia, and among many others (Jeppesen et al., 2011; Maiuri et al., 2017). Dysfunctional DDR are also implicated in several neurodegenerative polyQ diseases such as SCA3 and HD. A genome-wide association analysis found that genes involved in mismatch repair can modulate HD's age of onset (Lee et al., 2015). Other studies also indicate that DNA repair enzymes significantly modify the onset age in polyQ disorders including SCAs and HD (Bettencourt et al., 2016; Moss et al., 2017). DNA damage and apoptosis have also been linked to spinocerebellar ataxia with axonal neuropathy (SCAN1) pathogenesis (Takashima et al., 2002). Mutant AT1 and mutant HTT, responsible for SCA1 and HD, respectively, are shown to reduce the level of HMGB1/2, involved in regulating transcription and DNA repair (Muller et al., 2001; Travers, 2003). And HMGB1/2 complementation ameliorates mutant protein-induced pathology in neurons and in *Drosophila* model (Qi et al., 2007). Another systematic analysis of SCA1 *Drosophila* reveals the roles of aberrant DNA damage repair in SCA1 (Barclay et al., 2014). In addition, spinal and bulbar muscular atrophy (SBMA), another polyQ disorder, is caused by polyQ expansion in androgen receptor (AR). Mutant AR inhibits recruitment of PITP, a DNA repair protein, to damage sites, resulting in sensitivity to DNA damage and genome instability. And a higher level of DNA damage and activation of DDR are observed in SBMA mice (Xiao et al., 2012). Abnormal DDR might be a common underlying molecular mechanism in these neurodegenerative disease, and represent a potential therapeutic target.

ATM

Ataxia-telangiectasia mutated (ATM) is a central kinase of DNA damage response. Phosphorylated H2AX mediated by ATM serves as a platform to recruit other DNA damage repair proteins (Ciccia and Elledge, 2010). Aberrant ATM pathway exerts important role in the onset of SCA3: mutant but not wild-type ATX3 expression in SH-SY5Y cells remarkably activates ATM signaling pathway, as indicated by phosphorylation of ATM and its downstream targets including H2AX, Chk2 and p53, and phosphorylation of p53 and Chk2 is diminished by ATM inhibitor KU-55933, suggesting that DDR evoked by mutant ATX3 relies on ATM. Moreover, mutant ATX3 activates pro-apoptotic pathway by activating ATM, which can be restored by ATM inhibition (Gao et al., 2015). And ectopic expression of mutant HTT results in increased ROS levels, DNA damage and ATM activation (Giuliano et al., 2003; Illuzzi et al., 2009; Bertoni et al., 2011). Elevated ATM signaling and γH2AX levels was also observed in cells from HD patients and HD mouse (Giuliano et al., 2003; Enokido et al., 2010). These results imply that inhibition of ATM signaling might be protective against genotoxicity induced by mutant HTT. Indeed, ATM reduction alleviates motor deficits caused by mutant HTT in *drosophila* and mouse models, and pharmacological inhibition of ATM by KU-60019 or KU-55933 also exerts neuroprotective effects in rat striatal neurons and HD patient iPSC-derived neurons (Lu et al., 2014). Hence, ATM might be a potential therapeutic target for SCA3 and HD.

PNKP

Recently, both mutant ATX3 and mutant HTT were reported to impair PNKP activity, disrupting strand break repair and transcription. Consistently, there is a higher level of DNA breaks in transcribed genes in affected brain regions of SCA3 patients and mice, and brains of HD patients and mice also show DNA damage accumulation as compared to control (Gao et al., 2019; Chakraborty et al., 2020). In addition, mutant HTT impairs ATX3 activity, which promotes ubiquitination and degradation of CBP, negatively impacting transcription (Gao et al., 2019). More importantly, upregulation of PNKP activity rescues deficient DSB repair and neurotoxicity in SCA3 *Drosophila*, and PNKP overexpression significantly rescues cell toxicity induced by mutant HTT (Gao et al., 2019; Chakraborty et al., 2020). These studies indicate the potential of PNKP as a therapeutic target for SCA3 and HD.

In addition, elevated ADP-ribose levels after DNA damage are observed in PNKP-patient cells (Hoch et al., 2017). Given that mutant ATX3 can inhibit phosphatase activity of PNKP and result in accumulation of DNA breaks (Gao et al., 2015), it might also cause PARP1 hyperactivation. To figure out the therapeutic potential of PAPR inhibition in SCA3 therapy, further studies are still needed.

Apoptosis as Therapy Targets

Apoptosis is regarded as the dominant mechanism underlying neurodegeneration in PD (Kountouras et al., 2012). A lot of studies also support the role of apoptosis in SCA3 and HD (Sawa et al., 1999; Wellington et al., 2000; Vis et al., 2005). Tumor suppressor protein p53 is known to play a crucial role in deciding cell fate under stress and suppressing the propagation of damaged cells. As mentioned above, mutant ATX3 causes neurodegeneration via apoptosis by upregulating p53 function, and neurodegeneration in animal (zebra fish and mouse) models is remarkably halted by p53 deficiency (Liu et al., 2016). Besides, mutant ATX3 activates apoptosis pathway mediated by p53 and PKC after prolonged accumulation of DNA damage (Gao

et al., 2015). Thus, inhibiting p53 activity in neurons could be a potential therapeutic strategy for SCA3.

It was previously reported that p53 is involved in the pathogenesis of HD (Steffan et al., 2000; Trettel et al., 2000) and ployQ-expanded HTT results in transcription dysregulation by interacting with transcription factors such as p53 (Yu et al., 2002; Schaffar et al., 2004; Bae et al., 2005; Cong et al., 2005). There are results indicating that p53 expression level is elevated in HD patients and mice, and that polyQ-induced toxicity is mediated by p53. Consistently, p53 perturbation by pharmacologic inhibitor pifithrin-α (PFT-α), RNAi or genetic deletion significantly rescue the neurodegeneration in HD models (Bae et al., 2005). Similarly, p53 inhibitor PFT-α and p53 knockdown can efficiently relieve polyQ-induced neuronal cell death (Anne et al., 2007). Moreover, PFT-α can enhance the survival of dopamine cell transplants and augment behavioral recovery in parkinsonian animals, which indicates that p53 may be also served as a potential therapeutic target for HD and PD (Chou et al., 2011).

CONCLUSION

Although significant advances have been made in establishing normal functions of ATX3 and etiology of SCA3, the underlying molecular mechanism of SCA3 pathogenesis is still urging for sussing out. The impaired functions of ATX3-interacting proteins, sequestered in the polyQ aggregates, is thought to associate with cellular toxicity and neurodegeneration in SCA3 (Paulson et al., 1997; Warrick et al., 1998; Chai et al., 1999a,b, 2002; Ferrigno and Silver, 2000; McCampbell et al., 2000; Schmidt et al., 2002). In the present context, we have tried to give a comprehensive overview of the novel physiological functions of ATX3 in DDR and apoptosis, which relies on interaction between ATX3 and key players in these pathways.

Given that the post-mitotic status of neurons and high level of oxygen metabolism in brain, efficient DDR is absolutely essential for neuronal function and survival. ROS are reported to be responsible for various neurological disorders such as AD and PD. Although the underlying mechanism that contributes to selective neuronal death and pathological changes remains to be investigated, it is thought that the role of ROS in the pathogenesis of these disorders is associated with proteins including a-synuclein, DJ-1, Amyloid β and tau protein (Jiang et al., 2016). For example, oxidative stress can result in upregulated expression of β-secretase and aberrant phosphorylation of tau (Lovell et al., 2004; Tamagno et al., 2005), and oxidative stress-induced damage may compromise the functions of crucial molecules such as Parkin. In comparison with these oxidative stress-induced changes of essential proteins and consequent pathology of AD or PD, ATX3 is directly involved in counteracting oxidative stress by enhancing the association between Bcl-xL and Bax or promoting the expression of antioxidant SOD2 (Araujo et al., 2011; Zhou et al., 2013). More particularly, ATX3 itself is involved in DNA strand break repair by stimulating the activity of PNKP and maintaining the accumulation of MDC1 at breaks, which are both essential for the removal of oxidative stress-induced DNA lesions. Importantly, aberrant polyQ expansion, which is defined as the cause of SCA3, compromises the crucial roles of ATX3 in counteracting oxidative stress and maintaining genome integrity, resulting in neuronal dysfunction and cell death. Current findings about the direct roles of ATX3 and HTT in DDR and apoptosis, and abnormal of which caused by polyQ expansion will help us decipher the molecular pathogenic mechanism of SCA3 and HD. Discussing the molecular changes and related pathways shared by these neurodegenerative diseases would lead to a better understanding of the network in these disorders and facilitating to develop therapeutic strategy for these disorders. Consistently, there are many studies indicating that targeted modulation of DDR and apoptosis can relieve the pathology of many neurodegenerative diseases including HD and SCA3 (Lu et al., 2014; Gao et al., 2015, 2019; Chakraborty et al., 2020).

DDR is also an important pathway in cancer genesis. Sharing the same pathway, it seemed that neurodegeneration and cancer have a subtle linkage, and this relationship alerts us that we need to cautiously assess the cancer risk if we plan to use drugs targeting DDR to slow down the progress of neurodegenerative diseases. For example, p53 is abnormally activated in SCA3, inhibiting the function of p53 may alleviate the degeneration disease, whereas bring about high risk of cancer. Therefore, although many preclinical studies indicate the efficiency of DDR and apoptosis modulation in improving the pathology of neurodegenerative diseases including SCA3, further investigation is undoubtedly needed to confirm target specificity and minimize side effects before their employment for therapeutic intervention. We hope that future studies regarding SCA3 and neurodegenerative diseases will provide effective solutions for clinical therapy.

AUTHOR CONTRIBUTIONS

All authors listed have made a substantial, direct and intellectual contribution to the work, and approved it for publication.

FUNDING

This work was supported by National Key Research and Development Program of China (2018YFA0108500), the Strategic Priority Research Program of the Chinese Academy of Sciences (XDA16010107), National Natural Science Foundation of China (31801198, 81901281, 82030033, and 91754204), and Natural Science Foundation of Beijing (5181001).

ACKNOWLEDGMENTS

The authors thank Hongmei Liu and Fengli Wang for helpful discussions.

REFERENCES

Acevedo-Torres, W., Berrios, L., Rosario, N., Dufault, V., Skatchkov, S., Eaton, M. J., et al. (2008). Mitochondrial DNA damage is a hallmark of chemically-induced and the r6/2 Transgenic models of Huntington's disease. *Environ. Mol. Mutagen* 49, 522–522. doi: 10.1016/j.dnarep.2008.09.004

Ackermann, L., Schell, M., Pokrzywa, W., Kevei, E., Gartner, A., Schumacher, B., et al. (2016). E4 ligase-specific ubiquitination hubs coordinate DNA double-strand-break repair and apoptosis. *Nat. Struct. Mol. Biol.* 23, 995–1002. doi: 10.1038/nsmb.3296

Alonso-de Vega, I., Martin, Y., and Smits, V. A. (2014). USP7 controls Chk1 protein stability by direct deubiquitination. *Cell Cycle* 13, 3921–3926. doi: 10.4161/15384101.2014.973324

Anne, S. L., Saudou, F., and Humbert, S. (2007). Phosphorylation of huntingtin by cyclin-dependent kinase 5 is induced by DNA damage and regulates wild-type and mutant huntingtin toxicity in neurons. *J. Neurosci.* 27, 7318–7328. doi: 10.1523/JNEUROSCI.1831-07.2007

Araujo, J., Breuer, P., Dieringer, S., Krauss, S., Dorn, S., Zimmermann, K., et al. (2011). FOXO4-dependent upregulation of superoxide dismutase-2 in response to oxidative stress is impaired in spinocerebellar ataxia type 3. *Hum. Mol. Genet.* 20, 2928–2941. doi: 10.1093/hmg/ddr197

Bae, B. I., Xu, H., Igarashi, S., Fujimuro, M., Agrawal, N., Taya, Y., et al. (2005). p53 mediates cellular dysfunction and behavioral abnormalities in Huntington's disease. *Neuron* 47, 29–41. doi: 10.1016/j.neuron.2005.06.005

Barclay, S. S., Tamura, T., Ito, H., Fujita, K., Tagawa, K., Shimamura, T., et al. (2014). Systems biology analysis of Drosophila *in vivo* screen data elucidates core networks for DNA damage repair in SCA1. *Hum. Mol. Genet.* 23, 1345–1364. doi: 10.1093/hmg/ddt524

Bennett, C. B., Lewis, A. L., Baldwin, K. K., and Resnick, M. A. (1993). Lethality induced by a single site-specific double-strand break in a dispensable yeast plasmid. *Proc. Natl. Acad. Sci. U.S.A.* 90, 5613–5617. doi: 10.1073/pnas.90.12.5613

Berke, S. J., Chai, Y., Marrs, G. L., Wen, H., and Paulson, H. L. (2005). Defining the role of ubiquitin-interacting motifs in the polyglutamine disease protein, ataxin-3. *J. Biol. Chem.* 280, 32026–32034. doi: 10.1074/jbc.M506084200

Berke, S. J., Schmied, F. A., Brunt, E. R., Ellerby, L. M., and Paulson, H. L. (2004). Caspase-mediated proteolysis of the polyglutamine disease protein ataxin-3. *J. Neurochem.* 89, 908–918. doi: 10.1111/j.1471-4159.2004.02369.x

Bertoni, A., Giuliano, P., Galgani, M., Rotoli, D., Ulianich, L., Adornetto, A., et al. (2011). Early and late events induced by PolyQ-expanded proteins identification of a common pathogenic property of polyQ-Expanded Proteins. *J. Biol. Chem.* 286, 4727–4741. doi: 10.1074/jbc.M110.156521

Bettencourt, C., Hensman-Moss, D., Flower, M., Wiethoff, S., Brice, A., Goizet, C., et al. (2016). DNA repair pathways underlie a common genetic mechanism modulating onset in polyglutamine diseases. *Ann. Neurol.* 79, 983–990. doi: 10.1002/ana.24656

Boeddrich, A., Gaumer, S., Haacke, A., Tzvetkov, N., Albrecht, M., Evert, B., et al. (2006). An arginine/lysine-rich motif is crucial for VCP/p97-mediated modulation of ataxin-3 fibrillogenesis. *EMBO J.* 25, 1547–1558. doi: 10.1038/sj.emboj.7601043

Bogdanov, M. B., Andreassen, O. A., Dedeoglu, A., Ferrante, R. J., and Beal, M. F. (2001). Increased oxidative damage to DNA in a transgenic mouse model of Huntington's disease. *J. Neurochem.* 79, 1246–1249. doi: 10.1046/j.1471-4159.2001.00689.x

Browne, S. E., Bowling, A. C., MacGarvey, U., Baik, M. J., Berger, S. C., Muqit, M. M. K., et al. (1997). Oxidative damage and metabolic dysfunction in Huntington's disease: selective vulnerability of the basal ganglia. *Ann. Neurol.* 41, 646–653. doi: 10.1002/ana.410410514

Burnett, B., Li, F., and Pittman, R. N. (2003). The polyglutamine neurodegenerative protein ataxin-3 binds polyubiquitylated proteins and has ubiquitin protease activity. *Hum. Mol. Genet.* 12, 3195–3205. doi: 10.1093/hmg/ddg344

Caldecott, K. W. (2003). XRCC1 and DNA strand break repair. *DNA Repair* 2, 955–969. doi: 10.1016/S1568-7864(03)00118-6

Chai, Y., Koppenhafer, S. L., Bonini, N. M., and Paulson, H. (1999a). Analysis of the role of heat shock protein (Hsp) molecular chaperones in polyglutamine disease. *J. Neurosci.* 19, 10338–10347. doi: 10.1523/JNEUROSCI.19-23-10338.1999

Chai, Y., Koppenhafer, S. L., Shoesmith, S. J., Perez, M., and Paulson, H. (1999b). Evidence for proteasome involvement in polyglutamine disease: localization to nuclear inclusions in SCA3/MJD and suppression of polyglutamine aggregation *in vitro*. *Hum. Mol. Genet.* 8, 673–682. doi: 10.1093/hmg/8.4.673

Chai, Y., Shao, J., Miller, V. M., Williams, A., and Paulson, H. (2002). Live-cell imaging reveals divergent intracellular dynamics of polyglutamine disease proteins and supports a sequestration model of pathogenesis. *Proc. Natl. Acad. Sci. U.S.A.* 99, 9310–9315. doi: 10.1073/pnas.152101299

Chakraborty, A., Tapryal, N., Venkova, T., Horikoshi, N., Pandita, R. K., Sarker, A. H., et al. (2016). Classical non-homologous end-joining pathway utilizes nascent RNA for error-free double-strand break repair of transcribed genes. *Nat. Commun.* 7:13049. doi: 10.1038/ncomms13049

Chakraborty, A., Tapryal, N., Venkova, T., Mitra, J., Vasquez, V., Sarker, A., et al. (2020). Deficiency in classical nonhomologous end-joining-mediated repair of transcribed genes is linked to SCA3 pathogenesis. *Proc. Natl. Acad. Sci. U.S.A.* 117, 8154–8165. doi: 10.1073/pnas.1917280117

Chang, J. R., Ghafouri, M., Mukerjee, R., Bagashev, A., Chabrashvili, T., Sawaya, B., et al. (2012). Role of p53 in neurodegenerative diseases. *Neurodegener. Dis.* 9, 68–80. doi: 10.1159/000329999

Chappell, C., Hanakahi, L. A., Karimi-Busheri, F., Weinfeld, M., and West, S. (2002). Involvement of human polynucleotide kinase in double-strand break repair by non-homologous end joining. *EMBO J.* 21, 2827–2832. doi: 10.1093/emboj/21.11.2827

Chatterjee, A., Saha, S., Chakraborty, A., Silva-Fernandes, A., Mandal, S. M., Neves-Carvalho, A., et al. (2015). The role of the mammalian DNA end-processing enzyme polynucleotide kinase 3'-phosphatase in spinocerebellar ataxia type 3 pathogenesis. *PLoS Genet.* 11:e1004749. doi: 10.1371/journal.pgen.1004749

Chen, C. M., Wu, Y. R., Cheng, M. L., Liu, J., Lee, Y. M., Lee, P. W., et al. (2007). Increased oxidative damage and mitochondrial abnormalities in the peripheral blood of Huntington's disease patients. *Biochem. Biophys. Res. Commun.* 359, 335–340. doi: 10.1016/j.bbrc.2007.05.093

Chen, D., Kon, N., Li, M., Zhang, W., Qin, J., and Gu, W. (2005). ARF-BP1/Mule is a critical mediator of the ARF tumor suppressor. *Cell* 121, 1071–1083. doi: 10.1016/j.cell.2005.03.037

Chen, X., Tang, T. S., Tu, H., Nelson, O., Pook, M., Hammer, R., et al. (2008). Deranged calcium signaling and neurodegeneration in spinocerebellar ataxia type 3. *J. Neurosci.* 28, 12713–12724. doi: 10.1523/JNEUROSCI.3909-08.2008

Cheng, E. H., Levine, B., Boise, L. H., Thompson, C. B., and Hardwick, J. M. (1996). Bax-independent inhibition of apoptosis by Bcl-XL. *Nature* 379, 554–556. doi: 10.1038/379554a0

Choo, Y. S., Johnson, G. V., MacDonald, M., Detloff, P. J., and Lesort, M. (2004). Mutant huntingtin directly increases susceptibility of mitochondria to the calcium-induced permeability transition and cytochrome c release. *Hum. Mol. Genet.* 13, 1407–1420. doi: 10.1093/hmg/ddh162

Chou, A. H., Yeh, T. H., Kuo, Y. L., Kao, Y. C., Jou, M. J., Hsu, C. Y., et al. (2006). Polyglutamine-expanded ataxin-3 activates mitochondrial apoptotic pathway by upregulating Bax and downregulating Bcl-xL. *Neurobiol. Dis.* 21, 333–345. doi: 10.1016/j.nbd.2005.07.011

Chou, J., Greig, N. H., Reiner, D., Hoffer, B. J., and Wang, Y. (2011). Enhanced survival of dopaminergic neuronal transplants in hemiparkinsonian rats by the p53 inactivator PFT-alpha. *Cell Transplant.* 20, 1351–1359. doi: 10.3727/096368910X557173

Ciccia, A., and Elledge, S. J. (2010). The DNA damage response: making it safe to play with knives. *Mol. Cell* 40, 179–204. doi: 10.1016/j.molcel.2010.09.019

Cong, S. Y., Pepers, B. A., Evert, B. O., Rubinsztein, D. C., Roos, R. A., van Ommen, G. J., et al. (2005). Mutant huntingtin represses CBP, but not p300, by binding and protein degradation. *Mol. Cell. Neurosci.* 30, 560–571. doi: 10.1016/j.mcn.2005.05.003

Cooper, J. K., Schilling, G., Peters, M. F., Herring, W. J., Sharp, A. H., Kaminsky, Z., et al. (1998). Truncated N-terminal fragments of huntingtin with expanded glutamine repeats form nuclear and cytoplasmic aggregates in cell culture. *Hum. Mol. Genet.* 7, 783–790. doi: 10.1093/hmg/7.5.783

Danial, N. N., and Korsmeyer, S. J. (2004). Cell death: critical control points. *Cell* 116, 205–219. doi: 10.1016/S0092-8674(04)00046-7

Donaldson, K. M., Li, W., Ching, K. A., Batalov, S., Tsai, C. C., and Joazeiro, C. A. (2003). Ubiquitin-mediated sequestration of normal cellular proteins

into polyglutamine aggregates. *Proc. Natl. Acad. Sci. U.S.A.* 100, 8892–8897. doi: 10.1073/pnas.1530212100

Dornan, D., Wertz, I., Shimizu, H., Arnott, D., Frantz, G. D., Dowd, P., et al. (2004). The ubiquitin ligase COP1 is a critical negative regulator of p53. *Nature* 429, 86–92. doi: 10.1038/nature02514

Dou, H., Huang, C., Singh, M., Carpenter, P., B., and Yeh, E. (2010). Regulation of DNA repair through deSUMOylation and SUMOylation of replication protein A complex. *Mol. Cell* 39, 333–345. doi: 10.1016/j.molcel.2010.07.021

Dragatsis, I., Levine, M. S., and Zeitlin, S. (2000). Inactivation of Hdh in the brain and testis results in progressive neurodegeneration and sterility in mice. *Nat. Genet.* 26, 300–306. doi: 10.1038/81593

Enokido, Y., Tamura, T., Ito, H., Arumughan, A., Komuro, A., Shiwaku, H., et al. (2010). Mutant huntingtin impairs Ku70-mediated DNA repair. *J. Cell Biol.*189, 425–443. doi: 10.1083/jcb.200905138

Feijoo, C., Hall-Jackson, C., Wu, R., Jenkins, D., Leitch, J., Gilbert, D., et al. (2001). Activation of mammalian Chk1 during DNA replication arrest: a role for Chk1 in the intra-S phase checkpoint monitoring replication origin firing. *J. Cell Biol.* 154, 913–923. doi: 10.1083/jcb.200104099

Ferlazzo, M. L., Sonzogni, L., Granzotto, A., Bodgi, L., Lartin, O., Devic, C., et al. (2014). Mutations of the Huntington's disease protein impact on the ATM-dependent signaling and repair pathways of the radiation-induced DNA Double-Strand Breaks: Corrective Effect Of Statins And Bisphosphonates. *Mol. Neurobiol.* 49, 1200–1211. doi: 10.1007/s12035-013-8591-7

Ferrigno, P., and Silver, P. A. (2000). Polyglutamine expansions: proteolysis, chaperones, and the dangers of promiscuity. *Neuron* 26, 9–12. doi: 10.1016/S0896-6273(00)81132-0

Friedberg, E. C. (2003). DNA damage and repair. *Nature* 421, 436–440. doi: 10.1038/nature01408

Friedberg, E. C., Walker, G. C., and Siede, W. (1995). *DNA Repair and Mutagenesis*. Washington, DC: ASM Press.

Galanty, Y., Belotserkovskaya, R., Coates, J., and Jackson, S. P. (2012). RNF4, a SUMO-targeted ubiquitin E3 ligase, promotes DNA double-strand break repair. *Genes Dev.* 26, 1179–1195. doi: 10.1101/gad.188284.112

Gao, R., Chakraborty, A., Geater, C., Pradhan, S., Gordon, K. L., Snowden, J., et al. (2019). Mutant huntingtin impairs PNKP and ATXN3, disrupting DNA repair and transcription. *Elife* 8:e42988. doi: 10.7554/eLife.42988

Gao, R., Liu, Y., Silva-Fernandes, A., Fang, X., Paulucci-Holthauzen, A., Chatterjee, A., et al. (2015). Inactivation of PNKP by mutant ATXN3 triggers apoptosis by activating the DNA damage-response pathway in SCA3. *PLoS Genet.* 11:e1004834. doi: 10.1371/journal.pgen.1004834

Ghavami, S., Shojaeid, S., Yeganeh, B., Ande, S. R., Jangamreddy, J. R., Mehrpour, M., et al. (2014). Autophagy and apoptosis dysfunction in neurodegenerative disorders. *Prog. Neurobiol.* 112, 24–49. doi: 10.1016/j.pneurobio.2013.10.004

Giuliano, P., de Cristofaro, T., Affaitati, A., Pizzulo, G., M., Feliciello, A., Criscuolo, C., et al. (2003). DNA damage induced by polyglutamine-expanded proteins. *Hum. Mol. Genet.* 12, 2301–2309. doi: 10.1093/hmg/ddg242

Green, D. R., and Kroemer, G. (2004). The pathophysiology of mitochondrial cell death. *Science* 305, 626–629. doi: 10.1126/science.1099320

Guervilly, J. H., Renaud, E., Takata, M., and Rosselli, F. (2011). USP1 deubiquitinase maintains phosphorylated CHK1 by limiting its DDB1-dependent degradation. *Hum. Mol. Genet.* 20, 2171–2181. doi: 10.1093/hmg/ddr103

Hackam, A. S., Singaraja, R., Wellington, C. L., Metzler, M., McCutcheon, K., Zhang, T., et al. (1998). The influence of huntingtin protein size on nuclear localization and cellular toxicity. *J. Cell Biol.* 141, 1097–1105. doi: 10.1083/jcb.141.5.1097

Harper, J. W., and Elledge, S. J. (2007). The DNA damage response: ten years after. *Mol. Cell* 28, 739–745. doi: 10.1016/j.molcel.2007.11.015

Hoch, N. C., Hanzlikova, H., Rulten, S. L., Tetreault, M., Komulainen, E., Ju, L. M., et al. (2017). XRCC1 mutation is associated with PARP1 hyperactivation and cerebellar ataxia. *Nature* 541, 87–91. doi: 10.1038/nature20790

Hodgson, J. G., Agopyan, N., Gutekunst, C. A., Leavitt, B. R., LePiane, F., Singaraja, R., et al. (1999). A YAC mouse model for Huntington's disease with full-length mutant huntingtin, cytoplasmic toxicity, and selective striatal neurodegeneration. *Neuron* 23, 181–192. doi: 10.1016/S0896-6273(00)80764-3

Hoeijmakers, J. H. (2009). DNA damage, aging, and cancer. *N. Engl. J. Med.* 361, 1475–1485. doi: 10.1056/NEJMra0804615

Huen, M. S., Grant, R., Manke, I., Minn, K., Yu, X., Yaffe, M., et al. (2007). RNF8 transduces the DNA-damage signal via histone ubiquitylation and checkpoint protein assembly. *Cell* 131, 901–914. doi: 10.1016/j.cell.2007.09.041

Illuzzi, J., Yerkes, S., Parekh-Olmedo, H., and Kmiec, E. B. (2009). DNA breakage and induction of DNA damage response proteins precede the appearance of visible mutant huntingtin aggregates. *J. Neurosci. Res.* 87, 733–747. doi: 10.1002/jnr.21881

Jackson, S. P., and Bartek, J. (2009). The DNA-damage response in human biology and disease. *Nature* 46, 1071–1078. doi: 10.1038/nature08467

Jeppesen, D. K., Bohr, V. A., and Stevnsner, T. (2011). DNA repair deficiency in neurodegeneration. *Prog. Neurobiol.* 94, 166–200. doi: 10.1016/j.pneurobio.2011.04.013

Jiang, T., Sun, Q., and Chen, S. (2016). Oxidative stress: a major pathogenesis and potential therapeutic target of antioxidative agents in Parkinson's disease and Alzheimer's disease. *Prog. Neurobiol.* 147, 1–19. doi: 10.1016/j.pneurobio.2016.07.005

Jilani, A., Ramotar, D., Slack, C., Ong, C., Yang, X. M., Scherer, S. W.,et al. (1999). Molecular cloning of the human gene, PNKP, encoding a polynucleotide kinase 3'-phosphatase and evidence for its role in repair of DNA strand breaks caused by oxidative damage. *J. Biol. Chem.* 274, 24176–24186. doi: 10.1074/jbc.274.34.24176

Karimi-Busheri, F., Rasouli-Nia, A., Allalunis-Turner, J., and Weinfeld, M. (2007). Human polynucleotide kinase participates in repair of DNA double-strand breaks by nonhomologous end joining but not homologous recombination. *Cancer Res.* 67, 6619–6625. doi: 10.1158/0008-5472.CAN-07-0480

Katyal, S., and McKinnon, P. J. (2008). DNA strand breaks, neurodegeneration and aging in the brain. *Mech. Ageing Dev.* 129, 483–491. doi: 10.1016/j.mad.2008.03.008

Kawaguchi, Y., Okamoto, T., Taniwaki, M., Aizawa, M., Inoue, M., Katayama, S., et al. (1994). CAG expansions in a novel gene for Machado-Joseph disease at chromosome 14q32.1. *Nat. Genet.* 8, 221–228. doi: 10.1038/ng1194-221

Kegel, K. B., Kim, M., Sapp, E., McIntyre, C., Castano, J. G., Aronin, N.,et al. (2000). Huntingtin expression stimulates endosomal-lysosomal activity, endosome tubulation, and autophagy. *J. Neurosci.* 20, 7268–7278. doi: 10.1523/JNEUROSCI.20-19-07268.2000

Koch, C. A., Agyei, R., Galicia, S., Metalnikov, P., O'Donnell, P., Starostine, A., et al. (2004). Xrcc4 physically links DNA end processing by polynucleotide kinase to DNA ligation by DNA ligase IV. *EMBO J.* 23, 3874–3885. doi: 10.1038/sj.emboj.7600375

Kops, G. J., Dansen, T. B., Polderman, P. E., Saarloos, I., Wirtz, K. W., Coffer, P. J., et al. (2002). Forkhead transcription factor FOXO3a protects quiescent cells from oxidative stress. *Nature* 419, 316–321. doi: 10.1038/nature01036

Kountouras, J., Zavos, C., Polyzos, S. A., Deretzi, G., Vardaka, E., Giartza-Taxidou, E., et al. (2012). *Helicobacter pylori* infection and Parkinson's disease: apoptosis as an underlying common contributor. *Eur. J. Neurol.* 19, e56–e56. doi: 10.1111/j.1468-1331.2012.03695.x

Kwon, M. J., Han, M. H., Bagley, J. A., Hyeon, D., Ko, B. S., Lee, Y. M., et al. (2018). Coiled-coil structure-dependent interactions between polyQ proteins and Foxo lead to dendrite pathology and behavioral defects. *Proc. Natl. Acad. Sci. U.S.A.* 115, E10748–E10757. doi: 10.1073/pnas.1807206115

Leavitt, B. R., Guttman, J. A., Hodgson, J. G., Kimel, G. H., Singaraja, R., Vogl, A. W., et al. (2001). Wild-type huntingtin reduces the cellular toxicity of mutant huntingtin *in vivo*. *Am. J. Hum. Genet.* 68, 313–324. doi: 10.1086/318207

Lebovitz, R. M., Zhang, H., Vogel, H., Cartwright, J. Jr., Dionne, L., Lu, N., et al. (1996). Neurodegeneration, myocardial injury, and perinatal death in mitochondrial superoxide dismutase-deficient mice. *Proc. Natl. Acad. Sci. U.S.A.* 93, 9782–9787. doi: 10.1073/pnas.93.18.9782

Lee, J. M., Wheeler, V. C., Chao, M. J., Vonsattel, J. P., Pinto, R. M., Lucente, D., et al. (2015). Identification of genetic factors that modify clinical onset of Huntington's disease. *Cell* 162, 516–526. doi: 10.1016/j.cell.2015.07.003

Leng, R. P., Lin, Y., Ma, W., Wu, H., Lemmers, B., Chung, S., et al. (2003). Pirh2, a p53-induced ubiquitin-protein ligase, promotes p53 degradation. *Cell* 112, 779–791. doi: 10.1016/S0092-8674(03)00193-4

Li, M., Brooks, C., L., Kon, N., and Gu, W. (2004). A dynamic role of HAUSP in the p53-Mdm2 pathway. *Mol. Cell* 13, 879–886. doi: 10.1016/S1097-2765(04)00157-1

Liu, H., Li, X., Ning, G., Zhu, S., Ma, X., Liu, X., et al. (2016). The Machado-Joseph disease deubiquitinase Ataxin-3 regulates the stability and apoptotic function of p53. *PLoS Biol.* 14:e2000733. doi: 10.1371/journal.pbio.2000733

Lovell, M. A., Xiong, S., Xie, C., Davies, P., and Markesbery, W. R. (2004). Induction of hyperphosphorylated tau in primary rat cortical neuron cultures mediated by oxidative stress and glycogen synthase kinase-3. *J. Alzheimers Dis.* 6, 659–671; discussion 673–681. doi: 10.3233/JAD-2004-6610

Lu, X. H., Mattis, V. B., Wang, N., Al-Ramahi, I., van den Berg, N. Fratantoni, S., A., et al. (2014). Targeting ATM ameliorates mutant Huntingtin toxicity in cell and animal models of Huntington's disease. *Sci. Transl. Med.* 6:268ra178. doi: 10.1126/scitranslmed.3010523

Lunkes, A., and Mandel, J. L. (1998). A cellular model that recapitulates major pathogenic steps of Huntington's disease. *Hum. Mol. Genet.* 7, 1355–1361. doi: 10.1093/hmg/7.9.1355

Luo, K., Zhang, H., Wang, L., Yuan, J., and Lou, Z. (2012). Sumoylation of MDC1 is important for proper DNA damage response. *EMBO J.* 31, 3008–3019. doi: 10.1038/emboj.2012.158

Maiuri, T., Mocle, A. J., Hung, C. L., Xia, J., van Roon-Mom, W. M. C., and Truant, R. (2017). Huntingtin is a scaffolding protein in the ATM oxidative DNA damage response complex. *Hum. Mol. Genet.* 26, 395–406. doi: 10.1093/hmg/ddw395

Matos, C. A., de Macedo-Ribeiro, S., and Carvalho, A. L. (2011). Polyglutamine diseases: the special case of ataxin-3 and Machado-Joseph disease. *Prog Neurobiol.* 95, 26–48. doi: 10.1016/j.pneurobio.2011.06.007

McCampbell, A., Taylor, J. P., Taye, A. A., Robitschek, J., Li, M., Walcott, J., et al. (2000). CREB-binding protein sequestration by expanded polyglutamine. *Hum. Mol. Genet.* 9, 2197–2202. doi: 10.1093/hmg/9.14.2197

Moss, D. J. H., Pardias, A. F., and Langbehn, D. (2017). Identification of genetic variants associated with Huntington's disease progression: a genome-wide association study (2017). *Lancet Neurol.* 16, 683–683. doi: 10.1016/S1474-4422(17)30161-8

Muller, P. A., and Vousden, K. H. (2013). p53 mutations in cancer. *Nat. Cell Biol.* 15, 2–8. doi: 10.1038/ncb2641

Muller, S., Scaffidi, P., Degryse, B., Bonaldi, T., Ronfani, L., Agresti, A., et al. (2001). New EMBO members' review: the double life of HMGB1 chromatin protein: architectural factor and extracellular signal. *EMBO J.* 20, 4337–4340. doi: 10.1093/emboj/20.16.4337

Nishi, R., Wijnhoven, P., le Sage, C., Tjeertes, J., Galanty, Y., Forment, J., et al. (2014). Systematic characterization of deubiquitylating enzymes for roles in maintaining genome integrity. *Nat. Cell Biol.* 16, 1016–1026, 1011–1018. doi: 10.1038/ncb3028

Olsson, A., Manzl, C., Strasser, A., and Villunger, A. (2007). How important are post-translational modifications in p53 for selectivity in target-gene transcription and tumour suppression? *Cell Death Differ.* 14, 1561–1575. doi: 10.1038/sj.cdd.4402196

Park, C., Suh, Y., and Cuervo, A. M. (2015). Regulated degradation of Chk1 by chaperone-mediated autophagy in response to DNA damage. *Nat. Commun.* 6: 6823. doi: 10.1038/ncomms7823

Parsons, J. L., Khoronenkova, S., Dianova, V. II., Ternette, N., Kessler, B. M., Datta, P. K., et al. (2012). Phosphorylation of PNKP by ATM prevents its proteasomal degradation and enhances resistance to oxidative stress. *Nucleic Acids Res.* 40, 11404–11415. doi: 10.1093/nar/gks909

Paulson, H. (2012). Machado-Joseph disease/spinocerebellar ataxia type 3. *Handb. Clin. Neurol.* 103, 437–449. doi: 10.1016/B978-0-444-51892-7.00027-9

Paulson, H. L., Perez, M. K., Trottier, Y., Trojanowski, J. Q., Subramony, S. H., Das, S. S., et al. (1997). Intranuclear inclusions of expanded polyglutamine protein in spinocerebellar ataxia type 3. *Neuron* 19, 333–344. doi: 10.1016/S0896-6273(00)80943-5

Pfeiffer, A., Luijsterburg, M. S., Acs, K., Wiegant, W. W., Helfricht, A., Herzog, L. K., et al. (2017). Ataxin-3 consolidates the MDC1-dependent DNA double-strand break response by counteracting the SUMO-targeted ubiquitin ligase RNF4. *EMBO J.* 36, 1066–1083. doi: 10.15252/embj.201695151

Qi, M. L., Tagawa, K., Enokido, Y., Yoshimura, N., Wada, Y., Watase, K., et al. (2007). Proteome analysis of soluble nuclear proteins reveals that HMGB1/2 suppress genotoxic stress in polyglutamine diseases. *Nat. Cell Biol.* 9, 402–414. doi: 10.1038/ncb1553

Rasouli-Nia, A., Karimi-Busheri, F., and Weinfeld, M. (2004). Stable down-regulation of human polynucleotide kinase enhances spontaneous mutation frequency and sensitizes cells to genotoxic agents. *Proc. Natl. Acad. Sci. U.S.A.* 101, 6905–6910. doi: 10.1073/pnas.0400099101

Reddy, P. H., Williams, M., Charles, V., Garrett, L., Pike-Buchanan, L., Whetsell, W., et al. (1998). Behavioural abnormalities and selective neuronal loss in HD transgenic mice expressing mutated full-length HD cDNA. *Nat. Genet.* 20, 198–202. doi: 10.1038/2510

Reynolds, J. J., Walker, A. K., Gilmore, E. C., Walsh, C. A., and Caldecott, K. W. (2012). Impact of PNKP mutations associated with microcephaly, seizures and developmental delay on enzyme activity and DNA strand break repair. *Nucleic Acids Res.* 40, 6608–6619. doi: 10.1093/nar/gks318

Riess, O., Rub, U., Pastore, A., Bauer, P., and Schols, L. (2008). SCA3: neurological features, pathogenesis and animal models. *Cerebellum* 7, 125–137. doi: 10.1007/s12311-008-0013-4

Rigamonti, D., Bauer, J. H., De-Fraja, C., Conti, L., Sipione, S., Sciorati, C., et al. (2000). Wild-type huntingtin protects from apoptosis upstream of caspase-3. *J. Neurosci.* 20, 3705–3713. doi: 10.1523/JNEUROSCI.20-10-03705.2000

Ross, C. A., Aylward, E. H., Wild, E. J., Langbehn, D. R., Long, J. D., Warner, J. H., et al. (2014). Huntington disease: natural history, biomarkers and prospects for therapeutics. *Nat. Rev. Neurol.* 10, 204–216. doi: 10.1038/nrneurol.2014.24

Sandell, L. L., and Zakian, V. A. (1993). Loss of a yeast telomere: arrest, recovery, and chromosome loss. *Cell* 75, 729–739. doi: 10.1016/0092-8674(93)90493-A

Sawa, A., Wiegand, G. W., Cooper, J., Margolis, R. L., Sharp, A. H., Lawler, J. F., et al. (1999). Increased apoptosis of Huntington disease lymphoblasts associated with repeat length-dependent mitochondrial depolarization. *Nat. Med.* 5, 1194–1198. doi: 10.1038/13518

Schaffar, G., Breuer, P., Boteva, R., Behrends, C., Tzvetkov, N., Strippel, N., et al. (2004). Cellular toxicity of polyglutamine expansion proteins: mechanism of transcription factor deactivation. *Mol. Cell* 15, 95–105. doi: 10.1016/j.molcel.2004.06.029

Schmidt, T., Landwehrmeyer, G. B., Schmitt, I., Trottier, Y., Auburger, G., Laccone, F., et al. (1998). An isoform of ataxin-3 accumulates in the nucleus of neuronal cells in affected brain regions of SCA3 patients. *Brain Pathol.* 8, 669–679. doi: 10.1111/j.1750-3639.1998.tb00193.x

Schmidt, T., Lindenberg, K. S., Krebs, A., Schols, L., Laccone, F., Herms, J., et al. (2002). Protein surveillance machinery in brains with spinocerebellar ataxia type 3: redistribution and differential recruitment of 26S proteasome subunits and chaperones to neuronal intranuclear inclusions. *Ann. Neurol.* 51, 302–310. doi: 10.1002/ana.10101

Schmitt, I., Linden, M., Khazneh, H., Evert, B. O., Breuer, P., Klockgether, T., et al. (2007). Inactivation of the mouse Atxn3 (ataxin-3) gene increases protein ubiquitination. *Biochem. Biophys. Res. Commun.* 362, 734–739. doi: 10.1016/j.bbrc.2007.08.062

Schols, L., Bauer, P., Schmidt, T., Schulte, T., and Riess, O. (2004). Autosomal dominant cerebellar ataxias: clinical features, genetics, and pathogenesis. *Lancet Neurol.* 3, 291–304. doi: 10.1016/S1474-4422(04)00737-9

Segal-Raz, H., Mass, G., Baranes-Bachar, K., Lerenthal, Y., Wang, S. Y., Chung, Y. M., et al. (2011). ATM-mediated phosphorylation of polynucleotide kinase/phosphatase is required for effective DNA double-strand break repair. *EMBO Rep.* 12, 713–719. doi: 10.1038/embor.2011.96

Shen, J., Gilmore, E. C., Marshall, C. A., Haddadin, M., Reynolds, J. J., Eyaid, W., et al. (2010). Mutations in PNKP cause microcephaly, seizures and defects in DNA repair. *Nat. Genet.* 42, 245–249. doi: 10.1038/ng.526

Singh, A. N., Oehler, J., Torrecilla, I., Kilgas, S., Li, S., Vaz, B., et al. (2019). The p97-Ataxin 3 complex regulates homeostasis of the DNA damage response E3 ubiquitin ligase RNF8. *EMBO J.* 38:e102361. doi: 10.15252/embj.2019102361

Stack, C., Ho, D., Wille, E., Calingasan, N. Y., Williams, C., Liby, K., et al. (2010). Triterpenoids CDDO-ethyl amide and CDDO-trifluoroethyl amide improve the behavioral phenotype and brain pathology in a transgenic mouse model of Huntington's disease. *Free Radic. Biol. Med.* 49, 147–158. doi: 10.1016/j.freeradbiomed.2010.03.017

Steffan, J. S., Kazantsev, A., Spasic-Boskovic, O., Greenwald, M., Zhu, Y. Z., Gohler, H., et al. (2000). The Huntington's disease protein interacts with p53 and CREB-binding protein and represses transcription. *Proc. Natl. Acad. Sci. U.S.A.* 97, 6763–6768. doi: 10.1073/pnas.100110097

Sugasawa, K., Ng, J., M., Masutani, C., Maekawa, T., Uchida, A., van der Spek, P. J., et al. (1997). Two human homologs of Rad23 are functionally interchangeable in complex formation and stimulation of XPC repair activity. *Mol. Cell. Biol.* 17, 6924–6931. doi: 10.1128/MCB.17.12.6924

Sun, X. X., Challagundla, K. B., and Dai, M. S. (2012). Positive regulation of p53 stability and activity by the deubiquitinating enzyme Otubain 1. *EMBO J.* 31, 576–592. doi: 10.1038/emboj.2011.434

Takai, H., Tominaga, K., Motoyama, N., Minamishima, Y. A., Nagahama, H., Tsukiyama, T., et al. (2000). Aberrant cell cycle checkpoint function and early embryonic death in Chk1(-/-) mice. *Genes Dev.* 14, 1439–1447.

Takashima, H., Boerkoel, C. F., John, J., Saifi, G. M., Salih, M. A. M., Armstrong, D., et al. (2002). Mutation of TDP1, encoding a topoisomerase I-dependent DNA damage repair enzyme, in spinocerebellar ataxia with axonal neuropathy. *Nat. Genet.* 32, 267–272. doi: 10.1038/ng987

Takiyama, Y., Nishizawa, M., Tanaka, H., Kawashima, S., Sakamoto, H., Karube, Y., et al. (1993). The gene for Machado-Joseph disease maps to human chromosome 14q. *Nat. Genet.* 4, 300–304. doi: 10.1038/ng0793-300

Tamagno, E., Parola, M., Bardini, P., Piccini, A., Borghi, R., Guglielmotto, M., et al. (2005). Beta-site APP cleaving enzyme up-regulation induced by 4-hydroxynonenal is mediated by stress-activated protein kinases pathways. *J. Neurochem.* 92, 628–636. doi: 10.1111/j.1471-4159.2004.02895.x

Todi, S. V., Scaglione, K. M., Blount, J. R., Basrur, V., Conlon, K. P., Pastore, A.,e t al. (2010). Activity and cellular functions of the deubiquitinating enzyme and polyglutamine disease protein ataxin-3 are regulated by ubiquitination at lysine 117. *J. Biol. Chem.* 285, 39303–39313. doi: 10.1074/jbc.M110.181610

Todi, S. V., Winborn, B. J., Scaglione, K. M., Blount, J. R., Travis, S. M., and Paulson, H. L., et al. (2009). Ubiquitination directly enhances activity of the deubiquitinating enzyme ataxin-3. *EMBO J.* 28, 372–382. doi: 10.1038/emboj.2008.289

Travers, A. A. (2003). Priming the nucleosome: a role for HMGB proteins? *EMBO Rep.* 4, 131–136. doi: 10.1038/sj.embor.embor741

Trettel, F., Rigamonti, D., Hilditch-Maguire, P., Wheeler, V. C., Sharp, A. H., Persichetti, F., et al. (2000). Dominant phenotypes produced by the HD mutation in STHdh(Q111) striatal cells. *Hum. Mol. Genet.* 9, 2799–2809. doi: 10.1093/hmg/9.19.2799

Tu, Y., Liu, H., Zhu, X., Shen, H., Ma, X., Wang, F., et al. (2017). Ataxin-3 promotes genome integrity by stabilizing Chk1. *Nucleic Acids Res.* 45, 4532–4549. doi: 10.1093/nar/gkx095

van der Horst, A., and Burgering, B. M. (2007). Stressing the role of FoxO proteins in lifespan and disease. *Nat. Rev. Mol. Cell Biol.* 8, 440–450. doi: 10.1038/nrm2190

Vis, J. C., Schipper, E., de Boer-van Huizen, R. T.,Verbeek, M. M., de Waal, R. M. W., Wesseling, P., et al. (2005). Expression pattern of apoptosis-related markers in Huntington's disease. *Acta Neuropathol.* 109, 321–328. doi: 10.1007/s00401-004-0957-5

Vyas, R., Kumar, R., Clermont, F., Helfricht, A., Kalev, P., Sotiropoulou, P., et al. (2013). RNF4 is required for DNA double-strand break repair *in vivo*. *Cell Death Differ.* 20, 490–502. doi: 10.1038/cdd.2012.145

Wang, G., Sawai, N., Kotliarova, S., Kanazawa, I., and Nukina, N. (2000). Ataxin-3, the MJD1 gene product, interacts with the two human homologs of yeast DNA repair protein RAD23, HHR23A and HHR23B. *Hum. Mol. Genet.* 9, 1795–1803. doi: 10.1093/hmg/9.12.1795

Wang, X., Zhu, S., Drozda, M., Zhang, W., Stavrovskaya, I., G., Cattaneo, E., et al. (2003). Minocycline inhibits caspase-independent and -dependent mitochondrial cell death pathways in models of Huntington's disease. *Proc. Natl. Acad. Sci. U.S.A.* 100, 10483–10487. doi: 10.1073/pnas.1832501100

Ward, J. F., Evans, J., W., Limoli, C., L., and Calabro-Jones, P. M. (1987). Radiation and hydrogen peroxide induced free radical damage to DNA. *Br. J. Cancer Suppl.* 8, 105–112.

Warrick, J. M., Paulson, H. L., Gray-Board, G. L., Bui, Q. T., Fischbeck, K. H., Pittman, R. N., et al. (1998). Expanded polyglutamine protein forms nuclear inclusions and causes neural degeneration in Drosophila. *Cell* 93, 939–949. doi: 10.1016/S0092-8674(00)81200-3

Weinfeld, M., Mani, R. S., Abdou, I., Aceytuno, R. D., and Glover, J. N. (2011). Tidying up loose ends: the role of polynucleotide kinase/phosphatase in DNA strand break repair. *Trends Biochem. Sci.* 36, 262–271. doi: 10.1016/j.tibs.2011.01.006

Wellington, C. L., Leavitt, B. R., and Hayden, M. R. (2000). Huntington disease: new insights on the role of huntingtin cleavage. *Adv. Res. Neurodegener.* 7, 1–17. doi: 10.1007/978-3-7091-6284-2_1

Williams, M. D., Van Remmen, H., Conrad, C. C., Huang, T. T., Epstein, C. J., and Richardson, A., et al. (1998). Increased oxidative damage is correlated to altered mitochondrial function in heterozygous manganese superoxide dismutase knockout mice. *J. Biol. Chem.* 273, 28510–28515. doi: 10.1074/jbc.273.43.28510

Winborn, B. J., Travis, S. M., Todi, S. V., Scaglione, K., Xu, P., Williams, A. J., et al. (2008). The deubiquitinating enzyme ataxin-3, a polyglutamine disease protein, edits Lys63 linkages in mixed linkage ubiquitin chains. *J. Biol. Chem.* 283, 26436–26443. doi: 10.1074/jbc.M803692200

Xiao, H., Yu, Z. G., Wu, Y. P., Nan, J., Merry, D. E., Sekiguchi, J. M., et al. (2012). A polyglutamine expansion disease protein sequesters PTIP to attenuate DNA repair and increase genomic instability. *Hum. Mol. Genet.* 21, 4225–4236. doi: 10.1093/hmg/dds246

Yin, Y., Seifert, A., Chua, J. S., Maure, J. F., Golebiowski, F., and Hay, R. T. (2012). SUMO-targeted ubiquitin E3 ligase RNF4 is required for the response of human cells to DNA damage. *Genes Dev.* 26, 1196–1208. doi: 10.1101/gad.189274.112

Youle, R. J., and Strasser, A. (2008). The BCL-2 protein family: opposing activities that mediate cell death. *Nat. Rev. Mol. Cell Biol.* 9. 47–59. doi: 10.1038/nrm2308

Yu, Z. X., Li, S., H., Nguyen, H., P., and Li, X. J. (2002). Huntingtin inclusions do not deplete polyglutamine-containing transcription factors in HD mice. *Hum. Mol. Genet.* 11, 905–914. doi: 10.1093/hmg/11.8.905

Yuan, J., Luo, K., Zhang, L., Cheville, J. C., and Lou, Z. (2010). USP10 regulates p53 localization and stability by deubiquitinating p53. *Cell* 140, 384–396. doi: 10.1016/j.cell.2009.12.032

Zeitlin, S., Liu, J. P., Chapman, D. L., Papaioannou, V. E., and Efstratiadis, A. (1995). Increased apoptosis and early embryonic lethality in mice nullizygous for the Huntington's disease gene homologue. *Nat. Genet.* 11,155–163. doi: 10.1038/ng1095-155

Zhang, P., Wei, Y., Wang, L., Debeb, B. G., Yuan, Y., Zhang, J., et al. (2014). ATM-mediated stabilization of ZEB1 promotes DNA damage response and radioresistance through CHK1. *Nat. Cell Biol.* 16, 864–875. doi: 10.1038/ncb3013

Zhong, X., and Pittman, R. N. (2006). Ataxin-3 binds VCP/p97 and regulates retrotranslocation of ERAD substrates. *Hum. Mol. Genet.* 15, 2409–2420. doi: 10.1093/hmg/ddl164

Zhou, L., Wang, H., Wang, P., Ren, H., Chen, D., Ying, Z., et al. (2013). Ataxin-3 protects cells against H2O2-induced oxidative stress by enhancing the interaction between Bcl-X(L) and Bax. *Neuroscience* 243, 14–21. doi: 10.1016/j.neuroscience.2013.03.047

Zolner, A. E., Abdou, I., Ye, R., Mani, R. S., Fanta, M., Yu, Y., et al. (2011). Phosphorylation of polynucleotide kinase/ phosphatase by DNA-dependent protein kinase and ataxia-telangiectasia mutated regulates its association with sites of DNA damage. *Nucleic Acids Res.* 39, 9224–9237. doi: 10.1093/nar/gkr647

Conflict of Interest: The authors declare that the research was conducted in the absence of any commercial or financial relationships that could be construed as a potential conflict of interest.

frontiers in Cell and Developmental Biology

ORIGINAL RESEARCH
published: 09 February 2021
doi: 10.3389/fcell.2020.609290

High Dosages of Equine Chorionic Gonadotropin Exert Adverse Effects on the Developmental Competence of IVF-Derived Mouse Embryos and Cause Oxidative Stress-Induced Aneuploidy

En Lin, Zhiling Li, Yue Huang, Gaizhen Ru and Pei He*

Department of Reproductive Center, The First Affiliated Hospital of Shantou University Medical College, Shantou University, Shantou, China

OPEN ACCESS

Edited by:
Chunlong Chen,
Institut Curie, France

Reviewed by:
Karen Schindler,
Rutgers, The State University of New Jersey, United States
Viviana Barra,
University of Palermo, Italy

****Correspondence:***
Zhiling Li
stlizhiling@126.com

Specialty section:
This article was submitted to Cell Growth and Division, a section of the journal Frontiers in Cell and Developmental Biology

Received: *23 September 2020*
Accepted: *21 December 2020*
Published: *09 February 2021*

Citation:
Lin E, Li Z, Huang Y, Ru G and He P (2021) High Dosages of Equine Chorionic Gonadotropin Exert Adverse Effects on the Developmental Competence of IVF-Derived Mouse Embryos and Cause Oxidative Stress-Induced Aneuploidy. Front. Cell Dev. Biol. 8:609290. doi: 10.3389/fcell.2020.609290

Gonadotropins play vital roles in the regulation of female reproductive ability and fertility. Our study aimed to determine the effects of superovulation induced by increasing doses of equine chorionic gonadotropin [eCG; also referred to as pregnant mare serum gonadotropin (PMSG)] on the developmental competence of mouse embryos and on aneuploidy formation during *in vitro* fertilization (IVF). eCG dose-dependently enhanced the oocyte yield from each mouse. Administration of 15 IU eCG significantly reduced the fertilization rate and the formation of four-cell embryos and blastocysts and increased the risk of chromosome aneuploidy. The IVF-derived blastocysts in the 15 IU eCG treatment group had the fewest total cells, inner cell mass (ICM) cells and trophectoderm (TE) cells. Moreover, more blastocysts and fewer apoptotic cells were observed in the 0, 5, and 10 IU eCG treatment groups than in the 15 IU eCG treatment group. We also investigated reactive oxygen species (ROS) levels and variations in several variables: mitochondrial membrane potential (MMP); active mitochondria; mitochondrial superoxide production; adenosine triphosphate (ATP) content; spindle structures; chromosome karyotypes; microfilament distribution; and the expression of Aurora B [an important component of the chromosomal passenger complex (CPC)], the spindle assembly checkpoint (SAC) protein mitotic arrest deficient 2 like 1 (MAD2L1), and the DNA damage response (DDR) protein γH2AX. Injection of 15 IU eCG increased ROS levels, rapidly reduced MMP, increased active mitochondria numbers and mitochondrial superoxide production, reduced ATP content, increased abnormal spindle formation rates, and induced abnormalities in chromosome number and microfilament distribution, suggesting that a high dose of eCG might alter developmental competence and exert negative effects on IVF-obtained mouse embryos. Additionally, the appearance of γH2AX and the significantly increased expression of Aurora B and MAD2L1 suggested that administration of relatively high doses of eCG caused Aurora B-mediated SAC activation triggered by ROS-induced

DNA damage in early mouse IVF-derived embryos for self-correction of aneuploidy formation. These findings improve our understanding of the application of gonadotropins and provide a theoretical basis for gonadotropin treatment.

Keywords: equine chorionic gonadotropin, aneuploidy, reactive oxygen species, DNA damage response, spindle assembly checkpoint, MAD2L1, Aurora B

INTRODUCTION

The use of gonadotropins is currently a considerable part of assisted reproductive technology (ART) because it enables procurement of large numbers of oocytes from a single *in vitro* fertilization (IVF) cycle (Zolbin et al., 2018). However, the side effects of ovulation induction treatments, such as ovarian hyperstimulation syndrome (OHSS) and the potential for increased long-term ovarian cancer risk (Farhud et al., 2019) are raising concerns regarding the safety of ovulation stimulants to the mother. Whether high doses of gonadotropins impact the fertilization potential of oocytes and the further developmental quality of the embryos is a subject of concern (Anderson et al., 2018; Wu et al., 2018). Increases in the levels of endogenous gonadotropins (e.g., due to the reduction in the ovarian reserve in aged females) or exogenous gonadotropins (e.g., due to ovulation stimulation in ART) are potential mechanisms of aneuploidy, a major factor in early fetal death and severe intellectual disability (Dursun et al., 2006). Additionally, hormonal stimulation can independently lead to cognitive dysplasia (Rumbold et al., 2017), and a high-quality study has shown that ovulation induction in the absence of ART increases the risk of developmental disorders in children (Bay et al., 2013). Furthermore, ovarian hyperstimulation might negatively affect cardiac metabolic outcomes in IVF offspring by altering the early environment of the oocytes and/or embryos, thus leading to epigenetic modifications of pivotal metabolic systems implicated in blood pressure regulation (La Bastide-Van Gemert et al., 2014; Seggers et al., 2014). Superovulated human oocytes show hypermethylation of H19 and demethylation at paternally expressed gene 1 (PEG1) (Sato et al., 2007), indicating that superovulation might lead to false imprinting (Lawrence and Moley, 2008; Calicchio et al., 2014).

Superovulation using equine chorionic gonadotropin (eCG) and human chorionic gonadotropin (HCG) in place of follicle-stimulating hormone (FSH) and luteinizing hormone (LH) is a widely used protocol for maximizing the numbers of oocytes and preimplantation embryos obtained from animals, respectively (Uysal et al., 2018). Results from animal studies have shown that gonadotropin stimulation can reduce the developmental potential of embryos *in vitro* (Karagenc et al., 2004; Wu et al., 2013; Swann, 2014), cause mitochondrial dysfunction in mouse oocytes (Ge et al., 2012), alter DNA methyltransferase protein expression (Uysal et al., 2018), affect the translational control of maternally stored messenger RNA (mRNA) (Ozturk et al., 2016) in early embryos, impair embryo quality and the uterine milieu (Ertzeid and Storeng, 2001), and change the appearance of imprinted genes in the midgestation mouse placenta (Fortier et al., 2008), resulting in delayed development (Ertzeid and Storeng, 1992; Ingrid and Thomas, 2001) or embryo death (Beaumont and Smith, 1975) and leading to an increased rate of offspring malformations (Sakai and Endo, 1987). Moreover, anti-eCG serum can effectively reduce the negative effect of eCG on the normal ovulation of mice (Lin et al., 2015).

Increasing amounts of evidence are showing that reactive oxygen species (ROS) play a crucial role in the regulation of oocyte maturation and fertilization (Lopes et al., 2010; Ge et al., 2012). Oocyte development and maturation depend on a dynamic balance between oxidant and antioxidant production (Kala et al., 2016; Han et al., 2017). Regardless of the sources of superoxide anion free radicals in female germ cells, when oxidative stimulation is well-balanced and suitable for physiological processes (e.g., zona pellucida hardening and oocyte maturation), H_2O_2 produced by disproportionation exerts positive effects. However, the overproduction of ROS is associated with negative outcomes (e.g., impaired mitochondrial function, aging, DNA damage and impaired chromosome segregation; Kala et al., 2016; Aitken, 2020). Mitochondrial dysfunction is linked to non-physiological ovarian stimulation and *in vitro* maturation (Ge et al., 2012). Mitochondria are the primary cellular sources of ROS, and these organelles are vulnerable to ROS-induced damage (Yamada-Fukunaga et al., 2013). ROS can disrupt the flow of electrons in the mitochondria and promote electron leakage and ROS production, thereby enhancing the generation of ROS in the positive feedback system. Because of this chemical reaction, oxidative stress persists and has a considerable effect on apoptosis (Aitken, 2020). Moreover, because eCG has a circulating half-life of 40–125 h, its residues often affect follicular maturation and ovulation and thereby induce persistent estrogen secretion from large anovulatory follicles, which might lead to supraphysiological levels of estrogen (Lin et al., 2015). It has been proposed that estrogen can generate ROS both directly by acting on mitochondria (Felty et al., 2005) and indirectly through IL-1β and TNF-α (Roy et al., 2007). Additionally, the exceedingly high estradiol concentrations induced by ovarian stimulation during IVF increase extramitochondrial ROS production in endometrial epithelial cells, which leads to mitochondrial dysfunction (Chou et al., 2020).

Aurora B kinase (Aurora B/AURKB) is an element of the chromosomal passenger complex (CPC) as well as a serine/threonine kinase that is well-known for its important functions in multiple events during mitosis, including sister chromosome adhesion, chromosome condensation, chromosome biorientation, kinetochore-microtubule (KT-MT) attachments, spindle assembly checkpoint (SAC) activation, cytokinesis, and chromosome segregation (Honma et al., 2014; Huang et al., 2019; Li et al., 2019; Zhang et al., 2020). Germ

cells that undergo meiosis also express an Aurora B homolog named Aurora C, which can play a role in the CPC as well (Ruchaud et al., 2007). During meiosis in mouse oocytes, Aurora B is directly involved in SAC function *via* the kinetochore recruitment of SAC components, while Aurora C is thought to play an indirect role in SAC activation through depolymerization of improper KT-MT attachments (Balboula and Schindler, 2014; Nguyen et al., 2014). In mitosis, among other functions, Aurora B directly participates in the maintenance of SAC activation by recruiting key factors to kinetochores and indirectly invokes SAC signaling by destabilizing incorrect KT-MT attachments (Ruchaud et al., 2007; Saurin et al., 2011; Balboula and Schindler, 2014). However, it is important to note that Aurora C is not inimitably essential for SAC activation or cytokinesis, and these events may be Aurora B specific (Yasui et al., 2004; Balboula and Schindler, 2014). Nguyen et al. (2018) described a unique requirement for Aurora B to negatively regulate Aurora C to prevent aneuploidy. Only Aurora B overexpression (not Aurora C overexpression) can rescue chromosome alignment defects (Shuda et al., 2009). Aurora B has been reported to potentiate Mps1 (also known as TTK) activation to quickly establish the mitotic checkpoint (Saurin et al., 2011); moreover, our previous findings have shown that mitotic arrest deficient 2 like 1 (MAD2L1; also referred to as MAD2) recruitment to kinetochores by TTK occurs at the onset of oxidative damage in embryos during SAC activation (Wu et al., 2017). In addition, MAD2 prevents chromosome segregation defects and maintains chromosome stability through modulation of the mitotic functions of Aurora B (Shandilya et al., 2016). In a previous study, we found that ROS-induced DNA damage triggers SAC activation *via* Aurora B to hinder aneuploidy in early IVF-derived mouse embryos and that Aurora B is an important regulator of mitosis that assists in self-correction when chromosomal abnormalities occur during embryo development (Li et al., 2019). Hence, Aurora C will not be discussed further in this article. The current study focused on the role of the critical CPC kinase Aurora B during mitosis in early IVF-derived mouse embryos. Our results have consistently shown that oxidative stress increases the probability of sex chromosome aneuploidy in male mouse embryos by inducing chromosome mis-segregation and inhibits the expression levels of male reproduction-related proteins; these effects might negatively affect the reproductive health of IVF-obtained male offspring (Huang et al., 2019). We consequently hypothesized that administration of high doses of eCG would affect the viability and development of IVF-derived mouse embryos and cause oxidative stress-induced aneuploidy, thereby triggering Aurora B-mediated SAC activation.

MATERIALS AND METHODS

Experimental Animals

Adult Kunming mice (male: aged 3–6 months; female: aged 6–8 weeks) were ordered from the animal center at Shantou University Medical College. The mice were randomly assigned to various groups. All work strictly abided by the International Guiding Principles for Biomedical Research Involving Animals (2012 edition) published by the Council for the International Organization of Medical Sciences, and all experimental protocols were approved by the Institutional Animal Care and Use Committee (IACUC) of Shantou University Medical College (SUMC2018-049).

Sperm Capacitation, Oocyte Collection, IVF, and Embryo/Blastocyst Culture

As described previously (Huang et al., 2019; Li et al., 2019), prior to oocyte collection, sperm were removed from the epididymal tails of male mice, moved to capacitation medium prepared in advance with human tubal fluid (HTF) medium (Cooper Surgical, USA) containing 1.5% bovine serum albumin (BSA) and immediately incubated in an incubator (37°C, 5% CO_2) for 60 min. Adult female mice were intraperitoneally injected with 0, 5, 10, or 15 IU eCG (Ningbo Second Hormone Factory, China); 48 h later, the mice received an injection of 10 IU HCG (Ningbo Second Hormone Factory, China). A dose of 10 IU eCG is the most commonly used dose for ovulation induction in female Kunming mice (Wu et al., 2016; Huang et al., 2019; Li et al., 2019). Therefore, we decided to use up to 15 IU eCG (a high dose of eCG) in our experiments. When injected, eCG or HCG was diluted with 0.9% NaCl solution. The same amount of 0.9% NaCl solution was given to the mice in the control (0 IU eCG) group. Superovulated but unmated female mice were euthanized at 13–15 h following HCG injection. Cumulus-oocyte complexes were collected from the ovaries and transferred to droplets, which were prepared by adding capacitated sperm to an HTF solution containing 0.4% BSA; the complex-containing droplets were then incubated in 5% CO_2 at 37°C for 6 h. After fertilization, the zygotes were washed three times in HTF medium at 37°C and cultured in new embryo culture medium (HTF medium with both 0.4% BSA and 10% fetal bovine serum) at 37°C under an atmosphere with 5% CO_2. For blastocyst culture, we used the same protocol described above but with blastocyst culture medium (Cooper Surgical, USA) instead of embryo culture medium.

Determination of Cytoplasmic ROS Products

DCFH-DA (Sigma, USA) is a cell-permeable fluorogenic probe useful for determining the degree of overall oxidative stress. The stock solution of DCFH-DA was diluted with HTF medium to a final concentration of 10 μmol/L. Zygotes from each treatment group were transferred into DCFH-DA droplets, incubated at 37°C for 30 min, washed three times in phosphate-buffered saline (PBS) and mounted on adhesive microscope slides. The glass slides were observed by fluorescence microscopy (Nikon Eclipse 90 Ni-E, Japan). The fluorescence intensity (FI) was detected *via* Image-Pro Plus 6.0 software (Media Cybernetics, USA).

Evaluation of Mitochondrial Membrane Potential (MMP)

JC-1 (Sigma, USA) is a type of cationic fluorescent membrane-permeable carbocyanine dye that can be used as a ratiometric indicator of MMP in zygotes. Mitochondria with high and low

membrane potentials are stained red and green, respectively, by this probe. A 5 mg/mL stock solution was prepared in dimethyl sulfoxide (DMSO), and this solution was diluted with PBS to a 1.25 μmol/L working solution. Zygotes were incubated for 30 min at 37°C in dye-containing medium and washed three times with PBS (3 min per wash) prior to experimental observation. Under an upright fluorescence microscope (Nikon Eclipse Ni-E, Japan), the J-monomer (green) was observed selectively with a 488-nm argon-ion laser source. The J-aggregate (red) was observed with a 568-nm argon-krypton laser line. The red/green FI in zygotes was detected using Image-Pro Plus 6.0 software.

Detection of Active Mitochondria and Superoxide Anion Production

MitoTracker™ Green FM (Invitrogen, USA) is a green fluorescent dye that stains mitochondria in embryos and accumulates in active mitochondria, and its accumulation is independent of the membrane potential. A small amount of 1 mM MitoTracker Green stock solution was added to HTF culture medium at a ratio of 1:5000–1:50000 to obtain a final concentration in the range of 20–200 nM. A 5 mM mitochondrial superoxide indicator MitoSOX™ Red (Invitrogen, USA) stock solution was then diluted in HTF culture medium to obtain a 5 μM MitoSOX Red working solution. One hundred microliters of MitoTracker Green or MitoSOX Red working solution was then applied to the embryos. The embryos were then incubated for 30 min at 37°C in the dark, gently washed three times with warm buffer and mounted in warm buffer on adhesive microscope slides for imaging. The fluorescence signal (FI value) for each embryo was measured with Image-Pro Plus 6.0 software.

Determination of the Adenosine Triphosphate (ATP) Content

The amount of ATP present in embryos was quantified using a CellTiter-Glo® 2.0 Assay (Promega, Madison, WI, USA) with a multimode microplate reader (Synergy H1, BioTek, USA). rATP (10 mM, Promega, USA) was used to generate a 14-point ATP standard curve for each analysis before addition of CellTiter-Glo® 2.0 reagent in the same 96-well plate in which samples were examined. The ATP content of each group was calculated with the formula obtained from linear regression of the standard curve. All embryos treated with increasing amounts of eCG were analyzed simultaneously to reduce any potential variability.

Immunofluorescence and DAPI Staining

The protocol used for the immunofluorescence staining of embryos was previously described by our research group (Huang et al., 2019; Li et al., 2019). The sections were visualized using an LSM 800 laser scanning microscope (ZEISS, Germany). F-actin was labeled with Alexa Fluor™ 488 phalloidin, which was purchased from Invitrogen (Carlsbad, CA, USA). A rabbit anti-gamma H2A.X antibody (phospho-S139), a rabbit anti-Aurora B antibody, DAPI staining solution and a goat anti-rabbit IgG H&L antibody (Alexa Fluor® 488) were obtained from Abcam (Cambridge, UK). An Alexa Fluor® 594-conjugated mouse anti-MAD2 antibody was obtained from Santa Cruz (Dallas, TX, USA). A mouse anti-α-tubulin-FITC monoclonal antibody was procured from Sigma-Aldrich (St. Louis, MO, USA).

Fluorescence *in situ* Hybridization (FISH)

RNA FISH probe mixes for hybridization to Aurora B (FAM-conjugated) and MAD2L1 (Cy3-conjugated) mRNA molecules were designed and synthesized by GenePharma (Shanghai, China). FISH assays were performed manually with an RNA FISH kit (GenePharma) following the manufacturer's recommended protocol. Embryos mounted on polylysine slides were fixed with 4% paraformaldehyde for 15 min, transferred to 0.1% Triton X-100 for 15 min, subjected to two 5-min rinses in PBS and treated sequentially with 2× saline sodium citrate (SSC; 30 min at 37°C), 70% ethanol (3 min at room temperature), 85% ethanol (3 min at room temperature), and anhydrous ethanol (3 min at room temperature) to enable RNA probe access. Target probe mixes for Aurora B and MAD2L1, diethyl pyrocarbonate (DEPC)-treated water and warm hybridization solution were added onto the slides, and the slides were then incubated in the dark for 5 min at 73°C for denaturation and in a humid atmosphere for 12–16 h at 37°C to allow the probe to hybridize with the RNA targets. The slides were subsequently washed with 0.1% Tween-20 for 5 min and incubated with two SSC solutions: 2× SSC (5 min at room temperature) and 1× SSC (5 min at room temperature). Chromatin was then stained with DAPI, and the slides were subjected to two 5-min washes in PBS. The Aurora B and MAD2L1 mRNA fluorescence signals were imaged under an LSM 800 laser-scanning microscope (ZEISS, Germany).

Karyotype Analysis

Typical protocols from our previous studies (Huang et al., 2019; Li et al., 2019) were used and are summarized below. Briefly, karyotype analysis of mouse embryos is a four-step procedure. In the first step, the embryos were added to HTF culture medium with 0.05 μg/mL podophyllotoxin and 0.05 μg/mL vinblastine and incubated for 12–16 h. Podophyllotoxin damages the microfilament system to prevent prokaryotic fusion, and vincristine interferes with tubulin polymerization, blocks spindle formation, and maintains embryos at the mid-cleavage stage. Subsequently, the embryos were immersed in 0.1% pancreatin to remove the zona pellucidae and mounted on adhesive slides. Ultrapure water containing 20% fetal bovine serum was mixed with a 0.9% sodium citrate solution at a ratio of 1:6 to form a hypotonic solution. The slides with the embryo samples were added to the preheated hypotonic solution, placed in an incubator at 37°C for 30 min, and then incubated with a series of conventional fixative solutions: fixative I (methanol:glacial acetic acid:ultrapure water = 15:3:1, 5 min at room temperature), fixative II (methanol:glacial acetic acid = 3:1, overnight at room temperature), and fixative III (methanol:glacial acetic acid:ultrapure water = 3:3:1, 1 min at room temperature). In the last step, the slides were stained in Giemsa staining solution for 30 min, washed with ultrapure water and dried in air. To prevent confusion, only one embryo was lysed after exposure to the fixative solutions and slowly "melted" onto one clean microscope slide. The slides were then scanned using a standard bright-field microscope (Nikon Eclipse 90 Ni-E).

Terminal Deoxynucleotidyl Transferase-Mediated dUTP Nick-End Labeling (TUNEL) Assay

A RiboAPO^{TM} One-Step TUNEL Apoptosis Detection Kit (Red) (RiboBio, China) was used to detect blastocyst apoptosis. The level of apoptosis and the blastocyst internal population of cells, which is termed the inner cell mass (ICM), were evaluated through a TUNEL assay and immunofluorescence staining of octamer-binding transcription factor 4 (Oct4), respectively. The apoptosis rate is expressed as the percentage of TUNEL-positive cells relative to the total number of cells (DAPI-stained cells) in a single blastocyst. The total cell number (as indicated by DAPI staining) in each blastocyst minus the ICM (as indicated by Oct4 staining) was calculated as the number of trophectoderm (TE) cells, and the ICM/TE cell ratio was then calculated. The cell counting method was described by Carstea et al. (2012). A rabbit anti-oct4 antibody and a goat anti-rabbit IgG H&L antibody (Alexa Fluor® 488), which were purchased from Abcam (Cambridge, UK), were used as the primary and secondary antibodies, respectively.

Real-Time Quantitative PCR (RT-PCR)

Approximately 150 zygotes were prepared, and RNA was extracted with an RNAprep Pure Micro Kit (Tiangen, China). High-quality RNA was used for cDNA synthesis with FastKing gDNA Dispelling RT SuperMix (Tiangen, China). The C_t values were determined by RT-PCR using a CFX Connect^{TM} Real-Time PCR Detection System (Bio-Rad, USA) and Talent qPCR PreMix (SYBR Green) (Tiangen, China). The expression of β-actin was used as an internal control. The relative mRNA expression level of each target gene is represented as the fold change calculated using the $2^{-\Delta\Delta Ct}$ method.

Protein Extraction From Zygotes

Lysates of 150 zygotes from each treatment group were prepared *via* addition of ice-cold RIPA lysis buffer (Beyotime, China) containing a protease and phosphatase inhibitor cocktail (Beyotime, China) to a final volume of 10 μL. A histone extraction kit (Abcam, UK) was used to extract histone proteins from zygotes. The protein concentrations were quantified using a BCA kit (Boster, China) with BSA as the standard.

Automated Western Immunoblotting

All primary rabbit antibodies used in automated capillary western immunoblotting were obtained from Abcam (Cambridge, UK). All dilutions were prepared in Antibody Diluent II buffer (ProteinSimple, USA). The anti-rabbit secondary antibody (ProteinSimple, USA) was ready-to-use without any handling. Automated western immunoblotting was performed using Wes Simple^{TM} (ProteinSimple, USA) in accordance with the manufacturer's instructions (Nelson et al., 2017; Sage et al., 2020).

Statistical Analysis

The results from at least three independent experiments were collected and analyzed with SPSS version 19.0 software (IBM, Armonk, NY, USA). The data are presented as the means ± standard deviations (*SD*s) and were assessed with Student's *t*-tests and ANOVA. Some values are expressed as percentages and were compared using the Pearson's chi-square test or Fisher's exact test. In all the statistical tests, differences were considered significant if $P < 0.05$.

RESULTS

Effects of Different eCG Doses on the Numbers of Oocytes Obtained From Mice

Increasing eCG doses (with 10 IU HCG injection) markedly and dose-dependently enhanced mouse oocyte yield. The mean numbers of oocytes retrieved from female Kunming mice after injections of 0, 5, 10, and 15 IU eCG were 11.00 ± 3.00, 22.00 ± 2.65, 45.67 ± 3.22, and 56.00 ± 4.58, respectively. The numbers of mouse oocytes increased with increasing doses of eCG ($P < 0.05$) (**Figure 1A**).

Effects of Different eCG Doses on the Development of IVF-Derived Mouse Embryos

To identify the effects of different eCG doses on the developmental potential, oocytes obtained after ovulation were fertilized and cultured *in vitro*. At 8–10 hpi, two-pronuclear (2PN) zygotes and/or the second polar body could be observed after the successful fertilization of normal mouse zygotes (**Figure 1C**). Nearly identical fertilization rates were found for the zygotes in the control (0 IU eCG injection) group (84.38 ± 7.94), 5 IU eCG injection group (82.23 ± 9.29) and 10 IU eCG injection group (80.91 ± 1.58) ($P > 0.05$). Compared with the experimental groups that received 0, 5, and 10 IU eCG, the group that received 15 IU eCG (59.22 ± 6.39) exhibited at significantly lower fertilization rate ($P < 0.05$) (**Figure 1B**). The rates of two-cell embryo formation in the groups of mice administered 0, 5, 10, and 15 IU eCG were 86.87 ± 5.65, 84.13 ± 5.16, 81.35 ± 3.87, and 80.54 ± 3.50, respectively. Increasing the eCG dose had no significant effect on the rate of two-cell embryo formation ($P > 0.05$). The rate of four-cell embryo formation was significantly lower in the 15 IU eCG (64.45 ± 1.72) treatment group than in the 0 IU eCG (78.60 ± 6.59), 5 IU eCG (75.91 ± 4.03), and 10 IU eCG (77.36 ± 3.46) treatment groups ($P < 0.05$). Similarly, administration of 15 IU eCG (44.68 ± 4.72) significantly reduced the rate of blastocyst formation ($P < 0.05$). Furthermore, the rate of blastocyst formation in the control group (74.72 ± 4.00) was higher than those in the 5, 10, and 15 IU eCG groups, but no significant difference was found between the 5 IU eCG (63.99 ± 3.53) and 10 IU eCG (61.21 ± 2.90) treatment groups (**Figures 1D,E**).

Effects of Different eCG Doses on ROS Concentrations in IVF-Derived Mouse Embryos

The total cytoplasmic and mitochondrial ROS levels of mouse embryos obtained after administration of different doses of eCG were tested using the cell-permeable fluorogenic probe DCFH-DA and the mitochondrial superoxide indicator MitoSOX^{TM} Red,

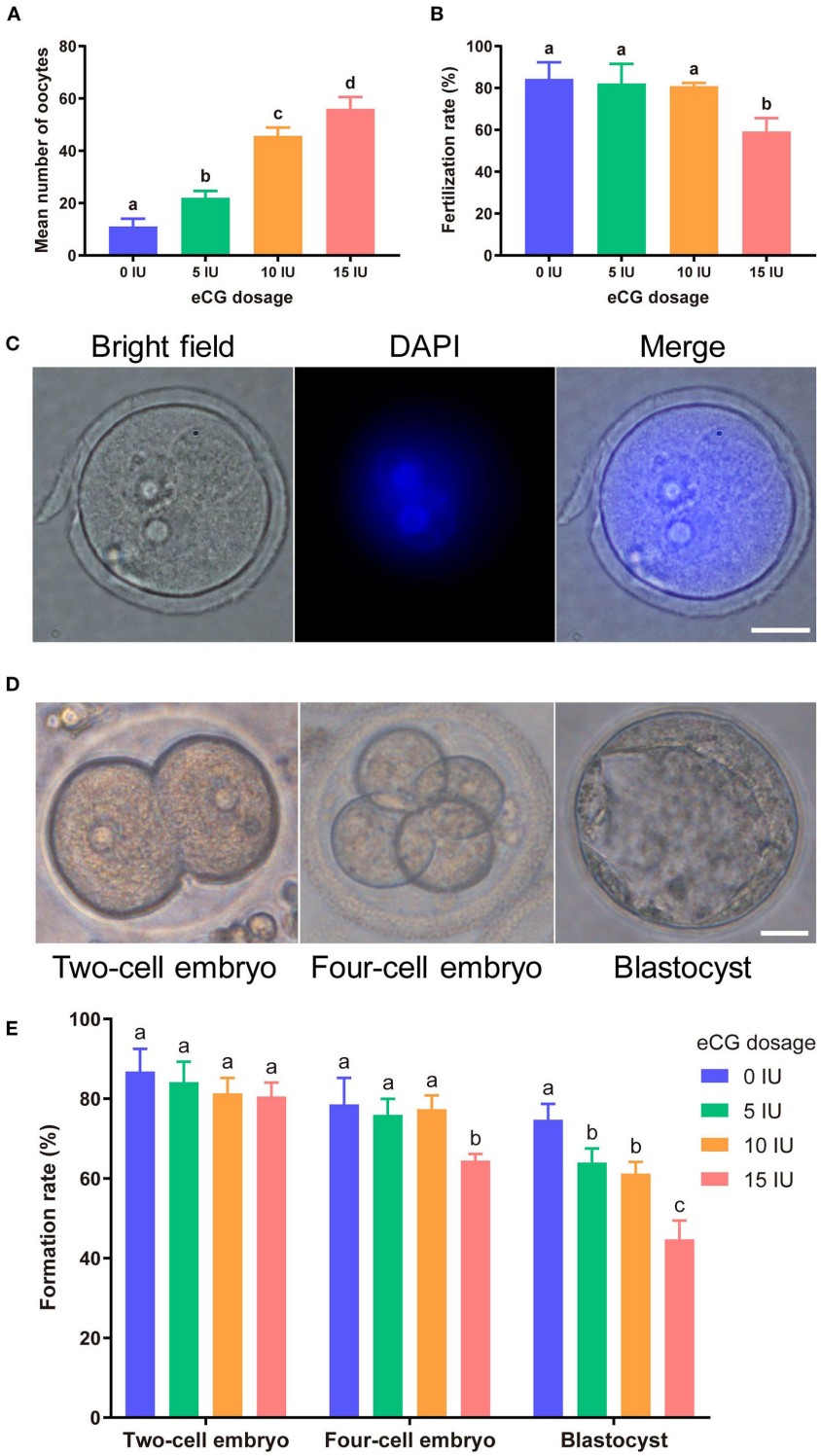

FIGURE 1 | Effects of different eCG doses on the development of IVF-derived mouse embryos. **(A)** Mean numbers (means ± *SD*s) of oocytes obtained after administration of 0, 5, 10, and 15 IU eCG (with 10 IU HCG injection). [a,b,c,d]Bars labeled with different letters are significantly different from each other ($P < 0.05$). **(B)** Fertilization rates after treatments with different eCG doses. [a,b]Bars labeled with different superscript letters are significantly different from each other ($P < 0.05$). **(C)** Representative images of 2PN zygotes in mouse embryos at 8–10 h post insemination (hpi) (scale bar = 20 μm). **(D)** Morphological appearances of a two-cell embryo, a four-cell mouse embryo and a single blastocyst. Scale bar = 20 μm. **(E)** Rates of two-cell embryo, four-cell embryo and blastocyst formation with different doses of eCG. The data are expressed as the means ± *SD*s. [a,b,c]Columns within a group marked with different superscript letters are significantly different from each other, $P < 0.05$.

respectively. Our results showed that the total cytoplasmic ROS levels (35.35 ± 3.50, $P < 0.001$) and mitochondrial ROS levels (70.57 ± 7.88, $P < 0.001$) of the embryos in the 15 IU eCG group were markedly higher than those of the embryos in the other three groups. The mean FIs of cytoplasmic and mitochondrial ROS produced in the embryos of the 10 IU eCG treatment group (4.40 ± 2.04 and 20.01 ± 6.38, respectively) were similar to those in the embryos of the 5 IU eCG treatment group (4.04 ± 1.12 and 17.09 ± 4.40, respectively) and the control group (4.22 ± 0.25 and 12.88 ± 5.24, respectively) (**Figure 2**).

Effects of Different eCG Doses on the Mitochondrial Function of IVF-Derived Mouse Embryos

To further verify the effects of different eCG doses on mitochondrial function in IVF mouse embryos, we monitored variations in MMP, active mitochondria, and ATP content.

Measurement of MMP

JC-1 tends to aggregate and thus fluoresce red when MMP is elevated. In contrast, JC-1 tends to appear as a monomer,

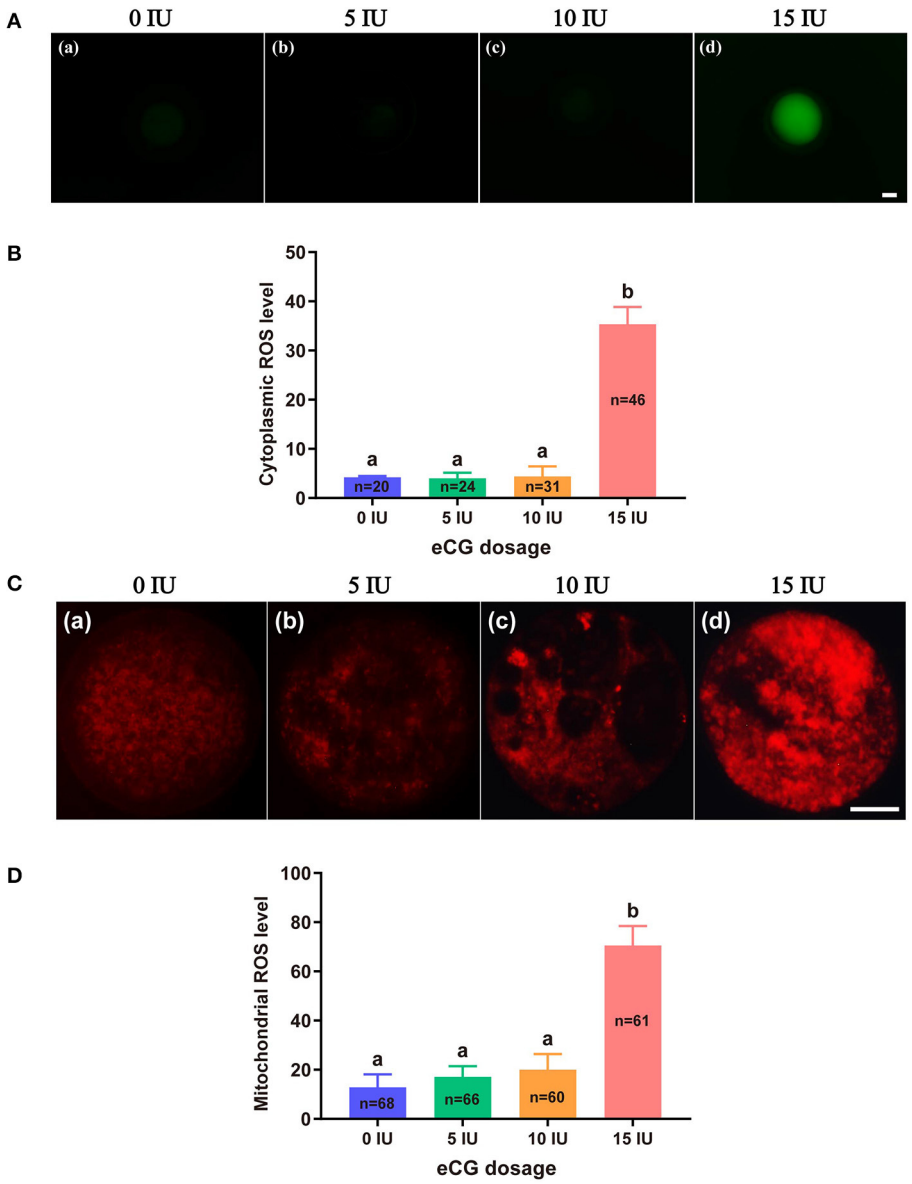

FIGURE 2 | Effects of different eCG doses on ROS concentrations in IVF-derived mouse embryos. **(A)** Representative images of cytoplasmic ROS in embryos after administration of eCG at doses of 0, 5, 10, and 15 IU (a–d). Scale bar = 20 μm. **(B)** ROS production in the cytoplasm was assessed by staining with DCFH-DA. The cytoplasmic ROS levels of the embryos in the group treated with the high dose (15 IU) of eCG were significantly higher than those of the embryos in the other three groups. **(C)** Representative images of mitochondrial ROS in embryos after administration of eCG at doses of 0, 5, 10, and 15 IU (a–d). Scale bar = 20 μm. **(D)** ROS production in mitochondria was assessed using the mitochondrial superoxide indicator MitoSOX™ Red. The mitochondrial ROS levels of the embryos in the group treated with the high dose (15 IU) of eCG were significantly higher than those of the embryos in the other three groups. The continuous FI data were analyzed using Student's *t*-test and ANOVA. [a,b]Bars labeled with different letters are significantly different from each other ($P < 0.05$). *n* shows the total number of embryos detected.

fluorescing green, when MMP is reduced. Thus, the FI ratio of these two colors of fluorescence (red/green ratio) is often used to evaluate changes in MMP. In this experiment, the mean red/green FI ratio obtained for the control group was set to 100%. No significant difference in MMP was found among the embryos from the 0, 5, and 10 IU eCG treatment groups. The relative red/green FI ratio for the embryos retrieved from the mice injected with 15 IU eCG was ∼2.5-fold lower than that for the embryos retrieved from the control mice (100 vs. 40.58% ± 4.72, $P < 0.001$) (**Figures 3A,B**).

Evaluation of Active Mitochondria

We used MitoTracker™ Green to assess the number of active mitochondria, which is expressed as the FI per embryo. The embryos obtained from the mice injected with 15 IU eCG showed higher mitochondrial activity than the IVF-derived embryos in the other three groups ($P < 0.001$). Moreover, administration of eCG at doses of 0, 5, and 10 IU did not significantly affect the number of active mitochondria. Although the number of active mitochondria was slightly increased in the 5 IU eCG treatment group, it was very similar to those in the 0 and 10 IU eCG treatment groups (**Figures 3C,D**).

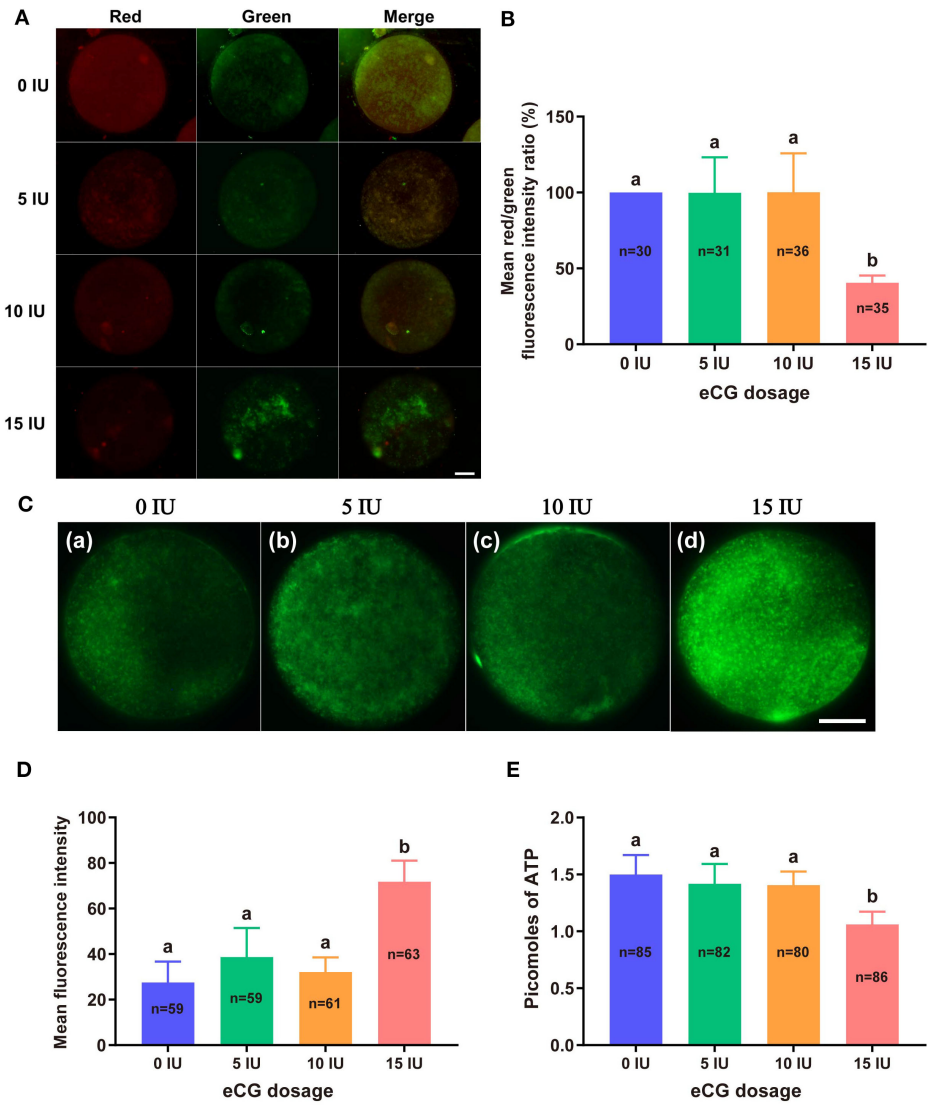

FIGURE 3 | Effects of different eCG doses on the mitochondrial function of IVF-derived mouse embryos. **(A)** Representative images of the MMP in embryos after administration of eCG at doses of 0, 5, 10, and 15 IU. Scale bar = 20 μm. **(B)** Ratios of the red/green FI following JC-1 staining. The mean red/green FI ratio of the control (0 IU eCG injection) group was set to 100%. **(C)** Representative images of mitochondrial activity in embryos after administration of eCG at doses of 0, 5, 10, and 15 IU (a–d). Scale bar = 20 μm. **(D)** Magnitude of mitochondrial activity in IVF-derived embryos after administration of different doses of eCG. The mitochondrial activity in the embryos is represented by the mean FI. **(E)** ATP content of individual embryos from mice administered different doses of eCG. All the values are presented as the means ± *SD*s. Different letters above the columns indicate significant differences ($P < 0.05$). Each experiment was performed in triplicate, and *n* shows the total number of embryos detected.

Quantification of ATP Content

A 14-point standard curve was generated in each experiment. The mean ATP content (1.06 ± 0.11, $P < 0.05$) in the IVF embryos obtained after injection of 15 IU eCG was lower than that in the embryos obtained from control mice. The mean ATP levels of the individual embryos obtained from the female mice administered 0, 5, and 10 IU eCG were 1.50 ± 0.17, 1.42 ± 0.18, and 1.41 ± 0.12, respectively, and no significant changes in ATP were detected in these three groups ($P > 0.05$) (**Figure 3E**).

Effects of Different eCG Doses on Chromosome Segregation and the Cytoskeleton in IVF-Derived Mouse Embryos

To study the effects of different eCG doses on chromosome segregation and the cytoskeletal system in embryos obtained from IVF, we explored lagging chromosomes, micronuclei and multinuclei through DAPI staining; determined the number of chromosomes by karyotype analysis; and detected the localization of α-tubulin (microtubules) and F-actin (microfilaments) by immunostaining.

Determination of Lagging Chromosomes, Micronuclei, and Multinuclei

The rates of lagging chromosome and/or micronucleus formation in IVF-derived embryos retrieved following administration of 0, 5, and 10 IU eCG were 2.04% (1/49), 4.44% (2/45), and 3.92% (2/51), respectively; these rates were significantly lower than that in the 15 IU eCG injection group (15.09%, 8/53, $P < 0.05$) (**Figures 4A,D**). A similar trend was observed for the rates of multinucleus formation in the various groups. The percentage of multinucleus formation among IVF-derived embryos from females treated with 5 (6.56%, 4/61) or 10 (6.90%, 4/58) IU eCG was comparable to that among embryos from control females (3.51%, 2/57) but significantly lower than that among embryos from females treated with 15 IU eCG (16.67%, 10/60) (**Figures 4B,E**).

Analysis of the Number of Chromosomes

Our chromosome karyotyping results suggested that the rates of chromosomal abnormalities (including hyperdiploidy and hypodiploidy) were significantly enhanced in IVF-derived embryos obtained with increasing doses of eCG up to 15 IU (36.67%, 11/30). Non-significant differences in the incidence of aneuploidy were observed among the groups of females injected with 0, 5, and 10 IU eCG; the rates of aneuploidy obtained for these groups were 5.00% (1/20), 4.35% (1/23), and 8.00% (2/25), respectively (**Figures 4C,F**).

Distribution of Microtubules and Microfilaments

The localization of α-tubulin (microtubules) is related to the formation of the spindle at the metaphase of mitosis. Importantly, the assembly and distribution of F-actin cytoskeletal components (microfilaments) are associated with cleavage in early-stage embryos. Similar trends in the rates of both abnormal microtubule formation and aberrant microfilament formation were found in all four groups. The rates of abnormal microtubule and aberrant microfilament formation in IVF-derived embryos obtained after ovarian stimulation with 15 IU eCG were 17.91% (12/67) and 19.23% (10/52), respectively; these values were substantially higher than those found for the embryos obtained after ovarian stimulation with 0 IU eCG (3.28%, 2/61 and 1.89%, 1/53, respectively), 5 IU eCG (5.00%, 3/60 and 3.64%, 2/55, respectively), and 10 IU eCG (4.62%, 3/65 and 4.00%, 2/50, respectively) (**Figures 4G–J**).

Effects of Different eCG Doses on Apoptosis and Cell Allocation in IVF-Derived Mouse Blastocysts

The developmental potential of IVF-derived blastocysts from groups of mice administered 0, 5, 10, and 15 IU eCG was evaluated with respect to apoptosis, total cell numbers and allocation of cells to the ICM and TE (**Figure 5**). As indicated in **Table 1**, increasing eCG doses up to 15 IU significantly enhanced the average apoptotic cell count and the mean apoptotic rate compared with the values obtained for IVF-derived blastocysts retrieved from mice primed with 0, 5, and 10 IU eCG ($P < 0.05$). The IVF-derived blastocysts in the 15 IU eCG treatment group had the lowest numbers of total cells, ICM cells, and TE cells and the lowest ICM/TE cell ratio ($P < 0.05$). Our results revealed that administration of 0, 5, and 10 IU eCG had no obvious effects on the total cell count, number of ICM cells, number of TE cells, or ICM/TE cell ratio in individual IVF-derived embryos, as shown in **Table 2**.

Effects of Different eCG Doses on the Expression Levels of γH2AX, Aurora B, and MAD2L1 in IVF-Derived Mouse Embryos

We subsequently investigated the roles of the DNA damage response (DDR), CPC and SAC in the response of IVF-derived mouse embryos to different eCG doses. We examined both the subcellular localization and the relative expression levels of γH2AX (a marker of DNA double-strand breaks), Aurora B (the central member of the CPC), and MAD2L1 (a pivotal component of the SAC).

Immunofluorescence Staining for γH2AX, Aurora B, and MAD2L1

To explore the relative protein expression levels of γH2AX, Aurora B, and MAD2L1, we further assessed the average FI values in IVF-derived mouse embryos belonging to all four groups with Image-Pro Plus 6.0 software. The outcomes are presented as the FI values in arbitrary units (a.u.) per embryo. High γH2AX expression was detected in a pair of daughter nuclei in IVF-derived embryos obtained from mice administered 15 IU eCG ($P < 0.01$). The average FI values of γH2AX in the groups of mice administered 0, 5, 10, and 15 IU eCG were 8.36 ± 1.56, 8.30 ± 0.63, 6.34 ± 0.43, and 27.95 ± 0.91, respectively. Strong enrichment of Aurora B-MAD2L1 foci on chromatin was observed in the 15 IU eCG treatment group, but weak expression was observed in the 0, 5, and 10 IU eCG treatment groups. The average FI values of Aurora B/MAD2L1 per embryo obtained

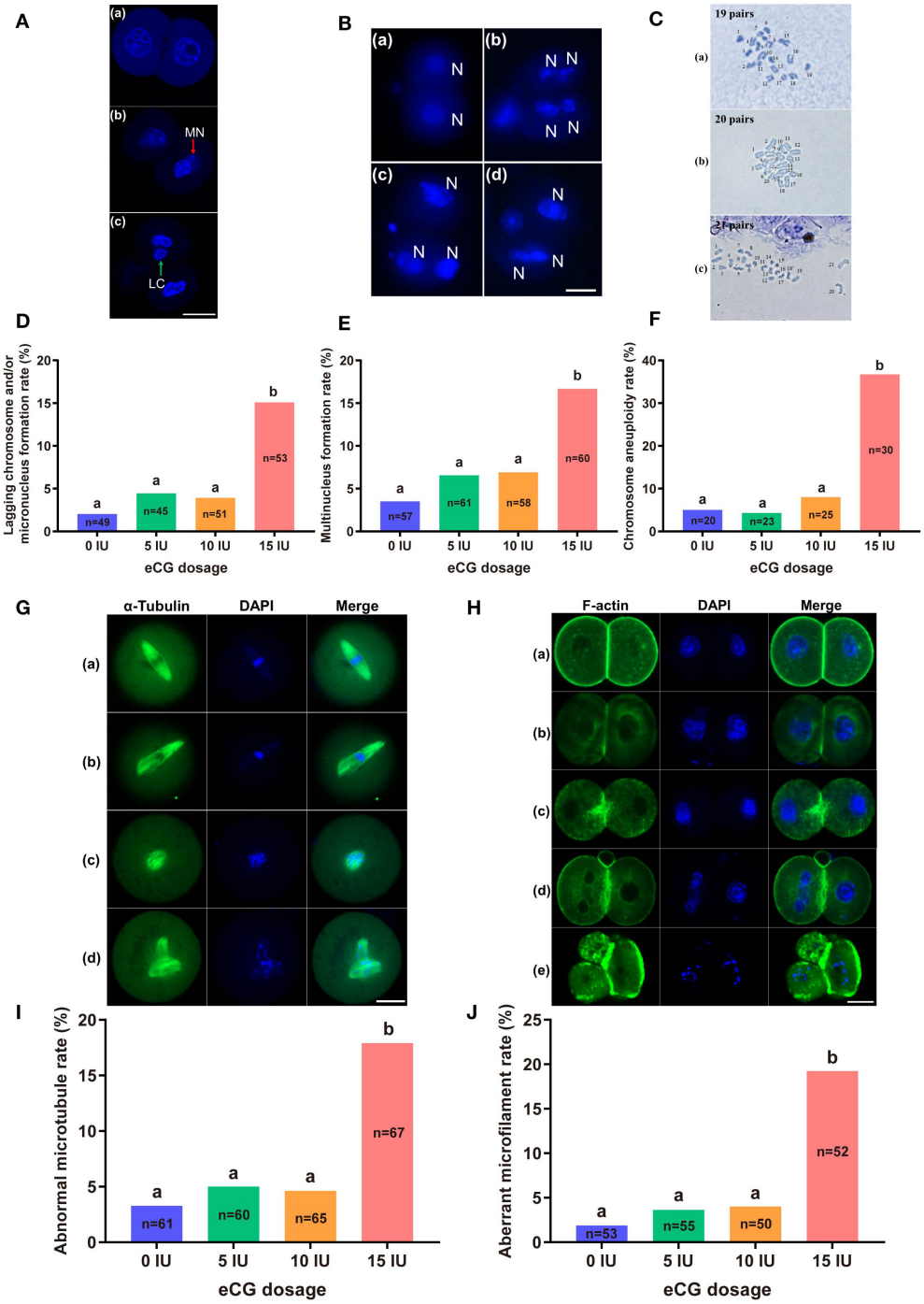

FIGURE 4 | Effects of different eCG doses on chromosome segregation and the cytoskeleton in IVF-derived mouse embryos during the first mitotic division. **(A)** Fluorescence photomicrograph of two normal daughter nuclei, micronuclei (red arrow) and lagging chromosomes (green arrow) (a–c, respectively) in IVF-derived mouse embryos during the first mitosis. Scale bar = 20 μm. MN and LC refer to micronuclei and lagging chromosomes, respectively. **(B)** Representative images of two new daughter nuclei (a) and multinuclei (b–d). Scale bar = 20 μm. *N* refers to nuclei. **(C)** Hypodiploidy: 19 pairs of chromosomes (a). Normal mice have 20 pairs of chromosomes (b). Hyperdiploidy: 21 pairs of chromosomes (c). **(D–F)** Bar graphs of the lagging chromosome and/or micronucleus formation rates, multinucleus formation rates, and chromosome aneuploidy rates for the four groups. **(G)** Confocal images of a normal spindle structure and shape (a) and abnormal spindle formation (b–d). Mouse embryos at metaphase were stained with anti-α-tubulin antibodies (green) to detect microtubules, namely, the spindle. Scale bar = 20 μm. **(H)** Mouse embryos were stained with Alexa Fluor™ 488 phalloidin (green) to visualize the configuration and distribution of microfilaments. Normal microfilaments were precisely located in the cell cortex around the contractile ring at telophase (a). Representative images of aberrant microfilament formation (b–e). Scale bar = 20 μm. **(I,J)** Bar graphs of the abnormal microtubule rates and aberrant microfilament rates, respectively. Different lowercase letters in the columns within each parameter indicate significant differences ($P < 0.05$). The nuclei were stained with DAPI (blue), and *n* shows the total number of embryos detected.

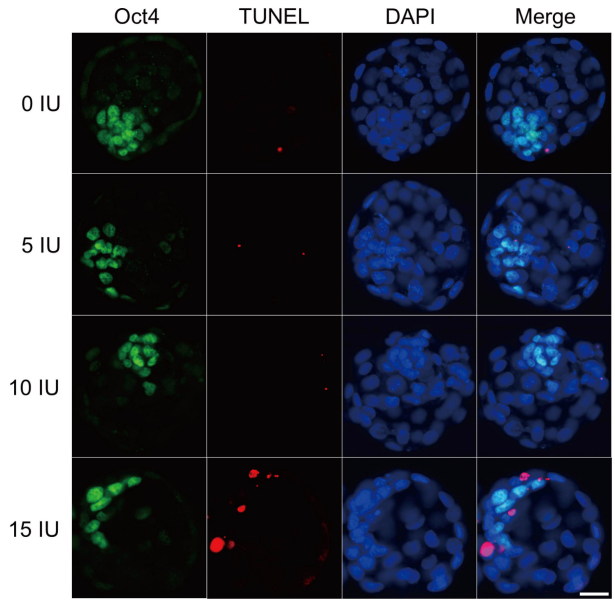

FIGURE 5 | Effects of different eCG doses on apoptosis and cell allocation in IVF-derived mouse blastocysts. Representative fluorescence micrographs of IVF-derived blastocysts obtained from groups primed with different doses of eCG are shown. The proportion of ICM cells was inferred by counting Oct4-positive (green) cells. The percentage of apoptotic nuclei was examined by detecting TUNEL-positive (red) cells. DAPI staining (blue) was used to analyze the total number of nuclei and thus estimate the total cell count of individual blastocysts. Scale bar = 20 μm.

TABLE 1 | Comparison of the average apoptotic cell counts and the mean apoptotic rates in IVF-derived blastocysts obtained from mice primed with different doses of eCG.

eCG dose (IU)	Number of blastocysts examined	Total cell count	Average apoptotic cell count	Mean apoptotic rate (%)
0	35	$50.26^{a} \pm 6.68$	$1.63^{a} \pm 1.03$	$3.16^{a} \pm 1.88$
5	35	$48.86^{a} \pm 5.77$	$1.71^{a} \pm 1.10$	$3.54^{a} \pm 2.28$
10	35	$48.43^{a} \pm 5.90$	$1.54^{a} \pm 1.04$	$3.17^{a} \pm 2.06$
15	35	$36.54^{b} \pm 4.66$	$5.46^{b} \pm 2.50$	$14.77^{b} \pm 6.56$

The values are shown as the means ± SDs.
^{a,b}Different superscripts within the same column indicate statistically significant differences ($P < 0.05$).

TABLE 2 | Comparison of the allocation to ICM and TE lineages in IVF-derived blastocysts derived from mice primed with different doses of eCG.

eCG dose (IU)	ICM cell count	TE cell count	ICM/TE cell ratio
0	$16.09^{a} \pm 2.32$	$34.17^{a} \pm 4.62$	$0.47^{a} \pm 0.04$
5	$16.14^{a} \pm 2.12$	$32.71^{a} \pm 4.36$	$0.50^{a} \pm 0.07$
10	$15.49^{a} \pm 2.08$	$32.94^{a} \pm 4.17$	$0.47^{a} \pm 0.05$
15	$10.29^{b} \pm 1.71$	$26.26^{b} \pm 4.35$	$0.40^{b} \pm 0.10$

The data are expressed as the means ± SDs.
^{a,b}Within a column, values with different superscripts are significantly different ($P < 0.05$).

after administration of 0, 5, 10, and 15 IU eCG were 1.43 ± 0.43/1.12 ± 0.19, 1.58 ± 0.45/1.40 ± 0.27, 1.64 ± 0.15/1.50 ± 0.09, and 3.42 ± 0.13/2.33 ± 0.10, respectively (**Figures 6A,B,D**).

Analysis of the Localization of Aurora B and MAD2L1 by FISH Assay

Due to the varied expression levels of Aurora B protein in different mouse strains and to differences in detection reagents, the presence of Aurora B protein in a single embryo cannot always be reliably detected using commercially available reagents (Schindler et al., 2012). Few studies have reported data resulting from detection of Aurora B expression in embryos *via* RNA *in situ* hybridization. To investigate the sensitivity of the RNA-FISH assay in detecting the localization of Aurora B and MAD2L1, we analyzed the subcellular localization of the corresponding mRNA molecules in IVF-derived mouse embryos. The double RNA-FISH results showed that Aurora B and MAD2L1 mRNA signals were strongly colocalized on chromatin in 11.21% (12/107) of IVF embryos derived from mice primed with 15 IU eCG. In contrast, enrichment of Aurora B and MAD2L1 signals on chromatin was detected in only 1.52% (1/66), 1.41% (1/71), and 2.25% (2/89) of the IVF embryos from female mice injected with 0, 5, and 10 IU eCG, respectively. In most other cases, Aurora B and MAD2L1 mRNA signals were localized in the cytoplasm (**Figures 6C,E**).

RT-PCR and Quantitative Immunocapillary Electrophoresis Analysis

Consistently, both the mRNA and protein expression levels of Aurora B and MAD2L1 in mouse embryos were significantly enhanced with increasing eCG doses up to 15 IU. Additionally, the relative protein expression levels of γH2AX and phospho-Aurora B (p-Aurora B; Aurora B phosphorylated at T232 and exhibiting maximal activation) were significantly higher in the 15 IU eCG treatment group than in the other three groups ($P < 0.05$). However, the mRNA expression of H2AX was not changed regardless of the eCG dose used ($P > 0.05$) (**Figures 6F,G**).

DISCUSSION

Traditional IVF ovarian stimulation strategies aim to maximize oocyte production. Recently, mild superovulation treatment protocols using lower doses and/or shorter durations of exogenous gonadotropin treatment have become increasingly popular, and the improvements in IVF technology have reduced the need for high oocyte production (Alper and Fauser, 2017). eCG mimics endogenous FSH with regard to its oocyte maturation-inducing effect, as observed in a mouse study (Behringer et al., 2018). In addition, a recent study has shown that high-dose FSH treatment should be discontinued during ovarian stimulation with IVF in predicted low responders because high FSH doses might not increase the rate of live births and might cause harm to women undergoing IVF treatment (Leijdekkers et al., 2019). Furthermore, studies on laboratory animals and women undergoing IVF have indicated that high doses of gonadotropin have harmful effects compared with low doses of gonadotropin (Bosch et al., 2016), and exposure to elevated

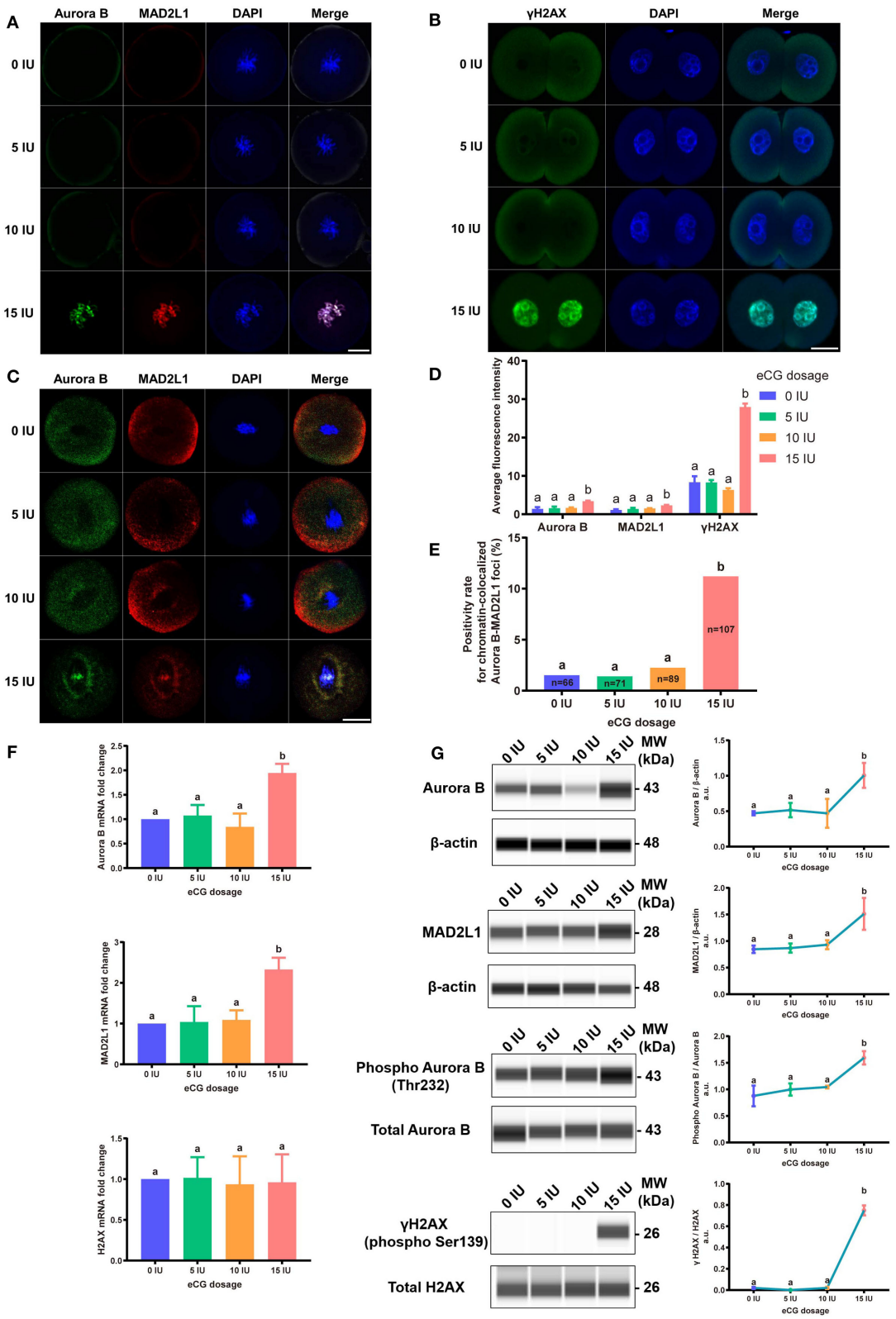

FIGURE 6 | Effects of different eCG doses on the expression profiles of γH2AX, Aurora B, and MAD2L1 in IVF-derived mouse embryos. **(A)** The subcellular colocalization between Aurora B (green) and MAD2L1 (red) in IVF-derived mouse embryos from groups treated with different eCG doses was observed by immunofluorescence staining. The nuclei were stained with DAPI (blue). Scale bar = 20 μm. **(B)** Representative photomicrographs of γH2AX in each group. In the

(Continued)

FIGURE 6 | 15 IU eCG treatment group, γH2AX (green) was strikingly expressed in two daughter nuclei (blue). Scale bar = 20 μm. **(C)** Confocal images of RNA FISH for endogenous Aurora B (green) and MAD2L1 (red) mRNA molecules in IVF-derived mouse embryos following administration of different doses of eCG. The embryo nuclei were counterstained with DAPI (blue). Scale bar = 20 μm. **(D)** Average FI of Aurora B/MAD2L1/γH2AX per IVF-derived mouse embryo in the groups treated with different eCG doses. The continuous FI data were analyzed using Student's *t*-test and ANOVA. [a,b]Different lowercase letters in the columns within each parameter indicate significant differences ($P < 0.05$). **(E)** Percentages of IVF-derived mouse embryos positive for local enrichment of Aurora B and MAD2L1 mRNA signals on chromatin (positivity rates for chromatin-colocalized Aurora B-MAD2L1 foci) in groups of mice administered eCG once at doses ranging from 0 to 15 IU. *n* shows the total number of embryos. Different letters in the columns depict statistical significance (for a and b, $P < 0.05$). **(F)** The relative mRNA expression levels of Aurora B, MAD2L1, and H2AX were analyzed by RT-PCR and normalized to those of β-actin. The differences in these continuous data were analyzed by Student's *t*-test and ANOVA. [a,b]Columns marked with different letters are significantly different from each other ($P < 0.05$). **(G)** Capillary-based immunodetection of protein extracts was performed using a Wes capillary-based device (ProteinSimple) to determine the average levels of Aurora B, MAD2L1, phospho-Aurora B (T232), and γH2AX. Every experiment was performed in triplicate. [a,b]Different superscripts above the error bars show significant differences ($P < 0.05$).

levels of gonadotropins after IVF treatment is considered a hazard factor for the development of ovarian tumors. In addition, the female reproductive system appears to be more susceptible to gonadotropin-related disorders than the male reproductive system (Rulli and Huhtaniemi, 2005). Nevertheless, the effects of high gonadotropin doses on IVF-derived embryos remain poorly understood (Alper and Fauser, 2017), particularly at the cellular level. Because previous studies on the use of gonadotropins have yielded contradictory and inconclusive results (Barash et al., 2017), we focused on IVF-derived embryos from eCG-primed mice to determine whether different doses of a single gonadotropin (eCG) affect the developmental competence of IVF-derived embryos and the formation of aneuploidy.

In this study, oocyte yield increased with increasing eCG doses; this result is similar to findings obtained previously (Edgar et al., 1987; Karagenc et al., 2004). Additionally, we observed that exposure of IVF-derived embryos to relatively high eCG doses reduced fertilization, four-cell embryo formation and blastocyst formation rates but did not significantly affect the two-cell embryo formation rate. Although we observed significant increases in oocyte yield in the presence of high doses of gonadotropin, the increases appeared meaningless because no effective increases in the numbers of high-quality embryos and blastocysts or in the live birth rate, which is the ultimate outcome, were observed (Leijdekkers et al., 2019). Undoubtedly, the success of IVF depends largely on the quality of the oocytes (Bosch et al., 2016). Notably, the development of diploid parthenogenetic oocytes is impaired by high eCG doses, which suggests that superovulation reduces both oocyte developmental potential and oocyte quality (Karagenc et al., 2004).

ROS can be derived from embryo metabolism and/or the environment surrounding embryos. Culture conditions and some other exogenous factors can accelerate the generation of ROS in embryos (Guérin et al., 2001). Oxidative stress plays a vital role in the process of ovulation, and ovulation leads to ROS-induced damage, which accumulates stage by stage in oocytes and related cells (Nie et al., 2018). We found higher total cytoplasmic and mitochondrial ROS levels in the embryos of the 15 IU eCG treatment group than in the embryos of the other groups, which indicated that IVF-derived embryos from mice primed with 15 IU eCG were in a state of oxidative stress. Ovarian stimulation during IVF can lead to supraphysiological estradiol concentrations, and elevated estradiol concentrations induce ROS production and mitochondrial dysfunction (Chou et al., 2020). In addition to genetic susceptibility factors, the quality of oocytes depends to a large extent on their maturation environment within the follicle and their independent viability after ovulation (Bradley and Swann, 2019). Superovulation increases the levels of ROS in the ovaries of mice, which demonstrates that ovaries are under high levels of oxidative stress after superovulation (Nie et al., 2018). Stimulation of the oviductal environment by gonadotropins impairs the development of embryos. Specifically, after superovulation, the presence of fluid in the fallopian tube appears to hinder embryo development (Chegini, 1996). Follicular fluid is the microenvironment of mature oocytes before fertilization, and the levels of ROS extracted from the follicular fluid of women undergoing ovarian stimulation is significantly negatively correlated with embryo formation and quality (Das et al., 2006). *In vitro* culture appears to compromise the development of IVF-derived embryos, particularly with respect to ROS levels, which indicates that non-ideal culture environments might be responsible for some of the observed results (Huang et al., 2019; Li et al., 2019) and that high doses of eCG may worsen these results.

It is important to consider that mitochondrial status and activity, which are susceptible to influence by non-physiological processes such as ovarian hyperstimulation and IVF, are key aspects affecting the quality of oocytes and the results of IVF (Ge et al., 2012). A mitochondrial ATP content above the threshold value of 2.0 pmol in human oocytes is connected with an increased likelihood of normal development and of early implantation of embryos after fertilization (Thouas et al., 2004). However, the ATP content and MMP of oocytes decrease after repeated ovarian stimulation (Combelles and Albertini, 2003; Ge et al., 2012). Hypoxia can increase MMP in mouse blastocysts cultured *in vitro* while elevating the expression levels of antioxidant genes and implantation proteins (Ma et al., 2017). In addition, MMP is involved in regulation of ROS and ATP generation (Romek et al., 2017), and a reduction in MMP is an early irreversible step in apoptosis (Zamzami et al., 1995; Green and Reed, 1998). The energy needed to maintain the normal development of preimplantation embryos is supplied in the form of ATP produced by mitochondria. Studies have shown that a suboptimal level of mitochondrial ATP production might lead to multiple embryo development defects and thus adversely affect the success rate of IVF (Fragouli and Wells, 2015). In this study, increasing doses of eCG decreased MMP

and sharply reduced the ATP content. In addition, the highest mitochondrial activity was obtained in the 15 IU eCG treatment group. Our findings are in good agreement with the "quiet embryo hypothesis" presented by Baumann et al. (2007) and Jing et al. (2019), who proposed that the active metabolism observed in embryos prior to the blastocyst stage is a signal that triggers multiple energy-consuming pathways for DNA damage repair. The viability of early embryos depends on their ability to maintain optimal metabolic levels (Bradley and Swann, 2019). Compared with less metabolically active embryos, embryos with more active metabolism show greater damage, and the surviving embryos exhibit lower oxidative phosphorylation activity and reduced oxygen consumption (Madrid Gaviria et al., 2019). The metabolism of an embryo before implantation is related to its developmental potential (Uyar and Seli, 2014). Quiet metabolism in early-stage embryos is associated with well-balanced embryo development. In contrast, active metabolism is related to subsequent suboptimal developmental outcomes (Leese et al., 2007). When external factors affect the viability of embryos, energy consumption increases to enable completion of the necessary repair processes. Active metabolism increases ROS levels with potentially harmful outcomes for embryos (Leese et al., 2007). Relatively low metabolic levels are most conducive to embryo survival (Leese, 2002). Notably, embryos cultured in 20% oxygen are capable of development and indeed exhibit reduced nutrient turnover (Leese et al., 2008). Suboptimal embryos cannot tolerate oxidative stress. Developmentally impaired or unhealthy embryos might have weakened defenses or reduced antioxidant capacities to cope with ROS and might therefore have to resort to other energy-consuming metabolic processes to maintain their redox stability. The quiet embryo hypothesis in this case refers to the ability of an embryo to respond to ROS (Gardner and Wale, 2013). Healthy embryos are metabolically inactive. Any non-physiological conditions that impair the function of an embryo trigger active metabolism, which may be reflected by an enhanced expenditure of energy substrates from the surrounding environment (D'Souza et al., 2016). Conceivably, to compensate for the oxidative damage caused by high-dose eCG-mediated induction of ovulation, the embryos in the current study underwent an energy-consuming repair process, which might explain the increases in active mitochondria and mitochondrial ROS production and the decreases in MMP and ATP content observed in the IVF mouse embryos belonging to the 15 IU eCG treatment group.

Sudden increases in the levels of blood gonadotropins (endogenous or exogenous) are potential mechanisms of aneuploidy (Dursun et al., 2006). In addition, gonadotropins might exert a mutagenic effect on DNA and increase sister chromatid exchange rates (Dursun et al., 2006). During the eight to sixteen-cell embryo stage, the dose of eCG and the probability of polyploidy show a dose-response relationship in CD-1 mice, and the probability of polyploidy increases from 2.9% with 10 IU eCG to 10.5% with 15 IU eCG (Ma et al., 1997). In our previous model, we revealed that ROS-induced damage increases the incidence of sex chromosome aneuploidy in IVF-obtained male mouse embryos and found that this effect occurs mainly *via* chromosome mis-segregation (Huang et al., 2019). The frequent observation of lagging chromosomes, micronuclei, and/or multinuclei suggests the existence of chromosomal aneuploidy (Zhao et al., 2010; Huang et al., 2019; Li et al., 2019). The formation of micronuclei in mouse embryos leads to permanent unilateral chromosomal inheritance (Vázquez-Diez et al., 2016). Our results demonstrate that a high gonadotropin dose leads to an elevated incidence of nuclear abnormalities; in other words, high-dose gonadotropin stimulation might induce chromosomal aneuploidy.

The side effects of exogenous gonadotropins may include cytoskeletal abnormalities. For example, spindle assembly and chromosome segregation might be affected by ovarian hormone stimulation (Mantikou et al., 2012), and abnormal spindle formation usually leads to aneuploidy (Zhao et al., 2010). Gonadotropins may also influence microtubule function in meiotic and mitotic spindles and thus increase aneuploidy rates (Dursun et al., 2006). Moreover, the correct assembly and distribution of the microfilament cytoskeleton in mouse embryos are closely related to the cleavage of early embryos (Wu et al., 2016). Different modes of microfilament formation have been found in the oocytes of superovulated hamsters (Lee et al., 2005). High doses of gonadotropins can induce aberrant microfilament distribution and decrease enrichment of cortical actin domains in oocytes, which might be associated with abnormal expression of actin-related genes (Lee et al., 2006). These findings, in conjunction with the findings of the current study, provide evidence showing that high-dose stimulation exerts negative effects on the spindle structure and microfilament distribution in IVF-derived mouse embryos.

The blastocyst stage is the optimal time period for screening of abnormalities (Bazrgar et al., 2013). The quality of blastocysts depends on the number of cells in the ICM, the number of TUNEL-positive nuclei, the ratio of ICM cells to TE cells, and the total number of cells (Wang et al., 2006; Maluf et al., 2009; Romek et al., 2017). Oct4-expressing ICM and TE cells are separated during blastocyst formation (Le Bin et al., 2014; Simmet et al., 2018). Compared with *in vivo* fertilization, IVF negatively affects the number of TE cells and ICM cells in blastocysts (Maluf et al., 2009). Additionally, compared with blastocysts obtained from naturally cycling mice, blastocysts obtained from superovulated mice present fewer surface microvilli, and the decrease in surface microvilli is accompanied by decreases in [^{35}S]-methionine uptake, cell number, mitotic index, and viability (Mitwally et al., 2005). According to studies conducted by Lee et al. (2005) the number of ICM cells is significantly reduced in golden hamsters after superovulation, and this reduction might be linked with alterations in mitochondrial function or number. One early study performed by our research team indicated that ROS increase the blastocyst apoptosis rate (Huang et al., 2019). A major consequence of unrepaired DNA damage is apoptosis. Mechanistically, it is likely that DNA damage causes developmental delay and micronuclei in embryos and ultimately leads to apoptosis in blastocysts. Normal embryos with DNA damage show increased genomic instability, which might affect implantation and postimplantation development (D'Souza et al., 2016). Notably, the total cell counts and ICM and TE cell counts of diploid parthenogenetic blastocysts are significantly lower after

application of 20 IU eCG than after application of 5 and 10 IU eCG (Karagenc et al., 2004). Similar to the results obtained with diploid parthenogenetic mouse blastocysts, rapid declines in the TE cell and ICM cell proportions, the ICM/TE cell ratios and the total cell counts in IVF-derived blastocysts were observed after stimulation with high doses of gonadotropin in this study.

Several hypotheses can be raised to explain the observed reductions in the developmental capacity of embryos in response to high doses of eCG. (1) Stimulation with high concentrations of eCG might have disrupted normal and critical intracellular signal transduction pathways that play crucial roles in the earliest phases of embryogenesis (Williams, 2002; Karagenc et al., 2004; Ducibella and Fissore, 2008). Gonadotropin-dependent follicles have their own microenvironments that transmit gonadotropin signals in different ways (Webb and Campbell, 2007). Tightly regulated signal transduction is important for embryonic functions (Lin et al., 2015), and high doses of eCG might disrupt the functions of normal signal transduction pathways at the early stages of development (Karagenc et al., 2004). (2) The administration of elevated levels of eCG for ovarian stimulation might have changed the levels and distributions of regulatory proteins in oocytes/embryos (Karagenc et al., 2004). (3) High-dose eCG treatment might have led to abnormalities in cytoskeletal dynamics and activity to negatively influence embryo proliferation and differentiation (Lee et al., 2005, 2006). (4) The high doses of eCG might have altered the mitochondrial number and activity in oocytes/embryos and induced mitochondrial dysfunction, resulting in insufficient energy or high oxidative stress (Lee et al., 2006). (5) The administration of high doses of gonadotropin might have induced production of a large quantity of low-potential oocytes. Low-potential oocytes are usually immature, with low mitochondrial counts and mitochondrial dysfunction, which lead to reduced rates of embryo development; such embryos might have been selected during the processes of fertilization and cleavage (Shu et al., 2016).

MAD2L1, a crucial component of the SAC complex, ensures chromosomal stability by regulating Aurora B (Shandilya et al., 2016). In a previous study, we first confirmed that ROS can arrest IVF-obtained mouse embryos in prophase/metaphase at the first mitotic cleavage through MAD2L1-mediated SAC activation (Wu et al., 2017). We then illustrated that SAC and DDR assist in repairing sex chromosome aneuploidy through the MAD2-mediated pathway (Huang et al., 2019). Subsequently, and most importantly, we demonstrated that Aurora B prevents aneuploidy *via* MAD2 in IVF-derived mouse embryos under oxidative stress (Li et al., 2019). In this study, we found that the expression of γH2AX was enhanced after administration of 15 IU eCG and that the expression of this protein remained restricted to two daughter nuclei at telophase in IVF-derived embryos. Furthermore, we detected distinctly upregulated expression and chromosomal enrichment of Aurora B and MAD2L1 in IVF-derived mouse embryos belonging to the high-stimulation (15 IU eCG) group. These results, combined with the research findings of our previous studies (Huang et al., 2019; Li et al., 2019) and the phenomenon of ROS elevation after high-dose stimulation, indicate that high-dose gonadotropin treatment induces ROS-mediated DNA damage and thereby triggers Aurora B-mediated SAC activation in early IVF-derived mouse embryos. Notably, it has previously been reported that partially activated Aurora B-mediated phosphorylation of H2AX at serine 121 (H2AX-pS121) can accelerate Aurora B full autophosphorylation, which is necessary for correct chromosome segregation in mitosis (Shimada and Nakanishi, 2016; Shimada et al., 2016). Given this information and our observations, we suspect that γH2AX plays a role similar to that of H2AX-pS121, but more experiments should be performed to confirm or refute this possibility. Further analysis *via* double mRNA FISH revealed that stimulation with 15 IU eCG increased the frequency of colocalization of Aurora B and MAD2L1 mRNA expression with chromatin in IVF-derived mouse embryos. The increased colocalization of these two mRNA populations with chromatin may be a sign of SAC activation. Our preliminary findings regarding Aurora B and MAD2L1 expression detected by mRNA FISH were similar to the immunofluorescence staining results. Due to the occasional failure of commercially available reagents to reliably detect Aurora B protein in individual oocytes and early embryos (Schindler et al., 2012; Nguyen and Schindler, 2017), mRNA FISH might be a more sensitive method than immunofluorescence for detecting Aurora B expression in IVF embryos. Findings obtained in mouse and Xenopus oocytes are in good agreement with our experimental results, suggesting that Aurora B may be detectable on all chromosomes during prometaphase (Ju et al., 2016). Moreover, Aurora B overexpression might partly rescue defects in chromosome alignment in mouse oocytes, specifically during the metaphase I stage (Shuda et al., 2009). Aurora B is also overexpressed in many tumors; however, this overexpression rarely leads to fatal aneuploidy because it limits chromosome segregation errors (Manzione et al., 2020). Aurora B enrichment on chromatin can also promote Aurora B activation (Kelly et al., 2007). Furthermore, estrogen induces the activity of Aurora B (Ruiz-Cortés et al., 2005). Notably, maximal Aurora B activation requires autophosphorylation at T232 in the activation loop (Shimada and Nakanishi, 2016). The capillary electrophoresis and immunodetection findings suggested that autophosphorylation of Aurora B at T232 was markedly strengthened by superovulation with 15 IU eCG, which supports the idea that Aurora B autoactivation is connected with SAC activation in IVF-derived embryos following administration of high doses of gonadotropin. The elevations in Aurora B and Aurora B autoactivation-triggered SAC activation (as indicated by increased expression of MAD2L1) seem designed to provide embryos with the chance to self-correct aneuploidies and repair their spindles during early embryo development (Wang et al., 2002; Bazrgar et al., 2013). Although chromosome instability is prevalent in cleavage-stage embryos during early IVF embryogenesis, mosaic embryos, including normal blastomeres, may still have the potential to be chromosomally normal fetuses (Vanneste et al., 2009). Of interest, some authors have reported that Aurora B p.L39P is a possible gain-of-function mutant protein with enhanced function in regulating the alignment of chromosomes at the metaphase plate (Nguyen et al., 2017). The expression and role of Aurora B in regeneration (Gwee et al., 2018; Shaalan and Proctor, 2019) and glycolysis metabolism (Zhou et al., 2018; He et al., 2019) have been explored over

the past few years. Accordingly, the potential role of Aurora B in IVF-derived mouse embryos needs to be further confirmed and investigated.

Collectively, the research findings obtained in the present study reveal that priming with high doses of eCG exerts marked adverse effects on certain developmental competences of IVF-derived mouse embryos. Based on these findings and the findings of our previous studies, we propose, for the first time, that a high dose of eCG is a contributing factor that might induce oxidative stress-related DNA damage to trigger Aurora B-mediated SAC activation in early IVF-derived mouse embryos for the self-correction of aneuploidy formation (**Figure 7**). Based on these considerations, the Aurora B protein and related agents likely play roles in preventing the birth of offspring with chromosomal diseases. It should be noted that this study examined only a mouse model, and there were some techniques and methods that we could not include; thus, the results might not be fully applicable to human ART, and suitable trials are needed to verify the findings. However, the lessons learned in studies on mice provide considerable evidence regarding the impact of gonadotrophin-induced superovulation on the developmental competence of IVF-derived embryos and its relationship with reproductive pathophysiology. The body surface area normalization method can be used to convert doses from mice to humans, especially in clinical trials (Reagan-Shaw et al., 2008). In the future, physiologic, pharmacokinetic, and toxicology data can also be used for scientific justification (Blanchard and Smoliga, 2015). Studies on mouse models have provided abundant new information on previously unknown mechanisms involved in the pathophysiological effects of gonadotrophins in both sexes and have clearly expanded the body of knowledge (Rulli and Huhtaniemi, 2005). In addition, new ART regimens involving low gonadotropin doses might be explored to improve pregnancy outcomes in women and to potentially avoid chromosome aneuploidy in embryos.

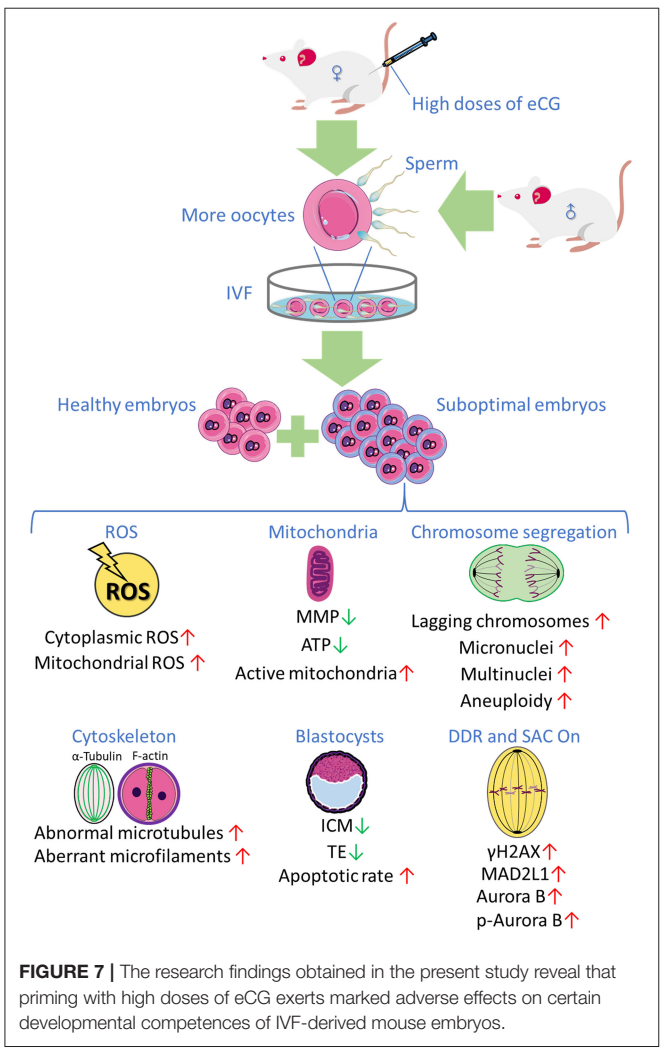

FIGURE 7 | The research findings obtained in the present study reveal that priming with high doses of eCG exerts marked adverse effects on certain developmental competences of IVF-derived mouse embryos.

DATA AVAILABILITY STATEMENT

All datasets generated for this study are included in the article/**Supplementary Material**.

ETHICS STATEMENT

The animal study was reviewed and approved by the Institutional Animal Care and Use Committee (IACUC) of Shantou University Medical College (SUMC2018-049).

AUTHOR CONTRIBUTIONS

ZL had the initial idea, supervised the experiments, and revised the manuscript. ZL, EL, and YH designed the experiments. EL, YH, GR, and PH performed the experiments and analyzed data. EL wrote the manuscript. All authors commented on the manuscript.

FUNDING

This research was supported by the National Natural Science Foundation of China (No. 81871223, No. 81671536, and No. 81471522), the Guangdong Provincial Science and Technology Project (No. 2016A020218015), and the Natural Science Foundation of Guangdong Province of China (No. 2014A030313482).

ACKNOWLEDGMENTS

The authors thank all of the participants in this study. **Figure 7** was partly produced using Servier Medical Art, available from https://smart.servier.com/ and licensed under a Creative Commons Attribution 3.0 Unported License.

SUPPLEMENTARY MATERIAL

The Supplementary Material for this article can be found online at: https://www.frontiersin.org/articles/10.3389/fcell.2020.609290/full#supplementary-material

REFERENCES

Aitken, R. J. (2020). Impact of oxidative stress on male and female germ cells: implications for fertility. *Reproduction*159, R189–R201. doi: 10.1530/REP-19-0452

Alper, M. M., and Fauser, B. C. (2017). Ovarian stimulation protocols for IVF: is more better than less? *Reprod. Biomed. Online* 34, 345–353. doi: 10.1016/j.rbmo.2017.01.010

Anderson, R. C., Newton, C. L., Anderson, R. A., and Millar, R. P. (2018). Gonadotropins and their analogs: current and potential clinical applications. *Endocr. Rev.* 39, 911–937. doi: 10.1210/er.2018-00052

Balboula, A. Z., and Schindler, K. (2014). Selective disruption of aurora C kinase reveals distinct functions from aurora B kinase during meiosis in mouse oocytes. *PLoS Genet.* 10:e1004194. doi: 10.1371/journal.pgen.1004194

Barash, O. O., Hinckley, M. D., Rosenbluth, E. M., Ivani, K. A., and Weckstein, L. N. (2017). High gonadotropin dosage does not affect euploidy and pregnancy rates in IVF PGS cycles with single embryo transfer. *Hum. Reprod.* 32, 2209–2217. doi: 10.1093/humrep/dex299

Baumann, C. G., Morris, D. G., Sreenan, J. M., and Leese, H. J. (2007). The quiet embryo hypothesis: molecular characteristics favoring viability. *Mol. Reprod. Dev.* 74, 1345–1353. doi: 10.1002/mrd.20604

Bay, B., Mortensen, E. L., Hvidtjørn, D., and Kesmodel, U. S. (2013). Fertility treatment and risk of childhood and adolescent mental disorders: register based cohort study. *BMJ* 347, f3978–f3978. doi: 10.1136/bmj.f3978

Bazrgar, M., Gourabi, H., Valojerdi, M. R., Yazdi, P. E., and Baharvand, H. (2013). Self-correction of chromosomal abnormalities in human preimplantation embryos and embryonic stem cells. *Stem Cells Dev.* 22, 2449–2456. doi: 10.1089/scd.2013.0053

Beaumont, H. M., and Smith, A. F. (1975). Embryonic mortality during the pre- and post-implantation periods of pregnancy in mature mice after superovulation. *J. Reprod. Fertil.* 45, 437–448. doi: 10.1530/jrf.0.0450437

Behringer, R., Gertsenstein, M., Nagy, K. V., and Nagy, A. (2018). Administration of gonadotropins for superovulation in mice. *Cold Spring Harb. Protoc.* 2018, 24–27. doi: 10.1101/pdb.prot092403

Blanchard, O. L., and Smoliga, J. M. (2015). Translating dosages from animal models to human clinical trials–revisiting body surface area scaling. *Faseb J.* 29, 1629–1634. doi: 10.1096/fj.14-269043

Bosch, E., Labarta, E., Kolibianakis, E., Rosen, M., and Meldrum, D. (2016). Regimen of ovarian stimulation affects oocyte and therefore embryo quality. *Fertil. Steril.* 105, 560–570. doi: 10.1016/j.fertnstert.2016.01.022

Bradley, J., and Swann, K. (2019). Mitochondria and lipid metabolism in mammalian oocytes and early embryos. *Int. J. Dev. Biol.* 63, 93–103. doi: 10.1387/ijdb.180355ks

Calicchio, R., Doridot, L., Miralles, F., Méhats, C., and Vaiman, D. (2014). DNA methylation, an epigenetic mode of gene expression regulation in reproductive science. *Curr. Pharmaceut. Design* 20, 1726–1750. doi: 10.2174/13816128113199990517

Carstea, C., Bogdan, A., Iudith, I., Cean, A., Ilie, D., and Vintilă, R. (2012). Effect of Intracytoplasmic Sperm Injection (ICSI) on mouse embryos preimplantational development. *Sci. Papers Anim. Sci. Biotechnol.* 45, 299–303. Available online at: http://spasb.ro/index.php/spasb/article/view/588/546

Chegini, N. (1996). Oviductal-derived growth factors and cytokines: implication in preimplantation. *Semin. Reprod. Endocrinol.* 14, 219–229. doi: 10.1055/s-2007-1016332

Chou, C.-H., Chen, S.-U., Chen, C.-D., Shun, C.-T., Wen, W.-F., Tu, Y.-A., et al. (2020). Mitochondrial dysfunction induced by high estradiol concentrations in endometrial epithelial cells. *J. Clin. Endocrinol. Metab.* 105:dgz015. doi: 10.1210/clinem/dgz015

Combelles, C. M., and Albertini, D. F. (2003). Assessment of oocyte quality following repeated gonadotropin stimulation in the mouse. *Biol. Reprod.* 68, 812–821. doi: 10.1095/biolreprod.102.008656

Das, S., Chattopadhyay, R., Ghosh, S., Ghosh, S., Goswami, S. K., Chakravarty, B. N., et al. (2006). Reactive oxygen species level in follicular fluid–embryo quality marker in IVF? *Human Reprod.* 21, 2403–2407. doi: 10.1093/humrep/del156

D'Souza, F., Pudakalakatti, S. M., Uppangala, S., Honguntikar, S., Salian, S. R., Kalthur, G., et al. (2016). Unraveling the association between genetic integrity and metabolic activity in pre-implantation stage embryos. *Sci. Rep.* 6:37291. doi: 10.1038/srep37291

Ducibella, T., and Fissore, R. (2008). The roles of Ca2+, downstream protein kinases, and oscillatory signaling in regulating fertilization and the activation of development. *Dev. Biol.* 315, 257–279. doi: 10.1016/j.ydbio.2007.12.012

Dursun, P., Gultekin, M., Yuce, K., and Ayhan, A. (2006). What is the underlying cause of aneuploidy associated with increasing maternal age? Is it associated with elevated levels of gonadotropins? *Med. Hypotheses* 66, 143–147. doi: 10.1016/j.mehy.2004.10.022

Edgar, D. H., Whalley, K. M., and Mills, J. A. (1987). Effects of high-dose and multiple-dose gonadotropin stimulation on mouse oocyte quality as assessed by preimplantation development following *in vitro* fertilization. *J. in vitro Fert. Embryo Transf.* 4, 273–276. doi: 10.1007/BF01555203

Ertzeid, G., and Storeng, R. (1992). Adverse effects of gonadotrophin treatment on pre- and postimplantation development in mice. *J. Reprod. Fertil.* 96, 649–655. doi: 10.1530/jrf.0.0960649

Ertzeid, G., and Storeng, R. (2001). The impact of ovarian stimulation on implantation and fetal development in mice. *Human Reprod.* 16, 221–225. doi: 10.1093/humrep/16.2.221

Farhud, D. D., Zokaei, S., Keykhaei, M., and Yeganeh, M. Z. (2019). Strong evidences of the ovarian carcinoma risk in women after IVF treatment: a review article. *Iran. J. Publ. Health* 48, 2124–2132. doi: 10.18502/ijph.v48i12.3543

Felty, Q., Xiong, W.-C., Sun, D., Sarkar, S., Singh, K. P., Parkash, J., et al. (2005). Estrogen-induced mitochondrial reactive oxygen species as signal-transducing messengers. *Biochemistry* 44, 6900–6909. doi: 10.1021/bi047629p

Fortier, A. L., Lopes, F. L., Darricarrere, N., Martel, J., and Trasler, J. M. (2008). Superovulation alters the expression of imprinted genes in the midgestation mouse placenta. *Hum. Mol. Genet.* 17, 1653–1665. doi: 10.1093/hmg/ddn055

Fragouli, E., and Wells, D. (2015). Mitochondrial DNA assessment to determine oocyte and embryo viability. *Semin. Reprod. Med.* 33, 401–409. doi: 10.1055/s-0035-1567821

Gardner, D. K., and Wale, P. L. (2013). Analysis of metabolism to select viable human embryos for transfer. *Fertil. Steril.* 99, 1062–1072. doi: 10.1016/j.fertnstert.2012.12.004

Ge, H., Tollner, T. L., Hu, Z., Da, M., Li, X., Guan, H., et al. (2012). Impaired mitochondrial function in murine oocytes is associated with controlled ovarian hyperstimulation and *in vitro* maturation. *Reprod. Fertil. Dev.* 24, 945–952. doi: 10.1071/RD11212

Green, D. R., and Reed, J. C. (1998). Mitochondria and apoptosis. *Science* 281, 1309–1312. doi: 10.1126/science.281.5381.1309

Guérin, P., El Mouatassim, S., and Ménézo, Y. (2001). Oxidative stress and protection against reactive oxygen species in the pre-implantation embryo and its surroundings. *Hum. Reprod. Update* 7, 175–189. doi: 10.1093/humupd/7.2.175

Gwee, S. S. L., Radford, R. A. W., Chow, S., Syal, M. D., Morsch, M., Formella, I., et al. (2018). Aurora kinase B regulates axonal outgrowth and regeneration in the spinal motor neurons of developing zebrafish. *Cell Mol. Life Sci.* 75, 4269–4285. doi: 10.1007/s00018-018-2780-5

Han, L., Wang, H., Li, L., Li, X., Ge, J., Reiter, R. J., et al. (2017). Melatonin protects against maternal obesity-associated oxidative stress and meiotic defects in oocytes *via* the SIRT3-SOD2-dependent pathway. *J. Pineal Res.* 63:e12431. doi: 10.1111/jpi.12431

He, J., Qi, Z., Zhang, X., Yang, Y., Liu, F., Zhao, G., et al. (2019). Aurora kinase B inhibitor barasertib (AZD1152) inhibits glucose metabolism in gastric cancer cells. *Anticancer Drugs* 30, 19–26. doi: 10.1097/CAD.0000000000000684

Honma, K., Nakanishi, R., Nakanoko, T., Ando, K., Saeki, H., Oki, E., et al. (2014). Contribution of Aurora-A and -B expression to DNA aneuploidy in gastric cancers. *Surg. Today* 44, 454–461. doi: 10.1007/s00595-013-0581-x

Huang, Y., Ha, S., Li, Z., Li, J., and Xiao, W. (2019). CHK1-CENP B/MAD2 is associated with mild oxidative damage-induced sex chromosome aneuploidy of male mouse embryos during *in vitro* fertilization. *Free Rad. Biol. Med.* 137, 181–193. doi: 10.1016/j.freeradbiomed.2019.04.037

Ingrid, V. d. A., and Thomas, D. H. (2001). Superovulation of female mice delays embryonic and fetal development. *Human Reprod.* 16, 1237–1243. doi: 10.1093/humrep/16.6.1237

Jing, Y., Li, L., Li, Y. Y., Ouyang, Y. C., Sun, Q. Y., Zhang, C. L., et al. (2019). Embryo quality, and not chromosome non-diploidy, affects mitochondrial DNA content in mouse blastocysts. *J. Cell Physiol.* 234, 10481–10488. doi: 10.1002/jcp.27713

Ju, S., Peng, X., Yang, X., Sozar, S., Muneri, C. W., Xu, Y., et al. (2016). Aurora B inhibitor barasertib prevents meiotic maturation and subsequent embryo development in pig oocytes. *Theriogenology* 86, 503–515. doi: 10.1016/j.theriogenology.2016.01.030

Kala, M., Shaikh, M. V., and Nivsarkar, M. (2016). Equilibrium between anti-oxidants and reactive oxygen species: a requisite for oocyte development and maturation. *Reprod. Med. Biol.* 16, 28–35. doi: 10.1002/rmb2.12013

Karagenc, L., Yalcin, E., Ulug, U., and Bahceci, M. (2004). Administration of increasing amounts of gonadotrophin compromises preimplantation development of parthenogenetic mouse embryos. *Reprod. Biomed. Online* 8, 628–634. doi: 10.1016/S1472-6483(10)61642-2

Kelly, A. E., Sampath, S. C., Maniar, T. A., Woo, E. M., Chait, B. T., and Funabiki, H. (2007). Chromosomal enrichment and activation of the aurora B pathway are coupled to spatially regulate spindle assembly. *Dev. Cell* 12, 31–43. doi: 10.1016/j.devcel.2006.11.001

La Bastide-Van Gemert, S., Seggers, J., Haadsma, M. L., Heineman, M. J., Middelburg, K. J., Roseboom, T. J., et al. (2014). Is ovarian hyperstimulation associated with higher blood pressure in 4-year-old IVF offspring? Part II: an explorative causal inference approach. *Human Reprod.* 29, 510–517. doi: 10.1093/humrep/det448

Lawrence, L. T., and Moley, K. H. (2008). Epigenetics and assisted reproductive technologies: human imprinting syndromes. *Semin. Reprod. Med.* 26, 143–152. doi: 10.1055/s-2008-1042953

Le Bin, G. C., Muñoz-Descalzo, S., Kurowski, A., Leitch, H., Lou, X., Mansfield, W., et al. (2014). Oct4 is required for lineage priming in the developing inner cell mass of the mouse blastocyst. *Development* 141, 1001–1010. doi: 10.1242/dev.096875

Lee, S. T., Han, H. J., Oh, S. J., Lee, E. J., Han, J. Y., and Lim, J. M. (2006). Influence of ovarian hyperstimulation and ovulation induction on the cytoskeletal dynamics and developmental competence of oocytes. *Mol. Reprod. Dev.* 73, 1022–1033. doi: 10.1002/mrd.20500

Lee, S. T., Kim, T. M., Cho, M. Y., Moon, S. Y., Han, J. Y., and Lim, J. M. (2005). Development of a hamster superovulation program and adverse effects of gonadotropins on microfilament formation during oocyte development. *Fertil. Steril.* 83(suppl.1), 1264–1274. doi: 10.1016/j.fertnstert.2004.09.039

Leese, H. J. (2002). Quiet please, do not disturb: a hypothesis of embryo metabolism and viability. *Bioessays* 24, 845–849. doi: 10.1002/bies.10137

Leese, H. J., Baumann, C. G., Brison, D. R., McEvoy, T. G., and Sturmey, R. G. (2008). Metabolism of the viable mammalian embryo: quietness revisited. *Mol. Hum. Reprod.* 14, 667–672. doi: 10.1093/molehr/gan065

Leese, H. J., Sturmey, R. G., Baumann, C. G., and McEvoy, T. G. (2007). Embryo viability and metabolism: obeying the quiet rules. *Hum. Reprod.* 22, 3047–3050. doi: 10.1093/humrep/dem253

Leijdekkers, J. A., Torrance, H. L., Schouten, N. E., van Tilborg, T. C., Oudshoorn, S. C., Mol, B. W. J., et al. (2019). Individualized ovarian stimulation in IVF/ICSI treatment: it is time to stop using high FSH doses in predicted low responders. *Hum. Reprod.* 35, 1954–1963. doi: 10.1093/humrep/dez184

Li, J., Ha, S., Li, Z., Huang, Y., Lin, E., and Xiao, W. (2019). Aurora B prevents aneuploidy *via* MAD2 during the first mitotic cleavage in oxidatively damaged embryos. *Cell Proliferation* 52:e12657. doi: 10.1111/cpr.12657

Lin, Z. L., Ni, H. M., Liu, Y. H., Sheng, X. H., Cui, X. S., Kim, N. H., et al. (2015). Effect of anti-PMSG on distribution of estrogen receptor alpha and progesterone receptor in mouse ovary, oviduct and uterus. *Zygote* 23, 695–703. doi: 10.1017/S0967199414000343

Lopes, A. S., Lane, M., and Thompson, J. G. (2010). Oxygen consumption and ROS production are increased at the time of fertilization and cell cleavage in bovine zygotes. *Human Reprod.* 25, 2762–2773. doi: 10.1093/humrep/deq221

Ma, S., Kalousek, D. K., Yuen, B. H., and Moon, Y. S. (1997). Investigation of effects of pregnant mare serum gonadotropin (PMSG) on the chromosomal complement of CD-1 mouse embryos. *J. Assist. Reprod. Genet.* 14, 162–169. doi: 10.1007/BF02766134

Ma, Y. Y., Chen, H. W., and Tzeng, C. R. (2017). Low oxygen tension increases mitochondrial membrane potential and enhances expression of antioxidant genes and implantation protein of mouse blastocyst cultured *in vitro*. *J. Ovarian Res.* 10:47. doi: 10.1186/s13048-017-0344-1

Madrid Gaviria, S., Morado, S. A., López Herrera, A., Restrepo Betancur, G., Urrego Álvarez, R. A., Echeverri Zuluaga, J., et al. (2019). Resveratrol supplementation promotes recovery of lower oxidative metabolism after vitrification and warming of *in vitro*-produced bovine embryos. *Reprod. Fertil. Dev.* 31, 521–528. doi: 10.1071/RD18216

Maluf, M., Perin, P. M., Foltran Januário, D. A., and Nascimento Saldiva, P. H. (2009). *In vitro* fertilization, embryo development, and cell lineage segregation after pre- and/or postnatal exposure of female mice to ambient fine particulate matter. *Fertil. Steril.* 92, 1725–1735. doi: 10.1016/j.fertnstert.2008.08.081

Mantikou, E., Wong, K. M., Repping, S., and Mastenbroek, S. (2012). Molecular origin of mitotic aneuploidies in preimplantation embryos. *Biochim. Biophys. Acta* 1822, 1921–1930. doi: 10.1016/j.bbadis.2012.06.013

Manzione, M. G., Rombouts, J., Steklov, M., Pasquali, L., Sablina, A., Gelens, L., et al. (2020). Co-regulation of the antagonistic RepoMan:Aurora-B pair in proliferating cells. *Mol. Biol. Cell* 31, 419–438. doi: 10.1091/mbc.E19-12-0698

Mitwally, M. F. M., Casper, R. F., and Diamond, M. P. (2005). The role of aromatase inhibitors in ameliorating deleterious effects of ovarian stimulation on outcome of infertility treatment. *Reprod. Biol. Endocrinol.* 3, 54–54. doi: 10.1186/1477-7827-3-54

Nelson, G. M., Guynn, J. M., and Chorley, B. N. (2017). Procedure and key optimization strategies for an automated capillary electrophoretic-based immunoassay method. *J. Visual. Exp.* 127:e55911. doi: 10.3791/55911

Nguyen, A. L., Drutovic, D., Vazquez, B. N., El Yakoubi, W., Gentilello, A. S., Malumbres, M., et al. (2018). Genetic interactions between the aurora kinases reveal new requirements for AURKB and AURKC during oocyte meiosis. *Curr. Biol.* 28, 3458–3468.e3455. doi: 10.1016/j.cub.2018.08.052

Nguyen, A. L., Gentilello, A. S., Balboula, A. Z., Shrivastava, V., Ohring, J., and Schindler, K. (2014). Phosphorylation of threonine 3 on histone H3 by haspin kinase is required for meiosis I in mouse oocytes. *J. Cell Sci.* 127, 5066–5078. doi: 10.1242/jcs.158840

Nguyen, A. L., Marin, D., Zhou, A., Gentilello, A. S., Smoak, E. M., Cao, Z., et al. (2017). Identification and characterization of Aurora kinase B and C variants associated with maternal aneuploidy. *Mol. Hum. Reprod.* 23, 406–416. doi: 10.1093/molehr/gax018

Nguyen, A. L., and Schindler, K. (2017). Specialize and divide (twice): functions of three aurora kinase homologs in mammalian oocyte meiotic maturation. *Trends Genet.* 33, 349–363. doi: 10.1016/j.tig.2017.03.005

Nie, X., Dai, Y., Zheng, Y., Bao, D., Chen, Q., Yin, Y., et al. (2018). Establishment of a mouse model of premature ovarian failure using consecutive superovulation. *Cell Physiol. Biochem.* 51, 2341–2358. doi: 10.1159/000495895

Ozturk, S., Yaba-Ucar, A., Sozen, B., Mutlu, D., and Demir, N. (2016). Superovulation alters embryonic poly(A)-binding protein (Epab) and poly(A)-binding protein, cytoplasmic 1 (Pabpc1) gene expression in mouse oocytes and early embryos. *Reprod. Fertil. Dev.* 28, 375–383. doi: 10.1071/RD14106

Reagan-Shaw, S., Nihal, M., and Ahmad, N. (2008). Dose translation from animal to human studies revisited. *Faseb J.* 22, 659–661. doi: 10.1096/fj.07-9574LSF

Romek, M., Gajda, B., Krzysztofowicz, E., Kucia, M., Uzarowska, A., and Smorag, Z. (2017). Improved quality of porcine embryos cultured with hyaluronan due to the modification of the mitochondrial membrane potential and reactive oxygen species level. *Theriogenology* 102, 1–9. doi: 10.1016/j.theriogenology.2017.06.026

Roy, D., Cai, Q., Felty, Q., and Narayan, S. (2007). Estrogen-induced generation of reactive oxygen and nitrogen species, gene damage, and estrogen-dependent cancers. *J. Toxicol. Environ. Health B Crit. Rev.* 10, 235–257. doi: 10.1080/15287390600974924

Ruchaud, S., Carmena, M., and Earnshaw, W. C. (2007). Chromosomal passengers: conducting cell division. *Nat. Rev. Mol. Cell Biol.* 8, 798–812. doi: 10.1038/nrm2257

Ruiz-Cortés, Z. T., Kimmins, S., Monaco, L., Burns, K. H., Sassone-Corsi, P., and Murphy, B. D. (2005). Estrogen mediates phosphorylation of histone H3 in ovarian follicle and mammary epithelial tumor cells *via* the mitotic kinase, Aurora B. *Mol. Endocrinol.* 19, 2991–3000. doi: 10.1210/me.2004-0441

Rulli, S. B., and Huhtaniemi, I. (2005). What have gonadotrophin overexpressing transgenic mice taught us about gonadal function? *Reproduction* 130, 283–291. doi: 10.1530/rep.1.00661

Rumbold, A. R., Moore, V. M., Whitrow, M. J., Oswald, T. K., Moran, L. J., Fernandez, R. C., et al. (2017). The impact of specific fertility treatments on cognitive development in childhood and adolescence: a systematic review. *Human Reprod.* 32, 1489–1507. doi: 10.1093/humrep/dex085

Sage, J. M., Hall, L., McVey, A., Barohn, R. J., Statland, J. M., Jawdat, O., et al. (2020). Use of capillary electrophoresis immunoassay to search for potential

biomarkers of amyotrophic lateral sclerosis in human platelets. *J. Vis. Exp.* 156:e60638. doi: 10.3791/60638

Sakai, N., and Endo, A. (1987). Potential teratogenicity of gonadotropin treatment for ovulation induction in the mouse offspring. *Teratology* 36, 229–233. doi: 10.1002/tera.1420360211

Sato, A., Otsu, E., Negishi, H., Utsunomiya, T., and Arima, T. (2007). Aberrant DNA methylation of imprinted loci in superovulated oocytes. *Human Reprod.* 22, 26–35. doi: 10.1093/humrep/del316

Saurin, A. T., van der Waal, M. S., Medema, R. H., Lens, S. M., and Kops, G. J. (2011). Aurora B potentiates Mps1 activation to ensure rapid checkpoint establishment at the onset of mitosis. *Nat. Commun.* 2:316. doi: 10.1038/ncomms1319

Schindler, K., Davydenko, O., Fram, B., Lampson, M. A., and Schultz, R. M. (2012). Maternally recruited Aurora C kinase is more stable than Aurora B to support mouse oocyte maturation and early development. *Proc. Natl. Acad. Sci. U. S. A.* 109, E2215–2222. doi: 10.1073/pnas.1120517109

Seggers, J., Haadsma, M. L., La Bastide-Van Gemert, S., Heineman, M. J., Middelburg, K. J., Roseboom, T. J., et al. (2014). Is ovarian hyperstimulation associated with higher blood pressure in 4-year-old IVF offspring? Part I: multivariable regression analysis. *Human Reprod.* 29, 502–509. doi: 10.1093/humrep/det396

Shaalan, A., and Proctor, G. (2019). Salivary glands require Aurora Kinase B for regeneration after transient innate immune-mediated injury. *Sci. Rep.* 9:11339. doi: 10.1038/s41598-019-47762-9

Shandilya, J., Medler, K. F., and Roberts, S. G. (2016). Regulation of AURORA B function by mitotic checkpoint protein MAD2. *Cell Cycle* 15, 2196–2201. doi: 10.1080/15384101.2016.1200773

Shimada, M., Goshima, T., Matsuo, H., Johmura, Y., Haruta, M., Murata, K., et al. (2016). Essential role of autoactivation circuitry on Aurora B-mediated H2AX-pS121 in mitosis. *Nat. Commun.* 7:12059. doi: 10.1038/ncomms12059

Shimada, M., and Nakanishi, M. (2016). Aurora B twists on histones for activation. *Cell Cycle* 15, 3321–3322. doi: 10.1080/15384101.2016.1224758

Shu, J., Xing, L.-L., Ding, G.-L., Liu, X.-M., Yan, Q.-F., and Huang, H.-F. (2016). Effects of ovarian hyperstimulation on mitochondria in oocytes and early embryos. *Reprod. Fertil. Dev.* 28, 1214–1222. doi: 10.1071/RD14300

Shuda, K., Schindler, K., Ma, J., Schultz, R. M., and Donovan, P. J. (2009). Aurora kinase B modulates chromosome alignment in mouse oocytes. *Mol. Reprod. Dev.* 76, 1094–1105. doi: 10.1002/mrd.21075

Simmet, K., Zakhartchenko, V., Philippou-Massier, J., Blum, H., Klymiuk, N., and Wolf, E. (2018). OCT4/POU5F1 is required for NANOG expression in bovine blastocysts. *Proc. Natl. Acad. Sci. U. S. A.* 115, 2770–2775. doi: 10.1073/pnas.1718833115

Swann (2014). *Effects of Ovarian Stimulation on Oocyte Development and Embryo Quality*. Nottingham: University of Nottingham.

Thouas, G. A., Trounson, A. O., Wolvetang, E. J., and Jones, G. M. (2004). Mitochondrial dysfunction in mouse oocytes results in preimplantation embryo arrest *in vitro*. *Biol. Reprod.* 71, 1936–1942. doi: 10.1095/biolreprod.104.033589

Uyar, A., and Seli, E. (2014). Metabolomic assessment of embryo viability. *Semin. Reprod. Med.* 32, 141–152. doi: 10.1055/s-0033-1363556

Uysal, F., Ozturk, S., and Akkoyunlu, G. (2018). Superovulation alters DNA methyltransferase protein expression in mouse oocytes and early embryos. *J. Assist. Reprod. Genet.* 35, 503–513. doi: 10.1007/s10815-017-1087-z

Vanneste, E., Voet, T., Le Caignec, C., Ampe, M., Konings, P., Melotte, C., et al. (2009). Chromosome instability is common in human cleavage-stage embryos. *Nat. Med.* 15, 577–583. doi: 10.1038/nm.1924

Vázquez-Diez, C., Yamagata, K., Trivedi, S., Haverfield, J., and FitzHarris, G. (2016). Micronucleus formation causes perpetual unilateral chromosome inheritance in mouse embryos. *Proc. Natl. Acad. Sci. U. S. A.* 113, 626–631. doi: 10.1073/pnas.1517628112

Wang, X., Jin, D. Y., Ng, R. W., Feng, H., Wong, Y. C., Cheung, A. L., et al. (2002). Significance of MAD2 expression to mitotic checkpoint control in ovarian cancer cells. *Cancer Res.* 62, 1662–1668. doi: 10.1158/0008-5472.CAN-18-1290

Wang, Y., Ock, S. A., and Chian, R. C. (2006). Effect of gonadotrophin stimulation on mouse oocyte quality and subsequent embryonic development *in vitro*. *Reprod. Biomed. Online* 12, 304–314. doi: 10.1016/S1472-6483(10)61002-4

Webb, R., and Campbell, B. K. (2007). Development of the dominant follicle: mechanisms of selection and maintenance of oocyte quality. *Soc. Reprod. Fertil. Suppl.* 64, 141–163. doi: 10.5661/RDR-VI-141

Williams, C. J. (2002). Signalling mechanisms of mammalian oocyte activation. *Hum. Reprod. Update* 8, 313–321. doi: 10.1093/humupd/8.4.313

Wu, B.-j., Xue, H.-y., Chen, L.-p., Dai, Y.-f., Guo, J.-t., and Li, X.-h. (2013). Effect of PMSG/hCG superovulation on mouse embryonic development. *J. Integr. Agri.* 12, 1066–1072. doi: 10.1016/S2095-3119(13)60485-2

Wu, D., Yu, D., Wang, X., and Yu, B. (2016). F-actin rearrangement is regulated by mTORC2/Akt/Girdin in mouse fertilized eggs. *Cell Prolif.* 49, 740–750. doi: 10.1111/cpr.12285

Wu, Q., Li, H., Zhu, Y., Jiang, W., Lu, J., Wei, D., et al. (2018). Dosage of exogenous gonadotropins is not associated with blastocyst aneuploidy or live-birth rates in PGS cycles in Chinese women. *Hum. Reprod.* 33, 1875–1882. doi: 10.1093/humrep/dey270

Wu, Q., Li, Z., Huang, Y., Qian, D., Chen, M., Xiao, W., et al. (2017). Oxidative stress delays prometaphase/metaphase of the first cleavage in mouse zygotes *via* the MAD2L1-mediated spindle assembly checkpoint. *Oxid. Med. Cell Longev.* 2017:2103190. doi: 10.1155/2017/2103190

Yamada-Fukunaga, T., Yamada, M., Hamatani, T., Chikazawa, N., Ogawa, S., Akutsu, H., et al. (2013). Age-associated telomere shortening in mouse oocytes. *Reprod. Biol. Endocrinol.* 11, 108–108. doi: 10.1186/1477-7827-11-108

Yasui, Y., Urano, T., Kawajiri, A., Nagata, K., Tatsuka, M., Saya, H., et al. (2004). Autophosphorylation of a newly identified site of Aurora-B is indispensable for cytokinesis. *J. Biol. Chem.* 279, 12997–13003. doi: 10.1074/jbc.M311128200

Zamzami, N., Marchetti, P., Castedo, M., Zanin, C., Vayssière, J. L., Petit, P. X., et al. (1995). Reduction in mitochondrial potential constitutes an early irreversible step of programmed lymphocyte death *in vivo*. *J. Exp. Med.* 181, 1661–1672. doi: 10.1084/jem.181.5.1661

Zhang, J., Lin, X., Wu, L., Huang, J.-J., Jiang, W.-Q., Kipps, T. J., et al. (2020). Aurora B induces epithelial-mesenchymal transition by stabilizing Snail1 to promote basal-like breast cancer metastasis. *Oncogene* 39, 2550–2567. doi: 10.1038/s41388-020-1165-z

Zhao, X., Jin, S., Song, Y., and Zhan, Q. (2010). Cdc2/cyclin B1 regulates centrosomal Nlp proteolysis and subcellular localization. *Cancer Biol. Ther.* 10, 945–952. doi: 10.4161/cbt.10.9.13368

Zhou, R., Zhang, Y., Du, G., Han, L., Zheng, S., Liang, J., et al. (2018). Down-regulated let-7b-5p represses glycolysis metabolism by targeting AURKB in asthenozoospermia. *Gene* 663, 83–87. doi: 10.1016/j.gene.2018.04.022

Zolbin, M. M., Nematin, S., Daghigh, F., Namdar, F., Madadian, M., Abbasi, M., et al. (2018). PMSG and HCG hormones effect on the development and growth of ovarian follicles. *J. Contemp. Med. Sci.* 4, 51–54. doi: 10.22317/jcms.03201811

Conflict of Interest: The authors declare that the research was conducted in the absence of any commercial or financial relationships that could be construed as a potential conflict of interest.

frontiers in Cell and Developmental Biology

REVIEW
published: 15 March 2021
doi: 10.3389/fcell.2021.657305

Human MUS81: A Fence-Sitter in Cancer

Sisi Chen[1,2], *Xinwei Geng*[2], *Madiha Zahra Syeda*[2], *Zhengming Huang*[2], *Chao Zhang*[2] *and Songmin Ying*[1,2]*

[1] International Institutes of Medicine, The Fourth Affiliated Hospital of Zhejiang University School of Medicine, Yiwu, China, [2] Key Laboratory of Respiratory Disease of Zhejiang Province, Department of Pharmacology and Department of Respiratory and Critical Care Medicine of the Second Affiliated Hospital, Zhejiang University School of Medicine, Hangzhou, China

MUS81 complex, exhibiting endonuclease activity on specific DNA structures, plays an influential part in DNA repair. Research has proved that MUS81 is dispensable for embryonic development and cell viability in mammals. However, an intricate picture has emerged from studies in which discrepant gene mutations completely alter the role of MUS81 in human cancers. Here, we review the recent understanding of how MUS81 functions in tumors with distinct genetic backgrounds and discuss the potential therapeutic strategies targeting MUS81 in cancer.

Keywords: human MUS81, endonuclease, DNA damage response, cancer therapy, chromosomal instability

OPEN ACCESS

Edited by:
Yunzhou Dong,
Boston Children's Hospital and Harvard Medical School, United States

Reviewed by:
Yanbin Zhang,
University of Miami, United States
Jianjun Wu,
University of Texas Southwestern Medical Center, United States

***Correspondence:**
Songmin Ying
yings@zju.edu.cn

Specialty section:
This article was submitted to Cell Growth and Division, a section of the journal Frontiers in Cell and Developmental Biology

Received: *22 January 2021*
Accepted: *10 February 2021*
Published: *15 March 2021*

Citation:
Chen S, Geng X, Syeda MZ, Huang Z, Zhang C and Ying S (2021) Human MUS81: A Fence-Sitter in Cancer. Front. Cell Dev. Biol. 9:657305. doi: 10.3389/fcell.2021.657305

INTRODUCTION

Mus81 was first identified by its cooperation with the homologous recombination (HR) protein Rad54 in yeast (Boddy et al., 2000; Interthal and Heyer, 2000; Haber and Heyer, 2001), indicating its possible role in DNA repair. Owing to its high evolutionary conservation, human MUS81 was subsequently discovered (Chen et al., 2001). The MUS81 protein possesses a characteristic ERCC4 nuclease domain containing the $VERKX_3D$ motif, which is indispensable for the endonuclease activity (Chen et al., 2001). The abundance of human MUS81 augments unequivocally when cells are exposed to replication stress (Chen et al., 2001). Human MUS81 localizes to damaged DNA sites under replication stress (Gao et al., 2003). MUS81-depleted U2OS cells exhibit elevated level of chromosomal bridges and micronuclei, characteristic features of DNA damage (Ying et al., 2013). MUS81-deficient cells and mice are intolerant to mitomycin C (MMC), an interstrand crosslinking agent, while MUS81 haploinsufficiency results in genomic instability (McPherson et al., 2004). Altogether, mammalian MUS81 is unambiguously a DNA damage repair protein.

DNA damage response (DDR) defects are common occurrences in multiple cancers, manifesting as mutation and inactivation of DDR-relative proteins. In recent findings, it is becoming increasingly evident that MUS81 has close relationships with cancers. Interestingly, MUS81 is helpful for tumor survival in some cases but lethal to them in other cases. For instance, endonuclease activity of MUS81 is crucial for survival of BRCA2-insufficient cancer cells (Lai et al., 2017; Lemaçon et al., 2017). Nevertheless, in WRN-depleted microsatellite instability (MSI) cancer cells, MUS81 complex shatters chromosomes, which causes apoptosis of cancer cells (van Wietmarschen et al., 2020).

Herein, this review focuses on recent understanding of how MUS81 works in distinct cancer cells and discuss why MUS81 causes such different consequences as black and white in tumors.

MECHANISMS OF MUS81 IN DNA REPAIR

Molecular Mechanism of Substrate Recognition and Cleavage by MUS81

Human MUS81 is a substrate selective endonuclease and exhibits a wide range of specificity for replication forks, 3′-flap structures, Holliday junctions (HJs), and D-loops (Chen et al., 2001; Constantinou et al., 2002; Zeng et al., 2009).

The crystal structure of human MUS81–essential meiotic structure-specific endonuclease 1 (MUS81–EME1) combined with 3′ flaps demonstrates the recognition and cleavage mechanism of MUS81 complex (Chang et al., 2008; Gwon et al., 2014). Binding of 3′-flap DNA induces rotation of the helix–hairpin–helix (HhH_2) heterodimer of the MUS81–EME1 complex. The disordered loop of the EME1 linker becomes ordered, which subsequently unmasks the hydrophobic wedge and forms the 5′ end binding pocket of MUS81 (Gwon et al., 2014). The binding pocket accommodates the 5′ nicked end of the 3′ flap DNA, which is pivotal for the substrate specificity (Tsodikov et al., 2005; Chang et al., 2008). HhH2 of EME1 and HhH2 of MUS81 are able to interact with the pre- and the postnick DNA strands, respectively, as a result of the conformational changes (Gwon et al., 2014). The wedge bends the substrate, which put the 3′ end into the ERCC4 site of MUS81 and assists the substrate cleavage (Enzlin and Schärer, 2002; Gwon et al., 2014).

MUS81–EME2 Promotes DNA Replication Completion in S Phase

Replication forks are prone to stall when encountering obstacles during DNA replication (Liao et al., 2018). The recovery of the replication forks is necessary for faithful DNA replication and cell division (Bryant et al., 2009). MUS81–EME2 can cleave reversed replication forks (Amangyeld et al., 2014) and D-loops (Pepe and West, 2014b) and is responsible for the restart of stalled forks in S phase (Gao et al., 2003; Pepe and West, 2014a). When replication forks are stalled in S phase, MUS81–EME2 complex is recruited to cleave the stalled replication forks and induces transient DNA double-strand break (DSB) formation (Gao et al., 2003; Pepe and West, 2014a). The cleavage of MUS81–EME2 restarts the stalled replication forks and promotes replication recovery (Hanada et al., 2007) via break-induced replication (BIR) pathway (Kramara et al., 2018).

MUS81–EME1 Promotes Faithful Chromosome Disjunction in M Phase

MUS81–EME1 Complex Triggers Common Fragile Site Expression

Common fragile sites (CFSs) are difficult-to-replicate foci that preferentially form breaks in chromosomes under replication stress and frequently rearrange in tumor cells (Durkin and Glover, 2007). We revealed that MUS81–EME1 complex promotes expression of CFSs and faithful disjunction of sister chromosomes in human cells (Naim et al., 2013; Ying et al., 2013). Under replication inhibitors, CFSs remain underreplicated at the end of S phase, are prone to form replication intermediates, and then give rise to sister-chromatid bridging in M phase, which contributes to chromosomal instability and oncogenesis (Chan et al., 2009). Nonetheless, MUS81–EME1 complex is phosphorylated and collected to underreplicated CFS loci in early mitosis. RECQ5 dismantles RAD51 from the single-strand DNA (ssDNA), which promotes the cleavage of MUS81–EME1 on stalled replication forks (Di Marco et al., 2017). MUS81–EME1 then cleaves the intertwined DNA strands, manifesting as breaks observed at CFSs (Naim et al., 2013; Ying et al., 2013). Ultimately, we identified that POLD3-dependent DNA synthesis, promoted by MUS81 cleavage, repairs the expressed CFSs and boosts faithful sister chromatid disjunction (Minocherhomji et al., 2015).

SLX–MUS Complex Contributes to Holliday Junction Resolution

HJs are cruciform-shaped chromosome junctions that arise temporarily during HR, and their resolution is critical for chromosomal disjunction and genome maintenance (West, 2009). There are three major HJ-resolving pathways in human cells, one of which involves synthetic lethal of unknown function protein 1 (SLX1)–SLX4–MUS81–EME1 (SLX–MUS) complex, a backup for Bloom syndrome protein (BLM)–TopoisomeraseIIIa–RecQ-mediated genome instability protein 1 (RMI1)–RMI2 (BTRR) pathway (Fekairi et al., 2009; Wyatt et al., 2013; Sarbajna et al., 2014). Cells, lacking SLX–MUS complex-associated proteins, show defective chromosome morphology and reduced survival (Wyatt et al., 2013; Sarbajna et al., 2014). After SLX4 and EME1 are phosphorylated by cyclin-dependent kinase, MUS81–MEM1 and SLX1–SLX4 associate and combine into a stable SLX–MUS complex at the G2/M phase (Wyatt et al., 2013). At that point, SLX–MUS complex triggers bilateral cleavage of intact HJs by a coordinated nicking and counternicking mechanism (Wyatt et al., 2013). Interestingly, MUS81–EME1 cleaves intact HJs inefficiently (Ciccia et al., 2003), and SLX1–SLX4 introduces nicks into intact HJs optionally. However, SLX–MUS complex mobilizes cleavage activity of both SLX1–SLX4 and MUS81–EME1 and exhibits a more orchestrated reaction for efficient HJs resolution (Wyatt et al., 2013).

RELEVANCE BETWEEN MUS81 AND CANCER

Involvement of MUS81 in Tumor Suppression

As defects in DNA damage repair are frequently interrelated with high predisposition to cancer, research has been carried out to demonstrate whether MUS81 suppresses tumors *in vivo*. Mus81-deficient mice are born at expected Mendelian frequencies (McPherson et al., 2004), indicating a non-essential role of MUS81 in murine meiotic recombination and oncogenesis. However, MUS81 deficiency, even MUS81 insufficiency, leads to a dramatic susceptibility to cancers, especially lymphomas in mice through the first year of life (McPherson et al., 2004). These tumors show a high frequency of DNA aneuploid

via cytogenetic analysis (McPherson et al., 2004). Strikingly, concomitant deficiency of MUS81 and P53 leads to an extremely high frequency in sarcoma development in mice, indicating the collaboration of MUS81 and P53 in tumor suppression (Pamidi et al., 2007). There is, however, a different voice suggesting that murine MUS81 is unnecessary for tumor suppression, based on evidence that no increased sign of tumors was detected in MUS81-deficient mice during a 15-month monitoring (Dendouga et al., 2005). The reason for the discrepant performance of murine MUS81 in tumor predisposition is still unclear. Thus, determining the role of MUS81 in tumor suppression requires further studies. Nonetheless, a growing number of evidence prove that MUS81 plays a dominant role in some specific gene-mutated cancer cells.

MUS81 Is Essential in BRCA2-Deficient Cancer Cells

Inheritance of *BRCA2* mutations is responsible for predisposing humans to breast cancer (Ford et al., 1998). Primary human cells with *BRCA2* deletion accumulate spontaneous DNA damage and go toward senescence and apoptosis (Carlos et al., 2013). Mice with homozygous *BRCA2* mutation show embryonic lethality (Jonkers et al., 2001). However, BRCA2-deficient cancer cells can survive in virtue of high tolerance of endogenous DNA damage (Pardo et al., 2020). Dual loss of BRCA2 and MUS81 results in obvious cancer cell death (Lai et al., 2017), indicating a pivotal role of MUS81 in *BRCA2*-mutated cancer cells (**Figure 1A**). Replication forks stall when they encounter DNA lesions upon drug treatment, and RAD51 promotes reversed fork formation (Zellweger et al., 2015; Lemaçon et al., 2017). Subsequently, BRCA2 is recruited to protect the regressed arms of nascent DNA strands at stalled forks by stabilizing RAD51 filaments from nucleolytic degradation (Schlacher et al., 2011; Lemaçon et al., 2017; Mijic et al., 2017). In the lack of BRCA2, MRE11, initiated by CtIP, targets unprotected reversed forks and starts fork resection by its endonuclease activity (Lemaçon et al., 2017). MRE11 resection leads to the ssDNA flap formation in reversed forks (Lemaçon et al., 2017). MUS81 cleaves these resected regressed forks and leads to transient DSB accumulation (Lemaçon et al., 2017). Finally, POLD3-dependent DNA synthesis repairs DSBs and restarts the MUS81-cleaved forks (Lemaçon et al., 2017). Conversely, in cancer cells with dual loss of BRCA2 and MUS81, resected forks cannot be restarted, which is supported by the observation that frequency of reversed forks with ssDNA is increased dramatically (Lemaçon et al., 2017).

Given that BRCA2 is best known for its function in HR repair, whether the synthetic lethality between MUS81 and BRCA2 can be stretched to other proteins involved in HR pathway, like BRCA1, was further explored. Surprisingly, BRCA1, RAD51, or RAD51C depletion, unlike BRCA2 depletion, cannot lead to synthetic lethality upon concomitant loss of MUS81 in cancer cells (Lai et al., 2017). BRCA1 functions upstream of BRCA2 in a common HR pathway (Roy et al., 2011) and is capable of protecting the reversed forks as BRCA2 does (Lemaçon et al., 2017). Nevertheless, MUS81 and POLD3 foci do not accumulate in BRCA1-insufficient cancer cells (Lemaçon et al., 2017). It would be interesting to uncover the mechanism by which MUS81 insufficiency leads to such different phenotypes between BRCA1- and BRCA2-deficient cancer cells (**Figure 1**).

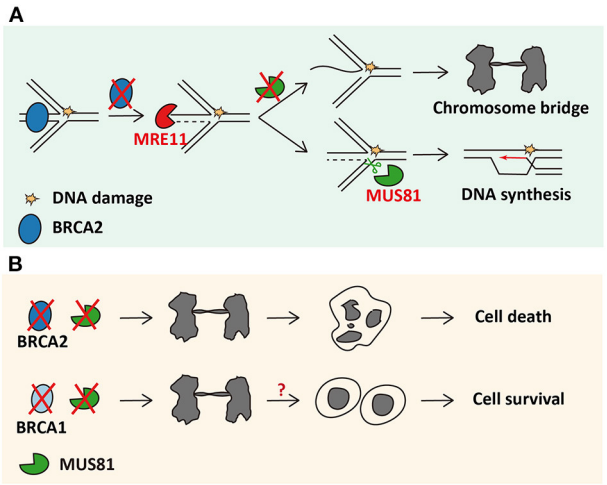

FIGURE 1 | MUS81 sustains survival of BRCA2-deficient cancer cells through rescuing reversed forks. **(A)** The mechanism of MUS81 resolving chromosomal interlinks in cells lacking BRCA2. **(B)** MUS81 is dispensable in BRCA1-deficient cells.

MUS81 Induces Chromosome Shattering in WRN-Deficient MSI Cancer Cells

MSI is characterized by a hypermutable state of nucleotide repeat regions, which is promoted by defects in DNA mismatch repair (MMR) (Kim et al., 2013). MSI facilitates occurrence of multiple cancers (Pal et al., 2008; Kim et al., 2013). Considering the vulnerabilities of MSI, WRN is identified as an essential gene in MSI cells (Chan et al., 2019). WRN depletion causes DSBs and chromosome shattering (van Wietmarschen et al., 2020) and reduces the cell viability (Chan et al., 2019) in MSI cells but neither in microsatellite stable (MSS) cancer cells nor in primary human cells. However, MUS81 exhaustion before WRN depletion notably cuts down the chromosome shattering and DSBs formation at TA repeats (van Wietmarschen et al., 2020), indicating that MUS81 cleavage contributes to apoptosis of MSI cells with WRN deficiency (**Figure 2**).

In MSI cells, TA repeats, which are highly unstable, encounter and accumulate large-scale expansions for some reason (van Wietmarschen et al., 2020). Cruciform structures form at the expanded TA repeats (Inagaki et al., 2009), which are tended to stall replication forks. WRN is then recruited and unwinds the secondary structures in virtue of its helicase activity rather than its exonuclease activity, which allows restart of the stalled replication forks (Chan et al., 2019), whereas, in the absence of WRN, cruciform structures of TA repeats cannot be unfolded. Instead, MUS81–EME1 cleaves the cruciform structures and causes DSBs. Interestingly, the cleavage sites are exactly adjacent to the border of expanded TA repeats (van Wietmarschen et al.,

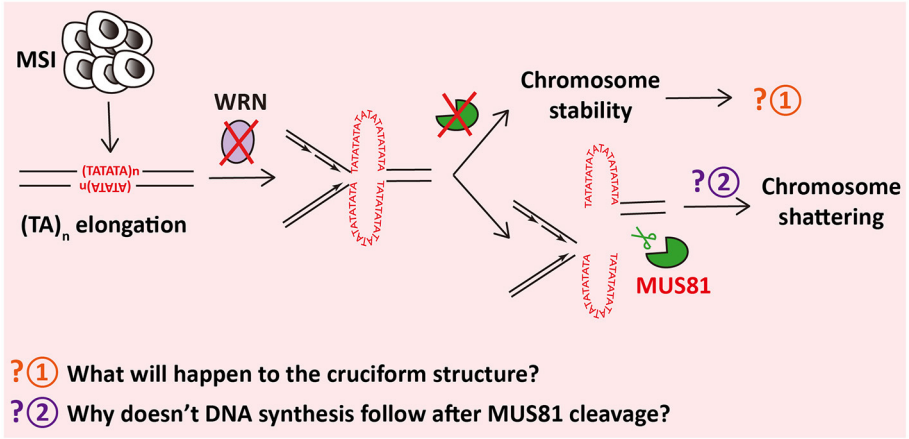

FIGURE 2 | MUS81 shatters chromosomes in WRN-insufficient microsatellite instability (MSI) cells by cleaving $(TA)_n$-formed cruciform structures.

2020). Furthermore, cleavage of MUS81 and accumulation of DSBs lead to massive chromosome shattering. Finally, WRN-deficient MSI cells ends in cell cycle arrest and apoptosis (van Wietmarschen et al., 2020).

A question, which remains to be answered, will be of considerable interest. Why does MUS81 cleavage in TA repeats lead to chromosome shattering rather than triggering POLD3-dependent DNA synthesis for DNA repair? It has been found that these TA repeats cannot be amplified *in vitro* and have extremely low sequencing depth (van Wietmarschen et al., 2020), indicating that secondary structures formed at TA repeats might restrain polymerase extension and inhibit DNA synthesis.

DISCUSSION

DDR pathways play crucial roles in genomic stability, and compromised DDR pathways are common in multiple tumors. Recent studies have unveiled the link between DDR deficiency and innate/adaptive immunity against tumor cells (Barber, 2015; Reisländer et al., 2020). Cyclic GMP–AMP synthase (cGAS) detects the cytosolic DNA caused by DDR deficiency in cancers and activates stimulator of interferon genes (STING), which triggers interferons (IFNs) signaling and antitumor immunity (Chen et al., 2016). DNA mismatch repair (MMR) inactivation-induced neoantigens in cancers boost adaptive immunity as well, which is independent of the cGAS–STING pathway (Germano et al., 2017). Therefore, targeting DDR pathways holds therapeutic potential against cancers.

DDR-directed therapies have been introduced in clinical trials recently (Pilié et al., 2019). However, chromosomal instability (CIN) is the dominant drawback of this strategy, which conversely underpins evolution and growth of tumor cells (Bakhoum and Cantley, 2018; Calzetta et al., 2020).Thus, knowledge of the interactions among multiple DDR pathways and understanding the discrepant functions of DDR-relevant proteins in various cancers contribute to efficient cancer therapy and needs to be further elucidated.

As this review demonstrates, human MUS81 is closely related to cancers but results in totally different fates of cancers bearing distinct mutated genes, indicating that the interactions between MUS81 and other DDR proteins master the cancer cell fate and MUS81 is a potential and intriguing target in specific cancer therapies. A further understanding of the precise mechanisms of MUS81 and the interactions among DDR pathways in discrepant cancers may pave the way toward improved cancer therapeutic strategies.

AUTHOR CONTRIBUTIONS

SC wrote the manuscript. XG, MS, ZH, CZ, and SY provided guidance and supervised the final version of the manuscript. All authors contributed to the article and approved the submitted version.

FUNDING

This work was funded by the Ministry of Science and Technology of the People's Republic of China (2016YFA0100301), the Natural Science Foundation of China (81870007, 81920108001), the Zhejiang Provincial Natural Science Foundation (LD19H160001), and the Zhejiang Provincial Program for the Cultivation of High-Level Innovative Health Talents (2016-63).

REFERENCES

Amangyeld, T., Shin, Y. K., Lee, M., Kwon, B., and Seo, Y. S. (2014). Human MUS81-EME2 can cleave a variety of DNA structures including intact Holliday junction and nicked duplex. *Nucleic Acids Res.* 42, 5846–5862. doi: 10.1093/nar/gku237

Bakhoum, S. F., and Cantley, L. C. (2018). The multifaceted role of chromosomal instability in cancer and its microenvironment. *Cell* 174, 1347–1360. doi: 10.1016/j.cell.2018.08.027

Barber, G. N. (2015). STING: infection, inflammation, and cancer. *Nat. Rev. Immunol.* 15, 760–770. doi: 10.1038/nri3921

Boddy, M. N., Lopez Girona, A., Shanahan, P., Interthal, H., Heyer, W. D., and Russell, P. (2000). Damage tolerance protein Mus81 associates with the FHA1 domain of checkpoint kinase Cds1. *Mol. Cell. Biol.* 20, 8758–8766. doi: 10.1128/MCB.20.23.8758-8766.2000

Bryant, H. E., Petermann, E., Schultz, N., Jemth, A. S., Loseva, O., Issaeva, N., et al. (2009). PARP is activated at stalled forks to mediate Mre11-dependent replication restart and recombination. *EMBO J.* 28, 2601–2615. doi: 10.1038/emboj.2009.206

Calzetta, N. L., Besteiro, M. A. G., and Gottifredi, V. (2020). Mus81-Eme1-dependent aberrant processing of DNA replication intermediates in mitosis impairs genome integrity. *Sci. Adv.* 6:eabc8257. doi: 10.1126/sciadv.abc8257

Carlos, A. R., Escandell, J. M., Kotsantis, P., Suwaki, N., Bouwman, P., Badie, S., et al. (2013). ARF triggers senescence in Brca2-deficient cells by altering the spectrum of p53 transcriptional targets. *Nat. Commun.* 4:2697. doi: 10.1038/ncomms3697

Chan, E. M., Shibue, T., McFarland, J. M., Gaeta, B., Ghandi, M., Dumont, N., et al. (2019). WRN helicase is a synthetic lethal target in microsatellite unstable cancers. *Nature* 568, 551–556. doi: 10.1038/s41586-019-1102-x

Chan, K. L., Palmai Pallag, T., Ying, S., and Hickson, I. D. (2009). Replication stress induces sister-chromatid bridging at fragile site loci in mitosis. *Nat. Cell Biol.* 11, 753–760. doi: 10.1038/ncb1882

Chang, J. H., Kim, J. J., Choi, J. M., Lee, J. H., and Cho, Y. (2008). Crystal structure of the Mus81-Eme1 complex. *Genes Dev.* 22, 1093–1106. doi: 10.1101/gad.1618708

Chen, Q., Sun, L., and Chen, Z. J. (2016). Regulation and function of the cGAS-STING pathway of cytosolic DNA sensing. *Nat. Immunol.* 17, 1142–1149. doi: 10.1038/ni.3558

Chen, X. B., Melchionna, R., Denis, C. M., Gaillard, P. H. L., Blasina, A., Van de Weyer, I., et al. (2001). Human Mus81-associated endonuclease cleaves Holliday junctions *in vitro*. *Mol. Cell* 8, 1117–1127. doi: 10.1016/S1097-2765(01)00375-6

Ciccia, A., Constantinou, A., and West, S. C. (2003). Identification and characterization of the human mus81-eme1 endonuclease. *J. Biol. Chem.* 278, 25172–25178. doi: 10.1074/jbc.M302882200

Constantinou, A., Chen, X. B., McGowan, C. H., and West, S. C. (2002). Holliday junction resolution in human cells: two junction endonucleases with distinct substrate specificities. *EMBO J.* 21, 5577–5585. doi: 10.1093/emboj/cdf554

Dendouga, N., Gao, H., Moechars, D., Janicot, M., Vialard, J., and McGowan, C. H. (2005). Disruption of murine Mus81 increases genomic instability and DNA damage sensitivity but does not promote tumorigenesis. *Mol. Cell. Biol.* 25, 7569–7579. doi: 10.1128/MCB.25.17.7569-7579.2005

Di Marco, S., Hasanova, Z., Kanagaraj, R., Chappidi, N., Altmannova, V., Menon, S., et al. (2017). RECQ5 helicase cooperates with MUS81 endonuclease in processing stalled replication forks at common fragile sites during mitosis. *Mol. Cell* 66, 658–671. doi: 10.1016/j.molcel.2017.05.006

Durkin, S. G., and Glover, T. W. (2007). Chromosome fragile sites. *Annu. Rev. Genet.* 41, 169–192. doi: 10.1146/annurev.genet.41.042007.165900

Enzlin, J. H., and Schärer, O. D. (2002). The active site of the DNA repair endonuclease XPF-ERCC1 forms a highly conserved nuclease motif. *EMBO J.* 21, 2045–2053. doi: 10.1093/emboj/21.8.2045

Fekairi, S., Scaglione, S., Chahwan, C., Taylor, E. R., Tissier, A., Coulon, S., et al. (2009). Human SLX4 is a Holliday junction resolvase subunit that binds multiple DNA repair/recombination endonucleases. *Cell* 138, 78–89. doi: 10.1016/j.cell.2009.06.029

Ford, D., Easton, D. F., Stratton, M., Narod, S., Goldgar, D., Devilee, P., et al. (1998). Genetic heterogeneity and penetrance analysis of the BRCA1 and BRCA2 genes in breast cancer families. The breast cancer linkage consortium. *Am. J. Hum. Genet.* 62, 676–689. doi: 10.1086/301749

Gao, H., Chen, X. B., and McGowan, C. H. (2003). Mus81 endonuclease localizes to nucleoli and to regions of DNA damage in human S-phase cells. *Mol. Biol. Cell* 14, 4826–4834. doi: 10.1091/mbc.e03-05-0276

Germano, G., Lamba, S., Rospo, G., Barault, L., Magrì, A., Maione, F., et al. (2017). Inactivation of DNA repair triggers neoantigen generation and impairs tumour growth. *Nature* 552, 116–120. doi: 10.1038/nature24673

Gwon, G. H., Jo, A., Baek, K., Jin, K. S., Fu, Y., Lee, J.-B., et al. (2014). Crystal structures of the structure-selective nuclease Mus81-Eme1 bound to flap DNA substrates. *EMBO J.* 33, 1061–1072. doi: 10.1002/embj.201487820

Haber, J. E., and Heyer, W. D. (2001). The fuss about Mus81. *Cell* 107, 551–554. doi: 10.1016/S0092-8674(01)00593-1

Hanada, K., Budzowska, M., Davies, S. L., van Drunen, E., Onizawa, H., Beverloo, H. B., et al. (2007). The structure-specific endonuclease Mus81 contributes to replication restart by generating double-strand DNA breaks. *Nat. Struct. Mol. Biol.* 14, 1096–1104. doi: 10.1038/nsmb1313

Inagaki, H., Ohye, T., Kogo, H., Kato, T., Bolor, H., Taniguchi, M., et al. (2009). Chromosomal instability mediated by non-B DNA: cruciform conformation and not DNA sequence is responsible for recurrent translocation in humans. *Genome Res.* 19, 191–198. doi: 10.1101/gr.079244.108

Interthal, H., and Heyer, W. D. (2000). MUS81 encodes a novel helix-hairpin-helix protein involved in the response to UV- and methylation-induced DNA damage in Saccharomyces cerevisiae. *Mol. Gen. Genet.* 263, 812–827. doi: 10.1007/s004380000241

Jonkers, J., Meuwissen, R., van der Gulden, H., Peterse, H., van der Valk, M., and Berns, A. (2001). Synergistic tumor suppressor activity of BRCA2 and p53 in a conditional mouse model for breast cancer. *Nat. Genet.* 29, 418–425. doi: 10.1038/ng747

Kim, T. M., Laird, P. W., and Park, P. J. (2013). The landscape of microsatellite instability in colorectal and endometrial cancer genomes. *Cell* 155, 858–868. doi: 10.1016/j.cell.2013.10.015

Kramara, J., Osia, B., and Malkova, A. (2018). Break-induced replication: the where, the why, and the how. *Trends Genet.* 34, 518–531. doi: 10.1016/j.tig.2018.04.002

Lai, X., Broderick, R., Bergoglio, V., Zimmer, J., Badie, S., Niedzwiedz, W., et al. (2017). MUS81 nuclease activity is essential for replication stress tolerance and chromosome segregation in BRCA2-deficient cells. *Nat. Commun.* 8:15983. doi: 10.1038/ncomms16171

Lemaçon, D., Jackson, J., Quinet, A., Brickner, J. R., Li, S., Yazinski, S., et al. (2017). MRE11 and EXO1 nucleases degrade reversed forks and elicit MUS81-dependent fork rescue in BRCA2-deficient cells. *Nat. Commun.* 8:860. doi: 10.1038/s41467-017-01180-5

Liao, H., Ji, F., Helleday, T., and Ying, S. (2018). Mechanisms for stalled replication fork stabilization: new targets for synthetic lethality strategies in cancer treatments. *EMBO Rep.* 19:e46263. doi: 10.15252/embr.201846263

McPherson, J. P., Lemmers, B., Chahwan, R., Pamidi, A., Migon, E., Matysiak Zablocki, E., et al. (2004). Involvement of mammalian Mus81 in genome integrity and tumor suppression. *Science (N. Y.)* 304, 1822–1826. doi: 10.1126/science.1094557

Mijic, S., Zellweger, R., Chappidi, N., Berti, M., Jacobs, K., Mutreja, K., et al. (2017). Replication fork reversal triggers fork degradation in BRCA2-defective cells. *Nat. Commun.* 8:859. doi: 10.1038/s41467-017-01164-5

Minocherhomji, S., Ying, S., Bjerregaard, V. A., Bursomanno, S., Aleliunaite, A., Wu, W., et al. (2015). Replication stress activates DNA repair synthesis in mitosis. *Nature* 528, 286–290. doi: 10.1038/nature16139

Naim, V., Wilhelm, T., Debatisse, M., and Rosselli, F. (2013). ERCC1 and MUS81-EME1 promote sister chromatid separation by processing late replication intermediates at common fragile sites during mitosis. *Nat. Cell Biol.* 15, 1008–1015. doi: 10.1038/ncb2793

Pal, T., Permuth Wey, J., Kumar, A., and Sellers, T. A. (2008). Systematic review and meta-analysis of ovarian cancers: estimation of microsatellite-high frequency and characterization of mismatch repair deficient tumor histology. *Clin. Cancer Res. Off. J. Am. Assoc. Cancer Res.* 14, 6847–6854. doi: 10.1158/1078-0432.CCR-08-1387

Pamidi, A., Cardoso, R., Hakem, A., Matysiak Zablocki, E., Poonepalli, A., Tamblyn, L., et al. (2007). Functional interplay of p53 and Mus81

in DNA damage responses and cancer. *Cancer Res.* 67, 8527–8535. doi: 10.1158/0008-5472.CAN-07-1161

Pardo, B., Moriel-Carretero, M., Vicat, T., Aguilera, A., and Pasero, P. (2020). Homologous recombination and Mus81 promote replication completion in response to replication fork blockage. *EMBO Rep.* 21:e49367. doi: 10.15252/embr.201949367

Pepe, A., and West, S. C. (2014a). MUS81-EME2 promotes replication fork restart. *Cell Rep.* 7, 1048–1055. doi: 10.1016/j.celrep.2014.04.007

Pepe, A., and West, S. C. (2014b). Substrate specificity of the MUS81-EME2 structure selective endonuclease. *Nucleic Acids Res.* 42, 3833–3845. doi: 10.1093/nar/gkt1333

Pilié, P. G., Tang, C., Mills, G. B., and Yap, T. A. (2019). State-of-the-art strategies for targeting the DNA damage response in cancer. *Nat. Rev. Clin. Oncol.* 16, 81–104. doi: 10.1038/s41571-018-0114-z

Reisländer, T., Groelly, F. J., and Tarsounas, M. (2020). DNA Damage and Cancer Immunotherapy: a STING in the Tale. *Mol. Cell* 80, 21–28. doi: 10.1016/j.molcel.2020.07.026

Roy, R., Chun, J., and Powell, S. N. (2011). BRCA1 and BRCA2: different roles in a common pathway of genome protection. *Nat. Rev. Cancer* 12, 68–78. doi: 10.1038/nrc3181

Sarbajna, S., Davies, D., and West, S. C. (2014). Roles of SLX1-SLX4, MUS81-EME1, and GEN1 in avoiding genome instability and mitotic catastrophe. *Genes Dev.* 28, 1124–1136. doi: 10.1101/gad.238303.114

Schlacher, K., Christ, N., Siaud, N., Egashira, A., Wu, H., and Jasin, M. (2011). Double-strand break repair-independent role for BRCA2 in blocking stalled replication fork degradation by MRE11. *Cell* 145, 529–542. doi: 10.1016/j.cell.2011.03.041

Tsodikov, O. V., Enzlin, J. H., Schärer, O. D., and Ellenberger, T. (2005). Crystal structure and DNA binding functions of ERCC1, a subunit of the DNA structure-specific endonuclease XPF-ERCC1. *Proc. Natl. Acad. Sci. U.S.A.* 102, 11236–11241. doi: 10.1073/pnas.0504341102

van Wietmarschen, N., Sridharan, S., Nathan, W. J., Tubbs, A., Chan, E. M., Callen, E., et al. (2020). Repeat expansions confer WRN dependence in microsatellite-unstable cancers. *Nature* 586, 292–298. doi: 10.1038/s41586-020-2769-8

West, S. C. (2009). The search for a human Holliday junction resolvase. *Biochem. Soc. Trans.* 37, 519–526. doi: 10.1042/BST0370519

Wyatt, H. D. M., Sarbajna, S., Matos, J., and West, S. C. (2013). Coordinated actions of SLX1-SLX4 and MUS81-EME1 for Holliday junction resolution in human cells. *Mol. Cell* 52, 234–247. doi: 10.1016/j.molcel.2013.08.035

Ying, S., Minocherhomji, S., Chan, K. L., Palmai Pallag, T., Chu, W. K., Wass, T., et al. (2013). MUS81 promotes common fragile site expression. *Nat. Cell Biol.* 15, 1001–1007. doi: 10.1038/ncb2773

Zellweger, R., Dalcher, D., Mutreja, K., Berti, M., Schmid, J. A., Herrador, R., et al. (2015). Rad51-mediated replication fork reversal is a global response to genotoxic treatments in human cells. *J. Cell Biol.* 208, 563–579. doi: 10.1083/jcb.201406099

Zeng, S., Xiang, T., Pandita, T. K., Gonzalez Suarez, I., Gonzalo, S., Harris, C. C., et al. (2009). Telomere recombination requires the MUS81 endonuclease. *Nat. Cell Biol.* 11, 616–623. doi: 10.1038/ncb1867

Conflict of Interest: The authors declare that the research was conducted in the absence of any commercial or financial relationships that could be construed as a potential conflict of interest.

frontiers in Cell and Developmental Biology

ORIGINAL RESEARCH
published: 16 March 2021
doi: 10.3389/fcell.2021.637064

Blocking DNA Damage Repair May Be Involved in Stattic (STAT3 Inhibitor)-Induced FLT3-ITD AML Cell Apoptosis

Yuxuan Luo[1,2†], Ying Lu[2,3†], Bing Long[2,4], Yansi Lin[5], Yanling Yang[2], Yichuang Xu[2], Xiangzhong Zhang[2,4] and Jingwen Zhang[2,4*]*

[1] Department of Pediatric, Guangzhou Women and Children's Medical Center, Guangzhou, China, [2] Department of Hematology, Third Affiliated Hospital of Sun Yat-sen University, Guangzhou, China, [3] Department of Blood Transfusion, Third Affiliated Hospital of Sun Yat-sen University, Guangzhou, China, [4] Sen Yat-sen Institute of Hematology, Guangzhou, China, [5] Department of General Medicine, Sun Yat-sen Memorial Hospital, Sun Yat-sen University, Guangzhou, China

OPEN ACCESS

Edited by:
Yunzhou Dong,
Boston Children's Hospital and Harvard Medical School, United States

Reviewed by:
Fan Jiang,
Shandong University, China
Hasan Rajabi,
Dana–Farber Cancer Institute, United States
Xiaolei Li,
The First Affiliated Hospital of Nanchang University, China

***Correspondence:**
Xiangzhong Zhang
zhxzhong@mail.sysu.edu.cn
Jingwen Zhang
linlin_jw@163.com

[†]These authors have contributed equally to this work

Specialty section:
This article was submitted to Cell Growth and Division, a section of the journal Frontiers in Cell and Developmental Biology

Received: 02 December 2020
Accepted: 23 February 2021
Published: 16 March 2021

Citation:
Luo Y, Lu Y, Long B, Lin Y, Yang Y, Xu Y, Zhang X and Zhang J (2021) Blocking DNA Damage Repair May Be Involved in Stattic (STAT3 Inhibitor)-Induced FLT3-ITD AML Cell Apoptosis. Front. Cell Dev. Biol. 9:637064. doi: 10.3389/fcell.2021.637064

The FMS-like tyrosine kinase 3 (FLT3)- internal tandem duplication (ITD) mutation can be found in approximately 25% of all acute myeloid leukemia (AML) cases and is associated with a poor prognosis. The main treatment for FLT3-ITD-positive AML patients includes genotoxic therapy and FLT3 inhibitors, which are rarely curative. Inhibiting STAT3 activity can improve the sensitivity of solid tumor cells to radiotherapy and chemotherapy. This study aimed to explore whether Stattic (a STAT3 inhibitor) affects FLT3-ITD AML cells and the underlying mechanism. Stattic can inhibit the proliferation, promote apoptosis, arrest cell cycle at G0/G1, and suppress DNA damage repair in MV4-11cells. During the process, through mRNA sequencing, we found that DNA damage repair-related mRNA are also altered during the process. In summary, the mechanism by which Stattic induces apoptosis in MV4-11cells may involve blocking DNA damage repair machineries.

Keywords: FLT3-ITD mutation, acute myeloid leukemia, DNA damage repair, apoptosis, STAT3

INTRODUCTION

FMS-like tyrosine kinase 3 (FLT3) mutations include the FLT3-internal tandem duplication (ITD) mutation (approximately 25% of all AML cases) and FLT3-tyrosine kinase domain mutation (approximately 7–10% of all AML cases). FLT3-ITD is a common driver mutation that presents a high leukemic burden and is associated with a poor prognosis in patients with AML (Daver et al., 2019). The FLT3-ITD mutation is the insertion of a repetitive segment of the gene encoding the membrane region of the FLT3 receptor. Its length varies from 3 to >400 base pairs, and the number of inserted bases is usually a multiple of three (Levis and Small, 2003). The MV4-11 cell line is a FLT3-ITD mutant leukemia cell line which is often used in research related to FLT3-ITD AML (Quentmeier et al., 2003).

Genome instability is one of the mechanisms of drug resistance. Previous studies have found that in FLT3-ITD AML cells, there is high spontaneous DNA damage and both the micro-homology-mediated alternative non-homologous end-joining (Alt-NHEJ) and homologous recombination (HR) pathways are active (Fan et al., 2010). Alt-NHEJ is error-prone and leads to gene mutations.

Although the HR pathway has high accuracy, it often leads to loss of heterozygosity (LOH). Clinically, patients with FLT3-ITD mutation recurrence often have new cytogenetic and molecular abnormalities and a higher FLT3-ITD/FLT3-wild-type (FLT3-WT) ratio (Stirewalt et al., 2014).

Radiotherapy and most chemotherapies induce apoptosis by causing DNA double-strand breaks (DSBs) in tumor cells. DNA damage repair (DDR) is initiated after the cell is genetically damaged. If DDR is not activated, the cell undergoes apoptosis (Takagi, 2017). Radiotherapy or chemotherapy resistance is related to the activity of DDR (Huang and Zhou, 2020). Inhibiting the repair of DNA damage in tumor cells is crucial for solving the drug resistance of tumor cells (Goldstein and Kastan, 2015).

Signal transducer and activator of transcription 3 (STAT3) is a vital regulatory factor of signal transduction and transcriptional activation and is essential for the proliferation, differentiation, and apoptosis of cells (Wang et al., 2018). In normal cells, the activation of STAT3 is rapid and transient; however, numerous studies have confirmed that the abnormal activation of STAT3 is involved in the development of tumors. In leukemia cells, abnormal expression and activation of STAT3 always occur, which accelerate proliferation, block differentiation, and inhibit apoptosis by inducing anti-apoptotic gene expression (Redell et al., 2011; Arora et al., 2018). A previous study found that the stimulation of FLT3-ITD AML cells (MV4-11) elevates p-STAT3 levels, which upregulates the expression of anti-apoptotic genes, thereby protecting AML cells from apoptosis (Zhou et al., 2009; Shi et al., 2018).

STAT3 is also related to the DDR process. Inhibiting its expression can increase the degree of DNA damage induced by radiation in tumor cells and promote apoptosis of tumor cells. Radiotherapy and chemotherapy promote apoptosis by causing DSBs (Takagi, 2017). For example, VP-16 (etoposide) is a traditional antitumor drug that acts on DNA topoisomerase II and promotes tumor cell apoptosis by inducing DSBs. However, many tumors are resistant to radiotherapy or chemotherapy because of active DDR pathways (Begg et al., 2011). STAT3 inhibitors can improve the sensitivity to radiotherapy and chemotherapy in solid tumors such as glioma (Han et al., 2016), esophageal cancer (Zhang et al., 2015), head and neck tumors (Adachi et al., 2012; Pan et al., 2013). Similarly, the decreased activity of STAT3 in mouse fibroblasts hindered the cell's ability to repair DSBs induced by reactive oxygen species (ROS) (Barry et al., 2010). This suggests that STAT3 is a key factor in DDR.

Stattic is a selective STAT3 inhibitor, which inhibits the function of the STAT3 SH2 domain without affecting STAT1 (Schust et al., 2006). In this study, we used Stattic to inhibit the activity of STAT3, explore its effect on DDR in FLT3-ITD AML cells, and find possible ways to harness this effect.

MATERIALS AND METHODS

Cell Lines and Reagents

Human AML cells HL60 and KG1a were obtained from the Guangzhou Institute of Biomedicine and Health, Chinese Academy of Sciences. Human AML cells MV4-11were obtained from the Shanghai Institutes of Biochemistry and Cell Biology, Chinese Academy of Sciences. All cell lines used in this examination were free of mycoplasma infection. Stattic was purchased from CAYMAN CHEMICAL COMPANY and dissolved in DMSO. VP16 was purchased from Sigma (United States) and diluted with DMSO.

Antibodies

Annexin-V-PI antibody was purchased from BD (United States). The γ-H2AX antibody was purchased from BioLegend (United States). Western blotting-related antibodies GPADH, Phospho-Stat3 (Tyr705), Anti-rabbit IgG, HRP-linked Antibody were purchased from CST (United States).

Flow Cytometry

Cells in the logarithmic growth phase were collected at a density of 1×10^6 per well, washed twice with 2% FBS solution, blocked by Fc (Fc: 2% FBS = 1:100), and placed on ice for 10–15 min. Next, the antibodies (1:200) were added, and the cells were incubated for another 15 min in the dark. Moreover, the blank tube and single stain tubes were set. In the end, the fluorescence intensity was detected using BD Bioscience C6 flow cytometry and analyzed with Flowjo software.

Cell Viability Assay

Cells were seeded at a density of 2.5×10^5 to 5×10^5 cells per mL and incubated in the presence or absence of Stattic for the indicated times. Cell viability was measured using the CCK8 assay kit according to the manufacturer's instructions (DOJINDO, Japan). Cell line experiments were repeated three times. Data were analyzed using the GraphPad Prism software.

DNA Sequencing

DNA was extracted using the Magen Hipure Tissue DNA Micro Kit (China) according to the manufacturer's instructions. DNA sequencing was performed by Sangon Biotech according to their established protocol, using the following primer sequences: (5′–3′): Flt3: forward GCA ATT TAG GTA TGA AAG CCA GC reverse CTT TCA GCA TTT TGA CGG CAA CC. Data were analyzed using the SnapGene software.

Western Blotting

Cells were lysed for 30 min in an ice-cold buffer containing RIPA lysate (approximately 5×10^5 cells/ml), PMSF (1:100), leupetin (1:1,000), and $NaVO_3$ (5:1,000), and the supernatant was collected. Subsequently, the OD value was obtained and the samples were prepared. Samples were electrophoresed at room temperature for 90 min and transferred on ice for 100 min; the required internal reference protein and target protein band were blocked at room temperature for 30 min to 1 h after being cut. Next, the samples were placed in TBST buffer with primary antibody overnight at 4°C followed by incubation with secondary antibody for 2 h and the addition of ECL solution. Finally, the samples were visualized using Image J software.

qRT-PCR

RNA was extracted by using the TAKARA RNA extraction kit (Japan); purity and concentration were determined; reverse transcription reaction was performed using the TAKARA reverse transcription kit and the TAKARA kit for polymerase chain reaction. Finally, data analysis was performed using GAPDH as the baseline and the $2^{-\Delta\Delta}$ct value analysis. Primer sequences were as follows (5′–3′): STAT3: forward ACCAGCA GTATAGCCGCTTC reverse GCCACAATCCGGGCAATCTG APDH: forward ACCACAGTCCATGCCATCAC reverse TCC ACCACCCTGTTGCTGTA.

RNA Sequencing Analysis

MV4-11 cells were treated with DMSO (control), Stattic (2.5 μM), or Stattic (2.5 μM) + VP16 (4 μg/ml) for 4.5 h. The experiment was repeated thrice. Transcriptome sequencing was conducted by OE Biotech Co., Ltd. (Shanghai, China) according to their established protocol. Briefly, total RNA was extracted from the sample; DNA was digested with DNase; and the eukaryotic mRNA was enriched with magnetic beads with Oligo (dT). Interruption reagents were added to obtain short fragments of mRNA. Using the interrupted mRNA as a template, a six-base random primer was used to synthesize the first-strand cDNA, and then the second-strand formation reaction system was prepared to synthesize the second-strand cDNA, and the double-stranded cDNA was purified using the Stranded cDNA kit. The purified double-stranded cDNA was subjected to end repair, a tail was added, the sequencing adapter was connected, the fragment size was selected, and finally, PCR amplification was performed. Agilent 2100 Bioanalyzer was used to control the quality of the constructed library. Illumina sequencer was then used for sequencing.

Image Processing and Statistical Analysis

Images were processed using Adobe Illustrator and GraphPad Prism. All data are expressed as means ± *SD*. All data were analyzed using SPSS Statistics 16.0 or GraphPad Prism software. One-way ANOVA was used for comparisons among groups and LSD-test was used for comparisons between two groups. The values were considered significant at $^{*}p < 0.05$, $^{**}p < 0.01$, $^{***}p < 0.001$, and $^{****}p < 0.0001$.

RESULTS

Confirmation of FLT3 Gene Sequence in Cell Lines

The MV4-11 cell line is often used in the study of FLT3-ITD mutant AML. First, DNA sequencing was used to confirm the sequences of the FLT3 gene in the MV4-11, KG1a, and HL60 cell lines. The results showed that the FLT3 sequences of KG1a and HL60 cell lines were consistent with those of the wild-type, whereas FLT3 of MV4-11 cells had an inserted 30 base pair sequence (**Figure 1**). This confirmed the presence of the FLT3-ITD mutation in the MV4-11 cell line and that of FLT3-WT in the KG1a and HL60 cell lines.

STAT3 Expression in MV4-11 and FLT3-WT Cell Lines and Inhibition of STAT3-pi by Stattic

The expression of STAT3 mRNA levels in MV4-11 and FLT3-WT cell lines detected by qRT-PCR is shown in **Figure 2A**. The expression of STAT3 in MV4-11 cell line was higher than that in HL60 and KG1a cell lines.

Stattic is a selective STAT3 inhibitor, which inhibits the expression of STAT3-pi. MV4-11 cells were treated with DMSO (as control) or increasing concentrations of Stattic (1, 2.5, and 5 μM) for 24 h. Using western blotting, we determined that Stattic can effectively inhibit STAT3-pi (**Figure 2B**).

Stattic Inhibits the Proliferation of MV4-11 Cells in a Dose- and Time-Dependent Manner

MV4-11 cells were treated with different concentrations of Stattic (1, 2.5, 5, and 10 μM) for 24 h and then subjected to a CCK8 assay to estimate the inhibition rate (IR) of cell proliferation. As shown in **Figure 3A**, the IR is dose-dependent, with an IC50 of 1.66 μM. When MV4-11 cells were treated with 2 μM Stattic or DMSO for 12, 24, 36, 48, and 60 h, the control group achieved higher proliferation than the Stattic group (**Figure 3B**), suggesting that the inhibition of cell proliferation by Stattic is dose- and time-dependent.

Stattic Blocks the Cell Cycle in the G0/G1 Phase

Flow cytometry was performed to detect the cell cycle distribution of MV4-11 cells treated with DMSO (as control) or different concentrations of Stattic (1, 2.5, and 5 μM) for 24 h. The proportion of cells in the G0/G1 phase significantly increased, whereas the proportion of cells in the G2/M phase significantly decreased in the Stattic group compared with that in the control group, suggesting that Stattic blocks the cell cycle (**Figure 4**).

Stattic Promotes Apoptosis in MV4-11 Cells

To further explore whether Stattic affects cell survival, we treated MV4-11 cells with DMSO (as control) or increasing concentrations of Stattic (1, 2.5, and 5 μM) for 24 h. Analysis of apoptosis using annexin-V/propidium iodide double staining showed that Stattic induces apoptosis in MV4-11 cells in a dose-dependent manner (**Figure 5**). Apoptosis rates are shown in **Figure 5A**.

Stattic Induces DSBs in MV4-11 Cells

To explore the effect of Stattic on the induction of DSBs, we treated MV4-11 cells with Stattic (2.5 μM) or DMSO (control) for 24 h. The mean fluorescence intensity (MFI) of γ-H2AX detected by flow cytometry was used to evaluate the level of DSBs. As shown in **Figure 6**, the MFI of the Stattic-treated group

1. *CTACGTTGATTTCAGAGAATATGAATATGATC*	*TCAAATGGGAGTTTCCAAGAGAAAATTTAGAGTT*
2. *CTACGTTGATTTCAGAGAATATGAATATGATC* *ACGTTGATTTCAGAGAATATGAATATGATC*	*TCAAATGGGAGTTTCCAAGAGAAAATTTAGAGTT*
3. *CTACGTTGATTTCAGAGAATATGAATATGATC*	*TCAAATGGGAGTTTCCAAGAGAAAATTTAGAGTT*
4. *CTACGTTGATTTCAGAGAATATGAATATGATC*	*TCAAATGGGAGTTTCCAAGAGAAAATTTAGAGTT*

FIGURE 1 | Confirmation of FLT3 gene sequence in cell lines. Partial FLT3 sequences of each cell line (1. FLT3-WT sequence from NCBI; 2. MV4-11 3. HL60 4. KG1a).

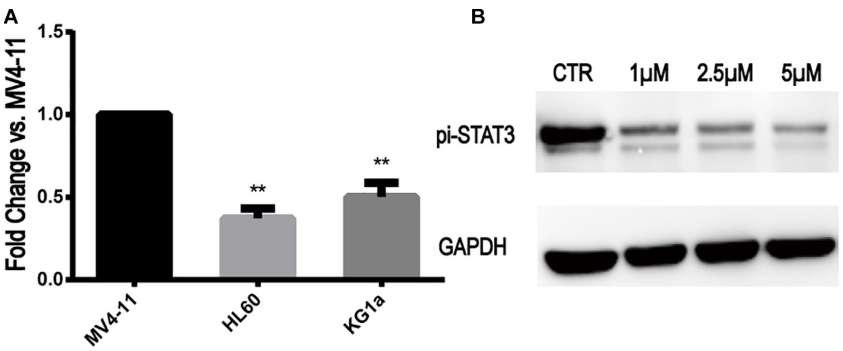

FIGURE 2 | STAT3 expression in MV4-11 and FLT3-WT cell lines and inhibition of STAT3-pi by Stattic. **(A)** The expression of STAT3 mRNA in HL60 cell line was 0.37 ± 0.05-fold ($n = 3$) of MV4-11 cell line, and the expression of STAT3 mRNA in KG1a cell line was 0.50 ± 0.07-fold ($n = 3$) of MV4-11 cell line (**$P < 0.01$). **(B)** Protein expression of STAT3-pi in MV4-11 cell line treated with different concentrations of Stattic (0, 1, 2.5, and 5 μM), as detected by western blotting.

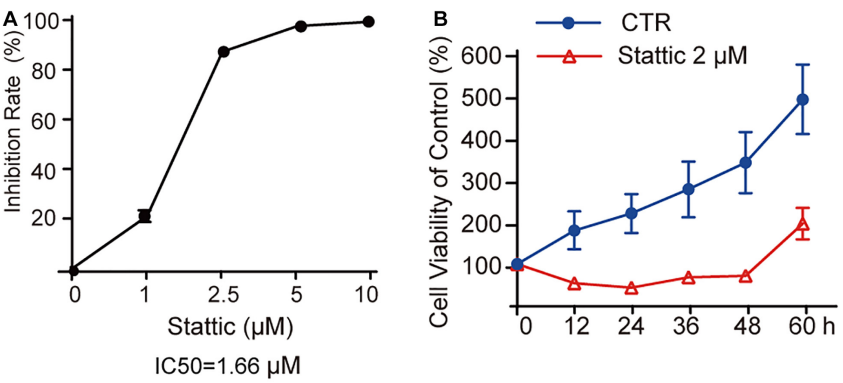

FIGURE 3 | Stattic inhibits the proliferation of MV4-11 cells in a dose-and time-dependent manner. Stattic inhibits the growth of MV4-11 cells. The cell proliferation inhibition induced by Stattic in MV4-11 cells is time- and dose-dependent. **(A)** MV4-11 cells were treated with 0, 1, 2.5, 5, and 10 μM Stattic for 24 h ($n = 3$, IR of MV4-11 cells treated with 1, 2.5, 5, and 10 μM Stattic for 24 h were 21.00 ± 2.33%, 86.45 ± 0.58%, 96.76 ± 0.51%, and 98.54 ± 0.53%, respectively). **(B)** MV4-11 cells were treated with 2 μM Stattic or DMSO (as control) and cell viability was tested by CCK at 12, 24, 36, 48, and 60 h ($n = 5$, cell viability of DMSO group at 12, 24, 36, 48, and 60 h were 180.04 ± 44.39%, 219.92 ± 46.07%, 276.84 ± 65.26%, 340.23 ± 72.34%, and 489.21 ± 82.07%, respectively; cell viability of Stattic group at 12, 24, 36, 48, and 60 h were 54.85 ± 6.34%, 45.01 ± 3.49%, 68.66 ± 6.61%, 73.22 ± 4.76%, 196.21 ± 36.97%, respectively.

was higher than that of the control group, suggesting that Stattic induces DSBs in MV4-11 cells.

Stattic Combined With VP-16 Promote MV4-11 Apoptosis

Vp-16, a traditional chemotherapy drug, is often used to treat leukemia. To explore the effect of Stattic combined with Vp-16 on FLT3-ITD mutant cells, we treated MV4-11 cells with Stattic (2.5 μM) and VP-16 (4 μg/ml) alone or in combination for 4.5 h. Apoptosis was then detected by flow cytometry. As shown in **Figure 7**, Stattic and VP-16 both promote apoptosis of MV4-11 cells. The early apoptosis, late apoptosis, and total apoptotic rates of the combined group were statistically increased compared with the VP16 or Stattic group.

MV4-11 Cells Repaired DNA Damages

The use of VP-16 causes DNA DSBs in leukemia cells; however, it is well-known that leukemia stem cells could repair DNA damage

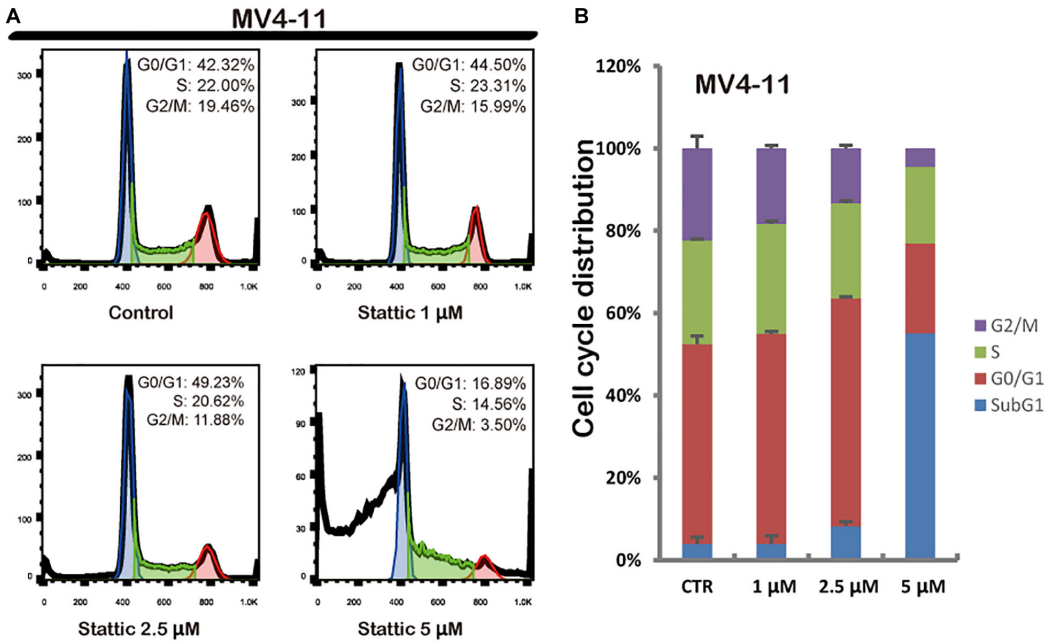

FIGURE 4 | Stattic blocks the cell cycle in the G0/G1 phase. Cells were treated with 0, 1, 2.5, and 5 μM Stattic for 24 h. All cell cycle analyses were conducted thrice. The cell cycle distribution was determined using propidium iodide staining **(A,B)**.

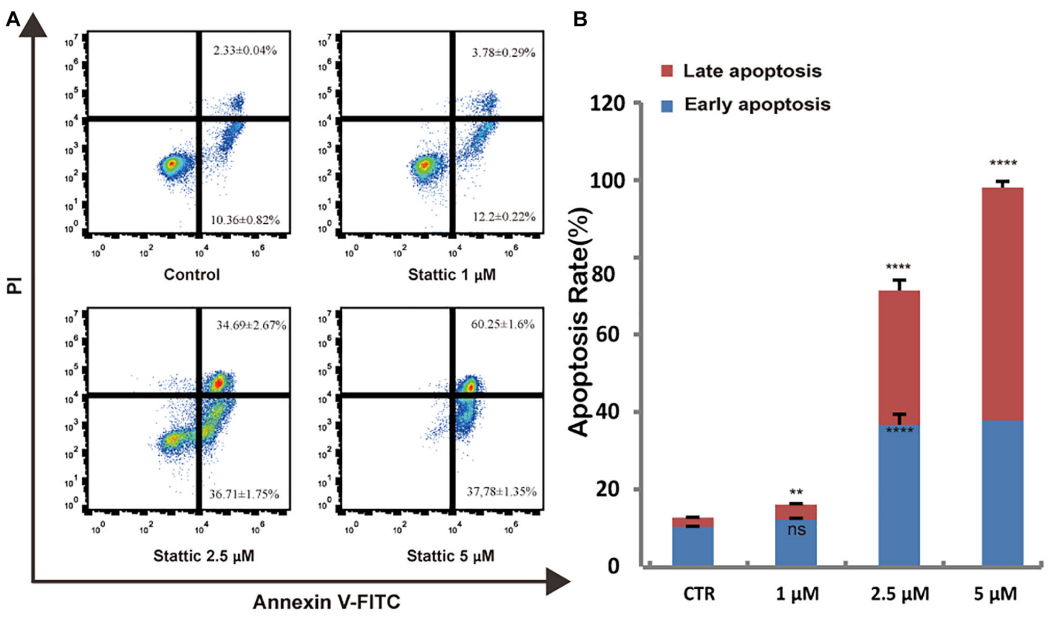

FIGURE 5 | Stattic promotes apoptosis in MV4-11 cells. Cells were treated with 1, 2.5, and 5 μM Stattic for 24 h. Apoptosis were quantified by flow cytometry. Data from three replica plates were plotted. Data are shown as mean ± *SD* **(A,B)**. $^{**}p < 0.01$ and $^{****}p < 0.0001$.

by DDR. To ascertain this, we pretreated MV4-11 cells with VP-16 and measured the MFI of γ-H2AX by flow cytometry over time. Right after drug elution, the MFI of pretreated cells was significantly higher than that of control cells, and it decreased gradually for 2 h. This indicates that MV4-11 cells can repair the DNA damage induced by VP-16 (**Figure 8**).

Stattic Blocks DDR in MV4-11 Cells

To investigate the effects of Stattic on the DNA repairing ability of MV4-11 cells, we induced DSBs using VP-16, and then cultured the cells in a medium containing Stattic and a medium without drug (control) for 4 h. We used flow cytometry to detect the expression of γH2AX, and the results are shown

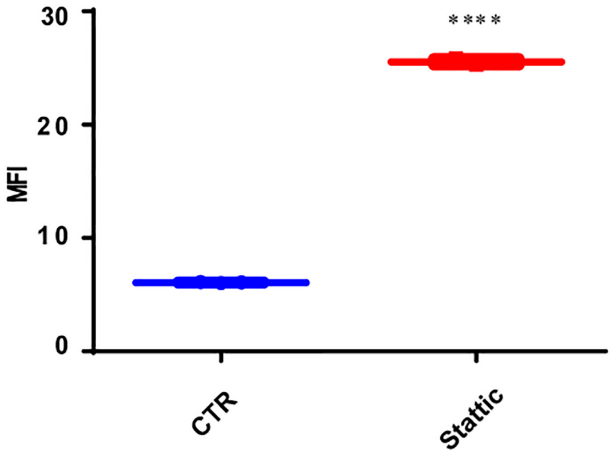

FIGURE 6 | Stattic induces DSBs in MV4-11 cells. Cells were treated with Stattic (2.5 μM) or DMSO (as control) for 24 h ($n = 3$). The DSB level was determined using H2AX staining and measured by mean fluorescence intensity. ****$p < 0.0001$.

in **Figure 9A**: MFI of the Stattic group was maintained at a higher level than that of the control group. This indicated that Stattic hinders the repair of VP-16-induced DSBs by cells (**Figure 9A**). To further distinguish that the higher γH2AX expression in Stattic group is caused by delayed repair of VP16-induced damages but not by Stattic itself, MV4-11 cells were treated with Stattic or DMSO (control) for 4 h; the results are presented in **Figure 9B**. There is no significant difference between the Stattic and control groups, indicating that Stattic did not cause higher γH2AX at 4 h treatment (**Figure 9B**).

Blocking DDR Participate in Apoptosis by Stattic in FLT3-ITD AML

To further explore the mechanism by which Stattic inhibits DDR in MV4-11 cells, MV4-11 cells were treated with different drugs [Stattic, Stattic combined with Vp-16, or DMSO (as control)] for 4.5 h, and then mRNA sequencing was performed. Data analysis was performed by OE Biotech Co., Ltd. (Shanghai, China). After KEGG analysis of genes with statistically significant changes in mRNA sequencing, it was found that in the DDR-related pathways (MMR, HR, etc. pathways), only the expression levels of some genes related to the HR pathway changed. The results showed that the Stattic group had lower ATM mRNA levels (**Figures 10A,C**). Cells treated with Stattic combined with VP-16 had a downregulated expression of BRCA1, RAD51, and polδ mRNA, which indicates that the combination of Stattic and VP-16 inhibited the expression of genes related to the HR pathway (**Figures 10B,D**). Therefore, the mechanism by which Stattic induces apoptosis in MV4-11 cells involves blocking the HR pathways of DDR pathways. However, the combined group shows upregulated expression of PRA and BRCA2, which are involved in the repair of DNA damage. The implications of this upregulation remain to be explored.

DISCUSSION

In 1995, Yu et al. (1995) discovered for the first time that the abnormal activation of STAT3 is related to the occurrence and

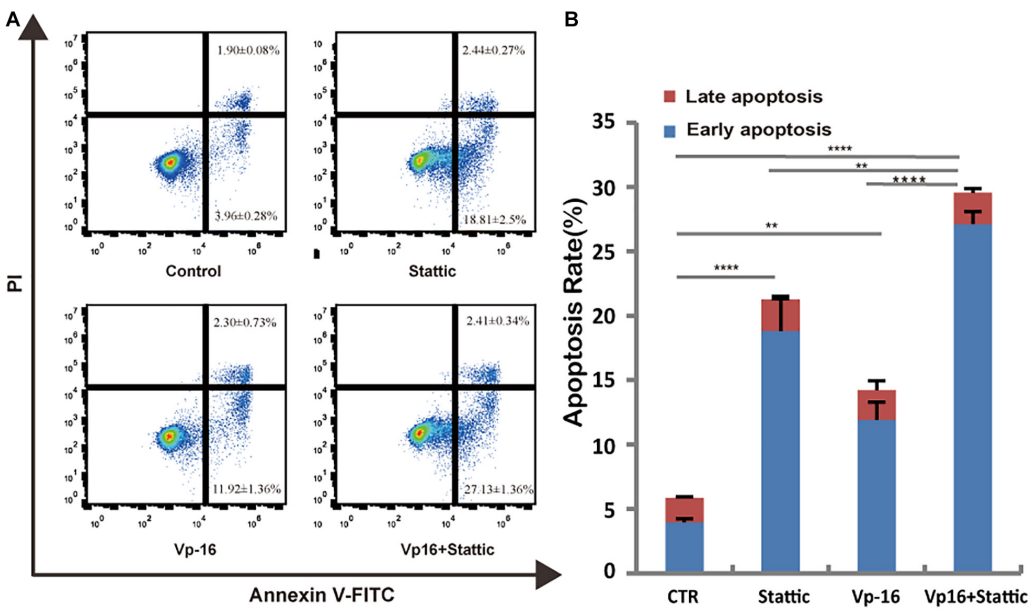

FIGURE 7 | Stattic combined with VP-16 promote MV4-11 apoptosis. MV4-11 cells were treated with DMSO (control), Stattic (2.5 μM), and VP-16 (4 μg/ml) alone or in combination for 4.5 h. Apoptosis was measured by flow cytometry. Data from three replica plates were plotted. Apoptosis rates were shown as mean ± *SD* **(A,B)**. *$p < 0.05$, **$p < 0.01$, and ****$p < 0.0001$.

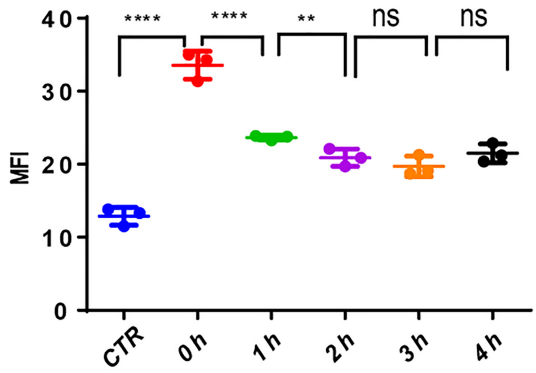

FIGURE 8 | MV4-11 cells repaired DNA damages. MV4-11 cells were pretreated with VP-16 for 2 h to induce DSB and then washed off. Cells were then incubated in fresh culture medium for 0, 1, 2, 3, and 4 h. The MFI of γ-H2AX was detected by flow cytometry to evaluate the level of DSBs at each stage. MV4-11 cells not pretreated with VP-16 were used as control. $^{**}p < 0.01$ and $^{****}p < 0.0001$.

development of tumors. This conclusion has been confirmed by other investigators. Activation of STAT3 is present in approximately 70% of all solid and hematological tumors (Kanna et al., 2018). STAT3 promotes the proliferation of leukemia cells through AKT/STAT3, Ras/Raf/MAPK and PI3K/AKT/mTOR, and other pathways (Badie et al., 1997). Simultaneously, aberrant STAT3 causes an increase in anti-apoptotic or a decrease in pro-apoptotic protein production and uncontrolled proliferation of cells (Kanna et al., 2018). Studies also found that inhibiting STAT3 activity can increase the degree of radiation damage to various solid tumor cells and promote tumor cell apoptosis (Pan et al., 2013; Zhang et al., 2015; Han et al., 2016).

Our experiments found that STAT3 inhibitors (Stattic) can effectively inhibit the proliferation of MV4-11 AML cells and promote apoptosis. Moreover, Stattic can also inhibit the DDR function of MV4-11 cells, delay the repair of DSBs, and thus enhance the induction of DSBs by VP-16 in AML cells. The mechanism may be related to the inhibition of the DDR pathway of AML cells. Our experimental results show that after treatment with Stattic, the level of ATM mRNA in leukemia cells is lower, and after Stattic and VP-16 treatment of cells, the expression of BRCA1, BARD1, RAD51, and polδ in the HR pathway are all downregulated. However, we also found that Stattic alone or in combination with VP-16 can upregulate the expression of some genes in the HR pathway, such as BRCA2 and RPA. This result seems to contradict the delay in repairing DSBs. We speculate that the dysregulation of various signaling molecules during HR repair is related to this paradox. In general, after DSBs occur in the cell, the damaged DNA ends are cut into 3′ single strands and combined with RPA to stabilize the single strand structure; next, RAD51 replaces RPA to form a RAD51-ssDNA complex and a D-loop at the DNA end. Finally, polδ performs DNA strand extension to complete DNA repair. It is noteworthy that assembly of the RAD51–ssDNA complex requires the participation of the following molecules: BRCA1, BRCA2, and RDA51 homologs (BARD1, RAD51D, RAD51B, and RAD51C) (Symington and Gautier, 2011; Iyama and Wilson, 2013; Kakarougkas and Jeggo, 2014; Fouquin et al., 2017). During this process, the increased expression levels of RPA and BRCA2 are conducive to the normal HR repair pathway. However, the downregulation of RAD51 and polδ expression downstream of RPA in the HR pathway may affect the normal repair of DSBs. Because the process of RAD51 replacing RPA requires the participation of BRCA1 and RAD51 homolog BARD1, the decrease in BRCA1 and BARD1 expression is not conducive to the successful assembly of RAD51–ssDNA complex and thus affects the normal progression of HR. However, the specific mechanism by which Stattic regulates the expression of genes such as BRCA1, BARD1, RAD51, and polδ mRNA still needs further study. In our experiments, we only showed changes in mRNA expressions of several HR-related factors; and our next step is to explore the effect of STAT3-inhibition on DDR pathway *in vivo*.

Besides hindering the repair of DSBs by affecting the HR pathway, Stattic can also induce DSBs. We speculate that Stattic affects the repair of spontaneously damaged DNA by accumulating DSBs in FLT3-ITD AML cells by inhibiting the HR repair pathway. This is because FLT3-ITD AML cells already have higher levels of DSBs. The continuous activation of the FLT3 receptor can activate the downstream PI3K/AKT,

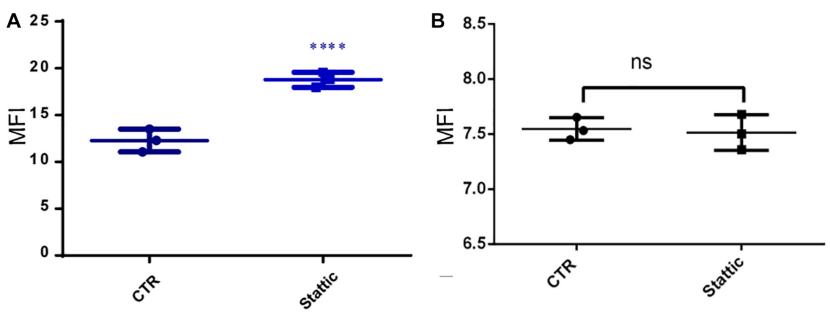

FIGURE 9 | Stattic blocks DDR in MV4-11 cells. **(A)** MV4-11 cells pretreated with VP-16 for 2 h and then incubated in fresh culture medium with DMSO (as control) or Stattic (2.5 μM) for 4 h. The mean fluorescence intensity (MFI) of γ-H2AX was detected by flow cytometry to estimate DSBs levels in both groups (**A**, $n = 3$, $^{****}P < 0.0001$). **(B)** MV4-11 cells were treated with Stattic (2.5 μM) or DMSO (control) for 4 h. The MFI of γ-H2AX was detected to estimate DSB levels in both groups. There is no significant difference between the Stattic and control groups (**B**, $n = 3$. $P > 0.5$).

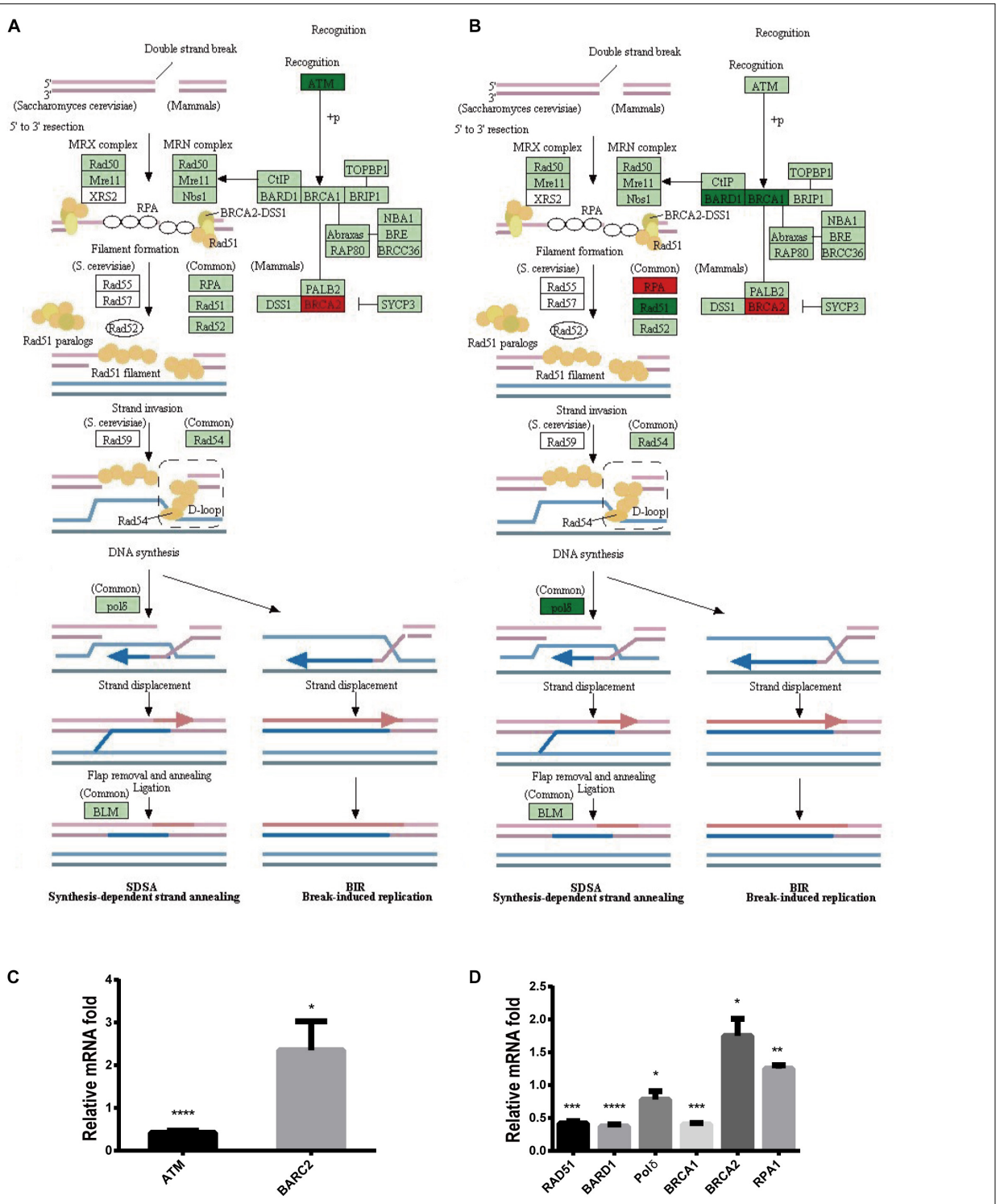

FIGURE 10 | Blocking DDR is involved in apoptosis induced by Stattic in FLT3-ITD AML. MV4-11 cells were treated with DMSO (as control), Stattic (2.5 μM), or Stattic (2.5 μM) combined with VP-16 (4 μg/ml) for 4.5 h, and then mRNA sequencing was performed ($n = 3$). **(A)** Compared with the control group, the Stattic group has low ATM mRNA levels and BRCA2 mRNA is upregulated. **(B)** Compared with the control group, Stattic + VP-16 group had downregulated expression of BRCA1, RAD51, and polδ mRNA in the HR pathway (red: upregulated, green: downregulated, light green: unchanged). **(C)** The expression of ATMmRNA, BRCA2mRNA in Stattic group were 0.41 ± 0.04-fold, 2.35 ± 0.55-fold of control group. **(D)** The expression of BAD51mRNA, BARD1mRNA, polδmRNA, BRCA1mRNA, BRCA2mRNA, RPA1mRNA in Stattic + VP-16 group were 0.42 ± 0.03-fold, 0.37 ± 0.03-fold, 0.78 ± 0.10 -fold, 0.4 ± 0.02-fold, 1.75 ± 0.21-fold, 1.25 ± 0.04-fold of control group.RNA sequencing data can be obtained from the following URL: https://www.ncbi.nlm.nih.gov/sra/?term=PRJNA685978# repository accession number PRJNA685978. *$p < 0.05$, **$p < 0.01$, ***$p < 0.001$, and ****$p < 0.0001$.

JAK/STAT, and Ras/MAPK pathways (Sellar and Losman, 2017). The RAS/PI3K/STAT pathway actively promotes the generation of ROS and then spontaneously induces the production of DSBs (Sallmyr et al., 2008).

Stattic can inhibit DDR function and hinder the repair of DSBs, thereby enhancing the sensitivity to chemotherapy drugs. Most traditional chemotherapeutic drugs kill leukemia cells by inducing DSBs, the accumulation of which leads to apoptosis (Goldstein and Kastan, 2015). Relapsed FLT3-ITD AML patients had an increased FLT3-ITD/FLT3-WT ratio in blasts of bone marrow as well as other new abnormalities in cellular and molecular level, which may be related to the HR pathway activity after DSBs AML cells. It may be related to LOH as well (Rebechi and Pratz, 2017). The results of this study provide a theoretical basis for the clinical treatment of FLT3-ITD AML by using STAT3 inhibitors combined with traditional chemotherapy drugs. This strategy could overcome the drug resistance of FLT3-ITD AML cells and improve the clinical prognosis of these patients.

In this study, we aims to explore the effect of Stattic on FLT3-ITD mutation AML cell lines (MV4-11) and the underlying mechanisms. We found Stattic can inhibit MV4-11 cell line proliferation and promote cell apoptosis, arrest cell cycle at G0/G1. Meanwhile, we also found the Stattic treatment suppress the HR pathway, which may be the mechanism of Stattic induced apoptosis. Our further investigation also found that Stattic can inhibit FLT3-WT cell line proliferation and promote cell apoptosis (**Supplementary Figures S1, S2**) by down regulate expression of STAT3-pi (**Supplementary Figure S3**); however, by comparing IC50 and apoptosis rate, we found that MV4-11 is more sensitive to Stattic than FLT3-WT cell line. Whether our conclusion from FLT3-ITD AML cells is applicable for multiple cell lines and animal models warrants further investigation.

DATA AVAILABILITY STATEMENT

The data presented in the study are deposited in the https://www.ncbi.nlm.nih.gov/sra/?term=PRJNA685978# repository, accession number PRJNA685978.

AUTHOR CONTRIBUTIONS

YXL and YL designed the study, conducted the experiments, and analyzed the data. BL, YSL, YY, and YX cultured cells. JZ supervised the study and wrote the manuscript. XZ corrected and approved the final version of the manuscript. All authors read and approved the final manuscript.

FUNDING

This work was supported by the Natural Science Foundation of Guangdong Province, China (No. 2018A0303130248) and Medical Scientific Research Foundation of Guangdong Province of China (A2018253).

SUPPLEMENTARY MATERIAL

The Supplementary Material for this article can be found online at: https://www.frontiersin.org/articles/10.3389/fcell.2021.637064/full#supplementary-material

Supplementary Figure 1 | Stattic inhibits the growth of HL60 cells and KG1a cells. **(A)** HL60 cells were treated with 0, 1, 2.5, 5, and 10 μM Stattic for 24 h ($n = 3$, IR of HL60 cells treated with 1, 2.5, 5, and 10 μM Stattic for 24 h were 12.33 ± 3.97%, 24.96 ± 3.11%, 79.17 ± 1.22%, and 90.35 ± 2.27% IC50 = 3.65 μM). **(B)** KG1a cells were treated with 0, 1, 2.5, 5, and 10 μM Stattic for 24 h ($n = 3$, IR of KG1a cells treated with 1, 2.5, 5, and 10 μM Stattic for 24 h were 7.12 ± 3.35%, 18.58 ± 4.11%, 34.45 ± 2.40%, and 61.86 ± 2.40% IC50 = 6.22 μM).

Supplementary Figure 2 | Stattic promotes apoptosis in KG1a and HL60 cells. KG1a cells and HL60 cells were treated with 1, 2.5, and 5 μM Stattic for 24 h. Apoptosis were quantified by flow cytometry. Data from three replica plates were plotted. Data are shown as mean ± *SD* **(A,B)**.

Supplementary Figure 3 | Inhibition of STAT3-pi by Stattic in KG1a and HL60 cells. Protein expression of STAT3-pi in KG1a and HL60 cells treated with different concentrations of Stattic (1,2.5, and 5 μM) for 24 h, as detected by western blotting **(A,B)**.

REFERENCES

Adachi, M., Cui, C., Dodge, C. T., Bhayani, M. K., and Lai, S. Y. (2012). Targeting STAT3 inhibits growth and enhances radiosensitivity in head and neck squamous cell carcinoma. *Oral Oncol.* 48, 1220–1226. doi: 10.1016/j.oraloncology.2012.06.006

Arora, L., Kumar, A. P., Arfuso, F., Chng, W. J., and Sethi, G. (2018). The role of signal transducer and activator of transcription 3 (STAT3) and its targeted inhibition in hematological malignancies. *Cancers (Basel)* 10:327. doi: 10.3390/cancers10090327

Badie, C., Goodhardt, M., Waugh, A., Doyen, N., Foray, N., Calsou, P., et al. (1997). A DNA double-strand break defective fibroblast cell line (180BR) derived from a radiosensitive patient represents a new mutant phenotype. *Cancer Res.* 57, 4600–4607.

Barry, S. P., Townsend, P. A., Knight, R. A., Scarabelli, T. M., Latchman, D. S., and Stephanou, A. (2010). STAT3 modulates the DNA damage response pathway. *Int. J. Exp. Pathol.* 91, 506–514. doi: 10.1111/j.1365-2613.2010.00734.x

Begg, A. C., Stewart, F. A., and Vens, C. (2011). Strategies to improve radiotherapy with targeted drugs. *Nat. Rev. Cancer* 11, 239–253. doi: 10.1038/nrc3007

Daver, N., Schlenk, R. F., Russell, N. H., and Levis, M. J. (2019). Targeting FLT3 mutations in AML: review of current knowledge and evidence. *Leukemia* 33, 299–312. doi: 10.1038/s41375-018-0357-9

Fan, J., Li, L., Small, D., and Rassool, F. (2010). Cells expressing FLT3/ITD mutations exhibit elevated repair errors generated through alternative NHEJ pathways: implications for genomic instability and therapy. *Blood* 116, 5298–5305. doi: 10.1182/blood-2010-03-272591

Fouquin, A., Guirouilh-Barbat, J., Lopez, B., Hall, J., Amor-Gueret, M., and Pennaneach, V. (2017). PARP2 controls double-strand break repair pathway choice by limiting 53BP1 accumulation at DNA damage sites and promoting end-resection. *Nucleic Acids Res.* 45, 12325–12339. doi: 10.1093/nar/gkx881

Goldstein, M., and Kastan, M. B. (2015). The DNA damage response: implications for tumor responses to radiation and chemotherapy. *Annu. Rev. Med.* 66, 129–143. doi: 10.1146/annurev-med-081313-121208

Han, T. J., Cho, B. J., Choi, E. J., Kim, D. H., Song, S. H., Paek, S. H., et al. (2016). Inhibition of STAT3 enhances the radiosensitizing effect of temozolomide in glioblastoma cells in vitro and in vivo. *J. Neurooncol.* 130, 89–98. doi: 10.1007/s11060-016-2231-9

Huang, R. X., and Zhou, P. K. (2020). DNA damage response signaling pathways and targets for radiotherapy sensitization in cancer. *Signal Transduct Target Ther.* 5:60.

Iyama, T., and Wilson, D. M. 3RD (2013). DNA repair mechanisms in dividing and non-dividing cells. *DNA Repair (Amst)* 12, 620–636. doi: 10.1016/j.dnarep.2013.04.015

Kakarougkas, A., and Jeggo, P. A. (2014). DNA DSB repair pathway choice: an orchestrated handover mechanism. *Br. J. Radiol.* 87:20130685. doi: 10.1259/bjr.20130685

Kanna, R., Choudhary, G., Ramachandra, N., Steidl, U., Verma, A., and Shastri, A. (2018). STAT3 inhibition as a therapeutic strategy for leukemia. *Leuk Lymphoma* 59, 2068–2074. doi: 10.1080/10428194.2017.1397668

Levis, M., and Small, D. (2003). FLT3: itdoes matter in leukemia. *Leukemia* 17, 1738–1752. doi: 10.1038/sj.leu.2403099

Pan, Y., Zhou, F., Zhang, R., and Claret, F. X. (2013). Stat3 inhibitor stattic exhibits potent antitumor activity and induces chemo- and radio-sensitivity in nasopharyngeal carcinoma. *PLoS One* 8:e54565. doi: 10.1371/journal.pone.0054565

Quentmeier, H., Reinhardt, J., Zaborski, M., and Drexler, H. G. (2003). FLT3 mutations in acute myeloid leukemia cell lines. *Leukemia* 17, 120–124. doi: 10.1038/sj.leu.2402740

Rebechi, M. T., and Pratz, K. W. (2017). Genomic instability is a principle pathologic feature of FLT3 ITD kinase activity in acute myeloid leukemia leading to clonal evolution and disease progression. *Leuk Lymphoma* 58, 1–11.

Redell, M. S., Ruiz, M. J., Alonzo, T. A., Gerbing, R. B., and Tweardy, D. J. (2011). Stat3 signaling in acute myeloid leukemia: ligand-dependent and -independent activation and induction of apoptosis by a novel small-molecule Stat3 inhibitor. *Blood* 117, 5701–5709. doi: 10.1182/blood-2010-04-280123

Sallmyr, A., Fan, J., and Rassool, F. V. (2008). Genomic instability in myeloid malignancies: increased reactive oxygen species (ROS), DNA double strand breaks (DSBs) and error-prone repair. *Cancer Lett.* 270, 1–9. doi: 10.1016/j.canlet.2008.03.036

Schust, J., Sperl, B., Hollis, A., Mayer, T. U., and Berg, T. (2006). Stattic: a small-molecule inhibitor of STAT3 activation and dimerization. *Chem. Biol.* 13, 1235–1242. doi: 10.1016/j.chembiol.2006.09.018

Sellar, R., and Losman, J. A. (2017). Targeting aberrant signaling in myeloid malignancies: promise versus reality. *Hematol. Oncol. Clin. North Am.* 31, 565–576. doi: 10.1016/j.hoc.2017.04.001

Shi, Y., Zhang, Z., Qu, X., Zhu, X., Zhao, L., Wei, R., et al. (2018). Roles of STAT3 in leukemia (review). *Int. J. Oncol.* 53, 7–20.

Stirewalt, D. L., Pogosova-Agadjanyan, E. L., Tsuchiya, K., Joaquin, J., and Meshinchi, S. (2014). Copy-neutral loss of heterozygosity is prevalent and a late event in the pathogenesis of FLT3/ITD AML. *Blood Cancer J.* 4:e208. doi: 10.1038/bcj.2014.27

Symington, L. S., and Gautier, J. (2011). Double-strand break end resection and repair pathway choice. *Annu. Rev. Genet.* 45, 247–271. doi: 10.1146/annurev-genet-110410-132435

Takagi, M. (2017). DNA damage response and hematological malignancy. *Int. J. Hematol.* 106, 345–356. doi: 10.1007/s12185-017-2226-0

Wang, L., Jiang, Z., Huang, D., Duan, J., Huang, C., Sullivan, S., et al. (2018). JAK/STAT3 regulated global gene expression dynamics during late-stage reprogramming process. *BMC Genomics* 19:183. doi: 10.1186/s12864-018-4507-2

Yu, C. L., Meyer, D. J., Campbell, G. S., Larner, A. C., Carter-su, C., Schwartz, J., et al. (1995). Enhanced DNA-binding activity of a Stat3-related protein in cells transformed by the Src oncoprotein. *Science* 269, 81–83. doi: 10.1126/science.7541555

Zhang, Q., Zhang, C., He, J., Guo, Q., Hu, D., Yang, X., et al. (2015). STAT3 inhibitor stattic enhances radiosensitivity in esophageal squamous cell carcinoma. *Tumour Biol.* 36, 2135–2142. doi: 10.1007/s13277-014-2823-y

Zhou, J., Bi, C., Janakakumara, J. V., Liu, S. C., Chng, W. J., Tay, K. G., et al. (2009). Enhanced activation of STAT pathways and overexpression of survivin confer resistance to FLT3 inhibitors and could be therapeutic targets in AML. *Blood* 113, 4052–4062. doi: 10.1182/blood-2008-05-156422

Conflict of Interest: The authors declare that the research was conducted in the absence of any commercial or financial relationships that could be construed as a potential conflict of interest.

frontiers in Cell and Developmental Biology

ORIGINAL RESEARCH
published: 07 May 2021
doi: 10.3389/fcell.2021.656795

Cytolethal Distending Toxin Promotes Replicative Stress Leading to Genetic Instability Transmitted to Daughter Cells

William Tremblay[1†], Florence Mompart[1†], Elisa Lopez[1], Muriel Quaranta[2], Valérie Bergoglio[3], Saleha Hashim[1], Delphine Bonnet[4], Laurent Alric[4], Emmanuel Mas[2,5], Didier Trouche[3], Julien Vignard[1], Audrey Ferrand[2], Gladys Mirey[1] and Anne Fernandez-Vidal[1,3]**

[1] Toxalim (Research Centre in Food Toxicology), Université de Toulouse, INRAE, ENVT, INP-Purpan, UPS, Toulouse, France, [2] IRSD, Université de Toulouse, INSERM, INRAE, ENVT, UPS, Toulouse, France, [3] MCD, Centre de Biologie Intégrative, Université de Toulouse, CNRS, UPS, Toulouse, France, [4] Department of Internale and Digestive Diseases, Pole Digestif, CHU Toulouse, Paul Sabatier University, Toulouse, France, [5] Unité de Gastroentérologie, Hépatologie, Nutrition, Diabétologie et Maladies Héréditaires du Métabolisme, Hôpital des Enfants, CHU de Toulouse, Toulouse, France

OPEN ACCESS

Edited by:
Lin Deng,
Shenzhen Bay Laboratory, China

Reviewed by:
Jian Yuan,
Tongji University, China
Armelle Menard,
Université de Bordeaux, France
Chih-Ho Lai,
Chang Gung University, Taiwan

***Correspondence:**
Gladys Mirey
gladys.mirey@inrae.fr
Anne Fernandez-Vidal
anne.fernandez2@univ-tlse3.fr

[†] These authors have contributed equally to this work

Specialty section:
This article was submitted to Cell Growth and Division, a section of the journal Frontiers in Cell and Developmental Biology

Received: *21 January 2021*
Accepted: *23 March 2021*
Published: *07 May 2021*

Citation:
Tremblay W, Mompart F, Lopez E, Quaranta M, Bergoglio V, Hashim S, Bonnet D, Alric L, Mas E, Trouche D, Vignard J, Ferrand A, Mirey G and Fernandez-Vidal A (2021) Cytolethal Distending Toxin Promotes Replicative Stress Leading to Genetic Instability Transmitted to Daughter Cells. Front. Cell Dev. Biol. 9:656795. doi: 10.3389/fcell.2021.656795

The cytolethal distending toxin (CDT) is produced by several Gram-negative pathogenic bacteria. In addition to inflammation, experimental evidences are in favor of a protumoral role of CDT-harboring bacteria such as *Escherichia coli*, *Campylobacter jejuni*, or *Helicobacter hepaticus*. CDT may contribute to cell transformation *in vitro* and carcinogenesis in mice models, through the genotoxic action of CdtB catalytic subunit. Here, we investigate the mechanism of action by which CDT leads to genetic instability in human cell lines and colorectal organoids from healthy patients' biopsies. We demonstrate that CDT holotoxin induces a replicative stress dependent on CdtB. The slowing down of DNA replication occurs mainly in late S phase, resulting in the expression of fragile sites and important chromosomic aberrations. These DNA abnormalities induced after CDT treatment are responsible for anaphase bridge formation in mitosis and interphase DNA bridge between daughter cells in G1 phase. Moreover, CDT-genotoxic potential preferentially affects human cycling cells compared to quiescent cells. Finally, the toxin induces nuclear distension associated to DNA damage in proliferating cells of human colorectal organoids, resulting in decreased growth. Our findings thus identify CDT as a bacterial virulence factor targeting proliferating cells, such as human colorectal progenitors or stem cells, inducing replicative stress and genetic instability transmitted to daughter cells that may therefore contribute to carcinogenesis. As some CDT-carrying bacterial strains were detected in patients with colorectal cancer, targeting these bacteria could be a promising therapeutic strategy.

Keywords: cytolethal distending toxin, replicative stress, genetic instability, DNA bridge, DNA damage, human colorectal organoid

Abbreviations: ATM, ataxia–telangiectasia mutated kinase; ATR, ataxia–telangiectasia and Rad-3-related kinase; ATRi, ATR inhibitor; CDT, cytolethal distending toxin; CDT Ec, cytolethal distending toxin from *E. coli*; CDT Hd, cytolethal distending toxin from *H. ducreyi*; CFS, common fragile sites; CldU, 5-chlorodeoxyuridine; DSB, double-strand break; EdU, 5-ethynyl-2′-deoxyuridine; FA, Fanconi anemia; IdU, 5 iododeoxyuridine; NHEJ, non-homologous end joining; RH, homologous recombination; RPA, replication protein A; SSB, single-strand breaks; SSBR, single-strand break repair.

INTRODUCTION

The cytolethal distending toxin (CDT) was first identified in 1988 in *Escherichia coli* (*E. coli*) strains isolated from patients with diarrhea (Johnson and Lior, 1988a,b). To date, around 30 proteobacteria, including *E. coli*, *Campylobacter jejuni* (*C. jejuni*), *Aggregatibacter actinomycetemcomitans* (*A. actinomycetemcomitans*), *Helicobacter hepaticus* (*H. hepaticus*), or *Haemophilus ducreyi* (*H. ducreyi*), were identified to produce this virulence factor [for review, see Scuron et al. (2016)]. The genital, urinary, and digestive tracts constitute the main niches where CDT-producing bacteria were found. The mechanism of CDT intoxication was characterized by nuclear and cytoplasmic enlargement of mammalian cells giving its name to the toxin (Pérés et al., 1997; Sugai et al., 1998; Blazkova et al., 2010). CDT is a heterotrimeric complex belonging to the AB2-type genotoxin, composed of three subunits, mostly CdtA, CdtB, and CdtC. CdtA and CdtC constitute the regulatory subunits and CdtB the catalytic subunit exhibiting phosphatase and DNase activities, the latter responsible for DNA break formation [for review, see Guerra et al. (2011); Jinadasa et al. (2011)]. It was initially reported that CDT induces direct DNA double-strand break (DSB) in mammalian cells (Frisan et al., 2003). However, further investigations demonstrated that low doses of CDT first induce single-strand breaks (SSB), later converted into DSB during the S phase (Fedor et al., 2013), which may be due to replicative fork inhibition and the induction of a replicative stress. Moreover, at the molecular level, CDT-induced DNA damage activates the ataxia–telangiectasia and Rad-3-related kinase (ATR) and ataxia–telangiectasia mutated kinase (ATM) that initiate the DNA damage repair pathway through the spreading of H2AX phosphorylation (defined as γH2AX) around the DNA lesions (Cortes-Bratti et al., 2001; Fahrer et al., 2014). Then, the following checkpoint kinases CHK1, CHK2, and p53 phosphorylation mediate cell cycle arrest at the G1/S and/or G2/M transitions, depending on cellular host p53 status, allowing DNA-repairing machinery to correct DNA damaging insults (Cortes-Bratti et al., 2001; Alaoui-El-Azher et al., 2010; Fahrer et al., 2014). Homologous recombination (RH), non-homologous end joining (NHEJ), Fanconi anemia (FA), and single-strand break repair (SSBR) pathways were depicted as the main mammalian repair mechanisms involved in the resistance to CDT intoxication to preserve the DNA integrity (Bezine et al., 2016). In case of massive unrepaired or misrepaired DNA damage, senescence or cell death by apoptosis is activated (Cortes-Bratti et al., 2001; Alaoui-El-Azher et al., 2010; Guerra et al., 2011; Jinadasa et al., 2011).

Cytolethal distending toxin has been associated to several diseases. In addition to inflammation, some *in vitro* and *in vivo* experiments support its involvement in cancer. CDT-producing *E. coli* are detected in 15.8% of patients with colorectal cancer while it is not detected in the non-cancer group (Buc et al., 2013). In murine models, CDT produced by *H. hepaticus* or *C. jejuni* enhances inflammation and promotes liver and intestinal tumorigenesis through CdtB (Ge et al., 2007, 2017; He et al., 2019). Moreover, precancerous human colon epithelial cells or rat embryonic fibroblasts chronically exposed to CDT from *E. coli*, *H. ducreyi*, or *H. hepaticus* exhibit cancer hallmarks, such as anchorage-independent growth and genetic instability. Indeed, enhanced frequency of mutagenesis, chromosomal aberrations, interphase and anaphase bridges, and micronuclei are observed in cells chronically intoxicated with CDT genotoxin (Guidi et al., 2013; Graillot et al., 2016).

These studies, relying on chronic infection of mice or cell lines with CDT-producing bacteria or intoxication with purified holotoxins, demonstrate the carcinogenic potential of CDT. However, they did not directly assess the mechanism at the root of genomic instability induced by CDT that supports cancer development, including the impact of CDT on the DNA replication program, the characterization of genetic alterations, and their fate in daughter cells. Ultimately, this approach will allow for a better understanding of CDT cellular target considering its proliferation status. To address these issues, we analyzed the direct consequences of CDT on the DNA replication process after acute exposure to CDT holotoxins in human cells. Both HeLa cells, widely manipulated to study CDT, and the well-characterized U2OS cell line for the analysis of fragile site expression were employed to study the molecular mechanism of CDT intoxication. In addition, RKO colorectal cell line and human colorectal organoids were used to investigate the physiological impact of CDT. Here, we report a slowing down of DNA replication velocity depending on CdtB catalytic activity, mainly in the late S phase. This effect was associated with fragile site expression, accumulation of chromosomal aberrations and chromatin bridges in daughter cells. Finally, we show that CDT holotoxin carries out its genotoxic activity especially in cycling cells of human colorectal organoids leading to defective growth. Collectively, these data suggest that highly proliferating cells could be more sensitive to CDT through induction of a replicative stress favoring the establishment of genomic instability transmitted to daughter cells and associated with tumor progression.

MATERIALS AND METHODS

Cell Lines and Treatments

HeLa, U2OS, and RKO human cells were cultured in Dulbecco's modified Eagle's medium (DMEM, Gibco, Life Technologies) supplemented with 10% heat-inactivated calf serum and 0.5 mg/ml penicillin/streptomycin (P/S). Cells lines were grown in a humidified incubator at 37°C in a 5% CO_2 atmosphere. All cell lines were checked and were mycoplasma-free.

The wild-type cytolethal distending toxin from *E. coli* (CDT Ec) or *H. ducreyi* (CDT Hd) and catalytic dead mutants (CDT^{H153A} and CDT^{D273R}, respectively) were produced and purified in the lab at 25 μg/ml (Fedor et al., 2013; Pons et al., 2019) and preserved in phosphate-buffered saline (PBS) (Sigma-Aldrich) with 10% glycerol.

When needed, HeLa cells were treated with ATR inhibitor (ATRi) (VE-821, Sigma-Aldrich, 5 μM).

Quiescence of RKO was induced by cultivation of cells until confluence followed by serum starvation for 2 days. The quiescent cells were treated or not with CDT for 7 h before γH2AX staining.

Human Samples

Biological samples were obtained from seven different patients treated at the Toulouse University Hospital. Patients gave informed consent and were included in the registered BioDIGE protocol approved by the ethics committee "comité de protection des personnes du Sud-ouest et Outre-mer II, agence régionale de Santé Midi-Pyrénées" and was financially supported by the Toulouse University Hospital (NCT 02874365). Colonic samples were obtained from biopsies of healthy patients undergoing endoscopy.

DNA Fiber Assay

HeLa or U2OS cells were treated with CDT for 16 or 24 h, respectively, before sequential pulse labeling with 50 μM CldU (5-chlorodeoxyuridine, Sigma-Aldrich), then 100 μM IdU (5 iododeoxyuridine, Sigma-Aldrich) for 20 min each, followed by a chase with 200 μM thymidine (Sigma-Aldrich) for 1 h. Cells were then collected and DNA fiber assays were performed as described previously (Fernandez-Vidal et al., 2019). IdU and CldU were detected with monoclonal mouse (1/50, BD347583, Becton Dickinson) and rat anti-BrdU antibodies (1/75, OBT0030G, Bio-Rad), respectively, and subsequently single-strand DNA with mouse antibody (1/50, MAB3034, Millipore). Images were analyzed using NIS Elements-AR Nikon software. The specific DNA staining allowed the exclusion of any signal due to broken or overlapping DNA fibers. IdU track length was determined if flanked by a CldU track. At least 400 fibers per condition were measured.

Cell Cycle Analysis by Flow Cytometry

Sixteen hours after CDT treatment (2.5 ng/ml), HeLa and U2OS cells were incubated with 5-ethynyl-2′-deoxyuridine (EdU; 5 μM) for 30 min. Cells were collected by trypsinization and fixed, and incorporated EdU was detected using the baseclick EdU flow cytometry kit (Sigma, BCK-FC488) according to the manufacturer's instructions. Cells were incubated in PBS containing DAPI (1 μg/ml) for 15 min before samples were processed using flow cytometry (Beckman Coulter CytoFLEX S). At least 10,000 events were analyzed per sample using the CytExpert software.

Metaphase Spreading and Fluorescence *in situ* Hybridization Analysis

U2OS cells were treated with CDT from *E. coli* at 250 pg/ml during 48 h before adding nocodazole (0.1 μM) for 5 h more. After mitotic shake off, the cells were resuspended in a hypotonic solution (75 mM KCl) and incubated for 20 min at 37°C. Then, the cells were fixed in a methanol/acetic acid solution (3:1) and dropped on slides to spread the chromosomes. The RP11-36B6 and RP11-281J9 BAC probes (mapped onto FRA7H and FRA16D loci, respectively) were labeled by nick translation according to the supplier's recommendations (VY Nick Translation Kit and VY green dUTP, Abbott Molecular), then precipitated with ethanol (70%), human Cot-1 DNA (0.1 μg/μl, Invitrogen), DNA MB grade (1 mg/ml, Roche), and ammonium acetate (0.3 M) overnight at −20°C. After washing with 70% ethanol, the precipitated DNA was incubated for 15 min at 37°C in hybridization mix composed of 50% formamide, 2X SSC, 10% dextran sulfate, and 1% Tween20 and stored at −20°C. Metaphase slides were incubated at 62°C for 1 h then in 4% formol during 5 min, washed with PBS, followed by dehydration process in successive ethanol baths (70, 80, 90, and 100%) for 1 min each. The probe was applied on metaphases, denatured for 5 min at 80°C, and hybridized overnight at 37°C. Finally, the chromosomes were stained with DAPI (2 μM, 10 min) before adding VECTASHIELD mounting medium (Vector Laboratories). Image acquisition of multiple random fields was performed on a wide-field microscope (model Nikon, Ci-S, × 60 objective).

EdU Staining and Immunofluorescence Analysis

Cells were grown on glass coverslips. After 23 h of CDT treatment, EdU (10 μM) wad added for 45 min. Then, cells were fixed with 4% paraformaldehyde for 15 min and permeabilized with 0.5% Triton X-100 for 20 min. Incorporated EdU was detected using the baseclick EdU kit (BCK-EdU488, Sigma-Aldrich) according to the manufacturer's instructions. Then, cells were blocked in 3% bovine serum albumin (BSA) and stained with primary antibodies in a blocking solution. For replication protein A (RPA) detection, a pre-extraction step (0.5% Triton X-100 for 5 min) was performed before fixation. Cyclin A (H3, Santa Cruz, sc-271645, 1/100) antibody was incubated overnight at 4°C, while RPA (Calbiochem, Ab-2, Mouse mAb, RPA34-19, NA18, 1/200) and RIF1 (Bethyl A300-568A-4, 1/1000) antibodies were incubated for 3 h at room temperature. Cells were washed three times with PBS 0.1% Tween20 and incubated with the secondary antibodies (dilution 1/1,000) for 2 h (AlexaFluor purchased from Invitrogen). DNA was stained with DAPI.

For γH2AX immunofluorescence, quiescent or proliferating RKO cells were treated with CDT for 7 h, then fixed and permeabilized with 4% paraformaldehyde and 0.1% Triton X-100 for 15 min, blocked in 1% BSA and 0.1% Triton X-100 for 1 h, and finally stained with γH2AX antibody (Merck/Millipore, 05–636, 1/400) in 1% BSA for 3 h. High-capacity acquisition of fluorescent cell images was obtained by using an ArrayScan HCS with a × 20 objective lens reader, and image analysis was carried out by using the Cellomics analysis software (Thermo Scientific). Cells were positive for γH2AX when > 4 foci/nuclei were detected. For each analysis, a minimum of 1,000 cells were analyzed in three independent experiments. Cell cycle position was determined by quantification of DAPI signal intensity using R software.

Organoid Culture, Treatment, and Immunofluorescence

Colorectal crypt isolation was performed as described previously (Sébert et al., 2018). Fresh Matrigel (Corning, 356255) was added to isolated crypts; 25 μl of Matrigel containing 50 crypts were plated in each well of a pre-warmed eight-well chamber (Ibidi, 80841). Once the Matrigel had polymerized for 20 min at 37°C, 250 μl of culture medium was added to each well as described previously (Sébert et al., 2018). Then, colorectal crypts

were treated or not (NT) with wild-type (25 and 2.5 ng/ml) or mutated (H153A, 25 ng/ml) CDT from *E. coli* and incubated in a humidified incubator at 37°C and 5% CO_2 for 16 h (day 0). Finally, CDT was removed (day 1), and the culture medium was changed every 3 days without N-acetylcysteine (NAC; Sigma, A9165-5G) and LY2157599 (Axon MedChem, 1941). At day 5, nicotinamide (Sigma, N0636), SB202190 (Sigma, 57067), and PGE2 (Sigma, P0409) were removed from the medium and Wnt3a-conditioned medium [supernatants from L Wnt-3A cells (ATCC® CRL-2647™)] reduced to 5%. At day 6, Wnt3a-conditioned medium was totally removed until day 8.

All cultures were stopped at day 4 or 8 for analysis. EdU (10 μM) was added to the culture medium, 16 h before organoid fixation with 2% of paraformaldehyde for 30 min at 37°C. Then, organoids were washed in PBS and permeabilized with 0.5% Triton X-100 for 40 min. Incorporated EdU was detected using the baseclick EdU kit (BCK-EdU488, Sigma-Aldrich) according to the manufacturer's instructions. Then, cells were blocked in 3% BSA and stained with γH2AX antibody (1/1,000) in a blocking solution overnight at 4°C. Organoids were washed three times in PBS and incubated with the secondary antibody (1/1,000) for 2 h (AlexaFluor purchased from Invitrogen). After washes, DNA was stained with DAPI (2 μg/ml) for 30 min. Finally, plates were mounted with VECTASHIELD mounting medium.

In order to measure the organoid size, image acquisition of organoids was performed on a bright-field microscope (×5 objective). All organoids present in wells were counted. For immunostaining, at least six random organoids were analyzed for each condition with an inverted confocal microscope (Leica SP8, × 40 objective). Images were analyzed using the ImageJ software from FiJi.

Statistical Analysis

The results are expressed as the mean ± SEM. Statistical analysis was assessed using Prism 9 software (GraphPad). Student's *t*-test, Mann–Whitney, and one-way or two-way ANOVA tests, followed by *post hoc* tests were used when appropriate. A p value <0.05 was considered significant. For DNA fiber assays, statistical analysis was performed using two-tailed Mann–Whitney test. For cell cycle and interphase bridge analysis, one-way ANOVA followed by Tukey's multiple comparison test was used. For fragile site expression, chromosomic aberration, and mitotic bridge analysis, Student's *t*-test was employed. For analysis of cells with DNA bridges after CDT and ATRi treatments, two-way ANOVA followed by Bonferroni's multiple comparison test was used in order to compare ATRi treatment effects at each dose of CDT exposure. Two-way ANOVA followed by Dunnett's multiple comparison test was used to study CDT dose effects in the absence or in the presence of ATRi treatment. Two-way ANOVA followed by Tukey's multiple comparison test was used for cell cycle analysis on cells linked or not with a bridge. To analyze RIF1-cyclin A immunofluorescence in cells linked or not by DNA thread, two-way ANOVA followed by Dunnett's and Sidak's multiple comparison tests was used. For γ-H2AX foci formation assays, two-way ANOVA followed by Sidak's multiple comparison test was performed. For organoid and nucleus size analysis and EdU-positive cell quantification, two-way ANOVA followed by Dunnett's and Sidak's multiple comparison tests was used, whereas one-way ANOVA followed by Dunnett's multiple comparison test was employed for γ-H2AX-positive cell quantification in proliferating cells (EdU plus).

RESULTS

CDT Intoxication Induces Replicative Stress in Human Cells

In order to investigate the mechanism by which CDT promotes genetic instability, we assessed the toxin impact on the DNA replication program, at a single-molecule level. To address this question, we performed DNA fiber assays and monitored the replication fork velocity. HeLa and U2OS cells were incubated with CDT holotoxins from *E. coli* or *H. ducreyi*, respectively. Then, the successive double-pulse labeling with two nucleotide analogs, CldU followed by IdU incorporation, was performed and IdU track lengths measured (**Figure 1A**). We observed a significant decrease in IdU track length, revealing a slowing down of replication fork speed in the presence of CDT compared to untreated cells, independently of CDT-producing strains and host cells (**Figures 1B,C**). The same experiment was performed in U2OS cells with a mutant CDT from *H. ducreyi* in which aspartic acid 273, essential for CdtB catalytic activity, is replaced by an arginine (CDT^{D273R}) (Guerra et al., 2005; Pons et al., 2019). U2OS cells cultivated in the presence of CDT^{D273R} displayed a fork speed close to that observed in untreated cells, revealing that CDT catalytic activity is crucial to mediate the slowing down of fork progression (**Figure 1D**). Altogether, these results demonstrate that CDT holotoxins induce a replicative stress in different host cells and underline the major role of CDT catalytic activity in this process.

We next analyzed the consequences of this replicative stress on the global cell distribution in the S phase by performing EdU incorporation experiments followed by flow cytometry analysis. In addition to the G2/M block, the examination of EdU incorporation according to DAPI staining showed a higher proportion of S phase cells (EdU-positive cells) at the border of G2/M after *E. coli* or *H. ducreyi* wild-type CDT exposure of HeLa cells compared to control cells (**Figure 2A**, red boxes and **Figure 2B**). Indeed, CDT treatment generated a significant increase in the proportion of cells in the late S phase with a low EdU incorporation, which is abolished with the mutant form. Very similar results were obtained in U2OS cells (**Figures 2C,D**). These experiments unveil a slowing down of DNA replication occurring probably mainly in the late S phase or a weak replication persisting in G2, after CDT intoxication. Despite the wild-type p53 status, a G1 block has not been detected in U2OS cells, in agreement with previous a work (Blazkova et al., 2010).

CDT Exposure Promotes Mitotic Abnormalities and Fragile Site Expression

Among the domains replicated in the late S phase, common fragile sites (CFS) constitute the major chromosomal regions

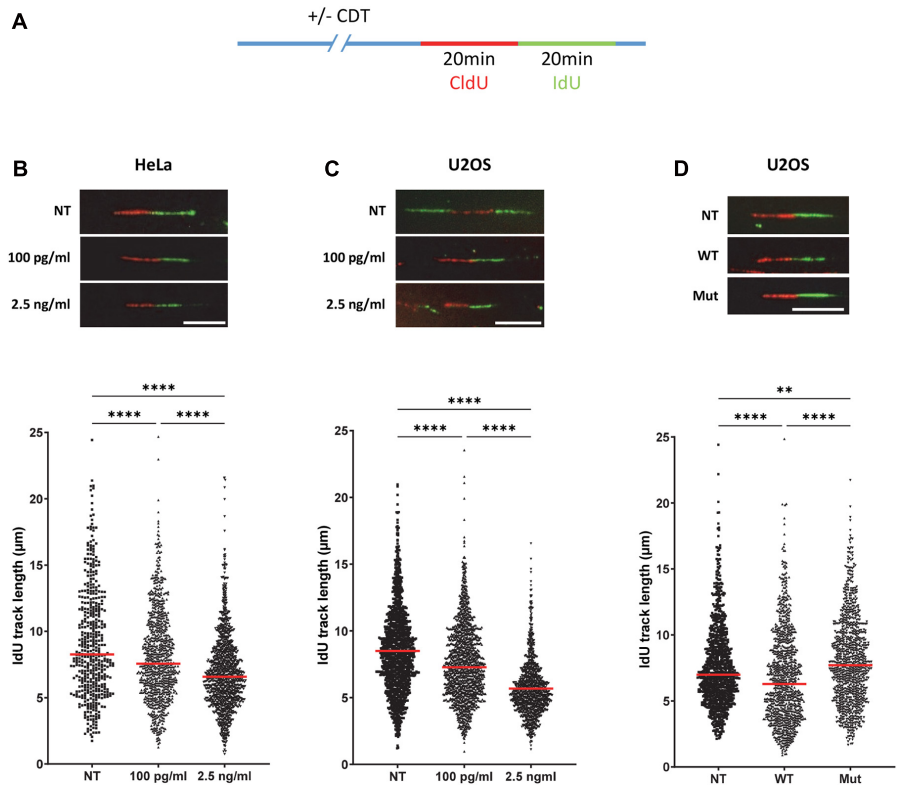

FIGURE 1 | The catalytic activity of cytolethal distending toxin (CDT) induces a replicative stress. **(A)** Cells were incubated or not with CDT holotoxins during several hours before successive pulse labeling with 5-chlorodeoxyuridine (CldU) and 5 iododeoxyuridine (IdU). Then, replication fork speed was analyzed by DNA fiber assay. IdU track length was determined. **(B–D)** Upper panel: representative images of replication tracks: CldU (red) and IdU (green) ($n > 400$ IdU tracks were measured with a wide-field fluorescent microscope, original magnification × 40, scale bar: 10 µm). Lower panel: horizontal red lines represent the median (**$P < 0.01$, ****$P < 0.0001$). **(B)** HeLa cells were treated or not (NT) with 100 pg/ml or 2.5 ng/ml of CDT from *E. coli* for 16 h before IdU and CldU staining. **(C)** U2OS cells were treated or not with the same doses of CDT from *H. ducreyi* for 24 h before the replication staining. **(D)** U2OS cells were treated or not with 2.5 ng/ml of wild-type (WT) or catalytically inactive mutant (Mut) of CDT from *H. ducreyi* for 24 h before IdU and CldU incorporation.

prone to breakage upon moderate replicative stress and the main source of genomic instability in precancerous lesions and cancer development (Gorgoulis et al., 2005; Durkin and Glover, 2007; Bignell et al., 2010; Georgakilas et al., 2014). Therefore, we explored CFS stability by using a FISH (fluorescence *in situ* hybridization)-based assay after cell treatment with CDT. We quantified the percentage of cells with rearrangements (translocation, amplification, or deletion) that localized to the FRA7H and FRA16D fragile sites. For that, we used U2OS cell line in which these fragile sites are not already rearranged. As shown in **Figures 3A,B**, we highlighted a significant increase in the expression of both fragile sites in cells exposed to the genotoxin compared to control cells, supporting that the replicative stress induced by CDT may contribute to the establishment of genomic instability by at least expression of fragile sites.

Afterward, we investigated the consequences of CDT exposure on the global chromosomal integrity. Metaphase spreads revealed that after CDT intoxication, the U2OS cell proportion with structural abnormalities significantly increased compared to control cells (**Figures 3C,D**). Chromatid breaks, end-to-end fusions, and radial chromosomes were observed (see **Figure 3C** for examples), depicting a huge chromosomal instability induced by the toxin. Then, we monitored chromosome segregation in anaphase and highlighted a significant increase of cells with persistent physical connections between the two DNA batches called DNA bridges after CDT treatment compared to control cells (**Figures 3E,F** and **Supplementary Figure 1**). These results suggest that the chromosomal abnormalities induced by CDT impair proper chromosome segregation in anaphase.

Genetic Instability Driven by CDT Is Transmitted to Daughter Cells

To deeper understand the fate of cells presenting these mitotic defects, we monitored chromatin abnormalities in interphase. Strikingly, nuclei connected with a thin chromatin bridge stained with DAPI appeared more frequently after exposure to wild-type CDT from *E. coli* or *H. ducreyi* than in untreated HeLa cells or cells treated with the catalytic dead CDT mutant (**Figures 4A–C**). These persisting DNA double-stranded structures (DAPI-positive bridges) present in interphase between daughter cells could reflect a failure of anaphase bridge resolution during mitosis and transmitted to the next generation. To evaluate

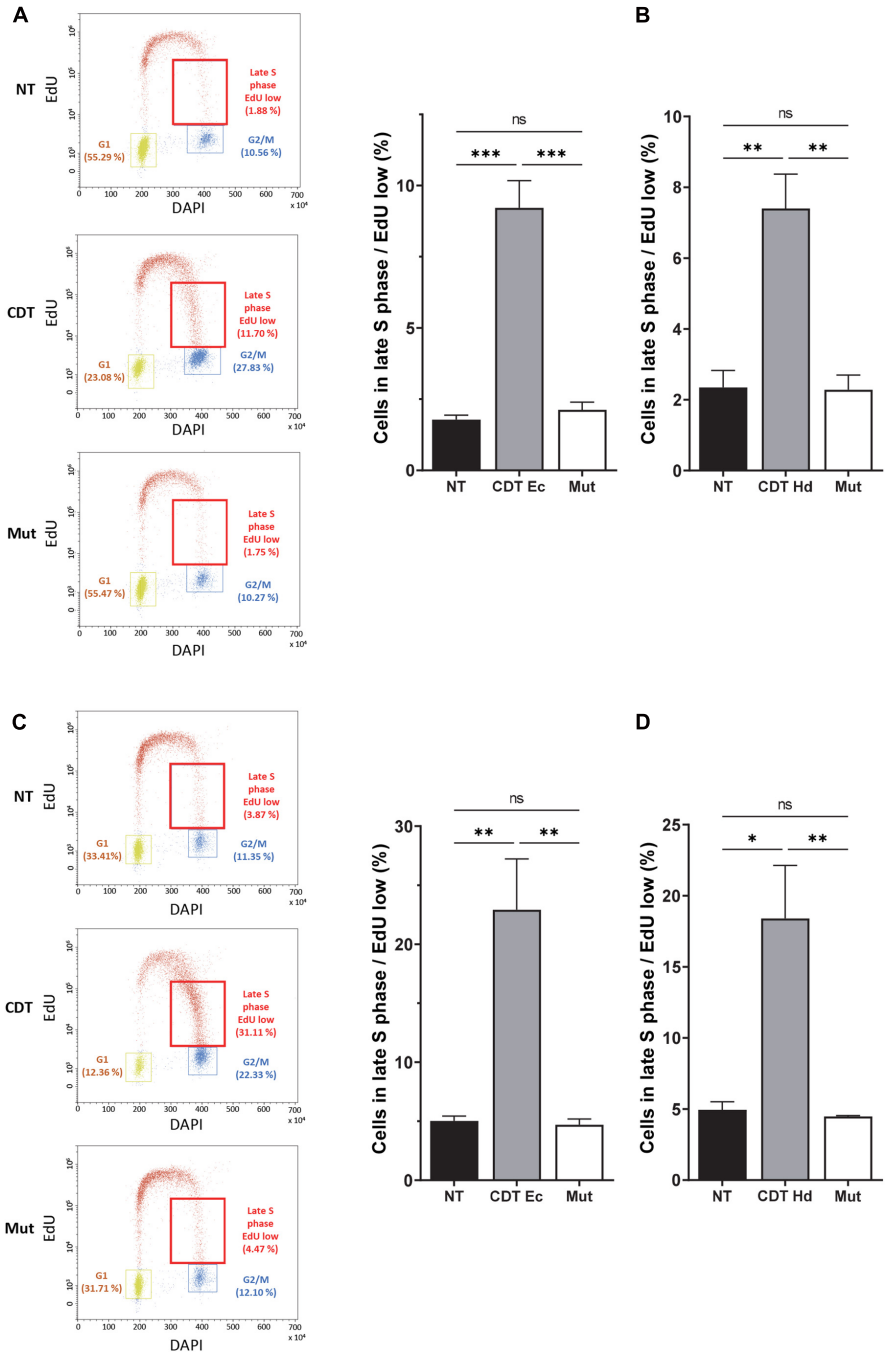

FIGURE 2 | CDT causes a slowdown of DNA replication in the late S phase. Cell cycle analysis by flow cytometry of HeLa **(A,B)** and U2OS **(C,D)** cells treated or not with 2.5 ng/ml of wild-type or catalytically inactive CDT mutant (Mut) from *E. coli* (CDT Ec) **(A,C)** or *H. ducreyi* (CDT Hd) **(B,D)** for 16 h was performed. **(A,C)** Left panel: representative flow cytometry of cells treated with CDT Ec is shown. EdU incorporation is plotted against the cellular DNA content (DAPI). Quantification of G1, G2, and late S cell population with low EdU (red boxes) is indicated. Right panel: data represent the percentage of EdU weakly positive cells in the late S phase. At least 10,000 events were analyzed per sample using the CytExpert software (mean ± SEM of at least three independent experiments) (*$P < 0.05$, **$P < 0.01$, ***$P < 0.001$, and ns, not significant).

whether the replicative stress induced by CDT exposure could be involved in the formation of DNA bridges observed in interphase, we quantified the percentage of cells in interphase presenting DNA bridge after or no treatment with an ATR inhibitor (ATRi). First, we confirmed that wild-type CDT, but not the catalytically inactive CDT mutant, induces the phosphorylation of replication protein A (RPA) on serine 33, an ATR-specific target. RPA phosphorylation was also impaired after ATRi

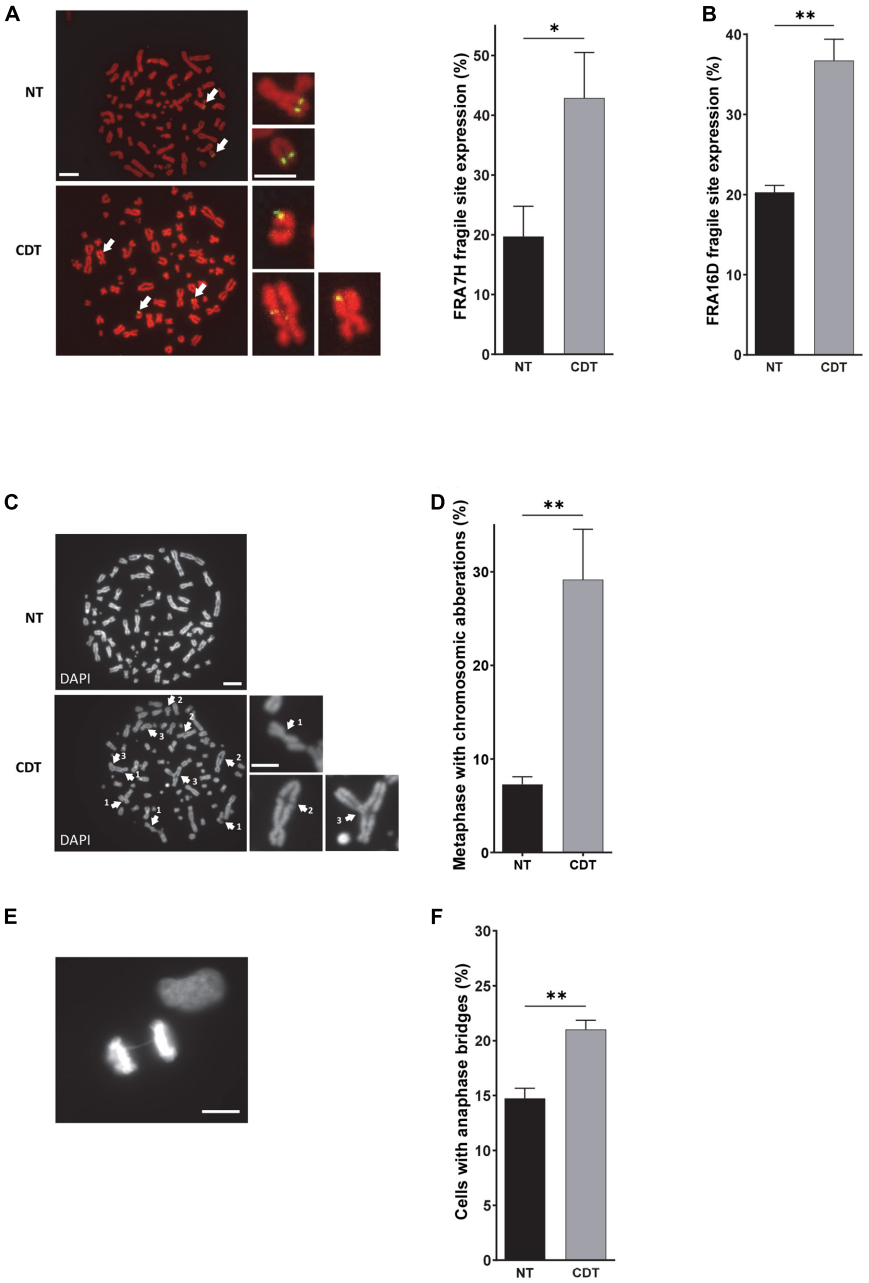

FIGURE 3 | CDT induces the expression of fragile sites, global chromosomic aberrations, and anaphase bridges. **(A)** Illustration and quantification of metaphases with the expression of the common fragile site FRA7F (green) analyzed by fluorescence *in situ* hybridization (FISH) in U2OS cells treated or not with 250 pg/ml of CDT from *E. coli* (CDT). The chromosomes were stained with DAPI (red). Images were obtained with a wide-field fluorescent microscope. $N > 30$ metaphases, scale bar: 10 μm (5 μm, chromosome magnification). **(B)** Quantification of metaphases with the expression of the common fragile site FRA16D analyzed by FISH in U2OS cells treated or not (NT) with *E. coli* CDT (CDT) for 53 h. Illustration **(C)** and quantification **(D)** of metaphases containing at least one chromosomic aberration in U2OS cells treated or not (NT) with 250 pg/ml of CDT from *E. coli* (CDT) during 53 h. The chromosomes were stained with DAPI (grayscale). Images were obtained with a wide-field fluorescent microscope. $N > 60$ metaphases; white arrows indicate chromosomal abnormalities such as DNA break (1), end-to-end fusion (2), and triradial chromosomes (3). Scale bar: 10 μm (5 μm, chromosome magnification). Representative image of DAPI (grayscale) staining **(E)** and quantification **(F)** of anaphases with DNA bridge in HeLa cells treated or not (NT) with 100 pg/ml of CDT from *E. coli* (CDT) for 24 h. $N > 90$ anaphases were analyzed with a wide-field fluorescent microscope. Scale bar: 10 μm (mean ± SEM of at least three independent experiments) [$^{*}P < 0.05$, $^{**}P < 0.01$, *versus* non-treated (NT)].

treatment (**Supplementary Figure 2**). Furthermore, as shown in **Figure 4D**, ATRi alone did not induce DNA bridges. However, the co-treatment with CDT and ATRi significantly increase the percentage of cells connected with a DAPI-positive DNA bridge compared to CDT-intoxicated cells without ATRi (14.9% *versus* 28.1% for the CDT highest dose). These data support the

major role of ATR to limit the formation of aberrant chromatin structure between daughter cells induced by CDT and sustain the involvement of replicative stress to drive genetic instability.

To further characterize the nature of DNA bridges formed after CDT intoxication, we asked whether single-stranded structures may link nuclei of daughter cells. To this end, we monitored the recruitment on the bridge of RPA, a protein known to cover and protect single-stranded DNA (**Figures 4E,F**). We found that CDT exposure stimulates the formation of RPA-positive bridges connecting the nuclei of daughter cells compared to untreated cells (2.5 *versus* 5.6%) but likely at a lesser extent compared to double-stranded bridges (compare **Figures 4B,F**). Altogether, these results demonstrate that single- and double-stranded DNA bridges connecting the nuclei of daughter cells increase after CDT intoxication, suggesting the transmission of aberrant chromatin structures to the next cell generation.

Then, we analyzed the impact of interphase bridges on cell cycle progression. To address this question, we performed EdU incorporation to track cells in the S phase, together with cyclin A immunostaining to monitor cells in the G1 phase (cyclin A-negative cells) (**Figure 4G**). We show that without CDT treatment, cells connected with a chromatin bridge are mainly in the G1 phase of the cell cycle (78.6%). In agreement with previously reported cell cycle arrest, CDT exposure seems to induce an accumulation of cells not linked with a DNA thread in the G2 phase (8.4% of untreated cells are in G2 *versus* 28.7% after treatment with 2.5 ng/ml of CDT) correlated with a decrease of G1 phase (41.5% of untreated cells are in G1 *versus* 21.5% after treatment with 2.5 ng/ml of CDT) (**Figures 2A**, **4G**). However, cells connected with a bridge are mainly in the G1 phase with a slight but not significant increase in the S phase after CDT treatment (**Figure 4G**). These data suggest that CDT intoxication promotes the emergence of DNA thread between cells mostly in the G1 phase of the cell cycle, probably until their resolution before or within the next S phase.

To determine whether replicative stress could be the cause of G1 cells connected with a thin DNA thread, we monitored Rap1 interacting factor 1 (RIF1) foci formation. RIF1 constitutes a major factor playing a crucial role in genome maintenance after replicative stress. Indeed, RIF1 is associated with stalled DNA replication forks favoring their restart (Buonomo et al., 2009; Alabert et al., 2014; Garzón et al., 2019; Mukherjee et al., 2019). Moreover, RIF1 was recently found to carry out its activity during and after a perturbed S phase to protect against replicative stress throughout the cell cycle and to ensure chromosome integrity (Harrigan et al., 2011; Lukas et al., 2011; Moreno et al., 2016; Watts et al., 2020). Whatever the presence or absence of chromatin bridges, CDT intoxication induces a significant increase in the percentage of RIF1-positive cells, compared to untreated cells (from 6.5 to 64.5% RIF1-positive cells among the cells not linked with a bridge and from 31.1 to 90.8% RIF1-positive cells among those connected with a DNA bridge) (**Figure 4H**). Moreover, a significant increase of RIF1-positive cells was observed in G1 (cyclin A-negative cells) for cells linked with DNA thread, in contrast to cells without DNA bridge. Indeed, among cells connected with a DNA bridge, 28.9% are RIF1 positive in the G1 phase in untreated condition compared to 69.2% after CDT exposure to 2.5 ng/ml. Our finding thus indicates that CDT treatment causes a massive RIF1 recruitment, not only in the G1 phase in nuclei linked with a DNA bridge but also in S and G2 in cells without an interphase bridge.

CDT Promotes γH2AX Foci Formation in Cycling Cells

As we observed that CDT intoxication leads to replicative stress, we hypothesized that proliferating cells could be more sensitive to the toxin compared to quiescent cells. To address this question, quiescence was induced in RKO human colonic cells by confluence and serum starvation (**Supplementary Figure 3**). Then, cycling or quiescent cells were incubated with CDT holotoxin from *E. coli*, and DNA damage induction was measured through γH2AX immunostaining and analyzed by the ArrayScan technology (**Figure 5A**). In cycling cells, cell cycle distribution was established according to DAPI signal intensity. In quiescent cells (G0) exposed to CDT, no significant variation of γH2AX foci number per cell or in the proportion of γH2AX-positive cells (with more than four foci) was observed (**Figures 5B,C**). However, CDT-intoxicated cycling cells presented more γH2AX foci per cell, and the percentage of γH2AX-positive cells significantly increased compared to untreated cells, especially in the S and G2 phases (**Figures 5B,C**). These data are consistent with the induction of replicative stress (**Figure 1**) and support the notion that proliferating cells could be more sensitive than quiescent cells to the genotoxicity induced by CDT.

To reinforce this finding in a more physiological model, we used human organoids in culture. As CDT-producing *E. coli* were associated with colorectal cancer (Buc et al., 2013), we performed human colorectal organoid culture in the presence of CDT holotoxin from *E. coli*. Human colon crypts were purified from fresh biopsies from healthy donors. In order to get as close as possible to the physiological context, isolated crypts were seeded in 3D Matrigel and directly incubated with the CDT holotoxin from *E. coli* during 16 h, time required for the opened crypts to seal and form cysts. Then, the free toxin was removed from the medium but not the one trapped in the cyst, and the organoid growth was monitored during 8 days. This protocol has the advantage of exposing fresh crypts to CDT and assessing the toxin impact on the organoid growth during several days without passaging and therefore maintaining their integrity. **Figures 6A,B** illustrates that colorectal organoid size was significantly smaller after 8 days of CDT exposure compared to untreated organoids. Organoids were also incubated with a mutated CDT (CDT^{H153A}), in which histidine 153, a crucial residue for the catalytic activity of CdtB, was replaced by an alanine (Elwell and Dreyfus, 2000). The organoid size was not significantly affected by exposure to the catalytic inactive CDT mutant. Then, we asked whether the CDT-induced organoid growth defect could be due to a slowing down of cell proliferation. To achieve this, we monitored proliferating cells with EdU incorporation after CDT intoxication of colorectal organoids (**Figure 6C**). First, as expected, we observed a significant decrease in the EdU-positive cell proportion from day 4 to day 8 without any treatment, confirming a decrease of cell proliferation during

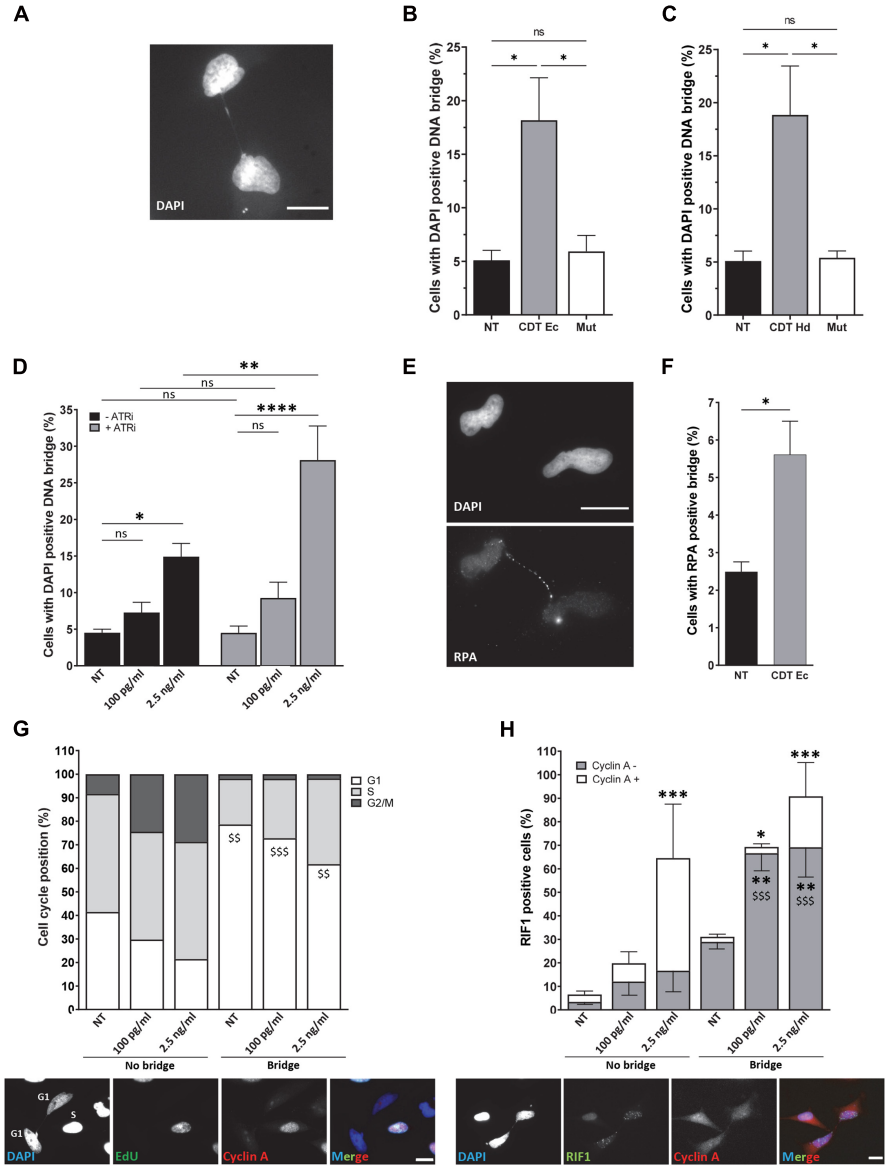

FIGURE 4 | ATR prevents the formation of persistent DNA bridges between G1 daughter cells. Illustration **(A)** and quantification **(B)** of HeLa cells with DAPI-positive DNA bridge (grayscale) after treatment or not (NT) with 2.5 ng/ml of wild-type (CDT Ec) or catalytically inactive CDT mutant (Mut) from *E. coli* for 24 h. $N > 500$ cells were analyzed with a wide-field fluorescent microscope. Scale bar: 20 μm. **(C)** Quantification of HeLa cells with DAPI-positive DNA bridge after treatment or no treatment (NT) with 2.5 ng/ml of wild-type (CDT Hd) or catalytically inactive CDT mutant (Mut) from *H. ducreyi* for 24 h. $N > 500$ cells were analyzed with a wide-field fluorescent microscope (mean ± SEM of four independent experiments) ($^{*}P < 0.05$, ns, not significant). **(D)** Quantification of HeLa cells with DAPI-positive DNA bridge after treatment or non-treatment (NT) with 100 pg/ml or 2.5 ng/ml of CDT from *E. coli* and ATR inhibitor (ATRi) for 24 h. $N > 500$ cells were analyzed with a wide-field fluorescent microscope (mean ± SEM of four independent experiments) ($^{*}P < 0.05$, $^{**}P < 0.01$, $^{****}P < 0.0001$; ns, not significant). **(E)** Representative images of replication protein A (RPA) immunostaining (grayscale) and quantification **(F)** of HeLa cells with RPA-positive DNA bridge after treatment or no treatment (NT) with 2.5 ng/ml of CDT from *E. coli* (CDT Ec) for 24 h. Nuclei were stained with DAPI (grayscale) and $n > 500$ cells were analyzed with a wide-field fluorescent microscope. Scale bar: 20 μm (mean ± SEM of four independent experiments) [$^{*}P < 0.05$, *versus* non-treated (NT)]. **(G)** Upper panel: quantification of cell cycle position of HeLa cells linked or not with a bridge after *E. coli* CDT treatment [100 pg/ml or 2.5 ng/ml or non-treated (NT)] for 24 h (mean ± SEM of three independent experiments). Cyclin A and EdU-negative cells are counted in G1, cyclin A, and EdU-positive cells in S and cyclin A-positive and EdU-negative cells in G2. Lower panel: representative images of EdU (grayscale) and cyclin A (grayscale) immunostaining of HeLa cells treated with CDT from *E. coli* (2.5 ng/ml) for 24 h. Nuclei were stained with DAPI (grayscale). Merge was performed with DAPI (blue), EdU (green), and cyclin A (red) images. $N > 100$ cells were analyzed with a wide-field fluorescent microscope. Scale bar: 20 μm ($^{\$\$}P < 0.01$, $^{\$\$\$}P < 0.001$ *versus* no bridge at the same CDT dose for the G1 phase). **(H)** Upper panel: quantification of positive HeLa cells for RIF1 ± cyclin A staining after *E. coli* CDT treatment [100 pg/ml or 2.5 ng/ml or non-treated (NT)] for 24 h (mean ± SEM of three independent experiments) [$^{*}P < 0.05$, $^{**}P < 0.01$, $^{***}P < 0.001$ *versus* non-treated (NT) and $^{\$\$\$}P < 0.001$ *versus* no bridge at the same CDT dose]. Lower panel: representative images of RIF1 (grayscale) and cyclin A (grayscale) immunostaining of HeLa cells treated with CDT from *E. coli* (2.5 ng/ml) for 24 h. Nuclei were stained with DAPI (grayscale). Merge was performed with DAPI (blue), RIF1 (green), and cyclin A (red) images. $N > 100$ cells were analyzed with a wide-field fluorescent microscope. Scale bar: 20 μm.

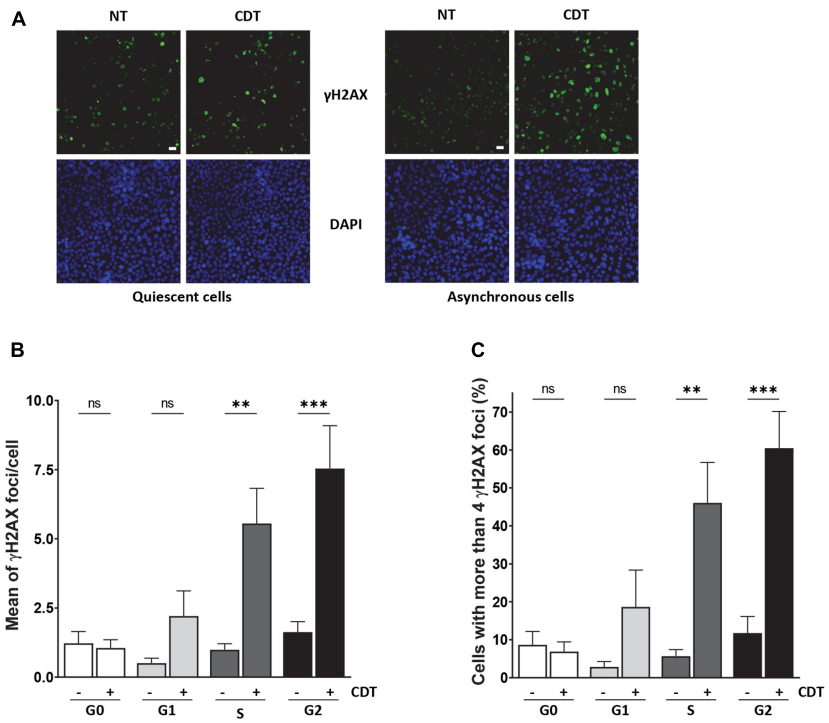

FIGURE 5 | CDT induces γH2AX foci formation preferentially in proliferating cells. **(A)** Representative images of γH2AX (green) immunostaining in quiescent or proliferating RKO cells after exposure or non-exposure (NT) with *E. coli* CDT (25 ng/ml) for 7 h. DNA was stained with DAPI (blue). Scale bar: 20 μm. **(B)** Quantification by ArrayScan analysis of γ-H2AX foci formation in quiescent or proliferating RKO cells sorted according to cell cycle phase after CDT treatment from *E. coli* (25 ng/ml) for 7 h. **(C)** Quantification of γH2AX-positive cells with > 4 foci/nuclei in cells treated as in **(B)**. For each analysis, a minimum of 1,000 cells were analyzed with a wide-field fluorescent microscope (ArrayScan technology) in three independent experiments [$^{**}P < 0.01$, $^{***}P < 0.001$ *versus* non-treated (NT); ns, not significant].

the organoid differentiation process. Moreover, exposure to wild-type CDT generated a huge decrease of cell proliferation at day 4, which was maintained until day 8. In contrast, treatment with CDT-catalytic-dead mutant did not significantly alter cell proliferation. Collectively, these data indicate that CDT affects cell proliferation through its catalytic activity, impairing organoid growth. Furthermore, as shown in **Figure 6D**, nucleus size increased from day 4 at both doses of CDT and became much larger on day 8 after CDT treatment at 25 ng/ml, highlighting a nuclear distension in human colorectal organoids, characteristic of CDT intoxication. However, we did not observe any significant variation after intoxication with the catalytic inactive mutant of CDT underlining the importance of its catalytic activity in this process. As CDT induces replicative stress (**Figure 1**), we finally wondered whether CDT intoxication could generate γH2AX accumulation in proliferating cells. For this purpose, we analyzed the proportion of γH2AX-positive cells in the EdU-positive cell population (**Figures 6E,F**). Interestingly, these experiments revealed that 4 days after toxin exposure with 25 ng/ml of CDT, the proportion of γH2AX-positive cells in proliferating cells (EdU+) was higher in intoxicated organoids compared to controls. In addition, 8 days after CDT intoxication, this increase was maintained in the cells, keeping their proliferation status. Finally, no significant variation was observed after intoxication of organoids with the CDT catalytic inactive mutant, indicating that γH2AX accumulation in proliferating cells of human colorectal organoids is dependent on its catalytic activity. Altogether, our results indicate that CDT induces γH2AX accumulation in proliferating cell population persisting through human colorectal organoid differentiation (day 8).

DISCUSSION

Cytolethal distending toxin produced by several bacterial strains was reported to promote not only cancer hallmark acquisition in chronically intoxicated cells but also tumorigenesis in mice models (Ge et al., 2007, 2017; Guidi et al., 2013; Graillot et al., 2016; He et al., 2019). Although some evidences support that CDT generates DNA breaks associated with genetic instability such as mutagenesis, chromatin and chromosomal abnormalities, and micronucleus formation (Frisan et al., 2003; Fedor et al., 2013; Guidi et al., 2013), the mechanism leading to cancer development is still unclear. Indeed, data are still lacking to explain how DNA breaks drive genetic instability transmitted to the next generation and to characterize CDT cellular targets allowing a better understanding of CDT *in vivo* tumorigenic properties. For this, mechanism-based approaches were led not only in HeLa cells, widely used for CDT studies, but also in U2OS cells, two well-characterized cellular models. In addition, RKO

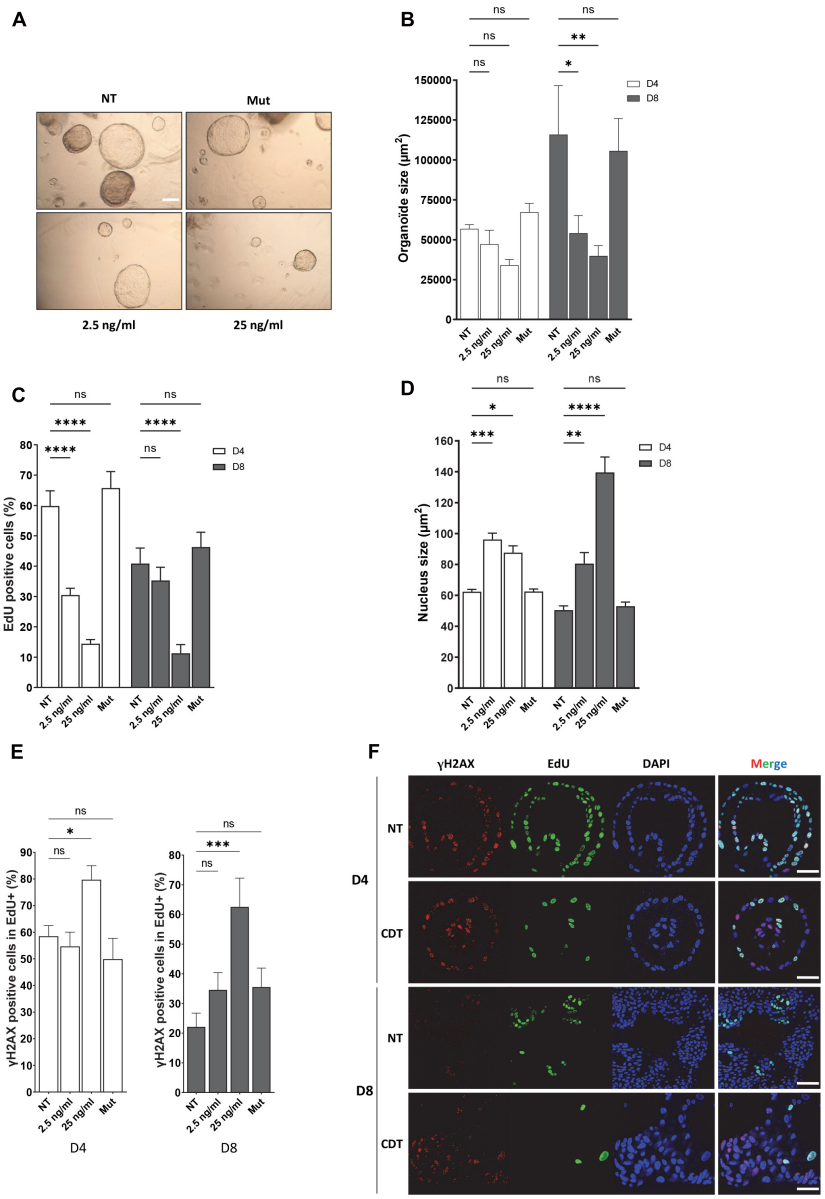

FIGURE 6 | CDT causes nuclear distension associated with DNA damage in cycling cells of human colorectal organoids leading to decrease of growth. Human colorectal crypts were treated at day 0 with wild-type (2.5 and 25 ng/ml) or catalytic inactive mutant (H153A, 25 ng/ml, Mut) of CDT from *E. coli* for 16 h. **(A)** Representative images of organoids at day 8 with a bright-field microscope. Scale bar: 200 µm. **(B)** At days 4 and 8 of culture, organoid size was measured. $N > 10$ organoids. **(C)** EdU was added to the organoid culture medium for 16 h before fixation. Then, EdU was revealed and EdU-positive cells per organoid were quantified by confocal analysis. $N > 6$ organoids. **(D)** At days 4 (D4) and 8 (D8) of culture, organoid nucleus size was analyzed by confocal microscopy. $N > 6$ organoids. **(E,F)** At day 4 (D4) or 8 (D8), EdU was added to the organoid culture medium for 16 h before fixation and revealed. Then, γH2AX immunostaining was performed and γH2AX-positive cells in proliferating cell population (EdU+) from organoids were quantified. $N > 6$ organoids. **(F)** Representative images of EdU (green) and γH2AX (red) immunostaining in human colorectal organoids at days 4 (D4) and 8 (D8) treated or non-treated (NT) with 25 ng/ml of *E. coli* CDT were obtained from confocal analysis. Scale bar: 50 µm (mean ± SEM of at least three independent experiments) [$^{*}P < 0.05$, $^{**}P < 0.01$, $^{***}P < 0.001$, $^{****}P < 0.0001$ *versus* non-treated (NT); ns, not significant].

colorectal cells and human colorectal organoids were used to investigate the physiological impact of CDT. Here, we report that CDT exposure leads to a replicative stress associated with mitotic aberrations and persistent chromatin abnormalities connecting daughter cells in G1. Our data start to fill the knowledge gap by highlighting that the proliferative status of CDT host cells may be crucial and determine the tumor cell fate. To our knowledge, this is the first time that the impact of CDT intoxication is directly addressed in human organoids from healthy donors.

First, we demonstrate that CDT exposure induces a dose-dependent slowing down of replicative fork dynamic in HeLa and U2OS cells. Since these results were independent of the

human cell type and CDT-producing strains, and given that the catalytic mutant has no effect on the fork velocity, we can speculate that the replicative stress induced by CDT could be a general mechanism consecutive to DNA breaks. These data reinforce our previous report indicating that CDT-induced SSB are converted into DSB upon DNA replication resulting in S phase delay (Fedor et al., 2013). Moreover, single-stranded DNA coated by RPA obtained after CDT treatment suggests uncoupling between replicative helicase and DNA polymerases (Fedor et al., 2013). Subsequently, ATR-dependent replicative stress response and FA pathway seem to be required to overcome the replication fork stalling induced by CDT (Fahrer et al., 2014; Bezine et al., 2016). Altogether, these evidences hint at a CDT-induced replicative stress that we definitively confirmed with replication fork progression defects on single DNA fibers. Our finding substantiates the importance of cell proliferation for CDT genotoxicity. Other workers have suggested that the S phase could be crucial for CDT intoxication. Indeed, Comayras et al. (1997) showed that most cells exposed to CDT in G2 and M were arrested only at the subsequent late G2 phase, in contrast to cells intoxicated in G1 or S phase, which were blocked in the G2 phase of the current cell cycle (Comayras et al., 1997; Sert et al., 1999). These results support that the passage through the S phase is required for CDT to exert its toxic effect in good agreement with the CDT-mediated replicative stress. Thus, it is reasonable to think that CDT activity may be mainly directed to single-stranded DNA predominantly generated during the DNA replication process. We can speculate that some DNA regions prone to adopt single-stranded DNA structure could also constitute CDT favor substrates. Moreover, since the slowing down of DNA replication occurs mainly in the late S phase after CDT exposure, CFS represent excellent target candidates. Indeed, in addition to their late replication and their high sensitivity to moderate replicative stress, their fragility can be explained by several features such as an enrichment in large genes, poor in DNA replication origins, forming secondary DNA structures due to AT-rich sequences and linked to 3D genome organization (Georgakilas et al., 2014; Sarni et al., 2020). Consequently, we detected a significant increase in FRA7H and FRA16D fragile site expression upon CDT exposure supporting our hypothesis and illustrating the consequences of the replicative stress. Furthermore, CDT-intoxicated cells displayed various chromosomal abnormalities in metaphase, showing that the host cells unsuccessfully repaired some CDT-induced DNA strand breaks. This suggests that CDT could also target DNA regions other than CFS that might be interesting to characterize in order to deepen CDT mode of action.

Interestingly, our finding revealed a higher frequency of anaphase and interphase DNA bridges after acute exposure to the genotoxin. These bridges may arise from end-to-end chromosome fusions after CDT-induced DNA breakage mentioned above or by incomplete DNA replication, as ATRi treatment amplified their occurrence. Since interphase bridges increase after CDT exposure, we can speculate that some anaphase chromosome bridges persist for many hours into the subsequent cell cycle without breaking as sustained by previous studies (Steigemann et al., 2009; Maciejowski et al., 2015; Pampalona et al., 2016; Umbreit et al., 2020). Finally, a recent work indicates that the bridges broke later, requiring actomyosin forces and initiating chromothripsis, which is further amplified through each mitosis leading to frequent mis-segregation (Umbreit et al., 2020). This is in accordance with our data showing that anaphase and interphase bridges appeared 1 or 2 days, respectively, after acute CDT treatment, thus constituting an early process in the genetic instability setting up. Moreover, they seem to be maintained after chronic intoxication to CDT (Guidi et al., 2013). We further showed that cells with a cytoplasmic DNA bridge are preferential in the G1 phase. This finding suggests that inheritance of lesions from previous cell cycle may correlate with a G1 delay in the next one. This data is in agreement with the work of Lezaja and Altmeyer (2018) highlighting the correlation between the amount of replication remnants and the next G1 duration. Therefore, unresolved DNA damage generated by CDT intoxication would be transmitted to the daughter cells and constitute a major source of genomic instability.

Then, we observed that human quiescent cells seem to be less sensitive to *E. coli* CDT exposure than proliferating cells, supporting the requirement of S phase progression for DNA damage expansion and genetic instability setting up. However, previous studies reported that, despite toxicity was dependent on cell differentiation stage, *A. actinomycetemcomitans*, *H. ducreyi*, or *C. jejuni* CDT can also intoxicate non-proliferating monocyte cells such as dendritic cells and macrophages, resulting in apoptosis cell death (Li et al., 2002; Xu et al., 2004; Hickey et al., 2005; Rabin et al., 2009). This suggests that CDT intoxication does not imperatively require replicative stress induction for killing its cell hosts. However, the previous works only focused on the CDT-mediated DNA damage and/or apoptosis but never monitored the fate of the genetic instability mediated by the toxin. To date, the importance of cell proliferation status on CDT toxicity was never addressed in non-hematological cells. Here, we address for the first time this question in colorectal cells. Thus, these discrepancies could be due to cell type specificity. Furthermore, the methodology that we employed constitutes a physiological process to push proliferating cells in quiescence by confluence and serum starvation. This protocol presents the advantage of comparing the same cell type in two different cell cycle stages (G0 phase *versus* cycling cells), without differentiation induction. Nonetheless, the cellular and molecular modifications induced by quiescence may not be comparable to those operating during the proliferation arrest accompanying the differentiation process. Finally, we cannot exclude that higher CDT doses could induce some DNA damage in quiescent cells. However, our data clearly established that cycling cells are far more sensitive.

To deeper understand the CDT mechanism of action in a more complex and physiological model, we used human colorectal organoids. Fresh human colorectal crypts from healthy donors were directly exposed to *E. coli* CDT until its trapping inside the cysts. This model mimics physiological CDT exposure to the crypts and allows us to monitor organoid growth during several days (8 days), without disrupting the structures, and address

different questions. Our data substantiate that, in addition to inducing nuclear distension, CDT intoxication strongly affects colorectal organoid growth by reducing the proliferating rate at least up to 8 days. However, the remaining cycling cells displayed a γH2AX increase a few days after CDT exposure, suggesting either the genotoxin is always active and continuously harms DNA or not all DNA lesions are completely repaired, meaning a persistence of DNA damage over time. After 8 days of organoid culture, stem cells and progenitors should constitute remaining cycling cells, suggesting that CDT could target these cell types and induce DNA injuries. Surprisingly, a high basal level of γH2AX was observed in untreated organoids at 4 days of culture, which can be explained by the high rate of proliferating cells (EdU+) owing to the greatly increased number of S phase occurring in these cells to quickly generate a mature organoid structure. Consequently, cycling cells from colorectal organoids could be more vulnerable to DNA damage during replication such as replication fork collapse leading to DNA breaks. Indeed, embryonic stem cells display marks of replicative stress associated with fast proliferation, and then the constitutive DNA damage response activation is rapidly abolished during differentiation (Ahuja et al., 2016). Moreover, the intestinal epithelium renewing supported by the intestinal stem cells is very frequent with a replacement every 4–5 days, revealing a huge proliferation rate to maintain the tissue homeostasis (Vermeulen and Snippert, 2014). Nevertheless, we cannot exclude that crypt isolation followed by the *in vitro* culture also generates cellular stress responsible for γH2AX induction during the first days.

In conclusion, this model highlights that human primary colorectal cells respond to CDT intoxication by a cell cycle arrest induction. However, a weak proportion of persistent cycling cells is present in mature organoids after CDT exposure. Because these cycling cells display more DNA lesions, probably due to their increased proliferation rate, they are likely to transmit DNA defects on the next generation. Unrepaired or incorrectly repaired lesions might then enhance the probability of mutation accrual, affecting genomic stability and promoting tumor initiation. Moreover, inflammatory context such as chronic inflammatory bowel disease may constitute a permissive environment for CDT intoxication predisposing to tumor progression. Finally, this work raises several questions such as the CDT impact on colorectal differentiation process, as well as its effect on epithelial barrier permeability. Further studies will be required to test these hypotheses, answer these questions, and fully understand CDT pathogenicity.

DATA AVAILABILITY STATEMENT

The original contributions presented in the study are included in the article/**Supplementary Material**, further inquiries can be directed to the corresponding author/s.

ETHICS STATEMENT

The studies involving human participants were reviewed and approved by the ethics committee "comité de protection des personnes du Sud-ouest et Outre-mer II, agence régionale de Santé Midi-Pyrénées" (NCT 02874365). Written informed consent to participate in this study was provided by the participants' legal guardian/next of kin.

AUTHOR CONTRIBUTIONS

AF-V designed, conceived, and supervised the study. AF-V, WT, EL, FM, and SH performed the experiments, analyzed the data, and prepared draft figures. EM, LA, and DB performed the endoscopies and the biopsies, and AF and MQ provided their expertise on organoid culture. JV purified CDT holotoxins and provided his expertise on CDT. VB provided BAC probes, material, and her expertise for FISH experiment and helped to edit the manuscript. AF-V prepared the manuscript draft with important intellectual input from JV, DT, AF, and GM. All authors approved the final manuscript. GM and AF-V obtained funding.

FUNDING

This work was supported by a grant from La Ligue Contre le Cancer (Haute-Garonne's committee) (AF-V) and ANR-10-CESA-0011 and ANR-14-CE21-0008 programs (GM).

ACKNOWLEDGMENTS

The authors would like to thank Thierry Gauthier, Brice Ronsin, and Stéphanie Bosch from the Imaging Core Facility of Toxalim/INRAE and CBI/CNRS, respectively, for their help with image acquisition and Mathieu Vigneau from ITAV for the ArrayScan training. Pr. Elisa Boutet-Robinet is also greatly acknowledged for the use of her Nikon wide-field microscope as well as the associated software for the DNA spreading experiments. The authors would also like to thank Yvan Canitrot for his advice on the manuscript. Finally, they would also like to thank the patients who have agreed on providing their tissues for research use and the DGOS (Organization de la Direction générale de l'offre de soins) for the funding of the Centre de référence des Maladies Rares Digestives.

SUPPLEMENTARY MATERIAL

The Supplementary Material for this article can be found online at: https://www.frontiersin.org/articles/10.3389/fcell.2021.656795/full#supplementary-material

REFERENCES

Ahuja, A. K., Jodkowska, K., Teloni, F., Bizard, A. H., Zellweger, R., Herrador, R., et al. (2016). A short G1 phase imposes constitutive replication stress and fork remodelling in mouse embryonic stem cells. *Nat. Commun.* 7:10660. doi: 10.1038/ncomms10660

Alabert, C., Bukowski-Wills, J.-C., Lee, S.-B., Kustatscher, G., Nakamura, K., de Lima Alves, F., et al. (2014). Nascent chromatin capture proteomics determines

chromatin dynamics during DNA replication and identifies unknown fork components. *Nat. Cell Biol.* 16, 281–293. doi: 10.1038/ncb2918

Alaoui-El-Azher, M., Mans, J. J., Baker, H. V., Chen, C., Progulske-Fox, A., Lamont, R. J., et al. (2010). Role of the ATM-checkpoint kinase 2 pathway in CDT-mediated apoptosis of gingival epithelial cells. *PLoS One* 5:e11714. doi: 10.1371/journal.pone.0011714

Bezine, E., Malaisé, Y., Loeuillet, A., Chevalier, M., Boutet-Robinet, E., Salles, B., et al. (2016). Cell resistance to the Cytolethal distending toxin involves an association of DNA repair mechanisms. *Sci. Rep.* 6:36022. doi: 10.1038/srep36022

Bignell, G. R., Greenman, C. D., Davies, H., Butler, A. P., Edkins, S., Andrews, J. M., et al. (2010). Signatures of mutation and selection in the cancer genome. *Nature* 463, 893–898. doi: 10.1038/nature08768

Blazkova, H., Krejcikova, K., Moudry, P., Frisan, T., Hodny, Z., and Bartek, J. (2010). Bacterial intoxication evokes cellular senescence with persistent DNA damage and cytokine signalling. *J. Cell. Mol. Med.* 14, 357–367. doi: 10.1111/j.1582-4934.2009.00862.x

Buc, E., Dubois, D., Sauvanet, P., Raisch, J., Delmas, J., Darfeuille-Michaud, A., et al. (2013). High prevalence of mucosa-associated *E. coli* producing cyclomodulin and genotoxin in colon cancer. *PLoS One* 8:e56964. doi: 10.1371/journal.pone.0056964

Buonomo, S. B. C., Wu, Y., Ferguson, D., and de Lange, T. (2009). Mammalian Rif1 contributes to replication stress survival and homology-directed repair. *J. Cell Biol.* 187, 385–398. doi: 10.1083/jcb.200902039

Comayras, C., Tasca, C., Pérès, S. Y., Ducommun, B., Oswald, E., and De Rycke, J. (1997). *Escherichia coli* cytolethal distending toxin blocks the HeLa cell cycle at the G2/M transition by preventing cdc2 protein kinase dephosphorylation and activation. *Infect. Immun.* 65, 5088–5095. doi: 10.1128/IAI.65.12.5088-5095.1997

Cortes-Bratti, X., Karlsson, C., Lagergård, T., Thelestam, M., and Frisan, T. (2001). The *Haemophilus ducreyi* cytolethal distending toxin induces cell cycle arrest and apoptosis via the DNA damage checkpoint pathways. *J. Biol. Chem.* 276, 5296–5302. doi: 10.1074/jbc.M008527200

Durkin, S. G., and Glover, T. W. (2007). Chromosome fragile sites. *Annu. Rev. Genet.* 41, 169–192. doi: 10.1146/annurev.genet.41.042007.165900

Elwell, C. A., and Dreyfus, L. A. (2000). DNase I homologous residues in CdtB are critical for cytolethal distending toxin-mediated cell cycle arrest. *Mol. Microbiol.* 37, 952–963. doi: 10.1046/j.1365-2958.2000.02070.x

Fahrer, J., Huelsenbeck, J., Jaurich, H., Dörsam, B., Frisan, T., Eich, M., et al. (2014). Cytolethal distending toxin (CDT) is a radiomimetic agent and induces persistent levels of DNA double-strand breaks in human fibroblasts. *DNA Repair.* 18, 31–43. doi: 10.1016/j.dnarep.2014.03.002

Fedor, Y., Vignard, J., Nicolau-Travers, M.-L., Boutet-Robinet, E., Watrin, C., Salles, B., et al. (2013). From single-strand breaks to double-strand breaks during S-phase: a new mode of action of the *Escherichia coli* Cytolethal Distending Toxin. *Cell. Microbiol.* 15, 1–15. doi: 10.1111/cmi.12028

Fernandez-Vidal, A., Arnaud, L. C., Maumus, M., Chevalier, M., Mirey, G., Salles, B., et al. (2019). Exposure to the fungicide captan induces DNA base alterations and replicative stress in mammalian cells. *Environ. Mol. Mutagen.* 60, 286–297. doi: 10.1002/em.22268

Frisan, T., Cortes-Bratti, X., Chaves-Olarte, E., Stenerlöw, B., and Thelestam, M. (2003). The *Haemophilus ducreyi* cytolethal distending toxin induces DNA double-strand breaks and promotes ATM-dependent activation of RhoA. *Cell. Microbiol.* 5, 695–707. doi: 10.1046/j.1462-5822.2003.00311.x

Garzón, J., Ursich, S., Lopes, M., Hiraga, S.-I., and Donaldson, A. D. (2019). Human RIF1-protein phosphatase 1 prevents degradation and breakage of nascent DNA on replication stalling. *Cell Rep.* 27, 2558–2566.e4.doi: 10.1016/j.celrep.2019.05.002

Ge, Z., Feng, Y., Ge, L., Parry, N., Muthupalani, S., and Fox, J. G. (2017). *Helicobacter* hepaticus cytolethal distending toxin promotes intestinal carcinogenesis in 129Rag2-deficient mice. *Cell. Microbiol.* 19:e12728. doi: 10.1111/cmi.12728

Ge, Z., Rogers, A. B., Feng, Y., Lee, A., Xu, S., Taylor, N. S., et al. (2007). Bacterial cytolethal distending toxin promotes the development of dysplasia in a model of microbially induced hepatocarcinogenesis. *Cell. Microbiol.* 9, 2070–2080. doi: 10.1111/j.1462-5822.2007.00939.x

Georgakilas, A. G., Tsantoulis, P., Kotsinas, A., Michalopoulos, I., Townsend, P., and Gorgoulis, V. G. (2014). Are common fragile sites merely structural domains or highly organized "functional" units susceptible to oncogenic stress? *Cell. Mol. Life Sci.* 71, 4519–4544. doi: 10.1007/s00018-014-1717-x

Gorgoulis, V. G., Vassiliou, L.-V. F., Karakaidos, P., Zacharatos, P., Kotsinas, A., Liloglou, T., et al. (2005). Activation of the DNA damage checkpoint and genomic instability in human precancerous lesions. *Nature* 434, 907–913. doi: 10.1038/nature03485

Graillot, V., Dormoy, I., Dupuy, J., Shay, J. W., Huc, L., Mirey, G., et al. (2016). Genotoxicity of Cytolethal Distending Toxin (CDT) on isogenic human colorectal cell lines: potential promoting effects for colorectal carcinogenesis. *Front. Cell. Infect. Microbiol.* 6:34. doi: 10.3389/fcimb.2016.00034

Guerra, L., Cortes-Bratti, X., Guidi, R., and Frisan, T. (2011). The biology of the cytolethal distending toxins. *Toxins* 3, 172–190. doi: 10.3390/toxins3030172

Guerra, L., Teter, K., Lilley, B. N., Stenerlöw, B., Holmes, R. K., Ploegh, H. L., et al. (2005). Cellular internalization of cytolethal distending toxin: a new end to a known pathway. *Cell. Microbiol.* 7, 921–934. doi: 10.1111/j.1462-5822.2005.00520.x

Guidi, R., Guerra, L., Levi, L., Stenerlöw, B., Fox, J. G., Josenhans, C., et al. (2013). Chronic exposure to the cytolethal distending toxins of Gram-negative bacteria promotes genomic instability and altered DNA damage response. *Cell. Microbiol.* 15, 98–113. doi: 10.1111/cmi.12034

Harrigan, J. A., Belotserkovskaya, R., Coates, J., Dimitrova, D. S., Polo, S. E., Bradshaw, C. R., et al. (2011). Replication stress induces 53BP1-containing OPT domains in G1 cells. *J. Cell Biol.* 193, 97–108. doi: 10.1083/jcb.201011083

He, Z., Gharaibeh, R. Z., Newsome, R. C., Pope, J. L., Dougherty, M. W., Tomkovich, S., et al. (2019). Campylobacter jejuni promotes colorectal tumorigenesis through the action of cytolethal distending toxin. *Gut* 68, 289–300. doi: 10.1136/gutjnl-2018-317200

Hickey, T. E., Majam, G., and Guerry, P. (2005). Intracellular Survival of *Campylobacter jejuni* in human monocytic cells and induction of apoptotic death by cytholethal distending toxin. *Infect. Immun.* 73, 5194–5197. doi: 10.1128/IAI.73.8.5194-5197.2005

Jinadasa, R. N., Bloom, S. E., Weiss, R. S., and Duhamel, G. E. (2011). Cytolethal distending toxin: a conserved bacterial genotoxin that blocks cell cycle progression, leading to apoptosis of a broad range of mammalian cell lineages. *Microbiology* 157(Pt 7), 1851–1875. doi: 10.1099/mic.0.049536-0

Johnson, W. M., and Lior, H. (1988a). A new heat-labile cytolethal distending toxin (CLDT) produced by *Campylobacter* spp. *Microb. Pathog.* 4, 115–126. doi: 10.1016/0882-401090053-8

Johnson, W. M., and Lior, H. (1988b). A new heat-labile cytolethal distending toxin (CLDT) produced by *Escherichia coli* isolates from clinical material. *Microb. Pathog.* 4, 103–113. doi: 10.1016/0882-401090052-6

Lezaja, A., and Altmeyer, M. (2018). Inherited DNA lesions determine G1 duration in the next cell cycle. *Cell Cycle* 17, 24–32. doi: 10.1080/15384101.2017.1383578

Li, L., Sharipo, A., Chaves-Olarte, E., Masucci, M. G., Levitsky, V., Thelestam, M., et al. (2002). The *Haemophilus ducreyi* cytolethal distending toxin activates sensors of DNA damage and repair complexes in proliferating and non-proliferating cells. *Cell. Microbiol.* 4, 87–99. doi: 10.1046/j.1462-5822.2002.00174.x

Lukas, C., Savic, V., Bekker-Jensen, S., Doil, C., Neumann, B., Sølvhøj Pedersen, R., et al. (2011). 53BP1 nuclear bodies form around DNA lesions generated by mitotic transmission of chromosomes under replication stress. *Nat. Cell Biol.* 13, 243–253. doi: 10.1038/ncb2201

Maciejowski, J., Li, Y., Bosco, N., Campbell, P. J., and de Lange, T. (2015). Chromothripsis and kataegis induced by telomere crisis. *Cell* 163, 1641–1654. doi: 10.1016/j.cell.2015.11.054

Moreno, A., Carrington, J. T., Albergante, L., Mamun, M. A., Haagensen, E. J., Komseli, E.-S., et al. (2016). Unreplicated DNA remaining from unperturbed S phases passes through mitosis for resolution in daughter cells. *Proc. Natl. Acad. Sci. U.S.A.* 113, E5757–E5764. doi: 10.1073/pnas.1603252113

Mukherjee, C., Tripathi, V., Manolika, E. M., Heijink, A. M., Ricci, G., Merzouk, S., et al. (2019). RIF1 promotes replication fork protection and efficient restart to maintain genome stability. *Nat. Commun.* 10:3287. doi: 10.1038/s41467-019-11246-1

Pampalona, J., Roscioli, E., Silkworth, W. T., Bowden, B., Genescà, A., Tusell, L., et al. (2016). Chromosome bridges maintain kinetochore-microtubule attachment throughout mitosis and rarely break during anaphase. *PLoS One* 11:e0147420. doi: 10.1371/journal.pone.0147420

Pérés, S. Y., Marchés, O., Daigle, F., Nougayréde, J. P., Herault, F., Tasca, C., et al. (1997). A new cytolethal distending toxin (CDT) from *Escherichia coli* producing CNF2 blocks HeLa cell division in G2/M phase. *Mol. Microbiol.* 1095–1107. doi: 10.1046/j.1365-2958.1997.4181785.x

Pons, B. J., Bezine, E., Hanique, M., Guillet, V., Mourey, L., Chicher, J., et al. (2019). Cell transfection of purified cytolethal distending toxin B subunits allows comparing their nuclease activity while plasmid degradation assay does not. *PLoS One* 14:e0214313. doi: 10.1371/journal.pone.0214313

Rabin, S. D. P., Flitton, J. G., and Demuth, D. R. (2009). *Aggregatibacter actinomycetemcomitans* cytolethal distending toxin induces apoptosis in nonproliferating macrophages by a phosphatase-independent mechanism. *Infect. Immun.* 77, 3161–3169. doi: 10.1128/IAI.01227-08

Sarni, D., Sasaki, T., Irony Tur-Sinai, M., Miron, K., Rivera-Mulia, J. C., Magnuson, B., et al. (2020). 3D genome organization contributes to genome instability at fragile sites. *Nat. Commun.* 11:3613. doi: 10.1038/s41467-020-17448-2

Scuron, M. D., Boesze-Battaglia, K., Dlakiæ, M., and Shenker, B. J. (2016). The cytolethal distending toxin contributes to microbial virulence and disease pathogenesis by acting as a tri-perditious toxin. *Front. Cell. Infect. Microbiol.* 6:168. doi: 10.3389/fcimb.2016.00168

Sébert, M., Denadai-Souza, A., Quaranta, M., Racaud-Sultan, C., Chabot, S., Lluel, P., et al. (2018). Thrombin modifies growth, proliferation and apoptosis of human colon organoids: a protease-activated receptor 1- and protease-activated receptor 4-dependent mechanism. *Br. J. Pharmacol.* 175, 3656–3668. doi: 10.1111/bph.14430

Sert, V., Cans, C., Tasca, C., Bret-Bennis, L., Oswald, E., Ducommun, B., et al. (1999). The bacterial cytolethal distending toxin (CDT) triggers a G2 cell cycle checkpoint in mammalian cells without preliminary induction of DNA strand breaks. *Oncogene* 18, 6296–6304. doi: 10.1038/sj.onc.1203007

Sugai, M., Kawamoto, T., Pérés, S. Y., Ueno, Y., Komatsuzawa, H., Fujiwara, T., et al. (1998). The cell cycle-specific growth-inhibitory factor produced by *Actinobacillus actinomycetemcomitans* is a cytolethal distending toxin. *Infect. Immun.* 66, 5008–5019. doi: 10.1128/IAI.66.10.5008-5019.1998

Steigemann, P., Wurzenberger, C., Schmitz, M. H. A., Held, M., Guizetti, J., Maar, S., et al. (2009). Aurora B-mediated abscission checkpoint protects against tetraploidization. *Cell* 136, 473–484. doi: 10.1016/j.cell.2008.12.020

Umbreit, N. T., Zhang, C.-Z., Lynch, L. D., Blaine, L. J., Cheng, A. M., Tourdot, R., et al. (2020). Mechanisms generating cancer genome complexity from a single cell division error. *Science* 368:eaba0712. doi: 10.1126/science.aba0712

Vermeulen, L., and Snippert, H. J. (2014). Stem cell dynamics in homeostasis and cancer of the intestine. *Nat. Rev. Cancer* 14, 468–480. doi: 10.1038/nrc3744

Watts, L. P., Natsume, T., Saito, Y., Garzon, J., Dong, Q., Boteva, L., et al. (2020). The RIF1-long splice variant promotes G1 phase 53BP1 nuclear bodies to protect against replication stress. *eLife* 9:e58020. doi: 10.7554/eLife.58020

Xu, T., Lundqvist, A., Ahmed, H. J., Eriksson, K., Yang, Y., and Lagergård, T. (2004). Interactions of *Haemophilus ducreyi* and purified cytolethal distending toxin with human monocyte-derived dendritic cells, macrophages and CD4+ T cells. *Microbes Infect.* 6, 1171–1181. doi: 10.1016/j.micinf.2004.07.003

Conflict of Interest: The authors declare that the research was conducted in the absence of any commercial or financial relationships that could be construed as a potential conflict of interest.

frontiers in Cell and Developmental Biology

MINI REVIEW
published: 10 May 2021
doi: 10.3389/fcell.2021.670392

Replication Fork Reversal and Protection

Shan Qiu[1,2,3†], Guixing Jiang[1†], Liping Cao[1] and Jun Huang[1,2*]*

[1] *Department of General Surgery, Sir Run Run Shaw Hospital, Zhejiang University School of Medicine, Hangzhou, China,* [2] *The MOE Key Laboratory of Biosystems Homeostasis and Protection, Zhejiang Provincial Key Laboratory for Cancer Molecular Cell Biology and Innovation Center for Cell Signaling Network, Life Sciences Institute, Zhejiang University, Hangzhou, China,* [3] *Zhejiang University-University of Edinburgh Institute, Zhejiang University School of Medicine, Zhejiang University, Haining, China*

During genome replication, replication forks often encounter obstacles that impede their progression. Arrested forks are unstable structures that can give rise to collapse and rearrange if they are not properly processed and restarted. Replication fork reversal is a critical protective mechanism in higher eukaryotic cells in response to replication stress, in which forks reverse their direction to form a Holliday junction-like structure. The reversed replication forks are protected from nuclease degradation by DNA damage repair proteins, such as BRCA1, BRCA2, and RAD51. Some of these molecules work cooperatively, while others have unique functions. Once the stress is resolved, the replication forks can restart with the help of enzymes, including human RECQ1 helicase, but restart will not be considered here. Here, we review research on the key factors and mechanisms required for the remodeling and protection of stalled replication forks in mammalian cells.

Keywords: replication stress, replication fork stalling, genome instability, replication fork reversal, DNA translocase

OPEN ACCESS

Edited by:
Huiqiang Lou,
China Agricultural University, China

Reviewed by:
Ian Grainge,
The University of Newcastle, Australia
Pietro Pichierri,
National Institute of Health (ISS), Italy

****Correspondence:***
Liping Cao
caolipingzju@zju.edu.cn
Jun Huang
jhuang@zju.edu.cn

† These authors have contributed equally to this study

Specialty section:
This article was submitted to Cell Growth and Division, a section of the journal Frontiers in Cell and Developmental Biology

Received: *21 February 2021*
Accepted: *19 April 2021*
Published: *10 May 2021*

Citation:
Qiu S, Jiang G, Cao L and Huang J (2021) Replication Fork Reversal and Protection. Front. Cell Dev. Biol. 9:670392. doi: 10.3389/fcell.2021.670392

INTRODUCTION

Faithful DNA replication during each cell cycle is essential for maintaining genome stability (Jeggo et al., 2016). However, the DNA replication process is frequently challenged by endogenous and exogenous sources of genotoxic stress, including DNA lesions, difficult to replicate sequences, and nucleotide depletion (Mehta and Haber, 2014; Kitao et al., 2018). These challenges, if not properly addressed, would ultimately cause genome instability, a hallmark of tumorigenesis (Jackson and Bartek, 2009; Ou and Schumacher, 2018). Fortunately, organisms have evolved multiple DNA damage repair pathways and DNA damage tolerance (DDT) mechanisms to maintain genome stability (Friedberg, 2005; Huen and Chen, 2010; Branzei and Psakhye, 2016).

DNA damage tolerance refers to the bypassing of DNA lesions and replication restart after the replication fork stalls (Friedberg, 2005). One mode of DDT is replication fork reversal. Proposed in 1976, replication fork reversal was long regarded as a pathological result of fork destabilization, but has now been accepted as a DDT based on recent observations of reversed fork structures *in vivo* and the identification of molecules involved in fork regression *in vitro* (Sakaguchi et al., 2009; Bermejo et al., 2011; Neelsen and Lopes, 2015; Berti et al., 2020a). Emerging evidence suggests that replication fork reversal is indispensable for maintaining genome stability in higher eukaryotic cells. For example, it actively slows down replication fork progression via multiple enzymes, such as the recombinase RAD51 and DNA translocase helicase-like transcription factor (HLTF), which

provides sufficient time for the DNA repair machinery to become involved and prevent double-strand break (DSB) formation (Poole and Cortez, 2017; Tye et al., 2020). Replication fork reversal also triggers template switching, where the nascent strand is used for error-free DNA synthesis (Zellweger et al., 2015). However, reversal can render replication forks susceptible to nucleolytic attack (Liao et al., 2018; Rickman and Smogorzewska, 2019). Recent studies have explored factors that can protect reversed forks against nuclease processing, like BRCA1, BRCA2, and components of the Fanconi anemia (FA) complex (Rickman and Smogorzewska, 2019; Tye et al., 2020).

This review focuses on the process of replication fork reversal, especially the enzymes, and molecules involved. First, changes in the replication fork structure after damage blockage, and the factors that promote fork regression, are summarized. The review then explores several mechanisms that protect the reversed fork structure. We hope that this review will provide comprehensive insight into replication fork reversal, thereby contributing to future therapies for diseases like cancers.

A TWO-STEP MECHANISM FOR REPLICATION FORK REVERSAL

In response to replication perturbation, the DNA fork structure changes depending on the type of damage. If a lesion occurs on the lagging strand, it will likely be bypassed because the semi-discontinuous characteristics of DNA replication allow the lagging strand to leave a single strand DNA (ssDNA) gap to be repaired afterward (McInerney and O'Donnell, 2004). However, if a lesion occurs on the leading strand, the fork structure will be altered. In this case, synthesis of the leading strand is inhibited at the blockage point due to polymerase dissociation (also called fork uncoupling), while the helicase continues to generate ssDNA for hundreds of bases (Atkinson and McGlynn, 2009; Berti et al., 2020a). Thus, stalling the synthesis of the leading strand results in an accumulation of ssDNA; this provides a platform for loading multiple enzymes, thereby promoting fork remodeling (Kolinjivadi et al., 2017).

PCNA Polyubiquitination and Fork Slowing

Proliferation cell nuclear antigen (PCNA) is a highly conserved homotrimer that serves as a DNA clamp and is crucial for DNA replication and associated processes (Boehm et al., 2016; Lee and Park, 2020). It is a critical regulator of DDT, in which PCNA monoubiquitination at lysine 164 (PCNA-Ub) facilitates error-prone translesion DNA synthesis and PCNA polyubiquitination (PCNA-Ub^n) promotes error-free damage bypass (Sale, 2013; Branzei and Szakal, 2017). In yeast, PCNA-Ub^n is mediated by E3 ubiquitin ligase Rad5, while in mammalian cells it is mediated by the Rad5 orthologs HLTF and SNF2 histone linker PHD RING helicase (SHPRH; Unk et al., 2010). Surprisingly, PCNA-Ub^n occurs in *Hltf/Shprh* double-deficient mouse embryonic fibroblasts (Krijger et al., 2011). Therefore, another E3 ligase must contribute to PCNA-Ub^n in mammalian cells. A recent *in vitro* study found that the HECT-type E3 ligase HECW2 interacted with PCNA and regulated its ubiquitination; its role in DDT needs further study (Krishnamoorthy et al., 2018). Strikingly, a recent study demonstrated that K63-linked, UBC13-dependent PCNA-Ub^n is required to slow and reverse replication forks in response to replication stress (Vujanovic et al., 2017).

Critical Enzymes in Fork Slowing and Reversal

Emerging evidence suggests that active replication fork slowing upon genotoxic stress is linked to replication fork reversal, which is at least partly regulated by SNF2 family chromatin remodelers, including SMARCAL1 (SWI/SNF-related, matrix-associated, actin-dependent, regulator of chromatin, and subfamily A-like 1), ZRANB3 (zinc finger, RAN-binding domain containing 3), and HLTF (Poole and Cortez, 2017; **Figure 1**). Mutations in *SMARCAL1* lead to Schimke immuno-osseous dysplasia (SIOD), while *HLTF/ZRANB3*-deficient cells are vulnerable to replication stress and contribute to tumorigenesis (Ciccia et al., 2009; Li et al., 2009; Weston et al., 2012; Helmer et al., 2019). Therefore, these helicase-like proteins play critical roles in DDT, and use energy from ATP hydrolysis to remodel chromatin structure (Hargreaves and Crabtree, 2011). They are recruited to the stalled replication forks by interactions with other proteins, like RPA or PCNA, and then bind DNA sequences via substrate-recognition domains. All three of these DNA translocases can catalyze replication fork regression both *in vitro* and *in vivo*, and have specific, distinct functions in fork remodeling (Blastyak et al., 2010; Achar et al., 2011; Betous et al., 2012).

SWI/SNF-related, matrix-associated, actin-dependent, regulator of chromatin, and subfamily A-like 1 is an annealing helicase that contains a replication protein A (RPA) binding domain. RPA, a eukaryotic ssDNA-binding protein that regulates various DNA metabolic processes, is required for SMARCAL1 localization to stalled forks (Ciccia et al., 2009; Yuan et al., 2009; Byrne and Oakley, 2019). SMARCAL1 interacts with RPA and catalyzes replication fork regression, which is regulated by the ATM and Rad3-related (ATR) protein kinase (Couch et al., 2013; Bhat and Cortez, 2018). While RPA stimulates SMARCAL1 fork reversal activity when it is bound to a ssDNA gap on the leading template strand, it inhibits SMARCAL1 when bound to a replication fork with a ssDNA gap on the lagging strand (Betous et al., 2013).

Zinc finger, RAN-binding domain containing 3 contains a PCNA-interacting protein box and an AIkB homology 2 PCNA interaction motif (APIM) to bind PCNA, which facilitates its localization to stalled forks (Ciccia et al., 2012; Weston et al., 2012; Yuan et al., 2012). Moreover, its NPL4 zinc-finger motif preferentially interacts with K63-linked polyubiquitinated PCNA and is also required for the localization of ZRANB3 at stalled replication forks (Vujanovic et al., 2017). Because of its homologous sequence, ZRANB3 has functions similar to SMARCAL1, including annealing complementary DNA strands and catalyzing fork reversal. Unlike SMARCAL1, however, RPA inhibits the fork reversal ability of ZRANB3 on the leading-strand

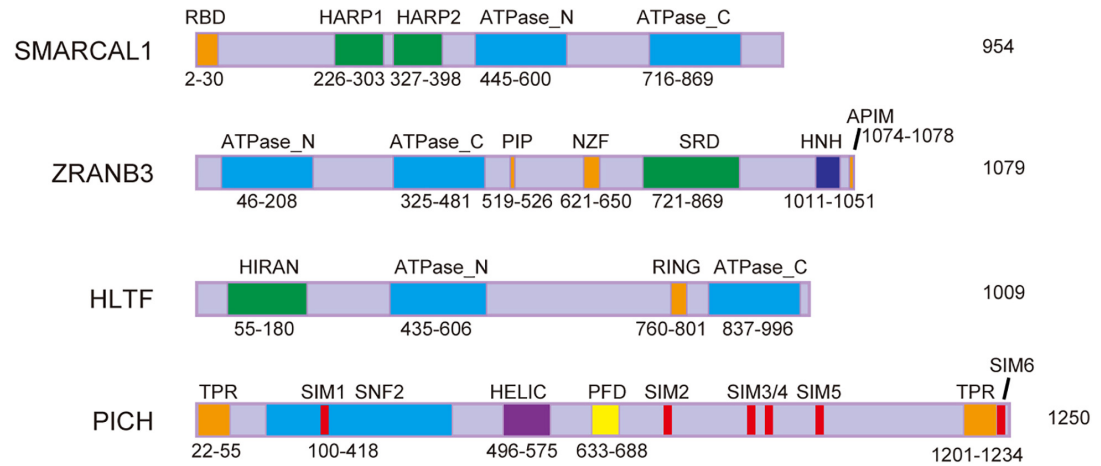

FIGURE 1 | Schematic representation of protein domains of SMARCAL1, ZRANB3, HLTF, and PICH. RBD, RPA-binding domain; HARP, HepA-related protein; PIP, PCNA-interacting protein box; NZF, Npl4 zinc-finger; SRD, substrate recognition domain; HNH, His-Asn-His protein; APIM, AlkB homolog 2 PCNA interacting motif; HIRAN, HIP116 and RAD5 *N*-terminal; RING, really interesting new gene; TPR, tetratricopeptide repeat; SIM, SUMO-interacting motif; SNF2, sucrose non-fermenting 2; HELIC, helicase superfamily *c*-terminal domain; and PFD, PICH family domain.

gaps substrates (Betous et al., 2013). Moreover, unlike other SNF2 family proteins, ZRANB3 exhibits structure-specific ATP-dependent endonuclease activity and can cleave fork DNA structures (Weston et al., 2012). Exactly how these enzymatic activities work together at stalled replication forks remains unknown.

Similar to SMARCAL1 and ZRANB3, HLTF can catalyze fork reversal via ATP hydrolysis. HLTF binds the leading strand via its *N*-terminal HIRAN domain to stimulate fork regression (Achar et al., 2015; Kile et al., 2015). In addition, it has been reported that HLTF partly counteracts the activity of the DNA helicase FANCJ at stalled forks to maintain fork remodeling and prevent unlimited replication (Peng et al., 2018). Unlike the other two DNA translocases, no protein interaction motifs have been discovered in HLTF, and how it is recruited to stalled forks requires further investigation. Although a study has demonstrated that RPA and Pax transactivation domain-interacting protein interacts with HLTF, future research should examine their roles in replication stress (MacKay et al., 2009). Since simultaneously depletion of SMARCAL1, ZRANB3, and HLTF did not show an additive effect on reversed fork frequency, these three DNA translocases may function at different stages of a common pathway (Taglialatela et al., 2017; Tian et al., 2021). It is also possible that each translocase works preferentially on specific substrates or genomic regions, which need further investigation (Taglialatela et al., 2017; Tian et al., 2021).

In addition to the SNF2 family proteins, it has been reported that RAD51 is required for replication fork regression. RAD51 is a highly conserved DNA recombinase that facilitates DNA DSB repair in vertebrates by promoting homologous recombination repair (Gachechiladze et al., 2017; Laurini et al., 2020; Sinha et al., 2020). A nascent chromatin capture screening study detected RAD51 on the replication forks (Alabert et al., 2014). Unlike homologous recombination repair, RAD51 has a non-canonical function in fork reversal, since BRCA2-modulated stable RAD51 filaments are not needed in this process (Bhat and Cortez, 2018). Although the mechanisms are not clear, it has been suggested that RAD51 paralogs (RAD51B, RAD51C, RAD51D, XRCC2, and XRCC3) may assist RAD51 and DNA translocases in promoting replication fork reversal (Berti et al., 2020b). The loaders and specific role of RAD51 in fork reversal warrant further investigation.

Other enzymes have also been reported to participate in the reversal of replication forks. For example, the branch point translocase FANCM (Fanconi anemia complementation group M) could convert a replication fork from a three-way junction to a four-way junction in an ATP-dependent manner (Gari et al., 2008). Moreover, a study showed that FBH1 (F-box DNA helicase 1) was recruited to the stalled forks and could unwind the lagging strands (Masuda-Ozawa et al., 2013). A more recent study demonstrated that the helicase activity of FBH1 was involved in replication fork regression, which was also dependent on ATP hydrolysis (Fugger et al., 2015). Although many related enzymes and molecules have been discovered, it is not clear whether these proteins work together to promote fork remodeling, or if they work independently in response to different replication obstacles. It will be necessary to explore the interactions among these enzymes in the future.

Although the above enzymes play significant roles in replication fork remodeling, they must be tightly regulated as too little or too much of their activities at stalled forks is deleterious for genomic stability. For example, ATR phosphorylates SMARCAL1 at Ser652 to limit its fork regression activity, thereby preventing replication fork collapse (Couch et al., 2013). Apart from ATR, RAD52 also limits SMARCAL1 activity at stalled forks by counteracting its loading (Malacaria et al., 2019). Moreover, the RPA-like single-strand DNA binding protein RADX antagonizes RAD51 filament formation to prevent

inappropriate replication fork reversal (Dungrawala et al., 2017; Schubert et al., 2017; Zhang et al., 2020; Adolph et al., 2021).

The ZATT-TOP2A-PICH Axis and Extensive Replication Fork Reversal

Extrusion of the leading and lagging strands from the template DNA during replication fork reversal, catalyzed by the above enzymes, would cause positive superhelical strain in the newly synthesized sister chromatids (Tian et al., 2021). The resulting superhelical strain prevents further regression of the stalled replication forks and must be dissipated by DNA topoisomerases for reversal to proceed efficiently (Tian et al., 2021). Our recent study found that DNA topoisomerase 2 (mainly TOP2A) can release the superhelical strain in newly synthesized chromatids generated by the DNA translocases SMARCAL1, ZRANB3, and HLTF during limited fork reversal (Tian et al., 2021; **Figure 2**). Our study also showed that, with replication stress, TOP2A is SUMOylated by the SUMO E3 ligase ZATT, mainly at lysines 1228 and 1240. SUMOylated TOP2A then recruits the SUMO-targeted DNA translocase PICH to stalled replication forks, where PICH branch migrates the Holliday junction structures and drives extensive replication fork reversal (Tian et al., 2021; **Figure 2**). Based on these findings, we proposed that replication fork reversal has two distinct stages, namely initiation and extension stages (Tian et al., 2021; **Figure 2**). Like SMARCAL1, ZRANB3, and HLTF, PICH is also a member of the SNF2 family (**Figure 1**). However, in contrast to SMARCAL1, ZRANB3, and HLTF, PICH possesses branch migration activity but not fork regression activity, indicating that PICH is specifically involved in the extension stage of replication fork reversal.

MECHANISMS FOR REPLICATION FORK MAINTENANCE AND STABILITY

Under replication stress, the replication fork reverses to form a four-way Holliday junction structure, as discussed above. However, the nascent strands in this structure resemble a one-ended DNA DSB, which is susceptible to nucleases such as MRE11, EXO1 (exonuclease1), DNA2 (DNA replication helicase/nuclease 2), and MUS81 (Thangavel et al., 2015; Lemacon et al., 2017; Mijic et al., 2017). To prevent excessive degradation at stalled forks, the nucleolytic activity of these enzymes has to be regulated accurately. Recent studies have identified several protective mechanisms that maintain replication fork structure and confer genomic stability.

BRCA1/2 AND RAD51

BRCA1/2-mediated stable RAD51 filament formation is required for its protective effect on the regressed arm (Carreira and Kowalczykowski, 2011; Schlacher et al., 2012). Consistent with this, wild-type RAD51, but not its DNA-binding mutant RAD51^{T131P}, stably associates with reversed forks and protects them from Mre11-mediated degradation (Kolinjivadi et al., 2017; Mijic et al., 2017). In addition, inhibition of RAD51 DNA-binding and strand exchange activities by the small molecule B02 destabilizes reversed forks, without causing the fork reversal defects observed upon RAD51 depletion (Taglialatela et al., 2017). Moreover, WRNIP1, a member of the AAA + ATPase family, interacts with the BRCA2/RAD51 complex and participates in the stabilization of RAD51 filaments from degradation by MRE11 (Leuzzi et al., 2016). These findings suggest that RAD51 has both a BRCA1/2-independent fork remodeling function and a BRCA1/2-dependent fork-protecting role. However, it is still unclear exactly how RAD51 protects regressed forks from nuclease-mediated degradation. Physical blocking of nuclease binding, or cooperation with other inhibitory proteins, are putative mechanisms. Furthermore, the RAD51 paralogs also participate in replication fork protection against MRE11 over-resection (Somyajit et al., 2015). Whether RAD51 paralogs dampen nucleases via the same mechanism as the BRCA1/2-RAD51 interaction requires further study.

FA Components

Fanconi anemia is a rare inherited disorder that results from mutations in *FA* genes, which play key roles in DNA replication and repair (Alter, 2014). The FA core complex is an ubiquitin ligase that detects DNA damage and monoubiquitinates the downstream proteins FANCD2 and FANCI to regulate DNA repair of inter-strand crosslinks (ICL) and homologous

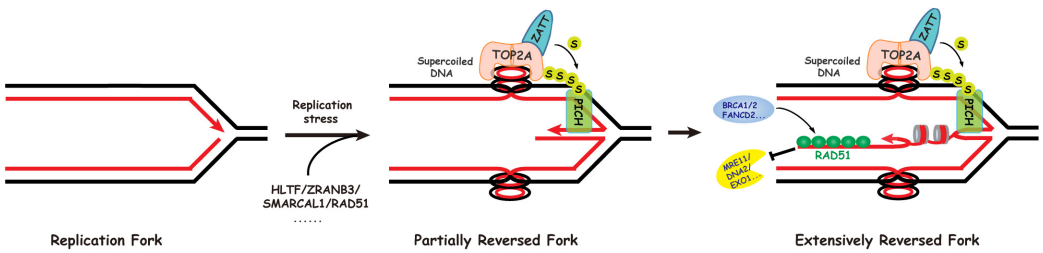

FIGURE 2 | Replication fork reversal occurs via a two-step mechanism. In the first step, SMARCAL1, HLTF, and ZRANB3 cooperate with RAD51 to initiate limited replication fork reversal, generating positive superhelical strain in the newly replicated sister chromatids. The initial fork reversal may be helped by the positive supercoiling ahead of the replication fork created during replication. In the second step, DNA topoisomerase IIalpha (TOP2A) promotes extensive fork reversal, on one hand through resolving the resulting topological barriers, and on the other hand via its role in recruiting the SUMO-targeted DNA translocase PICH to stalled replication forks.

recombination repair (Nepal et al., 2017; Liu et al., 2020). In addition to its canonical role in ICL repair, several FA proteins stabilize stalled forks. For example, the FA component FANCD2 prevents MRE11-mediated fork over-processing by stabilizing RAD51 nucleofilaments, similarly to BRCA2 (Schlacher et al., 2012; Kim et al., 2015). Interestingly, a recent study demonstrated that the novel protein BOD1L could also protect stalled forks from genome fragility (Higgs et al., 2015). Being downstream of FANCD2/BRCA2, BOD1L maintained fork stability by inhibiting BLM/FBH1 helicases and stabilizing RAD51 nucleoprotein filaments (Higgs et al., 2015). However, unlike FANCD2, BOD1L suppressed DNA2-mediated degradation rather than MRE11-dependent instability (Higgs et al., 2015). It may seem unintuitive that both FANCD2 and BOD1L stabilize RAD51 at sites of replication damage, but they prevent different types of nucleolytic attack. Future research is required to reveal the precise mechanism underlying RAD51 stabilization.

RecQ Family of DNA Helicases

The RecQ family of DNA helicases, including RECQL1/4/5, WRN (Werner syndrome protein), and BLM (Bloom's syndrome helicase), have been shown to be important for maintaining genome integrity (Croteau et al., 2014). These proteins are conserved from bacteria to humans, and mutations therein lead to diseases such as Werner syndrome and Bloom syndrome, as well as premature aging, and cancer proneness (Mojumdar, 2020). Since Werner and Bloom syndromes are both characterized by chromosome fragility and increased cancer predisposition, many studies have investigated whether the Bloom syndrome helicase BLM and Werner syndrome helicase WRN play roles in protecting stalled replication forks.

A previous study found that WRN helicase and exonuclease catalytic activities were needed to prevent MUS81-mediated breakage after HU-induced replication fork stalling (Murfuni et al., 2012). However, that study did not reveal how the different enzymatic activities of WRN collaborate at stalled forks. A more recent finding suggested that WRN exonuclease prevented MRE11/EXO1-dependent over-resection at nascent strands, while its helicase ensured the necessary exonucleolytic processing (Iannascoli et al., 2015). A non-enzymatic function of WRN was also reported (Su et al., 2014). The authors found that WRN could limit MRE11 exonuclease activity and prevent excessive degradation on nascent strands, possibly by stabilizing RAD51 (Su et al., 2014).

Bloom's syndrome helicase, another RecQ helicase, has also been implicated in replication fork protection upon replication stress. It was reported that BLM and FANCD2 co-localized at stalled forks in response to replication fork stalling agents (Pichierri et al., 2004). Moreover, the FA pathway was shown to be essential for BLM phosphorylation and assembly in nuclear foci in response to DNA interstrand crosslinking agents (Pichierri et al., 2004). Surprisingly, a recent study found that BLM helicase activity was also indispensable for FANCM recruitment and function at stalled forks (Ling et al., 2016). Therefore, it is reasonable to hypothesize that BLM and the FA pathway form a positive feedback loop to ensure sufficient protection of the stalled forks.

Other proteins, such as ABRO1, PALB2, and WRNIP, have also been implicated in stalled replication fork protection (Murphy et al., 2014; Liao et al., 2018; Bennett et al., 2020; Berti et al., 2020a). However, it is not clear how these factors interact in this process, or how they function in response to different replication obstacles.

CONCLUDING REMARKS

Recent studies have raised many questions about fork remodeling caused by replication stress. Although there are various well-established models of fork reversal and remodeling, some questions remain unanswered. For example, on what basis do cells choose one or several of these mechanisms upon encountering a DNA lesion? How do cells recognize and respond to different DNA lesions? How do factors with similar functions work in non-redundant ways? If helicase and polymerase are dissociated during fork reversal, how is the replisome reloaded onto the replication fork when the fork is restarted? Are other factors vital in the balance between fork reversal and restart? We believe that recent progress in our understanding of fork plasticity under genotoxic stress will spark interest in addressing these questions and clarifying the mechanistic link between fork remodeling and genomic instability. In turn, this should lead to a better understanding of the mechanisms underlying replication and the dynamic relationships among the involved processes, thereby leading to more efficient cancer therapies.

AUTHOR CONTRIBUTIONS

SQ and GJ wrote the manuscript. JH and LC reviewed and edited the manuscript. All authors contributed to the article and approved the submitted version.

FUNDING

This work was supported by National Natural Science Foundation of China (31730021, 31971220, and 31961160725), National Key Research and Development Program of China (2018YFC2000100), and the China's Fundamental Research Funds for the Central Universities.

ACKNOWLEDGMENTS

We apologize to colleagues whose work could not be cited because of space limitations. We thank all our colleagues in the Huang laboratory for helpful discussions.

REFERENCES

Achar, Y. J., Balogh, D., and Haracska, L. (2011). Coordinated protein and DNA remodeling by human HLTF on stalled replication fork. *Proc. Natl. Acad. Sci. U.S.A.* 108, 14073–14078. doi: 10.1073/pnas.1101951108

Achar, Y. J., Balogh, D., Neculai, D., Juhasz, S., Morocz, M., Gali, H., et al. (2015). Human HLTF mediates postreplication repair by its HIRAN domain-dependent replication fork remodelling. *Nucleic Acids Res.* 43, 10277–10291. doi: 10.1093/nar/gkv896

Adolph, M. B., Mohamed, T. M., Balakrishnan, S., Xue, C., Morati, F., Modesti, M., et al. (2021). RADX controls RAD51 filament dynamics to regulate replication fork stability. *Mol. Cell* 81, 1074 e1075–1083 e1075. doi: 10.1016/j.molcel.2020.12.036

Alabert, C., Bukowski-Wills, J. C., Lee, S. B., Kustatscher, G., Nakamura, K., de Lima Alves, F., et al. (2014). Nascent chromatin capture proteomics determines chromatin dynamics during DNA replication and identifies unknown fork components. *Nat. Cell Biol.* 16, 281–293. doi: 10.1038/ncb2918

Alter, B. P. (2014). Fanconi anemia and the development of leukemia. *Best Practice Res. Clin. Haematol.* 27, 214–221. doi: 10.1016/j.beha.2014.10.002

Atkinson, J., and McGlynn, P. (2009). Replication fork reversal and the maintenance of genome stability. *Nucleic Acids Res.* 37, 3475–3492. doi: 10.1093/nar/gkp244

Bennett, L. G., Wilkie, A. M., Antonopoulou, E., Ceppi, I., Sanchez, A., Vernon, E. G., et al. (2020). MRNIP is a replication fork protection factor. *Sci. Adv.* 6:eaba5974. doi: 10.1126/sciadv.aba5974

Bermejo, R., Capra, T., Jossen, R., Colosio, A., Frattini, C., Carotenuto, W., et al. (2011). The replication checkpoint protects fork stability by releasing transcribed genes from nuclear pores. *Cell* 146, 233–246. doi: 10.1016/j.cell.2011.06.033

Berti, M., Cortez, D., and Lopes, M. (2020a). The plasticity of DNA replication forks in response to clinically relevant genotoxic stress. *Nat. Rev. Mol. Cell Biol.* 21, 633–651. doi: 10.1038/s41580-020-0257-5

Berti, M., Teloni, F., Mijic, S., Ursich, S., Fuchs, J., Palumbieri, M. D., et al. (2020b). Sequential role of RAD51 paralog complexes in replication fork remodeling and restart. *Nat. Commun.* 11:3531. doi: 10.1038/s41467-020-17324-z

Betous, R., Couch, F. B., Mason, A. C., Eichman, B. F., Manosas, M., and Cortez, D. (2013). Substrate-selective repair and restart of replication forks by DNA translocases. *Cell Rep.* 3, 1958–1969. doi: 10.1016/j.celrep.2013.05.002

Betous, R., Mason, A. C., Rambo, R. P., Bansbach, C. E., Badu-Nkansah, A., Sirbu, B. M., et al. (2012). SMARCAL1 catalyzes fork regression and Holliday junction migration to maintain genome stability during DNA replication. *Genes Dev.* 26, 151–162. doi: 10.1101/gad.178459.111

Bhat, K. P., and Cortez, D. (2018). RPA and RAD51: fork reversal, fork protection, and genome stability. *Nat. Struct. Mol. Biol.* 25, 446–453. doi: 10.1038/s41594-018-0075-z

Blastyak, A., Hajdu, I., Unk, I., and Haracska, L. (2010). Role of double-stranded DNA translocase activity of human HLTF in replication of damaged DNA. *Mol. Cell. Biol.* 30, 684–693. doi: 10.1128/MCB.00863-09

Boehm, E. M., Gildenberg, M. S., and Washington, M. T. (2016). The many roles of PCNA in Eukaryotic DNA replication. *Enzymes* 39, 231–254. doi: 10.1016/bs.enz.2016.03.003

Branzei, D., and Psakhye, I. (2016). DNA damage tolerance. *Curr. Opin. Cell. Biol.* 40, 137–144. doi: 10.1016/j.ceb.2016.03.015

Branzei, D., and Szakal, B. (2017). Building up and breaking down: mechanisms controlling recombination during replication. *Crit. Rev. Biochem. Mol. Biol.* 52, 381–394. doi: 10.1080/10409238.2017.1304355

Byrne, B. M., and Oakley, G. G. (2019). Replication protein A, the laxative that keeps DNA regular: the importance of RPA phosphorylation in maintaining genome stability. *Semin. Cell. Dev. Biol.* 86, 112–120. doi: 10.1016/j.semcdb.2018.04.005

Carreira, A., and Kowalczykowski, S. C. (2011). Two classes of BRC repeats in BRCA2 promote RAD51 nucleoprotein filament function by distinct mechanisms. *Proc. Natl. Acad. Sci. U.S.A.* 108, 10448–10453. doi: 10.1073/pnas.1106971108

Ciccia, A., Bredemeyer, A. L., Sowa, M. E., Terret, M. E., Jallepalli, P. V., Harper, J. W., et al. (2009). The SIOD disorder protein SMARCAL1 is an RPA-interacting protein involved in replication fork restart. *Genes Dev.* 23, 2415–2425. doi: 10.1101/gad.1832309

Ciccia, A., Nimonkar, A. V., Hu, Y., Hajdu, I., Achar, Y. J., Izhar, L., et al. (2012). Polyubiquitinated PCNA recruits the ZRANB3 translocase to maintain genomic integrity after replication stress. *Mol. Cell.* 47, 396–409. doi: 10.1016/j.molcel.2012.05.024

Couch, F. B., Bansbach, C. E., Driscoll, R., Luzwick, J. W., Glick, G. G., Betous, R., et al. (2013). ATR phosphorylates SMARCAL1 to prevent replication fork collapse. *Genes Dev.* 27, 1610–1623. doi: 10.1101/gad.214080.113

Croteau, D. L., Popuri, V., Opresko, P. L., and Bohr, V. A. (2014). Human RecQ helicases in DNA repair, recombination, and replication. *Annu. Rev. Biochem.* 83, 519–552. doi: 10.1146/annurev-biochem-060713-035428

Dungrawala, H., Bhat, K. P., Le Meur, R., Chazin, W. J., Ding, X., Sharan, S. K., et al. (2017). RADX promotes genome stability and modulates chemosensitivity by regulating RAD51 at replication forks. *Mol. Cell.* 67:e375. doi: 10.1016/j.molcel.2017.06.023

Friedberg, E. C. (2005). Suffering in silence: the tolerance of DNA damage. *Nat. Rev. Mol. Cell. Biol.* 6, 943–953. doi: 10.1038/nrm1781

Fugger, K., Mistrik, M., Neelsen, K. J., Yao, Q., Zellweger, R., Kousholt, A. N., et al. (2015). FBH1 catalyzes regression of stalled replication forks. *Cell Rep.* 10, 1749–1757. doi: 10.1016/j.celrep.2015.02.028

Gachechiladze, M., Skarda, J., Soltermann, A., and Joerger, M. (2017). RAD51 as a potential surrogate marker for DNA repair capacity in solid malignancies. *Int. J. Cancer* 141, 1286–1294. doi: 10.1002/ijc.30764

Gari, K., Decaillet, C., Delannoy, M., Wu, L., and Constantinou, A. (2008). Remodeling of DNA replication structures by the branch point translocase FANCM. *Proc. Natl. Acad. Sci. U.S.A.* 105, 16107–16112. doi: 10.1073/pnas.0804777105

Hargreaves, D. C., and Crabtree, G. R. (2011). ATP-dependent chromatin remodeling: genetics, genomics and mechanisms. *Cell Res.* 21, 396–420. doi: 10.1038/cr.2011.32

Helmer, R. A., Kaur, G., Smith, L. A., and Chilton, B. S. (2019). Helicase-like transcription factor (Hltf) gene-deletion promotes oxidative phosphorylation (OXPHOS) in colorectal tumors of AOM/DSS-treated mice. *PLoS One* 14:e0221751. doi: 10.1371/journal.pone.0221751

Higgs, M. R., Reynolds, J. J., Winczura, A., Blackford, A. N., Borel, V., Miller, E. S., et al. (2015). BOD1L is required to suppress deleterious resection of stressed replication forks. *Mol. Cell.* 59, 462–477. doi: 10.1016/j.molcel.2015.06.007

Huen, M. S., and Chen, J. (2010). Assembly of checkpoint and repair machineries at DNA damage sites. *Trends Biochem. Sci.* 35, 101–108. doi: 10.1016/j.tibs.2009.09.001

Iannascoli, C., Palermo, V., Murfuni, I., Franchitto, A., and Pichierri, P. (2015). The WRN exonuclease domain protects nascent strands from pathological MRE11/EXO1-dependent degradation. *Nucleic Acids Res.* 43, 9788–9803. doi: 10.1093/nar/gkv836

Jackson, S. P., and Bartek, J. (2009). The DNA-damage response in human biology and disease. *Nature* 461, 1071–1078. doi: 10.1038/nature08467

Jeggo, P. A., Pearl, L. H., and Carr, A. M. (2016). DNA repair, genome stability and cancer: a historical perspective. *Nat. Rev. Cancer* 16, 35–42. doi: 10.1038/nrc.2015.4

Kile, A. C., Chavez, D. A., Bacal, J., Eldirany, S., Korzhnev, D. M., Bezsonova, I., et al. (2015). HLTF's Ancient HIRAN domain binds 3' DNA ends to drive replication fork reversal. *Mol. Cell* 58, 1090–1100. doi: 10.1016/j.molcel.2015.05.013

Kim, T. M., Son, M. Y., Dodds, S., Hu, L., Luo, G., and Hasty, P. (2015). RECQL5 and BLM exhibit divergent functions in cells defective for the Fanconi anemia pathway. *Nucleic Acids Res.* 43, 893–903. doi: 10.1093/nar/gku1334

Kitao, H., Iimori, M., Kataoka, Y., Wakasa, T., Tokunaga, E., Saeki, H., et al. (2018). DNA replication stress and cancer chemotherapy. *Cancer Sci.* 109, 264–271. doi: 10.1111/cas.13455

Kolinjivadi, A. M., Sannino, V., De Antoni, A., Zadorozhny, K., Kilkenny, M., Techer, H., et al. (2017). Smarcal1-mediated fork reversal triggers Mre11-Dependent degradation of nascent DNA in the absence of Brca2 and Stable Rad51 nucleofilaments. *Mol. Cell.* 67:e867. doi: 10.1016/j.molcel.2017.07.001

Krijger, P. H., Lee, K. Y., Wit, N., van den Berk, P. C., Wu, X., Roest, H. P., et al. (2011). HLTF and SHPRH are not essential for PCNA polyubiquitination, survival and somatic hypermutation: existence of an alternative E3 ligase. *DNA Repair (Amst)* 10, 438–444. doi: 10.1016/j.dnarep.2010.12.008

Krishnamoorthy, V., Khanna, R., and Parnaik, V. K. (2018). E3 ubiquitin ligase HECW2 targets PCNA and lamin B1. *Biochim. Biophys. Acta Mol. Cell. Res.* 1865, 1088–1104. doi: 10.1016/j.bbamcr.2018.05.008

Laurini, E., Marson, D., Fermeglia, A., Aulic, S., Fermeglia, M., and Pricl, S. (2020). Role of Rad51 and DNA repair in cancer: a molecular perspective. *Pharmacol. Ther.* 208:107492. doi: 10.1016/j.pharmthera.2020.107492

Lee, K. Y., and Park, S. H. (2020). Eukaryotic clamp loaders and unloaders in the maintenance of genome stability. *Exp. Mol. Med.* 52, 1948–1958. doi: 10.1038/s12276-020-00533-3

Lemacon, D., Jackson, J., Quinet, A., Brickner, J. R., Li, S., Yazinski, S., et al. (2017). MRE11 and EXO1 nucleases degrade reversed forks and elicit MUS81-dependent fork rescue in BRCA2-deficient cells. *Nat. Commun.* 8:860. doi: 10.1038/s41467-017-01180-5

Leuzzi, G., Marabitti, V., Pichierri, P., and Franchitto, A. (2016). WRNIP1 protects stalled forks from degradation and promotes fork restart after replication stress. *EMBO J.* 35, 1437–1451. doi: 10.15252/embj.201593265

Li, Y., Bolderson, E., Kumar, R., Muniandy, P. A., Xue, Y., Richard, D. J., et al. (2009). HSSB1 and hSSB2 form similar multiprotein complexes that participate in DNA damage response. *J. Biol. Chem.* 284, 23525–23531. doi: 10.1074/jbc.C109.039586

Liao, H., Ji, F., Helleday, T., and Ying, S. (2018). Mechanisms for stalled replication fork stabilization: new targets for synthetic lethality strategies in cancer treatments. *EMBO Rep.* 19:e46263. doi: 10.15252/embr.201846263

Ling, C., Huang, J., Yan, Z., Li, Y., Ohzeki, M., Ishiai, M., et al. (2016). Bloom syndrome complex promotes FANCM recruitment to stalled replication forks and facilitates both repair and traverse of DNA interstrand crosslinks. *Cell Discov.* 2:16047. doi: 10.1038/celldisc.2016.47

Liu, W., Palovcak, A., Li, F., Zafar, A., Yuan, F., and Zhang, Y. (2020). Fanconi anemia pathway as a prospective target for cancer intervention. *Cell. Biosci.* 10:39. doi: 10.1186/s13578-020-00401-7

MacKay, C., Toth, R., and Rouse, J. (2009). Biochemical characterisation of the SWI/SNF family member HLTF. *Biochem. Biophys. Res. Commun.* 390, 187–191. doi: 10.1016/j.bbrc.2009.08.151

Malacaria, E., Pugliese, G. M., Honda, M., Marabitti, V., Aiello, F. A., Spies, M., et al. (2019). Rad52 prevents excessive replication fork reversal and protects from nascent strand degradation. *Nat. Commun.* 10:1412. doi: 10.1038/s41467-019-09196-9

Masuda-Ozawa, T., Hoang, T., Seo, Y. S., Chen, L. F., and Spies, M. (2013). Single-molecule sorting reveals how ubiquitylation affects substrate recognition and activities of FBH1 helicase. *Nucleic Acids Res.* 41, 3576–3587. doi: 10.1093/nar/gkt056

McInerney, P., and O'Donnell, M. (2004). Functional uncoupling of twin polymerases: mechanism of polymerase dissociation from a lagging-strand block. *J. Biol. Chem.* 279, 21543–21551. doi: 10.1074/jbc.M401649200

Mehta, A., and Haber, J. E. (2014). Sources of DNA double-strand breaks and models of recombinational DNA repair. *Cold Spring Harb. Perspect Biol.* 6:a016428. doi: 10.1101/cshperspect.a016428

Mijic, S., Zellweger, R., Chappidi, N., Berti, M., Jacobs, K., Mutreja, K., et al. (2017). Replication fork reversal triggers fork degradation in BRCA2-defective cells. *Nat. Commun.* 8:859. doi: 10.1038/s41467-017-01164-5

Mojumdar, A. (2020). Mutations in conserved functional domains of human RecQ helicases are associated with diseases and cancer: a review. *Biophys. Chem.* 265:106433. doi: 10.1016/j.bpc.2020.106433

Murfuni, I., De Santis, A., Federico, M., Bignami, M., Pichierri, P., and Franchitto, A. (2012). Perturbed replication induced genome wide or at common fragile sites is differently managed in the absence of WRN. *Carcinogenesis* 33, 1655–1663. doi: 10.1093/carcin/bgs206

Murphy, A. K., Fitzgerald, M., Ro, T., Kim, J. H., Rabinowitsch, A. I., Chowdhury, D., et al. (2014). Phosphorylated RPA recruits PALB2 to stalled DNA replication forks to facilitate fork recovery. *J. Cell Biol.* 206, 493–507. doi: 10.1083/jcb.201404111

Neelsen, K. J., and Lopes, M. (2015). Replication fork reversal in eukaryotes: from dead end to dynamic response. *Nat. Rev. Mol. Cell. Biol.* 16, 207–220. doi: 10.1038/nrm3935

Nepal, M., Che, R., Zhang, J., Ma, C., and Fei, P. (2017). Fanconi anemia signaling and cancer. *Trends Cancer* 3, 840–856. doi: 10.1016/j.trecan.2017.10.005

Ou, H. L., and Schumacher, B. (2018). DNA damage responses and p53 in the aging process. *Blood* 131, 488–495. doi: 10.1182/blood-2017-07-746396

Peng, M., Cong, K., Panzarino, N. J., Nayak, S., Calvo, J., Deng, B., et al. (2018). Opposing roles of FANCJ and HLTF protect forks and restrain replication during stress. *Cell Rep.* 24, 3251–3261. doi: 10.1016/j.celrep.2018.08.065

Pichierri, P., Franchitto, A., and Rosselli, F. (2004). BLM and the FANC proteins collaborate in a common pathway in response to stalled replication forks. *EMBO J.* 23, 3154–3163. doi: 10.1038/sj.emboj.7600277

Poole, L. A., and Cortez, D. (2017). Functions of SMARCAL1, ZRANB3, and HLTF in maintaining genome stability. *Crit. Rev. Biochem. Mol. Biol.* 52, 696–714. doi: 10.1080/10409238.2017.1380597

Rickman, K., and Smogorzewska, A. (2019). Advances in understanding DNA processing and protection at stalled replication forks. *J. Cell. Biol.* 218, 1096–1107. doi: 10.1083/jcb.201809012

Sakaguchi, K., Ishibashi, T., Uchiyama, Y., and Iwabata, K. (2009). The multi-replication protein A (RPA) system–a new perspective. *FEBS J.* 276, 943–963. doi: 10.1111/j.1742-4658.2008.06841.x

Sale, J. E. (2013). Translesion DNA synthesis and mutagenesis in eukaryotes. *Cold Spring Harb. Perspect Biol.* 5:a012708. doi: 10.1101/cshperspect.a012708

Schlacher, K., Wu, H., and Jasin, M. (2012). A distinct replication fork protection pathway connects Fanconi anemia tumor suppressors to RAD51-BRCA1/2. *Cancer Cell* 22, 106–116. doi: 10.1016/j.ccr.2012.05.015

Schubert, L., Ho, T., Hoffmann, S., Haahr, P., Guerillon, C., and Mailand, N. (2017). RADX interacts with single-stranded DNA to promote replication fork stability. *EMBO Rep.* 18, 1991–2003. doi: 10.15252/embr.201744877

Sinha, A., Saleh, A., Endersby, R., Yuan, S. H., Chokshi, C. R., Brown, K. R., et al. (2020). RAD51-Mediated DNA homologous recombination is independent of PTEN mutational status. *Cancers (Basel)* 12:3178. doi: 10.3390/cancers12113178

Somyajit, K., Saxena, S., Babu, S., Mishra, A., and Nagaraju, G. (2015). Mammalian RAD51 paralogs protect nascent DNA at stalled forks and mediate replication restart. *Nucleic Acids Res.* 43, 9835–9855. doi: 10.1093/nar/gkv880

Su, F., Mukherjee, S., Yang, Y., Mori, E., Bhattacharya, S., Kobayashi, J., et al. (2014). Nonenzymatic role for WRN in preserving nascent DNA strands after replication stress. *Cell Rep.* 9, 1387–1401. doi: 10.1016/j.celrep.2014.10.025

Taglialatela, A., Alvarez, S., Leuzzi, G., Sannino, V., Ranjha, L., Huang, J. W., et al. (2017). Restoration of replication fork stability in BRCA1- and BRCA2-deficient cells by inactivation of SNF2-family fork remodelers. *Mol. Cell* 68:e418. doi: 10.1016/j.molcel.2017.09.036

Thangavel, S., Berti, M., Levikova, M., Pinto, C., Gomathinayagam, S., Vujanovic, M., et al. (2015). DNA2 drives processing and restart of reversed replication forks in human cells. *J. Cell Biol.* 208, 545–562. doi: 10.1083/jcb.201406100

Tian, T., Bu, M., Chen, X., Ding, L., Yang, Y., Han, J., et al. (2021). The ZATT-TOP2A-PICH Axis Drives Extensive Replication Fork Reversal to Promote Genome Stability. *Mol. Cell.* 81, 198 e196–211 e196. doi: 10.1016/j.molcel.2020.11.007

Tye, S., Ronson, G. E., and Morris, J. R. (2020). A fork in the road: where homologous recombination and stalled replication fork protection part ways. *Semin. Cell. Dev. Biol. [Online ahead of print]* S1084–S9521. doi: 10.1016/j.semcdb.2020.07.004

Unk, I., Hajdu, I., Blastyak, A., and Haracska, L. (2010). Role of yeast Rad5 and its human orthologs, HLTF and SHPRH in DNA damage tolerance. *DNA Repair (Amst)* 9, 257–267. doi: 10.1016/j.dnarep.2009.12.013

Vujanovic, M., Krietsch, J., Raso, M. C., Terraneo, N., Zellweger, R., Schmid, J. A., et al. (2017). Replication fork slowing and reversal upon DNA damage require PCNA Polyubiquitination and ZRANB3 DNA translocase activity. *Mol. Cell.* 67, 882–890e885. doi: 10.1016/j.molcel.2017.08.010

Weston, R., Peeters, H., and Ahel, D. (2012). ZRANB3 is a structure-specific ATP-dependent endonuclease involved in replication stress response. *Genes Dev.* 26, 1558–1572. doi: 10.1101/gad.193516.112

Yuan, J., Ghosal, G., and Chen, J. (2009). The annealing helicase HARP protects stalled replication forks. *Genes Dev.* 23, 2394–2399. doi: 10.1101/gad.1836409

Yuan, J., Ghosal, G., and Chen, J. (2012). The HARP-like domain-containing protein AH2/ZRANB3 binds to PCNA and participates in cellular response to replication stress. *Mol. Cell* 47, 410–421. doi: 10.1016/j.molcel.2012.05.025

Zellweger, R., Dalcher, D., Mutreja, K., Berti, M., Schmid, J. A., Herrador, R., et al. (2015). Rad51-mediated replication fork reversal is a global response to genotoxic treatments in human cells. *J. Cell. Biol.* 208, 563–579. doi: 10.1083/jcb.201406099

Zhang, H., Schaub, J. M., and Finkelstein, I. J. (2020). RADX condenses single-stranded DNA to antagonize RAD51 loading. *Nucleic Acids Res.* 48, 7834–7843. doi: 10.1093/nar/gkaa559

Conflict of Interest: The authors declare that the research was conducted in the absence of any commercial or financial relationships that could be construed as a potential conflict of interest.

frontiers in Cell and Developmental Biology

REVIEW
published: 25 June 2021
doi: 10.3389/fcell.2021.702584

The Replication Stress Response on a Narrow Path Between Genomic Instability and Inflammation

Hervé Técher and Philippe Pasero**

Institut de Génétique Humaine, CNRS, Université de Montpellier, Equipe Labellisée Ligue Contre le Cancer, Montpellier, France

The genome of eukaryotic cells is particularly at risk during the S phase of the cell cycle, when megabases of chromosomal DNA are unwound to generate two identical copies of the genome. This daunting task is executed by thousands of micro-machines called replisomes, acting at fragile structures called replication forks. The correct execution of this replication program depends on the coordinated action of hundreds of different enzymes, from the licensing of replication origins to the termination of DNA replication. This review focuses on the mechanisms that ensure the completion of DNA replication under challenging conditions of endogenous or exogenous origin. It also covers new findings connecting the processing of stalled forks to the release of small DNA fragments into the cytoplasm, activating the cGAS-STING pathway. DNA damage and fork repair comes therefore at a price, which is the activation of an inflammatory response that has both positive and negative impacts on the fate of stressed cells. These new findings have broad implications for the etiology of interferonopathies and for cancer treatment.

Keywords: DNA replication dynamics, fork progression, fork processing, fork reversal, cGAS-STING, inflammation

OPEN ACCESS

Edited by:
Yuanliang Zhai,
The University of Hong Kong, Hong Kong

Reviewed by:
Filippo Roselli,
UMR 9019 Center for the National Scientific Research (CNRS), France
Alexandre Maréchal,
Université de Sherbrooke, Canada

****Correspondence:***
Hervé Técher
herve.techer@igh.cnrs.fr
Philippe Pasero
philippe.pasero@igh.cnrs.fr

Specialty section:
This article was submitted to Cell Growth and Division, a section of the journal Frontiers in Cell and Developmental Biology

Received: *29 April 2021*
Accepted: *03 June 2021*
Published: *25 June 2021*

Citation:
Técher H and Pasero P (2021) The Replication Stress Response on a Narrow Path Between Genomic Instability and Inflammation. Front. Cell Dev. Biol. 9:702584. doi: 10.3389/fcell.2021.702584

INTRODUCTION

Eukaryotic DNA replication refers to a complex set of biological processes that duplicate chromosomal DNA during the S phase of the cell cycle. Briefly, DNA replication is pre-set in G_1, when origins of replication are "licensed" through the assembly of the pre-replication complex (pre-RC) on chromatin (Mechali, 2010). During this process, the six-subunit origin recognition complex (ORC) provides a platform to load the minichromosome maintenance (MCM) complex in a Cdc6- and Cdt1-dependent manner (**Figure 1A**). Upon entry into S phase, cyclin-dependent kinases (CDKs), and Dbf4-Cdc7 (DDK) activate a subset of these potential replication origins (pre-RCs). A critical step is the formation and activation of the replicative helicase, namely the CMG (CDC45-MCMs-GINS) complex, which opens the DNA duplex, leading to the formation of a replication bubble onto which the replication machinery—composed of two replisomes—assembles and initiates DNA synthesis. A replication bubble is composed of two replication forks traveling in opposite directions. In metazoans, the nature of replication origins is still poorly understood. It appears that diverse cues at the level of the DNA sequence and chromatin conformation contribute to the establishment of the pool of potential origins and the efficiency of origin firing (Mechali, 2010; Hyrien, 2015; Urban et al., 2015; Valton and Prioleau, 2016).

During the S phase, hundreds to thousands of origins fire sequentially at defined times to ensure the completion of DNA replication before chromosome segregation. Origin firing follows a specific spatial and temporal program—not yet understood in the very details—that is cell-type specific and is determined epigenetically by the chromosome environment (Rivera-Mulia and Gilbert, 2016). In mammals, the timing and efficiency of origin activation correlates also with ORC density, as indicated by chromatin immunoprecipitation experiments (Miotto et al., 2016). Only a fraction of all licensed origins is used during a normal S phase. The pool of "licensed" but inactive origins, also known as dormant origins, serves as backup to complete DNA synthesis in case of fork slowing or stalling (Blow et al., 2011; Técher et al., 2017).

DNA replication is often challenged by events of exogenous or endogenous origin that impede the rate and fidelity of DNA synthesis, and as a consequence affect the integrity of chromosomes. These events are collectively referred to as replication stress (RS). They include DNA lesions caused by ultraviolet (UV) light or oxidative DNA damage, shortage of deoxyribonucleotides (dNTPs) or exposure to a broad panel of genotoxic agents used in chemotherapy to target DNA replication. In all eukaryotes, RS is detected and signaled through a conserved pathway involving the Mec1 and Rad53 kinases in budding yeast (Pardo et al., 2017) and the ATR and CHK1 kinases in mammals (Zeman and Cimprich, 2014). The ATR-CHK1 pathway senses and signals the presence of single-stranded (ss) DNA at impaired replication forks and on damaged DNA.

The mechanisms that regulate DNA replication during the cell cycle and coordinate the cellular responses to RS have been extensively discussed elsewhere (Mechali, 2010; Renard-Guillet et al., 2014; Zeman and Cimprich, 2014; Bellelli and Boulton, 2021). This review addresses the events that perturb the progression, the structure and the stability of replication forks, with a focus on the links between the stability of nascent DNA at stalled replication forks and the cellular responses to self DNA by the cGAS-STING pathway. Although we discuss conceptual advances obtained from model systems such as yeast and *Xenopus* egg extracts, this review focuses on mammalian models because of recent advances on the links between RS and innate immunity. This connection has major implications for cancer therapy by opening new avenues for the development of innovative strategies exploiting RS-induced inflammation.

DNA REPLICATION UNDER NORMAL AND PATHOLOGICAL CONDITIONS

Normal Fork Progression

Eukaryotic replication forks progress at a median speed of 1–2 kb per min in unperturbed growth conditions (Tuduri et al., 2010; Guilbaud et al., 2011; Técher et al., 2013). Determination of fork speed was made possible with the development of DNA fiber autoradiography (Huberman and Riggs, 1966) and related immunofluorescence-based assays called DNA fiber spreading (Jackson and Pombo, 1998), DNA combing (Michalet et al., 1997) and SMARD (Single Molecule Analysis of Replicated DNA) (Norio and Schildkraut, 2001). In these assays, ongoing DNA synthesis is labeled with halogenated thymidine analogs and the length of labeled tracks is measured to determine the speed of individual replication forks.

Fork speed shows a broad distribution in a population of cells, reflecting either cell-to-cell differences or locus-specific variations. DNA synthesis requires a constant supply of histones (Groth et al., 2007; Mejlvang et al., 2014) and dNTPs (Anglana et al., 2003; Poli et al., 2012) that can fluctuate during S phase and thus could affect the overall speed of replication forks. In human HCT116 cells, forks are slower in early S phase than in late S phase (Malinsky et al., 2001; Bianco et al., 2019), presumably because dNTP levels are lower upon entry into S phase (Malinsky et al., 2001). This is reminiscent of *S. cerevisiae* cells, which enter S phase with suboptimal dNTP pools and activate the Mec1^{ATR} pathway to induce dNTP synthesis and complete bulk DNA synthesis (Forey et al., 2020). However, differences between early and late DNA synthesis were not observed in other cell types (Guilbaud et al., 2011; Eykelenboom et al., 2013). Further work is therefore needed to elucidate the complex interplay between replication timing, dNTP levels and fork speed.

In addition to global changes in replication rate, specific DNA sequences or chromosomal structures may locally impede fork progression. For instance, a variety of programmed replication pause sites have been identified in the genome of unicellular eukaryotes by two-dimensional gel electrophoresis (Deshpande and Newlon, 1996; Mirkin and Mirkin, 2007; Lambert and Carr, 2013). In large genomes, DNA fiber analysis is a method of choice to monitor site-specific events when combined with fluorescence *in situ* hybridization (FISH) to identify loci of interest along individual DNA fibers. This strategy was used to compare fork speed at specific loci relative to bulk DNA synthesis (Norio and Schildkraut, 2001; Pasero et al., 2002; Lebofsky et al., 2006) and led to contrasting results. Forks do not slow down at difficult-to-replicate loci such as the common fragile site (CFS) FRA3B (Letessier et al., 2011) and at the immunoglobulin heavy chain (IgH) locus (Guilbaud et al., 2011). However, they are slower at the AT-rich FRA16C CFS (Ozeri-Galai et al., 2011) and stall at CGG/CCG trinucleotide repeats located at the FMR1/fragile X locus (Gerhardt et al., 2014). Reduced fork velocity is also observed at centromeric and pericentromeric regions containing G4 (G-quadruplex)-forming sequences (Mendez-Bermudez et al., 2018), which are susceptible to breakage under replication stress conditions (Crosetto et al., 2013). Together, these studies indicate that although non-B DNA structures could locally slow down fork progression at specific loci, the mechanisms that govern the overall distribution of fork velocity in a population of cells remain poorly understood. At the level of the FRA3B CFS, completion of replication is challenged by the late timing of replication of this region and the lack of replication origins (Letessier et al., 2011). Difficult-to-replicate loci, such as some CFS, are thus not only defined by DNA sequence-driven impediments to fork passage, other important cues include replication timing, availability of replication origins, proficiency for restart and repair mechanisms, all of which being impacted by specific chromatin context. Interestingly, it has been recently reported that identical DNA molecules replicated *in vitro*

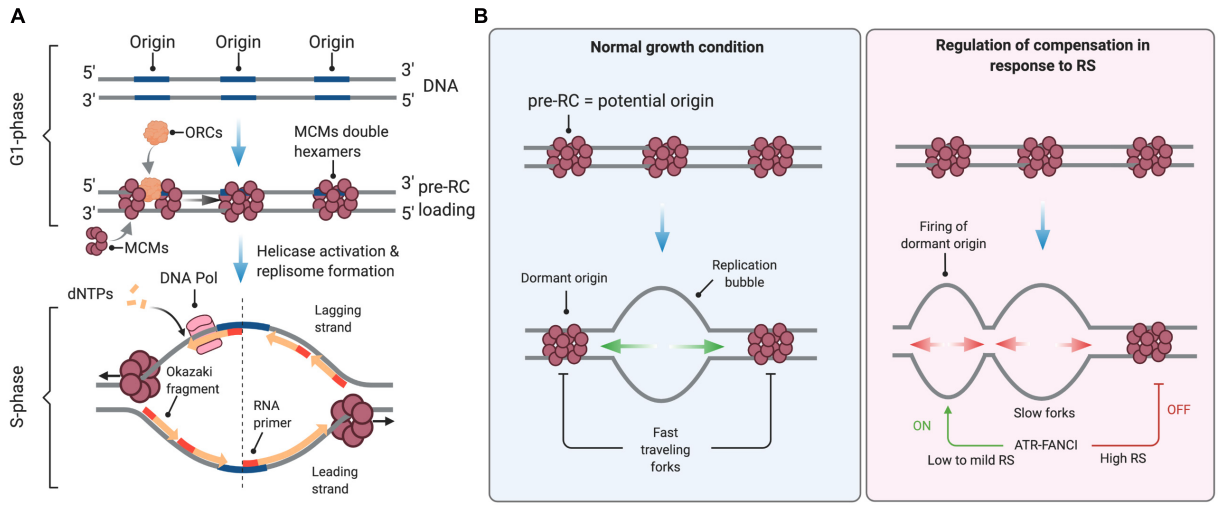

FIGURE 1 | Control of DNA replication origin firing. **(A)** Origins of replication are licensed during the G1 phase of the cell cycle through the sequential loading of the ORC and MCM complexes to form the pre-replication (pre-RC) complex. At the S-phase onset, S-CDK and DDK activate the replicative helicase by recruiting CDC45 and the GINS complex, enabling DNA unwinding and the formation of active replisomes. dNTPs are the essential building blocks used by the replicative DNA polymerases to elongate nascent DNA. **(B)** In normal growth conditions, firing is limited to a few licensed origins. Forks travel at full speed, inactivating neighboring unfired origins. Under conditions of low to mild RS, cells compensate for slow elongation by activating backup origins known as dormant origins. Under acute RS conditions, the ATR-FANCI pathway restrains the activation of new origins. See the text for further details. This figure has been created with BioRender.com.

by reconstituted replisomes also show a wide distribution of fork speed (Graham et al., 2017; Kurat et al., 2017; Yeeles et al., 2017), suggesting that replication forks stochastically pause and restart in a locus-independent manner.

Regulation of Fork Progression Under Replication Stress

Conditions that slow down or block replication fork progression are collectively referred to as RS (Zeman and Cimprich, 2014; Bellelli and Boulton, 2021). RS is often detected indirectly by measuring the activity of the ATR-CHK1 pathway (Toledo et al., 2017). It can also be more directly assessed with DNA fiber assays by comparing the length of replicated tracks before and after exposing cells to exogenous inducers of RS (Técher et al., 2013; Toledo et al., 2017). The impact of RS on fork velocity has been extensively documented by many groups. For example, fork progression is dramatically impacted by DNA alkylating agents (Merrick et al., 2004) and by hydroxyurea (HU), an inhibitor of ribonucleotide reductase (RNR) inducing dNTP starvation (Técher et al., 2016, 2017). Aphidicolin (APH), an inhibitor of replicative DNA polymerases, is also commonly used to slow down DNA synthesis (Koundrioukoff et al., 2013). Although, slowdown of replication forks is probably the most direct manifestation of RS, which can be directly assessed with DNA fiber analysis, there are other causes of RS, such as a paucity in initiation events or an acceleration of replication forks.

DNA fiber analysis is also instrumental to detect spontaneous fork pausing events at a global level by measuring differences in the progression of sister replication forks. Indeed, when two unchallenged forks progressing from a given replication origin are labeled with successive pulses of IdU and CldU, the length of labeled tracks should be nearly identical. In contrast, pausing or stalling of one of the forks should result in an asymmetric pattern (Conti et al., 2007; Tuduri et al., 2009). Differences between the length of adjacent IdU and CldU tracks generated by a given fork is also indicative of increased pausing or stalling (Conti et al., 2007; Técher et al., 2013; Quinet et al., 2017).

Mild RS, defined as a reduction of fork rate lower than 50% compared to untreated cells, is well tolerated by mammalian cells. For instance, low doses of APH or HU do not activate the ATR-CHK1 pathway and do not induce detectable levels of DNA breaks even though they induce a significant slowdown of fork velocity (Bergoglio et al., 2013; Koundrioukoff et al., 2013; Toledo et al., 2013; Wilhelm et al., 2014; Saxena et al., 2018). This tolerance to mild RS conditions is due to the coordinated action of RS response pathways that stabilize, assist and restart paused forks (Toledo et al., 2017; Bellelli and Boulton, 2021). Tolerance to RS also depends on dormant replication origins (**Figure 1B**), which are present in large excess on chromosomes and act as backup to rescue stalled or collapsed forks (Técher et al., 2017).

In untreated cells, the rate of fork progression inversely correlates with the density of active origins (Anglana et al., 2003; Woodward et al., 2006; Ge et al., 2007; Courbet et al., 2008). Under low to mild HU or APH treatment, cells also activate dormant origins to compensate for slower forks (Ge et al., 2007; Courbet et al., 2008; Técher et al., 2016). This regulation operates within replication foci, which correspond to clusters of replication origins that are activated in a coordinated manner (Jackson and Pombo, 1998; Anglana et al., 2003; Conti et al., 2007). Within these replication foci, initiation events are distributed every 100–150 kb on average. When forks slow down, inter-origin distances (IODs) decrease due to the passive activation of dormant origins and via an active process mediated by ATR (Shechter et al., 2004; Lossaint et al., 2013; Chen et al., 2015). In response to low levels of RS (e.g., low dose of HU)

the activation of dormant origins is promoted by FANCI and inhibited by FANCD2, likely through the phosphorylation of MCMs by the CDC7 kinase (Chen et al., 2015). The lack of ATR activation under low RS conditions is thus compatible with the firing of extra origins (Koundrioukoff et al., 2013). In contrast, initiation is repressed in response to high levels of RS (e.g., high doses of HU; Costanzo et al., 2003; Shechter et al., 2004; Ge and Blow, 2010). Under these conditions, ATR phosphorylates also FANCI, which then loses its ability to stimulate origin firing but promotes fork stability and restart together with FANCD2 (Lossaint et al., 2013; Chen et al., 2015; **Figure 1B**).

The ability to activate dormant origins near paused or arrested forks represents a strategy of choice to resume replication. Indeed, the excess of MCMs loaded onto chromatin is critical to maintain the availability of dormant origins in cancer cell lines. Under RS conditions, the partial depletion of MCMs abrogates the capacity of these cells to mobilize extra-origins and leads to increased chromosomal instability and cell death (Ge et al., 2007; Ibarra et al., 2008). In contrast, non-transformed cells are less dependent on high MCM levels to tolerate fork slowing.

Although this RS tolerance mechanism is very robust, it has some inherent limitations. The deleterious consequences of massive fork arrest or destabilization cannot be compensated by the firing of dormant origins and can even promote genome instability. Indeed, the activation of a large number of extra origins stresses the system by exhausting limiting factors. Work from the Lukas and Debatisse laboratories has shown that high levels of RS resulting from the combination of APH and ATR inhibition leads to replication catastrophe (Koundrioukoff et al., 2013; Toledo et al., 2013). In this context, the single-stranded (ss) DNA binding factor RPA becomes limiting, impacting both fork stability and checkpoint activation (Toledo et al., 2013). Moreover, activation of additional origins on a damaged template increases the number of stalled forks and generates additional substrates for structure-specific nucleases, contributing therefore to genomic instability (Pasero and Vindigni, 2017). In addition, dNTPs become limiting when too many origins are activated simultaneously in yeast and in mammalian cells (Petermann et al., 2010b; Mantiero et al., 2011).

Interestingly, dNTP levels also drop to suboptimal levels when budding yeast cells enter S phase and activate early replication origins. This dNTP shortage interferes with fork progression and activates the $Mec1^{ATR}$ kinase, leading to the upregulation of RNR and to replication resumption (Forey et al., 2020). This transient RS represents therefore the physiological signal to coordinate the production of dNTPs with the onset of S phase. Finally, ATR is also important to couple S phase completion with mitosis onset during normal growth conditions in human cells. ATR inhibition or depletion results in premature entry into mitosis with genomic loci not being fully replicated. Under-replication leads to mitotic aberrations such as anaphase bridges and formation of chromosomal breaks (Eykelenboom et al., 2013; Saldivar et al., 2018).

In addition to the initiation rate, RS can also modulate fork speed. Somyajit and colleagues have recently shown that fork slowing in HU-treated cells depends on the sensing of oxidative stress by replisome components such as Timeless (Somyajit et al., 2017). Moreover, the ATR-CHK1 pathway actively reduces fork speed in response to RS. In human primary dermal fibroblasts exposed to HU, ATR slows down forks by targeting the MCM complex in a FANCD2-dependent manner (Lossaint et al., 2013). When forks face discrete impediments such as those caused by inter-strand crosslinks (ICLs), ATR signaling can also downregulate distant forks, although to a lesser extent than ICLs themselves (Mutreja et al., 2018). In budding yeast, replication forks progress faster when cells exposed to MMS or to low levels of DSBs are unable to activate $Rad53^{CHK1}$, indicating that the DNA damage response actively reduces elongation (Bacal et al., 2018). Global fork slowing also relies on the CHK1 kinase in human cells exposed to low doses of the topoisomerase I inhibitor camptothecin (CPT) (Seiler et al., 2007). In CHK1-depleted cells, DNA lesions indirectly slow fork progression through the activation of the DNA damage response, notably via the ATM-p53 axis (Técher et al., 2016). In this latter case, fork slowing has been proposed to be, at least in part, the consequence dNTP starvation because the pool of dNTP has to be shared between repair and replication events (Técher et al., 2016).

PATHOLOGICAL CONSEQUENCES OF REPLICATION STRESS

The RS response is activated in a variety of physiological and pathological situations. This chapter focuses on RS conditions that promote genomic instability and addresses how RS can be exploited in cancer treatment as a mean to overload tumor cells with an unbearable amount of DNA lesions (O'Connor, 2015). The pathological situations triggering an acute RS response differ significantly from the milder RS situations described above, in which functional checkpoint and repair pathways promote tolerance to low levels of RS. Acute RS situations are typically observed in cells defective for homologous recombination (HR) and ATR-CHK1 pathways, which accumulate RS and DNA damage markers (Kolinjivadi et al., 2017a; Técher et al., 2017). Hereafter, specific examples are discussed in which failure in one of these key pathways unveil their essential function in genome maintenance under RS conditions.

Single-Stranded DNA Gaps at Stalled Forks

The RAD51 recombinase is a key HR factor that binds protruding 3′ single-stranded DNA (ssDNA) ends formed at resected double-strand breaks (DSBs) to form RAD51 filaments (Jasin and Rothstein, 2013). Resection of DNA ends is initiated by the endonuclease and 3′–5′ exonuclease MRE11 (Shibata et al., 2014) and is further extended by the long-range resection nucleases DNA2 and EXO1 (Jasin and Rothstein, 2013; Pasero and Vindigni, 2017). The key function of the RAD51 filament is to invade a donor DNA duplex harboring sequence homology to serve as template for DNA repair synthesis.

Pioneering work from Costanzo and colleagues using an electron microscopy (EM) approach developed by Jose Sogo (Sogo et al., 2002; Vindigni and Lopes, 2017) revealed that inactivation of RAD51 in *Xenopus* egg extract leads to the formation of ssDNA gaps at arrested forks (Hashimoto et al.,

2010). Together with studies from the Jasin group (Schlacher et al., 2011, 2012), these seminal observations unveiled a novel role for HR factors in the protection of nascent DNA at stalled forks. In this process, RAD51 is loaded on newly replicated chromatin by BRCA1 and BRCA2, as shown by iPOND (isolation of proteins on nascent DNA) and related assays (Petermann et al., 2010a; Zellweger et al., 2015; Kolinjivadi et al., 2017b), to prevent the excessive degradation of nascent DNA strands by MRE11 (Hashimoto et al., 2010; Schlacher et al., 2011). The fork protection mechanism mediated by RAD51 depends on its ability to form a fully functional nucleofilament (Zadorozhny et al., 2017).

Fork resection is a conserved mechanism that has been reported in different species, from yeast to *Xenopus*, mice and human (Schlacher et al., 2011, 2012; Somyajit et al., 2015; Ait Saada et al., 2017; Kolinjivadi et al., 2017b; Lemacon et al., 2017; Mijic et al., 2017; Delamarre et al., 2020). Importantly, fork resection is not a pathological process *per se*, but rather a physiological event promoting HR-mediated fork repair and contributing to the activation of the ATR-CHK1 pathway (Coquel et al., 2018; García-Rodríguez et al., 2018; Menin et al., 2018; Villa et al., 2018; Delamarre et al., 2020). Accordingly, fork resection has been reported in a variety of HU-treated human cells, including U2OS, HeLa, and HEK293T cells (Thangavel et al., 2015; Bhat et al., 2018; Coquel et al., 2018). However, nascent DNA resection must be tightly controlled to prevent irreversible fork collapse.

The nature of MRE11 substrates at stalled forks is currently the subject of intense research (**Figure 2**). In RAD51-deficient *Xenopus* egg extracts, ssDNA gaps are detected both immediately behind stalled forks and at internal sites on daughter strands (Hashimoto et al., 2010). Only internal gaps depend on MRE11, the ssDNA gaps observed at the fork junction potentially resulting from an uncoupling between DNA polymerase and helicase activities (Zou and Elledge, 2003; Byun et al., 2005). Interestingly, most internal gaps show an asymmetric distribution on daughter strands (Hashimoto et al., 2010; Kolinjivadi et al., 2017b). An attractive possibility could be that incomplete Okazaki fragment processing on the lagging strand provides entry points for MRE11-mediated degradation. This view is supported by the fact that RAD51 interacts with DNA polymerase alpha (Pol α) and that RAD51 depletion leads to a decreased loading of Pol α at forks, leading to incomplete Okazaki fragments synthesis

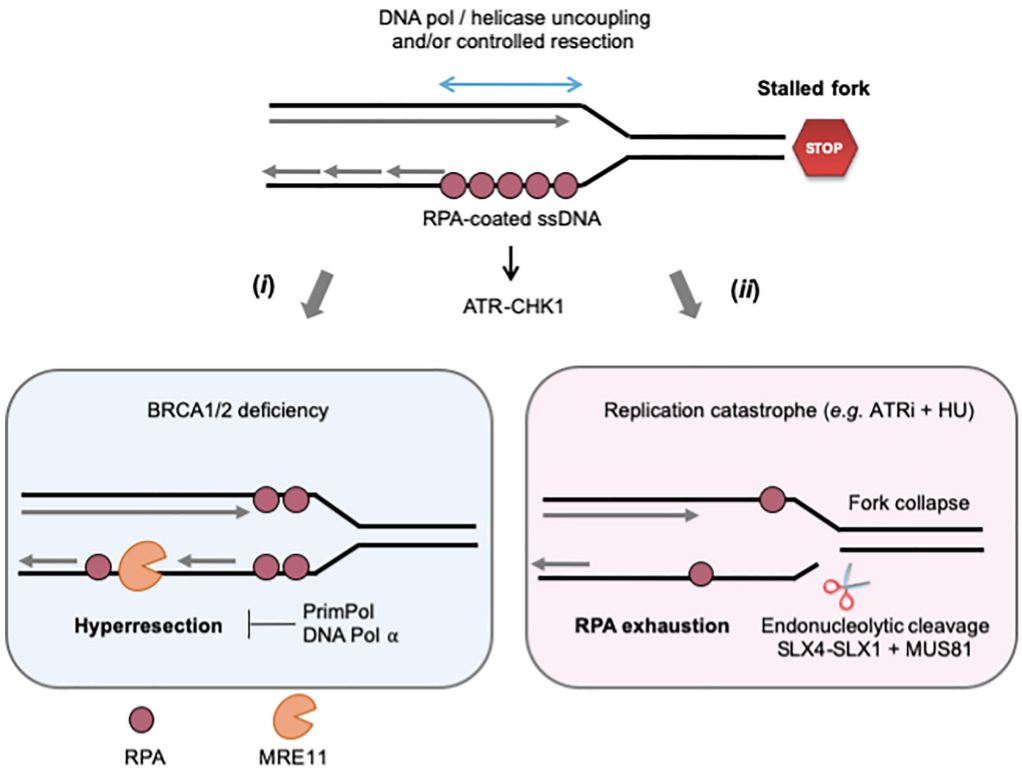

FIGURE 2 | Controlled and pathological formation of ssDNA at stalled forks. When cells are exposed to RS, ssDNA forms at stalled forks through the uncoupling of replicative helicase and polymerase activities and/or the controlled degradation of nascent DNA by MRE11 and other nucleases. The ssDNA exposed is covered by the ssDNA-binding protein RPA, which serves as platform to recruit and activate ATR-CHK1 signaling. (*i*) In BRCA2-deficient cells, large ssDNA gaps form as the result of uncontrolled MRE11-mediated nascent DNA degradation (hyperresection). DNA pol α and PrimPol could either fill these gaps or promote lesion bypass while creating additional gaps in the process. (*ii*) The ATR-CHK1 pathway represses initiation when cells are exposed to acute RS conditions (high doses of APH or HU). In the presence of ATRi, the increased number of stalled forks depletes RPA and cells suffer from replication catastrophe, an event characterized by increased ssDNA exposure and massive fork collapse. Fork breakage may also result from uncontrolled nuclease activities, such as MUS81, SLX4-1. See text for further details.

(Kolinjivadi et al., 2017a,b). Moreover, inhibition of Pol α with the small-molecule inhibitor CD437 interferes with lagging strand synthesis and also leads to the accumulation of ssDNA gaps on one of the daughter strands (Ercilla et al., 2020). Although current EM techniques cannot discriminate between leading and lagging strands, these data strongly suggest that MRE11 acts on the lagging strand to generate ssDNA gaps in *Xenopus* egg extracts. In other organisms, it has been proposed that MRE11 can also act by enlarging ssDNA gaps generated upon repriming of DNA synthesis after a lesion on the leading strand (García-Rodríguez et al., 2018; Quinet et al., 2020; Somyajit et al., 2021). As it is the case for DSB end resection, the exonuclease activity of MRE11 is stimulated by its interaction with CtIP and SAMHD1 (Daddacha et al., 2017; Coquel et al., 2018). Moreover, long-range resection at stalled forks involves additional nucleases and DNA helicases such as EXO1 and BLM (Berti and Vindigni, 2016; Pasero and Vindigni, 2017).

Fork Reversal as a Mechanism to Protect and Restart Arrested Forks

Reversed forks (RVFs) result from the extensive remodeling of stalled forks into branched structures resembling Holliday junctions (HJs). HJs are formed during HR by strand invasion of a homologous template in a RAD51-dependent manner. Similarly, reversed forks (RVFs) result from the reannealing of parental DNA strands, zipping the fork backwards and allowing the concomitant pairing of newly synthesized strands (**Figure 3A**). RVFs were first visualized in budding yeast by EM, using psoralen-crosslinked DNA samples to prevent branch migration after DNA extraction (Sogo et al., 2002). EM analysis remains the gold standard to monitor RVF formation and stability in large vertebrate genomes (Vindigni and Lopes, 2017).

RVFs were initially observed in HU-treated yeast mutants deficient for the checkpoint kinase Rad53^{CHK1}, but not in wild-type cells (Sogo et al., 2002). This led to the assumption that RVFs are pathological structures corresponding to terminally arrested forks. However, several lines of evidence indicate that fork reversal is rather an active process contributing to the protection and the repair of arrested forks through an HR-mediated process that does not require the formation of a DSB (Berti and Vindigni, 2016; Giannattasio and Branzei, 2017; Teixeira-Silva et al., 2017). This raises important questions regarding (*i*) the conditions under which fork reverse, (*ii*) the factors that regulate fork reversal, (*iii*) the consequences of fork reversal in normal and pathological situations, and (*iv*) the requirement of a fork reversal for resection.

Conditions That Promote Fork Reversal

RVFs are rarely detected in unchallenged conditions (Sogo et al., 2002; Ray Chaudhuri et al., 2012; Zellweger et al., 2015; Kolinjivadi et al., 2017a), indicating either that fork reversal does not occur at natural pause sites and spontaneous DNA lesions or is too transient to be detected by EM. The frequency of RVFs increases dramatically when yeast cells and Xenopus egg extracts are exposed to low doses of the topoisomerase I inhibitor CPT (Ray Chaudhuri et al., 2012; Menin et al., 2018). Since topoisomerases release positive DNA supercoiling accumulating ahead of the replication fork, these data suggest that DNA torsional stress contributes to fork reversal. However, RVFs are also frequently detected in human cell lines exposed to a large panel of DNA damaging agents that do not necessarily accumulate DNA supercoiling (Zellweger et al., 2015). For instance, 20–30% of the replication intermediates (RIs) detected under mild RS conditions (40–60% fork slowdown) correspond to RVFs (Zellweger et al., 2015). These results suggest that fork reversal may significantly contribute to reduce fork rates. They also indicate that besides torsional stress, cellular factors may actively promote fork reversal. Fork reversal may also constitute a structure prone to recruit repair factors and allowing access to DNA damage on the template (Neelsen and Lopes, 2015; Berti and Vindigni, 2016).

Factors Regulating Fork Reversal

The DNA translocase SMARCAL1 is one of the first protein shown to cause fork reversal *in vivo* and *in vitro* (Bétous et al., 2012; Couch et al., 2013). This factor is responsible for half of RVFs in APH-treated *Xenopus* egg extract (Kolinjivadi et al., 2017b) and it plays a predominant role in fork reversal in BRCA1/2-deficient mammalian cells (Taglialatela et al., 2017). Other DNA translocases such as FBH1, HLTF, and ZRANB3 also play roles in the formation of RVFs, depending on the cell-type and the drugs used to induce RS (Fugger et al., 2015; Mijic et al., 2017; Vujanovic et al., 2017; Bai et al., 2020). It has been proposed that SNF2-family of DNA translocases may act hierarchically, SMARCAL1 and HLTF being first recruited on RPA-coated ssDNA to initiate fork reversal. In a second step, HLTF would recruit ZRANB3 through poly-ubiquitylation of PCNA to extend fork reversal (Taglialatela et al., 2017; Vujanovic et al., 2017; Bai et al., 2020). Further extension of RVFs downstream of SNF2-fork remodelers is mediated by topoisomerase II and the helicase PICH (Tian et al., 2021). In topoisomerase II- or PICH-depleted cells, reversed forks are less frequent and they show shorter regressed arms, suggesting that they are less stable. These translocases may also act on different substrates or fork structures, which would explain this apparent functional redundancy. It has been recently shown that 53BP1 protects forks that are reversed by FBH1 in U2OS cells (Liu et al., 2020), whereas BRCA2 protects SNF2-remodeled forks. These results point to the existence of several mechanisms of fork reversion and stabilization.

ATR phosphorylates SMARCAL1 in response to RS (Couch et al., 2013) and could therefore regulate fork reversal. It has been shown that ATR inhibits SMARCAL1 activity *in vitro* and, as a consequence, it has been proposed that ATR activity restrains fork reversal. This hypothesis is supported by the finding that more ssDNA is exposed in ATR-inhibited cells in a SMARCAL1-dependent manner (Couch et al., 2013). However, this view is not consistent with recent EM studies from Lopes and co-workers, showing that ATR inhibition abrogates fork reversal under diverse RS conditions (Mutreja et al., 2018). However, ATR inhibition has pleiotropic effects and could affect fork reversal indirectly, for instance by interfering with the localization or the

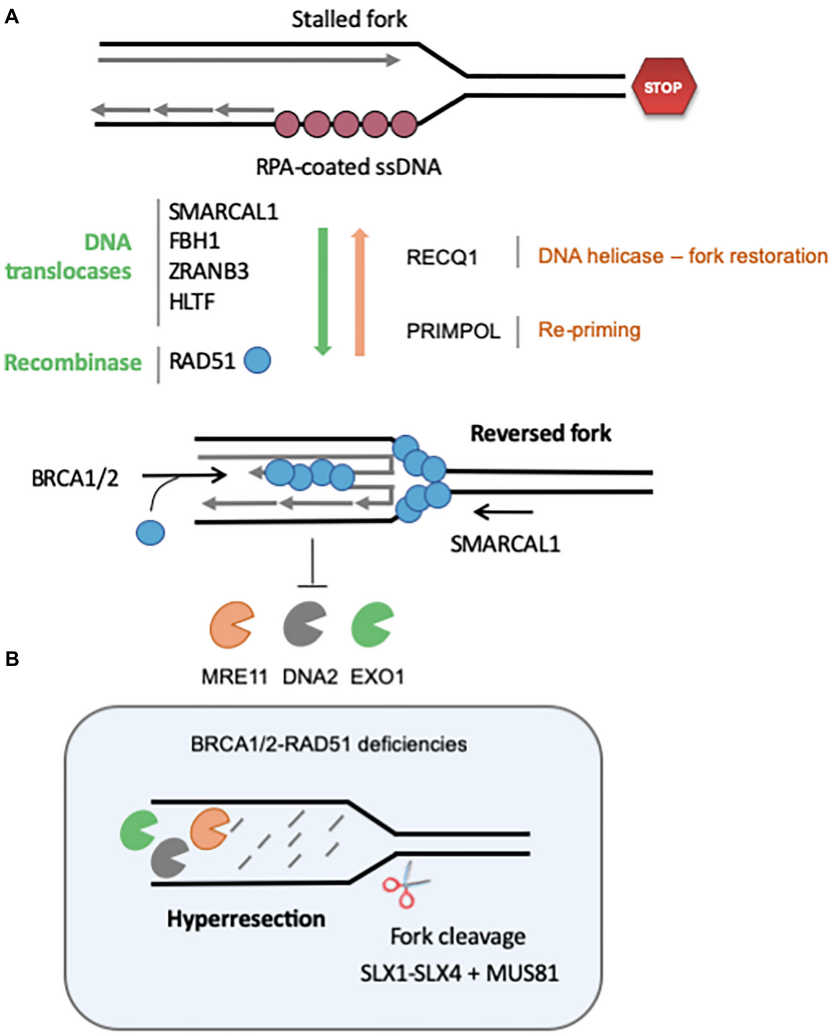

FIGURE 3 | Regulation of the formation and stability of reversed fork. **(A)** Fork reversal results from the re-annealing of parental strands, zipping the fork backward and promoting the pairing of nascent strands. Fork reversal is highly regulated, and many factors are currently known to regulate the balance between RVF formation, stabilization and restart. Redundant DNA translocases, namely SMARCAL1, FBH1, ZRANB3, and HLTF, have been described to promote fork regression *in vitro* and *in vivo*. The recombinase RAD51 also promotes fork reversion in a BRCA2-independent manner, although it is not clear whether its strand invasion property is required. RECQ1 is the major helicase known to promote restoration of the normal fork structure. PARP1 inhibits RECQ1-mediated fork restoration. Re-priming of DNA synthesis through PrimPol favors fork restart and reduces the frequency of fork regression. Once formed, RVF are stabilized by BRCA2-mediated loading of RAD51 on the regressed arm. **(B)** If BRCA-RAD51 fork protection is not functional, the regressed arm is extensively degraded by MRE11, DNA2 and EXO1. Eventually, the SLX1-SLX4-MUS81 endonucleases can cleave these structures to rescue forks. See text for further details.

function of HR factors such as RAD51 (Sorensen et al., 2005; Buisson et al., 2017).

RAD51 is another key regulator of fork reversal. Indeed, the partial depletion of RAD51 decreases the frequency of RVFs in human cells (Zellweger et al., 2015) and in *Xenopus* egg extracts (Kolinjivadi et al., 2017b). Moreover, SMARCAL1 and RAD51 depletion have additive effects on fork regression, showing that their mechanism of action is different. Interestingly, this function of RAD51 is also distinct from its role in the protection of nascent DNA against MRE11-dependent degradation. Since MRE11 acts on reversed forks, RAD51 could therefore promote fork resection both by contributing to fork reversal in a BRCA2-independent manner and by protecting nascent DNA from degradation in a BRCA2-dependent manner (Kolinjivadi et al., 2017b; Lemacon et al., 2017; Mijic et al., 2017).

RVFs can also form when DNA Pol α function is compromised in yeast primase mutants (Fumasoni et al., 2015) and in the absence of TIM (Timeless) and Tipin (Errico et al., 2007, 2014), two components of the fork protection complex (FPC). Since TIM and Tipin promote the recruitment of Pol α to chromatin (Errico et al., 2014), this suggests the existence of a link between RVFs and defects in Pol α-dependent DNA synthesis. Importantly, both Pol α and the FPC prevent the accumulation of ssDNA gaps at forks. Indeed, Pol α is required for lagging strand synthesis and the FPC coordinates the activity of DNA polymerases and helicases (Katou et al., 2003; Errico et al., 2009;

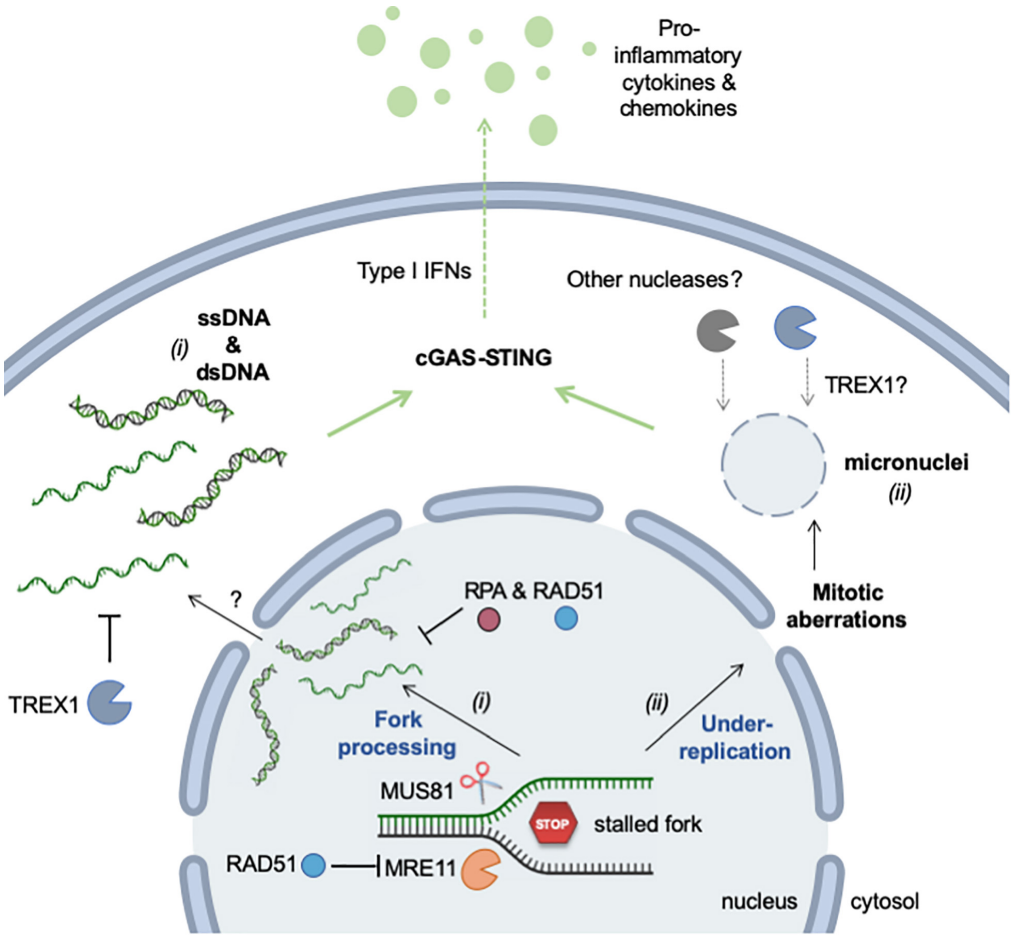

FIGURE 4 | Mechanisms of RS-induced accumulation of cytosolic (self-) DNA. Self DNA accumulates in the cytosol when mammalian cells are exposed to RS-inducing agents (e.g., HU, APH, CPT) or when cells are deficient for factors promoting replication fork stability (e.g., SAMHD1). The release of genomic DNA occurs in two different ways. (*i*) DNA fragments (ssDNA and dsDNA) are released from stalled forks by nucleolytic cleavage (MRE11 and MUS81). The mechanism by which these fragments exit the nucleus is currently unknown, but it is repressed by RPA and RAD51. TREX1 is the major cytosolic exonuclease that degrades DNA to prevent the activation of the cGAS-STING pathway. (*ii*) Incomplete replication, known as under-replication, induces chromosome segregation defects and leads to the formation of micronuclei and to other mitotic defects. Upon rupture of their membrane, cGAS localizes to micronuclei and activates STING. Whether TREX1 or other nucleases can access DNA inside micronuclei is not known. See text for additional details. This figure was created in part with BioRender.com.

Kurat et al., 2017; Abe et al., 2018). In addition, Pol α may reprime DNA synthesis at stalled forks and contribute to the filling of post-replicative ssDNA gaps, presumably through the interaction between Pol α and RAD51 (Kolinjivadi et al., 2017b). This balance between resection and repriming is well documented at unprotected telomeres, where EXO1-mediated resection is compensated by Pol α gap filling (Wu et al., 2012) and could also occurs during DSB repair (Mirman et al., 2018). Moreover, the Pol α interactor AND1 is important to promote both fork progression and protection (Abe et al., 2018). Increased fork reversal upon AND1 or Tipin depletion suggests that ssDNA gaps promote RVFs (Errico et al., 2014; Abe et al., 2018), as illustrated by the presence of single-stranded tails at RVFs (Thangavel et al., 2015; Kolinjivadi et al., 2017b; Lemacon et al., 2017).

Another important regulator of fork reversal is the poly-ADP-ribose polymerase 1 (PARP1). In particular, PARP1 promotes RVF in response to topoisomerase I inhibition by CPT (Ray Chaudhuri et al., 2012; Berti et al., 2013), but the mechanism involved remains elusive. PARP1 interacts with RECQ1, a DNA helicase involved in the resolution of RVFs (Berti et al., 2013) and PARP1 inhibition reduces the frequency of CPT-induced RVFs in controls cells but not in RECQ1-depleted cells. RECQ1 could therefore be the main target of PARP1 to stabilize RVFs by preventing their resolution by RECQ1.

The expression of p53 has been shown to restrain fork progression and to promote recombination events in absence or presence of exogenous RS inducers (Hampp et al., 2016; Biber et al., 2021). P53 interacts with the translesion synthesis polymerase ι (POLι) and PCNA that promote a mechanism called "idling," which acts as a replication barrier and gives time for HLTF to poly-ubiquitylate PCNA. The DNA binding and interaction with RPA of p53 are required for this DNA damage tolerance pathway, but transcription regulation is not (Biber et al., 2021). It has been suggested that this "idling" mechanism

promotes fork reversal by the combined action of HLTF and ZRANB3, leading to the observed fork deceleration and increase frequency of recombinational events during S phase.

PrimPol, a DNA polymerase with primase activity, has recently been discovered and acts in a parallel pathway to fork reversal (Bianchi et al., 2013; Mourón et al., 2013; Wan et al., 2013). PrimPol promotes fork progression under RS conditions induced by UV irradiation or HU treatment by repriming DNA synthesis at stalled forks. PrimPol defects lead to the persistence of ssDNA gaps (Vallerga et al., 2015). In the absence of RAD51, cells accumulate ssDNA gaps in a PrimPol dependent-manner, indicating that PrimPol promotes constant re-priming in these cells, at the expense of nascent DNA integrity (Vallerga et al., 2015). Moreover, PrimPol restrains nascent DNA degradation in BRCA-deficient cells by preventing fork reversal (Quinet et al., 2020). Conversely, inhibition of fork reversal by SMARCAL1 or HLTF depletion favors PrimPol-mediated repriming (Bai et al., 2020; Quinet et al., 2020). The balance between RAD51-SMARCAL1 and PrimPol dictates the choice between fork reversal and repriming, with potential consequences on the degradation of RVFs by MRE11 (i.e., in BRCA deficient background) or the persistence of ssDNA gaps.

Importantly, the balance between fork reversal and repriming also impacts on the speed of replication forks, as measured by DNA fiber assays. Indeed, the fork slowdown induced by MMC or CPT in human cells depends on RAD51 (Zellweger et al., 2015) and the effect of Cisplatin and UV on chicken DT40 cells depends on the RAD51 paralog XRCC3 (Henry-Mowatt et al., 2003). Since XRCC3 regulates RAD51 activity, both factors could indirectly regulate fork speed by promoting fork reversal. Along the same line, the depletion of SMARCAL1 or PARP1 increases fork speed in a variety of contexts (Berti et al., 2013; Mijic et al., 2017; Vujanovic et al., 2017; Maya-Mendoza et al., 2018) and p53 expression leads to fork deceleration (Biber et al., 2021). Altogether, these studies show that the apparent speed of replication forks inversely correlates with the rate of fork reversal.

Fork Reversal in Pathological Situations

A large body of evidence indicates that the controlled resection of nascent DNA by nucleases such as MRE11, EXO1 and DNA2 contributes to the recovery of stalled forks (Trenz et al., 2006; Thangavel et al., 2015). However, this control is lost in the absence of BRCA1/2 and hyper-resection leads to fork collapse and chromosome breaks (Schlacher et al., 2011, 2012; Wilhelm et al., 2014; Feng and Jasin, 2017; Taglialatela et al., 2017; **Figure 3B**). Hyper-resection of nascent DNA in BRCA-deficient cells generates structures that need to be cleaved by MUS81 to resume replication (Lemacon et al., 2017). SMARCAL1 causes genomic instability in BRCA1-deficient cells by promoting the formation of large ssDNA gaps (>300 nt) at stalled forks in a MRE11-dependent manner, which may in turn generate ultrafine chromatin bridges in mitosis (Vujanovic et al., 2017). In BRCA1/2-deficient cells, SMARCAL1 depletion restores replication fork stability and reduces the formation of replication stress-induced DNA breaks and chromosomal aberrations (Taglialatela et al., 2017).

Fork resection depends on PTIP, a protein interacting with members of a family of histone H3K4 methyltransferases known as MLL (Mixed Lineage Leukemia). PTIP promotes MRE11 and RAD51 loading to chromatin at the level of nascent DNA. In BRCA1/2-deficient cells, PTIP knock-out (KO) alleviates hyper-resection of nascent DNA and chromosome breaks (Ray Chaudhuri et al., 2016). These results suggest that chromatin modifications may influence fork stability, presumably through the recruitment of nucleases. Moreover, it has been recently shown that the lysine acetyltransferase KAT2B (also known as PCAF) that acetylates core histones promotes nascent DNA degradation in BRCA-deficient cells. PCAF acetylates H4 at lysine 8 at the level of stalled forks, promoting the recruitment of the MRE11 and EXO1 nucleases (Kim et al., 2020). BRCA2-deficient tumor cells have been shown to resist to cisplatin treatment in the absence of the nucleosome remodeler CHD4 (part of NuRD complex) through an increase level of translesion synthesis (Guillemette et al., 2015). Cisplatin resistance in this latter context has not been correlated to a particular state of chromatin but it has been shown that CHD4 loss restores fork stability in BRCA2-deficient cells (Ray Chaudhuri et al., 2016).

Nascent DNA degradation also depends on PARP1 status. As mentioned earlier, PARP1 inhibition decreases the level of RVFs and blocks fork resection in BRCA-deficient cells (Ray Chaudhuri et al., 2012, 2016; Ding et al., 2016). Either PARP inhibition or PARP1 depletion has been shown to promote the viability of BRCA1-2 deficient cells, especially in the context of ESCs (Embryonic Stem Cells) (Ding et al., 2016). Along the same line, MRE11 depletion or inhibition with Mirin treatment restores the viability of BRCA2$^{-/-}$ ESCs (Ray Chaudhuri et al., 2016). Together, these data indicate that the lethality of ESCs caused by BRCA1-2 deficiency stems from the degradation of nascent strands at RVFs in a mechanism dependent on PARP1 and MRE11. These results contrast with the known sensitivity of BRCA-deficient cancer cells to PARPi. In these BRCA-deficient cancer cells, survival depends on PARP-mediated DNA repair as an alternative to HR.

In conclusion, a large body of evidence supports the view that fork reversal is a physiological process protecting replication forks against exogenous sources of RS. Recently, this role was extended to oncogene induced-RS. Indeed, both SMARCAL1 and ZRANB3 protect cells against Myc-induced RS (Puccetti et al., 2019) and behave therefore as tumor suppressors. Preventing fork reversal through the chemical inhibition of SMARCAL1 or ZRANB3 could provide a new line of anticancer treatment. This strategy would be especially relevant in combination to drugs that induce RS or in genetic backgrounds associated with fork instability.

REPLICATION STRESS INDUCES FORK CLEAVAGE AND MITOTIC DEFECTS

Although cells generally manage to complete S phase under mild RS conditions, they usually display increased levels of

mitotic aberrations and chromosomal abnormalities, such as metaphase breaks or anaphase bridges. Moderate RS levels also increase chromosome breaks at CFS (Debatisse et al., 2012), at least in part through the cleavage of late-replication intermediates by the ERCC1 and MUS81-EME1 nucleases (Naim et al., 2013; Ying et al., 2013) and by preventing the complete duplication of these loci until the onset of mitosis. Interestingly, depletion of MUS81-EME1 in aphidicolin-treated cells reduces chromosomal breaks at the expense of a sharp increase of anaphase bridges. These data indicate that the MUS81 and ERCC1 cleave under-replicated DNA in mitosis to avoid more deleterious consequences associated with the persistence of entangled chromosomes. Indeed, chromatin bridges have a high likelihood to break during anaphase, resulting in the loss of genomic DNA and the formation of micronuclei. It has been shown that MUS81 cleavage at CFSs triggers a mitotic mechanism of DNA synthesis and repair involving POLD3 (Minocherhomji et al., 2015). This mitotic DNA synthesis (MIDAS) represents the last opportunity to complete the duplication of under-replicated CFSs, presumably through the cleavage of RVFs in G_2/M. Fugger *et al*. have shown that RVFs are formed by FBH1 and then cleaved by MUS81, forming DSBs (Fugger et al., 2013, 2015), suggesting that RVFs are a good substrate for structure-specific nucleases and are cleaved to promote fork recovery. This is consistent with the fact that MUS81 promotes cell viability in the presence of APH or HU by inducing DSBs (Hanada et al., 2007). Failure to resolve these late intermediates leads to the formation of 53BP1 bodies in the next cell cycle (Lukas et al., 2011).

HR deficiency leads to the accumulation of bulky anaphase bridges, reflecting the persistence of repair intermediates or under-replicated DNA in mitosis (Wilhelm et al., 2014; Ait Saada et al., 2017; Feng and Jasin, 2017; Lai et al., 2017). In BRCA-deficient cells, this phenotype is further increased by the depletion of MUS81 (Lai et al., 2017), which is reminiscent of CFS breakage under mild RS condition. In budding yeast, survival to CPT relies on both HR factors, namely Rad51 and Rad52, and the structure specific Mus81 endonuclease (Pardo et al., 2020). In both *rad51* and *rad52* mutants, replication tracks are shorter upon CPT-treatment, indicating that the formation of recombination structures (i.e., D-loop) protects arrested forks. In this context, MUS81 is important to resolve intermediates in G_2/M phase of the cell cycle. The fact that Mus81 acts in G_2/M in response to CPT suggests that the stalled fork, after being protected through Rad52-Rad51-mediated strand invasion, is joined by a converging fork, enabling completion of the replication after Mus81 cleavage. This model is consistent with the fact that late replication intermediates at human CFSs are also resolved, at least in part, by MUS81 in G_2/M (Naim et al., 2013; Ying et al., 2013). Replication forks are slower in BRCA2- and RAD51-deficient cells (Wilhelm et al., 2014, 2016; Lai et al., 2017), but restoration of normal fork progression by supplementing cells with nucleotide precursors and anti-oxidants also abolishes mitotic defects (Wilhelm et al., 2014, 2016). These results show that fork slowing in HR-deficient cells mimics low RS and leads to incomplete DNA replication and mitotic aberrations.

As discussed above, the controlled cleavage of RVFs and other replication intermediates promotes tolerance to RS. However in some instances uncontrolled cleavage of DNA by nucleases leads to the accumulation of high load of DNA breaks that is detrimental to cells (Pasero and Vindigni, 2017; **Figures 2**, **3**). This is the case when S-phase checkpoints are not fully functional. For instance, CHK1 deficiency leads to the accumulation of DNA lesions formed by MUS81-EME2 and MRE11 (Syljuasen et al., 2005; Técher et al., 2016; Calzetta et al., 2020). This uncontrolled cleavage may reflect the unscheduled activation of CDKs in the absence of CHK1, which is known to regulate both MUS81 and MRE11 activities. Consistently, inhibition of CDK by Roscovitine abolishes the appearance of DNA damages in CHK1-deficient cells (Syljuasen et al., 2005).

SELF DNA AND ACTIVATION OF THE INFLAMMATORY RESPONSE

Cancer cells bear a high load of chromosomal instability and suffer from replication defects, which both induce inflammation. This inflammation arises from the pathological accumulation of genomic DNA fragments in the cytoplasm when chromosome integrity is compromised. The pioneering work of Nelson Gekara's group revealed that genomic instability correlates with induction of inflammation (Härtlova et al., 2015). These authors found that ATM deficiency and DNA damage inducers such as γ-irradiation and Etoposide, promote the accumulation of cytosolic DNA molecules and trigger a type I interferon (IFN) response. However, the nature and the origin of cytosolic DNA species remained poorly understood.

Early studies from Costanzo and colleagues have shown that in *Xenopus* egg extracts, the processing of DSBs by the MRE11 nuclease leads to the release of short oligonucleotides from DNA ends, which contribute to activate ATM (Jazayeri et al., 2008). Irradiation of human cells also leads to the release of soluble ssDNA oligos (Jazayeri et al., 2008). More recently, a variety of agents used in radiotherapy and chemotherapy were shown to promote the accumulation of ssDNA fragments in the cytosol and the activation of a type I interferon response (Erdal et al., 2017). The impact of this DNA damage-induced inflammatory response has broad consequences for cancer therapy, as acute inflammation promotes tumor rejection by the immune system (Erdal et al., 2017; Harding et al., 2017; Mackenzie et al., 2017). However, chronic inflammation associated with chromosomal instability in some cancer types may also promote cancer development by stimulating metastasis (Bakhoum et al., 2018), stressing the importance of better understanding the links between RS and inflammation.

The Aicardi-Goutières Syndrome

Recent advances in the analysis of genes frequently mutated in the Aicardi-Goutières syndrome (AGS) has shed new light into the molecular mechanisms linking RS and inflammation. AGS is a severe interferonopathy associated with microcephaly and chronic inflammation (Crow and Manel, 2015). Cells from AGS patients accumulate cytosolic nucleic acids and show a chronic induction of type I IFNs via the cGAS (cyclic GMP-AMP synthase)-STING (stimulator of interferon genes) pathway. cGAS is a DNA sensor producing cyclic GMP-AMP (cGAMP) as

a second messenger upon binding to dsDNA and activating the transcription of interferon genes via the STING-TBK1-IRF3 axis (Li and Chen, 2018).

The mechanism by which AGS cells accumulate self DNA in their cytoplasm has long remained elusive. However, recent evidence indicates that byproducts of nuclear DNA repair and/or replication fork processing could represent a major source of cytosolic DNA in AGS cells (Erdal et al., 2017; Mackenzie et al., 2017; Yang et al., 2007; Coquel et al., 2018). This is consistent with the genetics of AGS, involving several enzymes processing nucleic acids, such as the cytoplasmic exonuclease TREX1, the ribonuclease RNase H2 or the dNTPase SAMHD1 (Crow and Manel, 2015).

TREX1 degrades cytosolic DNA species (Yang et al., 2007; Stetson et al., 2008) and has been proposed to process "abnormal" DNA structures at hard-to-replicate telomeres (Maciejowski et al., 2015), even though this role was challenged by a more recent study (Umbreit et al., 2020). The ssDNA binding factors RPA and RAD51 protect TREX1-deficient cells from inflammation by sequestering DNA fragments in the nucleus (Wolf et al., 2016; Vanpouille-Box et al., 2017). These results are consistent with the hypothesis that byproducts of DNA repair reactions induce inflammatory signals in AGS cells.

SAMHD1 mutations are implicated in several human diseases among which AGS (Rice et al., 2009), viral infection and cancers (Crow and Manel, 2015). SAMHD1 is a dNTP triphosphohydrolase (dNTPase) that degrades dNTPs and enables cells to control dNTP pools level and balance (Franzolin et al., 2013). In addition to dNTP control, SAMHD1 also impacts replication and repair fidelity through its DNA binding and interaction with the CtIP-MRE11 nuclease (Seamon et al., 2015; Daddacha et al., 2017; Coquel et al., 2018). SAMHD1-deficient cells accumulate cytosolic DNA fragments in response to RS (Coquel et al., 2018).

RNase H2 is a three-subunit enzyme involved in the removal of different types of RNA:DNA hybrids. Mutations in RNase H2 subunit are associated with AGS (Crow et al., 2006) and with chromosomal instability (Mackenzie et al., 2017). Deletion of RNase H2 genes is embryonic lethal in mouse (Reijns et al., 2012). RNase H2 removes ribonucleotides misincorporated into DNA (Reijns et al., 2012; Sparks et al., 2012) and processes R-loops (Lim et al., 2015). It has been recently proposed that micronuclei formation in absence of RNase H2 is the source of pro-inflammatory self DNA (Mackenzie et al., 2017).

Origin of Cytosolic DNA in Cancer Cells

RS and DNA damage induce the accumulation of cytosolic DNA, especially in TREX1-deficent cells (Yang et al., 2007; Stetson et al., 2008). But how are these chromosomal DNA fragments released from the nucleus? Two main mechanisms have been described in response to genotoxic insults. On the one hand, incomplete DNA replication or defective DSB repair generate large chromosome fragments devoid of centromeres that form micronuclei after mitosis. In different contexts, including RNase H2 deficiency, γ-irradiation, Ras overexpression and BRCA2 mutation, the rupture of these micronuclei releases DNA fragments in the cytosol and activates the cGAS-STING pathway (Dou et al., 2017; Gluck et al., 2017; Mackenzie et al., 2017; Reisländer et al., 2019). On the other hand, small DNA fragments are directly released from DNA ends (Jazayeri et al., 2008; Erdal et al., 2017) and escape the nucleus (Wolf et al., 2016). In SAMHD1-deficient cells, nascent DNA is displaced from stalled forks as a consequence of aberrant fork processing by RECQ1 and MRE11 (Coquel et al., 2018). This is reminiscent of the BLM- and EXO1-dependent release of ssDNA from damaged DNA (Erdal et al., 2017) and indicates that alterations of classical resection pathways contribute to the release of DNA fragments from the nucleus.

A growing body of evidence indicates that stalled and reversed forks represent a major source of cytosolic DNA when cells are exposed to genotoxic agents interfering with DNA replication. Central to this process is the role of endonucleases that release DNA fragments from arrested forks. In prostate cancer cells, the structure-specific endonuclease MUS81 is necessary for the accumulation of cytosolic DNA fragments (Shen et al., 2015; Ho et al., 2016). Interestingly, this process depends also on PARP1 and ATR (Ho et al., 2016; Kidiyoor et al., 2020), which are involved in fork reversal and restart. However, the role of RVFs in the production of cytosolic DNA remains to be established.

In conclusion, RS promotes the accumulation of cytosolic DNA via two distinct mechanisms: (*i*) the formation and rupture of micronuclei resulting from the missegregation of chromosomes during mitosis and (*ii*) the aberrant processing of stalled replication forks (**Figure 4**). These two mechanisms generate DNA fragments of different size and structure, but are not mutually exclusive. They may represent the two faces of the same coin, activating inflammation in response to different types of replication stress.

Exploiting Replication Stress-Induced Inflammation in Cancer Treatment

Inflammation is a two-edged sword in the context of cancer treatment. Although inflammation induced by irradiation or chemotherapeutic agents contributes to tumor cell rejection (Erdal et al., 2017; Gluck et al., 2017; Mackenzie et al., 2017), chronic inflammation contributes to cancer development by promoting metastasis (Bakhoum et al., 2018). Exploiting RS-mediated inflammation to potentiate the effect of current cancer therapies requires therefore a thorough understanding of the molecular mechanisms involved.

Immunotherapy has made considerable progress during the past decade with the development of potent immune checkpoint inhibitors to unlock the immune rejection of cancer cells. However, these inhibitors are useless against "cold" tumors that escape detection by the immune system. Stimulating inflammation in these tumors in a controlled manner could represent a promising strategy to increase tumor infiltration by immune cells and potentiate the action of immune checkpoint inhibitors. Actionable targets to modulate this response include TREX1 and the STING pathway. Indeed, TREX1 is an upstream regulator of radiation-driven anti-tumor immunity (Vanpouille-Box et al., 2017) and STING is essential to promote tumor rejection in immunocompetent mice treated with the

anticancer agent Topotecan (Kitai et al., 2017). The cGAS-STING pathway is also often deregulated in cancer cells, supporting the view that it interferes with tumor growth (Lau et al., 2015). Strategies targeting DNA integrity and the DNA damage response could also have additive or synergistic effects with immunotherapies. Thus, it has been recently shown that ERCC1-deficient non-small cell lung cancer (NSCLC) cells accumulate cytosolic chromatin fragments and consecutively induce type I IFNs in response to PARP inhibition (Chabanon et al., 2019). NSCLC cells treated with PARP inhibitors (PARPi) induce the cell surface expression of the PD-L1 immune checkpoint inhibitor and secrete the CCL5 chemokine (Chabanon et al., 2019). In patient tumor samples, ERCC1-deficiency is associated with increased levels of lymphocyte infiltration, indicating that the type I IFN response observed in cultured cells occurs *in vivo*, promoting the attraction of immune cells. This proof-of-concept was also recently established *in vivo* using an elegant preclinical model of small cell lung cancer (Sen et al., 2019). In these mice, anti-PD-L1, PARPi or CHK1 inhibitors (CHK1i) have only a modest effect on tumor growth when used alone. However, both PARPi and CHK1i have synergistic effects on tumor growth when administrated in combination with anti-PD-L1 immunotherapy in mice proficient for the cGAS-STING pathway. In STING- or cGAS-deficient mice, the combination of PARPi/antiPD-L1 or CHK1i/antiPD-L1 had no effect on tumor growth (Sen et al., 2019). These data show that under these circumstances, self-DNA sensing is essential to promote the immune rejection of cancer cells.

Beyond cGAS DNA Sensing

It has been recently shown that cGAS localizes to the nucleus and is recruited to DNA damage foci, where it inhibits HR-mediated DNA repair (Liu et al., 2018; Jiang et al., 2019). Through its chromatin occupancy and DNA compaction, cGAS impedes RAD51 strand invasion during repair, impacting genome integrity and cell survival to DNA insults (Jiang et al., 2019). It is thus important to consider this STING-independent function of cGAS in particular when investigating the contribution of the cGAS-STING pathway to the response to chemotherapy.

Although DNA sensing by cGAS-STING plays a major role in the response to cancer therapy, as described above, it should be noted that RNA in various forms can contribute to the inflammatory response under conditions that challenge genome integrity. For instance the inhibition of ATR in irradiated cells induces type I IFNs by the RNA sensing pathway RIG-I/MDA5 (Feng et al., 2020). Moreover, TLR9 and its adaptor protein MyD88 or cGAS have been shown to detect RNA:DNA hybrids (Mankan et al., 2014; Rigby et al., 2014). R-loops have been extensively described as a potential source of fork impediment and DNA damage (Zeman and Cimprich, 2014). Yet, whether R-loop processing generates cytosolic RNA:DNA hybrids under RS conditions remains to be established.

Here, the discussion focused on cytosolic DNA of nuclear origin, in connection with the RS response. However it is worth mentioning that mitochondria can also represent a significant source of inflammatory RNA and DNA fragments under conditions of DNA damage. Upon breakage of mitochondrial DNA, the RIG-I—MAVS pathway senses RNA to activate IFNs (Tigano et al., 2021). Even after γ-irradiation, part of the inflammatory response depends on mitochondrial DNA damage (Tigano et al., 2021). MRE11 deficiency can also lead to the release of mitochondrial DNA, activating the inflammasome via AIM2 and NLRP3, and mediating cell death (Li et al., 2019).

PERSPECTIVES

Events threatening genome stability during DNA replication can produce a large amount of cytosolic DNA fragments, sensed by the cGAS-STING pathway to induce type I IFNs. This link between RS and inflammation has major implications for cancer treatment and immunotherapy. Potential targets to modulate this interplay include factors regulating the homeostasis of cytosolic DNA. For instance, TREX1 is a druggable enzyme that could be inhibited to prevent the degradation of RS-induced cytosolic DNA and promote inflammation during cancer treatment. However, the regulation of TREX1 levels and activity remain poorly understood at the molecular level. In particular, TREX1 could have nuclear or mitotic functions that need to be further investigated to ensure that its inhibition would not further increase genomic instability in cancer patients.

Cytosolic DNA results, at least in part, from the action of endo- and exonucleases. A better characterization of the substrates of MRE11, EXO1 and MUS81 at stalled forks is therefore important to understand how these enzymes contribute to inflammation. It would also be important to develop reliable methods to extract, concentrate and sequence cytosolic DNA in order to determine its origin. Indeed, under mild RS conditions, structure-specific nucleases such as MUS81 cleave replication intermediates accumulating within late-replicating regions of the genome, which should be overrepresented in cytosolic DNA. In contrast, the large chromosome fragments present in micronuclei should not display such a replication timing bias. In both cases, the ability of cells to modulate the rates of initiation and elongation in response to RS will determine the persistence of unreplicated DNA at the end of S phase and will therefore impact both the stability of the genome and the production of pro-inflammatory cytokines.

Recent evidence indicates that RS can also be caused by an increased fork velocity (Maya-Mendoza et al., 2018). Since ISG15, one of the interferon-stimulated genes induced by the cGAS-STING pathway, can also promote RS by accelerating forks in a RECQ1-dependent manner (Raso et al., 2020), it is tempting to speculate that inflammation induces RS in the same way that RS induces inflammation. This view is supported by a recent report showing a STING-dependent acceleration of replication forks in *Hidradenitis suppurativa*, a chronic inflammatory skin disease affecting hair follicle stem cells (Orvain et al., 2020). Another example of the unexpected links between RS and inflammation concerns the poor survival of female embryos that are deficient for the replicative helicase component MCM ($MCM4^{chaos3}$) can be suppressed by the

administration of the anti-inflammatory drug ibuprofen to gestating mice (McNairn et al., 2019). Male embryos are protected from lethality presumably through the anti-inflammatory effect of testosterone. This result suggests that RS generated *in vivo* by deregulated origin usage results in a chronic inflammatory response that compromises embryonic viability. Together, these findings indicate that the interplay between RS and inflammation has broad physiological consequences beyond cancer and aging.

AUTHOR CONTRIBUTIONS

HT wrote the original draft and assembled the figures. HT and PP wrote, reviewed, and edited the text and the figures. Both authors approved the submitted version of the article.

FUNDING

HT thanks AIRC and the European Union's Horizon 2020 Research and Innovation Program under the Marie Skłodowska-Curie grant agreement no 800924. Work in the PP lab was supported by grants from the Agence Nationale pour la Recherche (ANR), Institut National du Cancer (INCa), the Ligue Nationale Contre le Cancer (équipe labéllisée), and the Fondation MSDAvenir.

ACKNOWLEDGMENTS

We thank Yea-Lih Lin and Benjamin Pardo for comments. HT thanks AIRC under the iCARE-2 fellowship program for support.

REFERENCES

Abe, T., Kawasumi, R., Giannattasio, M., Dusi, S., Yoshimoto, Y., Miyata, K., et al. (2018). AND-1 fork protection function prevents fork resection and is essential for proliferation. *Nat. Commun.* 9:3091.

Ait Saada, A., Teixeira-Silva, A., Iraqui, I., Costes, A., Hardy, J., Paoletti, G., et al. (2017). Unprotected Replication Forks Are Converted into Mitotic Sister Chromatid Bridges. *Mol. Cell* 66, 398.e–410.e.

Anglana, M., Apiou, F., Bensimon, A., and Debatisse, M. (2003). Dynamics of DNA replication in mammalian somatic cells: nucleotide pool modulates origin choice and interorigin spacing. *Cell* 114, 385–394. doi: 10.1016/s0092-8674(03)00569-5

Bacal, J., Moriel-Carretero, M., Pardo, B., Barthe, A., Sharma, S., Chabes, A., et al. (2018). Mrc1 and Rad9 cooperate to regulate initiation and elongation of DNA replication in response to DNA damage. *EMBO J.* 37:e99319.

Bai, G., Kermi, C., Stoy, H., Schiltz, C. J., Bacal, J., Zaino, A. M., et al. (2020). HLTF Promotes Fork Reversal, Limiting Replication Stress Resistance and Preventing Multiple Mechanisms of Unrestrained DNA Synthesis. *Mol. Cell* 78, 1237.e–1251.e.

Bakhoum, S. F., Ngo, B., Laughney, A. M., Cavallo, J. A., Murphy, C. J., Ly, P., et al. (2018). Chromosomal instability drives metastasis through a cytosolic DNA response. *Nature* 553, 467–472. doi: 10.1038/nature25432

Bellelli, R., and Boulton, S. J. (2021). Spotlight on the Replisome: Aetiology of DNA Replication-Associated Genetic Diseases. *Trends Genet.* 37, 317–336. doi: 10.1016/j.tig.2020.09.008

Bergoglio, V., Boyer, A. S., Walsh, E., Naim, V., Legube, G., Lee, M. Y., et al. (2013). DNA synthesis by Pol eta promotes fragile site stability by preventing under-replicated DNA in mitosis. *J. Cell Biol.* 201, 395–408. doi: 10.1083/jcb.201207066

Berti, M., and Vindigni, A. (2016). Replication stress: Getting back on track. *Nat. Struct. Mol. Biol.* 23, 103–109. doi: 10.1038/nsmb.3163

Berti, M., Chaudhuri, A. R., Thangavel, S., Gomathinayagam, S., Kenig, S., Vujanovic, M., et al. (2013). Human RECQ1 promotes restart of replication forks reversed by DNA topoisomerase I inhibition. *Nat. Struct. Mol. Biol.* 20, 347–354. doi: 10.1038/nsmb.2501

Bétous, R., Mason, A. C., Rambo, R. P., Bansbach, C. E., Badu-Nkansah, A., Sirbu, B. M., et al. (2012). SMARCAL1 catalyzes fork regression and holliday junction migration to maintain genome stability during DNA replication. *Genes Dev.* 26, 151–162. doi: 10.1101/gad.178459.111

Bhat, K. P., Krishnamoorthy, A., Dungrawala, H., Garcin, E. B., Modesti, M., and Cortez, D. (2018). RADX Modulates RAD51 Activity to Control Replication Fork Protection. *Cell Rep.* 24, 538–545. doi: 10.1016/j.celrep.2018.06.061

Bianchi, J., Rudd, S. G., Jozwiakowski, S. K., Bailey, L. J., Soura, V., Taylor, E., et al. (2013). Primpol bypasses UV photoproducts during eukaryotic chromosomal DNA replication. *Mol. Cell* 52, 566–573. doi: 10.1016/j.molcel.2013.10.035

Bianco, J. N., Bergoglio, V., Lin, Y. L., Pillaire, M. J., Schmitz, A. L., Gilhodes, J., et al. (2019). Overexpression of Claspin and Timeless protects cancer cells from replication stress in a checkpoint-independent manner. *Nat. Commun.* 10:910.

Biber, S., Pospiech, H., Gottifredi, V., and Wiesmüller, L. (2021). Multiple biochemical properties of the p53 molecule contribute to activation of polymerase iota-dependent DNA damage tolerance. *Nucleic Acids Res.* 48, 12188–12203. doi: 10.1093/nar/gkaa974

Blow, J. J., Ge, X. Q., and Jackson, D. A. (2011). How dormant origins promote complete genome replication. *Trends Biochem. Sci.* 36, 405–414. doi: 10.1016/j.tibs.2011.05.002

Buisson, R., Niraj, J., Rodrigue, A., Ho, C. K., Kreuzer, J., Foo, T. K., et al. (2017). Coupling of Homologous Recombination and the Checkpoint by ATR. *Mol. Cell* 65, 336–346. doi: 10.1016/j.molcel.2016.12.007

Byun, T. S., Pacek, M., Yee, M. C., Walter, J. C., and Cimprich, K. A. (2005). Functional uncoupling of MCM helicase and DNA polymerase activities activates the ATR-dependent checkpoint. *Genes Dev.* 19, 1040–1052. doi: 10.1101/gad.1301205

Calzetta, N. L., Besteiro, M. A. G., and Gottifredi, V. (2020). Mus81-Eme1-dependent aberrant processing of DNA replication intermediates in mitosis impairs genome integrity. *Sci. Adv.* 6:eabc8257. doi: 10.1126/sciadv.abc8257

Chabanon, R. M., Muirhead, G., Krastev, D. B., Adam, J., Morel, D., Garrido, M., et al. (2019). PARP inhibition enhances tumor cell–intrinsic immunity in ERCC1-deficient non–small cell lung cancer. *J. Clin. Invest.* 129, 1211–1228. doi: 10.1172/jci123319

Chen, Y. H., Jones, M. J., Yin, Y., Crist, S. B., Colnaghi, L., Sims, R. J. III, et al. (2015). ATR-mediated phosphorylation of FANCI regulates dormant origin firing in response to replication stress. *Mol. Cell* 58, 323–338. doi: 10.1016/j.molcel.2015.02.031

Conti, C., Sacca, B., Herrick, J., Lalou, C., Pommier, Y., and Bensimon, A. (2007). Replication fork velocities at adjacent replication origins are coordinately modified during DNA replication in human cells. *Mol. Biol. Cell* 18, 3059–3067. doi: 10.1091/mbc.e06-08-0689

Coquel, F., Silva, M. J., Técher, H., Zadorozhny, K., Sharma, S., Nieminuszczy, J., et al. (2018). SAMHD1 acts at stalled replication forks to prevent interferon induction. *Nature* 557, 57–61. doi: 10.1038/s41586-018-0050-1

Costanzo, V., Shechter, D., Lupardus, P. J., Cimprich, K. A., Gottesman, M., and Gautier, J. (2003). An ATR- and Cdc7-dependent DNA damage checkpoint that inhibits initiation of DNA replication. *Mol. Cell* 11, 203–213. doi: 10.1016/s1097-2765(02)00799-2

Couch, F. B., Bansbach, C. E., Driscoll, R., Luzwick, J. W., Glick, G. G., Betous, R., et al. (2013). ATR phosphorylates SMARCAL1 to prevent replication fork collapse. *Genes Dev.* 27, 1610–1623. doi: 10.1101/gad.214080.113

Courbet, S., Gay, S., Arnoult, N., Wronka, G., Anglana, M., Brison, O., et al. (2008). Replication fork movement sets chromatin loop size and origin choice in mammalian cells. *Nature* 455, 557–560. doi: 10.1038/nature07233

Crosetto, N., Mitra, A., Silva, M. J., Bienko, M., Dojer, N., Wang, Q., et al. (2013). Nucleotide-resolution DNA double-strand break mapping by next-generation sequencing. *Nat. Methods* 10, 361–365. doi: 10.1038/nmeth.2408

Crow, Y. J., and Manel, N. (2015). Aicardi-Goutieres syndrome and the type I interferonopathies. *Nat. Rev. Immunol.* 15, 429–440. doi: 10.1038/nri3850

Crow, Y. J., Leitch, A., Hayward, B. E., Garner, A., Parmar, R., Griffith, E., et al. (2006). Mutations in genes encoding ribonuclease H2 subunits cause Aicardi-Goutières syndrome and mimic congenital viral brain infection. *Nat. Genet.* 38, 910–916. doi: 10.1038/ng1842

Daddacha, W., Koyen, A. E., Bastien, A. J., Head, P. E., Dhere, V. R., Nabeta, G. N., et al. (2017). SAMHD1 Promotes DNA End Resection to Facilitate DNA Repair by Homologous Recombination. *Cell Rep.* 20, 1921–1935.

Debatisse, M., Le Tallec, B., Letessier, A., Dutrillaux, B., and Brison, O. (2012). Common fragile sites: mechanisms of instability revisited. *Trends Genet.* 28, 22–32. doi: 10.1016/j.tig.2011.10.003

Delamarre, A., Barthe, A., de la Roche Saint-André, C., Luciano, P., Forey, R., Padioleau, I., et al. (2020). MRX Increases Chromatin Accessibility at Stalled Replication Forks to Promote Nascent DNA Resection and Cohesin Loading. *Mol. Cell* 77, 395.e–410.e.

Deshpande, A. M., and Newlon, C. S. (1996). DNA replication fork pause sites dependent on transcription. *Science* 272, 1030–1033. doi: 10.1126/science.272.5264.1030

Ding, X., Chaudhuri, A. R., Callen, E., Pang, Y., Biswas, K., Klarmann, K. D., et al. (2016). Synthetic viability by BRCA2 and PARP1/ARTD1 deficiencies. *Nat. Commun.* 7:12425.

Dou, Z., Ghosh, K., Vizioli, M. G., Zhu, J., Sen, P., Wangensteen, K. J., et al. (2017). Cytoplasmic chromatin triggers inflammation in senescence and cancer. *Nature* 550, 402–406. doi: 10.1038/nature24050

Ercilla, A., Benada, J., Amitash, S., Zonderland, G., Baldi, G., Somyajit, K., et al. (2020). Physiological Tolerance to ssDNA Enables Strand Uncoupling during DNA Replication. *Cell Rep.* 30, 2416.e–2429.e.

Erdal, E., Haider, S., Rehwinkel, J., Harris, A. L., and McHugh, P. J. (2017). A prosurvival DNA damage-induced cytoplasmic interferon response is mediated by end resection factors and is limited by Trex1. *Genes Dev.* 31, 353–369. doi: 10.1101/gad.289769.116

Errico, A., Aze, A., and Costanzo, V. (2014). Mta2 promotes Tipin-dependent maintenance of replication fork integrity. *Cell Cycle* 13, 2120–2128. doi: 10.4161/cc.29157

Errico, A., Cosentino, C., Rivera, T., Losada, A., Schwob, E., Hunt, T., et al. (2009). Tipin/Tim1/And1 protein complex promotes Polα chromatin binding and sister chromatid cohesion. *EMBO J.* 28, 3681–3692. doi: 10.1038/emboj.2009.304

Errico, A., Costanzo, V., and Hunt, T. (2007). Tipin is required for stalled replication forks to resume DNA replication after removal of aphidicolin in Xenopus egg extracts. *Proc. Natl. Acad. Sci. U S A.* 104, 14929–14934. doi: 10.1073/pnas.0706347104

Eykelenboom, J. K., Harte, E. C., Canavan, L., Pastor-Peidro, A., Calvo-Asensio, I., Llorens-Agost, M., et al. (2013). ATR activates the S-M checkpoint during unperturbed growth to ensure sufficient replication prior to mitotic onset. *Cell Rep.* 5, 1095–1107. doi: 10.1016/j.celrep.2013.10.027

Feng, W., and Jasin, M. (2017). BRCA2 suppresses replication stress-induced mitotic and G1 abnormalities through homologous recombination. *Nat. Commun.* 8:525.

Feng, X., Tubbs, A., Zhang, C., Tang, M., Sridharan, S., Wang, C., et al. (2020). ATR inhibition potentiates ionizing radiation-induced interferon response via cytosolic nucleic acid-sensing pathways. *EMBO J.* 39:e104036.

Forey, R., Poveda, A., Sharma, S., Barthe, A., Padioleau, I., Renard, C., et al. (2020). Mec1 Is Activated at the Onset of Normal S Phase by Low-dNTP Pools Impeding DNA Replication. *Mol. Cell* 78, 396.e–410.e.

Franzolin, E., Pontarin, G., Rampazzo, C., Miazzi, C., Ferraro, P., Palumbo, E., et al. (2013). The deoxynucleotide triphosphohydrolase SAMHD1 is a major regulator of DNA precursor pools in mammalian cells. *Proc. Natl. Acad. Sci. U S A.* 110, 14272–14277. doi: 10.1073/pnas.1312033110

Fugger, K., Chu, W. K., Haahr, P., Kousholt, A. N., Beck, H., Payne, M. J., et al. (2013). FBH1 co-operates with MUS81 in inducing DNA double-strand breaks and cell death following replication stress. *Nat. Commun.* 4:1423.

Fugger, K., Mistrik, M., Neelsen, K. J., Yao, Q., Zellweger, R., Kousholt, A. N., et al. (2015). FBH1 Catalyzes Regression of Stalled Replication Forks. *Cell Rep.* 10, 1749–1757. doi: 10.1016/j.celrep.2015.02.028

Fumasoni, M., Zwicky, K., Vanoli, F., Lopes, M., and Branzei, D. (2015). Error-Free DNA Damage Tolerance and Sister Chromatid Proximity during DNA Replication Rely on the Polα/Primase/Ctf4 Complex. *Mol. Cell* 57, 812–823. doi: 10.1016/j.molcel.2014.12.038

García-Rodríguez, N., Morawska, M., Wong, R. P., Daigaku, Y., and Ulrich, H. D. (2018). Spatial separation between replisome- and template-induced replication stress signaling. *EMBO J.* 37:e98369.

Ge, X. Q., and Blow, J. J. (2010). Chk1 inhibits replication factory activation but allows dormant origin firing in existing factories. *J. Cell Biol.* 191, 1285–1297. doi: 10.1083/jcb.201007074

Ge, X. Q., Jackson, D. A., and Blow, J. J. (2007). Dormant origins licensed by excess Mcm2-7 are required for human cells to survive replicative stress. *Genes Dev.* 21, 3331–3341. doi: 10.1101/gad.457807

Gerhardt, J., Tomishima, M. J., Zaninovic, N., Colak, D., Yan, Z., Zhan, Q., et al. (2014). The DNA Replication Program Is Altered at the FMR1 Locus in Fragile X Embryonic Stem Cells. *Mol. Cell* 53, 19–31. doi: 10.1016/j.molcel.2013.10.029

Giannattasio, M., and Branzei, D. (2017). S-phase checkpoint regulations that preserve replication and chromosome integrity upon dNTP depletion. *Cell. Mol. Life Sci.* 74, 2361–2380. doi: 10.1007/s00018-017-2474-4

Gluck, S., Guey, B., Gulen, M. F., Wolter, K., Kang, T. W., Schmacke, N. A., et al. (2017). Innate immune sensing of cytosolic chromatin fragments through cGAS promotes senescence. *Nat. Cell Biol.* 19, 1061–1070. doi: 10.1038/ncb3586

Graham, J. E., Marians, K. J., and Kowalczykowski, S. C. (2017). Independent and Stochastic Action of DNA Polymerases in the Replisome. *Cell* 169, 1201.e–1213.e.

Groth, A., Corpet, A., Cook, A. J., Roche, D., Bartek, J., Lukas, J., et al. (2007). Regulation of replication fork progression through histone supply and demand. *Science* 318, 1928–1931. doi: 10.1126/science.1148992

Guilbaud, G., Rappailles, A., Baker, A., Chen, C. L., Arneodo, A., Goldar, A., et al. (2011). Evidence for sequential and increasing activation of replication origins along replication timing gradients in the human genome. *PLoS Comput. Biol.* 7:e1002322. doi: 10.1371/journal.pcbi.1002322

Guillemette, S., Serra, R. W., Peng, M., Hayes, J. A., Konstantinopoulos, P. A., Green, M. R., et al. (2015). Resistance to therapy in BRCA2 mutant cells due to loss of the nucleosome remodeling factor CHD4. *Genes Dev.* 29, 489–494. doi: 10.1101/gad.256214.114

Hampp, S., Kiessling, T., Buechle, K., Mansilla, S. F., Thomale, J., Rall, M., et al. (2016). DNA damage tolerance pathway involving DNA polymerase ι and the tumor suppressor p53 regulates DNA replication fork progression. *Proc. Natl. Acad. Sci. U S A.* 113, E4311–E4319.

Hanada, K., Budzowska, M., Davies, S. L., Van Drunen, E., Onizawa, H., Beverloo, H. B., et al. (2007). The structure-specific endonuclease Mus81 contributes to replication restart by generating double-strand DNA breaks. *Nat. Struct. Mol. Biol.* 14, 1096–1104. doi: 10.1038/nsmb1313

Harding, S. M., Benci, J. L., Irianto, J., Discher, D. E., Minn, A. J., and Greenberg, R. A. (2017). Mitotic progression following DNA damage enables pattern recognition within micronuclei. *Nature* 548, 466–470. doi: 10.1038/nature23470

Härtlova, A., Erttmann, S. F., Raffi, F. A. M., Schmalz, A. M., Resch, U., Anugula, S., et al. (2015). DNA Damage Primes the Type I Interferon System via the Cytosolic DNA Sensor STING to Promote Anti-Microbial Innate Immunity. *Immunity* 42, 332–343. doi: 10.1016/j.immuni.2015.01.012

Hashimoto, Y., Chaudhuri, A. R., Lopes, M., and Costanzo, V. (2010). Rad51 protects nascent DNA from Mre11-dependent degradation and promotes continuous DNA synthesis. *Nat. Struct. Mol. Biol.* 17, 1305–1311. doi: 10.1038/nsmb.1927

Henry-Mowatt, J., Jackson, D., Masson, J. Y., Johnson, P. A., Clements, P. M., Benson, F. E., et al. (2003). XRCC3 and Rad51 modulate replication fork progression on damaged vertebrate chromosomes. *Mol. Cell* 11, 1109–1117. doi: 10.1016/s1097-2765(03)00132-1

Ho, S. S., Zhang, W. Y., Tan, N. Y., Khatoo, M., Suter, M. A., Tripathi, S., et al. (2016). The DNA Structure-Specific Endonuclease MUS81 Mediates DNA Sensor STING-Dependent Host Rejection of Prostate Cancer Cells. *Immunity* 44, 1177–1189. doi: 10.1016/j.immuni.2016.04.010

Huberman, J. A., and Riggs, A. D. (1966). Autoradiography of chromosomal DNA fibers from Chinese hamster cells. *Proc. Natl. Acad. Sci. U S A.* 55, 599–606. doi: 10.1073/pnas.55.3.599

Hyrien, O. (2015). Peaks cloaked in the mist: the landscape of mammalian replication origins. *J. Cell Biol.* 208, 147–160. doi: 10.1083/jcb.201407004

Ibarra, A., Schwob, E., and Mendez, J. (2008). Excess MCM proteins protect human cells from replicative stress by licensing backup origins of replication. *Proc. Natl. Acad. Sci. U S A.* 105, 8956–8961. doi: 10.1073/pnas.0803978105

Jackson, D. A., and Pombo, A. (1998). Replicon clusters are stable units of chromosome structure: Evidence that nuclear organization contributes to the efficient activation and propagation of S phase in human cells. *J. Cell Biol.* 140, 1285–1295. doi: 10.1083/jcb.140.6.1285

Jasin, M., and Rothstein, R. (2013). Repair of strand breaks by homologous recombination. *Cold Spring Harb. Perspect. Biol.* 5:a012740.

Jazayeri, A., Balestrini, A., Garner, E., Haber, J. E., and Costanzo, V. (2008). Mre11-Rad50-Nbs1-dependent processing of DNA breaks generates oligonucleotides that stimulate ATM activity. *EMBO J.* 27, 1953–1962. doi: 10.1038/emboj.2008.128

Jiang, H., Xue, X., Panda, S., Kawale, A., Hooy, R. M., Liang, F., et al. (2019). Chromatin-bound cGAS is an inhibitor of DNA repair and hence accelerates genome destabilization and cell death. *EMBO J.* 38:e102718.

Katou, Y., Kanoh, Y., Bando, M., Noguchi, H., Tanaka, H., Ashikari, T., et al. (2003). S-phase checkpoint proteins Tof1 and Mrc1 form a stable replication-pausing complex. *Nature* 424, 1078–1083. doi: 10.1038/nature01900

Kidiyoor, G. R., Li, Q., Bastianello, G., Bruhn, C., Giovannetti, I., Mohamood, A., et al. (2020). ATR is essential for preservation of cell mechanics and nuclear integrity during interstitial migration. *Nat. Commun.* 11, 1–16.

Kim, J. J., Lee, S. Y., Choi, J. H., Woo, H. G., Xhemalce, B., and Miller, K. M. (2020). PCAF-Mediated Histone Acetylation Promotes Replication Fork Degradation by MRE11 and EXO1 in BRCA-Deficient Cells. *Mol. Cell* 80, 327.e–344.e.

Kitai, Y., Kawasaki, T., Sueyoshi, T., Kobiyama, K., Ishii, K. J., Zou, J., et al. (2017). DNA-Containing Exosomes Derived from Cancer Cells Treated with Topotecan Activate a STING-Dependent Pathway and Reinforce Antitumor Immunity. *J. Immunol.* 198, 1649–1659. doi: 10.4049/jimmunol.1601694

Kolinjivadi, A. M., Sannino, V., de Antoni, A., Técher, H., Baldi, G., and Costanzo, V. (2017a). Moonlighting at replication forks – a new life for homologous recombination proteins BRCA1, BRCA2 and RAD51. *FEBS Lett.* 591, 1083–1100. doi: 10.1002/1873-3468.12556

Kolinjivadi, A. M., Sannino, V., De Antoni, A., Zadorozhny, K., Kilkenny, M., Técher, H., et al. (2017b). Smarcal1-Mediated Fork Reversal Triggers Mre11-Dependent Degradation of Nascent DNA in the Absence of Brca2 and Stable Rad51 Nucleofilaments. *Mol. Cell* 67, 867.e–881.e.

Koundrioukoff, S., Carignon, S., Técher, H., Letessier, A., Brison, O., and Debatisse, M. (2013). Stepwise Activation of the ATR Signaling Pathway upon Increasing Replication Stress Impacts Fragile Site Integrity. *PLoS Genet.* 9:e1003643. doi: 10.1371/journal.pgen.1003643

Kurat, C. F., Yeeles, J. T., Patel, H., Early, A., and Diffley, J. F. (2017). Chromatin Controls DNA Replication Origin Selection, Lagging-Strand Synthesis, and Replication Fork Rates. *Mol. Cell* 65, 117–130. doi: 10.1016/j.molcel.2016.11.016

Lai, X., Broderick, R., Bergoglio, V., Zimmer, J., Badie, S., Niedzwiedz, W., et al. (2017). MUS81 nuclease activity is essential for replication stress tolerance and chromosome segregation in BRCA2-deficient cells. *Nat. Commun.* 8:16171.

Lambert, S., and Carr, A. M. (2013). Impediments to replication fork movement: Stabilisation, reactivation and genome instability. *Chromosoma* 122, 33–45. doi: 10.1007/s00412-013-0398-9

Lau, A., Gray, E. E., Brunette, R. L., and Stetson, D. B. (2015). DNA tumor virus oncogenes antagonize the cGAS-STING DNA-sensing pathway. *Science* 350, 568–571. doi: 10.1126/science.aab3291

Lebofsky, R., Heilig, R., Sonnleitner, M., Weissenbach, J., and Bensimon, A. (2006). DNA replication origin interference increases the spacing between initiation events in human cells. *Mol. Biol. Cell* 17, 5337–5345. doi: 10.1091/mbc.e06-04-0298

Lemacon, D., Jackson, J., Quinet, A., Brickner, J. R., Li, S., Yazinski, S., et al. (2017). MRE11 and EXO1 nucleases degrade reversed forks and elicit MUS81-dependent fork rescue in BRCA2-deficient cells. *Nat. Commun.* 8:860.

Letessier, A., Millot, G. A., Koundrioukoff, S., Lachagès, A. M., Vogt, N., Hansen, R. S., et al. (2011). Cell-type-specific replication initiation programs set fragility of the FRA3B fragile site. *Nature* 470, 120–123. doi: 10.1038/nature09745

Li, T., and Chen, Z. J. (2018). The cGAS-cGAMP-STING pathway connects DNA damage to inflammation, senescence, and cancer. *J. Exp. Med.* 215, 1287–1299. doi: 10.1084/jem.20180139

Li, Y., Shen, Y., Jin, K., Wen, Z., Cao, W., Wu, B., et al. (2019). The DNA Repair Nuclease MRE11A Functions as a Mitochondrial Protector and Prevents T Cell Pyroptosis and Tissue Inflammation. *Cell Metab.* 30, 477.e–492.e.

Lim, Y. W., Sanz, L. A., Xu, X., Hartono, S. R., and Chédin, F. (2015). Genome-wide DNA hypomethylation and RNA:DNA hybrid accumulation in Aicardi–Goutières syndrome. *Elife* 4:e08007.

Liu, H., Zhang, H., Wu, X., Ma, D., Wu, J., Wang, L., et al. (2018). Nuclear cGAS suppresses DNA repair and promotes tumorigenesis. *Nature* 563, 131–136. doi: 10.1038/s41586-018-0629-6

Liu, W., Krishnamoorthy, A., Zhao, R., and Cortez, D. (2020). Two replication fork remodeling pathways generate nuclease substrates for distinct fork protection factors. *Sci. Adv.* 6, 3598–3611.

Lossaint, G., Larroque, M., Ribeyre, C., Bec, N., Larroque, C., Decaillet, C., et al. (2013). FANCD2 binds MCM proteins and controls replisome function upon activation of s phase checkpoint signaling. *Mol. Cell* 51, 678–690. doi: 10.1016/j.molcel.2013.07.023

Lukas, C., Savic, V., Bekker-Jensen, S., Doil, C., Neumann, B., Pedersen, R. S., et al. (2011). 53BP1 nuclear bodies form around DNA lesions generated by mitotic transmission of chromosomes under replication stress. *Nat. Cell Biol.* 13, 243–253. doi: 10.1038/ncb2201

Maciejowski, J., Li, Y., Bosco, N., Campbell, P. J., and de Lange, T. (2015). Chromothripsis and Kataegis Induced by Telomere Crisis. *Cell* 163, 1641–1654. doi: 10.1016/j.cell.2015.11.054

Mackenzie, K. J., Carroll, P., Martin, C. A., Murina, O., Fluteau, A., Simpson, D. J., et al. (2017). cGAS surveillance of micronuclei links genome instability to innate immunity. *Nature* 548, 461–465. doi: 10.1038/nature23449

Malinsky, J., Koberna, K., Stanek, D., Masata, M., Votruba, I., and Raska, I. (2001). The supply of exogenous deoxyribonucleotides accelerates the speed of the replication fork in early S-phase. *J. Cell Sci.* 114, 747–750. doi: 10.1242/jcs.114.4.747

Mankan, A. K., Schmidt, T., Chauhan, D., Goldeck, M., Höning, K., Gaidt, M., et al. (2014). Cytosolic RNA:DNA hybrids activate the cGAS –STING axis. *EMBO J.* 33, 2937–2946. doi: 10.15252/embj.201488726

Mantiero, D., Mackenzie, A., Donaldson, A., and Zegerman, P. (2011). Limiting replication initiation factors execute the temporal programme of origin firing in budding yeast. *EMBO J.* 30, 4805–4814. doi: 10.1038/emboj.2011.404

Maya-Mendoza, A., Moudry, P., Merchut-Maya, J. M., Lee, M., Strauss, R., and Bartek, J. (2018). High speed of fork progression induces DNA replication stress and genomic instability. *Nature* 559, 279–284. doi: 10.1038/s41586-018-0261-5

McNairn, A. J., Chuang, C. H., Bloom, J. C., Wallace, M. D., and Schimenti, J. C. (2019). Female-biased embryonic death from inflammation induced by genomic instability. *Nature* 567, 105–108. doi: 10.1038/s41586-019-0936-6

Mechali, M. (2010). Eukaryotic DNA replication origins: many choices for appropriate answers. *Nat. Rev. Mol. Cell Biol.* 11, 728–738. doi: 10.1038/nrm2976

Mejlvang, J., Feng, Y., Alabert, C., Neelsen, K. J., Jasencakova, Z., Zhao, X., et al. (2014). New histone supply regulates replication fork speed and PCNA unloading. *J. Cell Biol.* 204, 29–43. doi: 10.1083/jcb.201305017

Mendez-Bermudez, A., Lototska, L., Bauwens, S., Giraud-Panis, M. J., Croce, O., Jamet, K., et al. (2018). Genome-wide Control of Heterochromatin Replication by the Telomere Capping Protein TRF2. *Mol. Cell* 70, 449.e–461.e.

Menin, L., Ursich, S., Trovesi, C., Zellweger, R., Lopes, M., Longhese, M. P., et al. (2018). Tel1/ ATM prevents degradation of replication forks that reverse after topoisomerase poisoning. *EMBO Rep.* 19:e45535.

Merrick, C. J., Jackson, D., and Diffley, J. F. (2004). Visualization of altered replication dynamics after DNA damage in human cells. *J. Biol. Chem.* 279, 20067–20075. doi: 10.1074/jbc.m400022200

Michalet, X., Ekong, R., Fougerousse, F., Rousseaux, S., Schurra, C., Hornigold, N., et al. (1997). Dynamic molecular combing: Stretching the whole human genome for high- resolution studies. *Science* 277, 1518–1523. doi: 10.1126/science.277.5331.1518

Mijic, S., Zellweger, R., Chappidi, N., Berti, M., Jacobs, K., Mutreja, K., et al. (2017). Replication fork reversal triggers fork degradation in BRCA2-defective cells. *Nat. Commun.* 8:859.

Minocherhomji, S., Ying, S., Bjerregaard, V. A., Bursomanno, S., Aleliunaite, A., Wu, W., et al. (2015). Replication stress activates DNA repair synthesis in mitosis. *Nature* 528, 286–290. doi: 10.1038/nature16139

Miotto, B., Ji, Z., and Struhl, K. (2016). Selectivity of ORC binding sites and the relation to replication timing, fragile sites, and deletions in cancers. *Proc. Natl. Acad. Sci. U S A.* 113, E4810–E4819.

Mirkin, E. V., and Mirkin, S. M. (2007). Replication fork stalling at natural impediments. *Microbiol. Mol. Biol. Rev.* 71, 13–35. doi: 10.1128/mmbr.00030-06

Mirman, Z., Lottersberger, F., Takai, H., Kibe, T., Gong, Y., Takai, K., et al. (2018). 53BP1–RIF1–shieldin counteracts DSB resection through CST- and Polα-dependent fill-in. *Nature* 560, 112–116. doi: 10.1038/s41586-018-0324-7

Mourón, S., Rodriguez-Acebes, S., Martínez-Jiménez, M. I., García-Gómez, S., Chocrón, S., Blanco, L., et al. (2013). Repriming of DNA synthesis at stalled replication forks by human PrimPol. *Nat. Struct. Mol. Biol.* 20, 1383–1389. doi: 10.1038/nsmb.2719

Mutreja, K., Krietsch, J., Hess, J., Ursich, S., Berti, M., Roessler, F. K., et al. (2018). ATR-Mediated Global Fork Slowing and Reversal Assist Fork Traverse and Prevent Chromosomal Breakage at DNA Interstrand Cross-Links. *Cell Rep.* 24, 2629–2642e5.

Naim, V., Wilhelm, T., Debatisse, M., and Rosselli, F. (2013). ERCC1 and MUS81-EME1 promote sister chromatid separation by processing late replication intermediates at common fragile sites during mitosis. *Nat. Cell Biol.* 15, 1008–1015. doi: 10.1038/ncb2793

Neelsen, K. J., and Lopes, M. (2015). Replication fork reversal in eukaryotes: from dead end to dynamic response. *Nat. Rev. Mol. Cell Biol.* 16, 207–220. doi: 10.1038/nrm3935

Norio, P., and Schildkraut, C. L. (2001). Visualization of DNA replication on individual Epstein-Barr virus episomes. *Science* 294, 2361–2364. doi: 10.1126/science.1064603

O'Connor, M. J. (2015). Targeting the DNA Damage Response in Cancer. *Mol. Cell* 60, 547–560.

Orvain, C., Lin, Y. L., Jean-Louis, F., Hocini, H., Hersant, B., Bennasser, Y., et al. (2020). Hair follicle stem cell replication stress drives IFI16/STING-dependent inflammation in hidradenitis suppurativa. *J. Clin. Invest.* 130, 3777–3790. doi: 10.1172/jci131180

Ozeri-Galai, E., Lebofsky, R., Rahat, A., Bester, A. C., Bensimon, A., and Kerem, B. (2011). Failure of origin activation in response to fork stalling leads to chromosomal instability at fragile sites. *Mol. Cell* 43, 122–131. doi: 10.1016/j.molcel.2011.05.019

Pardo, B., Crabbé, L., and Pasero, P. (2017). Signaling pathways of replication stress in yeast. *FEMS Yeast Res.* 17:fow101. doi: 10.1093/femsyr/fow101

Pardo, B., Moriel-Carretero, M., Vicat, T., Aguilera, A., and Pasero, P. (2020). Homologous recombination and Mus81 promote replication completion in response to replication fork blockage. *EMBO Rep.* 21:e49367.

Pasero, P., and Vindigni, A. (2017). Nucleases Acting at Stalled Forks: How to Reboot the Replication Program with a Few Shortcuts. *Annu. Rev. Genet.* 51, 477–499. doi: 10.1146/annurev-genet-120116-024745

Pasero, P., Bensimon, A., and Schwob, E. (2002). Single-molecule analysis reveals clustering and epigenetic regulation of replication origins at the yeast rDNA locus. *Genes Dev.* 16, 2479–2484. doi: 10.1101/gad.232902

Petermann, E., Orta, M. L., Issaeva, N., Schultz, N., and Helleday, T. (2010a). Hydroxyurea-stalled replication forks become progressively inactivated and require two different RAD51-mediated pathways for restart and repair. *Mol. Cell* 37, 492–502. doi: 10.1016/j.molcel.2010.01.021

Petermann, E., Woodcock, M., and Helleday, T. (2010b). Chk1 promotes replication fork progression by controlling replication initiation. *Proc. Natl. Acad. Sci. U S A.* 107, 16090–16095. doi: 10.1073/pnas.1005031107

Poli, J., Tsaponina, O., Crabbé, L., Keszthelyi, A., Pantesco, V., Chabes, A., et al. (2012). dNTP pools determine fork progression and origin usage under replication stress. *EMBO J.* 31, 883–894. doi: 10.1038/emboj.2011.470

Puccetti, M. V., Adams, C. M., Kushinsky, S., and Eischen, C. M. (2019). SMARCAL1 and ZrAnB3 protect replication forks from MYC-induced DNA replication stress. *Cancer Res.* 79, 1612–1623. doi: 10.1158/0008-5472.can-18-2705

Quinet, A., Carvajal-Maldonado, D., Lemacon, D., and Vindigni, A. (2017). DNA Fiber Analysis: Mind the Gap! *Methods Enzymol.* 591, 55–82. doi: 10.1016/bs.mie.2017.03.019

Quinet, A., Tirman, S., Jackson, J., Šviković, S., Lemaçon, D., Carvajal-Maldonado, D., et al. (2020). PRIMPOL-Mediated Adaptive Response Suppresses Replication Fork Reversal in BRCA-Deficient Cells. *Mol. Cell* 77, 461.e–474.e.

Raso, M. C., Djoric, N., Walser, F., Hess, S., Schmid, F. M., Burger, S., et al. (2020). Interferon-stimulated gene 15 accelerates replication fork progression inducing chromosomal breakage. *J. Cell Biol.* 219:e202002175.

Ray Chaudhuri, A., Callen, E., Ding, X., Gogola, E., Duarte, A. A., Lee, J. E., et al. (2016). Replication fork stability confers chemoresistance in BRCA-deficient cells. *Nature* 535, 382–387. doi: 10.1038/nature18325

Ray Chaudhuri, A., Hashimoto, Y., Herrador, R., Neelsen, K. J., Fachinetti, D., Bermejo, R., et al. (2012). Topoisomerase i poisoning results in PARP-mediated replication fork reversal. *Nat. Struct. Mol. Biol.* 19, 417–423. doi: 10.1038/nsmb.2258

Reijns, M. A., Rabe, B., Rigby, R. E., Mill, P., Astell, K. R., Lettice, L. A., et al. (2012). Enzymatic removal of ribonucleotides from DNA is essential for mammalian genome integrity and development. *Cell* 149, 1008–1022. doi: 10.1016/j.cell.2012.04.011

Reisländer, T., Lombardi, E. P., Groelly, F. J., Miar, A., Porru, M., Di Vito, S., et al. (2019). BRCA2 abrogation triggers innate immune responses potentiated by treatment with PARP inhibitors. *Nat. Commun.* 10:3143.

Renard-Guillet, C., Kanoh, Y., Shirahige, K., and Masai, H. (2014). Temporal and spatial regulation of eukaryotic DNA replication: from regulated initiation to genome-scale timing program. *Semin. Cell Dev. Biol.* 30, 110–120. doi: 10.1016/j.semcdb.2014.04.014

Rice, G. I., Bond, J., Asipu, A., Brunette, R. L., Manfield, I. W., Carr, I. M., et al. (2009). Mutations involved in Aicardi-Goutieres syndrome implicate SAMHD1 as regulator of the innate immune response. *Nat. Genet.* 41, 829–832.

Rigby, R. E., Webb, L. M., Mackenzie, K. J., Li, Y., Leitch, A., Reijns, M. A. M., et al. (2014). RNA:DNA hybrids are a novel molecular pattern sensed by TLR9. *EMBO J.* 33, 542–558. doi: 10.1002/embj.201386117

Rivera-Mulia, J. C., and Gilbert, D. M. (2016). Replicating Large Genomes: Divide and Conquer. *Mol. Cell* 62, 756–765. doi: 10.1016/j.molcel.2016.05.007

Saldivar, J. C., Hamperl, S., Bocek, M. J., Chung, M., Bass, T. E., Cisneros-Soberanis, F., et al. (2018). An intrinsic S/G2 checkpoint enforced by ATR. *Science* 361, 806–810. doi: 10.1126/science.aap9346

Saxena, S., Somyajit, K., and Nagaraju, G. (2018). XRCC2 Regulates Replication Fork Progression during dNTP Alterations. *Cell Rep.* 25, 3273.e–3282.e.

Schlacher, K., Christ, N., Siaud, N., Egashira, A., Wu, H., and Jasin, M. (2011). Double-strand break repair-independent role for BRCA2 in blocking stalled replication fork degradation by MRE11. *Cell* 145, 529–542. doi: 10.1016/j.cell.2011.03.041

Schlacher, K., Wu, H., and Jasin, M. (2012). A distinct replication fork protection pathway connects Fanconi anemia tumor suppressors to RAD51-BRCA1/2. *Cancer Cell* 22, 106–116. doi: 10.1016/j.ccr.2012.05.015

Seamon, K. J., Sun, Z., Shlyakhtenko, L. S., Lyubchenko, Y. L., and Stivers, J. T. (2015). SAMHD1 is a single-stranded nucleic acid binding protein with no active site-associated nuclease activity. *Nucleic Acids Res.* 43, 6486–6499. doi: 10.1093/nar/gkv633

Seiler, J. A., Conti, C., Syed, A., Aladjem, M. I., and Pommier, Y. (2007). The intra-S-phase checkpoint affects both DNA replication initiation and elongation: single-cell and -DNA fiber analyses. *Mol. Cell Biol.* 27, 5806–5818. doi: 10.1128/mcb.02278-06

Sen, T., Rodriguez, B. L., Chen, L., Della Corte, C. M., Morikawa, N., Fujimoto, J., et al. (2019). Targeting DNA damage response promotes antitumor immunity through STING-mediated T-cell activation in small cell lung cancer. *Cancer Discov.* 9, 646–661. doi: 10.1158/2159-8290.cd-18-1020

Shechter, D., Costanzo, V., and Gautier, J. (2004). ATR and ATM regulate the timing of DNA replication origin firing. *Nat. Cell Biol.* 6, 648–655. doi: 10.1038/ncb1145

Shen, Y. J., Le Bert, N., Chitre, A. A., Koo, C. X., Nga, X. H., Ho, S. S., et al. (2015). Genome-derived cytosolic DNA mediates type I interferon-dependent rejection

of B cell lymphoma cells. *Cell Rep.* 11, 460–473. doi: 10.1016/j.celrep.2015.03.041

Shibata, A., Moiani, D., Arvai, A. S., Perry, J., Harding, S. M., Genois, M. M., et al. (2014). DNA double-strand break repair pathway choice is directed by distinct MRE11 nuclease activities. *Mol. Cell* 53, 7–18.

Sogo, J. M., Lopes, M., and Foiani, M. (2002). Fork reversal and ssDNA accumulation at stalled replication forks owing to checkpoint defects. *Science* 297, 599–602. doi: 10.1126/science.1074023

Somyajit, K., Gupta, R., Sedlackova, H., Neelsen, K. J., Ochs, F., Rask, M. B., et al. (2017). Redox-sensitive alteration of replisome architecture safeguards genome integrity. *Science* 358, 797–802. doi: 10.1126/science.aao3172

Somyajit, K., Saxena, S., Babu, S., Mishra, A., and Nagaraju, G. (2015). Mammalian RAD51 paralogs protect nascent DNA at stalled forks and mediate replication restart. *Nucleic Acids Res.* 43, 9835–9855.

Somyajit, K., Spies, J., Coscia, F., Kirik, U., Rask, M. B., Lee, J. H., et al. (2021). Homology-directed repair protects the replicating genome from metabolic assaults. *Dev. Cell* 56, 461.e–477.e.

Sorensen, C. S., Hansen, L. T., Dziegielewski, J., Syljuasen, R. G., Lundin, C., Bartek, J., et al. (2005). The cell-cycle checkpoint kinase Chk1 is required for mammalian homologous recombination repair. *Nat. Cell Biol.* 7, 195–201. doi: 10.1038/ncb1212

Sparks, J. L., Chon, H., Cerritelli, S. M., Kunkel, T. A., Johansson, E., Crouch, R. J., et al. (2012). RNase H2-Initiated Ribonucleotide Excision Repair. *Mol. Cell* 47, 980–986. doi: 10.1016/j.molcel.2012.06.035

Stetson, D. B., Ko, J. S., Heidmann, T., and Medzhitov, R. (2008). Trex1 Prevents Cell-Intrinsic Initiation of Autoimmunity. *Cell* 134, 587–598. doi: 10.1016/j.cell.2008.06.032

Syljuasen, R. G., Sorensen, C. S., Hansen, L. T., Fugger, K., Lundin, C., Johansson, F., et al. (2005). Inhibition of human Chk1 causes increased initiation of DNA replication, phosphorylation of ATR targets, and DNA breakage. *Mol. Cell Biol.* 25, 3553–3562. doi: 10.1128/mcb.25.9.3553-3562.2005

Taglialatela, A., Alvarez, S., Leuzzi, G., Sannino, V., Ranjha, L., Huang, J. W., et al. (2017). Restoration of Replication Fork Stability in BRCA1- and BRCA2-Deficient Cells by Inactivation of SNF2-Family Fork Remodelers. *Mol. Cell* 68, 414.e–430.e.

Técher, H., Koundrioukoff, S., Azar, D., Wilhelm, T., Carignon, S., Brison, O., et al. (2013). Replication dynamics: Biases and robustness of DNA fiber analysis. *J. Mol. Biol.* 425, 4845–4855. doi: 10.1016/j.jmb.2013.03.040

Técher, H., Koundrioukoff, S., Carignon, S., Wilhelm, T., Millot, G. A., Lopez, B. S., et al. (2016). Signaling from Mus81-Eme2-Dependent DNA Damage Elicited by Chk1 Deficiency Modulates Replication Fork Speed and Origin Usage. *Cell Rep.* 14, 1114–1127. doi: 10.1016/j.celrep.2015.12.093

Técher, H., Koundrioukoff, S., Nicolas, A., and Debatisse, M. (2017). The impact of replication stress on replication dynamics and DNA damage in vertebrate cells. *Nat. Rev. Genet.* 18, 535–550. doi: 10.1038/nrg.2017.46

Teixeira-Silva, A., Ait Saada, A., Hardy, J., Iraqui, I., Nocente, M. C., Fréon, K., et al. (2017). The end-joining factor Ku acts in the end-resection of double strand break-free arrested replication forks. *Nat. Commun.* 8, 1–14.

Thangavel, S., Berti, M., Levikova, M., Pinto, C., Gomathinayagam, S., Vujanovic, M., et al. (2015). DNA2 drives processing and restart of reversed replication forks in human cells. *J. Cell Biol.* 208, 545–562. doi: 10.1083/jcb.201406100

Tian, T., Bu, M., Chen, X., Ding, L., Yang, Y., Han, J., et al. (2021). The ZATT-TOP2A-PICH Axis Drives Extensive Replication Fork Reversal to Promote Genome Stability. *Mol. Cell* 81, 198.e–211.e.

Tigano, M., Vargas, D. C., Tremblay-Belzile, S., Fu, Y., and Sfeir, A. (2021). Nuclear sensing of breaks in mitochondrial DNA enhances immune surveillance. *Nature* 591, 477–481. doi: 10.1038/s41586-021-03269-w

Toledo, L. I., Altmeyer, M., Rask, M. B., Lukas, C., Larsen, D. H., Povlsen, L. K., et al. (2013). ATR prohibits replication catastrophe by preventing global exhaustion of RPA. *Cell* 155, 1088–1103. doi: 10.1016/j.cell.2013.10.043

Toledo, L., Neelsen, K. J., and Lukas, J. (2017). Replication Catastrophe: When a Checkpoint Fails because of Exhaustion. *Mol. Cell* 66, 735–749. doi: 10.1016/j.molcel.2017.05.001

Trenz, K., Smith, E., Smith, S., and Costanzo, V. (2006). ATM and ATR promote Mre11 dependent restart of collapsed replication forks and prevent accumulation of DNA breaks. *EMBO J.* 25, 1764–1774. doi: 10.1038/sj.emboj.7601045

Tuduri, S., Crabbe, L., Conti, C., Tourriere, H., Holtgreve-Grez, H., Jauch, A., et al. (2009). Topoisomerase I suppresses genomic instability by preventing interference between replication and transcription. *Nat. Cell Biol.* 11, 1315–1324. doi: 10.1038/ncb1984

Tuduri, S., Tourriere, H., and Pasero, P. (2010). Defining replication origin efficiency using DNA fiber assays. *Chromosom. Res.* 18, 91–102. doi: 10.1007/s10577-009-9098-y

Umbreit, N. T., Zhang, C. Z., Lynch, L. D., Blaine, L. J., Cheng, A. M., Tourdot, R., et al. (2020). Mechanisms generating cancer genome complexity from a single cell division error. *Science* 368:eaba0712. doi: 10.1126/science.aba0712

Urban, J. M., Foulk, M. S., Casella, C., and Gerbi, S. A. (2015). The hunt for origins of DNA replication in multicellular eukaryotes. *F1000Prime Rep.* 7:30.

Vallerga, M. B., Mansilla, S. F., Federico, M. B., Bertolin, A. P., and Gottifredi, V. (2015). Rad51 recombinase prevents Mre11 nuclease-dependent degradation and excessive PrimPol-mediated elongation of nascent DNA after UV irradiation. *Proc. Natl. Acad. Sci. U S A.* 112, E6624–E6633.

Valton, A. L., and Prioleau, M. N. (2016). G-Quadruplexes in DNA Replication: A Problem or a Necessity? *Trends Genet.* 32, 697–706. doi: 10.1016/j.tig.2016.09.004

Vanpouille-Box, C., Alard, A., Aryankalayil, M. J., Sarfraz, Y., Diamond, J. M., Schneider, R. J., et al. (2017). DNA exonuclease Trex1 regulates radiotherapy-induced tumour immunogenicity. *Nat. Commun.* 8:15618.

Villa, M., Bonetti, D., Carraro, M., and Longhese, M. P. (2018). Rad9/53BP1 protects stalled replication forks from degradation in Mec1/ATR-defective cells. *EMBO Rep.* 19, 351–367. doi: 10.15252/embr.201744910

Vindigni, A., and Lopes, M. (2017). Combining electron microscopy with single molecule DNA fiber approaches to study DNA replication dynamics. *Biophys. Chem.* 225, 3–9. doi: 10.1016/j.bpc.2016.11.014

Vujanovic, M., Krietsch, J., Raso, M. C., Terraneo, N., Zellweger, R., Schmid, J. A., et al. (2017). Replication Fork Slowing and Reversal upon DNA Damage Require PCNA Polyubiquitination and ZRANB3 DNA Translocase Activity. *Mol. Cell* 67, 882–890e5.

Wan, L., Lou, J., Xia, Y., Su, B., Liu, T., Cui, J., et al. (2013). HPrimpol1/CCDC111 is a human DNA primase-polymerase required for the maintenance of genome integrity. *EMBO Rep.* 14, 1104–1112. doi: 10.1038/embor.2013.159

Wilhelm, T., Magdalou, I., Barascu, A., Techer, H., Debatisse, M., and Lopez, B. S. (2014). Spontaneous slow replication fork progression elicits mitosis alterations in homologous recombination-deficient mammalian cells. *Proc. Natl. Acad. Sci. U S A.* 111, 763–768. doi: 10.1073/pnas.1311520111

Wilhelm, T., Ragu, S., Magdalou, I., Machon, C., Dardillac, E., Técher, H., et al. (2016). Slow Replication Fork Velocity of Homologous Recombination-Defective Cells Results from Endogenous Oxidative Stress. *PLoS Genet.* 12:e1006007. doi: 10.1371/journal.pgen.1006007

Wolf, C., Rapp, A., Berndt, N., Staroske, W., Schuster, M., Dobrick-Mattheuer, M., et al. (2016). RPA and Rad51 constitute a cell intrinsic mechanism to protect the cytosol from self DNA. *Nat. Commun.* 7:11752.

Woodward, A. M., Gohler, T., Luciani, M. G., Oehlmann, M., Ge, X., Gartner, A., et al. (2006). Excess Mcm2-7 license dormant origins of replication that can be used under conditions of replicative stress. *J. Cell Biol.* 173, 673–683. doi: 10.1083/jcb.200602108

Wu, P., Takai, H., and De Lange, T. (2012). Telomeric 3' overhangs derive from resection by Exo1 and apollo and fill-in by POT1b-associated CST. *Cell* 150, 39–52. doi: 10.1016/j.cell.2012.05.026

Yang, Y. G., Lindahl, T., and Barnes, D. E. (2007). Trex1 Exonuclease Degrades ssDNA to Prevent Chronic Checkpoint Activation and Autoimmune Disease. *Cell* 131, 873–886. doi: 10.1016/j.cell.2007.10.017

Yeeles, J. T., Janska, A., Early, A., and Diffley, J. F. (2017). How the Eukaryotic Replisome Achieves Rapid and Efficient DNA Replication. *Mol. Cell* 65, 105–116. doi: 10.1016/j.molcel.2016.11.017

Ying, S., Minocherhomji, S., Chan, K. L., Palmai-Pallag, T., Chu, W. K., Wass, T., et al. (2013). MUS81 promotes common fragile site expression. *Nat. Cell Biol.* 15, 1001–1007. doi: 10.1038/ncb2773

Zadorozhny, K., Sannino, V., Beláň, O., Mlčoušková, J., Špírek, M., Costanzo, V., et al. (2017). Fanconi-Anemia-Associated Mutations Destabilize RAD51 Filaments and Impair Replication Fork Protection. *Cell Rep.* 21, 333–340. doi: 10.1016/j.celrep.2017.09.062

Zellweger, R., Dalcher, D., Mutreja, K., Berti, M., Schmid, J. A., Herrador, R., et al. (2015). Rad51-mediated replication fork reversal is a global response to genotoxic treatments in human cells. *J. Cell Biol.* 208, 563–579. doi: 10.1083/jcb.201406099

Zeman, M. K., and Cimprich, K. A. (2014). Causes and consequences of replication stress. *Nat. Cell Biol.* 16, 2–9. doi: 10.1038/ncb2897

Zou, L., and Elledge, S. J. (2003). Sensing DNA damage through ATRIP recognition of RPA-ssDNA complexes. *Science* 300, 1542–1548. doi: 10.1126/science.1083430

Conflict of Interest: The authors declare that the research was conducted in the absence of any commercial or financial relationships that could be construed as a potential conflict of interest.

frontiers in Cell and Developmental Biology

MINI REVIEW
published: 28 June 2021
doi: 10.3389/fcell.2021.699966

Coordinated Cut and Bypass: Replication of Interstrand Crosslink-Containing DNA

Qiuzhen Li[1†], Kata Dudás[1†], Gabriella Tick[2] and Lajos Haracska[1]*

[1] HCEMM-BRC Mutagenesis and Carcinogenesis Research Group, Institute of Genetics, Biological Research Centre, Szeged, Hungary, [2] Mutagenesis and Carcinogenesis Research Group, Institute of Genetics, Biological Research Centre, Szeged, Hungary

DNA interstrand crosslinks (ICLs) are covalently bound DNA lesions, which are commonly induced by chemotherapeutic drugs, such as cisplatin and mitomycin C or endogenous byproducts of metabolic processes. This type of DNA lesion can block ongoing RNA transcription and DNA replication and thus cause genome instability and cancer. Several cellular defense mechanism, such as the Fanconi anemia pathway have developed to ensure accurate repair and DNA replication when ICLs are present. Various structure-specific nucleases and translesion synthesis (TLS) polymerases have come into focus in relation to ICL bypass. Current models propose that a structure-specific nuclease incision is needed to unhook the ICL from the replication fork, followed by the activity of a low-fidelity TLS polymerase enabling replication through the unhooked ICL adduct. This review focuses on how, in parallel with the Fanconi anemia pathway, PCNA interactions and ICL-induced PCNA ubiquitylation regulate the recruitment, substrate specificity, activity, and coordinated action of certain nucleases and TLS polymerases in the execution of stalled replication fork rescue via ICL bypass.

Keywords: interstrand crosslink, DNA repair, translesion synthesis polymerases, PCNA ubiquitylation, structure-specific nuclease

OPEN ACCESS

Edited by:
Lin Deng,
Shenzhen Bay Laboratory, China

Reviewed by:
Jun Huang,
Zhejiang University, China
Indrajit Chaudhury,
University of Minnesota Morris, United States
Jing Zhang,
Tongji University, China

****Correspondence:***
Lajos Haracska
haracska.lajos@brc.hu

† These authors have contributed equally to this work

Specialty section:
This article was submitted to Cell Growth and Division, a section of the journal Frontiers in Cell and Developmental Biology

Received: *24 April 2021*
Accepted: *07 June 2021*
Published: *28 June 2021*

Citation:
Li Q, Dudás K, Tick G and Haracska L (2021) Coordinated Cut and Bypass: Replication of Interstrand Crosslink-Containing DNA. Front. Cell Dev. Biol. 9:699966. doi: 10.3389/fcell.2021.699966

INTRODUCTION

Our genome is constantly exposed to different exogenous and endogenous DNA damaging factors. Chemotherapeutic drugs, such as cisplatin or mitomycin C and metabolites like those from lipid peroxidation can cause interstrand crosslinks (ICLs), covalent links between the opposite strands of the DNA (reviewed in Stone et al., 2008). ICLs prevent strand separation, physically blocking replication and transcription. Stalled replication forks may collapse, causing DNA double-strand breaks, which can lead to chromosomal rearrangements, carcinogenesis, or cell death (reviewed in Negrini et al., 2010; Lenart and Krejci, 2016). ICLs have significant clinical relevance; inactivation of the Fanconi Anemia (FA) ICL repair pathway leads to FA. Patients diagnosed with FA suffer from progressive bone marrow failure and have a higher risk of developing cancer (reviewed in Shimamura and Alter, 2010). Due to their high cytotoxicity, ICL-inducing agents are the earliest and most commonly applied chemotherapeutic drugs (Rosenberg et al., 1969).

Since ICLs pose a high risk to cell survival and genome integrity, cells have developed multiple pathways to repair this type of DNA lesion. Nucleotide excision repair (NER) is able to recognize and remove ICL lesions in non-S-phase cells as well, while when ICLs block ongoing replication forks, in higher eukaryotic cells, the Fanconi anemia complementation group (FANC) DNA repair

proteins that belong to the Fanconi Anemia (FA) pathway are believed to be the main operating defense system (reviewed in Wood, 2010). Activation of the FA pathway leads to the recruitment of structure-specific nucleases and translesion DNA synthesis (TLS) polymerases to enable the bypass of the lesion as well as facilitate the recombination-dependent rescue system (Howlett et al., 2002; Sarkar et al., 2006; Hicks et al., 2010; Kim and D'Andrea, 2012). However, a general defense system, the so-called Rad6-18 postreplication repair system, also comes into play when replication encounters unrepaired DNA damage, such as ICLs (Shen et al., 2006). Rad6-Rad18-dependent monoubiquitination of proliferating cell nuclear antigen (PCNA) initiates a number of subsequent replication fork rescue processes and is believed to serve as a key regulatory step in stalled replication fork rescue (reviewed in Chang and Cimprich, 2009).

Although the FA as well as the Rad6-Rad18 postreplication repair pathway become activated when replication stalls at ICLs, their interplay has been less characterized. In this review, we are placing the focus on sensors of ICLs, nucleases for ICL unhooking, and TLS polymerases for ICL adduct bypass with particular emphasis on parallels and possible interplays between their regulation by ubiquitylation of the FANCI and FANCD2 heterodimer (ID2) and ubiquitylation of PCNA during the rescue of replication forks stalled at ICLs.

SENSORS AND TRANSDUCERS OF ICL REPAIR PATHWAYS

ICL repair is mostly activated during the S phase, but there are secondary mechanisms that are active in quiescent cells as well (Williams et al., 2012). Although these pathways have distinct mechanisms depending on the cell cycle, they all have common key steps. First, the lesion is recognized by sensor proteins that recruit other downstream regulators. During the G0/G1 phase, mainly nucleotide excision repair (NER) pathways monitor the genome, searching for ICL-caused distortion in the DNA. The XPA (Xeroderma pigmentosum A) and RPA (replicative protein A) protein, after having been recruited to the damaged area, load the structure-specific nuclease ERCC1-XPF onto the DNA (Volker et al., 2001; Tsodikov et al., 2007).

In the S phase of the cell cycle, ICLs cause replication fork stalling followed by activation of Ataxia telangiectasia (ATR)-dependent damage signaling, which will prevent dormant replication fork firing, while stabilizing the stalled replication fork (Luke-Glaser et al., 2010; Schwab et al., 2010). As shown in **Figure 1A**, the binding of FANCM at the site of the ICL has an essential role since it provides a platform for anchoring other FA proteins (Collis et al., 2008; Deans and West, 2009). Although FANCM seems to be an upstream regulator of ATR, its activity is also induced by ATR-dependent phosphorylation (Ciccia et al., 2007; Collis et al., 2008; Singh et al., 2013). When the phosphorylated FANCM recognizes ICLs, it recruits the FA core complex, which has a ubiquitin ligase activity transferring the ubiquitin with the help of FANCL, a RING-domain containing E3, from the UBE2T/FANCT, an E2 enzyme, to the FANCI and FANCD2 heterodimer (ID2) at lysines 523 and 561, respectively (Smogorzewska et al., 2007; Alpi et al., 2008; Huang et al., 2014). Prior to monoubiquitination, ID2 seems to be recruited by the FANC core complex to the damage where its DNA-binding generates the needed conformational change in FANCD2 for its ubiquitylation. Ubiquitylation closes the ID2 complex into a clamp conformation (Liang et al., 2015; Alcón et al., 2020; Tan et al., 2020). The activated ID2 complex then serves as a central hub for subsequent molecular events by enabling the recruitment of proteins that provide finally the rescue of the replication fork stalled at the ICL. These proteins include nucleases for unhooking ICLs, TLS polymerases for bypass of the unhooked adduct, repair factors for ICL elimination, and several factors of homologous recombination (**Figure 1A**).

Interestingly, in addition to the FANCM-dependent mechanism, other ICL-sensors, such as the Ubiquitin-Like PHD And RING Finger Domain-Containing Protein 1 (UHRF1) was also identified (Liang et al., 2015). UHRF1 and its paralog, UHRF2, can recruit FANCD2 to the site of the ICL and stimulate monoubiquitination of the ID2 complex (Motnenko et al., 2018).

PCNA UBIQUITYLATION, A SENSOR AND SIGNAL TRANSDUCER IN THE REPLICATION OF ICL LESIONS

The homotrimer PCNA is the master regulator of the replication fork. PCNA forms a sliding clamp over the DNA double strand and serves as a processivity factor for replicative polymerases. Encountering an unrepaired DNA lesion, such as an ICL results in the stalling of the replicative polymerase, which leads to the recruitment of Rad6-Rad18, a ubiquitin conjugating-ligase protein complex, which facilitates PCNA monoubiquitination (Bailly et al., 1997; Yoon et al., 2012). Monoubiquitinated PCNA can recruit TLS polymerases, which synthesize DNA across the damaged region either in an error-free or an error-prone mode, depending on the actual lesion and the TLS polymerase accessed (reviewed in Prakash et al., 2005). Many TLS polymerases, such as Pol eta, Pol kappa, and Pol iota exhibit conserved PCNA-interacting (PIP) as well as ubiquitin-binding (UBD) domains, by which they can strongly associate with monoubiquitinated PCNA (Ub-PCNA), which provides their timely access to the primer ends at stalled forks when replication encounters a barrier (Haracska et al., 2001a; Plosky et al., 2006). The PIP and UBD domains are also exhibited in certain nucleases implicated in ICL repair, such as SNM1A and FAN1, which raises the possibility that, similarly to Ub-ID2, Ub-PCNA can also play a role in their targeting to replication-stalling ICLs (Yang et al., 2010; Porro et al., 2017). Monoubiquitinated PCNA can also undergo polyubiquitylation in an Mms2–Ubc13 (E2)- and HTLF-SHPRH (E3)-dependent manner (Unk et al., 2008). Polyubiquitylated PCNA can initiate template switching, an error-free pathway for stalled replication fork rescue, which can involve fork reversal. Fork reversal can place ICL back to a general double-stranded DNA region, making it accessible for excision repair pathways, such as NER. Interestingly, RAD18 also has a function in ICL repair, independent of ubiquitinated PCNA. RAD18 has been shown to indirectly regulate the ubiquitination and loading of

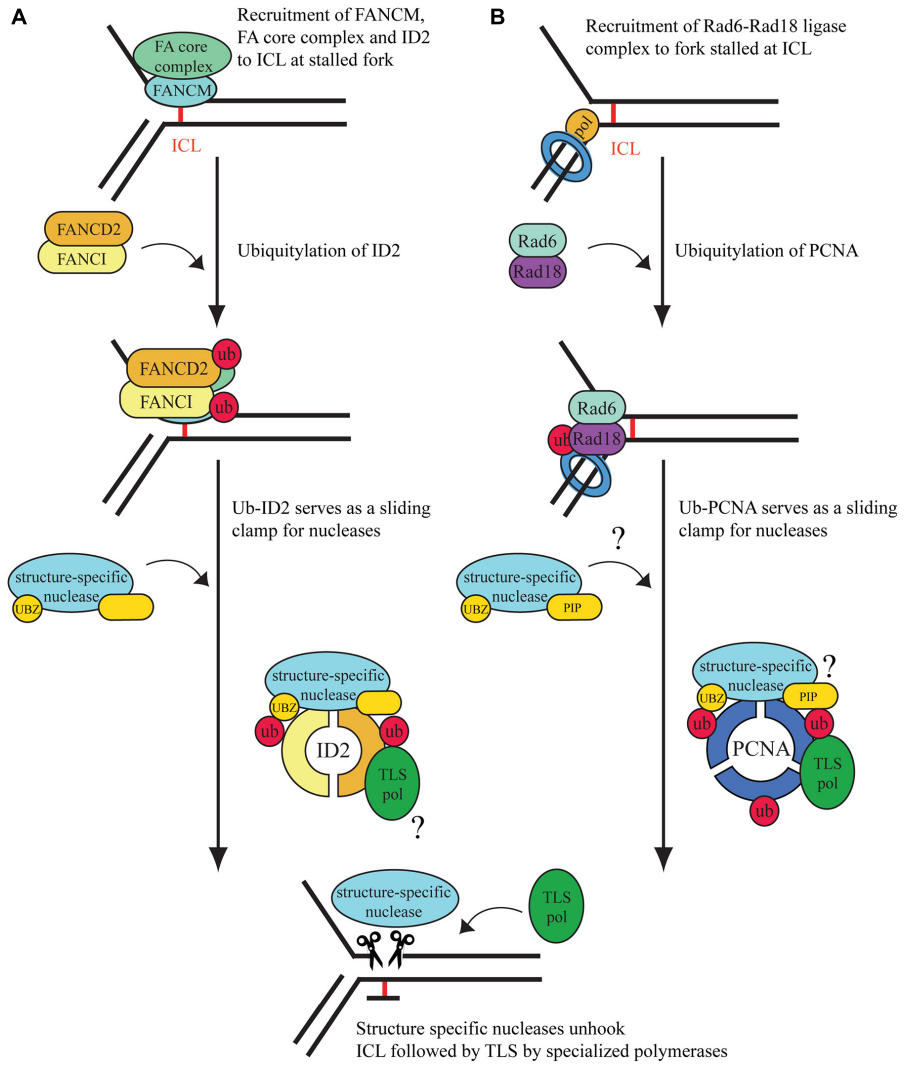

FIGURE 1 | Interstrand crosslink repair pathways at the stalled replication fork. **(A)** Replication-dependent ICL repair is considered to be carried out mainly by the Fanconi anemia pathway. After damage recognition, the ID2 complex is ubiquitylated by the activated FA core complex. The monoubiquitinated ID2 complex can further recruit structure-specific nucleases for unhooking. Gap filling is carried out by TLS polymerases, but the mechanism behind the recruitment of the polymerases is yet unknown. We hypothesize that Ub-ID2 serves as a DNA- encircling sliding clamp for TLS polymerases and nucleases. **(B)** When the ongoing DNA replication fork is blocked by DNA lesions, such as ICLs, upstream factors recognize it, and PCNA is monoubiquitinated by RAD6/RAD18. We hypothesize that monoubiquitinated PCNA acts as a hub for the recruitment of certain PIP box- and UBZ domain-containing structure-specific nucleases to unhook the ICL lesion. Translesion synthesis polymerases are also recruited to the site of damage by Ub-PCNA, which complete the bypass of the DNA damage. The covalent bond of the monoadduct is removed by nucleotide excision repair.

FANCD2 and FANCI in S phase, which suggests a possible role for RAD18 as an E3 ligase of the FA core complex (Williams et al., 2011). Recently, the RING finger and WD repeat domain-containing protein 3 (RFWD3) has been identified as an activator of various rescue mechanisms at the stalled replication fork, such as translesion synthesis and homologous recombination (HR) (Elia et al., 2015; Inano et al., 2017). Importantly for ICL repair, RFWD3 was suggested to be a FA gene since its biallelic mutation was found in a child with FA, which was also supported by results in cellular systems and animal model (Knies et al., 2017). Indicating complex interplays, the interaction of RFWD3 and PCNA stabilizes RFWD3 to the replication fork, and PCNA also interacts with FANCM, pointing to its possible function in lesion recognition (Rohleder et al., 2016; Lin et al., 2018).

STRUCTURE-SPECIFIC NUCLEASES AS EXECUTORS OF ICL UNHOOKING AT THE STALLED REPLICATION FORK

Following lesion recognition, the ICL is released from one of the DNA strands by a process called unhooking. During unhooking, structure-specific nucleases nick the DNA on both sides of the ICL, removing it from one of the parental strands. Several

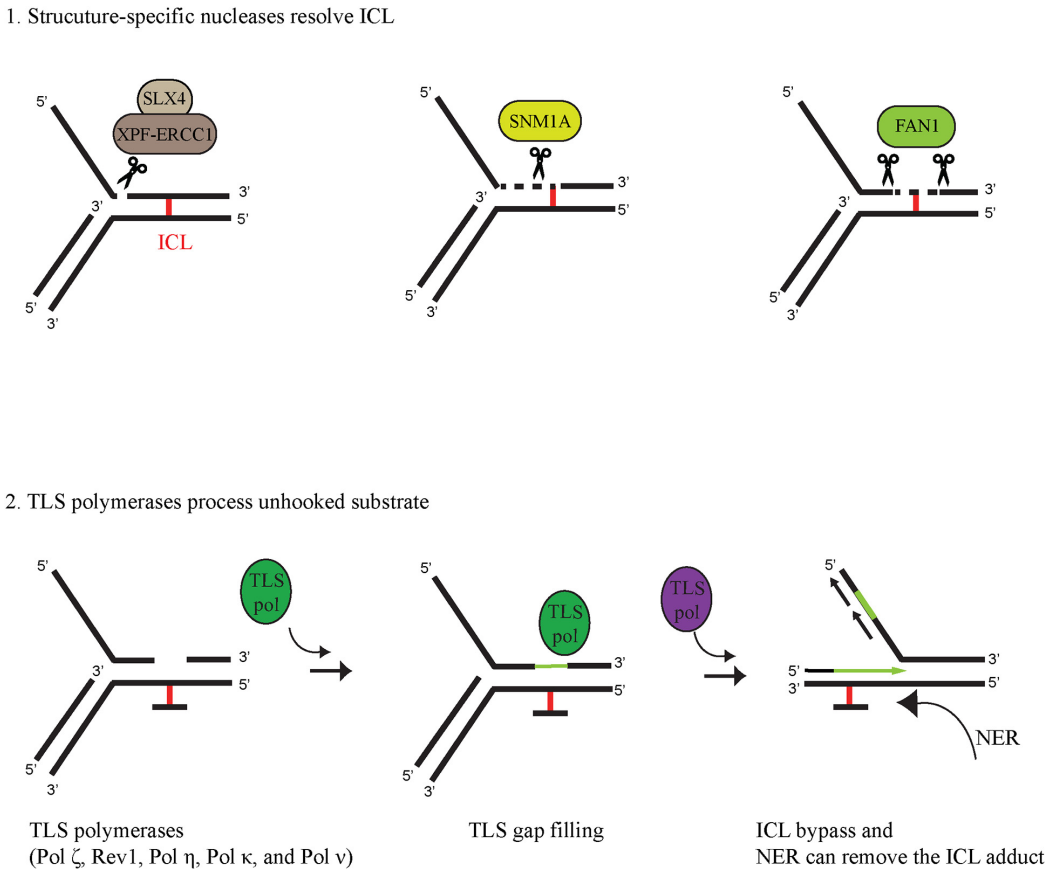

FIGURE 2 | Coordinated activity of structure-specific nucleases and TLS polymerases in ICL bypass (1) Structure-specific nucleases unhook ICL-containing DNA. SLX4 serves as a scaffold protein for XPF-ERCC1 to digest the dsDNA phosphodiester bond at the 5′ primer of the junction between dsDNA and ssDNA. The digested substrate can be further processed by the 5′-3′ exonuclease activity of SNM1A. FAN1 can completely unhook the ICL-containing substrate due to its 5′-3′ endo/exonuclease activity. (2) TLS polymerases can process the unhooked ICL-containing DNA by filling in the gap generated by ICL-unhooking nucleases and by extending the primer through the unhooked ICL adduct. Finally, the ICL monoadduct can be removed by another DNA repair pathway, such as nucleotide excision repair (NER).

nucleases have been implicated in ICL unhooking, such as XPF-ERCC1, MUS81-EME1, SLX1, SNM1A, and FAN1 the deficiency of which renders cells sensitive to ICL-generating agents. These nucleases alone or in collaboration can cleave the DNA on both sites of the ICL, leaving a gap, which can be filled in subsequently by TLS polymerases (**Figure 2**). XPF and SLX1 nucleases are considered to incise at 3′- and 5′-sides of the ICL (Kuraoka et al., 2000; Fricke and Brill, 2003), respectively, while MUS81 cuts at 3′-sides in specific cases (Ciccia et al., 2003). Various interactions can modulate the cleavage specificity of these enzymes; the nuclease activity of SLX1 can be extremely enhanced by its interaction with SLX4 (Fricke and Brill, 2003). As a scaffold protein, SLX4 can interact with several other nucleases and via its UBZ-domain-mediated binding to Ub-ID2 it can recruit XPF-ERCC1-MUS81-EME1-SLX1-SLX4 to the ICL (Fekairi et al., 2009; Castor et al., 2013). Ub-ID2 might play a role in the recruitment of other nucleases, as well, as it was proposed for FAN1; however, here we put more focus on interaction of SNM1A and FAN1 with Ub-PCNA in the ICL repair process. The SNM1A nuclease contains a ubiquitin—binding zinc finger (UBZ) domain at the N-terminal and a PIP box in the middle region of the protein (Yang et al., 2010). SNM1A has an intrinsic 5′ to 3′ exonuclease activity and was shown to be epistatic with the XPF-ERCC1 endonuclease that can nick the DNA 5′ from the ICL (Wang et al., 2011). Their coordinated action in ICL unhooking was shown; the XPF-ERCC1-generated nick provided an entry point for SNM1A exonuclease activity (Wang et al., 2011). Recently, SNM1A has been shown to have single-strand-specific endonuclease activity as well (5′ and 3′overhangs, hairpins, flaps, and gapped substrates) (Buzon et al., 2018).

The FAN1 nuclease also possesses a UBZ domain and a PIP box at the N-terminal end (Smogorzewska et al., 2007; Pennell et al., 2014). Originally, several reports described FAN1 as a member of the FA pathway since its action on ICL-containing DNA was described to be dependent on monoubiquitinated FANCD2 (Kratz et al., 2010; Liu et al., 2010; MacKay et al., 2010). However, later on, it turned out that patients with biallelic FAN1 mutations do not develop FA, and FAN1 does not show epistasis with other FA genes, which indicates some other role for FAN1 in ICL repair (Zhou et al., 2012; Lachaud et al., 2016b).

FAN1 has an endonuclease activity and is able to incise 5′ to the ICL at the 4th nucleotide after the replication fork junction on the 5′ flap model substrate (**Figure 2**). FAN1 has a 5′ → 3′ exonuclease activity as well, initiating cleavage 4 nt from the 5′ end on single- and double-stranded DNA (MacKay et al., 2010; Lachaud et al., 2016a). FAN1 is able to unhook nitrogen mustard-induced interstrand crosslinks *in vitro* due to its nuclease activity (Pizzolato et al., 2015). FAN1 also interacts with ubiquitin-PCNA and enhances PCNA ubiquitylation after mitomycin C treatment (Porro et al., 2017).

TLS POLYMERASES PROCESS SUBSTRATES UNHOOKED BY NUCLEASES

Replicative polymerases, such as the human Pol δ and Pol ε have high fidelity and possess 3′ → 5′ exonuclease activity as a proofreading function to ensure precise DNA replication (Johnson et al., 2015). However, there is a cost of high fidelity since DNA contains many lesions, such as base adducts, photoproducts, intrastrand and interstrand crosslinks, which cannot be accommodated by the tight active sites of the replicative polymerases, leading to blocked replication fork machinery (Bezalel-Buch et al., 2020). Stalling of replication can lead to strand breaks, chromosomal rearrangement, and other genome-destabilizing events; to avoid this, the so-called DNA damage tolerance (DDT) pathways, such as the Rad6-Rad18-dependent PCNA-monoubiquitination-mediated one come into play upon fork stalling (Davies et al., 2008). One sub-branch of these DDT pathways is translesion synthesis, in which, at the damage, low-fidelity polymerases take over the 3′ primer end from the replicative polymerase and insert either the correct or uncorrect nucleotide opposite the lesion, leading to error-free or error-prone bypass. As shown in **Figure 2**, bypass of ICL may involve TLS polymerase action at two points; in the gap filling after the nuclease has unhooked the ICL and in the replication through the adduct. Based on genetic assays with TLS polymerase-deficient cells as well as biochemical findings, many TLS polymerases have been implicated in the bypass of the unhooked ICL (Ho et al., 2011; Roy et al., 2016; Bezalel-Buch et al., 2020). Sensitivity assays performed by treating cells with various crosslinking agents revealed ICL-repair functions for Pol ζ, Rev1, Pol η, Pol κ, and Pol ν (reviewed in Ho and Schärer (2010). Although various crosslinking agents can produce a wide variety of ICLs requiring different TLS polymerases for bypass, based on cisplatin and mitomycin C exposure, REV3-encoded Pol ζ and REV1 are believed to be among the main players of ICL bypass (Hicks et al., 2010). Genetic evidence also supports the involvement of Pol η in a more general role in ICL bypass, while Pol κ seems to be more restricted to minor groove DNA adducts and Pol ν to major groove ICL bypass (Zhang et al., 2000; Acharya et al., 2008; Yamanaka et al., 2010; Roy et al., 2016). TLS polymerases can bypass DNA lesions in a two-step fashion, first inserting a nucleotide opposite the lesion and then extending opposite from the lesion (Johnson et al., 2000; Haracska et al., 2001b). Certain TLS polymerases can carry out both steps, but often it requires the collaboration of two polymerases: an inserter and an extender (reviewed in Ho and Schärer, 2010). Even though the deficiency of a certain TLS polymerase does not cause strong hypersensitivity to crosslinking agents, its involvement in ICL bypass cannot be ruled out because cells can use multiple TLS polymerases as inserters as well as extenders. Although purified REV1 together with Pol ζ show complete bypass synthesis, experiments using Xenopus egg extracts indicate that Pol ζ and REV1 are required only for the extension step past a cisplatin-induced ICL (Bezalel-Buch et al., 2020). Pol η alone is able to carry out both the insertion and the extension steps across various major ICL lesions (Roy et al., 2016). Pol η and many other TLS polymerases, such as Pol κ and Pol ι contain PIP and ubiquitin-binding motif (UBM)/UBZ domains allowing them to interact with Ub-PCNA, which can target them to the site of the stalled fork at the ICL as well as stimulate their synthetic activity (Haracska et al., 2001a; Plosky et al., 2006).

DISCUSSION

Cytotoxic ICL lesions pose a considerable threat to cells regardless of cell phase. Cells can remove ICLs by NER during the G0/G1 phase, but some may escape repair and cause stalling of the replication machinery. In higher eukaryotic cells, the FA pathway is considered the main defense system to repair ICLs during the S phase of the cell cycle. In this review, we compare the FA pathway to a more general defense system, the Rad6-RAD18-dependent PCNA monoubiquitination, which is activated when replication stalls at various lesions, including ICLs. We also point out the similarities between the FA and Rad6-Rad18 pathways in dealing with the ICL at the stalled replication fork (**Figure 1**) and summarize our current knowledge on ICL-unhooking nucleases and ICL bypass polymerases (**Figure 2**), and reach the following conclusions. First, when replication encounters an ICL, monoubiquitation of the central hub proteins, ID2 and PCNA, is a critical step for the operation of the FA and Rad6-Rad18 pathways, respectively. Second, several proteins implicated in ICL repair can interact with Ub-ID2 as well as Ub-PCNA, such as the FAN1 nuclease, which exhibits PIP and UBZ domains for timely binding to the stalled fork (Buzon et al., 2018). Interestingly, deficiency of FAN1 can be partially complemented by the SNM1A nuclease, which also exhibits PIP and UBZ domains (Yang et al., 2010; Buzon et al., 2018). Third, ubiquitylation can provide access to unhooked ICL adduct bypass of various TLS polymerases exhibiting PIP and, in most cases, UBZ domains as well, which indicates similarities between the recruitment of nucleases and polymerases. Fourth, after completion of the repair process, both FA and Rad6-Rad18 DDT pathways are terminated by USP1-dependent deubiquitylation of their central hub proteins (Nijman et al., 2005; Huang et al., 2006). Importantly, PCNA encircles DNA as a homotrimeric sliding clamp, and each of its subunit can be ubiquitylated, providing three binding surfaces for PIP- and UBZ-domain-containing proteins. Thus, it is possible that proteins exhibiting these two domains, such as an ICL-unhooking nuclease like FAN1 and a TLS polymerase like Pol η, can bind to a Ub-PCNA

ring at the same time, which would provide a high degree of coordination between ICL unhooking and bypass. Interestingly, recent structural studies revealed that ubiquitylation of the ID2 complex results in its conformational change which converts the ID2 to a clamp encircling the DNA (Alcón et al., 2020; Wang et al., 2020). The structural analogy between Ub-PCNA and Ub-ID2 is tempting and forces one to speculate whether Ub-ID2 can serve as a sliding clamp for TLS polymerases in ICL bypass. Also, it would be interesting to explore whether the Ub-PCNA and Ub-ID2 sliding clamps can bind ICL nucleases and TLS polymerases at the same time for efficient bypass. Finally, it remains to be explored whether Ub-PCNA and Ub-ID2 rings can interact and provide a joint sliding clamp for protein exchange and higher coordination between the FA and Ub-PCNA ICL damage bypass pathways.

AUTHOR CONTRIBUTIONS

QL and KD reviewed the literature and wrote the first draft of the manuscript. GT and LH revised and edited the manuscript. All authors approved the final version of the manuscript for submission.

FUNDING

This project received funding from the European Union's Horizon 2020 Research and Innovation Programme under Grant Agreement No. 739593. This work was also supported by the National Research, Development and Innovation Office GINOP-2.3.2–15-2016–00024 and GINOP-2.3.2–15-2016–00026.

REFERENCES

Acharya, N., Yoon, J.-H., Gali, H., Unk, I., Haracska, L., Johnson, R. E., et al. (2008). Roles of PCNA-binding and ubiquitin-binding domains in human DNA polymerase η in translesion DNA synthesis. *Proc. Natl. Acad. Sci.* 105, 17724–17729. doi: 10.1073/pnas.0809844105

Alcón, P., Shakeel, S., Chen, Z. A., Rappsilber, J., Patel, K. J., and Passmore, L. A. (2020). FANCD2–FANCI is a clamp stabilized on DNA by monoubiquitination of FANCD2 during DNA repair. *Nat. Struct. Mol. Biol.* 27, 240–248. doi: 10.1038/s41594-020-0380-1

Alpi, A. F., Pace, P. E., Babu, M. M., and Patel, K. J. (2008). Mechanistic insight into site-restricted monoubiquitination of FANCD2 by Ube2t, FANCL, and FANCI. *Mol. Cell* 32, 767–777. doi: 10.1016/j.molcel.2008.12.003

Bailly, V., Lauder, S., Prakash, S., and Prakash, L. (1997). Yeast DNA repair proteins Rad6 and Rad18 form a heterodimer that has ubiquitin conjugating, DNA binding, and ATP hydrolytic activities. *J. Biol. Chem.* 272, 23360–23365. doi: 10.1074/jbc.272.37.23360

Bezalel-Buch, R., Cheun, Y. K., Roy, U., Schärer, O. D., and Burgers, P. M. (2020). Bypass of DNA interstrand crosslinks by a Rev1–DNA polymerase ζ complex. *Nucleic Acids Res.* 48, 8461–8473. doi: 10.1093/nar/gkaa580

Buzon, B., Grainger, R., Huang, S., Rzadki, C., and Junop, M. S. (2018). Structure-specific endonuclease activity of SNM1A enables processing of a DNA interstrand crosslink. *Nucleic Acids Res.* 46, 9057–9066. doi: 10.1093/nar/gky759

Castor, D., Nair, N., Déclais, A. C., Lachaud, C., Toth, R., Macartney, T. J., et al. (2013). Cooperative control of holliday junction resolution and DNA repair by the SLX1 and MUS81-EME1 nucleases. *Mol. Cell* 52, 221–233. doi: 10.1016/j.molcel.2013.08.036

Chang, D. J., and Cimprich, K. A. (2009). DNA damage tolerance: when it's ok to make mistakes. *Nat. Chem. Biol.* 5, 82–90. doi: 10.1038/nchembio.139

Ciccia, A., Constantinou, A., and West, S. C. (2003). Identification and characterization of the human Mus81-Emel endonuclease. *J. Biol. Chem.* 278, 25172–25178. doi: 10.1074/jbc.m302882200

Ciccia, A., Ling, C., Coulthard, R., Yan, Z., Xue, Y., Meetei, A. R., et al. (2007). Identification of FAAP24, a fanconi anemia core complex protein that interacts with FANCM. *Mol. Cell* 25, 331–343. doi: 10.1016/j.molcel.2007.01.003

Collis, S. J., Ciccia, A., Deans, A. J., Horejsí, Z., Martin, J. S., Maslen, S. L., et al. (2008). FANCM and FAAP24 function in ATR-mediated checkpoint signaling independently of the Fanconi anemia core complex. *Mol. Cell* 32, 313–324. doi: 10.1016/j.molcel.2008.10.014

Davies, A. A., Huttner, D., Daigaku, Y., Chen, S., and Ulrich, H. D. (2008). Activation of ubiquitin-dependent DNA damage bypass is mediated by replication protein a. *Mol. Cell* 29, 625–636. doi: 10.1016/j.molcel.2007.12.016

Deans, A. J., and West, S. C. (2009). FANCM connects the genome instability disorders bloom's syndrome and fanconi anemia. *Mol. Cell* 36, 943–953. doi: 10.1016/j.molcel.2009.12.006

Elia, A. E. H., Wang, D. C., Willis, N. A., Boardman, A. P., Hajdu, I., Adeyemi, R. O., et al. (2015). RFWD3-dependent ubiquitination of RPA regulates repair at stalled replication forks. *Mol. Cell* 60, 280–293. doi: 10.1016/j.molcel.2015.09.011

Fekairi, S., Scaglione, S., Chahwan, C., Taylor, E. R., Tissier, A., Coulon, S., et al. (2009). Human SLX4 Is a holliday junction resolvase subunit that binds multiple DNA repair/recombination endonucleases. *Cell* 138, 78–89. doi: 10.1016/s9999-9994(09)20375-8

Fricke, W. M., and Brill, S. J. (2003). Slx1 - Slx4 is a second structure-specific endonuclease functionally redundant with Sgs1 - Top3. *Genes Dev.* 17, 1768–1778. doi: 10.1101/gad.1105203

Haracska, L., Kondratick, C. M., Unk, I., Prakash, S., and Prakash, L. (2001a). Interaction with PCNA is essential for yeast DNA polymerase eta function. *Mol. Cell* 8, 407–415. doi: 10.1016/s1097-2765(01)00319-7

Haracska, L., Unk, I., Johnson, R. E., Johansson, E., Burgers, P. M., Prakash, S., et al. (2001b). Roles of yeast DNA polymerases delta and zeta and of Rev1 in the bypass of abasic sites. *Genes Dev.* 15, 945–954. doi: 10.1101/gad.882301

Hicks, J. K., Chute, C. L., Paulsen, M. T., Ragland, R. L., Howlett, N. G., Guéranger, Q., et al. (2010). Differential roles for DNA polymerases Eta, Zeta, and REV1 in lesion bypass of intrastrand versus interstrand DNA cross-links. *Mol. Cell. Biol.* 30, 1217–1230. doi: 10.1128/mcb.00993-09

Ho, T. V., and Schärer, O. D. (2010). Translesion DNA synthesis polymerases in DNA interstrand crosslink repair. *Environ. Mol. Mutagen.* 51, 552–566.

Ho, T. V., Guainazzi, A., Derkunt, S. B., Enoiu, M., and Schärer, O. D. (2011). Structure-dependent bypass of DNA interstrand crosslinks by translesion synthesis polymerases. *Nucleic Acids Res.* 39, 7455–7464. doi: 10.1093/nar/gkr448

Howlett, N. G., Taniguchi, T., Olson, S., Cox, B., Waisfisz, Q., De Die-Smulders, C., et al. (2002). Biallelic inactivation of BRCA2 in Fanconi anemia. *Science* 297, 606–609. doi: 10.1126/science.1073834

Huang, T. T., Nijman, S. M. B., Mirchandani, K. D., Galardy, P. J., Cohn, M. A., Haas, W., et al. (2006). Regulation of monoubiquitinated PCNA by DUB autocleavage. *Nat. Cell Biol.* 8, 341–347. doi: 10.1038/ncb1378

Huang, Y., Leung, J. W. C., Lowery, M., Matsushita, N., Wang, Y., Shen, X., et al. (2014). Modularized functions of the Fanconi anemia core complex. *Cell Rep.* 7, 1849–1857. doi: 10.1016/j.celrep.2014.04.029

Inano, S., Sato, K., Katsuki, Y., Kobayashi, W., Tanaka, H., Nakajima, K., et al. (2017). RFWD3-mediated ubiquitination promotes timely removal of both RPA and RAD51 from DNA damage sites to facilitate homologous recombination. *Mol. Cell* 66, 622–634.e8.

Johnson, R. E., Klassen, R., Prakash, L., and Prakash, S. (2015). A major role of DNA Polymerase δ in replication of both the leading and lagging DNA strands. *Mol. Cell* 59, 163–175. doi: 10.1016/j.molcel.2015.05.038

Johnson, R. E., Washington, M. T., Haracska, L., Prakash, S., and Prakash, L. (2000). Eukaryotic polymerases ι and ζ act sequentially to bypass DNA lesions. *Nature* 406, 1015–1019. doi: 10.1038/35023030

Kim, H., and D'Andrea, A. D. (2012). Regulation of DNA cross-link repair by the *Fanconi anemia*/BRCA pathway. *Genes Dev.* 26, 1393–1408. doi: 10.1101/gad.195248.112

Knies, K., Inano, S., Ramírez, M. J., Ishiai, M., Surrallés, J., Takata, M., et al. (2017). Biallelic mutations in the ubiquitin ligase RFWD3 cause *Fanconi anemia*. *J. Clin. Invest.* 127, 3013–3027. doi: 10.1172/jci92069

Kratz, K., Schöpf, B., Kaden, S., Sendoel, A., Eberhard, R., Lademann, C., et al. (2010). Deficiency of FANCD2-associated nuclease KIAA1018/FAN1 sensitizes cells to interstrand crosslinking agents. *Cell* 142, 77–88. doi: 10.1016/j.cell.2010.06.022

Kuraoka, I., Kobertz, W. R., Ariza, R. R., Biggerstaff, M., Essigmann, J. M., and Wood, R. D. (2000). Repair of an interstrand DNA cross-link initiated by ERCC1-XPF repair/recombination nuclease. *J. Biol. Chem.* 275, 26632–26636. doi: 10.1074/jbc.c000337200

Lachaud, C., Moreno, A., Marchesi, F., Toth, R., Blow, J. J., and Rouse, J. (2016a). Ubiquitinated Fancd2 recruits Fan1 to stalled replication forks to prevent genome instability. *Science* 351, 846–849. doi: 10.1126/science.aad5634

Lachaud, C., Slean, M., Marchesi, F., Lock, C., Odell, E., Castor, D., et al. (2016b). Karyomegalic interstitial nephritis and DNA damage-induced polyploidy in Fan1 nuclease-defective knock-in mice. *Genes Dev.* 30, 639–644. doi: 10.1101/gad.276287.115

Lenart, P., and Krejci, L. (2016). DNA, the central molecule of aging. *Mutat. Res.* 786, 1–7. doi: 10.1016/j.mrfmmm.2016.01.007

Liang, C. C., Zhan, B., Yoshikawa, Y., Haas, W., Gygi, S. P., and Cohn, M. A. (2015). UHRF1 Is a sensor for DNA interstrand crosslinks and recruits FANCD2 to initiate the *Fanconi anemia* pathway. *Cell Rep.* 10, 1947–1956. doi: 10.1016/j.celrep.2015.02.053

Lin, Y. C., Wang, Y., Hsu, R., Giri, S., Wopat, S., Arif, M. K., et al. (2018). PCNA-mediated stabilization of E3 ligase RFWD3 at the replication fork is essential for DNA replication. *Proc. Natl. Acad. Sci. U. S. A.* 115, 13282–13287. doi: 10.1073/pnas.1814521115

Liu, T., Ghosal, G., Yuan, J., Chen, J., and Huang, J. (2010). FAN1 acts with FANCI-FANCD2 to promote DNA interstrand cross-link repair. *Science* 329, 693–696. doi: 10.1126/science.1192656

Luke-Glaser, S., Luke, B., Grossi, S., and Constantinou, A. (2010). FANCM regulates DNA chain elongation and is stabilized by S-phase checkpoint signalling. *EMBO J.* 29, 795–805. doi: 10.1038/emboj.2009.371

MacKay, C., Déclais, A.-C., Lundin, C., Agostinho, A., Deans, A. J., MacArtney, T. J., et al. (2010). Identification of KIAA1018/FAN1, a DNA repair nuclease recruited to DNA damage by monoubiquitinated FANCD2. *Cell* 142, 65–76. doi: 10.1016/j.cell.2010.06.021

Motnenko, A., Liang, C. C., Yang, D., Lopez-Martinez, D., Yoshikawa, Y., Zhan, B., et al. (2018). Identification of UHRF2 as a novel DNA interstrand crosslink sensor protein. *PLoS Genet.* 14:e1007643. doi: 10.1371/journal.pgen.1007643

Negrini, S., Gorgoulis, V. G., and Halazonetis, T. D. (2010). Genomic instability an evolving hallmark of cancer. *Nat. Rev. Mol. Cell Biol.* 11, 220–228. doi: 10.1038/nrm2858

Nijman, S. M. B., Huang, T. T., Dirac, A. M. G., Brummelkamp, T. R., Kerkhoven, R. M., D'Andrea, A. D., et al. (2005). The deubiquitinating enzyme USP1 regulates the *Fanconi anemia* pathway. *Mol. Cell* 17, 331–339. doi: 10.1016/j.molcel.2005.01.008

Pennell, S., Déclais, A.-C., Li, J., Haire, L. F., Berg, W., Saldanha, J. W., et al. (2014). FAN1 activity on asymmetric repair intermediates is mediated by an atypical monomeric virus-type replication-repair nuclease domain. *Cell Rep.* 8, 84–93. doi: 10.1016/j.celrep.2014.06.001

Pizzolato, J., Mukherjee, S., Schärer, O. D., and Jiricny, J. (2015). FANCD2-associated nuclease 1, but not exonuclease 1 or flap endonuclease 1, is able to unhook DNA interstrand cross-links in vitro. *J. Biol. Chem.* 290, 22602–22611. doi: 10.1074/jbc.m115.663666

Plosky, B. S., Vidal, A. E., Fernández, de Henestrosa, A. R., McLenigan, M. P., McDonald, J. P., et al. (2006). Controlling the subcellular localization of DNA polymerases iota and eta via interactions with ubiquitin. *EMBO J.* 25, 2847–2855. doi: 10.1038/sj.emboj.7601178

Porro, A., Berti, M., Pizzolato, J., Bologna, S., Kaden, S., Saxer, A., et al. (2017). FAN1 interaction with ubiquitylated PCNA alleviates replication stress and preserves genomic integrity independently of BRCA2. *Nat. Commun.* 8:1073.

Prakash, S., Johnson, R. E., and Prakash, L. (2005). Eukaryotic translesion synthesis DNA polymerases: specificity of structure and function. *Annu. Rev. Biochem.* 74, 317–353. doi: 10.1146/annurev.biochem.74.082803.133250

Rohleder, F., Huang, J., Xue, Y., Kuper, J., Round, A., Seidman, M., et al. (2016). FANCM interacts with PCNA to promote replication traverse of DNA interstrand crosslinks. *Nucleic Acids Res.* 44, 3219–3232. doi: 10.1093/nar/gkw037

Rosenberg, B., Vancamp, L., Trosko, J. E., and Mansour, V. H. (1969). Platinum compounds: a new class of potent antitumour agents. *Nature* 222, 385–386. doi: 10.1038/222385a0

Roy, U., Mukherjee, S., Sharma, A., Frank, E. G., and Schärer, O. D. (2016). The structure and duplex context of DNA interstrand crosslinks affects the activity of DNA polymerase η. *Nucleic Acids Res.* 44, 7281–7291.

Sarkar, S., Davies, A. A., Ulrich, H. D., and McHugh, P. J. (2006). DNA interstrand crosslink repair during G1 involves nucleotide excision repair and DNA polymerase zeta. *EMBO J.* 25, 1285–1294. doi: 10.1038/sj.emboj.7600993

Schwab, R. A., Blackford, A. N., and Niedzwiedz, W. (2010). ATR activation and replication fork restart are defective in FANCM-deficient cells. *EMBO J.* 29, 806–818. doi: 10.1038/emboj.2009.385

Shen, X., Jun, S., O'Neal, L. E., Sonoda, E., Bemark, M., Sale, J. E., et al. (2006). REV3 and REV1 play major roles in recombination-independent repair of DNA interstrand cross-links mediated by monoubiquitinated proliferating cell nuclear antigen (PCNA). *J. Biol. Chem.* 281, 13869–13872. doi: 10.1074/jbc.c600071200

Shimamura, A., and Alter, B. P. (2010). Pathophysiology and management of inherited bone marrow failure syndromes. *Blood Rev.* 24, 101–122. doi: 10.1016/j.blre.2010.03.002

Singh, T. R., Ali, A. M., Paramasivam, M., Pradhan, A., Wahengbam, K., Seidman, M. M., et al. (2013). ATR-dependent phosphorylation of FANCM at serine 1045 is essential for FANCM functions. *Cancer Res.* 73, 4300–4310. doi: 10.1158/0008-5472.can-12-3976

Smogorzewska, A., Matsuoka, S., Vinciguerra, P., McDonald, E. R., Hurov, K. E., Luo, J., et al. (2007). Identification of the FANCI protein, a monoubiquitinated FANCD2 paralog required for DNA repair. *Cell* 129, 289–301. doi: 10.1016/j.cell.2007.03.009

Stone, M. P., Cho, Y., Huang, Kim, H.-Y., Kozekov, I. V., Kozekov, A., et al. (2008). Interstrand DNA cross-links induced by α,β-Unsaturated aldehydes derived from lipid peroxidation and environmental sources. *Acc. Chem. Res.* 41, 793–804. doi: 10.1021/ar700246x

Tan, W., van Twest, S., Leis, A., Bythell-Douglas, R., Murphy, V. J., Sharp, M., et al. (2020). Monoubiquitination by the human Fanconi anemia core complex clamps FANCI:FANCD2 on DNA in filamentous arrays. *Elife* 9:e54128.

Tsodikov, O. V., Ivanov, D., Orelli, B., Staresincic, L., Shoshani, I., and Oberman, R. (2007). Structural basis for the recruitment of ERCC1-XPF to nucleotide excision repair complexes by XPA. *EMBO J.* 26, 4768–4776. doi: 10.1038/sj.emboj.7601894

Unk, I., Hajdú, I., Fátyol, K., Hurwitz, J., Yoon, J. H., Prakash, L., et al. (2008). Human HLTF functions as a ubiquitin ligase for proliferating cell nuclear antigen polyubiquitination. *Proc. Natl. Acad. Sci. U. S. A.* 105, 3768–3773. doi: 10.1073/pnas.0800563105

Volker, M., Moné, M. J., Karmakar, P., van Hoffen, A., Schul, W., Vermeulen, W., et al. (2001). Sequential assembly of the nucleotide excision repair factors in vivo. *Mol. Cell* 8, 213–224. doi: 10.1016/s1097-2765(01)00281-7

Wang, A. T., Sengerová, B., Cattell, E., Inagawa, T., Hartley, J. M., Kiakos, K., et al. (2011). Human SNM1A and XPF-ERCC1 collaborate to initiate DNA interstrand cross-link repair. *Genes Dev.* 25, 1859–1870. doi: 10.1101/gad.15699211

Wang, R., Wang, S., Dhar, A., Peralta, C., and Pavletich, N. P. (2020). DNA clamp function of the monoubiquitinated *Fanconi anaemia* ID complex. *Nature* 580, 278–282. doi: 10.1038/s41586-020-2110-6

Williams, H. L., Gottesman, M. E., and Gautier, J. (2012). Replication-independent repair of DNA interstrand crosslinks. *Mol. Cell* 47, 140–147. doi: 10.1016/j.molcel.2012.05.001

Williams, S. A., Longerich, S., Sung, P., Vaziri, C., and Kupfer, G. M. (2011). The E3 ubiquitin ligase RAD18 regulates ubiquitylation and chromatin loading of FANCD2 and FANCI. *Blood* 117, 5078–5087. doi: 10.1182/blood-2010-10-311761

Wood, R. D. (2010). Mammalian nucleotide excision repair proteins and interstrand crosslink repair. *Environ. Mol. Mutagen.* 51, 520–526.

Yamanaka, K., Minko, I. G., Takata, K., Kolbanovskiy, A., Kozekov, I. D., Wood, R. D., et al. (2010). Novel enzymatic function of DNA Polymerase ν in

translesion DNA synthesis past major groove DNA-Peptide and DNA-DNA cross-links. *Chem. Res. Toxicol.* 23, 689–695. doi: 10.1021/tx900449u

Yang, K., Moldovan, G. L., and D'Andrea, A. D. (2010). RAD18-dependent recruitment of SNM1A to DNA repair complexes by a ubiquitin-binding zinc finger. *J. Biol. Chem.* 285, 19085–19091. doi: 10.1074/jbc.m109.100032

Yoon, J.-H., Prakash, S., and Prakash, L. (2012). Requirement of Rad18 protein for replication through DNA lesions in mouse and human cells. *Proc. Natl. Acad. Sci.* 109, 7799–7804. doi: 10.1073/pnas.1204105109

Zhang, Y., Yuan, F., Wu, X., Wang, M., Rechkoblit, O., Taylor, J.-S., et al. (2000). Error-free and error-prone lesion bypass by human DNA polymerase κ in vitro. *Nucleic Acids Res.* 28, 4138–4146. doi: 10.1093/nar/28.21.4138

Zhou, W., Otto, E. A., Cluckey, A., Airik, R., Hurd, T. W., and Chaki, M. (2012). FAN1 mutations cause karyomegalic interstitial nephritis, linking chronic kidney failure to defective DNA damage repair. *Nat. Genet.* 44, 910–915. doi: 10.1038/ng.2347

Conflict of Interest: The authors declare that the research was conducted in the absence of any commercial or financial relationships that could be construed as a potential conflict of interest.

frontiers in Cell and Developmental Biology

MINI REVIEW
published: 21 July 2021
doi: 10.3389/fcell.2021.658003

The Fate of Two Unstoppable Trains After Arriving Destination: Replisome Disassembly During DNA Replication Termination

*Yisui Xia**

The MRC Protein Phosphorylation and Ubiquitylation Unit, School of Life Sciences, University of Dundee, Dundee, United Kingdom

In eukaryotes, the perfect duplication of the chromosomes is executed by a dynamic molecular machine called the replisome. As a key step to finishing DNA replication, replisome disassembly is triggered by ubiquitylation of the MCM7 subunit of the helicase complex CMG. Afterwards, the CDC48/p97 "unfoldase" is recruited to the ubiquitylated helicase to unfold MCM7 and disassemble the replisome. Here we summarise recently discovered mechanisms of replisome disassembly that are likely to be broadly conserved in eukaryotes. We also discuss two crucial questions that remain to be explored further in the future. Firstly, how is CMG ubiquitylation repressed by the replication fork throughout elongation? Secondly, what is the biological significance of replisome disassembly and what are the consequences of failing to ubiquitylate and disassemble the CMG helicase?

Keywords: p97/CDC48/VCP, SCF^{Dia2}, CUL2^{LRR1}, CMG, ubiquitylation, replisome disassembly

OPEN ACCESS

Edited by:
Lin Deng,
Shenzhen Bay Laboratory, China

Reviewed by:
Anyong Xie,
Zhejiang University, China
Selwin K. Wu,
National University of Singapore, Singapore

***Correspondence:**
Yisui Xia
yyxia@dundee.ac.uk

Specialty section:
This article was submitted to Cell Growth and Division, a section of the journal Frontiers in Cell and Developmental Biology

Received: *24 January 2021*
Accepted: *14 June 2021*
Published: *21 July 2021*

Citation:
Xia Y (2021) The Fate of Two Unstoppable Trains After Arriving Destination: Replisome Disassembly During DNA Replication Termination. Front. Cell Dev. Biol. 9:658003. doi: 10.3389/fcell.2021.658003

OVERVIEW OF DNA REPLICATION TERMINATION

The accurate and complete duplication of the chromosomes is essential for the inheritance of genetic information. It is initiated during the S-phase of the cell cycle by the assembly of a pair of bi-directional replisome complexes at many origins of DNA replication, followed by semi-conservative DNA synthesis until each chromosome is perfectly duplicated (O'Donnell et al., 2013; Bell and Labib, 2016). Every beginning has an end, so as DNA replication. Its final processes define its termination. When two replication forks from neighbouring origins converge with each other, replication terminates and the remaining stretch of parental DNA between the two replisomes is unwound. Subsequently, a single-stranded gap exists between the 3′ end of the leading strand of one fork and the downstream Okazaki fragment of the opposing fork. This gap is then filled and the Okazaki fragment processed, leading to completion of DNA synthesis for a given replicon. The replicated sister chromatids are still linked by catenanes that are resolved subsequently by topoisomerase II, which is important to ensure that chromosome segregation can proceed successfully during mitosis (Dewar et al., 2015; Dewar and Walter, 2017).

The key regulated step during DNA replication termination is the disassembly of the replisome. In eukaryotes, the replisome is a large multi-protein super-complex (Baretic et al., 2020). The core of the replisome is the replicative helicase known as CMG (Cdc45-MCM-GINS), which is formed by the six Mcm2-7 ATPases, the Cdc45 protein, and the GINS complex. CMG encircles the leading strand template DNA strand and functions as a 3′–5′ DNA helicase during replication fork progression (Eickhoff et al., 2019; Yuan et al., 2020). It is important that CMG remains tightly

associated with replication forks throughout replication elongation, since the Mcm2-7 catalytic core can only be loaded around DNA during G1-phase. The remarkably stable association of CMG with replication forks implies that an active mechanism is required to disassemble the helicase and thus trigger replisome dissolution during DNA replication termination. Disassembly of CMG then leads to unloading of the associated replisome factors from chromatin, once DNA synthesis has been completed (Maric et al., 2014; Moreno et al., 2014).

CMG disassembly is initiated by ubiquitylation of its Mcm7 subunit, which then is rapidly unfolded by the Cdc48/p97 AAA + ATPase in association with its major adaptors Npl4 and Ufd1 (Deegan et al., 2020). In this review, we focus on the mechanism of CMG disassembly during eukaryotic DNA replication termination.

FORK CONVERGENCE

Except at chromosome ends or at nicks or breaks in the DNA template, fork convergence is an essential pre-requisite for replisome disassembly during termination. During fork progression, DNA unwinding by the replicative helicase causes torsional strain that induces positive supercoils ahead of each replisome. Type I or II topoisomerases remove these supercoils and are essential for continued fork progression in both prokaryotes and eukaryotes. However, when two forks converge and are less than ∼150 bp apart, there is no longer space to form DNA supercoils ahead of the two replisomes. Under these conditions, the topological stress that results from unwinding the final stretch of parental DNA is resolved by replisome rotation, which leads to precatenane formation behind the converging replisomes. In bacteria and viruses, the removal of precatenanes by type II topoisomerases is crucial to allow converging replisomes to unwind the final stretch of parental DNA (Dewar and Walter, 2017). However, depletion of type II topoisomerase does not block fork convergence in budding yeast cells (Baxter and Diffley, 2008), although Top2 does make a minor contribution to the efficiency of fork convergence when replication terminates in a reconstituted DNA replication system (Deegan et al., 2019; Devbhandari and Remus, 2020). A similar result was reported in egg extracts of *Xenopus laevis*, in which Top2α promotes fork convergence by preventing the accumulation of topological stress from earlier stages of replication (Heintzman et al., 2019).

The fact that *Saccharomyces cerevisiae* DNA replication can be reconstituted with purified proteins *in vitro* gives a unique opportunity to study the molecular mechanism of termination (Yeeles et al., 2015, 2017). In reactions containing all the factors that are essential for initiation and elongation, converging replication forks were seen to stall even in the presence of topoisomerases (Deegan et al., 2019). This observation led to the identification of a role for the Pif1 family of DNA helicases during DNA replication termination (**Figure 1A**). Budding yeast Pif1 and Rrm3 are monomeric DNA helicases that have low processivity and 5′–3′ unwinding polarity. Both Pif1 and Rrm3 can support termination in the reconstituted budding yeast DNA replication system, in contrast to other 5′–3′ helicases including a bacterial Pif1 orthologue that is highly active as a helicase *in vitro* (Deegan et al., 2019). These findings suggest that budding yeast Pif1/Rrm3 might rely on specific interactions with the yeast replisome, though this remains to be determined.

In vivo studies have also implicated the single fission yeast Pif1 helicase (Pfh1) in the convergence of DNA replication forks during termination (Steinacher et al., 2012). The situation in metazoa is likely to be more complicated, given the greater number of 5′–3′ DNA helicases in metazoan species. It will be interesting in future studies to investigate whether other such helicases or other uncovered pathways can also promote fork convergence.

CMG DISASSEMBLY IN BUDDING YEAST

CMG ubiquitylation is blocked when converging replication fork arrest in the absence of Pif1-family DNA helicases, indicating that the helicase is normally only ubiquitylated after DNA synthesis has been completed (**Figures 1A,B**; Deegan et al., 2020). The trigger for CMG-Mcm7 ubiquitylation during DNA replication termination is still understood poorly. Inhibiting CMG ubiquitylation throughout elongation is likely to be important for the preservation of genome integrity, otherwise forks could become permanently arrested. A recent study in *S. cerevisiae* and *X. laevis* egg extract suggested that CMG ubiquitylation is inhibited throughout elongation by the Y-shaped DNA structure of a replication fork, with which the helicase associates (**Figures 1A**, **2A**; Deegan et al., 2020; Low et al., 2020). The mechanism of such inhibition remains to be determined.

Once CMG ubiquitylation is activated, a replisome associated E3 ubiquitin ligase drives the poly-ubiquitylation of CMG-Mcm7. The first such ligase to be characterised was the cullin 1-RING ligase in budding yeast known as SCF^{Dia2} (Maric et al., 2014). Ubiquitylation by as SCF^{Dia2} begins with the action of the E1 ubiquitin-activating enzyme known as Uba1, which transfers activated ubiquitin to the E2 ubiquiting conjugating enzyme Cdc34 (Deegan et al., 2020). In other species, the ubiquitin-like protein NEDD8 is essential for the function of cullin-RING ligase. The budding yeast NEDD8 orthologue Rub1 modifies the cullin scaffold as in other species, but is a non-essential protein. CMG ubiquitylation in *rub1*Δ cells was only reduced modestly, indicating that neddylation has little impact on the regulation of SCF^{Dia2} (Mukherjee and Labib, 2019).

SCF^{Dia2} is recruited to the CMG helicase by two components of budding yeast replisome, known as Ctf4 and Mrc1 (Morohashi et al., 2009; Maculins et al., 2015). These two factors jointly ensure the very high efficiency of CMG ubiquitylation by SCF^{Dia2}, thereby pushing ubiquitylated Mcm7 over a ubiquitin threshold that governs the action of the Cdc48/p97 ATPase (**Figure 1C**; Deegan et al., 2020). Cdc48/p97 ATPase is a hexameric ATPase that disrupts protein structure and transports unfolded polypeptides through its central channel (Bodnar and Rapoport, 2017; Cooney et al., 2019; Twomey et al., 2019). In budding

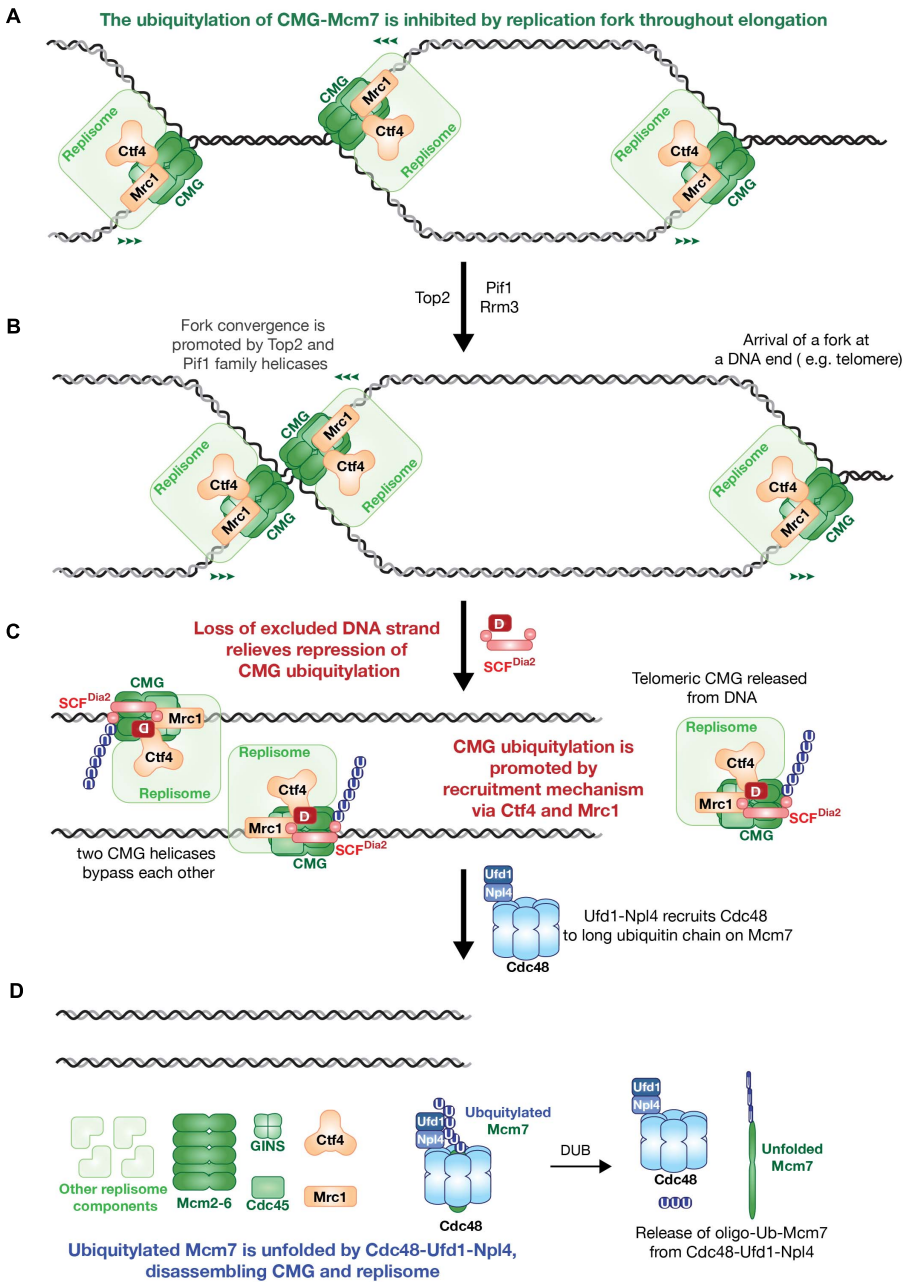

FIGURE 1 | The model of *Saccharomyces cerevisiae* replisome disassembly during DNA replication termination. **(A)** CMG ubiquitylation is inhibited by replication fork during replication elongation. **(B)** Fork convergence is promoted by type II topoisomerases and Pif1 family helicases. **(C)** Loss of excluded strand relieves repression of CMG ubiquitylation, then SCF^{Dia2} dependent Mcm7 ubiquitylation is promoted by recruitment mechanism via replisome components Ctf4 and Mrc1. **(D)** Ufd1-Npl4 recruits Cdc48 to ubiquitylated CMG to unfold poly-ubiquitylated Mcm7 subunit and disassemble replisome.

yeast, Cdc48 is recruited to ubiquitylated substrates by its Ufd1-Npl4 cofactors. A combination of biochemical and structural studies have shown that Cdc48-Ufd1-Npl4 can only unfold proteins that are conjugated to at least five ubiquitins (Twomey et al., 2019; Deegan et al., 2020). The replisome-recruitment mechanism of SCF^{Dia2} guarantees that CMG disassembly is highly efficient during DNA replication termination. In addition, the requirement of Cdc48 for long ubiquitin chains on its substrates provides a form of quality control. Unscheduled ubiquitylation events during replication elongation are likely to be inefficient and would only produce short ubiquitin chains, thereby preventing premature Cdc48-Ufd1-Npl4 dependent CMG disassembly (**Figure 1D**; Deegan et al., 2020).

The mechanism by which Cdc48-Ufd1-Npl4 disassembles ubiquitylated CMG involves the specific unfolding of the ubiquitylated Mcm7 subunit (Deegan et al., 2020), likely initiated

by unfolding of one of the ubiquitin moieties conjugated to Mcm7 (Twomey et al., 2019). Unfolding of Mcm7 collapses CMG and leads to disassembly of the replisome. The fate of unfolded Mcm7 is probably to be degraded by proteasome (**Figure 1D**; Deegan et al., 2020).

CMG DISASSEMBLY IN METAZOA

Studies of CMG disassembly in *Caenorhabditis elegans* and *X. laevis* have shown that CMG is ubiquitylated on its MCM7 subunit as in budding yeast, and disassembled by the CDC48/p97 ATPase (Dewar et al., 2017; Sonneville et al., 2017). However, orthologues of the F-box protein Dia2 are not apparent in metazoa and studies of *C. elegans* early embryos, *X. laevis* egg extracts, and mouse ES cells showed that a different E3 ligase known as CUL-2^{LRR-1} drives the poly-ubiquitylation of MCM7 during DNA replication termination (**Figures 2C,D**; Dewar et al., 2017; Sonneville et al., 2017; Villa et al., 2021). Work with *X. laevis* egg extracts showed that $CUL2^{LRR1}$ is only recruited to the replisome during replication termination. A very recent study indicates that recruitment of $CUL2^{LRR1}$ is blocked throughout elongation by the association of CMG with the DNA replication fork (Dewar et al., 2017), mirroring the regulation of yeast SCF^{Dia2}.

The action of cullin-RING ubiquitin ligases is more complex in metazoa than in budding yeast. Work with human cells showed that cullin-RING ligases are activated by neddylation of the cullin subunit (Baek et al., 2020). Furthermore, the first ubiquitin is conjugated to substrates of metazoan cullin-RING ligases by different enzymes to those that subsequently elongate the K48-linked ubiquitin chain. Such priming of ubiquitylation can occur in two different ways. Firstly, the RING subunit of the cullin-RING ligase can activate the E2 UBE2D (UBCH5) to add the first ubiquitin to the substrate. Alternatively, a "RING between RING" or RBR ligase of the Ariadne family can associate with neddylated cullin scaffold and receive activated ubiquitin from a cognate E2, before transferring ubiquitin to substrate (Scott et al., 2016; Baek et al., 2020). Subsequently, the E2 enzymes UBE2R1/2/CDC34 and UBE2G1 function redundantly to elongate a K48-linked ubiquitin chain (Hill et al., 2019).

CMG ubiquitylation in *Xenopus* egg extracts is inhibited by MLN4924, a specific inhibitor of the E1 enzyme for the NEDD8 pathway (Dewar et al., 2015). However, until recently the ubiquitylation of metazoan CMG had not been reconstituted *in vitro*, and the enzymes responsible for ubiquitin priming and elongation on CMG had not been characterised in any metazoan species. However, *C. elegans* CMG ubiquitylation was recently reconstituted with a set of purified proteins (Xia et al., 2021). Orthologues of human UBCH5 and the Ariandne ligase ARIH1 cooperate redundantly with neddylated CUL-2^{LRR-1} to prime ubiquitylation of CMG-MCM-7 (**Figure 2C**), as predicted by studies of human cullin-RING ligases. Moreover, a ubiquitin-chain on primed CMG-MCM-7 is then extended redundantly by two E2s, UBC-3 (nematode orthologue of human CDC34/UBC2R) and UBC-7 (orthologue of human UBE2G1) (**Figure 2D**).

Interestingly, the replisome components TIM-1_TIPN-1, whose orthologues are TIMELESS-TIPIN in mammalian cells, were found to recruit CUL-2^{LRR-1} to worm CMG (Xia et al., 2021). Depletion of TIM-1_TIPN-1 dramatically compromises the ubiquitylation of MCM-7 both *in vitro* and *in vivo* (**Figures 2C,D**). These findings indicate that the metazoan and yeast replisomes use different but analogous recruitment mechanisms for CUL-2^{LRR-1} and SCF^{Dia2}, in order to push CMG-MCM-7 ubiquitylation over the ubiquitin threshold of the CDC48/p97 ATPase.

In addition to UFD1-NPL4, metazoan cells contain a range of other partners of CDC48/p97 that are thought to recruit the unfoldase to specific targets or particular subcellular locations. In *C. elegans*, together with CDC-48_UFD-1_NPL-4, an adaptor protein known as UBXN-3 (the nematode orthologue of human FAF1) was shown to be required for a second pathway of CMG disassembly in *C. elegans* early embryos that acts during mitosis (Sonneville et al., 2017), in order to process sites of incomplete DNA replication (Sonneville et al., 2019). Recent work showed that UBXN-3 is also critical for CMG helicase unloading during DNA replication termination, in worms depleted for TIM-1_TIPN-1 (Xia et al., 2021). Moreover, UBXN-3 stimulates the ability of CDC-48_UFD-1_NPL-4 to disassemble poly-ubiquitylated CMG *in vitro* (**Figure 2E**), revealing a more complicated mechanism for the metazoan CMG disassembly machinery. It remains to be determined why metazoan cell need an additional adaptor in order to disassemble ubiquitylated CMG, especially when p97-UFD1-NPL4 is able to unfold a model ubiquitylated protein *in vitro* (Pan et al., 2021). The unfolding mechanism for ubiquitylated MCM-7 is probably similar in metazoa to that observed in yeast, but greater insight is likely to come from structural studies in the future.

PERSPECTIVE

It is now clear that the termination of eukaryotic DNA replication is regulated just as carefully as the initiation of DNA synthesis. Replisome disassembly is the key regulated step during termination and although the principal steps have now been identified, several critical questions await further investigation.

The first question is in regard to the beginning of this process. What is the signal of MCM7 ubiquitylation? As discussed above, a series of observations with yeast and *Xenopus* egg extracts indicate that CMG ubiquitylation is inhibited throughout elongation by the DNA structure of a replication fork. It means the termination of DNA replication removes the Y-shaped DNA structure of a fork, thereby exposing CMG to ubiquitylation by SCF^{Dia2} in budding yeast or $CUL2^{LRR1}$ in metazoa. The same mechanism would apply when two forks converge and when a single fork arrives at a DNA end (Deegan et al., 2020; Low et al., 2020). However, the mechanism by which the Y-shaped fork DNA structure represses CMG ubiquitylation still remains unclear. The timing of recruitment of SCF^{Dia2} to the yeast replisome is not known, but $CUL2^{LRR1}$ isn't recruited at stall fork but terminated fork in *X. laevis* egg extract (Dewar et al., 2017). Moreover, the E3 ligases are recruited by members of replisome components

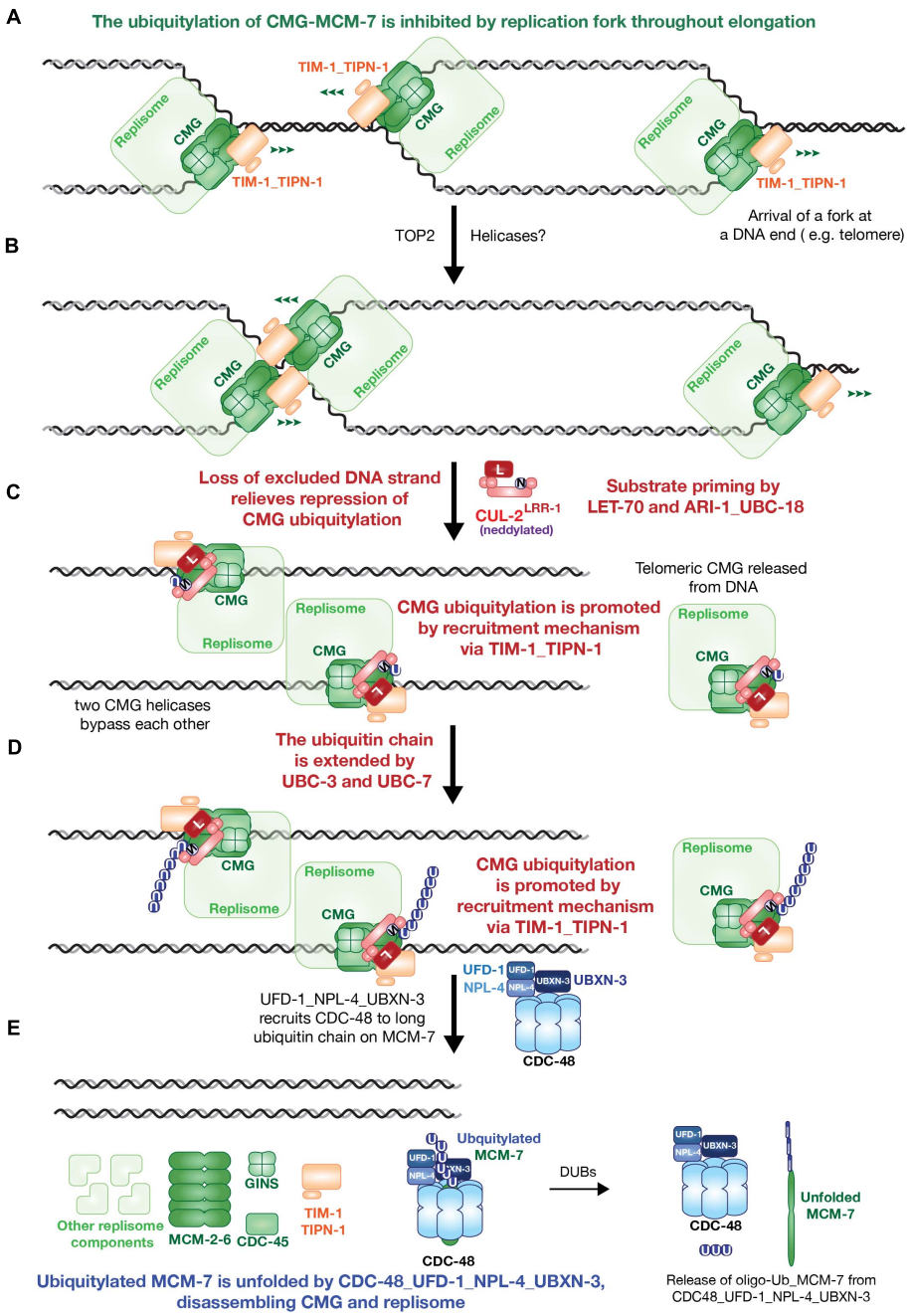

FIGURE 2 | A possible model of *Caenorhabditis elegans* replisome disassembly during DNA replication termination. **(A)** Replication fork structure blocks CMG ubiquitylation during replication elongation. **(B)** Fork convergence is supported by type II topoisomerases or other uncovered pathways **(C)** CMG ubiquitylation starts with substrate priming step via LET-70 or ARI-1_UBC-18 with neddylated CUL-2^{LRR-1} when the repression from fork DNA is eliminated. **(D)** E2s UBC-3 or UBC-7 work with neddylated CUL-2^{LRR-1} to extend ubiquitin chain on MCM-7. Both of substrate priming and ubiquitin chain extension are stimulated by recruitment of CUL-2^{LRR-1} via TIM-1_TIPN-1. **(E)** UFD-1_NPL-4_UBXN-3 recruits CDC-48 to ubiquitylated CMG, as a result, MCM-7 is unfolded and replisome is disassembled.

to ensure efficient ubiquitylation in yeast and nematode (Deegan et al., 2020; Xia et al., 2021), which suggests the possibility that this kind of recruitment of E3 ligase is inhibited by repressive fork DNA structure. Furthermore, there is another possibility that ubiquitylation sites on MCM7 are protected by fork DNA structure. During unwinding, CMG encircles and translocates along the leading strand while excluding the lagging strand template. It is still difficult to interpret how the flexible lagging strand can prevent the lysine sites located at the N-terminal of MCM7 from being ubiquitylated. It may suggest the possibility that the lagging strand machinery also contributes to protecting progressive replisome. In subsequent studies, structural biology

will be important to determine how the yeast and metazoan E3 ligases engage with the replisome and gain access to their cognate ubiquitylation sites on MCM7.

Another important question regards the physiological importance of replisome disassembly during DNA replication termination. In budding yeast, Dia2 is a non-essential gene, but *dia2*Δ shows cold-sensitive growth defect and hyper-sensitive to the replication stress (Morohashi et al., 2009; Maculins et al., 2015). Similarly, LRR-1 is an essential gene that supports the normal growth in *C. elegans* (Ossareh-Nazari et al., 2016; Sonneville et al., 2017). In addition, FAF1, the orthologues of *C. elegans* UBXN-3 in human, is a tumour suppressor. These important genes' being involved in CMG disassembly reveals the significance of this process. A clear S phase delay was observed in *lrr-1* depleted worm embryo (Sonneville et al., 2017) implies that the recycle of CMG subunits during S phase might be important to efficiently complete DNA synthesis. Although there is no evidence yet to confirm MCM7 is the primary substrate of SCF^{Dia2} or $CUL2^{LRR1}$, the importance of CMG disassembly can be studied by generating MCM7 ubiquitylation sites mutated alleles in the future. Additionally, there is a back-up pathway of CMG ubiquitylation in metazoan. If CMG is failed to be disassembled during termination, MCM7 will be ubiquitylated by another RING E3 ligase TRAIP in mitosis (Deng et al., 2019). This mechanism increases the complexity of the significance of $CUL2^{LRR1}$ dependent CMG ubiquitylation. The genomes fail to complete replication in S phase when the cells are challenged by replication stress. The regions of incompletely replicated DNA are processed in early mitosis via a process known as mitotic DNA repair synthesis (MiDAS; Minocherhomji et al., 2015). In this situation, the CMG cannot be disassembled by $CUL2^{LRR1}$ for the incomplete DNA synthesis, as well as TRAIP is essential for MiDAS. It implies that the un-disassembled CMG complex becomes a potential barrier to the MiDAS pathway (Deng et al., 2019; Sonneville et al., 2019). It also provides a possibility that accumulated CMG complex could interfere with other processes on chromosomes. Moreover, TRAIP also leads to disassembly of post-termination CMG helicases in worms, frog egg extracts, and mammalian cells that lack the activity of $CUL\text{-}2^{LRR-1}$ (Deng et al., 2019; Villa et al., 2021). It remains to be determined why TRAIP is unable to compensate for the lethal consequences of deleting the LRR-1 gene, both in *C. elegans* and also in mammalian cells where LRR1 is also an essential gene (from IMPC Viability Primary Screen [IMPC_VIA_001]).

The eukaryotic replisome is equivalent to an unstoppable train that proceeds inexorably throughout each replicon from initiation until DNA synthesis is finished. Subsequently, CMG disassembly removes the formerly unstoppable train from the track, upon arrival at the destination. Much still remains to be learnt about this highly complicated process, which appears to have diverged considerably during the course of eukaryotic evolution. The cullin-RING ubiquitin ligases SCF^{Dia2} and $CUL2^{LRR1}$ are not found in other branches of eukarya such as plants, and it will be important to explore whether replisome disassembly during DNA replication termination follows universal principles in diverse eukaryotes, or else has evolved repeatedly and is not always dependent upon MCM7 ubiquitylation.

AUTHOR CONTRIBUTIONS

The author confirms being the sole contributor of this work and has approved it for publication.

ACKNOWLEDGMENTS

I am very grateful for financial support from the Medical Research Council (core grant MC_UU_12016/13) and Cancer Research UK (Programme Grant C578/A24558). I sincerely thank Karim Labib and Tom Deegan for helpful discussions and feedback on the manuscript and Huimei Liang for proofreading.

REFERENCES

Baek, K., Krist, D. T., Prabu, J. R., Hill, S., Klugel, M., Neumaier, L. M., et al. (2020). NEDD8 nucleates a multivalent cullin-RING-UBE2D ubiquitin ligation assembly. *Nature* 578, 461–466. doi: 10.1038/s41586-020-2000-y

Baretic, D., Jenkyn-Bedford, M., Aria, V., Cannone, G., Skehel, M., and Yeeles, J. T. P. (2020). Cryo-EM structure of the fork protection complex bound to CMG at a replication fork. *Mol. Cell* 78, 926–940.e913.

Baxter, J., and Diffley, J. F. (2008). Topoisomerase II inactivation prevents the completion of DNA replication in budding yeast. *Mol. Cell* 30, 790–802. doi: 10.1016/j.molcel.2008.04.019

Bell, S. P., and Labib, K. (2016). Chromosome duplication in *Saccharomyces* cerevisiae. *Genetics* 203, 1027–1067. doi: 10.1534/genetics.115.186452

Bodnar, N. O., and Rapoport, T. A. (2017). Molecular mechanism of substrate processing by the Cdc48 ATPase complex. *Cell* 169, 722–735.e729.

Cooney, I., Han, H., Stewart, M. G., Carson, R. H., Hansen, D. T., Iwasa, J. H., et al. (2019). Structure of the Cdc48 segregase in the act of unfolding an authentic substrate. *Science* 365, 502–505. doi: 10.1126/science.aax0486

Deegan, T. D., Baxter, J., Ortiz Bazan, M. A., Yeeles, J. T. P., and Labib, K. P. M. (2019). Pif1-Family helicases support fork convergence during DNA replication termination in eukaryotes. *Mol. Cell* 74, 231–244.e239.

Deegan, T. D., Mukherjee, P. P., Fujisawa, R., Polo Rivera, C., and Labib, K. (2020). CMG helicase disassembly is controlled by replication fork DNA, replisome components and a ubiquitin threshold. *Elife* 9:e60371.

Deng, L., Wu, R. A., Sonneville, R., Kochenova, O. V., Labib, K., Pellman, D., et al. (2019). Mitotic CDK promotes replisome disassembly, fork breakage, and complex DNA rearrangements. *Mol. Cell* 73, 915–929.e916.

Devbhandari, S., and Remus, D. (2020). Rad53 limits CMG helicase uncoupling from DNA synthesis at replication forks. *Nat. Struct. Mol. Biol.* 27, 461–471. doi: 10.1038/s41594-020-0407-7

Dewar, J. M., and Walter, J. C. (2017). Mechanisms of DNA replication termination. *Nat. Rev. Mol. Cell Biol.* 18, 507–516.

Dewar, J. M., Budzowska, M., and Walter, J. C. (2015). The mechanism of DNA replication termination in vertebrates. *Nature* 525, 345–350. doi: 10.1038/nature14887

Dewar, J. M., Low, E., Mann, M., Raschle, M., and Walter, J. C. (2017). CRL2Lrr1 promotes unloading of the vertebrate replisome from chromatin during replication termination. *Genes Dev.* 31, 275–290. doi: 10.1101/gad.291799.116

Eickhoff, P., Kose, H. B., Martino, F., Petojevic, T., Abid Ali, F., Locke, J., et al. (2019). Molecular basis for ATP-hydrolysis-driven DNA translocation by the CMG helicase of the eukaryotic replisome. *Cell Rep.* 28, 2673–2688.e2678.

Heintzman, D. R., Campos, L. V., Byl, J. A. W., Osheroff, N., and Dewar, J. M. (2019). Topoisomerase II is crucial for fork convergence during vertebrate replication termination. *Cell Rep.* 29, 422–436.e425.

Hill, S., Reichermeier, K., Scott, D. C., Samentar, L., Coulombe-Huntington, J., Izzi, L., et al. (2019). Robust cullin-RING ligase function is established by a multiplicity of poly-ubiquitylation pathways. *Elife* 8:e51163.

Low, E., Chistol, G., Zaher, M. S., Kochenova, O. V., and Walter, J. C. (2020). The DNA replication fork suppresses CMG unloading from chromatin before termination. *Genes Dev.* 34, 1534–1545. doi: 10.1101/gad.339739.120

Maculins, T., Nkosi, P. J., Nishikawa, H., and Labib, K. (2015). Tethering of SCF(Dia2) to the replisome promotes efficient ubiquitylation and disassembly of the CMG helicase. *Curr. Biol.* 25, 2254–2259. doi: 10.1016/j.cub.2015.07.012

Maric, M., Maculins, T., De Piccoli, G., and Labib, K. (2014). Cdc48 and a ubiquitin ligase drive disassembly of the CMG helicase at the end of DNA replication. *Science* 346:1253596. doi: 10.1126/science.1253596

Minocherhomji, S., Ying, S., Bjerregaard, V. A., Bursomanno, S., Aleliunaite, A., Wu, W., et al. (2015). Replication stress activates DNA repair synthesis in mitosis. *Nature* 528, 286–290. doi: 10.1038/nature16139

Moreno, S. P., Bailey, R., Campion, N., Herron, S., and Gambus, A. (2014). Polyubiquitylation drives replisome disassembly at the termination of DNA replication. *Science* 346, 477–481. doi: 10.1126/science.1253585

Morohashi, H., Maculins, T., and Labib, K. (2009). The amino-terminal TPR domain of Dia2 tethers SCF(Dia2) to the replisome progression complex. *Curr. Biol.* 19, 1943–1949. doi: 10.1016/j.cub.2009.09.062

Mukherjee, P. P., and Labib, K. P. M. (2019). In vitro reconstitution defines the minimal requirements for Cdc48-dependent disassembly of the CMG helicase in budding yeast. *Cell Rep.* 28, 2777–2783.e2774.

O'Donnell, M., Langston, L., and Stillman, B. (2013). Principles and concepts of DNA replication in bacteria, archaea, and eukarya. *Cold Spring Harb. Perspect. Biol.* 5:a010108. doi: 10.1101/cshperspect.a010108

Ossareh-Nazari, B., Katsiarimpa, A., Merlet, J., and Pintard, L. (2016). RNAi-Based suppressor screens reveal genetic interactions between the CRL2LRR-1 E3-Ligase and the DNA replication machinery in caenorhabditis elegans. *G3 (Bethesda)* 6, 3431–3442. doi: 10.1534/g3.116.033043

Pan, M., Zheng, Q., Yu, Y., Ai, H., Xie, Y., Zeng, X., et al. (2021). Seesaw conformations of Npl4 in the human p97 complex and the inhibitory mechanism of a disulfiram derivative. *Nat. Commun.* 12:121.

Scott, D. C., Rhee, D. Y., Duda, D. M., Kelsall, I. R., Olszewski, J. L., Paulo, J. A., et al. (2016). Two distinct types of E3 ligases work in unison to regulate substrate ubiquitylation. *Cell* 166, 1198–1214.e1124.

Sonneville, R., Bhowmick, R., Hoffmann, S., Mailand, N., Hickson, I. D., and Labib, K. (2019). TRAIP drives replisome disassembly and mitotic DNA repair synthesis at sites of incomplete DNA replication. *Elife* 8:e48686.

Sonneville, R., Moreno, S. P., Knebel, A., Johnson, C., Hastie, C. J., Gartner, A., et al. (2017). CUL-2LRR-1 and UBXN-3 drive replisome disassembly during DNA replication termination and mitosis. *Nat. Cell Biol.* 19, 468–479. doi: 10.1038/ncb3500

Steinacher, R., Osman, F., Dalgaard, J. Z., Lorenz, A., and Whitby, M. C. (2012). The DNA helicase Pfh1 promotes fork merging at replication termination sites to ensure genome stability. *Genes Dev.* 26, 594–602. doi: 10.1101/gad.184663.111

Twomey, E. C., Ji, Z., Wales, T. E., Bodnar, N. O., Ficarro, S. B., Marto, J. A., et al. (2019). Substrate processing by the Cdc48 ATPase complex is initiated by ubiquitin unfolding. *Science* 365:eaax1033. doi: 10.1126/science.aax1033

Villa, F., Fujisawa, R., Ainsworth, J., Nishimura, K., Lie, A. L. M., Lacaud, G., et al. (2021). CUL2LRR1, TRAIP and p97 control CMG helicase disassembly in the mammalian cell cycle. *EMBO Rep.* 22:e52164.

Xia, Y., Fujisawa, R., Deegan, T. D., Sonneville, R., and Labib, K. (2021). TIMELESS-TIPIN and UBXN-3 promote replisome disassembly during DNA replication terminatiosn in C. elegans. *EMBO J.* 40:e108053.

Yeeles, J. T. P., Janska, A., Early, A., and Diffley, J. F. X. (2017). How the Eukaryotic Replisome Achieves Rapid and Efficient DNA Replication. *Mol. Cell* 65, 105–116. doi: 10.1016/j.molcel.2016.11.017

Yeeles, J. T., Deegan, T. D., Janska, A., Early, A., and Diffley, J. F. (2015). Regulated eukaryotic DNA replication origin firing with purified proteins. *Nature* 519, 431–435. doi: 10.1038/nature14285

Yuan, Z., Georgescu, R., Bai, L., Zhang, D., Li, H., and O'Donnell, M. E. (2020). DNA unwinding mechanism of a eukaryotic replicative CMG helicase. *Nat. Commun.* 11:688.

Conflict of Interest: The author declares that the research was conducted in the absence of any commercial or financial relationships that could be construed as a potential conflict of interest.

frontiers in Cell and Developmental Biology

ORIGINAL RESEARCH
published: 26 July 2021
doi: 10.3389/fcell.2021.714868

RECQ1 Promotes Stress Resistance and DNA Replication Progression Through PARP1 Signaling Pathway in Glioblastoma

*Jing Zhang[1,2], Hao Lian[1], Kui Chen[1], Ying Pang[1], Mu Chen[1], Bingsong Huang[1], Lei Zhu[1], Siyi Xu[1], Min Liu[1] and Chunlong Zhong[1]**

[1] Department of Neurosurgery, Shanghai East Hospital, School of Medicine, Tongji University, Shanghai, China, [2] Institute for Advanced Study, Tongji University, Shanghai, China

OPEN ACCESS

Edited by:
Lin Deng,
Shenzhen Bay Laboratory, China

Reviewed by:
Cong Liu,
Sichuan University, China
Sheng Yi,
Nantong University, China
Xiaoping Xu,
National Cancer Institute at Frederick, United States

***Correspondence:**
Chunlong Zhong
drchunlongzhong@tongji.edu.cn

Specialty section:
This article was submitted to Cell Growth and Division, a section of the journal Frontiers in Cell and Developmental Biology

Received: 26 May 2021
Accepted: 29 June 2021
Published: 26 July 2021

Citation:
Zhang J, Lian H, Chen K, Pang Y, Chen M, Huang B, Zhu L, Xu S, Liu M and Zhong C (2021) RECQ1 Promotes Stress Resistance and DNA Replication Progression Through PARP1 Signaling Pathway in Glioblastoma. Front. Cell Dev. Biol. 9:714868. doi: 10.3389/fcell.2021.714868

Glioblastoma (GBM) is the most common aggressive primary malignant brain tumor, and patients with GBM have a median survival of 20 months. Clinical therapy resistance is a challenging barrier to overcome. Tumor genome stability maintenance during DNA replication, especially the ability to respond to replication stress, is highly correlated with drug resistance. Recently, we identified a protective role for RECQ1 under replication stress conditions. RECQ1 acts at replication forks, binds PCNA, inhibits single-strand DNA formation and nascent strand degradation in GBM cells. It is associated with the function of the PARP1 protein, promoting PARP1 recruitment to replication sites. RECQ1 is essential for DNA replication fork protection and tumor cell proliferation under replication stress conditions, and as a target of RECQ1, PARP1 effectively protects and restarts stalled replication forks, providing new insights into genomic stability maintenance and replication stress resistance. These findings indicate that tumor genome stability targeting RECQ1-PARP1 signaling may be a promising therapeutic intervention to overcome therapy resistance in GBM.

Keywords: genomic stability, drug resistance, DNA replication stress, fork reversal, RECQ1, PARP1

INTRODUCTION

Glioblastoma (GBM) is the most common, aggressive adult primary brain tumor and is associated with profound genomic heterogeneity and limited cure development to date (Stupp et al., 2017). The capacity for DNA replication damage repair and genome stability maintenance during tumor proliferation is thought to contribute to therapy resistance. The DNA replication machinery must duplicate genomic information, overcome numerous obstacles established by endogenous and exogenous replication stress that impair replication fork progression and DNA synthesis during DNA replication (Zeman and Cimprich, 2014). Under replication stress, protection of DNA

replication is critical for the maintenance of genomic integrity, driving functional "protection" for the survival of rapidly dividing tumor cells, which also leads to resistance to cancer drug therapy. In addition, cells suffer uncontrolled degradation and replication fork collapse, promoting DNA damage and genomic instability.

Human RecQ helicases (WRN, BLM, RECQ4, RECQ5, and RECQ1) play critical roles in protecting and stabilizing the genome (Hickson, 2003; Opresko et al., 2004). Depending on their ability to unwind various DNA structures, multiple cellular functions have been associated with RecQ proteins, including those with roles in stabilizing damaged DNA replication forks, telomere maintenance, and homologous recombination (Sharma et al., 2006; Bohr, 2008; Ouyang et al., 2008). Of the five human RecQ families, three are genetically linked to cancer syndromes and premature diseases, such as Bloom's syndrome (BLM gene mutations), Werner's syndrome (WRN gene mutations), Rothmund-Thomson syndrome (RTS), RAPADILINO, and Baller-Gerold syndrome (caused by mutation of RECQ4) (Ellis et al., 1995; Yu et al., 1996; Kitao et al., 1999; Siitonen et al., 2003). As the most abundant of the five human RecQ proteins, although the clinical importance of RECQ1 has only been partially revealed, the currently mysterious, unknown, unique, and important roles of RECQ1 in cellular DNA metabolism need to be discovered.

RECQ1 is overexpressed in rapidly dividing cells and multiple cancer cells, including human GBM, ovarian cancer, and hypopharyngeal cancer (Mendoza-Maldonado et al., 2011; Viziteu et al., 2017; Debnath and Sharma, 2020). However, the function and mechanism of RECQ1 activity in cancer proliferation remain unknown. We hypothesized that RECQ1 plays a particularly important role in facilitating DNA replication stress in cancer cells that undergo rapid proliferation. RECQ1 has recently been reported to confer specific oncogene effects, including cell cycle progression in the S-phase, to tumors, and systemic depletion of RECQ1 has been shown to prevent tumor growth in murine models (Futami et al., 2008; Arai et al., 2011; Mendoza-Maldonado et al., 2011), but a direct role for RECQ1 in DNA replication and cellular processes has not been identified.

In this study, we demonstrate that RECQ1 plays an essential role in DNA replication fork protection and thus maintains genome stability in response to replication stress. RECQ1 is located at replication sites and associates with proliferating cell nuclear antigen (PCNA) and physically interacts with poly[ADP-ribose] polymerase 1 (PARP1), which binds to unresected stalled DNA replication forks and recruit XRCC1 to mediate repair and promote replication restart, thereby protecting replication fork stability (Ying et al., 2016; Thakar et al., 2020). We show that RECQ1 depletion results in increased nascent strand degradation and fork stalling, DNA double-strand breaks (DSBs) and a decreased cell proliferation rate under replication stress, supporting the notion that RECQ1 plays a specific role in the maintenance of genomic stability. In addition, RECQ1-depleted cells are hypersensitive to methyl methanesulfonate (MMS) and temozolomide (TMZ) treatment. Glioblastoma is the most common and aggressive malignant histotype of brain tumor, and patients with glioblastoma have a poor prognosis (Lefranc et al., 2005; Stupp et al., 2009). Although considerable advancements in glioblastoma treatment have been investigated in recent years, new therapeutic strategies are still urgently needed. Considering these data, we propose that RECQ1 regulates PARP1 protein function and protects DNA replication fork stability to maintain genomic stability under replication stress conditions and contributes to the drug resistance of GBM cells. This study provides a novel approach to GBM suppression whereby mediating the DNA repair RECQ1-PARP1 signaling pathway function inhibits DNA replication.

MATERIALS AND METHODS

Cell Culture

M059K, U251, U87MG, and RPE1 cells were purchased from American Type Culture Collection (ATCC). Cells free of mycoplasma contamination were maintained in Dulbecco's modified Eagle's medium (DMEM) or a 1:1 mixture of DMEM and Ham's F12 medium supplemented with 2.5 mM L-glutamine, 15 mM HEPES, 0.5 mM sodium pyruvate, 1.2 g/L sodium bicarbonate, 0.05 mM non-essential amino acids and 10% fetal bovine serum. Cells were cultured at 37°C in a humidified atmosphere containing 5% CO2.

siRNA and Transfection

Cells were seeded in six-well plates and transfected with indicated siRNA. The siRNA-targeting sequences used were: siRECQ1: (Dharmacon SMARTpool, GAGCUUAUGUUACCAGUUA, CUACGGCUUUGGAGAUAUA, GAUUAUAAGGCACUUGG UA, GGGCAAGCAAUGAAU AUGA). siPARP1: UUCUCCGA ACGUGUCACGUTT, GAGGAAGGUAUCAACAAAUTT, GA GCACUUCAUGAAAUUAUTT, GAGACCCAAUAGGUUAAU TT. Negative Control siRNA and siPARP1 (GAGGAAGGUA UCAACAAA UTT) (Qiagen). PARP1 expression ORF was purchased from OriGene Technologies, transfection by using Lipofectamine transfection reagent (L3000015, Thermo Fisher Scientific) according to the manufacturer's instructions. Cells were harvested on day 4 after transfection for further analyses.

Antibodies and Reagents

The antibodies anti-RECQ1 (ab151501, 1:200 dilution), anti-53BP1 (ab175933, 1:200 dilution), anti-RPA (ab2175, 1: 1000 dilution), anti-PARP1 (ab191217, 1:1000 dilution) and anti-BrdU (ab6326, 1:200), anti-RPA2-pS4/S8 (ab87277, 1:200 dilution) were purchased from Abcam. Antibodies anti-γH2AX (2577, 1:800 dilution), α-Tubulin (2144, 1:1000 dilution) and PCNA antibody (2586, 1:200 dilution) were purchased from Cell Signaling. Mouse anti-BrdU (347580, 1:40) was purchased from BD Biosciences. AF647 (A-21247, 1:1000) and AF488 (A-11001, 1:1000) were purchased from Thermo Fisher Scientific. BMN673 (S7048, Talazoparib) was purchased from Selleck Chemicals.

Immunofluorescence Staining

M059K cells were cultured in 35 mm plates and transfected with siRECQ1, siPARP1 or PARP1 OE, followed indicated treatment. Then cells were washed with PBS and fixed with 4% formaldehyde. Cells were permeabilized with Triton X-100 (0.05%) for 10 min, blocked with 3% BSA in PBS and then incubated overnight at 4°C with primary antibodies. Next, cells were washed and incubated with AF488 or AF647-conjugated secondary antibody. Finally, cells were washed with PBST for three times and stained with DAPI for 10 min at RT. Images of the mounted slides were acquired with a Zeiss Axiovert 200 M microscope.

DNA Fiber Spreading Analysis

DNA fiber spreading assays were performed as followed. Briefly, cells were transfected with siRECQ1, siPARP1 or PARP1 OE, followed by incubation with 10 μM CldU for 30 min and then with 100 μM IdU for another 30 min. For treatment, cells were exposed to 2 mM HU or 50 μM MMS before or after IdU incubation. Cells were then suspended in PBS, and ∼200 cells placed on a glass microscope slide (Newcomer Glass) and 10 μl of lysis buffer (0.5% SDS in 200 mM Tris–HCl pH 7.5, 50 mM EDTA) added. DNA fibers were spread and fixed in methanol: acetic acid (3:1), denatured with 2.5 M HCl for 1 h, neutralized in 0.4 M Tris–HCl pH 7.5 for 5 min, washed in PBS, and immunostained using anti-BrdU primary and corresponding secondary antibodies. The slides were mounted in ProLong Gold Anti-fade Mounting medium. Images were acquired using a Zeiss Axiovert 200 M microscope at ×63 magnification with the Axio Vision software packages (Zeiss).

In situ Proximity Ligation Assay (PLA)

Cells were grown on 35 mm MatTek glass bottomed plates followed by transfection with siRECQ1 in the presence or absence of MMS, then cells were incubated with 0.1% formaldehyde for 5 min and treated twice total 10 min with CSK-R buffer (10 mM PIPES, pH 7.0, 100 mM NaCl, 300 mM sucrose, 3 mM MgCl2, 0.5% Triton X-100, 300 μg/ml RNAse), and fixed in 4% formaldehyde in PBS (W/V) for 10 min at RT, followed by incubation in pre-cold methanol for 20 min at −20°C. After washing with PBS for three times, cells were treated with 100 μg/ml RNAse in 5 mM EDTA buffer for 30 min at 37°C. *In situ* PLA was performed using the Duolink PLA kit (Sigma-Aldrich) according to the manufacturer's instructions. Briefly, the cells were blocked for 30 min at 37°C and incubated with primary antibodies for 30 min at 37°C. Following three times washing with PBST (phosphate buffered saline, 0.1% Tween), anti-mouse PLUS and anti-rabbit MINUS PLA probes were coupled to the primary antibodies for 1 h at 37°C. After three times washing with buffer A (0.01 M Tris, 0.15 M NaCl, and 0.05% Tween-20) for 5 min, PLA probes were ligated for 30 min at 37°C. After three times washing with buffer A, amplification using Duolink *In Situ* Detection Reagents (Sigma) was performed at 37°C for 100 min. After amplification, the plates were washed for 5 min three times with wash buffer B (0.2 M Tris 0.1 M NaCl). Finally, they were coated with mounting medium containing DAPI (Prolong Gold, Invitrogen) and imaged using a Zeiss Axiovert 200 M microscope.

Cell Survival Assay and Cell Viability Assay

Cell survival fraction was assessed by evaluating the colony-forming ability. In brief, M059K and U251 cells were seeded in six-well plates (500 cells per well) after transfection with siRECQ1, siNC, in the presence of different concentration of TMZ and were subsequently incubated for 10 days to allow colonies to develop. Cells were finally fixed with cold methanol, and the colonies were stained with crystal violet (in a 100% methanol solution) for manual counting.

The viability of M059K and U251 cells was assessed with a Cell Counting Kit-8 (CCK8) kit (DOJINDO Laboratories) according to the manufacturer's instructions. Cells were seeded in 96-well plates and cultured in a 37°C incubator for up to 4 days after treatment, and the OD at 450 nm was measured. All cell-based assays were performed in at least triplicate.

Nuclear Morphology Assay

The chromosome breakage assay was performed as described previously (van der Crabben et al., 2016). In brief, M059K cells were treated with siRECQ1. After 4 days of culture, cells were incubated with hypotonic solution (0.56% KCl) at room temperature for 30 min and then in a 37°C water bath for 5 min. Fixation with pre-cooled fixation buffer (methanol: acetic acid = 3:1) was repeated three times, and a dropper was used to place cells onto a clean slide. Spread cells were incubated at 55°C overnight and stained with Giemsa solution (GS-500, Sigma) for image acquisition of aberrant chromosomes with a Zeiss Axiovert 200 M microscope.

Western Blot Analysis

Cells transfected with siRECQ1, siPARP1, or PARP1 OE were harvested and lysed in lysis buffer (50 mM Tris–HCl (pH 7.4), 0.15 M NaCl, and 1% Triton X-100 in PBS, supplemented with protease and phosphatase inhibitors) on ice for 30 min. Proteins were separated by SDS-PAGE on an 8–16% gel (Invitrogen) and transferred to a PVDF membrane. The membranes were blocked in 5% dry milk in 0.1% Tween-20 in PBS and detected with indicated antibodies. After incubation with horseradish peroxidase (HRP)-conjugated secondary antibodies (Bio-Rad), then immunoreactions were visualized using ECL western blot detection reagents (Pierce Biotechnology) and Image Lab 5.1 gel densitometry analysis system. ImageJ software (version 1.8.0.) was used to analyze protein bands.

Statistical Analysis

Statistical significance of PLA experiments was analyzed using the Mann–Whitney rank-sum test and expressed as mean ± SEM values. Fiber patterns and immunoblotting were analyzed using a two-sided unpaired *t*-test, and the exact *P*-values are given

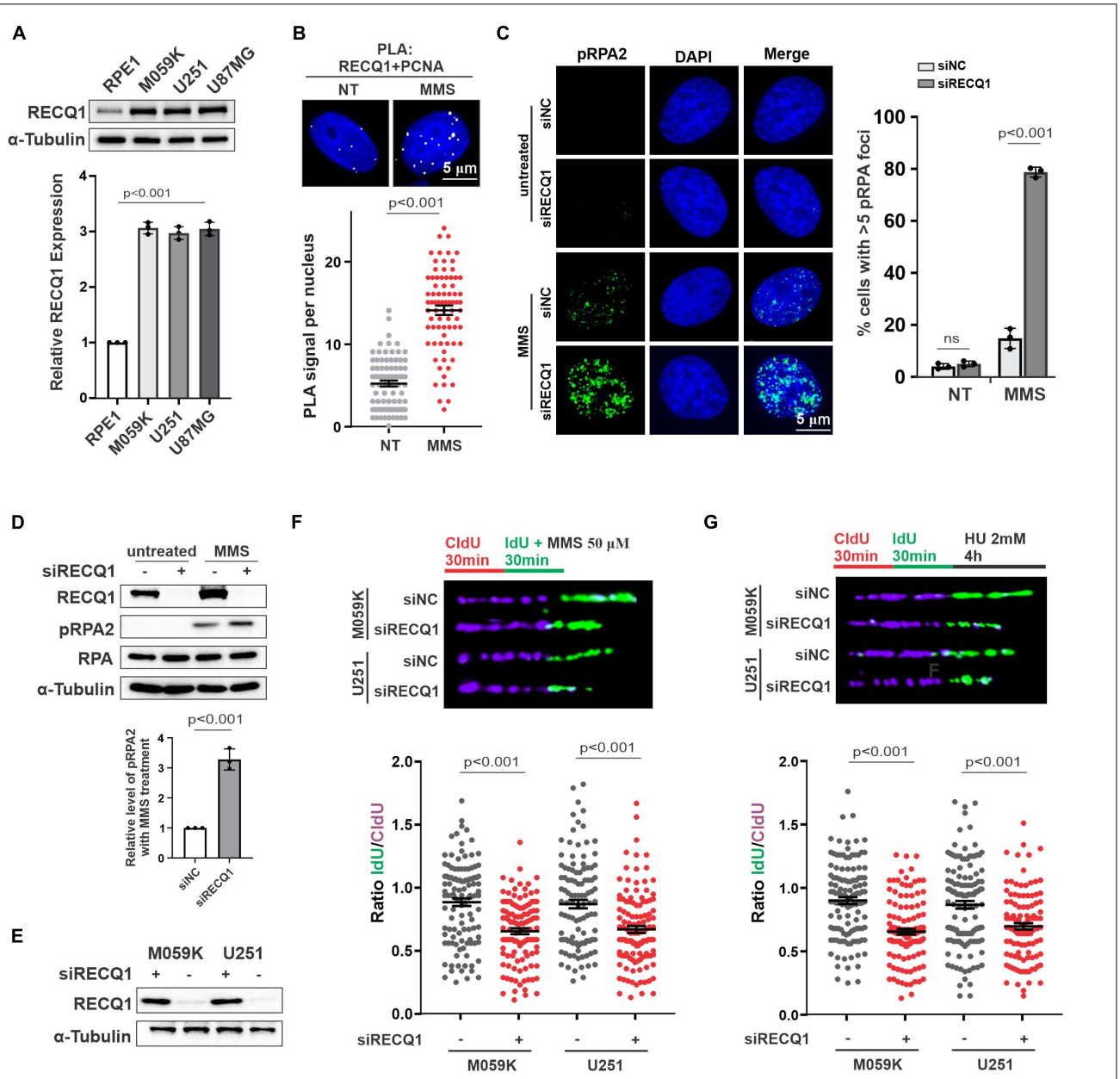

FIGURE 1 | RECQ1 is critical for replication fork restoration in response to replication stress. **(A)** Whole-cell lysates from different cell lines were analyzed by western blotting using indicated antibodies against RECQ1 and α-Tubulin, indicating RECQ1 is overexpressed in GBM cell lines. **(B)** Detection of RECQ1-PCNA interaction was carried out by PLA labeling in M059K cells treated with or without 50 μM MMS. Representative images are shown. Scale bars, 5 μm. The scatterplot displays quantification of the PLA signals per nucleus from three independent experiments. Data are mean ± SEM. **(C)** M059K cells were transfected with siNC or siRECQ1 for 48 h and then treated with the MMS or not. Immunofluorescence labeling was performed to detect level of pRPA2 for ssDNA accumulation analysis. Quantitation of pRPA2 was presented from three independent replicates. Data are mean ± SD. **(D,E)** Whole-cell lysates from different cell lines with MMS treatment or not were analyzed by western blotting using the indicated antibodies. **(F,G)** Schematic of the CldU/IdU pulse-labeling analysis used to investigate nascent Strand degradation upon MMS or HU treatment in M059K and U251 cells transfected with siRECQ1 targeting RECQ1 for 48 h. Representative images of CldU and IdU replication tracks (top) and scatterplot of IdU/CldU-tract length ratios (bottom) for replication forks are shown. Fiber evaluated from at least 100 events from three independent experiments. Data are mean ± SEM. A two-sided Mann–Whitney rank-sum test was used to determine if differences were significant **(B,F,G)**. A two-sided unpaired *t*-test was used to calculate *P*-values **(C)**. Significant: $p < 0.05$; NS, not significant: $P > 0.05$.

in each case. These data are expressed as the mean and standard deviation (mean ± SD) values. Statistical analysis was performed using Student's independent *t*-test, and two-sided *p*-values. All experiments data were calculated via GraphPad Prism 8.4.2 software to assess the significance of differences between experimental groups. For all tests: significant: $P < 0.05$, NS (not significant): $P > 0.05$. All experiments were performed at least three times.

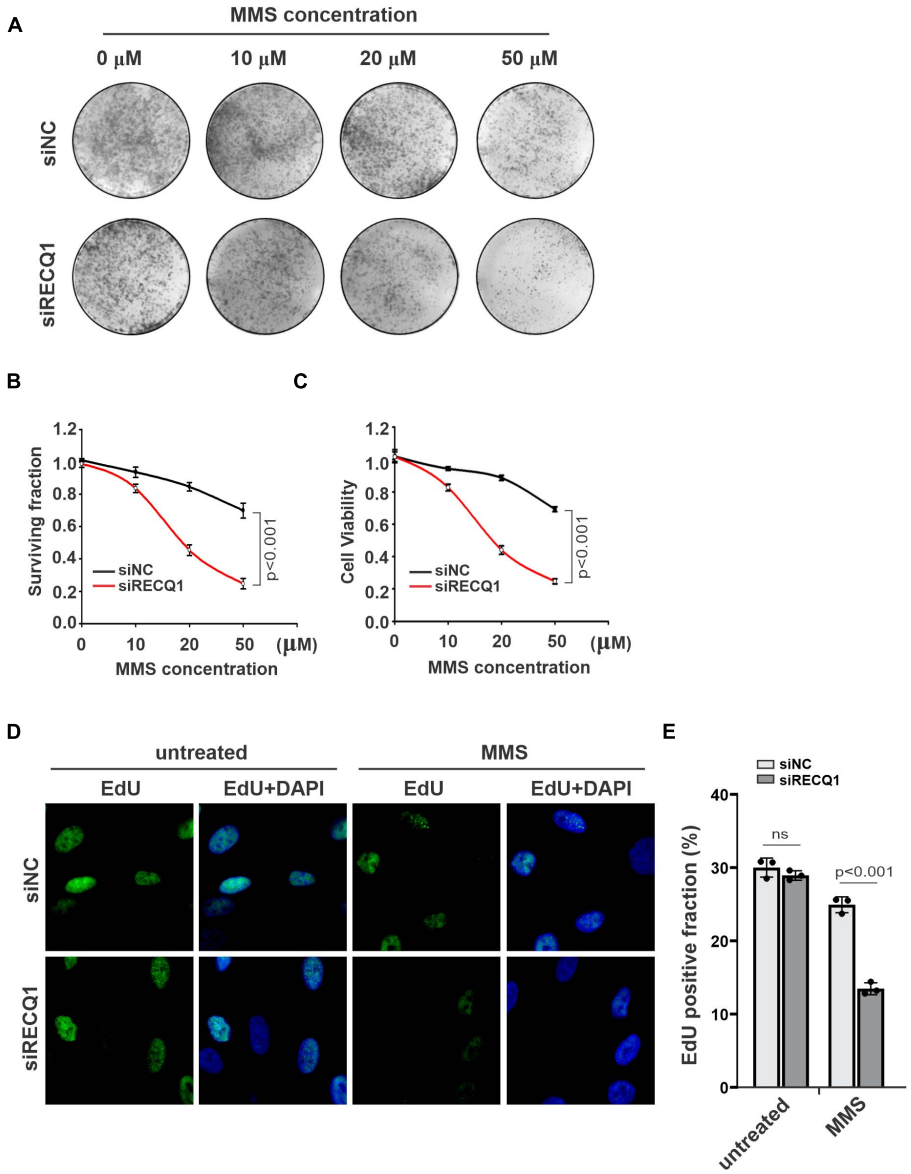

FIGURE 2 | RECQ1 depletion impaired GBM cells cellular progression. **(A)** Colony formation assay of M059K cells treated with different concentration of MMS after transfection with siNC or siRECQ1. Representative images are shown. **(B)** Quantification are represented as means ± SD from at least three independent experiments. **(C)** The viability of siRECQ1 transfected M059K cells was measured with a CCK8 kit. Data are represented as means ± SD from at least three independent experiments. **(D)** Cell proliferation was measured by an EdU labeling of immunofluorescence. **(E)** Quantification are represented as means ± SD from at least three independent experiments. A two-sided unpaired *t*-test was used to calculate *P*-values. Significant: $p < 0.05$; NS, not significant: $P > 0.05$.

RESULTS

RECQ1 Depletion Causes Nascent Strand Degradation Under Replication Stress

Given the characteristic RECQ1 overexpression in glioblastoma patient tumor tissue, RECQ1 has been suggested to play a probable role in GBM tumorigenesis and progression. To determine whether the glioblastoma cell lines used in this study express high levels of RECQ1, the RECQ1 protein levels in the M059K, and U251MG glioblastoma cell lines were compared to those in the RPE1 non-cancerous retina pigmented epithelium cell line by western blot assay (**Figure 1A**). A quantitative analysis confirmed that M059K, U251 and U87MG glioblastoma cells express a higher level of RECQ1 than RPE1 cells, which is in line with previous studies.

To investigate the function of RECQ1 in GBM cell proliferation, we first carried out proximity ligation assays (*in situ* PLA) using antibodies against RECQ1 and PCNA, which bind and indicate DNA replication intermediates during DNA replication. We detected PLA signals in untreated M059K

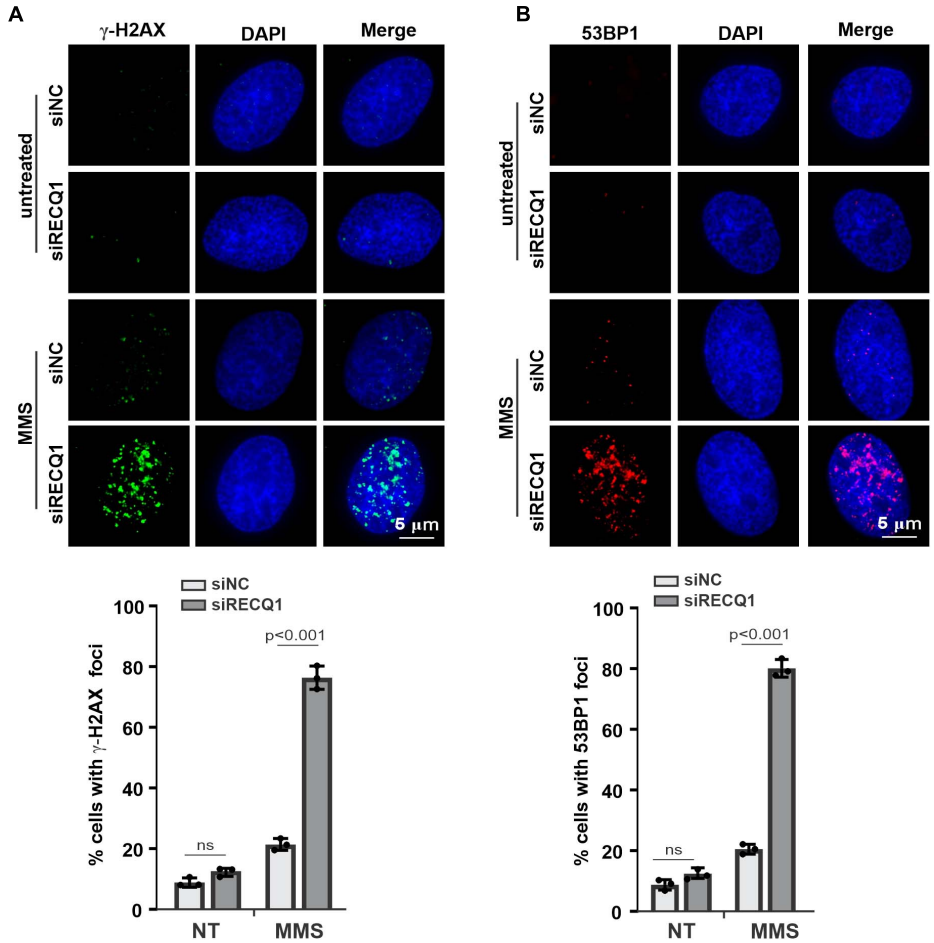

FIGURE 3 | RECQ1 deficiency leads to GBM cells DSB repair defects. **(A,B)** Treatment of M059K cells with siRECQ1 exposed to MMS resulted in DSBs accumulation, as indicated by nuclear γ-H2AX and 53BP1 staining. Quantification are represented as means ± SD from at least three independent experiments. A two-sided unpaired *t*-test was used to calculate *P*-values. Significant: $p < 0.05$; NS, not significant: $P > 0.05$.

cells but significantly increased PLA signals in cells treated with methyl methanesulfonate (MMS), an alkylating agent that transiently arrests fork progression by causing replication fork stalling. The increased nuclear PLA signals suggested an enhanced interaction of RECQ1 and replication sites in response to replication stress (**Figure 1B**). RPA-coated ssDNA is a universal feature of stalled replication forks that presents a recruiting platform for downstream repair factors and checkpoint kinases, such as ATR and CHK1 (Marechal and Zou, 2013). Therefore, phosphorylation of RPA2 at serine 4 and serine 8 (S4/S8) is a commonly used marker of DNA replication stress (Lossaint et al., 2013; Fugger et al., 2015). We compared the impact of RECQ1 deficiency on RPA2 phosphorylation levels upon MMS treatment. As shown in **Figure 1C**, RECQ1 depletion resulted in a dramatic increase in RPA2 phosphorylation in cells exposed to MMS, indicating that RECQ1 inhibited ssDNA accumulation and RPA binding to chromatin in response to replication stress. The increased expression of RPA2 phosphorylation was confirmed by western blot analysis with RECQ1-depleted M059K cells, showing that RECQ1 stabilizes stalled replication forks by limiting ssDNA formation (**Figure 1D**).

Prolonged fork stalling upon MMS treatment has been previously shown to result in fork collapse by uncontrolled nucleolytic degradation and ultimately results in replication-coupled DSB formation (Toledo et al., 2013). In the present study, western blot analysis showed decreased expression of RECQ1 in cells with RECQ1 siRNA transfection (**Figure 1E**). To gain further insights into the mechanism of RECQ1 depletion-induced ssDNA accumulation during DNA synthesis under replication stress conditions, we performed a DNA spreading assay. Nascent replication strands were sequentially labeled with chlorodeoxyuridine (CldU) and iododeoxyuridine (IdU) for 30 min, and then, they were subjected to 50 μM MMS treatment. RECQ1 deficiency resulted in a dramatic shortening of nascent replication strands in two distinct GBM cell lines, M059K, U251, and U87MG cells (**Figure 1F**), indicating that the forks damaged upon MMS exposure underwent excessive nuclease degradation upon RECQ1 depletion. A similar phenotype was observed in GBM cells treated with hydroxyurea (HU), a drug that causes

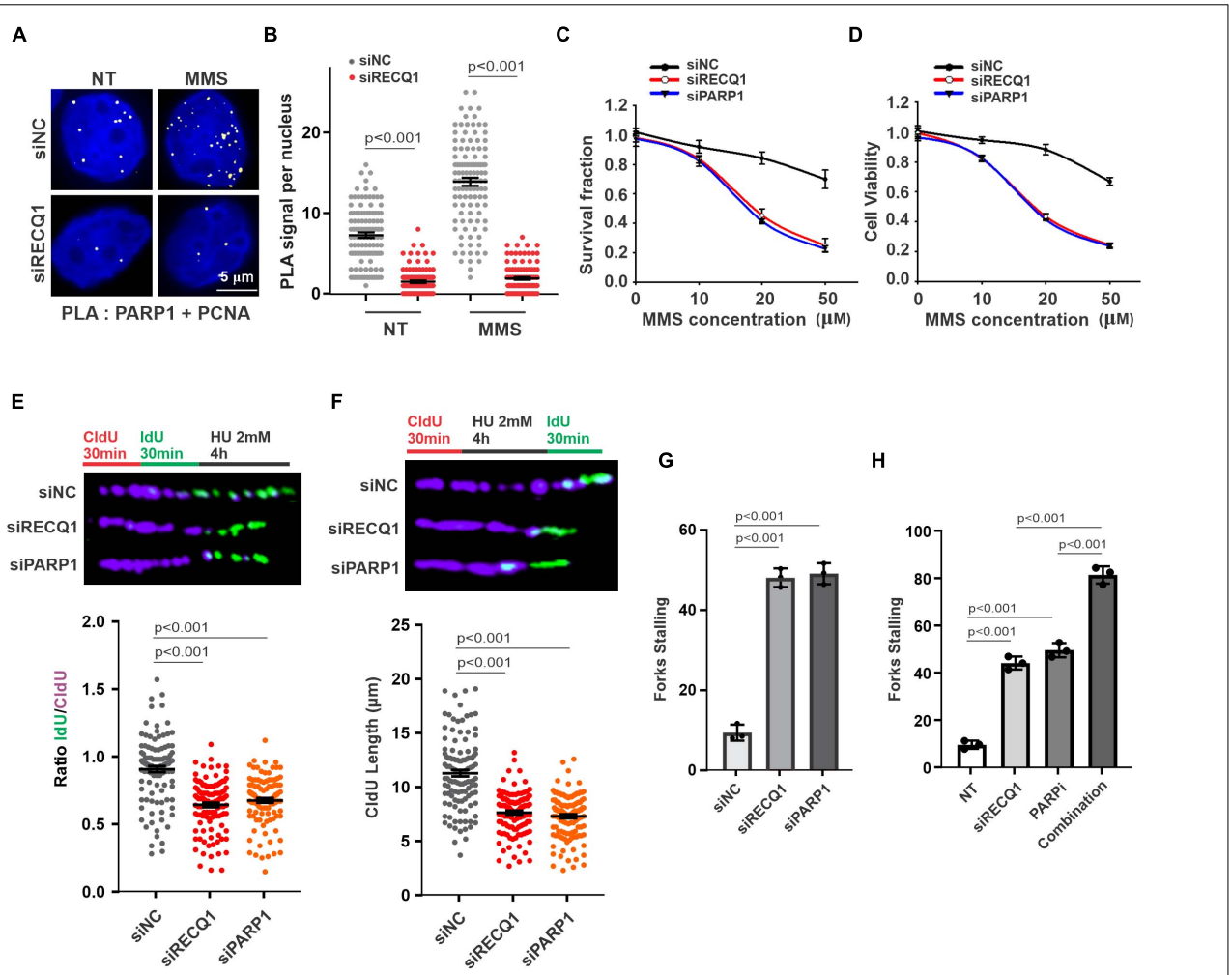

FIGURE 4 | RECQ1 function on GBM cells growth by mediating PARP1 pathway. **(A)** Detection of PARP1-PCNA interaction was carried out by PLA labeling in M059K cells treated with or without 50 μM MMS after transfection with siNC or siRECQ1. Representative images are shown. Scale bars, 5 μm. **(B)** The scatterplot displays quantification of the PLA signals per nucleus from three independent experiments. Data are mean ± SEM. **(C)** Quantification of colony formation assay of cells transfected with siNC, siRECQ1 or siPARP1 exposed to different concentration of MMS. **(D)** The viability of siRECQ1 transfected M059K cells was measured with a CCK8 kit. **(E)** Schematic of the CldU/IdU pulse-labeling analysis used to investigate replication fork degradation upon HU treatment in M059K cells transfected with siRECQ1 or siPARP1 for 48 h. Representative images of CldU and IdU replication tracks (top) and scatterplot of IdU/CldU-tract length ratios (bottom) for replication forks are shown. Fiber evaluated from at least 100 events from three independent experiments. Data are mean ± SEM. **(F–H)** Schematic of an alternative CldU/IdU pulse-labeling protocol to investigate fork degradation and fork stalling upon HU treatment in M059K cells of CldU tracking length and stalled forks are assayed. Fiber evaluated from at least 120 events from three independent experiments. Data are mean ± SEM. A two-sided Mann–Whitney rank-sum test was used to determine if differences were significant **(B,E,F)**. A two-sided unpaired *t*-test was used to calculate *P*-values **(C,D)**. Significant: $p < 0.05$; NS, not significant: $P > 0.05$.

fork stalling by depleting the pool of nucleotides available for DNA synthesis (**Figure 1G**). In light of these findings, we proposed that the helicase RECQ1 can prevent ssDNA formation and nascent strand degradation upon replication stress in GBM cells.

RECQ1 Depletion Inhibit GBM Cells Growth Upon Replication Stress

To investigate the role of RECQ1 in promoting glioblastoma cell growth and proliferation, we assayed the colony formation properties of M059K cells treated with different concentrations of MMS. Compared with cells transfected with control siRNA (causing an approximate 20% reduction in colony formation), the cells transfected with RECQ1 siRNA exhibited an approximate 80% reduction in colony formation (**Figures 2A,B**). Similar results were also found with a viability CCK-8 cell viability assay (**Figure 2C**). The cell survival curves with increasing MMS concentrations indicated that RECQ1-deficient cells were hypersensitive to MMS treatment and further confirmed the impairment of the repair function of RECQ1 in DNA replication fork progression with accumulated DNA damage caused by increased replication stress. To provide further evidence for suppressed cell proliferation due to RECQ1 deficiency, we

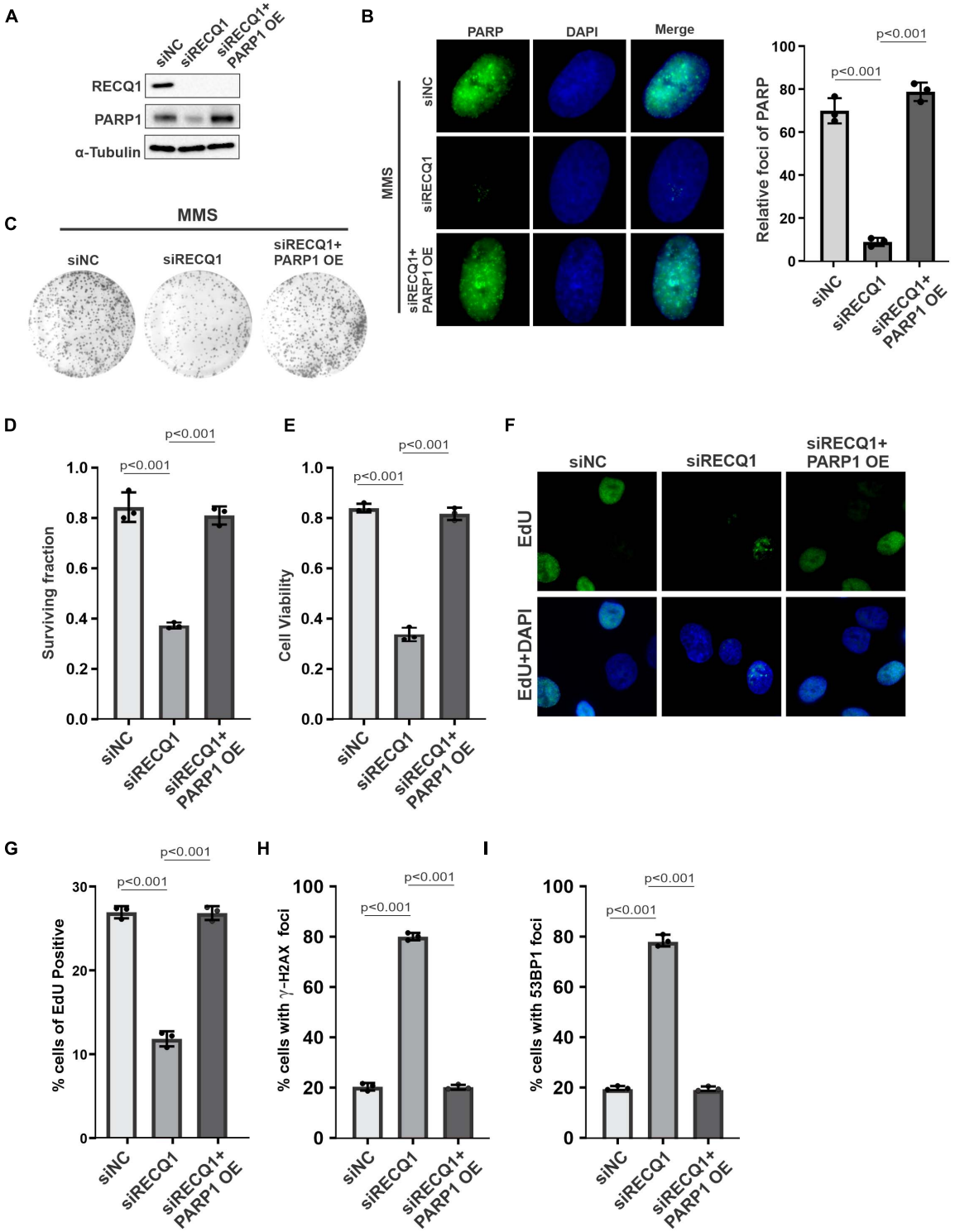

FIGURE 5 | PARP1 compensated RECQ1 dysfunction on GBM cells growth upon replication stress. **(A)** Whole-cell lysates from M059K cells transfected with siNC, siRECQ1, or siRECQ1 and PARP1 OE (overexpression plasmid) were analyzed by western blotting using the indicated antibodies. **(B)** Immunofluorescence indicates PARylation in cells transfected with siNC, siRECQ1, or siRECQ1 and PARP1 OE. **(C)** Representative images of colonies. **(D)** Quantification of colony formation assay of cells transfected with siNC, siRECQ1 or siRECQ1 and PARP1 OE exposed to MMS. **(E)** The viability of transfected M059K cells was measured with a CCK8 kit. **(F,G)** Cell proliferation was measured by an EdU labeling of immunofluorescence. Quantification of EdU positive cells were calculated. **(H,I)** γ-H2AX and 53BP1 staining indicated DSB accumulation. Quantification are represented as means ± SD from at least three independent experiments. A two-sided unpaired *t*-test was used to calculate *P*-values. Significant: $p < 0.05$; NS, not significant: $P > 0.05$.

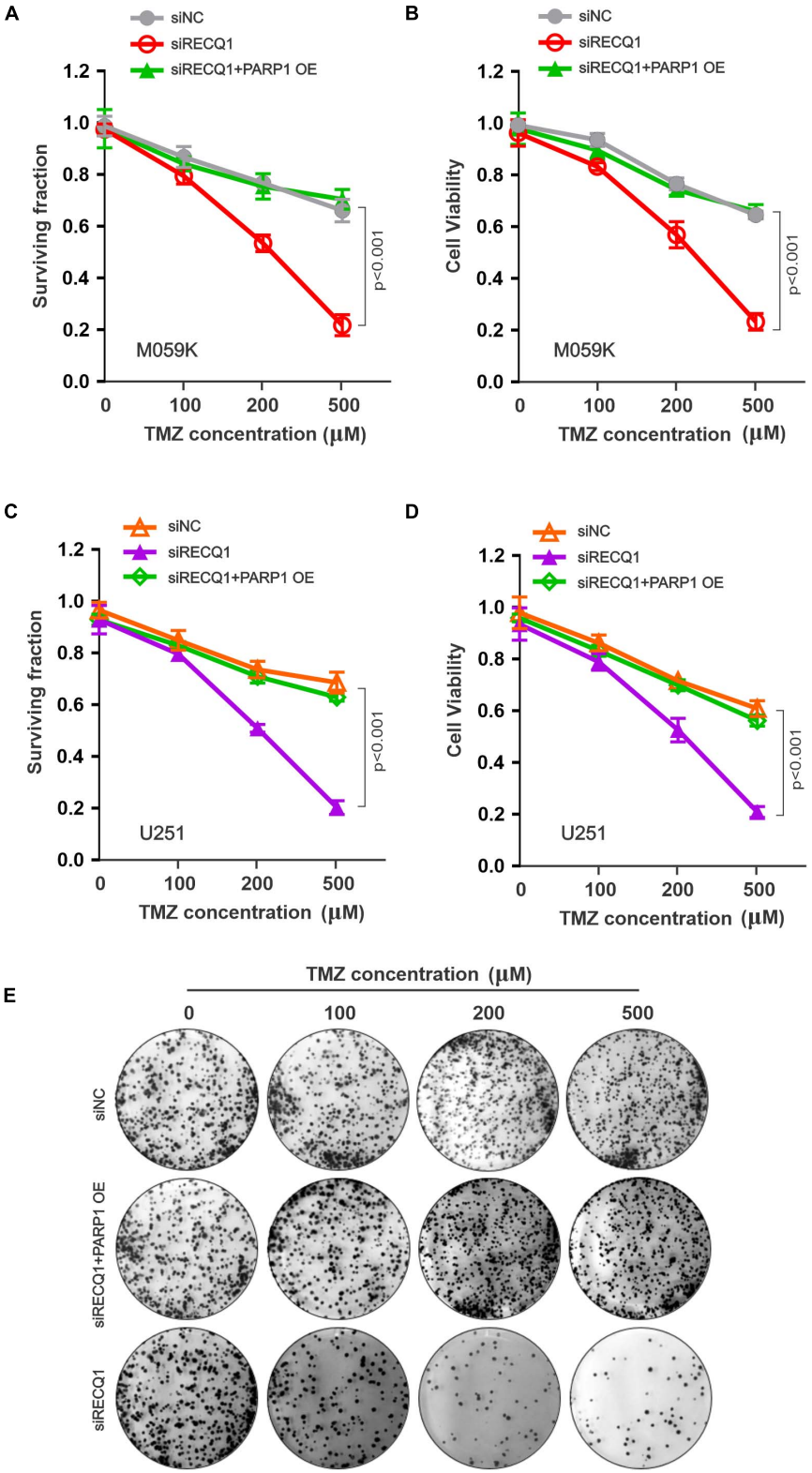

FIGURE 6 | RECQ1 deficient glioblastoma cells are hypersensitive to TMZ treatment. **(A)** Cellular surviving fractions and **(B)** cell viability was measured at different concentration of TMZ in M059K cells transfected with siNC, siRECQ1 or combined with PARP1 OE. Surviving fraction and viability values are indicated as mean ± SD from three independent experiments. **(C,D)** TMZ sensitivity analysis carried out in additional U251 cells. **(E)** Representative clone images were shown. A two-sided unpaired *t*-test was used to calculate *P*-values. Significant: $p < 0.05$; NS, not significant: $P > 0.05$.

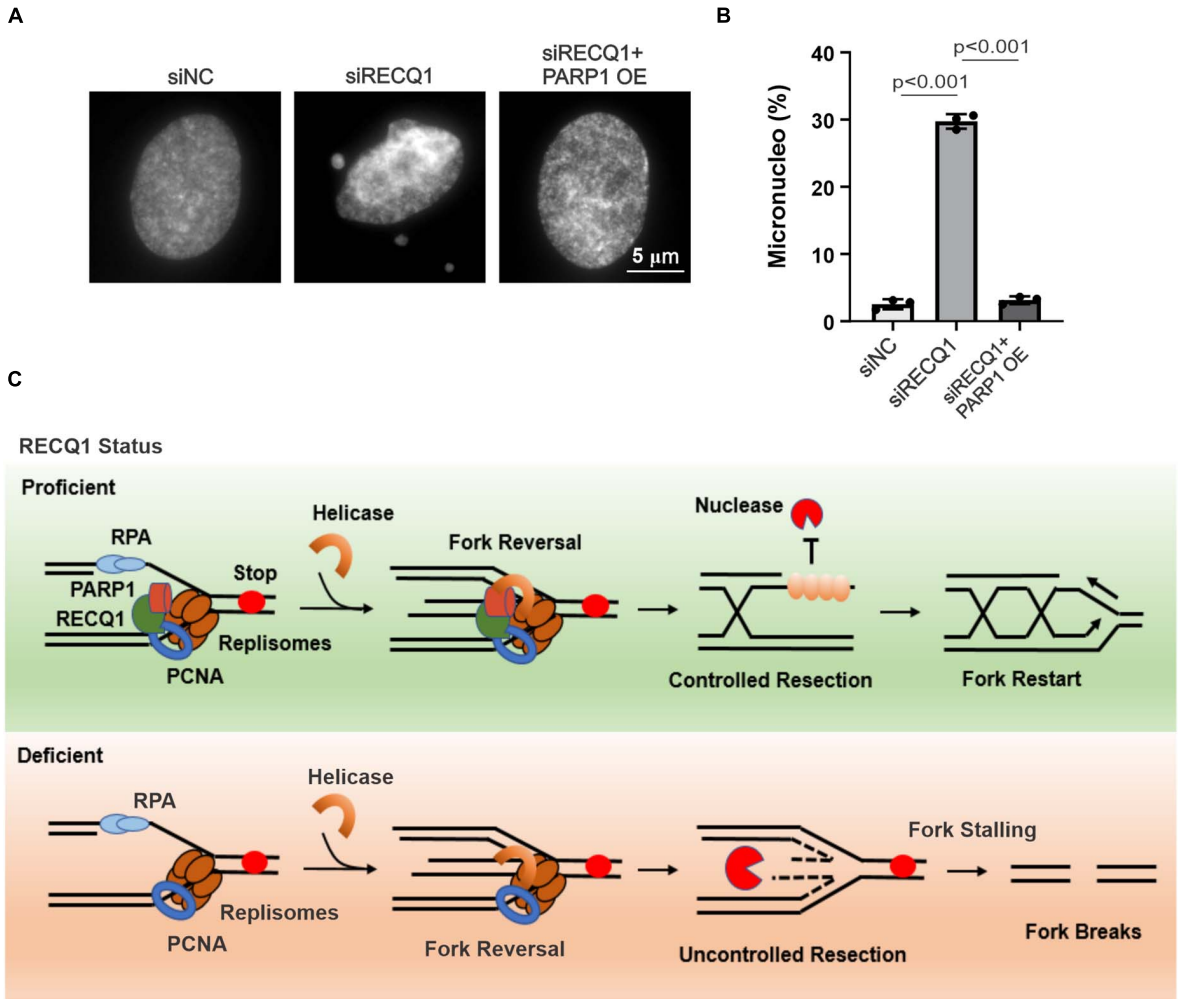

FIGURE 7 | RECQ1 deficient glioblastoma cells raised genomic instability. **(A)** Chromosomal abnormalities were showed by micronucleus formation in M059K cells treated with siRECQ1. **(B)** Quantification are represented as means ± SD from at least three independent experiments. **(C)** Model of RECQ1-PARP1 function. A two-sided unpaired *t*-test was used to calculate *P*-values. Significant: $p < 0.05$; NS, not significant: $P > 0.05$.

performed EdU staining of RECQ1-depleted M059K cells and showed that the number of EdU positive cells reduced by 50% (**Figures 2D,E**) indicating a slowed cellular progression upon RECQ1 depletion under replication stress conditions. These data confirmed that the downregulation of RECQ1 significantly suppressed the proliferation capacity of GBM cells by interfering with DNA synthesis and DNA replication fork progression under DNA replication stress. Thus, underlining the potential implications of these findings for GBM tumor growth, depletion of RECQ1 resulted in a progressive proliferative defect in GBM cells.

RECQ1 Deficiency in Glioblastoma Cells Results in Accumulated DNA Damage

RecQ helicases have been previously reported to associate with the stabilization and restarting of damaged DNA replication forks in response to multiple replication stresses (Brosh and Bohr, 2007). Long-term fork stalling and failure to restart damaged forks can lead to DNA breaks (Andreassen et al., 2006). Given the previous studies that RECQ1-deficient cells showed a mildly increased level of DNA damage with homologous recombination (HR) repair impairment under the untreated condition (Mendoza-Maldonado et al., 2011), we sought to evaluate whether RECQ1 depletion can trigger DNA damage upon MMS treatment. We analyzed the extent of spontaneous γ-H2AX and 53BP1 foci formation in M059K cells transfected with RECQ1 siRNA or siNC in the presence or absence of MMS; H2AX and 53BP1 are well-known markers of DNA double-strand breaks in damaged cells. Immunofluorescence analysis indicated that RECQ1 depletion resulted in a dramatic increase in γ-H2AX and 53BP1 foci formation in M059K cells exposed to MMS compared to unchallenged cells, confirming that the depletion of RECQ1 was associated with defects in DSB repair (**Figures 3A,B**). Approximately 80% of the RECQ1-deficient cells harbored more

than five γ-H2AX and 53BP1 foci per nucleus, compared to approximately 20% in the RECQ1-proficient cells, implying that the DNA repair capacity of RECQ1-deficiency cells was diminished upon MMS treatment. There was a much lower detectable percentage of cells with DSB damage among the untreated cells, indicating that specific DNA damage repair is mediated under different conditions. Increased DNA damage is often associated with growth inhibition, which is specific to cancer cells, as they rapidly proliferate and exhibit more DNA damage (Gangopadhyay et al., 2014; Qu et al., 2014). Therefore, the results of DNA damage accumulation demonstrated the suppressed growth of GBM cells with RECQ1 deficiency in response to MMS-induced replication stress.

RECQ1 Depletion Inhibit the Growth of GBM Cells by Impairing PARP1 Function

Earlier studies demonstrated that RECQ1 is directly associated with PAPR1 and contributes to fork restoration (Berti et al., 2013). To investigate the mechanism of RECQ1 in protecting replication forks upon DNA replication stress in GBM cells, we evaluated the response of PARP1 to replication stress. In stark contrast to the finding that RECQ1-deficient cells activated PARP1 in a specific response to H_2O_2 treatment, PARP1 was shown to be significantly recruited to the replication site, as indicated by PLA assay performed to test the interaction between PAPR1 and PCNA upon specific MMS treatment (**Figures 4A,B**). These results suggested the possibility that RECQ1 protects damaged forks by regulating PARP1 function and performs different mechanisms in response to various types of DNA damage. Survival and viability analyses validated the finding showing that cells deficient in RECQ1 and PARP1 were sensitive to replication stress induced by MMS (**Figures 4C,D**).

M059K cells were next transfected with PARP1 siRNA and scramble siNC prior to a DNA replication progression assay. PARP1-deficient cells contained shortened IdU strands, representing unprotected damaged replication forks similar to those captured in cells lacking RECQ1 in the presence of HU (**Figure 4E**). To evaluate the importance of PARP1 in the protection of stalled DNA replication forks, cells were exposed to long-term HU exposure before IdU labeling was performed a second time. The results from a DNA fiber analysis showed that nascent CldU strands in PARP1-deficient M059K cells were shortened during replication fork stalling, compared with the strands in PARP1-proficient cells, which was consistent with the observations of RECQ1-deficient cells (**Figure 4F**). Consistent with the expectation that RECQ1 and PARP1 function in stalled fork restarting, increased fork stalling was observed in both RECQ1- and PARP1-depleted cells (**Figure 4G**). In addition, RECQ1 depletion increased fork stalling to PARP inhibitor, suggesting a combined effect of RECQ1 and PARP on fork stability under replication stress (**Figure 4H**). Together, these observations raised the possibility that RECQ1 and PARP1 collaboratively protect stalled DNA forks and maintain cellular proliferation under specific replication stress conditions.

PARP1 Restored Cell Growth With RECQ1 Depletion Under Replication Stress

To confirm the role of RECQ1-PARP1 signaling in mediating GBM cell malignant growth, we transfected a PARP1 overexpression plasmid into RECQ1-depleted M059K cells and evaluated the compensatory influence of PARP1 on cell growth. A protein quantification analysis showed PARP1 downregulation in RECQ1-deficient cells, suggesting that PARP1 function was influenced by decreased RECQ1 abundance, while PARP1 expression increased with PARP1 overexpression plasmid transfection (**Figure 5A**). A decreased poly(ADP-ribosyl)ation (PARylation) was observed with RECQ1 depletion, while overexpression of PARP restored the modification, which indicated a protective role of PARP1 overexpression with RECQ1 deficiency (**Figure 5B**). We found that PARP1 overexpression dramatically increased the clonogenic formation capacity of RECQ1-deficient M059K cells after MMS treatment (**Figures 5C,D**). In agreement with the survival assay, similar results were found through the viability analysis performed by CCK-8 test (**Figure 5E**). Interestingly, in both EdU labeling and cell cycle assays based on flow cytometry, we consistently found that PARP1 overexpression abolished RECQ1 deficiency-mediated M059K growth inhibition, indicating that the downregulation of PARP1 induced by RECQ1 depletion was a key event in the PARP1 effect on cellular proliferation (**Figures 5F,G**). Moreover, we also observed dramatically decreased DSB accumulation with PARP1 overexpression, as marked by γ-H2AX and 53BP1 labeling, suggesting that the DNA damage accumulation was largely decreased through PARP1 compensatory activity (**Figures 5H,I**). Together, our results showed that proficient RECQ1 and PARP1 function in M059K cells was essential for the DNA damage repair induced by MMS. A greater DNA repair capacity can protect M059K cells from overcoming DNA damage that occurred endogenously or upon MMS replication stress, as well as prevent dramatic cellular proliferation.

RECQ1 Depletion Increased Micronucleus Formation With Hypersensitive to Temozolomide

Because RECQ1 was found to be overexpressed in glioblastomas, we next investigated the sensitivity of glioblastoma cells to temozolomide (TMZ), which is an anticancer alkylating agent commonly used for the treatment of human brain tumors. Nevertheless, TMZ resistance is a major common challenge to effective clinical therapy (Lefranc et al., 2005, 2007; Stupp et al., 2009). We explored the possibility of RECQ1-PARP1 being a promising signaling target for TMZ hypersensitivity, which would suppress glioblastoma cell proliferation. The surviving cell fraction and viability assays performed with a range of TMZ concentrations showed that RECQ1-depleted M059K cells were hypersensitive to TMZ treatment, while PARP1 overexpression contributed to a robust recovery of cell cycle progression (**Figures 6A,B**), confirming the role of RECQ1-PARP1 regulation

in DNA repair pathways related to DNA replication and chemoresistance. Similar to the effect in M059K cells, knocking down RECQ1 expression sensitized U251 glioblastoma cells to TMZ treatment, while PARP1 supplementation restored GBM cell survival rates and viability (**Figures 6C,D**), confirming that RECQ1-PARP1 regulation causes significant resistance of glioblastoma cells to the influence of the methylating drug TMZ. Representative clone formation images of U251 cells with the indicated treatment are presented (**Figure 6E**).

Consistent with the micronucleus being a typical sign of genotoxic events and chromosomal instability, RECQ1-deficient cells have been reported to display spontaneous genomic instability (Lucic et al., 2011; Zhang et al., 2015). Thus, we next aimed to explore whether RECQ1 depletion results in an increase in micronuclei changes in response to TMZ. As expected, there was an approximately twenty-fold increase in micronucleus formation in RECQ1-deficient M059K cells treated with TMZ (**Figures 7A,B**). Collectively, these data indicated the crucial role of RECQ1 in restoring DNA replication progression and protecting GBM cell genomic integrity. Our study also suggested that glioblastoma cells were reliant on this mechanism to escape clinical treatment through drug resistance; therefore, RECQ1-PARP1 signaling may be a suitable target for GBM tumor therapy.

DISCUSSION

DNA replication stress is considered a major driving force of genome instability and tumorigenesis promotion (Gaillard et al., 2015; Petropoulos et al., 2019). Rapidly proliferating tumor cells also encounter multiple blockades, including altered DNA secondary structures, oncogene activation, and DNA damage drugs, during replication and are usually reliant on overexpressed DNA damage repair factors to overcome these blockades to maintain cancer cell genome integrity (Hurley, 2001; Prado, 2014; Gupta et al., 2018); therefore, these cells are more susceptible to DNA damage response (DDR) inhibition than normal cells, which maintain full DNA repair capacity and provide potential therapeutic alternative strategies for interfering with these repair processes. Accumulating evidence has shown that RECQ1 is involved in several cellular functions, including DNA repair, cell cycle and growth, telomere maintenance, and transcription (Berti et al., 2013; Lu et al., 2013). Earlier studies demonstrated the unique role of RECQ1 in ensuring chromosomal stability and cancer (Sharma et al., 2006). Selectively highly expressed RECQ1 was identified in multiple GBM cells and might be related to the malignancy of tumors and drug resistance to clinical treatment (Bochman, 2014). Therefore, our findings provide a mechanistic rationale for RECQ1-PARP1 regulation of cellular progression, indicating that it may be a promising therapeutic target for the mitigation of glioblastoma progression.

In this study, we reported that the RECQ helicase family member RECQ1 is crucial for restoring stalled replication forks and maintaining GBM cell genomic stability by regulating PARP1 in response to various DNA replication stresses. Associated with PCNA, RECQ1 accumulates at stalled replication forks and recruits PARP1 to limit unprogrammed nucleolytic degradation and assure effective replication fork restart (**Figure 7C**). RECQ1 depletion increases ssDNA formation and nascent strand degradation under replication stress conditions. PARP1 deletion led to the acquisition of a phenotype similar to that of RECQ1-deficient cells, with increased replication fork stalling, a significant reduction of cellular proliferation and accumulated DNA damage in GBM cells. Consistent with a previous report showing that RECQ1 is important for HeLa cell proliferation and plays a unique role in the maintenance of genome integrity, our results suggest that RECQ1 is essential for DNA replication fork protection and GBM tumor cell malignant proliferation under replication stress conditions. We also found that RECQ1 depletion results in spontaneous γ-H2AX and 53BP1 foci formation in response to MMS exposure, suggesting that RECQ1 plays an essential role in preventing DNA damage accumulating during DNA replication upon replication stress. In addition, the resistance of GBM cells to chemotherapeutic agents is one of the challenges hindering clinical treatment (Roos et al., 2004; Happold et al., 2012). Our study shows that the hypersensitivity of RECQ1-deficient GBM cells to TMZ supports the notion of RECQ1-PARP1 regulation as a contributor to the resistance of glioblastoma cells to the methylating drug temozolomide and represents a promising target pathway for anticancer therapies that inhibit DNA replication and proliferation of GBM cells.

Other human helicases, such as BLM and WRN, are also upregulated in multiple tumors, driving cancer cells to rapidly proliferate, supporting oncogenic activation and potentially playing distinct functions in driving DNA replication stress. Dysregulation of these genes has been associated with cell genetic disorders related to cancer predisposition or promotion (Sidorova et al., 2013; Orlovetskie et al., 2017). Therefore, to determine whether these helicases play functions incompatible to GBM cell growth or have synthetic effects, further study is needed. Cancer cells might utilize these stress-resistant mechanisms during the process of DNA replication to enhance tumorigenesis and chemoresistance; thus, a better understanding of these important mechanisms may benefit GBM clinical therapy. Therefore, combining the newly identified RECQ1-PARP1 signaling function in genome stability and clinical resistance of GBM cells, further studies to discover how these complexities can be resolved to promote fork restarting and progression and the possible synthetic interactions with other human helicases will provide new insights into the mechanism of GBM progression.

DATA AVAILABILITY STATEMENT

The raw data supporting the conclusions of this article will be made available by the authors, without undue reservation.

AUTHOR CONTRIBUTIONS

JZ and CZ had the initial idea, supervised the experiments, and wrote and revised the manuscript. JZ, ML, and HL designed the experiments. KC, MC, BH, LZ, and SX performed the

experiments and analyzed the data. YP reviewed and reedited the manuscript. All authors commented on the manuscript.

FUNDING

This study was supported by grants from the Key Discipline Construction Project of Pudong Health Bureau of Shanghai (PWZxk2017-23), Outstanding Leaders Training Program of Pudong Health Bureau of Shanghai (PWR12018-07), and Top-Level Clinical Discipline Project of Shanghai Pudong (PWYgf2018-05).

SUPPLEMENTARY MATERIAL

The Supplementary Material for this article can be found online at: https://www.frontiersin.org/articles/10.3389/fcell.2021.714868/full#supplementary-material

REFERENCES

Andreassen, P. R., Ho, G. P., and D'Andrea, A. D. (2006). DNA damage responses and their many interactions with the replication fork. *Carcinogenesis* 27, 883–892. doi: 10.1093/carcin/bgi319

Arai, A., Chano, T., Futami, K., Furuichi, Y., Ikebuchi, K., Inui, T., et al. (2011). RECQL1 and WRN proteins are potential therapeutic targets in head and neck squamous cell carcinoma. *Cancer Res.* 71, 4598–4607. doi: 10.1158/0008-5472.can-11-0320

Berti, M., Chaudhuri, A. R., Thangavel, S., Gomathinayagam, S., Kenig, S., Vujanovic, M., et al. (2013). Human RECQ1 promotes restart of replication forks reversed by DNA topoisomerase I inhibition. *Nat. Struct. Mol. Biol.* 20, 347–354. doi: 10.1038/nsmb.2501

Bochman, M. L. (2014). Roles of DNA helicases in the maintenance of genome integrity. *Mol. Cell Oncol.* 1:e963429. doi: 10.4161/23723548.2014.963429

Bohr, V. A. (2008). Rising from the RecQ-age: the role of human RecQ helicases in genome maintenance. *Trends Biochem. Sci.* 33, 609–620. doi: 10.1016/j.tibs.2008.09.003

Brosh, R. M. Jr., and Bohr, V. A. (2007). Human premature aging, DNA repair and RecQ helicases. *Nucleic Acids Res.* 35, 7527–7544. doi: 10.1093/nar/gkm1008

Debnath, S., and Sharma, S. (2020). RECQ1 helicase in genomic stability and cancer. *Genes* 11:622. doi: 10.3390/genes11060622

Ellis, N. A., Groden, J., Ye, T. Z., Straughen, J., Lennon, D. J., Ciocci, S., et al. (1995). The Bloom's syndrome gene product is homologous to RecQ helicases. *Cell* 83, 655–666. doi: 10.1016/0092-8674(95)90105-1

Fugger, K., Mistrik, M., Neelsen, K. J., Yao, Q., Zellweger, R., Kousholt, A. N., et al. (2015). FBH1 catalyzes regression of stalled replication forks. *Cell Rep.* 10, 1749–1757. doi: 10.1016/j.celrep.2015.02.028

Futami, K., Kumagai, E., Makino, H., Sato, A., Takagi, M., Shimamoto, A., et al. (2008). Anticancer activity of RecQL1 helicase siRNA in mouse xenograft models. *Cancer Sci.* 99, 1227–1236. doi: 10.1111/j.1349-7006.2008.00794.x

Gaillard, H., Garcia-Muse, T., and Aguilera, A. (2015). Replication stress and cancer. *Nat. Rev. Cancer* 15, 276–289.

Gangopadhyay, N. N., Luketich, J. D., Opest, A., Landreneau, R., and Schuchert, M. J. (2014). PARP inhibitor activates the intrinsic pathway of apoptosis in primary lung cancer cells. *Cancer Invest.* 32, 339–348. doi: 10.3109/07357907.2014.919303

Gupta, R., Somyajit, K., Narita, T., Maskey, E., Stanlie, A., Kremer, M., et al. (2018). DNA repair network analysis reveals Shieldin as a key regulator of NHEJ and PARP inhibitor sensitivity. *Cell* 173, 923–988.e23.

Happold, C., Roth, P., Wick, W., Schmidt, N., Florea, A. M., Silginer, M., et al. (2012). Distinct molecular mechanisms of acquired resistance to temozolomide in glioblastoma cells. *J. Neurochem.* 122, 444–455. doi: 10.1111/j.1471-4159.2012.07781.x

Hickson, I. D. (2003). RecQ helicases: caretakers of the genome. *Nat. Rev. Cancer* 3, 169–178. doi: 10.1038/nrc1012

Hurley, L. H. (2001). Secondary DNA structures as molecular targets for cancer therapeutics. *Biochem. Soc. Trans.* 29, 692–696. doi: 10.1042/bst0290692

Kitao, S., Lindor, N. M., Shiratori, M., Furuichi, Y., and Shimamoto, A. (1999). Rothmund-thomson syndrome responsible gene, RECQL4: genomic structure and products. *Genomics* 61, 268–276. doi: 10.1006/geno.1999.5959

Lefranc, F., Brotchi, J., and Kiss, R. (2005). Possible future issues in the treatment of glioblastomas: special emphasis on cell migration and the resistance of migrating glioblastoma cells to apoptosis. *J. Clin. Oncol.* 23, 2411–2422. doi: 10.1200/jco.2005.03.089

Lefranc, F., Facchini, V., and Kiss, R. (2007). Proautophagic drugs: a novel means to combat apoptosis-resistant cancers, with a special emphasis on glioblastomas. *Oncologist* 12, 1395–1403. doi: 10.1634/theoncologist.12-12-1395

Lossaint, G., Larroque, M., Ribeyre, C., Bec, N., Larroque, C., Decaillet, C., et al. (2013). FANCD2 binds MCM proteins and controls replisome function upon activation of s phase checkpoint signaling. *Mol. Cell* 51, 678–690. doi: 10.1016/j.molcel.2013.07.023

Lu, X., Parvathaneni, S., Hara, T., Lal, A., and Sharma, S. (2013). Replication stress induces specific enrichment of RECQ1 at common fragile sites FRA3B and FRA16D. *Mol. Cancer* 12:29. doi: 10.1186/1476-4598-12-29

Lucic, B., Zhang, Y., King, O., Mendoza-Maldonado, R., Berti, M., Niesen, F. H., et al. (2011). A prominent beta-hairpin structure in the winged-helix domain of RECQ1 is required for DNA unwinding and oligomer formation. *Nucleic Acids Res.* 39, 1703–1717. doi: 10.1093/nar/gkq1031

Marechal, A., and Zou, L. (2013). DNA damage sensing by the ATM and ATR kinases. *Cold Spring Harb. Perspect. Biol.* 5:a012716. doi: 10.1101/cshperspect.a012716

Mendoza-Maldonado, R., Faoro, V., Bajpai, S., Berti, M., Odreman, F., Vindigni, M., et al. (2011). The human RECQ1 helicase is highly expressed in glioblastoma and plays an important role in tumor cell proliferation. *Mol. Cancer* 10:83. doi: 10.1186/1476-4598-10-83

Opresko, P. L., Cheng, W. H., and Bohr, V. A. (2004). Junction of RecQ helicase biochemistry and human disease. *J. Biol. Chem.* 279, 18099–18102. doi: 10.1074/jbc.r300034200

Orlovetskie, N., Serruya, R., Abboud-Jarrous, G., and Jarrous, N. (2017). Targeted inhibition of WRN helicase, replication stress and cancer. *Biochim. Biophys. Acta Rev. Cancer* 1867, 42–48. doi: 10.1016/j.bbcan.2016.11.004

Ouyang, K. J., Woo, L. L., and Ellis, N. A. (2008). Homologous recombination and maintenance of genome integrity: cancer and aging through the prism of human RecQ helicases. *Mech. Ageing Dev.* 129, 425–440. doi: 10.1016/j.mad.2008.03.003

Petropoulos, M., Champeris Tsaniras, S., Taraviras, S., and Lygerou, Z. (2019). Replication licensing aberrations, replication stress, and genomic instability. *Trends Biochem. Sci.* 44, 752–764. doi: 10.1016/j.tibs.2019.03.011

Prado, F. (2014). Homologous recombination maintenance of genome integrity during DNA damage tolerance. *Mol. Cell. Oncol.* 1:e957039. doi: 10.4161/23723548.2014.957039

Qu, A., Wang, H., Li, J., Wang, J., Liu, J., Hou, Y., et al. (2014). Biological effects of (125)i seeds radiation on A549 lung cancer cells: G2/M arrest and enhanced cell death. *Cancer Invest.* 32, 209–217. doi: 10.3109/07357907.2014.905585

Roos, W., Baumgartner, M., and Kaina, B. (2004). Apoptosis triggered by DNA damage O6-methylguanine in human lymphocytes requires DNA replication and is mediated by p53 and Fas/CD95/Apo-1. *Oncogene* 23, 359–367. doi: 10.1038/sj.onc.1207080

Sharma, S., Doherty, K. M., and Brosh, R. M. Jr. (2006). Mechanisms of RecQ helicases in pathways of DNA metabolism and maintenance of genomic stability. *Biochem. J.* 398, 319–337. doi: 10.1042/bj20060450

Sidorova, J. M., Kehrli, K., Mao, F., and Monnat, R. Jr. (2013). Distinct functions of human RECQ helicases WRN and BLM in replication fork recovery and progression after hydroxyurea-induced stalling. *DNA Repair* 12, 128–139. doi: 10.1016/j.dnarep.2012.11.005

Siitonen, H. A., Kopra, O., Kaariainen, H., Haravuori, H., Winter, R. M., Saamanen, A. M., et al. (2003). Molecular defect of RAPADILINO syndrome expands the phenotype spectrum of RECQL diseases. *Hum. Mol. Genet.* 12, 2837–2844. doi: 10.1093/hmg/ddg306

Stupp, R., Hegi, M. E., Mason, W. P., van den Bent, M. J., Taphoorn, M. J., Janzer, R. C., et al. (2009). Effects of radiotherapy with concomitant and adjuvant temozolomide versus radiotherapy alone on survival in glioblastoma in a randomised phase III study: 5-year analysis of the EORTC-NCIC trial. *Lancet Oncol.* 10, 459–466. doi: 10.1016/s1470-2045(09)70025-7

Stupp, R., Taillibert, S., Kanner, A., Read, W., Steinberg, D., Lhermitte, B., et al. (2017). Effect of tumor-treating fields plus maintenance Temozolomide vs Maintenance Temozolomide Alone on Survival in Patients With Glioblastoma: a randomized clinical trial. *JAMA* 318, 2306–2316. doi: 10.1001/jama.2017.18718

Thakar, T., Leung, W., Nicolae, C. M., Clements, K. E., Shen, B., Bielinsky, A. K., et al. (2020). Ubiquitinated-PCNA protects replication forks from DNA2-mediated degradation by regulating Okazaki fragment maturation and chromatin assembly. *Nat. Commun.* 11:2147.

Toledo, L. I., Altmeyer, M., Rask, M. B., Lukas, C., Larsen, D. H., Povlsen, L. K., et al. (2013). ATR prohibits replication catastrophe by preventing global exhaustion of RPA. *Cell* 155, 1088–1103. doi: 10.1016/j.cell.2013.10.043

van der Crabben, S. N., Hennus, M. P., McGregor, G. A., Ritter, D. I., Nagamani, S. C., Wells, O. S., et al. (2016). Destabilized SMC5/6 complex leads to chromosome breakage syndrome with severe lung disease. *J. Clin. Invest.* 126, 2881–2892. doi: 10.1172/jci82890

Viziteu, E., Klein, B., Basbous, J., Lin, Y. L., Hirtz, C., Gourzones, C., et al. (2017). RECQ1 helicase is involved in replication stress survival and drug resistance in multiple myeloma. *Leukemia* 31, 2104–2113. doi: 10.1038/leu.2017.54

Ying, S., Chen, Z., Medhurst, A. L., Neal, J. A., Bao, Z., Mortusewicz, O., et al. (2016). DNA-PKcs and PARP1 bind to unresected stalled DNA replication forks where they recruit XRCC1 to mediate repair. *Cancer Res.* 76, 1078–1088. doi: 10.1158/0008-5472.can-15-0608

Yu, C. E., Oshima, J., Fu, Y. H., Wijsman, E. M., Hisama, F., Alisch, R., et al. (1996). Positional cloning of the Werner's syndrome gene. *Science* 272, 258–262.

Zeman, M. K., and Cimprich, K. A. (2014). Causes and consequences of replication stress. *Nat. Cell Biol.* 16, 2–9. doi: 10.1038/ncb2897

Zhang, C. Z., Spektor, A., Cornils, H., Francis, J. M., Jackson, E. K., Liu, S., et al. (2015). Chromothripsis from DNA damage in micronuclei. *Nature* 522, 179–184. doi: 10.1038/nature14493

Conflict of Interest: The authors declare that the research was conducted in the absence of any commercial or financial relationships that could be construed as a potential conflict of interest.

Publisher's Note: All claims expressed in this article are solely those of the authors and do not necessarily represent those of their affiliated organizations, or those of the publisher, the editors and the reviewers. Any product that may be evaluated in this article, or claim that may be made by its manufacturer, is not guaranteed or endorsed by the publisher.

frontiers in Cell and Developmental Biology

ORIGINAL RESEARCH
published: 29 July 2021
doi: 10.3389/fcell.2021.707049

MiR-92b-3p Inhibits Proliferation of HER2-Positive Breast Cancer Cell by Targeting circCDYL

Gehao Liang[1,2†], Yun Ling[1,3†], Qun Lin[1], Yu Shi[1], Qing Luo[1], Yinghuan Cen[1], Maryam Mehrpour[5], Ahmed Hamai[5], Jun Li[4] and Chang Gong[1]**

[1] Breast Tumor Center, Sun Yat-sen Memorial Hospital, Sun Yat-sen University, Guangzhou, China, [2] Department of Breast Oncology, Sun Yat-sen University Cancer Center, Sun Yat-sen University, Guangzhou, China, [3] Department of Breast Surgery, The Second Affiliated Hospital, Guangzhou Medical University, Guangzhou, China, [4] Department of Biochemistry, Zhongshan School of Medicine, Sun Yat-sen University, Guangzhou, China, [5] Institut Necker-Enfants Malades (INEM), Inserm U1151-CNRS UMR 8253, Paris, France

Objectives: Circular RNA (circRNA) is a novel class of RNA, which exhibits powerful biological function in regulating cellular fate of various tumors. Previously, we had demonstrated that over-expression of circRNA circCDYL promoted progression of HER2-negative (HER2$^-$) breast cancer *via* miR-1275-ULK1/ATG7-autophagic axis. However, the role of circCDYL in HER2-positive (HER2$^+$) breast cancer, in particular its role in modulating cell proliferation, one of the most important characteristics of cellular fate, is unclear.

Materials and methods: qRT-PCR and *in situ* hybridization analyses were performed to examine the expression of circCDYL and miR-92b-3p in breast cancer tissues or cell lines. The biological function of circCDYL and miR-92b-3p were assessed by plate colony formation and cell viability assays and orthotopic animal models. In mechanistic study, circRNAs pull-down, RNA immunoprecipitation, dual luciferase report, western blot, immunohistochemical and immunofluorescence staining assays were performed.

Results: CircCDYL was high-expressed in HER2$^+$ breast cancer tissue, similar with that in HER2$^-$ breast cancer tissue. Silencing HER2 gene had no effect on expression of circCDYL in HER2$^+$ breast cancer cells. Over-expression of circCDYL promoted proliferation of HER2$^+$ breast cancer cells but not through miR-1275-ULK1/ATG7-autophagic axis. CircRNA pull down and miRNA deep-sequencing demonstrated the binding of miR-92b-3p and circCDYL. Interestingly, circCDYL did not act as miR-92b-3p sponge, but was degraded in miR-92b-3p-dependent silencing manner. Clinically, expression of circCDYL and miR-92b-3p was associated with clinical outcome of HER2$^+$ breast cancer patients.

Conclusion: MiR-92b-3p-dependent cleavage of circCDYL was an essential mechanism in regulating cell proliferation of HER2$^+$ breast cancer cells. CircCDYL was proved to be a potential therapeutic target for HER2$^+$ breast cancer, and both circCDYL and miR-92b-3p might be potential biomarkers in predicting clinical outcome of HER2$^+$ breast cancer patients.

Keywords: MiR-92b-3p, circCDYL, cell proliferation, HER2-positive breast cancer, RNA induced silencing complex

OPEN ACCESS

Edited by:
Chunlong Chen, Institut Curie, France

Reviewed by:
Hexin Chen, University of South Carolina, United States
Jianwei Zhou, Nanjing Medical University, China

****Correspondence:***
Jun Li
lijun37@mail.sysu.edu.cn
Chang Gong
gchang@mail.sysu.edu.cn

† These authors have contributed equally to this work

Specialty section:
This article was submitted to Cell Growth and Division, a section of the journal Frontiers in Cell and Developmental Biology

Received: *08 May 2021*
Accepted: *02 July 2021*
Published: *29 July 2021*

Citation:
Liang G, Ling Y, Lin Q, Shi Y, Luo Q, Cen Y, Mehrpour M, Hamai A, Li J and Gong C (2021) MiR-92b-3p Inhibits Proliferation of HER2-Positive Breast Cancer Cell by Targeting circCDYL. Front. Cell Dev. Biol. 9:707049. doi: 10.3389/fcell.2021.707049

INTRODUCTION

Breast cancer (BC) has become the most common malignant tumor and leading cause of death by tumor among female worldwide (Bray et al., 2018). Approximately 15–20% of these BC patients exhibits over-expression/amplification of human epidermal growth factor receptor 2 (HER2), and this BC subtype is named as HER2-positive ($HER2^+$) breast cancer. Although anti-HER2 therapy together with operation and chemotherapy contribute to a favorable clinical outcome of $HER2^+$ BC patients, around 10% $HER2^+$ patients still suffer recurrence or metastasis with the reasons unknown (DeSantis et al., 2019). The underlying mechanisms, especially non-coding RNA, in progression of $HER2^+$ BC progression are not elucidated clearly.

Circular RNAs (circRNAs), a novel class of RNAs with covalently closed loop, are stable and abundant in mammalian cells (Yu and Kuo, 2019). Importantly, circRNAs exhibit disease-specific and disease progression-specific characteristics, indicating that circRNAs exhibit a biomarker potential in early diagnosis and predicting prognosis of human disease (Jahani et al., 2020). Several researches demonstrated that circRNAs could act as miRNA sponges (Memczak et al., 2013; Yang et al., 2019; Zhou C. et al., 2020), and certain circRNAs with open reading frame (ORF) and internal ribosome entry site (IREs) acted as templates for protein translation (Legnini et al., 2017; Yang et al., 2018; Zhang et al., 2018), while the circRNAs located in nucleus regulated expression of certain genes by interacting with RNA polymerase II (Zhang et al., 2013; Li et al., 2015). In addition, circRNAs display powerful biological functions such as proliferation, migration, invasion and chemotherapy resistance in HER2-negative ($HER2^-$) subtype of breast cancer (Yang et al., 2019; Zhou Y. et al., 2020; Wang L. et al., 2021). Nevertheless, the role of circRNAs in regulating the cellular fate of $HER2^+$ BC cells is rarely elucidated.

Our previous study identified an autophagy-associated circRNA circCDYL, which promoted autophagosome formation and proliferation of $HER2^-$ breast cancer cells by sponging miR-1275 (Liang et al., 2020). However, the roles of circCDYL, especially cellular fate including proliferation and autophagy in $HER2^+$ BC, has not been investigated. In this study, circCDYL was found to promote the cell proliferation as well, but exhibited little effect on autophagic level in $HER2^+$ BC cells. Mechanism study demonstrated that little miR-1275 was found to bind circCDYL, as miR-1275 rarely expressed in $HER2^+$ BC cell lines. By miRNA sequencing, miR-92b-3p was screened out to bind with circCDYL in $HER2^+$ BC cell lines. Interestingly, circCDYL did not act as miR-92b-3p sponge, but was degraded in a miR-92b-3p dependent silencing manner.

MATERIALS AND METHODS

Cell Culture and Treatment

Normal human mammary epithelial cells (MCF-10A), HER2-negative BC cell lines (MCF-7, MDA-MB-231, and ZR75-1) and HER2-positive BC cell lines (AU565, MDA-MB-361, SK-BR-3, and BT474) were used in this study. All these cell lines were cultured as ATCC recommended. For transient transfection, 125 ng circCDYL over-expressing plasmid or 3 pmol siRNA (siRNA sequence shown in **Supplementary Table 1**) was added to cells with lipofectamine 3000 (Invitrogen, United States). Total RNA or protein was extracted 48 h after transfection.

Plate Colony Formation Assay

The SK-BR-3 or BT474 cells (3×10^3) were seeded in 6-well plates and were cultured for 3 weeks. The colonies were fixed with 4% formaldehyde for 10 min and stained with 1% crystal violet for 30 min. Image J software was used to calculate the colonies in each group.

Cell Counting Kit-8 Assay

The SK-BR-3 or BT474 cells (3×10^3) after treatment were seeded in 96-well plates. After 5 days, cellular viability of each group was determined by Cell Counting Kit-8 (Tongren, Japan).

Cell Counting Assay

Total of 5×10^4 SK-BR-3 or BT474 cells after treatment were cultured in 12-well plates. In continuous 5 days, cells were digested by trypsin, and re-suspended. Then cell suspension was added into cell-counting plate (Ruiyu Bio-science, China), and the cell number was calculated by cell counter (Countstar Bio-tech, IC100, China).

RNA Isolation and qRT-PCR

The total RNA of cell lines was collected by TRIzol reagent (Invitrogen, United States). The RNA was reverse transcribed to cDNA using RT SuperMix (Vazyme Biotech, China) according to the manufacturer's protocol. The real-time quantitative polymerase chain reaction (qRT-PCR) was performed by SYBR qRT-PCR Master Mix (Vazyme Biotech, China) on LightCycler 480 II system (Roche, Switzerland). The sequence of primers in this study were shown in **Supplementary Table 2**.

Western Blot Analysis

Cells were lysed in RIPA lysis buffer (BCA) kit (Lot 30342, Cwbio, China) was used to detect the concentration of protein. In electrophoresis process, 12% SDS-PAGE was used. The protein in the gels were transferred to PVDF membrane, and the membrane was incubated with 5% non-fat milk at room temperature. Primary antibody anti-β-actin (Cell Signaling Technology, 1:1,000), anti-PI3K (Cell Signaling Technology, 1:1,000), anti-p-PI3K (Cell Signaling Technology, 1:1,000), anti-AKT (Cell Signaling Technology, 1:1,000), anti-p-AKT (Cell Signaling Technology, 1:1,000) and anti-LC3 (Sigma-Aldrich, 1:1,000) were, respectively, added to the membrane and incubated at 4°C overnight. Secondary antibody (Cell Signaling Technology, 1:3,000) was added and incubated for 2 h at room temperature. Finally, the blots were detected by enhanced chemoluminescence kit (P90719, Millipore, United States) under Image Lab Software.

MiRNA Pull-Down Assay

MiRNA pulldown experiment was processed according to previous publication. Briefly, SK-BR-3 cells were transfected with

biotinylated miR-92b-3p mimic. After 24 h, transfected cells were harvested and fixed with formaldehyde for 30 min. Then the cells were lysed by co-IP buffer. C1 streptavid in magnetic beads was added to the mixture. Finally, total RNA was extracted as described and followed by qRT-PCR detection of circCDYL.

miRNAs Deep-Sequencing

RNA samples enriched by circCDYL probes in circRNAs pull-down assay was sent to Kangchen Bio-tech Company (Shanghai, China) for miRNA deep-sequencing and subsequent analysis. The raw data of miRNA deep-sequencing was uploaded to GEO database (GSE174541).

In situ Hybridization and Fluorescence *in situ* Hybridization

In situ hybridization (ISH) was performed to detect the expression of circCDYL and miR-92b-3p in paraffin-embedded sections from BC tissues or animal tumors. Briefly, the sections were digested with pepsin after dewaxing and rehydration, and hybridized with the digoxin-labeled circCDYL probe at 37°C overnight. Then the sections were incubated with anti-digoxin antibody overnight at 4°C and were stained with nitro blue tetrazolium/5-bromo-4-chloro-3-indolylphosphate. The staining scores were determined based on both the intensity and proportion of circCDYL. Total score = Σproportion × intensity. Intensity was recorded as 0 (no staining), 1 (light purple), 2 (purple blue), or 3 (dark purple). As for fluorescence *in situ* hybridization (FISH), Cy3-labeled probe for circCDYL and FAM-labeled probe for miR-92b-3p were used. These probes were designed and synthesized by Synbio-Tech Company (Guangzhou, China). Briefly, cells were cultured in a glass-bottom dish overnight and incubated with pre-hybridization solution at room temperature for 30 min. 20 μM of probes in hybridization solution was added to dish and hybridized overnight. After washing by SSC (saline sodium citrate), the dishes were incubated with DAPI for 10 min. Finally, the dishes were covered with coverslip and observed by confocal microscope.

CircRNA Pull-Down

CircRNA pull-down was performed as previously reported (Liang et al., 2020; Zhou C. et al., 2020). Briefly, SK-BR-3 was fixed with 1% formaldehyde and lysed by co-IP buffer and the cluster was sonicated. CircCDYL-specific and NC biotinylated probes were added to mixture to bind circCDYL. Next, C1 streptavidin magnetic beads was added to pull down circCDYL and circCDYL-binding RNA. Finally, total RNA was extracted from the magnetic beads and followed by qRT-PCR detection of circCDYL and miR-92b-3p.

Dual Luciferase Reporter Assay

Full-length sequence of circCDYL was inserted into psiCHECK-2 vectors (Synbio-tech, China). psiCHECK-2 vectors carrying NC mimic or miR-92b-3p mimic were co-transfected to SK-BR-3 cells, respectively. Dual-luciferase reporter assay system (Vazyme, Nanjing, China) was performed to detect luciferase activity of the transfected cells after 48 h transfection.

In vivo Breast Cancer Orthotopic Model

The breast cancer orthotopic model were performed in Forevergen Medical Corporation (Guangzhou, China), and all procedures were in accordance with the ethical guidelines of the institution. Briefly, we purchased 4-week-old female Balb/c nude mice from Nanjing Biomedical Research Institute of Nanjing University (Nanjing, China). SK-BR-3 cells (1×10^7) transduced with sh-NC or sh-circCDYL lentivirus were injected into the fourth left mammary fat pads of the nude mice ($n = 6$/group). The tumor growth of each group was recorded. After 44 days since tumor cell plantation, the mice were executed, and the tumor was made into paraffin-embedded sections.

Patient and Clinical Database

In this study, 50 $HER2^+$ BC patients and 70 $HER2^-$ BC patients from Sun Yat-sen Memorial Hospital (SYSMH) were enrolled. Enrolled patients were firstly diagnosed without any distant metastasis between 1st January 2010 and 31th December 2017. Paraffin-embedded BC tissue sections were collected for *in situ* hybridization (ISH). Clinicopathological material, such as age, molecular subtype, stage, survival, was collected and analyzed.

Statistical Analysis

GraphPad Prism 5 software was used for statistical analyses in this study. Student's *t*-test was performed to test statistical differences between two subgroups. X^2-test was applied to analyze the correlations between circCDYL expression and clinicopathological characterization of $HER2^+$ BC patients. Survival analysis of $HER2^+$ patients was evaluated by Kaplan–Meier plots and Log-rank tests. The univariate analyses were evaluated by Cox proportional hazards model. $P < 0.05$ was considered statistically significant.

RESULTS

CircCDYL Expression in HER2 + Breast Cancer Is Similar With That in $HER2^-$ Breast Cancer

To determine the expression of circCDYL in $HER2^+$ breast cancer, 50 $HER2^+$ patients and 70 $HER2^-$ patients were enrolled. *ISH* analysis revealed that circCDYL was elevated up to 1.63-folds in tumor tissues, compared to adjacent normal tissues of $HER2^+$ BC patients (n = 24) (**Figure 1A**). However, the expression level of circCDYL in $HER2^+$ BC tissues was similar to that in $HER2^-$ BC tissues (**Figure 1B**). In addition, the expression of circCDYL was detected by qRT-PCR in normal mammary epithelial cells (MCF-10A), $HER2^-$ BC cell lines (MCF-7, MDA-MB-231, and ZR75-1) and $HER2^+$ BC cell lines (AU565, MDA-MB-361, SK-BR-3, BT474). CircCDYL expression was obviously higher expressed in $HER2^+$ BC cell lines than normal mammary epithelial cells, slightly higher than that in

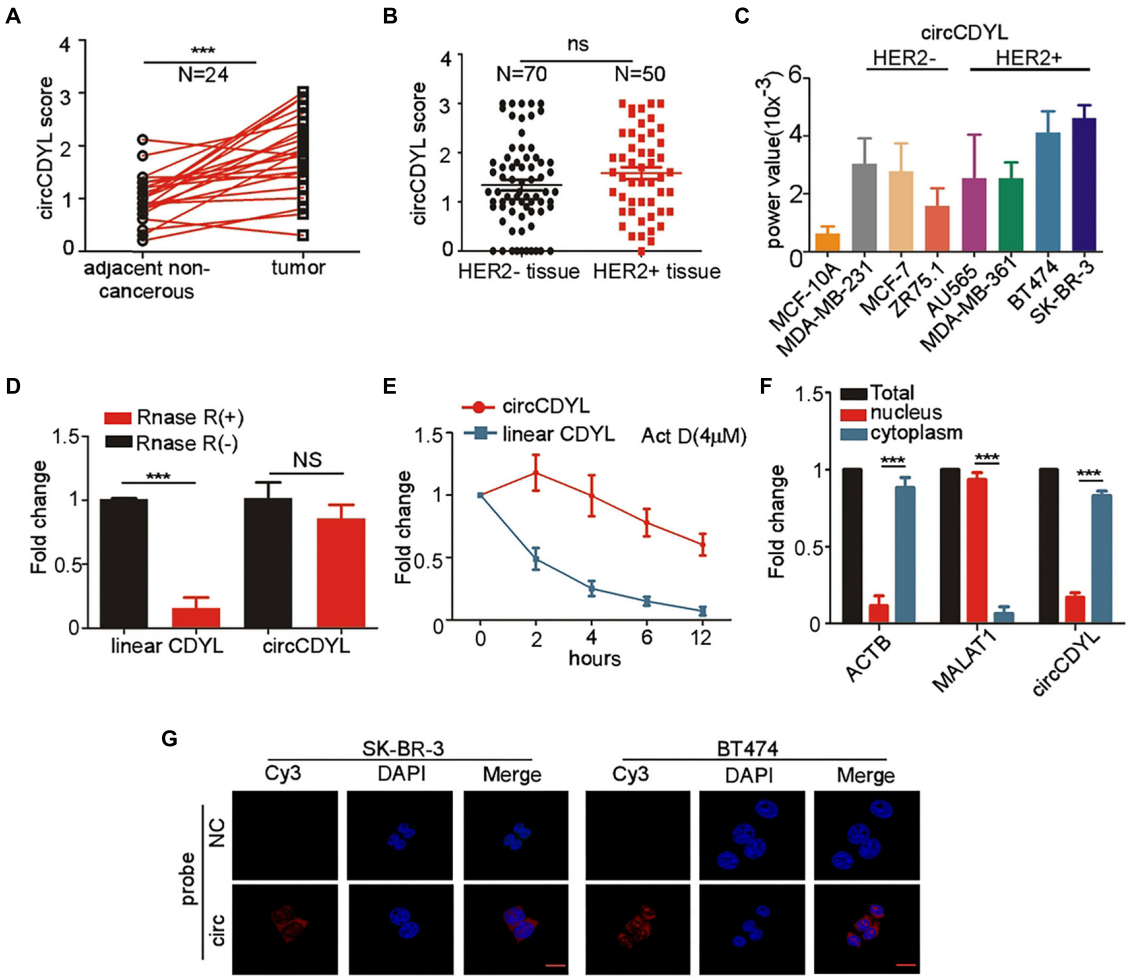

FIGURE 1 | CircCDYL is high-expressed in HER2$^+$ BC. **(A)** Comparison of circCDYL expression between HER2$^+$ BC tissues and paired adjacent non-cancerous tissues by *ISH* (n = 24). **(B)** Expression of circCDYL in HER2$^-$ BC tissues (n = 70) and HER2$^+$ BC tissues (n = 50), as detected by *ISH*. **(C)** Expression of circCDYL in normal mammary epithelial cells (MCF-10A), HER2$^-$ BC cell lines (MCF-7, MDA-MB-231, and ZR75-1) and HER2$^+$ BC cell lines (AU565, MDA-MB-361, SK-BR-3, and BT474), as detected by qRT-PCR. **(D)** Linear CDYL and circCDYL before or after RNase R digestion was detected by qRT-PCR. **(E)** qRT-PCR detection of circCDYL and linear CDYL in SK-BR-3 cells treated with Actinomycin D (4 μM) at various times. **(F)** qPCR analysis of circCDYL in the cytoplasm and nuclear separated from SK-BR-3 cells. **(G)** Cellular location of circCDYL in SK-BR-3 and BT474 cells, as detected by FISH. All experiments above were done for at least three times. ***P < 0.005. Error bars indicate Standard Error of Mean (S.E.M).

HER2$^-$ BC cell lines (**Figure 1C**). In addition, silencing HER2 gene in SK-BR-3 cells and over-expression of HER2 gene in HER2$^-$ BC cells (MCF- 7 and MDA-MB-231) had no effect on expression of circCDYL, indicating that HER2 gene do not regulate the expression circCDYL in HER2$^+$ cell (**Supplementary Figures 1A,B**).

CircCDYL (chr6:4,858,880-4,925,679) is derived from exon 4 of gene Chromodomain Y Like (CDYL). We further examined the characteristic of circCDYL. As shown in **Figures 1D,E**, circCDYL was more stable than parent CDYL linear RNA after RNase R digestion and more stable than CDYL linear RNA in living cells after inhibiting transcription of SK-BR-3 cells by actinomycin D (Act D, a transcription inhibitor). Moreover, we found that circCDYL mainly located in cytoplasm, as detected by nuclear-cytoplasm separation experiments (**Figure 1F**) and FISH in SK-BR-3 and BT474 cells (**Figure 1G**).

Over-Expression of circCDYL Promotes Cell Proliferation of HER2$^+$ BC Cells

Our previous study has showed that up-regulation of circCDYL augmented the cell proliferation and autophagy of HER2$^-$ BC cells (Liang et al., 2020), but the biological function of circCDYL in HER2$^+$ BC cells was not explored. Therefore, we investigated whether circCDYL could modulate the cell proliferation, one of the most important characteristics of cellular fates, in HER2$^+$ BC cells. In this study, silencing circCDYL by specific siRNAs or over-expressing circCDYL by plasmids could successfully decrease or increase circCDYL in HER2$^+$ BC cells without

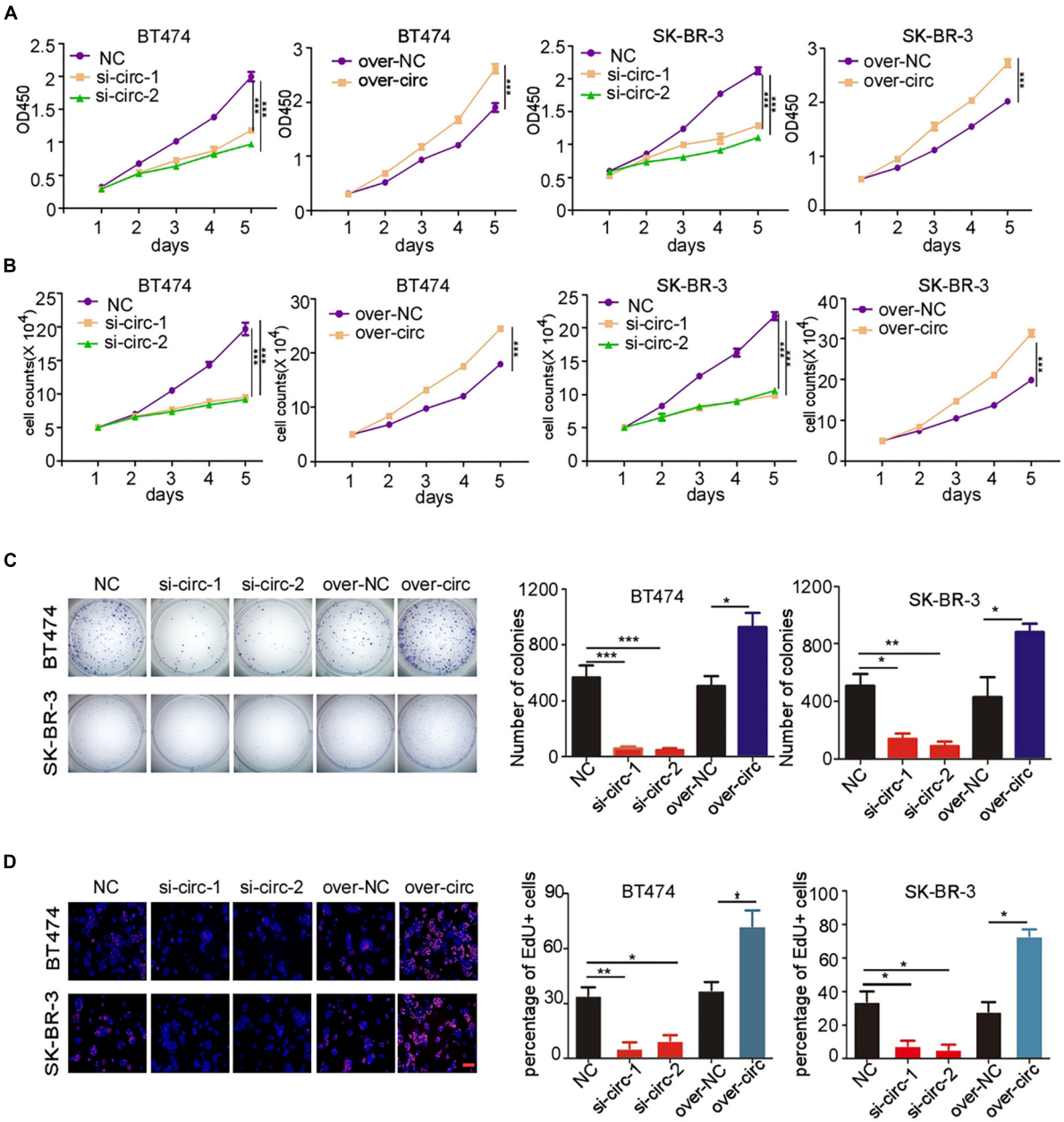

FIGURE 2 | circCDYL promotes proliferation of HER2$^+$ BC cells. **(A,B)** The proliferation of SK-BR-3 and BT474 cells after silencing circCDYL or over-expressing circCDYL, as detected by CCK-8 assay **(A)** and cell counting experiments **(B)**. **(C)** Proliferation of SK-BR-3 and BT474 cells, as detected by plate colony formation (left) and quantitative analysis of colonies of each group (right). **(D)** EdU staining in SK-BR-3 and BT474 cells under siRNA or over-expressing plasmid treatment (left) and the percentage of EdU positive cell in each group (right). *NC: negative control*. All experiments above were repeated at least three times. $^*P < 0.05$, $^{**}P < 0.01$, and $^{***}P < 0.005$. Error bars indicate S.E.M.

affecting the expression of CDYL linear RNA, as detected by qRT-PCR (**Supplementary Figures 1C,D**). Cell proliferation rate of HER2$^+$ BC cell lines SK-BR-3 and BT474 was impaired after silencing circCDYL but was augmented after over-expressing circCDYL, as detected by CCK-8 (**Figure 2A**) and cell-counting assays (**Figure 2B**). Similarly, plate colony formation and EdU staining experiments also indicated that circCDYL promoted the proliferation of HER2$^+$ BC cells (**Figures 2C,D**). As reported previously, circCDYL promoted the autophagosome formation of HER2$^-$ BC cells. However, silencing or over-expression of circCDYL had no effect on the autophagic level of SK-BR-3 in this study (**Supplementary Figure 1E**). All these suggest that circCDYL does not play similar roles in HER2$^+$ and HER2$^-$ BC cells, therefore, we next investigated the role of circCDYL in HER2$^+$ BC cells. Mechanically, over-expression of circCDYL promoted the activation of PI3K/AKT signal pathway

in SK-BR-3 cells (**Supplementary Figure 2A**). The promoting effect of circCDYL over-expression on proliferation was partly impaired by AKT inhibitor capivasertib (0.5 μM), as detected by CCK8 experiment (**Supplementary Figure 2B**), indicating that circCDYL promotes proliferation of HER2$^-$ BC cells through activating of PI3K/AKT signaling pathway.

CircCDYL Promotes Tumorigenesis of HER2$^+$ BC *in vivo*

To further investigate the biological role of circCDYL in HER2$^+$ BC *in vivo*, we established BC orthotopic model in Balb/c nude mice. The tumors derived from SK-BR-3 cells with stable knockdown of circCDYL grew slower than the control group (**Figure 3A**). The average tumor size of circCDYL knocking-down group was much smaller than NC group by measuring tumor sizes after tumor excision (**Figures 3B,C**). In addition, the percentage of Ki67 positive cells in circCDYL knocking-down tumors was significantly less than that in NC group (**Figure 3D**). The results above demonstrate that over-expression of circCDYL promotes the tumorigenesis of HER2$^+$ BC *in vivo*.

CircCDYL Is Degraded in a miR-92b-3p-Dependent Manner

MiRNA sponge was the most frequently reported mechanism of circRNAs, and circRNAs that can form circRNA-AGO2 complex are reported to have a potential to act as miRNA sponge. The AGO2 RIP experiment was performed in SK-BR-3 cells and showed that circCDYL was abundantly enriched by AGO2 antibody (**Figure 4A**). In our previous study, circCDYL acted as miR-1275 sponge in HER2$^-$ BC cells (MCF7 and MDA-MB-231) (Liang et al., 2020). However, circRNA pull-down experiments in SK-BR-3 indicated that miR-1275 was rarely enriched by circCDYL probes (**Supplementary Figure 3A**), which might be due to low expression of miR-1275 in HER2$^+$ BC cells (**Supplementary Figure 3B**). To find out circCDYL-binding miRNAs, miRNA deep-sequencing was performed to detect the RNA sample enriched by circCDYL pull-down experiment, and miRNAs candidates that were enriched by 10-folds or over were screened out (**Figure 4B**). Among the top 5 miRNA candidates, qRT-PCR analysis showed that only miR-92b-3p was verified to enrich by circCDYL probes in circRNA pull-down in SK-BR-3 cells (**Figure 4C** and **Supplementary Figure 3C**). Similarly, miRNA pull-down assay indicated that miR-92b-3p probes obviously enriched circCDYL (**Figure 4D**). By RNA hybrid online database, the 565nt of circCDYL was a strong binding site for miR-92b-3p (**Supplementary Figure 3D**). Co-location assay by FISH indicated that miR-92b-3p and circCDYL were overlapped in cytoplasm in both SK-BR-3 and BT474 cells (**Figure 4E**).

It has been reported that CREB3L2, TSC1, SGK3, and MEF2D are downstream genes of miR-92b-3b (Hu et al., 2017; Li T. et al., 2019; Ye et al., 2020; Huang et al., 2021). In HER2$^+$ BC cells, we found that these genes were down-regulated after miR-92b-3p mimics transfection in SK-BR-3 cells (**Supplementary Figure 3E**). However, silencing circCDYL had no effect on expression of CREB3L2, TSC1, SGK3 and MEF2D mRNA in SK-BR-3 cells (**Figure 4F**), suggesting that circCDYL may not act as miR-92b-3p sponge. Interestingly, circCDYL was down-regulated after miR-92b-3p mimic transfection and up-regulated after miR-92b-3p inhibitor transfection (**Figure 4G**), while silencing circCDYL had no effect on expression of miR-92b-3p in SK-BR-3 cells (**Supplementary Figure 3F**). AGO2, as an essential component of RNA-induced silencing complex (RISC), leads to gene silence in a siRNA or miRNA-dependent manner (Marzec, 2020). Therefore, we speculated whether circCDYL could be silenced in a miR-92b-3p dependent RISC manner. After silencing AGO2 or GW182 (another component in RISC complex) in SK-BR-3, expression of circCDYL was up-regulated significantly (**Supplementary Figure 3G**), suggesting that circCDYL was degraded in a RISC manner. In addition, a dual luciferase reporter (inserted full length of circCDYL) assay was performed, and miR-92b-3p mimic reduced the luciferase reporter activity by 68% (**Figure 4H**). While silencing either AGO2 or GW182 in SK-BR-3 cells, miR-92b-3p mimic transfection exhibited slight effect on circCDYL expression (**Figure 4I**), indicating circCDYL is silenced in a miR-92b-3p dependent RISC manner in HER2$^+$ cell.

Interestingly, miR-92b-3p mimic transfection decreased the expression of circCDYL in HER2$^-$ BC cells (MCF-7 and MDA-MB-231 cells) as well. When silencing either AGO2 or GW182 in MCF-7 and MDA-MB-231 cells, miR-92b-3p mimic transfection exhibited slight effect on circCDYL expression (**Supplementary Figure 4A**), indicating that miR-92b-3p- dependent RISC manner in degradation of circCDYL existed in HER2$^-$ BC cells as well as in HER2$^+$ BC cells. We compared the expression of miR-92b-3p in HER2$^-$ and HER2$^+$ BC cells, and miR-92b-3p was obviously higher expressed in HER2$^+$ BC cells than that in HER2$^-$ BC cells (**Supplementary Figure 4B**), indicating that miR-92b-3p- dependent RISCI manner on circCDYL may exhibit more effect in HER2$^+$ BC cells than in HER2$^-$ BC cells.

MiR-92b-3p Inhibits Cell Proliferation of HER2$^+$ BC Cells by Silencing circCDYL

Since the function of miR-92b-3p in BC was still unclear, we next investigated whether miR-92b-3p was involved in cell proliferation through regulation of circCDYL. CCK-8 assay showed that miR-92b-3p mimic transfection impaired proliferation rate of SK-BR-3 and BT474 cells (**Figure 5A**). The inhibitory effect of miR-92b-3p mimic in HER2$^+$ BC cells was partly rescued by over-expression of circCDYL (**Figure 5A**). The result of cell-counting assays and plate colony formation assay drew the similar conclusion (**Figures 5B,C**), indicating miR-92b-3p inhibits cell proliferation of HER2$^+$ BC cells *via* circCDYL degradation.

CircCDYL and miR-92b-3p Expression Correlates With Clinical Outcome of HER2$^+$ BC Patients

Expression of circCDYL and miR-92b-3p in tumor sections of 50 HER2$^+$ BC patients was detected by *ISH*. Pearson correlation analysis showed that miR-92b-3p expression was negatively correlated with circCDYL level (**Figure 6A**). We further analyzed

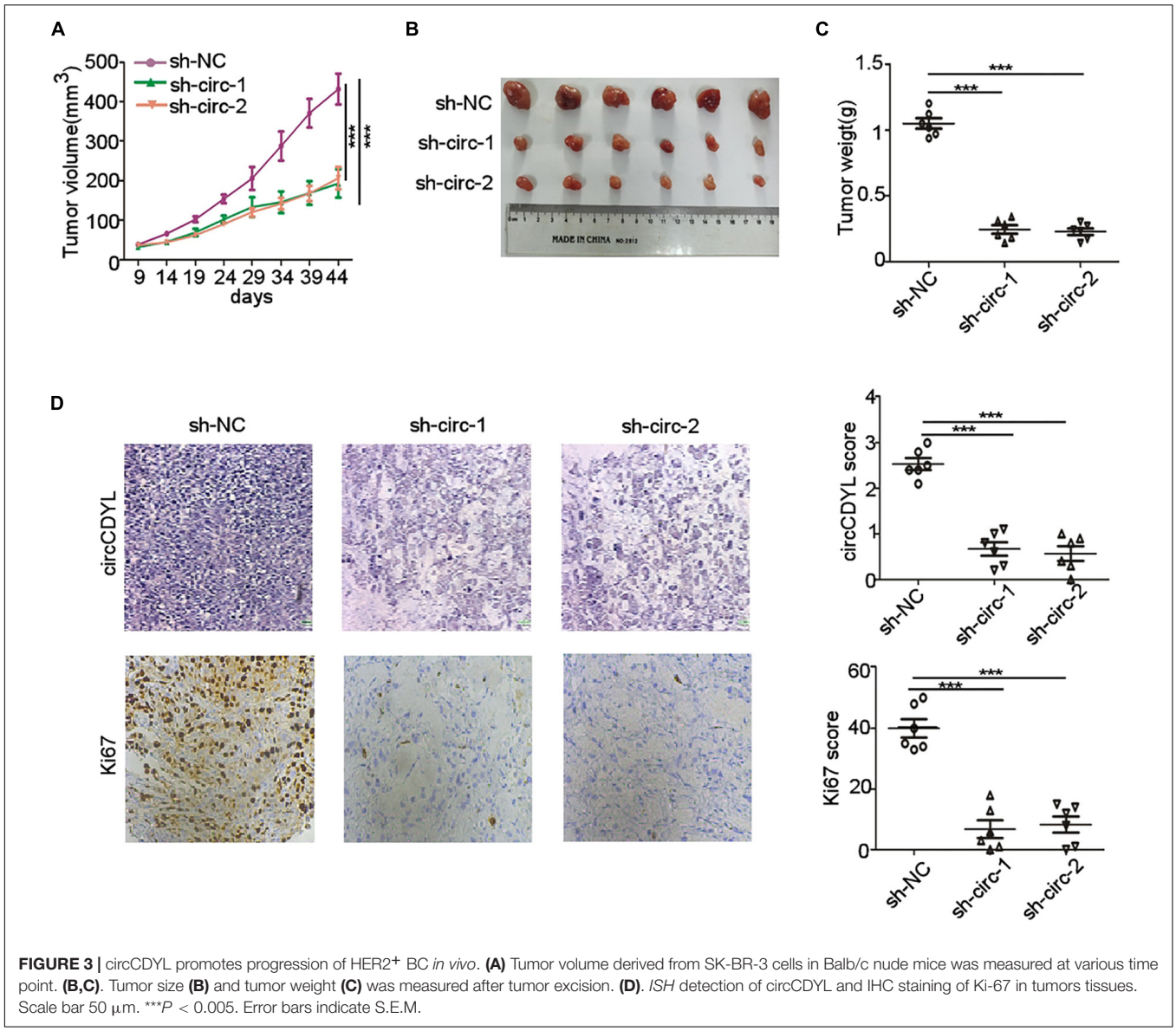

FIGURE 3 | circCDYL promotes progression of HER2$^+$ BC *in vivo*. **(A)** Tumor volume derived from SK-BR-3 cells in Balb/c nude mice was measured at various time point. **(B,C)**. Tumor size **(B)** and tumor weight **(C)** was measured after tumor excision. **(D)**. *ISH* detection of circCDYL and IHC staining of Ki-67 in tumors tissues. Scale bar 50 μm. ***$P < 0.005$. Error bars indicate S.E.M.

the relationship between the proliferative marker Ki67 and expression of circCDYL or miR-92b-3p, and found that the tumor with higher Ki67 index tended to have a lower expression of miR-92b-3p and higher expression of circCDYL (**Figure 6B**). Importantly, Kaplan–Meier analysis indicated that HER2$^+$ BC patients with higher expression of circCDYL exhibited a poorer disease-free survival (DFS) (HR = 6.327, $P = 0.0178$) (**Figure 6C**). Though patients with low expression of miR-92b-3p showed poorer DFS as well, the statistical significance was not found between miR-92b-3p low group and high group (HR = 0.296, $P = 0.113$) (**Figure 6C**).

DISCUSSION

Breast cancer (BC) is the most common malignant tumor and leading cause of death by tumor among female worldwide (Bray et al., 2018). Among these BC cases, around 15-20% is HER2$^+$ subtype, and the positive status of HER2 indicates poorer clinical outcome of BC patients. Tough numerous researches reveal the mechanism of HER2$^+$ BC progression, the underlying mechanisms, especially non-coding RNA, in progression of HER2$^+$ BC patients are not clear. Our previous study identified an autophagy-associated circRNA circCDYL, which promoted cell proliferation and autophagosome formation of HER2$^-$ BC cells *via* miR-1275 sponge. However, the role of circCDYL in regulating cellular fate of HER2$^+$ BC cells was not elucidated (Liang et al., 2020). Biological functional experiments proved that circCDYL promoted the proliferation of HER2$^+$ BC cells, but had no influence on autophagic level. Mechanism study indicated that circCDYL did not act as miR-1275 sponge in HER2$^+$ BC cells, as miR-1275 rarely expressed in HER2$^+$ BC cell lines.

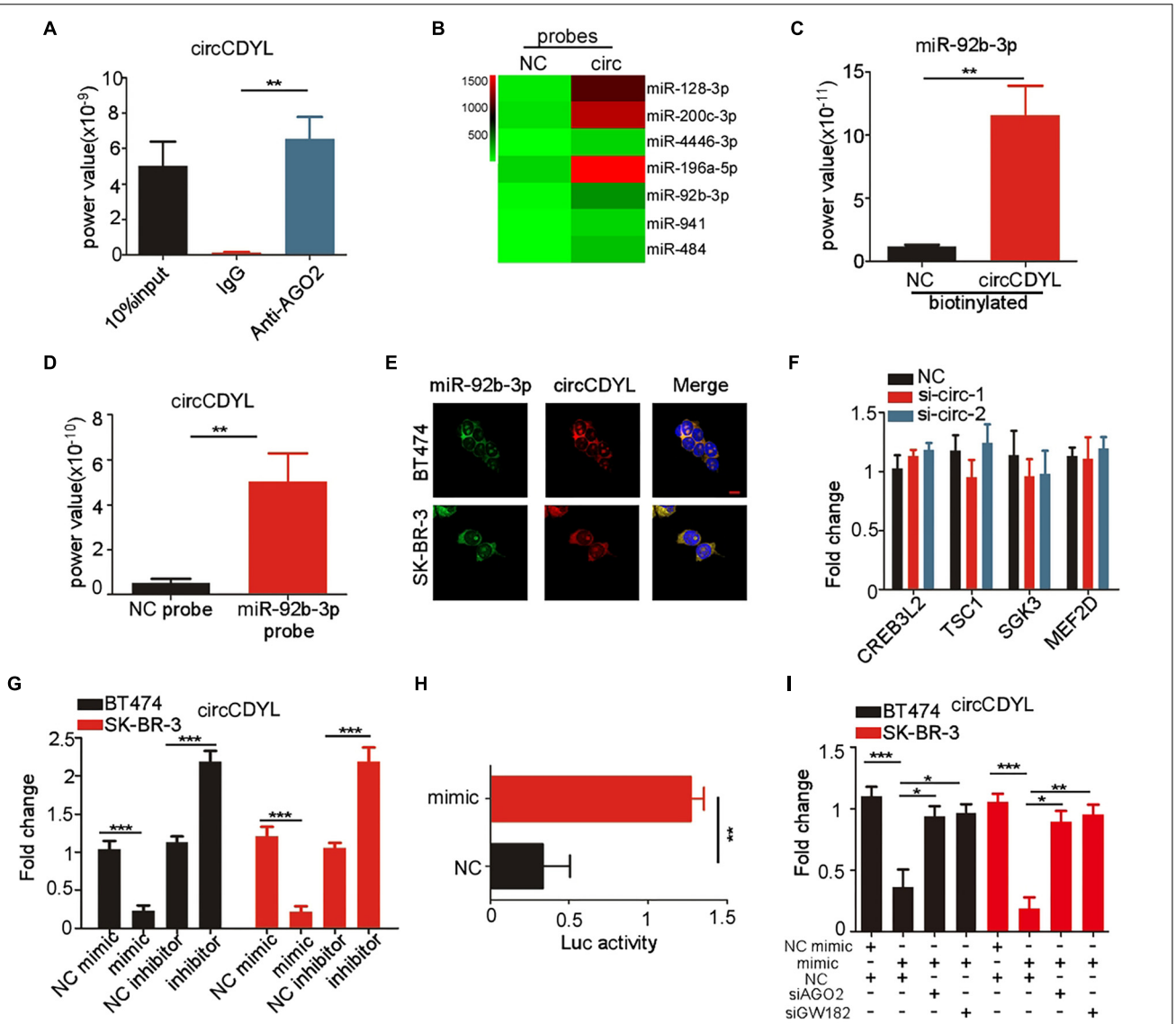

FIGURE 4 | circCDYL is degraded in miR-92b-3p-dependent RISC manner. **(A)** qRT-PCR detection of circCDYL in RNA sample pulled down by AGO2 antibody in RIP experiment. **(B)** MiRNA profile of RNA sample pulled down by circCDYL probes in circRNA pull-down assay, as detected by miRNA deep-sequencing. **(C)** qRT-PCR detection of miR-92b-3p in RNA sample pulled down by circCDYL probes in circRNA pull-down assay. **(D)** qRT-PCR detection of circCDYL in RNA sample pulled down by miR-92b-3p probes in miRNA pull-down assay. **(E)** FISH assay to detect the co-location of circCDYL and miR-92b-3p in BT474 and SK-BR-3 cells. **(F)** qRT-PCR detection of miR-92b-3p targeted genes (CREB3L2, TSC1, SGK3, and MEF2D) in SK-BR-3 cells after silencing circCDYL. **(G)** qRT-PCR detection of circCDYL in SK-BR-3 and BT474 cells after miR-92b-3p mimic or inhibitor transfection. **(H)** Dual luciferase assay in SK-BR-3 cells co-transfected with miR-92b-3p mimic and luciferase reporter plasmid (inserted with full length of circCDYL). **(I)** qRT-PCR detection of circCDYL in SK-BR-3 and BT474 cells after transfection of miR-92b-3p mimic or con-transfection of miR-92b-3p mimic and AGO2 or GW182 siRNA. All experiments above were repeated at least three times. $^{*}P < 0.05$, $^{**}P < 0.01$, and $^{***}P < 0.005$. Error bars indicate S.E.M.

The relationship between circCDYL and HER2 gene was further investigated. CircCDYL was commonly high-expressed in BC, no matter the statue of HER2 gene. Knocking down HER2 gene in HER2^{+} BC cells and over-expressing HER2 gene in HER2^{-} BC cell lines did not change the expression of circCDYL, indicating that HER2 gene did not regulate the expression of circCDYL. Though circCDYL promoted proliferation of both HER2^{+} and HER2^{-} BC cells, several mechanism of circCDYL was specific in HER2^{+} BC. Firstly, circCDYL promoted progression of BC mainly *via* miR-1275-ATG7/ULK1-autophagy axic in HER2^{-} BC (Liang et al., 2020), while circCDYL promoted progression of HER2^{+} BC *via* activation of PI3K-AKT pathway. Secondly, the manner of miR-92b-3p-dependent cleavage on circCDYL was specific in HER2^{+} BC cells, as miR-92b-3p rarely expressed in HER2- BC cells.

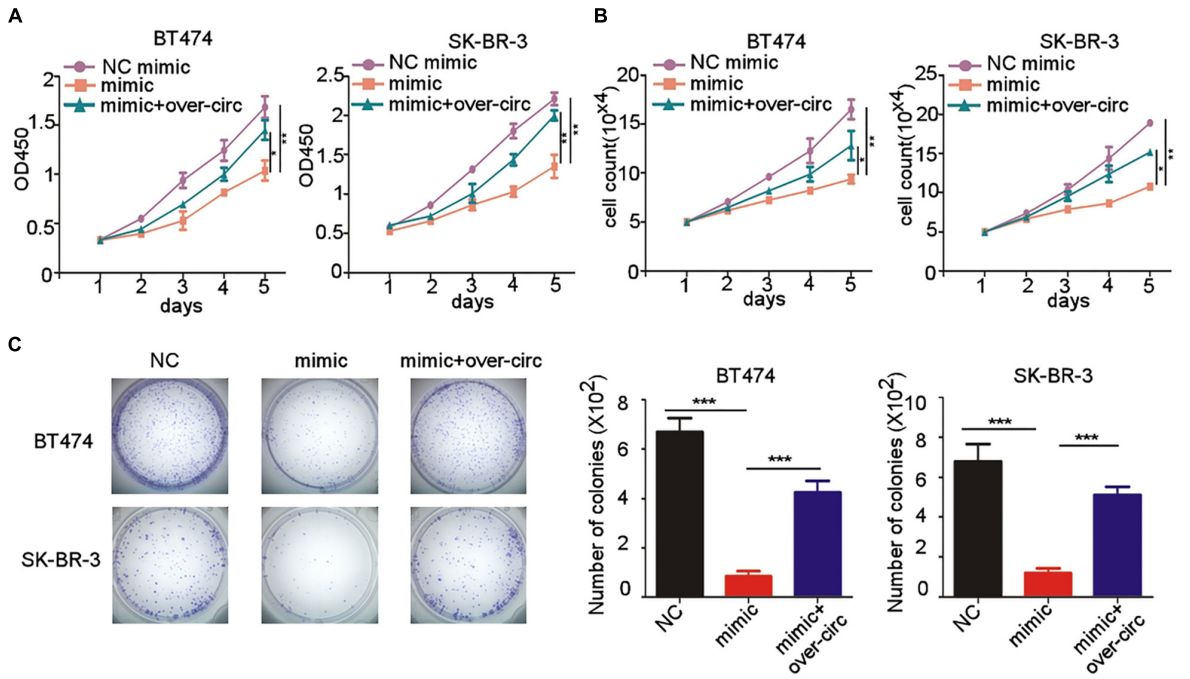

FIGURE 5 | miR-92b-3p inhibits proliferation of HER2$^+$ BC cells by down-regulation of circCDYL. **(A,B)** The proliferation of SK-BR-3 and BT474 cells after transfection of miR-92b-3p mimic or co-transfection of miR-92b-3p mimic and circCDYL over-expressing plasmid, as detected by CCK-8 assay **(A)** and cell counting experiments **(B)**. **(C)** Plate colony formation to detect the proliferation of SK-BR-3 and BT474 cells after transfection of miR-92b-3p mimic or co-transfection of miR-92b-3p mimic and circCDYL over-expressing plasmid (left), and quantitative analysis of colonies of each group (right). $^*P < 0.05$, $^{**}P < 0.01$, and $^{***}P < 0.005$. Error bars indicate S.E.M.

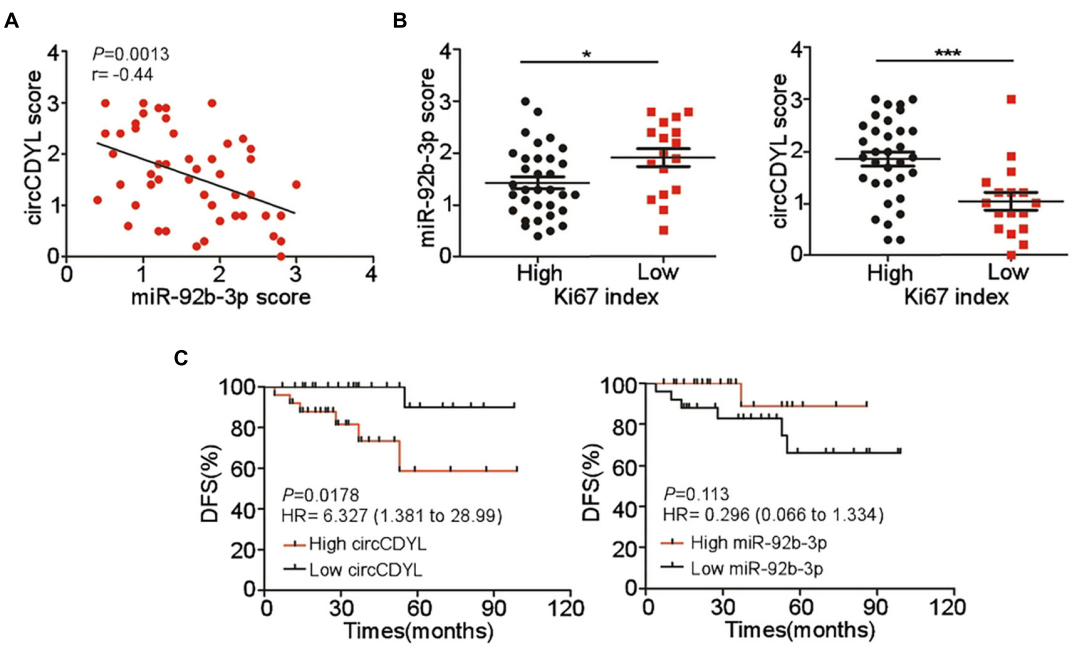

FIGURE 6 | Clinical significance of circCDYL and miR-92b-3p in HER2$^+$ BC. **(A)** The correlations between the expression of circCDYL and miR-92b-3p, as detected by ISH in 50 HER2$^+$ BC patient. **(B)** The expression of miR-92b-3p and circCDYL in HER2$^+$ BC patients with high Ki67 index (> 14%) and low Ki67 index (< =14%). **(C)** Kaplan–Meier analysis of Disease-free survival of HER2$^+$ BC patients (n = 50) with high/low expression of circCDYL (left) or miR-92b-3p (right).

In addition, several interesting findings in mechanism of circRNA were reported in this study. Firstly, published evidences shows that the circRNAs act as miRNA sponge if these circRNAs can form AGO2-circRNA complex (Huang et al., 2019; Liang et al., 2020; Zhou C. et al., 2020). In this study, we found that circCDYL could form AGO2-circCDYL complex, and could strongly interact with miR-92b-3p in $HER2^+$ BC cells. However, circCDYL had no influence on expression of miR-92b-3p targeted genes, indicating that circCDYL did not act as miR-92b-3p sponge in $HER2^+$ BC cell lines. The results above suggested that AGO2-circRNA complex was not a gold standard to reveal miRNA sponge potential of circRNAs. Secondly, AGO2 is an important component of RISC complex, and RISC complex exhibits nuclease function in degradation of RNA (Marzec, 2020). Interestingly, miR-92b-3p mimic transfection resulted in down-regulation of circCDYL in both $HER2^+$ and $HER2^-$ BC cells, and AGO2 silencing could almost prevent the down-regulation of circCDYL from miR-92b-3p mimic transfection, indicating that circCDYL was degraded in a miR-92b-3p dependent RISC manner. Several researches have discussed about the degradation of circRNA. For example, RNase L was reported to degrade circRNAs when the cell was infected by virus (Liu et al., 2019), and structure-mediated RNA decay induced by UPF1 and G3BP1 protein was important pathway for degradation of circRNAs (Fischer et al., 2020). Our study provides a new mechanism of circRNA degradation that miRNA-dependent RISC manner is an alternative way for cleanup of circRNAs in eukaryotic cells. Thirdly, circCDYL acted as miR-1275 sponge in $HER2^-$ BC cells (Liang et al., 2020), but did not act the same way in $HER2^+$ BC cell, as miR-1275 was rarely expressed in $HER2^-$ BC cell lines. These findings indicated that mechanism of circRNAs was various in different subtypes of breast cancer, and mechanism of circRNA was dependent on the expression of downstream genes.

The role of miR-92b-3p in cancer is contentious. MiR-92b-3p exhibited tumor-promoting role in proliferation, migration and invasion of colorectal, renal, gastric and prostate cancer cells (Gong et al., 2018; Li C. et al., 2019; Wang et al., 2020; Wang G. et al., 2021). On the contrary, miR-92b-3p suppresses tumor progression of pancreatic cancer by targeting Gabra3 (Long et al., 2017). However, the role of miR-92b-3p is unclear in BC, and this is the first study to reveal the biological function of miR-92b-3p in BC. In this study, we found that MiR-92b-3p acted as a tumor-repressive miRNA and inhibited cell proliferation of BC cells by down-regulation of circCDYL.

Breast cancer is a subtype with poor clinical outcome, and identifying new biomarkers for predicting prognosis of BC patients is of tremendous clinical significance. CircRNA and miRNA are proved to be stable and abundant, and exhibits disease-specific characteristic in eukaryotic cells, for which both of them are considered to be ideal biomarkers for human diseases (Jahani et al., 2020; Galvão-Lima et al., 2021). In this study, we identified the stability of circCDYL in $HER2^+$ BC cells. CircCDYL was up-regulated in tumor tissues of $HER2^+$ BC patients when comparing with the adjacent normal tissues. Importantly, high expression of circCDYL or low expression of miR-92b-3p was associated with poor disease-free survival of $HER2^+$ BC patients. Therefore, our finding provided two potential biomarkers for $HER2^+$ BC patients. For the patients with high expression of circCDYL or low expression of miR-92b-3p, more aggressive treatment or closer follow-up should be considered. CircCDYL exhibited powerful biological function in regulating cellular fate in both $HER2^+$ and $HER2^-$ BC cells, for which circCDYL might be a potential therapeutic target for BC patients.

In this study, circCDYL was proved to promote proliferation of $HER2^+$ BC cells *via* the activation of PI3K/AKT signal pathway, however, the downstream mechanism how circCDYL promoted activation of PI3K/AKT signal pathway remain largely unknown. In this research, no other miRNAs except miR-92b-3p was found to interact with circRNAs, and we had no evidence to prove the miRNA sponge potential of circCDYL in $HER2^+$ BC cells. In addition, circCDYL mainly located in the cytoplasm of $HER2^+$ BC cell and could not promote transcription of gene by interacting with pol-II protein. Moreover, circCDYL exhibited little possibility to be a protein translation template, for the reason that circCDYL did not have open reading frame (ORF) and internal ribosome entry site (IREs), as predicted by circRNAdb online database. Enormous studies determine that circRNAs can regulate biological function of cancer cells by interacting with protein (Du et al., 2016, 2018; Sun et al., 2019). CircCDYL might promote cell proliferation of $HER2^+$ BC cells by interacting with certain protein, which involve in the activation of PI3K/AKT pathway.

DATA AVAILABILITY STATEMENT

The datasets presented in this study can be found in online repositories. The names of the repository/repositories and accession number(s) can be found below: https://www.ncbi.nlm.nih.gov/geo/query/acc.cgi?acc=GSE174541, accession number: GSE174541.

ETHICS STATEMENT

The studies involving human participants were reviewed and approved by Sun Yat-sen Memorial Hospital, Sun Yat-sen University. The patients/participants provided their written informed consent to participate in this study. The animal study was reviewed and approved by Forevergen Medical Corporation (Guangzhou, China), and all procedures were in accordance with the ethical guidelines of the institution.

AUTHOR CONTRIBUTIONS

GL and YL contributed to the acquisition, analysis, and interpretation of the data and drafting of the manuscript. QL, YS, QL, YC, MM, and AH contributed to the data collections and manuscript review and drafting of the manuscript. CG and JL supervised the study. All authors read and approved the final manuscript.

FUNDING

This work was supported by the National Key R&D Program of China (2017YFC1309103 and 2017YFC1309104); the Natural Science Foundation of China (81672594, 81772836, 81872139, 82072907, and 8203000408); Clinical Innovation Project of Bioland Laboratory (Guangzhou Regenerative Medicine and Health Guangdong Laboratory, 2018GZR0201004); Sun Yat-sen memorial hospital cultivation project for clinical research (SYS-C-201805); Key Projects of The National Natural Science Foundation of China (51861125203); Project of The Beijing Xisike Clinical Oncology Research Foundation (Y-Roche2019/2-0078); Technology Development Program of Guangdong Province (2021A0505030082); and Project of The Guangdong Provincial Key Laboratory of Malignant Tumor Epigenetics and Gene Regulation (2020B1212060018OF007).

SUPPLEMENTARY MATERIAL

The Supplementary Material for this article can be found online at: https://www.frontiersin.org/articles/10.3389/fcell.2021.707049/full#supplementary-material

REFERENCES

Bray, F., Ferlay, J., Soerjomataram, I., Siegel, R. L., and Torre, L. A. (2018). Global cancer statistics 2018: globocan estimates of incidence and mortality worldwide for 36 cancers in 185 countries. *CA Cancer J. Clin.* 68, 394–424. doi: 10.3322/caac.21492

DeSantis, C. E., Ma, J., Gaudet, M. M., Newman, L. A., Miller, K. D., Sauer, A., et al. (2019). Breast cancer statistics, 2019. *CA: Cancer J. Clin.* 69, 438–451. doi: 10.3322/caac.21583

Du, W. W., Yang, W., Li, X., Awan, F. M., and Yang, Z. (2018). A circular RNA circDNMT1 enhances breast cancer progression by activating autophagy. *Oncogene* 37, 5829–5842. doi: 10.1038/s41388-018-0369-y

Du, W. W., Yang, W., Liu, E., Yang, Z., Dhaliwal, P., Yang, B. B., et al. (2016). Foxo3 circular RNA retards cell cycle progression via forming ternary complexes with p21 and CDK2. *Nucleic Acids Res.* 44, 2846–2858. doi: 10.1093/nar/gkw027

Fischer, J. W., Busa, V. F., Shao, Y., and Leung, A. (2020). Structure-mediated RNA decay by UPF1 and G3BP1. *Mol. Cell* 78, 70–84. doi: 10.1016/j.molcel.2020.01.021

Galvão-Lima, L. J., Morais, A., Valentim, R., and Barreto, E. (2021). MiRNAs as biomarkers for early cancer detection and their application in the development of new diagnostic tools. *Biomed. Eng. Online* 20:21. doi: 10.1186/s12938-021-00857-9

Gong, L., Ren, M., Lv, Z., Yang, Y., and Wang, Z. (2018). MiR-92b-3p promotes colorectal carcinoma cell proliferation, invasion, and migration by inhibiting FBXW7 in vitro and in vivo. *DNA Cell Biol.* 37, 501–511. doi: 10.1089/dna.2017.4080

Hu, Z. Q., Luo, J. F., Yu, X. J., Zhu, J. N., and Huang, L. (2017). Targeting myocyte-specific enhancer factor 2D contributes to the suppression of cardiac hypertrophic growth by miR-92b-3p in mice. *Oncotarget* 8, 92079–92089. doi: 10.18632/oncotarget.20759

Huang, W., Fang, K., Chen, T. Q., Zeng, Z. C., and Sun, Y. M. (2019). CircRNA circAF4 functions as an oncogene to regulate MLL-AF4 fusion protein expression and inhibit MLL leukemia progression. *J. Hematol. Oncol.* 12:103. doi: 10.1186/s13045-019-0800-z

Huang, W., Ji, R., Ge, S., Zhou, D., and Liu, Z. (2021). MicroRNA-92b-3p promotes the progression of liver fibrosis by targeting CREB3L2 through the JAK/STAT signaling pathway. *Pathol. Res. Pract.* 219:153367. doi: 10.1016/j.prp.2021.153367

Jahani, S., Nazeri, E., Majidzadeh-A, K., Jahani, M., and Esmaeili, R. (2020). Circular RNA; A new biomarker for breast cancer: a systematic review. *J. Cell Physiol.* 235, 5501–5510. doi: 10.1002/jcp.29558

Legnini, I., Di Timoteo, G., Rossi, F., Morlando, M., and Briganti, F. (2017). Circ-ZNF609 is a circular RNA that can be translated and functions in myogenesis. *Mol. Cell* 66, 22–37. doi: 10.1016/j.molcel.2017.02.017

Li, C., Huo, B., Wang, Y., and Cheng, C. (2019). Downregulation of microRNA-92b-3p suppresses proliferation, migration, and invasion of gastric cancer SGC-7901 cells by targeting Homeobox D10. *J. Cell Biochem.* 120, 17405–17412. doi: 10.1002/jcb.29005

Li, T., Liu, X., Gong, X., E, Q., and Zhang, X. (2019). MicroRNA 92b-3p regulates primordial follicle assembly by targeting TSC1 in neonatal mouse ovaries. *Cell Cycle* 18, 824–833. doi: 10.1080/15384101.2019.1593648

Li, Z., Huang, C., Bao, C., Chen, L., Lin, M., Wang, X., et al. (2015). Exon-intron circular RNAs regulate transcription in the nucleus. *Nat. Struct. Mol. Biol.* 22, 256–264. doi: 10.1038/nsmb.2959

Liang, G., Ling, Y., Mehrpour, M., Saw, P. E., Liu, Z., Tan, W., et al. (2020). Autophagy-associated circRNA circCDYL augments autophagy and promotes breast cancer progression. *Mol. Cancer* 19:65. doi: 10.1186/s12943-020-01152-2

Liu, C. X., Li, X., Nan, F., Jiang, S., Gao, X., Gao, S. K., et al. (2019). Structure and degradation of circular RNAs regulate PKR activation in innate immunity. *Cell* 177, 865–880. doi: 10.1016/j.cell.2019.03.046

Long, M., Zhan, M., Xu, S., Yang, R., Chen, W., Zhang, S., et al. (2017). MiR-92b-3p acts as a tumor suppressor by targeting Gabra3 in pancreatic cancer. *Mol. Cancer* 16:167. doi: 10.1186/s12943-017-0723-7

Marzec, M. (2020). New insights into the function of mammalian Argonaute2. *PLoS Genet.* 16:e1009058. doi: 10.1371/journal.pgen.1009058

Memczak, S., Jens, M., Elefsinioti, A., Torti, F., Krueger, J., Rybak, A., et al. (2013). Circular RNAs are a large class of animal RNAs with regulatory potency. *Nature* 495, 333–338. doi: 10.1038/nature11928

Sun, S., Wang, W., Luo, X., Li, Y., Liu, B., Li, Z., et al. (2019). Circular RNA circ-ADD3 inhibits hepatocellular carcinoma metastasis through facilitating EZH2 degradation via CDK1-mediated ubiquitination. *Am. J. Cancer Res.* 9, 1695–1707.

Wang, C., Uemura, M., Tomiyama, E., Matsushita, M., Koh, Y., Nakano, K., et al. (2020). MicroRNA-92b-3p is a prognostic oncomiR that targets TSC1 in clear cell renal cell carcinoma. *Cancer Sci.* 111, 1146–1155. doi: 10.1111/cas.14325

Wang, G., Cheng, B., Jia, R., Tan, B., and Liu, W. (2021). Altered expression of microRNA-92b-3p predicts survival outcomes of patients with prostate cancer and functions as an oncogene in tumor progression. *Oncol. Lett.* 21:4. doi: 10.3892/ol.2020.12265

Wang, L., Yi, J., Lu, L. Y., Zhang, Y. Y., Wang, L., Hu, G., et al. (2021). Estrogen-induced circRNA, circPGR, functions as a ceRNA to promote estrogen receptor-positive breast cancer cell growth by regulating cell cycle-related genes. *Theranostics* 11, 1732–1752. doi: 10.7150/thno.45302

Yang, R., Xing, L., Zheng, X., Sun, Y., Wang, X., Chen, J., et al. (2019). The circRNA circAGFG1 acts as a sponge of miR-195-5p to promote triple-negative breast cancer progression through regulating CCNE1 expression. *Mol. Cancer* 18:4. doi: 10.1186/s12943-018-0933-7

Yang, Y., Gao, X., Zhang, M., Yan, S., and Sun, C. (2018). Novel role of FBXW7 circular RNA in repressing glioma tumorigenesis. *JNCI: J. Natl. Cancer Institute* 110, 304–315. doi: 10.1093/jnci/djx166

Ye, Z., Shi, J., Ning, Z., Hou, L., Hu, C. Y., Wang, C., et al. (2020). MiR-92b-3p inhibits proliferation and migration of C2C12 cells. *Cell Cycle* 19, 2906–2917. doi: 10.1080/15384101.2020.1827511

Yu, C. Y., and Kuo, H. C. (2019). The emerging roles and functions of circular RNAs and their generation. *J. Biomed. Sci.* 26:29. doi: 10.1186/s12929-019-0523-z

Zhang, M., Zhao, K., Xu, X., Yang, Y., Yan, S., Wei, P., et al. (2018). A peptide encoded by circular form of LINC-PINT suppresses oncogenic transcriptional elongation in glioblastoma. *Nat. Commun.* 9:4475. doi: 10.1038/s41467-018-06862-2

Zhang, Y., Zhang, X. O., Chen, T., Xiang, J. F., Yin, Q. F., Xing, Y., et al. (2013). Circular intronic long noncoding RNAs. *Mol. Cell* 51, 792–806. doi: 10.1016/j.molcel.2013.08.017

Zhou, C., Liu, H. S., Wang, F. W., Hu, T., and Liang, Z. X. (2020). CircCAMSAP1 promotes tumor growth in colorectal cancer via the miR-328-5p/E2F1 axis. *Mol. Ther.* 28, 914–928. doi: 10.1016/j.ymthe.2019.12.008

Zhou, Y., Liu, X., Lan, J., Wan, Y., and Zhu, X. (2020). Circular RNA circRPPH1 promotes triple-negative breast cancer progression via the miR-556-5p/YAP1 axis. *Am. J. Transl. Res.* 12, 6220–6234.

Conflict of Interest: The authors declare that the research was conducted in the absence of any commercial or financial relationships that could be construed as a potential conflict of interest.

Publisher's Note: All claims expressed in this article are solely those of the authors and do not necessarily represent those of their affiliated organizations, or those of the publisher, the editors and the reviewers. Any product that may be evaluated in this article, or claim that may be made by its manufacturer, is not guaranteed or endorsed by the publisher.

frontiers in Cell and Developmental Biology

MINI REVIEW
published: 12 August 2021
doi: 10.3389/fcell.2021.727429

Opposite Roles for ZEB1 and TMEJ in the Regulation of Breast Cancer Genome Stability

Mélanie K. Prodhomme[1,2†], Sarah Péricart[3], Roxane M. Pommier[4], Anne-Pierre Morel[1,2], Anne-Cécile Brunac[3], Camille Franchet[3], Caroline Moyret-Lalle[1,2], Pierre Brousset[3], Alain Puisieux[1,5], Jean-Sébastien Hoffmann[3] and Agnès Tissier[1,2]**

[1] INSERM 1052, CNRS 5286, Centre Léon Bérard, Cancer Research Centre of Lyon, Équipe Labellisée Ligue Contre le Cancer, Université de Lyon, Université Claude Bernard Lyon 1, Lyon, France, [2] LabEx DEVweCAN, Université de Lyon, Lyon, France, [3] Laboratoire d'Excellence Toulouse Cancer (TOUCAN), Laboratoire de Pathologie, Institut Universitaire du Cancer-Toulouse, Toulouse, France, [4] Gilles Thomas Bioinformatics Platform, Centre Léon Bérard, Cancer Research Centre of Lyon, Lyon, France, [5] Institut Curie, Versailles Saint-Quentin-en-Yvelines University, PSL Research University, Paris, France

Breast cancer cells frequently acquire mutations in faithful DNA repair genes, as exemplified by BRCA-deficiency. Moreover, overexpression of an inaccurate DNA repair pathway may also be at the origin of the genetic instability arising during the course of cancer progression. The specific gain in expression of *POLQ*, encoding the error-prone DNA polymerase Theta (POLθ) involved in theta-mediated end joining (TMEJ), is associated with a characteristic mutational signature. To gain insight into the mechanistic regulation of *POLQ* expression, this review briefly presents recent findings on the regulation of *POLQ* in the claudin-low breast tumor subtype, specifically expressing transcription factors involved in epithelial-to-mesenchymal transition (EMT) such as ZEB1 and displaying a paucity in genomic abnormality.

Keywords: epithelial to mesenchymal transition, DNA Repair, TMEJ, DNA polymerase theta, replicative stress

OPEN ACCESS

Edited by:
Lin Deng,
Shenzhen Bay Laboratory, China

Reviewed by:
Zhuobin Liang,
Shenzhen Bay Laboratory, China
Xiangyu Liu,
Shenzhen University, China

***Correspondence:**
Jean-Sébastien Hoffmann
jean-sebastien.hoffmann@inserm.fr
Agnès Tissier
agnes.tissier@inserm.fr

†Present address:
Mélanie K. Prodhomme,
Department of Epigenetics and Molecular Carcinogenesis, University of Texas MD Anderson Cancer Center, Houston, TX, United States

Specialty section:
This article was submitted to Cell Growth and Division, a section of the journal Frontiers in Cell and Developmental Biology

Received: *18 June 2021*
Accepted: *23 July 2021*
Published: *12 August 2021*

Citation:
Prodhomme MK, Péricart S, Pommier RM, Morel A-P, Brunac A-C, Franchet C, Moyret-Lalle C, Brousset P, Puisieux A, Hoffmann J-S and Tissier A (2021) Opposite Roles for ZEB1 and TMEJ in the Regulation of Breast Cancer Genome Stability. Front. Cell Dev. Biol. 9:727429. doi: 10.3389/fcell.2021.727429

INTRODUCTION

Genetic abnormalities have been largely described as a major hallmark of cancer. Typically, dysfunctional faithful DNA repair is at the origin of the numerous genomic aberrations driving malignant transformation by endowing cells with adaptive and proliferative advantages (Hanahan and Weinberg, 2011).

DNA double-strand break (DSB) repair pathways are generally classified into two categories, namely homologous recombination (HR) and canonical non-homologous end joining (cNHEJ). HR requires 5′ to 3′ end resection, RAD51 loading, strand invasion and DNA synthesis using an intact homologous template. In contrast, cNHEJ does not necessitate a homologous template and is instead dependent on the KU complex, DNA-PKcs, and XRCC4/LIG4. Alternative end joining pathways (Alt-EJ) including microhomology-mediated end joining (MMEJ) has also been described, which in contrast to cNHEJ acts on the 5′ to 3′ resected DSB HR intermediates. Additionally, MMEJ relies on DNA synthesis directed by short tracts of flanking microhomology leading to typical patterns of microhomology-flanked deletions and insertions. The proteins involved in MMEJ include the 5′ to 3′ resection factors MRE11, RAD50, NBN, CtIP, and EXO1 as well as PARP1 and LIG3. However, the most prominent factor associated with MMEJ is the DNA polymerase Theta (POLθ) encoded by the *POLQ* gene. POLθ is a unique multifunctional enzyme with an N-terminal helicase-like domain linked by a central region to a C-terminal A-family DNA

polymerase domain (Seki et al., 2003). As a consequence of the major involvement of POLθ, MMEJ has also been termed theta-mediated end joining (TMEJ) (Schimmel et al., 2017, 2019).

Recently, in the context of mammary cancer, high *POLQ* expression was observed in the most genomically unstable breast cancer subgroup containing HR-deficient tumors (Prodhomme et al., 2021). Conversely, in a subgroup distinguished by low genomic instability, a low frequency of TP53 mutations (Morel et al., 2017) and expression of epithelial-to-mesenchymal transition (EMT) features, as well as low *POLQ* expression were detected (Prodhomme et al., 2021). The EMT program, naturally inducing a phenotypic switch during embryonic development or adult tissue homeostasis by the transcriptional repression of epithelial factors, such as E-cadherin (CDH1 gene), may be expressed during tumorigenesis to confer epithelial-to-mesenchymal plasticity to cancer cells, which then acquire stem-like properties (Ye and Weinberg, 2015; Brabletz et al., 2018; Stemmler et al., 2019). Various transcription factors have been shown to orchestrate EMT, named the EMT inducing-transcription factors (EMT-TF), as Zinc finger E-box binding homeobox 1 (ZEB1). ZEB1 is associated with chemo-resistance and radio-resistance properties partly attributed to phosphorylation of ZEB1 by Ataxia-telangiectasia-mutated (ATM) (Zhang et al., 2014) and to the ZEB1 transcriptional activation of ATM (Zhang et al., 2018). ATM is a central regulator of DNA damage response (DDR) signaling which channels DSB repair into the process of HR.

Several aspects of the mechanisms underlying the choice of DNA repair pathway remain unanswered. Numerous studies have shown that individually both DNA damage repair pathways and the EMT process can be hijacked to promote cancer. What if these mechanisms were interconnected during cancer initiation and/or progression? Here, we address the relationship between replication stress generated by tumor initiation and/or progression and TMEJ or EMT features, and how these factors/processes ultimately contribute to genomic stability.

SUBSECTIONS:

Replication Stress, Genomic Instability, and Cancer Progression

Genome stability is compromised by exogenous insults such as chemical carcinogens and ionizing radiation. Endogenously-induced DNA damage generated during the process of chromosome duplication can also affect the stability of the genome. Then, DNA replication forks can be slowed down or stalled by various natural replication barriers, a process referred to as replication stress (RS) (Zeman and Cimprich, 2014; Macheret and Halazonetis, 2015). RS is detected at early stages of tumorigenesis and is generally considered to be the driving force behind cancer progression (Bartkova et al., 2005; Gorgoulis et al., 2005; Negrini et al., 2010). Indeed, oncogene-driven cell proliferation induces a high level of RS, arising notably from the perturbation of replication origin activation and timing as well as increased conflicts between replication and transcription. It results in under-replicated regions and the persistence of stalled and collapsed forks become major sources of chromosome breakage and instability. If two converging replication forks stall with no licensed origin in-between, a double fork stalling event occurs and the replication of this stretch of DNA has a high probability of being compromised. The main consequence of a double fork stalling event is the generation of under-replicated parental DNA (UR-DNA; also called "unreplicated DNA"), which can persist when the cells enter mitosis and lead to chromosomal breaks inheritable by the next generation of cells (Bertolin et al., 2020; Franchet and Hoffmann, 2020). Generally, collapsed forks also lead to DSBs, hence RS is also largely associated with the generation of DSBs, major threats to genome integrity and cell viability. These chromosomal breakages and alterations provide a permanent sub-population of cellular variants upon which selection could act, a proposed driving mechanism for tumor heterogeneity and development of drug resistance. Clonal evolution in cancer can result from the multiple forms of selective pressures that allow some mutant sub-clones to multiply while others become extinct.

While genomic instability is generally associated with poor prognosis, excessive chromosomal instability is deleterious for cell fitness and is correlated with enhanced cancer outcome, arguing in favor of an appropriate threshold in cancer cells for limiting extremely risky RS and DSBs (Sansregret and Swanton, 2017; Maiorano et al., 2021). Therefore, one of the most important features of cancer cells is the need to adapt to severe replicative defects and the ensuing excessive DSBs that are normally incompatible with cell survival. Importantly, several of these adaptive responses currently represent a very active area of research as they are considered to be therapeutically exploitable. First is the ATR-CHK1 checkpoint response which coordinates the stability of arrested forks and fork repair processes, preventing premature entry into mitosis and ensuring the completion of DNA replication (Saldivar et al., 2017). High expression of the genes encoding the checkpoint mediators CHK1, Claspin and Timeless known to stabilize stalled replication forks upon RS and that could counteract excessive RS in cancer cells, was correlated with poor patient survival (David et al., 2016; Bianco et al., 2019). The second adaptive response corresponds to molecular factors including RAD52 of mitotic DNA synthesis (MiDAS), a process that differs from semi-conservative DNA replication in S-phase and which neutralizes potentially lethal chromosome mis-segregation and non-disjunction by restraining the persistence of under-replicated DNA in mitosis (Franchet and Hoffmann, 2020). MiDAS is described as a form of HR-based DNA repair highly prevalent in aneuploid cancer cells, where it counteracts DNA replication stress that arises at "difficult-to-replicate" loci such as common fragile sites (Bergoglio et al., 2013). The third category, which will be developed in the next paragraph, includes the *POLQ* gene encoding POLθ.

TMEJ Limits Loss of Chromosomal Integrity

Although *POLQ* orthologs are present in multiple species (Seki et al., 2003; Seki and Wood, 2008), in normal cells, TMEJ activity for DSB repair is very low and *POLQ* deficiency in several species has been shown to have a minor impact on

organismal development (Alexander et al., 2016; Thyme and Schier, 2016). In contrast, in cells that are deficient in HR or NHEJ, including BRCA1/2 mutated cancer cells, POLθ becomes essential, indicative of synthetic lethal genetic interactions between the backup POLθ/TMEJ repair pathway and HR or NHEJ (Ceccaldi et al., 2015; Mateos-Gomez et al., 2015; Feng et al., 2019; Kamp et al., 2020; Carvajal-Garcia et al., 2021; Patel et al., 2021). It has been proposed that POLθ favors end joining of two separated DSBs (distal end joining) (Hwang et al., 2020). Moreover, a study recently revealed a broader landscape of synthetic lethality with POLθ, emphasizing a critical and general role for POLθ in protecting cells from the accumulation of non-productive HR intermediates at sites of DNA replication-associated DSBs, even when canonical DSB repair pathways are functional (Feng et al., 2019), notably TMEJ has been proposed to contribute to the repair of single-ended DSBs at collapsed forks (Wang et al., 2019; **Figure 1**). Because of its high inaccuracy, TMEJ has been originally considered as a backup DNA repair pathway. However, TMEJ has been proposed to be essential in the repair of collapsed replication forks with sister chromatids containing an inter-strand crosslink (Wyatt et al., 2016; Feng et al., 2019; Schrempf et al., 2021) as well as the repair of G4 quadruplex structures (Koole et al., 2014). Nevertheless, the regulation of TMEJ versus HR need to be further explored for this particular DNA damage. POLθ contains an exonuclease-like domain but lacks $3' \rightarrow 5'$ proofreading activity, explaining why POLθ is an error-prone polymerase (Arana et al., 2008). Because of its low fidelity and the unique thumb domain that holds positively charged residues to grasp the unstable primer terminus, POLθ has the ability to extend DNA from mismatched primers (Zahn et al., 2015). In the TMEJ process, microhomologies are identified by a bidirectional progression to a maximum of 15 nucleotides into flanking DNA through a scanning mechanism initiated from the 3′ terminus (Carvajal-Garcia et al., 2020). Aborted synthesis is frequent for POLθ as it is not sufficiently processive, leading to additional rounds of microhomology search, annealing and synthesis which can be observed in some cancer genomic scars (Pettitt et al., 2020), such as insertions of 3 to 30 bp of sequences identical to flanking DNA. Despite these mutagenic features, POLθ/TMEJ has been clearly demonstrated to prevent some chromosome translocations and mis-segregations by fixing DSB *per se*, i.e., limiting loss of chromosomal integrity (Hwang et al., 2020). Hence, it is possible that the high expression of POLθ observed in multiple cancers, frequently defined as a bad prognostic marker (Lemee et al., 2010; Pillaire et al., 2010; Allera-Moreau et al., 2012), has evolved to cope with chromosome fragility and assist the completion of DNA replication to prevent catastrophically large deletions and aberrant chromosome segregation. The increase in mutational frequency as well as short deletions and insertions associated with TMEJ could be the price to pay for cancer cell survival (**Figure 1**). Several companies are now considering POLθ as a strong therapeutic target and are on the verge of launching POLθ inhibitors, targeting especially breast and ovarian cancers with BRCA1/2 deficiency.

ZEB1 Controls TMEJ

Initially, indirect evidence highlighted a role for EMT in the regulation of TMEJ. The expression of ZEB1 is activated by the cytokine transforming growth factor-β (TGFβ) signaling pathway (Shirakihara et al., 2007), the inhibition of which compromises the HR and cNHEJ DSB repair mechanisms and increases the reliance on the error prone alt-EJ/TMEJ pathway. TGFβ signaling impediment leads to a significant increase in chromosomal aberrations in irradiated cells from human papilloma virus-positive head and neck squamous cell carcinoma (HNSC) (Liu et al., 2018). More recently, TGFβ was confirmed to broadly control the DNA damage response and to transcriptionally inhibit alt-EJ/TMEJ genes, such as those of *POLQ*, *PARP1,* and *LIG1*. Interestingly, the identified TGFβ and alt-EJ gene signatures were anticorrelated in HNSC, in glioblastoma, squamous cell lung cancer, and serous ovarian cancers. Furthermore, tumors classified as low TGFβ and high alt-EJ were characterized by an insertion-deletion mutation signature containing short microhomologies across several cancers (Liu et al., 2021).

Further insights have been recently gained when ZEB1 was shown to modulates TMEJ activity by directly inhibiting *POLQ* expression (Prodhomme et al., 2021). Essentially, ZEB1 and *POLQ* expression are mutually exclusive in breast tumors. Secondly, ZEB1 inhibits *POLQ* transcription by directly binding to the *POLQ* promoter. Transcription inhibition and the resulting reduction of POLθ protein levels strongly impacts TMEJ activity. The use of a functional HPRT assay clearly demonstrated that ZEB1 limits TMEJ-associated genomic instability through the regulation of *POLQ* transcription (Prodhomme et al., 2021).

This new piece of evidence showing the reduction of TMEJ activity by ZEB1 contributes to explaining the paucity of genomic aberrations displayed by ZEB1-expressing tumors. ZEB1 expression is a hallmark of claudin-low breast tumors (Morel et al., 2012; Fougner et al., 2019; Stemmler et al., 2019; Pommier et al., 2020) and ZEB1 counteracts the onset of oxidative stress in response to oncogene-induced replicative insults (Morel et al., 2017). Moreover, *POLQ* expression level is low in all CL tumors as compared to other breast cancer subtypes (Prodhomme et al., 2021). However, the characterization of three separate claudin-low subgroups, namely CL1, CL2 and CL3, with distinct transcriptomic, epigenetic, and genetic features led us to speculate on the correlation between the expression of TMEJ factors and ZEB1 levels in each subgroup (Pommier et al., 2020). Indeed, we showed here that *POLQ* expression is the lowest in CL1, displaying the highest level of ZEB1 while *POLQ* shows the highest expression in CL3, presenting the lowest level of ZEB1 (**Figure 2**). CL1 was shown to be enriched in stem-cell-related signatures (Pommier et al., 2020) with low proliferation activity. In contrast to CL1, the CL3 subgroup, containing the majority of BRCA-deficient tumors and showing lower levels of ZEB1, lower levels of ATM and higher levels of *POLQ*, displays stronger basal-related characteristics. In basal-like tumor subtypes with BRCA-mutations, ZEB1 expression may occur late in the oncogenic process depending on high *POLQ* expression in order to survive with the HR deficiency. In this case, even though

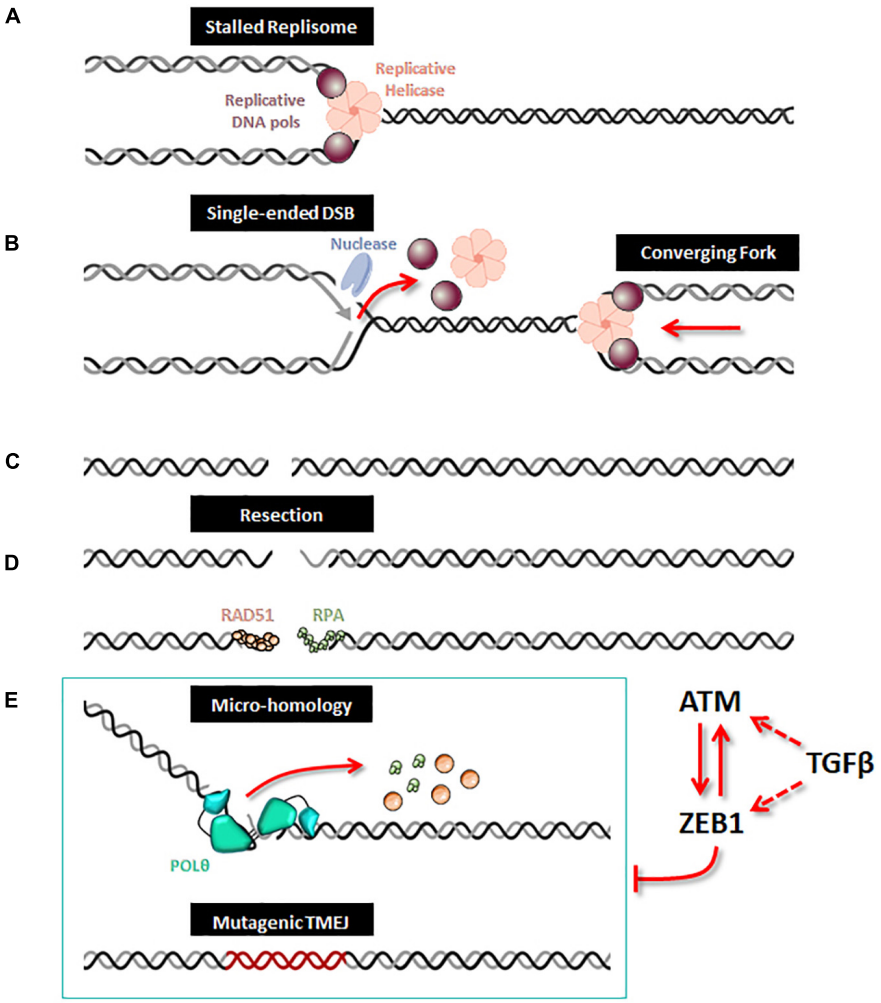

FIGURE 1 | ZEB1/EMT controls TMEJ. When a replication fork is stalled **(A)**, unloading of the replicative helicase and DNA polymerases leads to incision by a DNA nuclease, which creates a single-ended DSB **(B)**. After replication forks completion, a DSB is generated **(C)**. A 5′ to 3′ end resection generates single-stranded DNA, along which RPA and Rad51 loading can occur **(D)**. When homologous recombination is defective, the alternative TMEJ pathway can operate on this resected DSB **(E)**; POLθ is recruited as a dimer which facilitates the proximity of DNA ends and stabilizes synapsed intermediates; the helicase domain of POLθ can displace either RPA or RAD51 and the polymerase domain executes a bidirectional scanning initiated from the 3′ termini to identify internal microhomologies which can be annealed, thus generating 3′ flaps. POLθ then removes the 3′ flaps and starts DNA synthesis with poor processivity and frequent aborted synthesis resulting in a high rate of mutations including deletions and insertions from template switching events. When ZEB1 is expressed and stabilized by ATM, the expression of *POLQ* (encoding the POLθ protein) is decreased and therefore impedes the action of the alternative mutagenic TMEJ pathway on the resected DSB. The TMEJ inhibition by ZEB1 combined with ATM activity enhances accurate homologous recombination. Moreover, ZEB1 activates the transcription of ATM, both being under direct or indirect control of TGFβ signaling.

ZEB1 downregulates *POLQ* expression, *POLQ* expression level remains higher than normal, yet slightly lower than in the basal-like subgroup. Interestingly, *ATM* expression follows *ZEB1* in all CL subtypes as anticipated with the already described mechanism of recruitment of the transcriptional coactivators p300/PCAF by ZEB1 to the *ATM* promoter (Zhang et al., 2018). Similarly, ATM-mediated stabilization of ZEB1 plays an important role for the enhanced accurate DNA repair ability by HR pathway of radioresistant tumor cells (Zhang et al., 2014). *POLQ* and *ATM* were firstly described in mice as synthetic semi-lethality. Indeed, Atm-/- Polq-/- double mutant mice showed marked developmental disadvantage (Shima et al., 2004). Moreover, the co-inhibition of *ATM* and *POLQ* enhanced the sensitivity to radiotherapy or chemotherapy (Goff et al., 2009; Pan et al., 2020). All these data suggested a unique role of Polq in maintaining genomic integrity, which is probably distinctive from the major HR pathway regulated by ATM as evidenced by the extensive evidence for synthetic lethality between HR and TMEJ. ZEB1, stabilized by ATM, probably then acts as an inhibitor of TMEJ to promote accurate HR DNA repair.

Moreover, downregulation of *POLQ* by ZEB1 was reported to foster micronuclei formation (Prodhomme et al., 2021). Indeed, it was shown in several organisms and under various conditions that POLθ prevents micronuclei formation, whereas the loss of POLθ expression leads to an increase in micronuclei (Shima et al., 2004; Goff et al., 2009; Yousefzadeh et al.,

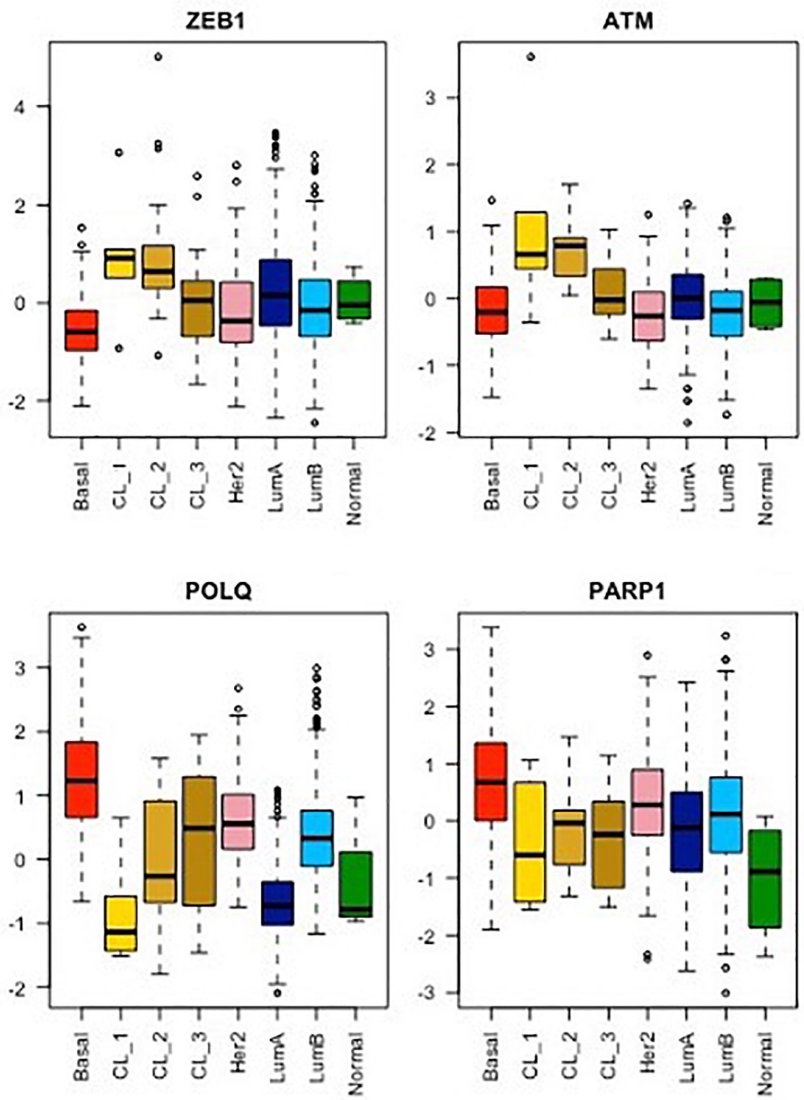

FIGURE 2 | mRNA expression analysis of ZEB1, ATM, POLQ, and PARP1 for each breast cancer molecular subtype from the METABRIC cohort. As already shown, the CL1 subgroup shows the highest stemness and EMT phenotype, exemplify here by *ZEB1* expression, while CL2 and CL3 subgroups display an intermediate stemness and EMT phenotype compared to their relative luminal/basal counterparts and CL1 tumors (Pommier et al., 2020). The mRNA levels of *ATM,* a major player in DDR signaling, as well as of *POLQ* and *PARP1*, two major players in TMEJ, were analyzed for all breast cancer subtypes using the same method. Wilcoxon tests. Boxplot: center line, median; box limits, upper and lower quartiles; whiskers, minimum to maximum; all data points are shown.

2014). These observations strengthened the notion that TMEJ is a full-fledged pathway, since the absence of TMEJ in claudin-low tumors leads to micronuclei originating most likely from unrepaired DNA damage (Prodhomme et al., 2021). However, in this specific breast tumor subtype, micronuclei abundance, generally considered to be a hallmark of genome instability (Jdey et al., 2017), is associated with low genomic instability (Morel et al., 2017). We postulated that one of the reasons explaining why micronuclei have no apparent incidence on claudin-low genome stability is that a small fraction of claudin-low cells with excessive micronuclei and/or unrepaired DNA damage would die. This hypothesis is illustrated in the analysis of neutral comet tail moments after the simultaneous deletion of TGFβ and TMEJ pathways, where an increase in DNA fragmentation is observed after cell irradiation (Liu et al., 2018). Consequently, an augmentation of unrepaired DNA may lead to cell death. Notably, radiosensitivity is highest when both TGFβ signaling and *POLQ* function are inactive (Liu et al., 2018). Further characterization of upcoming ZEB1-expressing tumor cells is needed to confirm this hypothesis, but one may suggest that ZEB1 and *POLQ* have opposite and complementary roles in the control of both the stability and integrity of breast cancer cell genomes. In normal cells, endogenous levels of POLθ and ZEB1 offer a compromise between the role of ZEB1 in protecting the stability of the genome and that of POLθ in protecting its

integrity. In pathological conditions such as breast cancer, this balance is possibly disturbed due to high replicative stress, except in ZEB1-expressing cells, as formerly demonstrated (Morel et al., 2017). This dysregulation may contribute to *POLQ* dependence for survival, especially in a BRCA-deficient context.

DISCUSSION

Recent studies have underlined the role of EMT in DNA repair pathway choice and in particular, TMEJ activity in breast cancers. TMEJ protects from replication stress by preserving genomic integrity at the cost of mutations in most breast cancer subtypes, except in BRCA non-mutated claudin-low subtypes, in which the important contribution of ZEB1 as a protective actor in both early and late steps of tumor development has been demonstrated (Morel et al., 2017; Pommier et al., 2020; Prodhomme et al., 2021).

Uncovering the mechanisms of TMEJ regulation in cancer progression remains an ongoing task. We have shown that the EMT transcription factor, ZEB1 interacts directly with the *POLQ* promoter to control the expression of the *POLQ* gene and prevent TMEJ activity. However, the mechanisms underlying the upregulation of *POLQ* expression, in particular in BRCA-deficient cancers, are still unknown.

POLθ was recently identified as a potential target in the treatment of numerous breast tumors, especially BRCA-deficient tumors. ZEB1 could constitute an important biomarker to exclude BRCA non-mutated, claudin-low tumors from future therapy with POLθ inhibitors. Conversely, considering the repressive role of ZEB1 on TMEJ activity, the identification of a ZEB1 inhibitor could be used to systematically stimulate TMEJ and render those tumors more sensitive to POLθ inhibition.

AUTHOR CONTRIBUTIONS

MP, J-SH and AT contributed to original draft preparation and editing. All authors contributed to the conceptualization of the review, the research of the pertinent literature and writing.

FUNDING

This work was supported by funding from the Ligue contre le Cancer (EL2016.LNCC/AIP and EL2019.LNCC/AIP), SIRIC LYriCAN (INCa-DGOS-Inserm_12563), and Laboratoire d'Excellence Toulouse Cancer (TOUCAN).

REFERENCES

Alexander, J. L., Beagan, K., Orr-Weaver, T. L., and McVey, M. (2016). Multiple mechanisms contribute to double-strand break repair at rereplication forks in *Drosophila* follicle cells. *Proc. Natl. Acad. Sci. U.S.A.* 113, 13809–13814. doi: 10.1073/pnas.1617110113

Allera-Moreau, C., Rouquette, I., Lepage, B., Oumouhou, N., Walschaerts, M., Leconte, E., et al. (2012). DNA replication stress response involving PLK1, CDC6, POLQ, RAD51 and CLASPIN upregulation prognoses the outcome of early/mid-stage non-small cell lung cancer patients. *Oncogenesis* 1:e30. doi: 10.1038/oncsis.2012.29

Arana, M. E., Seki, M., Wood, R. D., Rogozin, I. B., and Kunkel, T. A. (2008). Low-fidelity DNA synthesis by human DNA polymerase theta. *Nucleic Acids Res.* 36, 3847–3856. doi: 10.1093/nar/gkn310

Bartkova, J., Hořejší, Z., Koed, K., Krämer, A., Tort, F., Zleger, K., et al. (2005). DNA damage response as a candidate anti-cancer barrier in early human tumorigenesis. *Nature* 434, 864–870. doi: 10.1038/nature03482

Bergoglio, V., Boyer, A. S., Walsh, E., Naim, V., Legube, G., Lee, M. Y. W. T., et al. (2013). DNA synthesis by pol η promotes fragile site stability by preventing under-replicated DNA in mitosis. *J. Cell Biol.* 201, 395–408. doi: 10.1083/jcb.201207066

Bertolin, A. P., Hoffmann, J. S., and Gottifredi, V. (2020). Under-replicated DNA: the byproduct of large genomes? *Cancers* 12:2764. doi: 10.3390/cancers12102764

Bianco, J. N., Bergoglio, V., Lin, Y. L., Pillaire, M. J., Schmitz, A. L., Gilhodes, J., et al. (2019). Overexpression of claspin and timeless protects cancer cells from replication stress in a checkpoint-independent manner. *Nat. Commun.* 10:910. doi: 10.1038/s41467-019-08886-8

Brabletz, T., Kalluri, R., Nieto, M. A., and Weinberg, R. A. (2018). EMT in cancer. *Nat. Rev. Cancer* 18, 128–134. doi: 10.1038/nrc.2017.118

Carvajal-Garcia, J., Cho, J. E., Carvajal-Garcia, P., Feng, W., Wood, R. D., Sekelsky, J., et al. (2020). Mechanistic basis for microhomology identification and genome scarring by polymerase theta. *Proc. Natl. Acad. Sci. U.S.A.* 117, 8476–8485. doi: 10.1073/pnas.1921791117

Carvajal-Garcia, J., Crown, K. N., Ramsden, D. A., and Sekelsky, J. (2021). DNA polymerase theta suppresses mitotic crossing over. *PLoS Genet.* 17:e1009267. doi: 10.1371/journal.pgen.1009267

Ceccaldi, R., Liu, J. C., Amunugama, R., Hajdu, I., Primack, B., Petalcorin, M. I. R., et al. (2015). Homologous-recombination-deficient tumours are dependent on Polθ-mediated repair. *Nature* 518, 258–262. doi: 10.1038/nature14184

David, L., Fernandez-Vidal, A., Bertoli, S., Grgurevic, S., Lepage, B., Deshaies, D., et al. (2016). CHK1 as a therapeutic target to bypass chemoresistance in AML. *Sci. Signal.* 9:ra90. doi: 10.1126/scisignal.aac9704

Feng, W., Simpson, D. A., Carvajal-Garcia, J., Price, B. A., Kumar, R. J., Mose, L. E., et al. (2019). Genetic determinants of cellular addiction to DNA polymerase theta. *Nat. Commun.* 10:4286. doi: 10.1038/s41467-019-12234-1

Fougner, C., Bergholtz, H., Kuiper, R., Norum, J. H., and Sørlie, T. (2019). Claudin-low-like mouse mammary tumors show distinct transcriptomic patterns uncoupled from genomic drivers. *Breast Cancer Res.* 21:85. doi: 10.1186/s13058-019-1170-8

Franchet, C., and Hoffmann, J. S. (2020). When RAD52 allows mitosis to accept unscheduled dna synthesis. *Cancers* 12:26. doi: 10.3390/cancers12010026

Goff, J. P., Shields, D. S., Seki, M., Choi, S., Epperly, M. W., Dixon, T., et al. (2009). Lack of DNA Polymerase θ (POLQ) radiosensitizes bone marrow stromal cells in vitro and increases reticulocyte micronuclei after total-body irradiation. *Radiat. Res.* 172, 165–174. doi: 10.1667/RR1598.1

Gorgoulis, V., Vassiliou, L.-V. F., Karakaidos, P., Zacharatos, P., Kotsinas, A., Liloglou, T., et al. (2005). Activation of the DNA damage checkpoint and genomic instability in human precancerous lesions. *Nature* 434, 907–913. doi: 10.1038/nature03485

Hanahan, D., and Weinberg, R. A. (2011). Hallmarks of cancer: the next generation. *Cell* 144, 646–674. doi: 10.1016/j.cell.2011.02.013

Hwang, T., Reh, S., Dunbayev, Y., Zhong, Y., Takata, Y., Shen, J., et al. (2020). Defining the mutation signatures of DNA polymerase θ in cancer genomes. *NAR Cancer* 2:zcaa017. doi: 10.1093/narcan/zcaa017

Jdey, W., Thierry, S., Popova, T., Stern, M. H., and Dutreix, M. (2017). Micronuclei frequency in tumors is a predictive biomarker for genetic instability and sensitivity to the DNA repair inhibitor AsiDNA. *Cancer Res.* 77, 4207–4216. doi: 10.1158/0008-5472.CAN-16-2693

Kamp, J. A., van Schendel, R., Dilweg, I. W., and Tijsterman, M. (2020). BRCA1-associated structural variations are a consequence of polymerase theta-mediated end-joining. *Nat. Commun.* 11:3615. doi: 10.1038/s41467-020-17455-3

Koole, W., Schendel, R., Van Karambelas, A. E., Heteren, J. T., Van, Okihara, K. L., et al. (2014). A Polymerase theta-dependent repair pathway suppresses

extensive genomic instability at endogenous G4 DNA sites. *Nat. Commun.* 5:3216. doi: 10.1038/ncomms4216

Lemee, F., Bergoglio, V., Fernandez-Vidal, A., Machado-Silva, A., Pillaire, M.-J., Bieth, A., et al. (2010). DNA polymerase up-regulation is associated with poor survival in breast cancer, perturbs DNA replication, and promotes genetic instability. *Proc. Natl. Acad. Sci. U.S.A.* 107, 13390–13395. doi: 10.1073/pnas.0910759107

Liu, Q., Ma, L., Jones, T., Palomero, L., Pujana, M. A., Martinez-Ruiz, H., et al. (2018). Subjugation of TGFb signaling by human papilloma virus in head and neck squamous cell carcinoma shifts DNA repair from homologous recombination to alternative end joining. *Clin. Cancer Res.* 24, 6001–6014. doi: 10.1158/1078-0432.CCR-18-1346

Liu, Q., Palomero, L., Moore, J., Guix, I., Espín, R., Aytés, A., et al. (2021). Loss of TGFB signaling increases alternative end-joining DNA repair that sensitizes to genotoxic therapies across cancer types. *Sci. Transl. Med.* 13:eabc4465. doi: 10.1126/scitranslmed.abc4465

Macheret, M., and Halazonetis, T. D. (2015). DNA replication stress as a hallmark of cancer. *Annu. Rev. Pathol.* 10, 425–448. doi: 10.1146/annurev-pathol-012414-040424

Maiorano, D., El Etri, J., Franchet, C., and Hoffmann, J. S. (2021). Translesion synthesis or repair by specialized dna polymerases limits excessive genomic instability upon replication stress. *Int. J. Mol. Sci.* 22:3924. doi: 10.3390/ijms22083924

Mateos-Gomez, P. A., Gong, F., Nair, N., Miller, K. M., Lazzerini-Denchi, E., and Sfeir, A. (2015). Mammalian polymerase θ promotes alternative NHEJ and suppresses recombination. *Nature* 518, 254–257. doi: 10.1038/nature14157

Morel, A.-P., Ginestier, C., Pommier, R. M., Cabaud, O., Ruiz, E., Wicinski, J., et al. (2017). A stemness-related ZEB1-MSRB3 axis governs cellular pliancy and breast cancer genome stability. *Nat. Med.* 23, 568–578. doi: 10.1038/nm.4323

Morel, A.-P. P., Hinkal, G. W., Thomas, C. C., Fauvet, F. F., Courtois-Cox, S. S., Wierinckx, A., et al. (2012). EMT inducers catalyze malignant transformation of mammary epithelial cells and drive tumorigenesis towards claudin-low tumors in transgenic mice. *PLoS Genet.* 8:e1002723. doi: 10.1371/journal.pgen.1002723

Negrini, S., Gorgoulis, V. G., and Halazonetis, T. D. (2010). Genomic instability an evolving hallmark of cancer. *Nat. Rev. Mol. Cell Biol.* 11, 220–228. doi: 10.1038/nrm2858

Pan, Y.-R., Wu, C.-E., and Yeh, C.-N. (2020). ATM inhibitor suppresses gemcitabine-resistant btc growth in a polymerase θ deficiency-dependent manner. *Biomolecules* 10:1529. doi: 10.3390/biom10111529

Patel, P. S., Algouneh, A., and Hakem, R. (2021). Exploiting synthetic lethality to target BRCA1/2-deficient tumors: where we stand. *Oncogene* 40, 3001–3014. doi: 10.1038/s41388-021-01744-2

Pettitt, S. J., Frankum, J. R., Punta, M., Lise, S., Alexander, J., Chen, Y., et al. (2020). Clinical brca1/2 reversion analysis identifies hotspot mutations and predicted neoantigens associated with therapy resistance. *Cancer Discov.* 10, 1475–1488. doi: 10.1158/2159-8290.CD-19-1485

Pillaire, M. J., Selves, J., Gordien, K., Gouraud, P. A., Gentil, C., Danjoux, M., et al. (2010). A DNA replication signature of progression and negative outcome in colorectal cancer. *Oncogene* 29, 876–887. doi: 10.1038/onc.2009.378

Pommier, R. M., Sanlaville, A., Tonon, L., Kielbassa, J., Thomas, E., Ferrari, A., et al. (2020). Comprehensive characterization of claudin-low breast tumors reflects the impact of the cell-of-origin on cancer evolution. *Nat. Commun.* 11, 1–12. doi: 10.1038/s41467-020-17249-7

Prodhomme, M. K., Pommier, R. M., Franchet, C., Fauvet, F., Bergoglio, V., Brousset, P., et al. (2021). EMT transcription factor ZEB1 represses the mutagenic POLθ-mediated end-joining pathway in breast cancers. *Cancer Res.* 81, 1595–1606. doi: 10.1158/0008-5472.can-20-2626

Saldivar, J. C., Cortez, D., and Cimprich, K. A. (2017). The essential kinase ATR: ensuring faithful duplication of a challenging genome. *Nat. Rev. Mol. Cell Biol.* 18, 622–636. doi: 10.1038/nrm.2017.67

Sansregret, L., and Swanton, C. (2017). The role of aneuploidy in cancer evolution. *Cold Spring Harb. Perspect. Med.* 7:a028373. doi: 10.1101/cshperspect.a028373

Schimmel, J., Kool, H., van Schendel, R., and Tijsterman, M. (2017). Mutational signatures of non-homologous and polymerase theta-mediated end-joining in embryonic stem cells. *EMBO J.* 36, 3634–3649. doi: 10.15252/embj.201796948

Schimmel, J., van Schendel, R., den Dunnen, J. T., and Tijsterman, M. (2019). Templated insertions: a smoking gun for polymerase theta-mediated end joining. *Trends Genet.* 35, 632–644. doi: 10.1016/j.tig.2019.06.001

Schrempf, A., Slyskova, J., and Loizou, J. I. (2021). Targeting the DNA repair enzyme polymerase θ in cancer therapy. *Trends Cancer* 7, 98–111. doi: 10.1016/j.trecan.2020.09.007

Seki, M., Marini, F., and Wood, R. D. (2003). POLQ (Pol θ), a DNA polymerase and DNA-dependent ATPase in human cells. *Nucleic Acids Res.* 31, 6117–6126. doi: 10.1093/nar/gkg814

Seki, M., and Wood, R. D. (2008). DNA polymerase θ (POLQ) can extend from mismatches and from bases opposite a (6-4) photoproduct. *DNA Repair* 7, 119–127. doi: 10.1016/j.dnarep.2007.08.005

Shima, N., Munroe, R. J., and Schimenti, J. C. (2004). The mouse genomic instability mutation chaos1 is an allele of polq that exhibits genetic interaction with atm. *Mol. Cell. Biol.* 24, 10381–10389. doi: 10.1128/MCB.24.23.10381-10389.2004

Shirakihara, T., Saitoh, M., and Miyazono, K. (2007). Differential regulation of epithelial and mesenchymal markers by δEF1 proteins in epithelial-mesenchymal transition induced by TGF-β. *Mol. Biol. Cell* 18, 3533–3544. doi: 10.1091/mbc.E07-03-0249

Stemmler, M. P., Eccles, R. L., Brabletz, S., and Brabletz, T. (2019). Non-redundant functions of EMT transcription factors. *Nat. Cell Biol.* 21, 102–112. doi: 10.1038/s41556-018-0196-y

Thyme, S. B., and Schier, A. F. (2016). Polq-mediated end joining is essential for surviving dna double-strand breaks during early zebrafish development. *Cell Rep.* 15, 707–714. doi: 10.1016/j.celrep.2016.03.072

Wang, Z., Song, Y., Li, S., Kurian, S., Xiang, R., Chiba, T., et al. (2019). DNA polymerase θ (POLQ) is important for repair of DNA double-strand breaks caused by fork collapse. *J. Biol. Chem.* 294, 3909–3919. doi: 10.1074/jbc.RA118.005188

Wyatt, D. W., Feng, W., Conlin, M. P., Yousefzadeh, M. J., Roberts, S. A., Mieczkowski, P., et al. (2016). Essential roles for polymerase θ-mediated end joining in the repair of chromosome breaks. *Mol. Cell* 63, 662–673. doi: 10.1016/j.molcel.2016.06.020

Ye, X., and Weinberg, R. A. (2015). Epithelial-mesenchymal plasticity: a central regulator of cancer progression. *Trends Cell Biol.* 25, 675–686. doi: 10.1016/j.tcb.2015.07.012

Yousefzadeh, M. J., Wyatt, D. W., Takata, K., Mu, Y., Hensley, S. C., Tomida, J., et al. (2014). Mechanism of suppression of chromosomal instability by DNA polymerase POLQ. *PLoS Genet.* 10:e1004654. doi: 10.1371/journal.pgen.1004654

Zahn, K. E., Averill, A. M., Aller, P., Wood, R. D., and Doublié, S. (2015). Human DNA polymerase θ grasps the primer terminus to mediate DNA repair. *Nat. Struct. Mol. Biol.* 22, 304–311. doi: 10.1038/nsmb.2993

Zeman, M. K., and Cimprich, K. A. (2014). Causes and consequences of replication stress. *Nat. Cell Biol.* 16, 2–9. doi: 10.1038/ncb2897

Zhang, P., Wei, Y., Wang, L., Debeb, B. G., Yuan, Y., Zhang, J., et al. (2014). ATM-mediated stabilization of ZEB1 promotes DNA damage response and radioresistance through CHK1. *Nat. Cell Biol.* 16, 864–875. doi: 10.1038/ncb3013

Zhang, X., Zhang, Z., Zhang, Q., Zhang, Q., Sun, P., Xiang, R., et al. (2018). ZEB1 confers chemotherapeutic resistance to breast cancer by activating ATM. *Cell Death Dis.* 9:57. doi: 10.1038/s41419-017-0087-3

Conflict of Interest: The authors declare that the research was conducted in the absence of any commercial or financial relationships that could be construed as a potential conflict of interest.

Publisher's Note: All claims expressed in this article are solely those of the authors and do not necessarily represent those of their affiliated organizations, or those of the publisher, the editors and the reviewers. Any product that may be evaluated in this article, or claim that may be made by its manufacturer, is not guaranteed or endorsed by the publisher.

frontiers in Cell and Developmental Biology

REVIEW
published: 30 September 2021
doi: 10.3389/fcell.2021.735678

Biogenesis of Iron–Sulfur Clusters and Their Role in DNA Metabolism

*Ruifeng Shi[1,2], Wenya Hou[2], Zhao-Qi Wang[3,4] and Xingzhi Xu[1,2]**

[1] Shenzhen University-Friedrich Schiller Universität Jena Joint Ph.D. Program in Biomedical Sciences, Shenzhen University School of Medicine, Shenzhen, China, [2] Guangdong Key Laboratory for Genome Stability and Disease Prevention and Marshall Laboratory of Biomedical Engineering, Shenzhen University School of Medicine, Shenzhen, China, [3] Leibniz Institute on Aging—Fritz Lipmann Institute (FLI), Jena, Germany, [4] Faculty of Biological Sciences, Friedrich-Schiller-University Jena, Jena, Germany

Iron–sulfur (Fe/S) clusters (ISCs) are redox-active protein cofactors that their synthesis, transfer, and insertion into target proteins require many components. Mitochondrial ISC assembly is the foundation of all cellular ISCs in eukaryotic cells. The mitochondrial ISC cooperates with the cytosolic Fe/S protein assembly (CIA) systems to accomplish the cytosolic and nuclear Fe/S clusters maturation. ISCs are needed for diverse cellular functions, including nitrogen fixation, oxidative phosphorylation, mitochondrial respiratory pathways, and ribosome assembly. Recent research advances have confirmed the existence of different ISCs in enzymes that regulate DNA metabolism, including helicases, nucleases, primases, DNA polymerases, and glycosylases. Here we outline the synthesis of mitochondrial, cytosolic and nuclear ISCs and highlight their functions in DNA metabolism.

Keywords: iron-sulfur (Fe-S) clusters, genome stability, DNA replication, DNA repair, DNA metabolism

OPEN ACCESS

Edited by:
Chunlong Chen, Institut Curie, France

Reviewed by:
Jun Huang, Zhejiang University, China
Andrew Dancis, University of Pennsylvania, United States

***Correspondence:**
Xingzhi Xu
Xingzhi.Xu@szu.edu.cn

Specialty section:
This article was submitted to Cell Growth and Division, a section of the journal Frontiers in Cell and Developmental Biology

Received: *03 July 2021*
Accepted: *06 September 2021*
Published: *30 September 2021*

Citation:
Shi R, Hou W, Wang Z-Q and Xu X (2021) Biogenesis of Iron–Sulfur Clusters and Their Role in DNA Metabolism. Front. Cell Dev. Biol. 9:735678. doi: 10.3389/fcell.2021.735678

INTRODUCTION

Iron–sulfur (Fe/S) clusters (ISCs) are extremely ancient, small inorganic protein cofactors found in almost all organisms. Ferredoxin was discovered in the early 1960s, since then, the number of known Fe/S clusters-containing proteins has steadily increased. Until now, over 120 unique types of enzymes and proteins have been identified as ISC-containing proteins (Johnson et al., 2005). Until now, there are more than 200 known Fe/S proteins in human cells according to the UniProt database[1]. And bacteria contain a great variety of such proteins (Andreini et al., 2017). ISC proteins are found in the nucleus, cytosol, and mitochondria. The essentials of ISC proteins are reflected in the fact that they are required for many fundamental biochemical processes. For example, within mitochondria, the respiratory complexes I, II and III use many ISCs to transfer electrons which reduces ubiquinone by NADH or FADH, respectively. Within the nucleus, ISCs are functionally related to the maintenance of genome stability, RNA modification, and gene regulation. Specifically, ISCs are inserted into DNA repair enzymes, which fix DNA lesions according to the diffusing ability of an electron from an ISC along DNA (Arnold et al., 2016). Defects in mitochondrial ISC biogenesis can result in nuclear genomic instability (Veatch et al., 2009). Various nuclear DNA metabolic enzymes require ISCs to carry out DNA metabolism, including DNA primase, DNA polymerases (Klinge et al., 2007), DNA glycosylases (Alseth et al., 1999), and ATP-dependent DNA helicases (Rudolf et al., 2006; Gari et al., 2012; Stehling et al., 2012).

[1]https://www.uniprot.org/

MITOCHONDRIAL IRON–SULFUR (Fe/S) CLUSTER BIOGENESIS

There are three independent mechanisms that can synthesize ISCs in bacteria: the ISC assembly, methanoarchaeal sulfur mobilization (SUF) (Takahashi and Tokumoto, 2002), and nitrogen fixation (NIF) pathways (Mettert and Kiley, 2015). Each of these mechanisms shares the same steps: iron and sulfur ions are assembled at scaffold complexes. And then, the transfer system delivers the clusters to target proteins (Roche et al., 2013).

Eukaryotic mitochondria have one dedicated assembly pathway that inherits the ISC pathway from bacteria and integrate the NIF system components (Gisselberg et al., 2013; Roche et al., 2013). The ISCs in the cytoplasm and nucleus are assembled by the CIA pathway. In mammalian cells, there are two major forms of ISCs: 2Fe–2S and 4Fe–4S clusters (**Figure 1**). These two types of cofactors are generated by two related biochemical machineries in the cytosol (CIA pathway) and mitochondria (ISC pathway), respectively (Maio et al., 2020). The mitochondrial machinery assembly a necessary sulfur-containing intermediate that is exported to the cytoplasm and utilized for extramitochondrial ISCs assembly.

Mitochondrial ISC biogenesis has two functions: (1) to synthesize functional clusters in the mitochondria, and (2) to provide an essential precursor to the CIA pathway via the inner membrane exporter ABCB7 (Lill et al., 2015). Briefly, persulfide ions are generated by cysteine desulfurase (NFS1). Iron and sulfide ions are then delivered to a scaffold protein ISCU2 to form an initial 2Fe–2S cluster. Then chaperones transfer this 2Fe–2S cluster to a glutaredoxin, which subsequently delivers the 2Fe–2S cluster to the target protein or to the next Iron-sulfur assembly protein (ISA) complex. The ISA complex can condense two 2Fe–2S clusters into one 4Fe–4S center (Beilschmidt and Puccio, 2014). Major components involved in the ISC pathway are shown in **Table 1**. In sum, 2Fe-2S and 4Fe-4S proteins are made differently, with *de novo* 2Fe-2S clusters forming on the ISCU scaffold and 4Fe-4S clusters forming subsequently in a downstream step utilizing the ISA complex of proteins.

2Fe–2S Cluster Biogenesis

The 2Fe–2S clusters in rhombic form possess 2 sulfide ions and 2 irons, which coordinate four cysteinyl sulfhydryl side chains (**Figure 1A**). This rhombic-form cluster exhibits two oxidation states: the oxidized status with two Fe^{3++}, and the reduced status with one Fe^{3+} and one Fe^{2+}. As mentioned, the mitochondrial ISC pathway is essential for ISC biogenesis. This pathway starts with delivering iron and sulfur ions to scaffold protein ISCU2. ISCU has two isoforms: the mitochondrial isoform ISCU2 and cytosolic and nuclear isoform ISCU1. Cysteine desulfurase NFS1, which interacts with ISD11 and ACP to form a stable complex provides sulfur. However, the iron source of ISC is unknown yet. Frataxin (FXN) and ferredoxin2 (FDX2) are also important for ISCs *de novo* assembly. The former is thought to regulate NFS1 activity (Fox et al., 2019), while the latter is proposed to donate electrons for reduction (Cai et al., 2017; Gervason et al., 2019).

The eukaryotic cysteine desulfurase NFS1 is a pyridoxal phosphate-dependent enzyme. Sulfur is transferred from cysteine and activated into a persulfide form, which can be used for ISC assembly. In Cory et al. (2017), the first investigation into the eukaryotic NFS1 crystal structure revealed some key features: First, NFS1 binding to its substrate cysteine relies on a pyridoxal phosphate (PLP) cofactor. Second, there is a metal-binding cysteine site located in the C-terminus of NFS1. The activated sulfur abstracted is transferred to this cysteine site. Third, similar to the prokaryotic version of the enzyme, NFS1 forms a dimer. In the field of the enzymatic cycle, the PLP cofactor mediated the interaction of NFS1 and substrate cysteine. Then, NFS1 conformational change results in closing the activity site of cysteine with substrate and proceeding a nucleophilic attach (Johnson et al., 2005). During this second step, additional eukaryotic-specific subunits (ISD11 and ACP) interact with NFS1 and form a stable complex. ISD11 is a small protein of the LYR (Leu-Tyr-Arg motif) family, and ACP, which is an acyl carrier protein, regulates fatty acid synthesis. The long chain fatty acid of ACP is inserted into the helical center of the ISD11 subunit (Pandey et al., 2012; Parent et al., 2015; Cory et al., 2017). Finally, the persulfide sulfur is moved from NFS1 to the scaffold protein ISCU2 for ISC assembly.

The transfer of persulfur to the ISCU2 scaffold seems to be mediated by frataxin (Brancaccio et al., 2014; Fox et al., 2015). Frataxin is the earliest identified as a positive modulatory factor for NFS1 and ISC assembly. Frataxin interacts with NFS1 and enhance NFS1 cysteine desulfurase activity. Human neurodegenerative disease Friedreich's ataxia results from the deficient of frataxin. Deletion of the yeast orthologous gene, Yfh1, leads to excess iron accumulation in mitochondria (Campuzano et al., 1996; Babcock et al., 1997; Karthikeyan et al., 2002). Because of frataxin's weak Fe(II)-binding ability, it might be a potential iron donor to scaffold protein ISCU2 (Adamec et al., 2000; Yoon and Cowan, 2003). Structural studies have revealed that neither iron nor ISU oligomerization is essential for the interaction between bacterial frataxin, CyaY, and the ISU complex. Prokaryotic frataxin directly interacts with the bacterial desulfurase, IscS, but not the scaffold, IscU (Prischi et al., 2010). There are two apparently different reports for frataxin functions. One report suggested that frataxin promotes the interaction between NFS1 and substrate (Pandey et al., 2013), while frataxin was reported to promote sulfide transfer from NFS1 to ISCU1 (Parent et al., 2015). Furthermore, frataxin enhances sulfide transfer to ISCU1, forming a 2Fe–2S product on the ISCU scaffold (Bridwell-Rabb et al., 2014).

Transfer of 2Fe–2S Clusters

Once the initial 2Fe–2S cluster has been generated by the ISC system in mitochondria, it is transferred to the glutaredoxin 5 (GLRX5) dimer with the help of HSC20 and HSPA9. This process requires energy, which is supplied by ATP hydrolysis carried out by HSPA9 (Dutkiewicz et al., 2003). The binding of the chaperones HSC20 and HSPA9 leads to the dissociation of the assembly complex consisting NFS1/ISD11/ISCU/ACP/FXN. Competition of FXN with HSPA9 for the LPPVK binding site on ISCU acts as a molecular switch between assembly and

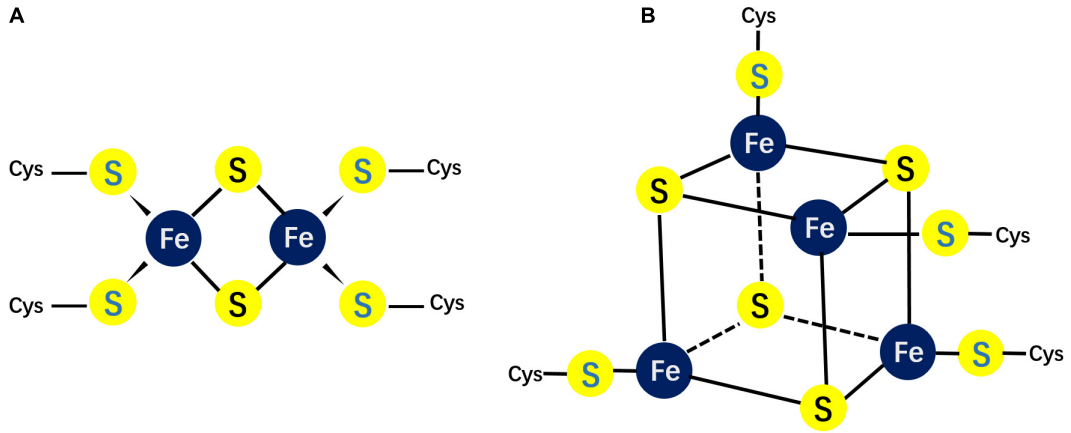

FIGURE 1 | Different possible structures of Fe/S clusters. **(A)** The structure of the rhombic 2Fe–2S cluster; **(B)** the structure of the cubane 4Fe–4S cluster.

transfer complexes (Majewska et al., 2013; Manicki et al., 2014). Cluster–bound GLRX5 includes a 2Fe–2S cluster connecting a GLRX5 dimer. Each GLRX5 contributes one cysteine ligand to the 2Fe–2S cluster, while a second thiolate ligand coming from a GLRX5–bound glutathione stably binds GLRX5 (Banci et al., 2014). *glrx5* deletion in yeast cells has dysfunctional phenotypes in both mitochondrial ISC *de novo* biogenesis and cytosolic ISC assembly (Muhlenhoff et al., 2003; Uzarska et al., 2013).

Mitochondrial 4Fe–4S Cluster Formation

The cubane-type cluster comprises 4 iron and 4 sulfide ions coordinated to four sulfhydryl side chains (**Figure 1**), which can be subdivided into low- or high-potential clusters[39]. The oxidation states of the low-potential clusters are the oxidized [$2Fe^{3+}$, $2Fe^{2+}$] and the reduced [Fe^{3+}, $3Fe^{2+}$] forms, while the oxidation states for the high potential clusters switch between the reduced [$2Fe^{3+}$, $2Fe^{2+}$] and the oxidized [$3Fe^{3+}$, Fe^{2+}] forms. Hence, the two ferric-two ferrous state is shared by the two families. Within a cell, the most common clusters are 4Fe–4S clusters. The ISA system mediates the transformation of 2Fe–2S clusters into 4Fe–4S clusters in the mitochondrial matrix. Unlikely to mitochondrial ISC biogenesis system, the cytoplasm contains different machineries to assembly 4Fe–4S clusters. The biogenesis of cytoplasmic 4Fe–4S clusters rely on substrate exported from the matrix by ABCB7 (Lill et al., 2015).

In brief, ISCA1, ISCA2, and IBA57 are responsible for the generation of mitochondrial 4Fe–4S clusters. ISCA1 and ISCA2 interact with each other (Muhlenhoff et al., 2011; Beilschmidt et al., 2017), and structure study reveals that ISCA2, but not ISCA1, is able to bind IBA57 (Muhlenhoff et al., 2011; Beilschmidt et al., 2017; Gourdoupis et al., 2018). Two GLRX5-derived 2Fe–2S clusters are converted to a 4Fe–4S cluster on the ISCA1-ISCA2 complex. This process required the presence of IBA57 and the electron transfer chain NADPH-FDXR-FDX2 (Weiler et al., 2020). Finally, NFU1 promotes the 4Fe–4S cluster transfer from the ISCA1-ISCA2-IBA57 complex to apoproteins. However, one biochemical study indicated that only ISCA1, but neither ISCA2 nor IBA57, is needed for the maturation of the 4Fe–4S cluster in mouse skeletal muscle and in primary neurons (Beilschmidt et al., 2017).

ISA system is only responsible for mitochondrial 4Fe–4S clusters biogenesis. In the absence of the ISA complex, cells showed mitochondrial function defects with uncompromised cellular viability, since the sulfur-containing component required for cytoplasmic Fe/S biogenesis still can be exported from mitochondria.

BIOGENESIS OF CYTOSOLIC AND NUCLEAR IRON–SULFUR (Fe/S) CLUSTERS

Except mitochondrial, there are also abundant ISC proteins located in cytosolic and nuclear in eukaryotic cells. And these proteins are involved in multiple biological processes. For example, DNA metabolism, iron regulation and metabolic catalysis. These processes are catalyzed by the CIA machinery. As discussed, the mitochondrial ISC assembly system generates an initial sulfur-containing intermediate and export the compound from mitochondria by the inner membrane ABC transporter, ABCB7 (Kispal et al., 1999; Gerber et al., 2004; Fosset et al., 2006; Lill et al., 2014). The exported intermediate is necessary for cytoplasmic ISC synthesis by the CIA system. However, chemical characterization and isolation of the intermediate is a subject of ongoing research. Glutathione (GSH) and the intermembrane space protein, ALR are important for this process (Kispal et al., 1999; Sipos et al., 2002; Pondarre et al., 2006; Cavadini et al., 2007). ALR is a FAD-dependent sulfhydryl oxidase. ALR inserts disulfide bridges into mitochondrial preproteins during their import into the intermembrane space (Mesecke et al., 2005). But another group reported that Cytosolic ISC protein maturation and iron regulation are independent of the mitochondrial Erv1/Mia40 import system. After the sulfur-containing compound was transferred to cytosolic, nine proteins of the CIA system are responsible for generating the cytosolic ISCs and inserting them into target proteins (Sharma et al., 2010;

TABLE 1 | Mitochondrial Fe/S cluster assembly components.

Complex	Human	Yeast	Function	Location
ISCU complex	ISCUs	Isu1/Isu2	Scaffold protein	Mitochondria, cytoplasm and nucleus
	NFS1	Nfs1	Cysteine desulfurase provides the sulfur	Mitochondria, cytoplasm and nucleus
	ISD11	Isd11	Stabilize binding partner of NFS1	Mitochondria and nucleus
	ACPM	Acp1	Bind to and stabilize Isd11	Mitochondria
	Ferredoxin	Yah1	Electron donor	Mitochondria
	Frataxin	Yfh1	Regulates NFS1 activity	Cytoplasm and nucleus
Cluster transfer complex	HSPA9	Ssq1	Co-chaperone of GLRX5	Mitochondria and nucleus
	HSC20	Jac1	Co-chaperone of GLRX5	Mitochondria, cytoplasm and nucleus
	GLRX5	Grx5	Transfers 2Fe–2S clusters to client proteins	Mitochondria
	ABCB7	Atm1	Exports Fe–S clusters from mitochondria	Mitochondria
	ALR	Erv1	Exports Fe–S clusters from mitochondria	Mitochondria and cytoplasm
ISA complex	ISCA1	Isa1	Assemble 4Fe–4S clusters	Mitochondria
	ISCA2	Isa2	Assemble 4Fe–4S clusters	Mitochondria
	IBA57	Iba57	Assemble 4Fe–4S clusters	Mitochondria
	NFU1	Nfu1	Transfer 4Fe–4S clusters to target proteins	Mitochondria

TABLE 2 | Cytosolic and nuclear Fe/S cluster assembly components.

Complex	Human	Yeast	Function	Location
CIA complex	CFD1	Cdf1	Scaffold protein	Cytoplasm
	NBP35	Nbp35	Scaffold protein	Cytoplasm and nucleus
	CIAPIN1	Dre2	Electron donor	Cytoplasm and nucleus
	NDOR1	Tah18	Electron donor	Cytoplasm
	IOP1	Nar1	Adaptor protein of CIA complex	Cytoplasm
	CIA1	Cia1	Transfer and insert Fe–S clusters into target proteins	Cytoplasm
	CIA2B	Cia2	Transfer and insert Fe–S clusters into target proteins	Cytoplasm and nucleus
	MMS19	Met18	Transfer and insert Fe–S clusters into target proteins	Cytoplasm and nucleus
	CIA2A	Absent	Specific maturation factor of IRP1	Cytoplasm

Basu et al., 2014; Netz et al., 2014). Major components involved in the CIA system are shown in **Table 2**. In the next section, the two essential steps of cytosolic and nuclear ISC assembly will be described.

Step 1 of Cytosolic and Nuclear Iron–Sulfur (Fe/S) Cluster Assembly

Similar to ISC biogenesis in mitochondria, the initial step of cytosolic and nuclear ISC synthesis is transient transfer a 4Fe–4S cluster to the cytosolic scaffold protein complex. This complex comprises two P-loop NTPases CFD1 and NBP35 (Roy et al., 2003; Hausmann et al., 2005; Netz et al., 2007; Stehling et al., 2018). CFD1 interact with NBP35 and form a heterotetrameric complex. This complex is able to coordinate two different types of 4Fe–4S clusters (Netz et al., 2012). One type of 4Fe–4S cluster can loosely bind to a conserved CX_2C motif that is located at the C-termini of CFD1 and NBP35. The second type of 4Fe–4S clusters bind at a ferredoxin-like $CX_{13}CX_2CX_5C$ motif, which is located at the N terminus of NBP35. This motif is essential for NBP35 function. Interestingly, a pulse-chase experiment with ^{55}Fe labeled yeast cells revealed the different labilities of the two ISCs associated with the CFD1–NBP35 complex (Pallesen et al., 2013). The 4Fe–4S cluster that binds to the N terminus of NBP35 is more stable than the 4Fe–4S cluster that binds the C-terminus, which transfers the loose-binding 4Fe–4S cluster to target proteins.

Another feature of cytosolic and nuclear ISC biogenesis that is similar to mitochondrial ISCs biogenesis is the dependency on a supply of electrons (Webert et al., 2014). The electron transfer chain of the CIA system comprises NADPH, NDOR1, and the Fe/S protein CIAPIN1 (Netz et al., 2010; Banci et al., 2013). NDOR1 is a key member of the electron transfer chain. It contains NADPH-, FAD- and FMN- binding domains. Protein-protein interaction and high-throughput studies have demonstrated that CIAPIN1 physically interacts with NDOR1 (Vernis et al., 2009). Dre2 is the CIAPIN1 yeast homolog: it is a crucial component of the cytosolic and nuclear ISC biogenesis system. The synthetically lethal effect was observed when deletion Dre2 and mitochondrial iron importers (Mrs3 and Mrs4) (Zhang et al., 2008). Dre2 contains a conserved C-terminal Fe/S domain which is responsible for coordinating one 2Fe–2S or one 4Fe–4S cluster by cysteine residues. The N-terminal of Dre2 is a SAM methyl-transferase-like domain, the middle linker domain of Dre2 mediate the connection of the N-terminus and C-terminus (Zhang et al., 2008; Netz et al., 2010, 2014).

Step 2 of Cytosolic and Nuclear Iron–Sulfur (Fe/S) Cluster Assembly

The second step of cytosolic ISC biogenesis is initialed by releasing the newly assembled 4Fe–4S cluster from the CFD1-NBP35 scaffold complex. Then, the 4Fe–4S cluster is inserted into targeted proteins (Balk et al., 2004, 2005; Song and Lee, 2008, 2011). Both the CIA targeting complex and

the iron-only hydrogenase-like protein, IOP1, are essential for this step reaction. Nar1 is the yeast ortholog of IOP1. Structure study of Nar1 revealed that the four conserved Cys residues, which are in the C-terminal of Nar1 are responsible for binding ISCs. The CIA targeting complex comprises CIA1, CIA2B, and human ortholog for the yeast methyl methanesulfonate-sensitivity protein 19 (MMS19). And these components physically interact with a large number of target proteins in the cytoplasm and nucleus (Srinivasan et al., 2007; Weerapana et al., 2010; van Wietmarschen et al., 2012; Stehling et al., 2013; Kassube and Thoma, 2020). The cytosolic ISC biogenesis contains two stages. In yeast, inactivation of early stage CIA assembles complex leads to the immaturity of Fe/S protein Nar1, while defect of late-stage proteins CIA1, CIA2B, and MMS19 do not affect ISC insert to target proteins (Balk et al., 2004). Base on this study, the early and late stage of CIA system is connected by Nar1via an unknown mode of action (Stehling et al., 2013).

CIA targeting complex component CIA1 contains seven WD40-repeat domains. The structural analysis demonstrated that these seven WD40-repeats distribute around a central axis, which functions as binding region docking site of the CIA targeting complex (Srinivasan et al., 2007). Point mutation of CIA1 has revealed that the conserved, surface-exposed residue R127 is responsible for assembling other subunits of cytosolic Fe/S protein (Paul and Lill, 2015). The conserved Cys residue is important for CIA2 function, which is also conserved in eukaryotes (Weerapana et al., 2010; Luo et al., 2012; Stehling et al., 2013). Knockout human CIA2B or its ortholog Cia2 suppresses the Fe/S proteins maturation (Chen et al., 2012). MMS19 contains 4 HEAT repeats at N-terminal. As the largest component of CIA, MMS19 is associated with the multitude of biological processes. For example, impaired chromosome segregation, defective double-strand break repair via homologous recombination, and immature cytosolic and nuclear Fe/S proteins (Prakash and Prakash, 1977; Lauder et al., 1996; Kou et al., 2008; Ito et al., 2010). For a long time, it was difficult to associate these phenotypes of MMS19-deficient cells with one molecular function. Until known that MMS19 is involved in cytosolic ISC biogenesis, this problem was resolved (Gari et al., 2012; Stehling et al., 2012). As a major determinant of the CIA targeting complex, MMS19 interacts with numerous target proteins and promotes the insertion of ISCs into them, including key enzymes in DNA synthesis (POLD1, PRIM2), DNA repair [XPD, DNA2 (DNA replication helicase/nuclease 2)], and telomere length regulation (RTEL1). Deletion of these enzymes, respectively, phenocopied variant MMS19 depletion defects.

THE CLOSE LINK BETWEEN IRON–SULFUR (Fe/S) CLUSTERS AND GENOME INTEGRITY

Mitochondria are organelles with a double-layer membrane found in most eukaryotic organisms. They generate most of the cellular chemical energy via oxidative phosphorylation. In addition to supplying energy, mitochondria are also involved in multitude of cellular biochemical processes such as programmed cell death, reactive oxygen species (ROS) production, and ISCs biogenesis. Biochemical studies revealed that mitochondrial DNA (mtDNA) defection result in nuclear genome instability and reduction of cells' viability in yeast. This effect is due to the important role of mitochondria ISC biogenesis (Veatch et al., 2009). As mentioned, down-regulation of Nar1 is sufficient to alter nuclear genome stability (Gari et al., 2012). Consistent with this study, deletion of Zim17, an important component of ISC biogenesis, leading to genomic instability (Diaz de la Loza Mdel et al., 2011; Stehling et al., 2013). Given that many enzymes that are required for DNA synthesis and repair harbor ISC cofactors, these observations suggest that defects in Fe/S biogenesis and distribution are likely to be the origin of genomic instability (Ben-Aroya et al., 2008; Veatch et al., 2009; Gari et al., 2012; Stehling et al., 2012; Stehling et al., 2013). For example, MMS19 was identified as a gene involved in transcription conducted by RNA polymerase II, nucleotide excision repair (NER), and methionine biosynthesis (Prakash and Prakash, 1977; Thomas et al., 1992). In yeast, the essential transcription factor IIH (TFIIH) complex is required for transcription-coupled NER (Lauder et al., 1996). MMS19 is not a component of the TFIIH complex, while numerous studies demonstrate that MMS19 is crucial to maintain the cellular Rad3 (XPD in human) protein level, a component of the TFIIH (Kou et al., 2008). Consistent with these findings, human MMS19 homolog also is reported to be involved in the NER pathway by regulating TFIIH function. In addition to regulating TFIIH function, MMS19 also directly interacts with CIA components CIA1 and CIA2B. And this interaction is important for regulating chromosome segregation and telomere length (Askree et al., 2004; Ito et al., 2010). All these MMS19 functional studies reveal the different phenotypes observed in MMS19 deficient cells (Gari et al., 2012; Stehling et al., 2012).

The function of MMS19 in DNA metabolism has been reported in multitude of ways. Many biochemical studies demonstrate that MMS19 and other CIA complex components directly interact with diverse DNA metabolism enzymes, such as DNA helicases [XPD, FANCJ (Fanconi anemia complementation group J)], and RTEL1, DNA polymerase subunits (POLD1, POLA1, and POLE1), the nuclease DNA2, the DNA glycosylase NTHL1, and the DNA primase PRI2. With the help of MMS19, these enzymes coordinate an ISC. Biochemical studies have revealed that MMS19 mediates the interaction of XPD and TFIIH, which is important for DNA metabolism. In yeast, deletion of Met18/Mms19, CIA complex components, increases phosphorylation of Rad3 and promotes Rad3-dependent gene expression (Gari et al., 2012; Stehling et al., 2012). Consist with this finding, cells lacking CIA complex proteins are very sensitive to DNA damage events, e.g., UV and chemical agents. Based on these studies, MMS19 not only is involved in the CIA complex for the maturity of target ISC proteins, but also plays a crucial role in DNA metabolism.

Recently, one biochemical study also indicated that inhibition of ISCs synthesis via NFS1 depletion in elevated O2 environment led to decreased POLE protein level. This perturbation reduces Pol ε activity and causes replication stress (Sviderskiy et al., 2020).

IRON–SULFUR (Fe/S) CLUSTERS AND DNA REPLICATION

High-fidelity DNA replication ensures the accurate transmission of parental genetic information to daughter cells. This process is coordinated by numerous enzymes (Bell and Dutta, 2002). Firstly, the DNA helicases open the double-stranded DNA. Then, the DNA primases initiate DNA synthesis via assembling short RNA primers, which are extended by DNA polymerases. DNA polymerases then utilize the two parental DNA strands as templates to synthesize complementary strands, but not to start *de novo* DNA replication (Bell and Dutta, 2002). During the DNA replication process, DNA2, a helicase/nuclease, is critical for lagging strand DNA replication via processing Okazaki fragment (Kang et al., 2010). The ISCs are critical for the proper functions of all three types of enzymes (**Table 3**). In the next section, we will describe the three types of replication factors that coordinate these crucial ISCs.

Iron–Sulfur (Fe/S) Clusters and Helicases

Helicases are a class of motor proteins that can unwind structured nucleic acids in an ATP-dependent manner. In this way, helicases can regulate many different processes that depend on strand separation during DNA metabolism (Lohman and Bjornson, 1996), including transcription, DNA replication, DNA repair, and telomere length regulation. Thus, helicases are important for genomic stability (Patel and Donmez, 2006; Brosh and Bohr, 2007; Lohman et al., 2008; Pyle, 2008). Helicases are classified into six super-families according to their primary amino acid sequences, and ISCs exist in numerous helicases.

In the helicase super-family 1, DNA2 is a multifunction enzyme not only involved in DNA replication, but also in double-strand DNA break (DSB) repair and telomere maintenance (Budd et al., 2005; Kang et al., 2010; Balakrishnan and Bambara, 2011). AddAB which contains a 4Fe–4S cluster, is a helicase-nuclease complex in bacteria. Eukaryotic helicase-nuclease DNA2 putative metal-binding motif was identified by sequence alignment with AddAB. Interestingly, structure studies revealed that four conserved Cys residues which are coordinated ISCs exist in the nuclease domain. This suggests that ISCs might function in stabilizing the nuclease domain conformation (Yeeles et al., 2009). Biochemical studies confirmed that yeast DNA2 coordinates ISCs by its conserved Cys residues (Pokharel and Campbell, 2012). ISC binding cysteine residues mutation results in nuclease activity and ATPase function defects in DNA2. However, the DNA binding ability of DNA2 is normal. Another biochemical study revealed that pro residue at position 504 of DNA2 is crucial to stabilize the ISC. These studies confirmed that the ISC regulates DNA2 nuclease and helicase activities by mediating conformational changes.

In the helicase super-family 2, an XPD homolog from Archaea was the first DNA repair helicase to be identified. A sequence alignment revealed that all the XPD helicase family members contain four highly conserved Cys residues. These conserved Cys residues which coordinate an ISC are crucial for 5′–3′ DNA helicases activity. The XPD helicase family comprises XPD and several related super-family 2 DNA helicases including DDX11/ChlR1 (DEAD/DEAH box helicase 11), RTEL1 (regulator of telomere elongation 1), and FANCJ (Fanconi anemia complementation group J). Many human diseases are linked to mutations in these three proteins (**Table 3**; White, 2009; Wu and Brosh, 2012).

XPD is a crucial subunit of the transcription initiation factor TFIIH, which is involved in NER and transcription (Compe and Egly, 2012). TFIIH comprises two major functional subcomplexes, a core complex (XPB, p8, p34, p44, p52, and p62), and a CAK (CDK–activating kinase) complex (cyclin H, CDK7, and MAT1). Helicase XPD is an important bridge between these two subcomplexes.

The mutations of XPD gene are related to three genetic diseases: xeroderma pigmentosum (XP), Cockayne syndrome (CS), and trichothiodystrophy (TTD) (White, 2009; Wu and Brosh, 2012). All three disorders have similar characteristics, with patients' skin being hypersensitive to sun exposure. This is due to the defect of the NER pathway (Lehmann, 2003). In 2006, biochemical and spectroscopic analyses indicated that XPD coordinates a 4Fe–4S cluster, which is a key determinant of XPD helicase activity. This finding significantly contributes to revealing the molecular differences of how mutations in a single gene result in different diseases (Stehling et al., 2012). Subsequently, structural analysis showed that the 4Fe–4S domain forms a channel with an arch domain, that can accommodate single-stranded DNA (ssDNA) (Fan et al., 2008; Liu et al., 2008; Wolski et al., 2008). Mutational analysis of conserved cysteine residues in the Fe/S domain of XPD indicated that an intact Fe/S domain is essential for helicase activity and/or stabilizing the protein structure (Liu et al., 2008; Pugh et al., 2008). For patients with XP, mutations in XPD primarily inhibit helicase activity without affecting the protein structure. Interestingly, all

TABLE 3 | DNA metabolism enzymes with Fe/S clusters.

Human	Yeast	Function	Associated disease
PRIM2	Pri2	Subunit of DNA primase, DNA synthesis and double-strand break repair	–
CHLR1	Chl1	Helicase, sister chromatid cohesion, heterochromatin organization	Warsaw breakage syndrome
DNA2	Dna2	Helicase/nuclease, DNA repair	–
FANCJ	Absent	Helicase	Fanconi anemia
RTEL1	Absent	Helicase	Hoyeraal–Hreidarsson syndrome
XPD	Rad3	Helicase	Xeroderma pigmentosum, Cockayne syndrome
POLA	Pol1	Catalytic subunit of polymerase α,	–
POLD1	Pol3	Catalytic subunit of polymerase δ,	–
POLE1	Pol2	Catalytic subunit of polymerase ε,	–
MUTYH	Absent	DNA glycosylase	–
NTHL1	Ntg2	DNA glycosylase	–

XP-causing mutations are conserved in archaeal XPD (Fan et al., 2008; Liu et al., 2008). However, most of the mutated residues in TTD are not conserved in the archaeal protein (Liu et al., 2008). In TTD patients, R112H exchange is the most common mutation. This amino acid substitution leads to loss of XPD helicase activity and deficiency of NER (Dubaele et al., 2003). Biochemical and structural studies demonstrated that this Arg residue is essential for the Fe/S domain. These findings underscore the structural role played by the ISC in helicase activity and highlight the close relationship between ISCs and DNA replication. In addition to these disease-associated mutations, other mutations of XPD destabilize the helicase structure and compromise interactions between the two TFIIH sub-complexes (Dubaele et al., 2003; Liu et al., 2008).

FANCJ, which was able to interact with the breast cancer C-terminal (BRCT) repeats of BRCA1, is another important member of the XPD helicase family (Cantor et al., 2001). FANCJ has been identified as the gene that is mutated in the J complementation group of Fanconi anemia (FA), a genome instability disorder with an elevated risk of developing cancer. FANCJ is known as an anti-oncogene because of its functions in DNA repair (Wu and Brosh, 2009). The substitution A349P in FANCJ is a common mutation seen in patients with FA (Wu et al., 2010). Although this alanine is not a conserved site in the XPD helicase family, the residue is near the fourth highly conserved cysteine residue in the ISC. Consistent with this, recombinant FANCJ-A349P protein was shown to decrease iron content and inhibit the separation of double-stranded DNA (dsDNA) (Wu et al., 2010). This finding indicates that, like XPD helicase, the catalytic activities of FANCJ critically rely on an intact Fe/S domain.

DDX11/CHLR is the third member of the XPD helicase family. The genetic disease Warsaw breakage syndrome (WABS) arises from a mutation in the human CHLR1 gene (van der Lelij et al., 2010). In *S. cerevisiae*, a mutation in *chl1* causes chromosome loss and unusual mating phenotypes (Liras et al., 1978). Consistent with this finding, mutations in *chl1* or CHLR1, the human homolog, show similar results (Skibbens, 2004; Parish et al., 2006). Unsurprisingly, patient-derived mutations also abolish helicase activity due to their perturbance of DNA binding and DNA-dependent ATPase activity (Wu et al., 2012).

Iron–Sulfur (Fe/S) Clusters and DNA Primase

A common feature of all DNA polymerases is that they are unable to initiate *de novo* synthesis of a DNA strand; they can only elongate an existing strand. Synthesis of a new strand can only begin from a primer with the 3′-OH end. Hence, a primase is required to catalyze the priming, form a primer, and initiate DNA replication. Primase in eukaryotic cells comprises two subunits, the catalytic PRIM1 subunit, and a large subunit PRIM2, both interacted with DNA polymerase-α (Frick and Richardson, 2001; Kang et al., 2010). Although only the PRIM1 subunit possesses catalytic activity, PRIM2 is also crucial for primase function (Zerbe and Kuchta, 2002). Spectroscopic analysis indicates that PRIM2 is able to bind a 4Fe–4S cluster, which is conserved from Archaea to eukaryotic cells (Weiner et al., 2007). Without this ISC, its enzymatic activity is compromised. High-resolution structural studies show that the conserved Lys314 in the C-terminal domain of human PRIM2 is supported by the 4Fe–4S cluster. This Lys314 mutant abolishes primer synthesis and DNA binding (Vaithiyalingam et al., 2010). This finding suggests that ISCs facilitate DNA binding via organizing the protein surface (Vaithiyalingam et al., 2010).

In addition, ISCs serve as a major determinant for regulation through their physical interactions with other proteins involved in DNA replication, the DNA damage response, stalled replication fork, and telomere maintenance (Weiner et al., 2007). The N- and C-terminal domains of PRIM2 folded together and are connected by a flexible 18-residue linker (Baranovskiy et al., 2018). Crystal structure studies reviewed that there are three metal-binding sites in the DNA primase, a Zn^{2+}-binding site, a PRIM1 catalytic site which coordinates two Mg^{2+} (or Mn^{2+}) ions, and a 4Fe–4S binding site in PRIM2. Furthermore, PRIM2 has four conserved Cys residues: Cys287, Cys367, Cys384, and Cys424, which are important for coordinating ISC. Point mutation of these Cys residues cause instability of both PRIM1 and PRIM2. The unstable structure of PRIM1 and PRIM2 lead to dysfunction of DNA polymerase-α primase complex and stalled replication fork (Liu and Huang, 2015). In fact, even a single point mutation of the conserved Cys residues is sufficient to reduce the activities of DNA primase and DNA polymerase. This result indicates that ISCs have an important role in enzyme functions[(12)].

Iron–Sulfur (Fe/S) Clusters and Polymerases

In eukaryotes, four types of class B family DNA polymerase complexes mediate replication and replication-associated genome maintenance. During normal replication, DNA polymerases (Pol) α, δ, and ε are responsible for replication fork extension. While the fourth polymerase, Polζ, is required for DNA synthesis at damaged sites (Johansson and Macneill, 2010). These polymerases are comprised of catalytic, regulatory, and accessory subunits (Burgers et al., 2001). Biochemical and structural studies demonstrate that there are two metal-binding motifs with conserved cysteine (CysA and CysB) located at Pol α, Pol δ, and Pol ε C-terminal catalytic subunits. At first, it was reported that these two metal-binding motifs coordinate Zn^{2+} ions (Evanics et al., 2003; Klinge et al., 2009). And they are essential for the stability of replisome. However, synthetically lethal effects are observed in yeast containing a single point mutant in the Pol3 CysB motif with essential components (DRE2, NBP35, and TAH18) of CIA complex (Chanet and Heude, 2003). Furthermore, pulse-chase ^{55}Fe experiment, UV–Vis, and electron paramagnetic resonance (EPR) spectroscopic studies proved that the CysB motifs of all B-family DNA polymerases coordinate ISCs rather than Zn^{2+} (Netz et al., 2011; Suwa et al., 2015; Ter Beek et al., 2019). Overexpression *S. cerevisiae* Polδ subunit Pol31 enhances the ability of binding ISCs (Sanchez Garcia et al., 2004). Consist with this study, Polζ catalytic subunit Rev3 also coordinates the

4Fe–4S cluster in CysB. And the 4Fe–4S cluster is crucial for stabilizing the polymerase complex (Baranovskiy et al., 2018). Together, these findings suggest that the proper activities of DNA polymerases require 4Fe–4S cluster coordination. In addition to CysB, CysA is also important for the interaction between PCNA with Polδ on DNA. PCNA is a major determinant for regulating DNA replication and cell cycle. Notably, the DNA polymerase and exonuclease of Polδ were regulated by coordinated ISC (Jozwiakowski et al., 2019). In addition to class B-family polymerase complex, biochemical studies revealed that D-family polymerases also coordinate ISCs in their CysB motif. Furthermore, ISCs are important for polymerase complex formation. Point mutation of conserved Cys residue in Pol3 results in the reduction of coordinated ISC and disassociation with Polδ subunits Pol31 and Pol32. Moreover, Pol3 and the Fe/S biosynthetic genes are synthetic lethal, indicate that ISC is an essential cofactor for DNA polymerase to regulate its structure and functions (Chanet and Heude, 2003).

IRON–SULFUR (Fe/S) CLUSTERS PROTEIN AND DNA REPAIR

Oxidation, deamination, and alkylation are likely to induce single base damage in DNA. Base excision repair (BER) is a highly conserved cellular biochemical process that repairs damaged bases throughout the cell cycle (Krokan and Bjoras, 2013). BER is started from DNA glycosylases, which recognize and remove damaged or inappropriate bases by forming AP sites. Then, these AP sites are cleaved by an AP endonuclease. Finally, according to the length of the resulting single-strand break, the damaged DNA can be repaired by short-patch or long-patch BER (Wallace, 2013). During this process, many DNA glycosylases contain Fe/S cofactor (Guan et al., 1998; Alseth et al., 1999; Hinks et al., 2002). The *E. coli* endonuclease III (Endo III) is the first known DNA glycosylase that coordinates a 4Fe–4S cluster. The interaction of Endo III with the DNA phosphate backbone is dependent on its ISC (Kuo et al., 1992). The *E. coli* MutY is an adenine DNA glycosylase involved in BER. Structurally like Endo III, MutY coordinates a 4Fe–4S cluster (Guan et al., 1998), which is important for MutY structure stability and recognition of substrates (Porello et al., 1998; Lu and Wright, 2003). Electrochemical studies showed that DNA binding of Endo III and MutY shifts the redox potentials of the 4Fe–4S clusters, which sense DNA lesions via electron transfer (Boal et al., 2005). Consist with MutY, the mammalian homolog MUTYH also functions in fixing oxidation caused DNA lesions (McGoldrick et al., 1995).

To date, there are no reports to suggest that DNA topoisomerase or ligase is coordinated with the ISC. However, both have been linked to cellular ISCs metabolism. Eukaryotic DNA topoisomerase II (Topo II) is able to modulate negative supercoiling DNA in an ATP-dependent manner. The inhibition of Topo II leads to a loss of chromosomal supercoiling and furthermore results in the upregulation of oxidative phosphorylation (Dahan-Grobgeld et al., 1998), which increases ROS levels (Nosal et al., 2014). The inhibition of Topo II induces the DNA damage response, upregulation of iron uptake, and ISC biosynthesis (Dwyer et al., 2007).

CONCLUDING REMARKS AND FUTURE PERSPECTIVES

Much research conducted over the past decade has greatly advanced our understanding of how the ISCs assemble and insert into target proteins in mitochondria, cytoplasm, and nucleus. However, there is still much to learn. For example, most of the proteins functioning in these pathways have been identified, but a complete picture of how ISC formation is regulated remains unclear. Recently, one group reported that acylated ACP1 may regulate ISCs *de novo* assembly via its dynamic interaction with ISD11. Upon high acetyl-CoA, mtFAS promotes long fatty acyl chain synthesis and acylated ACP1 binds to NFS1-ISD11. The long fatty acyl chain is able to stabilize the NFS1-ISD11-ACP1 complex and promote ISCs *de novo* assembly. On the contrary, cells that lack acylated ACP1 exhibit lower efficiency of ISCs assembly (Van Vranken et al., 2018). It is undeniable, however, that the regulation of ISC formation is crucial for cell survival.

ISC formation is controlled by several comprehensive mechanisms, including that (1) the Fe/S machinery requires delicate allosteric control, (2) the ISC delivery variations are regulated by carrier proteins, and (3) the expression levels of the Fe/S assembly protein are transcriptionally regulated. Despite great progress has been made, more research is needed to gain further insights into these processes.

Recent studies using mass spectrometry have identified many phosphorylation sites of NFS1; it has also been shown that mitochondria contribute to NFS1's phosphorylation, which is required for its activity. Since lacking sulfur from cysteine stops the ISC synthesis, this Nfs1 phosphorylation in mitochondria has the great potential to regulate the entire ISC assembly process (Rocha et al., 2018). However, although the crystal structure of the human NFS1/ISD11/ACP complex has been observed, the phosphorylated residues were not detected and remain unclear (Cory et al., 2017).

Similarly, in the cytoplasm of mammalian cells, ISCU is phosphorylated by mTORC1. This phosphorylation event enhances the stability of the protein and promotes ISC assembly (La et al., 2013).

The degradation mechanism of the ISC is also unclear. One unique feature of 4Fe–4S is that it can be cleaved to either one 3Fe–4S cluster or two 2Fe–2S clusters. For instance, the 4Fe–4S cluster in a nitrogenase Fe-protein can be converted into two 2Fe–2S clusters (Sen et al., 2004). ISCs can also serve as sulfur donors for other sulfur-containing protein cofactors, such as biotin and lipoic acid, in a self-sacrificing fashion. Exploring the mechanism of this cleavage is essential to understanding the function of these proteins. We believe that a combination of the developing approaches in the structural, biochemical, and cell biological fields will deepen our knowledge of the molecular mechanisms of assembly, insertion, and regulation of the ISCs in target proteins.

A steadily increasing number of ISC proteins that function in genome integrity maintenance have been identified. Thus, the next major research challenge is elucidating their molecular mechanisms. To date, most of the studies support that the ISC stabilizes the structure of DNA metabolism proteins (White and Dillingham, 2012). Besides that, Barton's group found that electron transport happens over a long distance of DNA. DNA lesions disrupt this charge transfer, which changes the redox-active status of the ISC in DNA. This proposes that, ISC is the key of how DNA glycosylases distinguish the intact and damaged bases. Similarly, primer synthesis by primase also requires the 4Fe–4S cluster although the underlying mechanisms remain unclear. One DNA-mediated electrochemistry experiment demonstrated that a reversible on/off switch in DNA primase for DNA binding is the oxidation state of the 4Fe–4S cluster. Moreover, primer synthesis is regulated by both the conserved charge transfer pathway through primase and DNA charge transport chemistry. This finding suggests that the primase uses DNA charge transport for redox signaling of 4Fe–4S clusters thus provides a chemical basis for understanding the precise regulation of primase activity and supports the notion of a fundamentally new redox switch model for substrate handoff (O'Brien et al., 2017).

Overall, the ISCs coordinate with key proteins in DNA metabolism. This coordination with the ISC regulates the target proteins via (1) stabilizing their structures, (2) mediating their local conformational changes, and (3) facilitating DNA charge transport. Improving our understanding of the critical roles played by ISCs in DNA replication and repair enzymes will ultimately help us solve the great mysteries around the DNA metabolism enzymes critical to life.

AUTHOR CONTRIBUTIONS

RS and XX conceived the scope and schemes of this review manuscript. RS wrote the first draft. WH, Z-QW, and XX revised and finalized the manuscript. All authors read and approved the submitted version.

FUNDING

This work was supported by the National Natural Science Foundation of China (Grants 31530016, 32090031, and 31761133012), the National Basic Research Program of China (Grant 2017YFA0503900), and the Shenzhen Science and Technology Innovation Commission (Grants JCYJ20180507182213033 and JCYJ20170412113009742).

ACKNOWLEDGMENTS

We would like to thank the members of the Xu lab for their insightful discussion and Dr. Jessica Tamanini for language editing prior to submission.

REFERENCES

Adamec, J., Rusnak, F., Owen, W. G., Naylor, S., Benson, L. M., Gacy, A. M., et al. (2000). Iron-dependent self-assembly of recombinant yeast frataxin: implications for Friedreich ataxia. *Am. J. Hum. Genet.* 67, 549–562. doi: 10.1086/303056

Alseth, I., Eide, L., Pirovano, M., Rognes, T., Seeberg, E., and Bjoras, M. (1999). The *Saccharomyces cerevisiae* homologues of endonuclease III from *Escherichia coli*, Ntg1 and Ntg2, are both required for efficient repair of spontaneous and induced oxidative DNA damage in yeast. *Mol. Cell Biol.* 19, 3779–3787. doi: 10.1128/mcb.19.5.3779

Andreini, C., Rosato, A., and Banci, L. (2017). The relationship between environmental dioxygen and iron-sulfur proteins explored at the genome level. *PLoS One* 12:e0171279. doi: 10.1371/journal.pone.0171279

Arnold, A. R., Grodick, M. A., and Barton, J. K. (2016). DNA charge transport: from chemical principles to the cell. *Cell Chem. Biol.* 23, 183–197. doi: 10.1016/j.chembiol.2015.11.010

Askree, S. H., Yehuda, T., Smolikov, S., Gurevich, R., Hawk, J., Coker, C., et al. (2004). A genome-wide screen for *Saccharomyces cerevisiae* deletion mutants that affect telomere length. *Proc. Natl. Acad. Sci. U.S.A.* 101, 8658–8663. doi: 10.1073/pnas.0401263101

Babcock, M., de Silva, D., Oaks, R., Davis-Kaplan, S., Jiralerspong, S., Montermini, L., et al. (1997). Regulation of mitochondrial iron accumulation by Yfh1p, a putative homolog of frataxin. *Science* 276, 1709–1712. doi: 10.1126/science.276.5319.1709

Balakrishnan, L., and Bambara, R. A. (2011). The changing view of Dna2. *Cell Cycle* 10, 2620–2621. doi: 10.4161/cc.10.16.16545

Balk, J., Aguilar Netz, D. J., Tepper, K., Pierik, A. J., and Lill, R. (2005). The essential WD40 protein Cia1 is involved in a late step of cytosolic and nuclear iron-sulfur protein assembly. *Mol. Cell Biol.* 25, 10833–10841. doi: 10.1128/mcb.25.24.10833-10841.2005

Balk, J., Pierik, A. J., Netz, D. J., Muhlenhoff, U., and Lill, R. (2004). The hydrogenase-like Nar1p is essential for maturation of cytosolic and nuclear iron-sulphur proteins. *EMBO J.* 23, 2105–2115. doi: 10.1038/sj.emboj.7600216

Banci, L., Bertini, I., Calderone, V., Ciofi-Baffoni, S., Giachetti, A., Jaiswal, D., et al. (2013). Molecular view of an electron transfer process essential for iron-sulfur protein biogenesis. *Proc. Natl. Acad. Sci. U.S.A.* 110, 7136–7141. doi: 10.1073/pnas.1302378110

Banci, L., Brancaccio, D., Ciofi-Baffoni, S., Del Conte, R., Gadepalli, R., Mikolajczyk, M., et al. (2014). [2Fe-2S] cluster transfer in iron-sulfur protein biogenesis. *Proc. Natl. Acad. Sci. U.S.A.* 111, 6203–6208. doi: 10.1073/pnas.1400102111

Baranovskiy, A. G., Siebler, H. M., Pavlov, Y. I., and Tahirov, T. H. (2018). Iron-sulfur clusters in DNA polymerases and primases of eukaryotes. *Methods Enzymol.* 599, 1–20. doi: 10.1016/bs.mie.2017.09.003

Basu, S., Netz, D. J., Haindrich, A. C., Herlerth, N., Lagny, T. J., Pierik, A. J., et al. (2014). Cytosolic iron-sulphur protein assembly is functionally conserved and essential in procyclic and bloodstream *Trypanosoma brucei*. *Mol. Microbiol.* 93, 897–910. doi: 10.1111/mmi.12706

Beilschmidt, L. K., Ollagnier de Choudens, S., Fournier, M., Sanakis, I., Hograindleur, M. A., Clemancey, M., et al. (2017). ISCA1 is essential for mitochondrial Fe4S4 biogenesis in vivo. *Nat. Commun.* 8:15124.

Beilschmidt, L. K., and Puccio, H. M. (2014). Mammalian Fe-S cluster biogenesis and its implication in disease. *Biochimie* 100, 48–60. doi: 10.1016/j.biochi.2014.01.009

Bell, S. P., and Dutta, A. (2002). DNA replication in eukaryotic cells. *Annu. Rev. Biochem.* 71, 333–374.

Ben-Aroya, S., Coombes, C., Kwok, T., O'Donnell, K. A., Boeke, J. D., and Hieter, P. (2008). Toward a comprehensive temperature-sensitive mutant repository of the essential genes of *Saccharomyces cerevisiae*. *Mol. Cell* 30, 248–258. doi: 10.1016/j.molcel.2008.02.021

Boal, A. K., Yavin, E., Lukianova, O. A., O'Shea, V. L., David, S. S., and Barton, J. K. (2005). DNA-bound redox activity of DNA repair glycosylases containing [4Fe-4S] clusters. *Biochemistry* 44, 8397–8407. doi: 10.1021/bi047494n

Brancaccio, D., Gallo, A., Mikolajczyk, M., Zovo, K., Palumaa, P., Novellino, E., et al. (2014). Formation of [4Fe-4S] clusters in the mitochondrial iron-sulfur cluster assembly machinery. *J. Am. Chem. Soc.* 136, 16240–16250. doi: 10.1021/ja507822j

Bridwell-Rabb, J., Fox, N. G., Tsai, C. L., Winn, A. M., and Barondeau, D. P. (2014). Human frataxin activates Fe-S cluster biosynthesis by facilitating sulfur transfer chemistry. *Biochemistry* 53, 4904–4913. doi: 10.1021/bi500532e

Brosh, R. M. Jr., and Bohr, V. A. (2007). Human premature aging, DNA repair and RecQ helicases. *Nucleic Acids Res.* 35, 7527–7544. doi: 10.1093/nar/gkm1008

Budd, M. E., Tong, A. H., Polaczek, P., Peng, X., Boone, C., and Campbell, J. L. (2005). A network of multi-tasking proteins at the DNA replication fork preserves genome stability. *PLoS Genet.* 1:e61. doi: 10.1371/journal.pgen.0010061

Burgers, P. M., Koonin, E. V., Bruford, E., Blanco, L., Burtis, K. C., Christman, M. F., et al. (2001). Eukaryotic DNA polymerases: proposal for a revised nomenclature. *J. Biol. Chem.* 276, 43487–43490.

Cai, K., Tonelli, M., Frederick, R. O., and Markley, J. L. (2017). Human mitochondrial ferredoxin 1 (FDX1) and ferredoxin 2 (FDX2) both bind cysteine desulfurase and donate electrons for iron-sulfur cluster biosynthesis. *Biochemistry* 56, 487–499. doi: 10.1021/acs.biochem.6b00447

Campuzano, V., Montermini, L., Molto, M. D., Pianese, L., Cossee, M., Cavalcanti, F., et al. (1996). Friedreich's ataxia: autosomal recessive disease caused by an intronic GAA triplet repeat expansion. *Science* 271, 1423–1427.

Cantor, S. B., Bell, D. W., Ganesan, S., Kass, E. M., Drapkin, R., Grossman, S., et al. (2001). BACH1, a novel helicase-like protein, interacts directly with BRCA1 and contributes to its DNA repair function. *Cell* 105, 149–160. doi: 10.1016/s0092-8674(01)00304-x

Cavadini, P., Biasiotto, G., Poli, M., Levi, S., Verardi, R., Zanella, I., et al. (2007). RNA silencing of the mitochondrial ABCB7 transporter in HeLa cells causes an iron-deficient phenotype with mitochondrial iron overload. *Blood* 109, 3552–3559. doi: 10.1182/blood-2006-08-041632

Chanet, R., and Heude, M. (2003). Characterization of mutations that are synthetic lethal with pol3-13, a mutated allele of DNA polymerase delta in *Saccharomyces cerevisiae*. *Curr. Genet.* 43, 337–350. doi: 10.1007/s00294-003-0407-2

Chen, K. E., Richards, A. A., Ariffin, J. K., Ross, I. L., Sweet, M. J., Kellie, S., et al. (2012). The mammalian DUF59 protein Fam96a forms two distinct types of domain-swapped dimer. *Acta Crystallogr. D Biol. Crystallogr.* 68, 637–648. doi: 10.1107/s0907444912006592

Compe, E., and Egly, J. M. (2012). TFIIH: when transcription met DNA repair. *Nat. Rev. Mol. Cell Biol.* 13, 343–354. doi: 10.1038/nrm3350

Cory, S. A., Van Vranken, J. G., Brignole, E. J., Patra, S., Winge, D. R., Drennan, C. L., et al. (2017). Structure of human Fe-S assembly subcomplex reveals unexpected cysteine desulfurase architecture and acyl-ACP-ISD11 interactions. *Proc. Natl. Acad. Sci. U.S.A.* 114, E5325–E5334.

Dahan-Grobgeld, E., Livneh, Z., Maretzek, A. F., Polak-Charcon, S., Eichenbaum, Z., and Degani, H. (1998). Reversible induction of ATP synthesis by DNA damage and repair in *Escherichia coli*. In vivo NMR studies. *J. Biol. Chem.* 273, 30232–30238. doi: 10.1074/jbc.273.46.30232

Diaz de la Loza Mdel, C., Gallardo, M., Garcia-Rubio, M. L., Izquierdo, A., Herrero, E., Aguilera, A., et al. (2011). Zim17/Tim15 links mitochondrial iron-sulfur cluster biosynthesis to nuclear genome stability. *Nucleic Acids Res.* 39, 6002–6015. doi: 10.1093/nar/gkr193

Dubaele, S., Proietti De Santis, L., Bienstock, R. J., Keriel, A., Stefanini, M., Van Houten, B., et al. (2003). Basal transcription defect discriminates between xeroderma pigmentosum and trichothiodystrophy in XPD patients. *Mol. Cell* 11, 1635–1646. doi: 10.1016/s1097-2765(03)00182-5

Dutkiewicz, R., Schilke, B., Knieszner, H., Walter, W., Craig, E. A., and Marszalek, J. (2003). Ssq1, a mitochondrial Hsp70 involved in iron-sulfur (Fe/S) center biogenesis. Similarities to and differences from its bacterial counterpart. *J. Biol. Chem.* 278, 29719–29727. doi: 10.1074/jbc.m303527200

Dwyer, D. J., Kohanski, M. A., Hayete, B., and Collins, J. J. (2007). Gyrase inhibitors induce an oxidative damage cellular death pathway in *Escherichia coli*. *Mol. Syst. Biol.* 3:91. doi: 10.1038/msb4100135

Evanics, F., Maurmann, L., Yang, W. W., and Bose, R. N. (2003). Nuclear magnetic resonance structures of the zinc finger domain of human DNA polymerase-alpha. *Biochim. Biophys. Acta* 1651, 163–171. doi: 10.1016/s1570-9639(03)00266-8

Fan, L., Fuss, J. O., Cheng, Q. J., Arvai, A. S., Hammel, M., Roberts, V. A., et al. (2008). XPD helicase structures and activities: insights into the cancer and aging phenotypes from XPD mutations. *Cell* 133, 789–800. doi: 10.1016/j.cell.2008.04.030

Fosset, C., Chauveau, M. J., Guillon, B., Canal, F., Drapier, J. C., and Bouton, C. (2006). RNA silencing of mitochondrial m-Nfs1 reduces Fe-S enzyme activity both in mitochondria and cytosol of mammalian cells. *J. Biol. Chem.* 281, 25398–25406. doi: 10.1074/jbc.m602979200

Fox, N. G., Das, D., Chakrabarti, M., Lindahl, P. A., and Barondeau, D. P. (2015). Frataxin accelerates [2Fe-2S] cluster formation on the human Fe-S assembly complex. *Biochemistry* 54, 3880–3889. doi: 10.1021/bi5014497

Fox, N. G., Yu, X., Feng, X., Bailey, H. J., Martelli, A., Nabhan, J. F., et al. (2019). Structure of the human frataxin-bound iron-sulfur cluster assembly complex provides insight into its activation mechanism. *Nat. Commun.* 10:2210.

Frick, D. N., and Richardson, C. C. (2001). DNA primases. *Annu. Rev. Biochem.* 70, 39–80. doi: 10.1146/annurev.biochem.70.1.39

Gari, K., Leon Ortiz, A. M., Borel, V., Flynn, H., Skehel, J. M., and Boulton, S. J. (2012). MMS19 links cytoplasmic iron-sulfur cluster assembly to DNA metabolism. *Science* 337, 243–245. doi: 10.1126/science.1219664

Gerber, J., Neumann, K., Prohl, C., Muhlenhoff, U., and Lill, R. (2004). The yeast scaffold proteins Isu1p and Isu2p are required inside mitochondria for maturation of cytosolic Fe/S proteins. *Mol. Cell Biol.* 24, 4848–4857. doi: 10.1128/mcb.24.11.4848-4857.2004

Gervason, S., Larkem, D., Mansour, A. B., Botzanowski, T., Muller, C. S., Pecqueur, L., et al. (2019). Physiologically relevant reconstitution of iron-sulfur cluster biosynthesis uncovers persulfide-processing functions of ferredoxin-2 and frataxin. *Nat. Commun.* 10:3566.

Gisselberg, J. E., Dellibovi-Ragheb, T. A., Matthews, K. A., Bosch, G., and Prigge, S. T. (2013). The suf iron-sulfur cluster synthesis pathway is required for apicoplast maintenance in malaria parasites. *PLoS Pathog.* 9:e1003655. doi: 10.1371/journal.ppat.1003655.g004

Gourdoupis, S., Nasta, V., Calderone, V., Ciofi-Baffoni, S., and Banci, L. (2018). IBA57 Recruits ISCA2 to form a [2Fe-2S] cluster-mediated complex. *J. Am. Chem. Soc.* 140, 14401–14412. doi: 10.1021/jacs.8b09061

Guan, Y., Manuel, R. C., Arvai, A. S., Parikh, S. S., Mol, C. D., Miller, J. H., et al. (1998). MutY catalytic core, mutant and bound adenine structures define specificity for DNA repair enzyme superfamily. *Nat. Struct. Biol.* 5, 1058–1064. doi: 10.1038/4168

Hausmann, A., Aguilar Netz, D. J., Balk, J., Pierik, A. J., Muhlenhoff, U., and Lill, R. (2005). The eukaryotic P loop NTPase Nbp35: an essential component of the cytosolic and nuclear iron-sulfur protein assembly machinery. *Proc. Natl. Acad. Sci. U.S.A.* 102, 3266–3271. doi: 10.1073/pnas.0406447102

Hinks, J. A., Evans, M. C., De Miguel, Y., Sartori, A. A., Jiricny, J., and Pearl, L. H. (2002). An iron-sulfur cluster in the family 4 uracil-DNA glycosylases. *J. Biol. Chem.* 277, 16936–16940. doi: 10.1074/jbc.m200668200

Ito, S., Tan, L. J., Andoh, D., Narita, T., Seki, M., Hirano, Y., et al. (2010). MMXD, a TFIIH-independent XPD-MMS19 protein complex involved in chromosome segregation. *Mol. Cell* 39, 632–640. doi: 10.1016/j.molcel.2010.07.029

Johansson, E., and Macneill, S. A. (2010). The eukaryotic replicative DNA polymerases take shape. *Trends Biochem. Sci.* 35, 339–347. doi: 10.1016/j.tibs.2010.01.004

Johnson, D. C., Dean, D. R., Smith, A. D., and Johnson, M. K. (2005). Structure, function, and formation of biological iron-sulfur clusters. *Annu. Rev. Biochem.* 74, 247–281. doi: 10.1146/annurev.biochem.74.082803.133518

Jozwiakowski, S. K., Kummer, S., and Gari, K. (2019). Human DNA polymerase delta requires an iron-sulfur cluster for high-fidelity DNA synthesis. *Life Sci. Alliance* 2:e201900321. doi: 10.26508/lsa.201900321

Kang, Y. H., Lee, C. H., and Seo, Y. S. (2010). Dna2 on the road to Okazaki fragment processing and genome stability in eukaryotes. *Crit. Rev. Biochem. Mol. Biol.* 45, 71–96. doi: 10.3109/10409230903578593

Karthikeyan, G., Lewis, L. K., and Resnick, M. A. (2002). The mitochondrial protein frataxin prevents nuclear damage. *Hum. Mol. Genet.* 11, 1351–1362. doi: 10.1093/hmg/11.11.1351

Kassube, S. A., and Thoma, N. H. (2020). Structural insights into Fe-S protein biogenesis by the CIA targeting complex. *Nat. Struct. Mol. Biol.* 27, 735–742. doi: 10.1038/s41594-020-0454-0

Kispal, G., Csere, P., Prohl, C., and Lill, R. (1999). The mitochondrial proteins Atm1p and Nfs1p are essential for biogenesis of cytosolic Fe/S proteins. *EMBO J.* 18, 3981–3989. doi: 10.1093/emboj/18.14.3981

Klinge, S., Hirst, J., Maman, J. D., Krude, T., and Pellegrini, L. (2007). An iron-sulfur domain of the eukaryotic primase is essential for RNA primer synthesis. *Nat. Struct. Mol. Biol.* 14, 875–877. doi: 10.1038/nsmb1288

Klinge, S., Nunez-Ramirez, R., Llorca, O., and Pellegrini, L. (2009). 3D architecture of DNA Pol alpha reveals the functional core of multi-subunit replicative polymerases. *EMBO J.* 28, 1978–1987. doi: 10.1038/emboj.2009.150

Kou, H., Zhou, Y., Gorospe, R. M., and Wang, Z. (2008). Mms19 protein functions in nucleotide excision repair by sustaining an adequate cellular concentration of the TFIIH component Rad3. *Proc. Natl. Acad. Sci. U.S.A.* 105, 15714–15719. doi: 10.1073/pnas.0710736105

Krokan, H. E., and Bjoras, M. (2013). Base excision repair. *Cold Spring Harb. Perspect. Biol.* 5:a012583.

Kuo, C. F., McRee, D. E., Cunningham, R. P., and Tainer, J. A. (1992). Crystallization and crystallographic characterization of the iron-sulfur-containing DNA-repair enzyme endonuclease III from *Escherichia coli*. *J. Mol. Biol.* 227, 347–351. doi: 10.1016/0022-2836(92)90703-m

La, P., Yang, G., and Dennery, P. A. (2013). Mammalian target of rapamycin complex 1 (mTORC1)-mediated phosphorylation stabilizes ISCU protein: implications for iron metabolism. *J. Biol. Chem.* 288, 12901–12909. doi: 10.1074/jbc.m112.424499

Lauder, S., Bankmann, M., Guzder, S. N., Sung, P., Prakash, L., and Prakash, S. (1996). Dual requirement for the yeast MMS19 gene in DNA repair and RNA polymerase II transcription. *Mol. Cell Biol.* 16, 6783–6793. doi: 10.1128/mcb.16.12.6783

Lehmann, A. R. (2003). DNA repair-deficient diseases, xeroderma pigmentosum, Cockayne syndrome and trichothiodystrophy. *Biochimie* 85, 1101–1111. doi: 10.1016/j.biochi.2003.09.010

Lill, R., Dutkiewicz, R., Freibert, S. A., Heidenreich, T., Mascarenhas, J., Netz, D. J., et al. (2015). The role of mitochondria and the CIA machinery in the maturation of cytosolic and nuclear iron-sulfur proteins. *Eur. J. Cell Biol.* 94, 280–291. doi: 10.1016/j.ejcb.2015.05.002

Lill, R., Srinivasan, V., and Muhlenhoff, U. (2014). The role of mitochondria in cytosolic-nuclear iron-sulfur protein biogenesis and in cellular iron regulation. *Curr. Opin. Microbiol.* 22, 111–119. doi: 10.1016/j.mib.2014.09.015

Liras, P., McCusker, J., Mascioli, S., and Haber, J. E. (1978). Characterization of a mutation in yeast causing nonrandom chromosome loss during mitosis. *Genetics* 88, 651–671. doi: 10.1093/genetics/88.4.651

Liu, H., Rudolf, J., Johnson, K. A., McMahon, S. A., Oke, M., Carter, L., et al. (2008). Structure of the DNA repair helicase XPD. *Cell* 133, 801–812.

Liu, L., and Huang, M. (2015). Essential role of the iron-sulfur cluster binding domain of the primase regulatory subunit Pri2 in DNA replication initiation. *Protein Cell* 6, 194–210. doi: 10.1007/s13238-015-0134-8

Lohman, T. M., and Bjornson, K. P. (1996). Mechanisms of helicase-catalyzed DNA unwinding. *Annu. Rev. Biochem.* 65, 169–214. doi: 10.1146/annurev.bi.65.070196.001125

Lohman, T. M., Tomko, E. J., and Wu, C. G. (2008). Non-hexameric DNA helicases and translocases: mechanisms and regulation. *Nat. Rev. Mol. Cell Biol.* 9, 391–401. doi: 10.1038/nrm2394

Lu, A. L., and Wright, P. M. (2003). Characterization of an *Escherichia coli* mutant MutY with a cysteine to alanine mutation at the iron-sulfur cluster domain. *Biochemistry* 42, 3742–3750. doi: 10.1021/bi0269198

Luo, D., Bernard, D. G., Balk, J., Hai, H., and Cui, X. (2012). The DUF59 family gene AE7 acts in the cytosolic iron-sulfur cluster assembly pathway to maintain nuclear genome integrity in *Arabidopsis*. *Plant Cell* 24, 4135–4148. doi: 10.1105/tpc.112.102608

Maio, N., Jain, A., and Rouault, T. A. (2020). Mammalian iron-sulfur cluster biogenesis: recent insights into the roles of frataxin, acyl carrier protein and ATPase-mediated transfer to recipient proteins. *Curr. Opin. Chem. Biol.* 55, 34–44. doi: 10.1016/j.cbpa.2019.11.014

Majewska, J., Ciesielski, S. J., Schilke, B., Kominek, J., Blenska, A., Delewski, W., et al. (2013). Binding of the chaperone Jac1 protein and cysteine desulfurase Nfs1 to the iron-sulfur cluster scaffold Isu protein is mutually exclusive. *J. Biol. Chem.* 288, 29134–29142. doi: 10.1074/jbc.m113.503524

Manicki, M., Majewska, J., Ciesielski, S., Schilke, B., Blenska, A., Kominek, J., et al. (2014). Overlapping binding sites of the frataxin homologue assembly factor and the heat shock protein 70 transfer factor on the Isu iron-sulfur cluster scaffold protein. *J. Biol. Chem.* 289, 30268–30278. doi: 10.1074/jbc.m114.596726

McGoldrick, J. P., Yeh, Y. C., Solomon, M., Essigmann, J. M., and Lu, A. L. (1995). Characterization of a mammalian homolog of the *Escherichia coli* MutY mismatch repair protein. *Mol. Cell Biol.* 15, 989–996. doi: 10.1128/mcb.15.2.989

Mesecke, N., Terziyska, N., Kozany, C., Baumann, F., Neupert, W., Hell, K., et al. (2005). relay system in the intermembrane space of mitochondria that mediates protein import. *Cell* 121, 1059–1069. doi: 10.1016/j.cell.2005.04.011

Mettert, E. L., and Kiley, P. J. (2015). How is Fe-S cluster formation regulated? *Annu. Rev. Microbiol.* 69, 505–526. doi: 10.1146/annurev-micro-091014-104457

Muhlenhoff, U., Gerber, J., Richhardt, N., and Lill, R. (2003). Components involved in assembly and dislocation of iron-sulfur clusters on the scaffold protein Isu1p. *EMBO J.* 22, 4815–4825. doi: 10.1093/emboj/cdg446

Muhlenhoff, U., Richter, N., Pines, O., Pierik, A. J., and Lill, R. (2011). Specialized function of yeast Isa1 and Isa2 proteins in the maturation of mitochondrial [4Fe-4S] proteins. *J. Biol. Chem.* 286, 41205–41216. doi: 10.1074/jbc.m111.296152

Netz, D. J., Mascarenhas, J., Stehling, O., Pierik, A. J., and Lill, R. (2014). Maturation of cytosolic and nuclear iron-sulfur proteins. *Trends Cell Biol.* 24, 303–312. doi: 10.1016/j.tcb.2013.11.005

Netz, D. J., Pierik, A. J., Stumpfig, M., Bill, E., Sharma, A. K., Pallesen, L. J., et al. (2012). A bridging [4Fe-4S] cluster and nucleotide binding are essential for function of the Cfd1-Nbp35 complex as a scaffold in iron-sulfur protein maturation. *J. Biol. Chem.* 287, 12365–12378. doi: 10.1074/jbc.m111.328914

Netz, D. J., Pierik, A. J., Stumpfig, M., Muhlenhoff, U., and Lill, R. (2007). The Cfd1-Nbp35 complex acts as a scaffold for iron-sulfur protein assembly in the yeast cytosol. *Nat. Chem. Biol.* 3, 278–286. doi: 10.1038/nchembio872

Netz, D. J., Stith, C. M., Stumpfig, M., Kopf, G., Vogel, D., Genau, H. M., et al. (2011). Eukaryotic DNA polymerases require an iron-sulfur cluster for the formation of active complexes. *Nat. Chem. Biol.* 8, 125–132. doi: 10.1038/nchembio.721

Netz, D. J., Stumpfig, M., Dore, C., Muhlenhoff, U., Pierik, A. J., and Lill, R. (2010). Tah18 transfers electrons to Dre2 in cytosolic iron-sulfur protein biogenesis. *Nat. Chem. Biol.* 6, 758–765. doi: 10.1038/nchembio.432

Nosal, R., Drabikova, K., Jancinova, V., Perecko, T., Ambrozova, G., Ciz, M., et al. (2014). On the molecular pharmacology of resveratrol on oxidative burst inhibition in professional phagocytes. *Oxid. Med. Cell Longev.* 2014:706269.

O'Brien, E., Holt, M. E., Thompson, M. K., Salay, L. E., Ehlinger, A. C., Chazin, W. J., et al. (2017). The [4Fe4S] cluster of human DNA primase functions as a redox switch using DNA charge transport. *Science* 355:eaag1789. doi: 10.1126/science.aag1789

Pallesen, L. J., Solodovnikova, N., Sharma, A. K., and Walden, W. E. (2013). Interaction with Cfd1 increases the kinetic lability of FeS on the Nbp35 scaffold. *J. Biol. Chem.* 288, 23358–23367. doi: 10.1074/jbc.m113.486878

Pandey, A., Golla, R., Yoon, H., Dancis, A., and Pain, D. (2012). Persulfide formation on mitochondrial cysteine desulfurase: enzyme activation by a eukaryote-specific interacting protein and Fe-S cluster synthesis. *Biochem. J.* 448, 171–187. doi: 10.1042/bj20120951

Pandey, A., Gordon, D. M., Pain, J., Stemmler, T. L., Dancis, A., and Pain, D. (2013). Frataxin directly stimulates mitochondrial cysteine desulfurase by exposing substrate-binding sites, and a mutant Fe-S cluster scaffold protein with frataxin-bypassing ability acts similarly. *J. Biol. Chem.* 288, 36773–36786. doi: 10.1074/jbc.m113.525857

Parent, A., Elduque, X., Cornu, D., Belot, L., Le Caer, J. P., Grandas, A., et al. (2015). Mammalian frataxin directly enhances sulfur transfer of NFS1 persulfide to both ISCU and free thiols. *Nat. Commun.* 6:5686.

Parish, J. L., Rosa, J., Wang, X., Lahti, J. M., Doxsey, S. J., and Androphy, E. J. (2006). The DNA helicase ChlR1 is required for sister chromatid cohesion in mammalian cells. *J. Cell Sci.* 119, 4857–4865. doi: 10.1242/jcs.03262

Patel, S. S., and Donmez, I. (2006). Mechanisms of helicases. *J. Biol. Chem.* 281, 18265–18268.

Paul, V. D., and Lill, R. (2015). Biogenesis of cytosolic and nuclear iron-sulfur proteins and their role in genome stability. *Biochim. Biophys. Acta* 1853, 1528–1539.

Pokharel, S., and Campbell, J. L. (2012). Cross talk between the nuclease and helicase activities of Dna2: role of an essential iron-sulfur cluster domain. *Nucleic Acids Res.* 40, 7821–7830. doi: 10.1093/nar/gks534

Pondarre, C., Antiochos, B. B., Campagna, D. R., Clarke, S. L., Greer, E. L., Deck, K. M., et al. (2006). The mitochondrial ATP-binding cassette transporter Abcb7 is essential in mice and participates in cytosolic iron-sulfur cluster biogenesis. *Hum. Mol. Genet.* 15, 953–964. doi: 10.1093/hmg/ddl012

Porello, S. L., Cannon, M. J., and David, S. S. (1998). A substrate recognition role for the [4Fe-4S]2+ cluster of the DNA repair glycosylase MutY. *Biochemistry* 37, 6465–6475. doi: 10.1021/bi972433t

Prakash, L., and Prakash, S. (1977). Isolation and characterization of MMS-sensitive mutants of *Saccharomyces cerevisiae*. *Genetics* 86, 33–55. doi: 10.1093/genetics/86.1.33

Prischi, F., Konarev, P. V., Iannuzzi, C., Pastore, C., Adinolfi, S., Martin, S. R., et al. (2010). Structural bases for the interaction of frataxin with the central components of iron-sulphur cluster assembly. *Nat. Commun.* 1:95.

Pugh, R. A., Honda, M., Leesley, H., Thomas, A., Lin, Y., Nilges, M. J., et al. (2008). The iron-containing domain is essential in Rad3 helicases for coupling of ATP hydrolysis to DNA translocation and for targeting the helicase to the single-stranded DNA-double-stranded DNA junction. *J. Biol. Chem.* 283, 1732–1743. doi: 10.1074/jbc.m707064200

Pyle, A. M. (2008). Translocation and unwinding mechanisms of RNA and DNA helicases. *Annu. Rev. Biophys.* 37, 317–336. doi: 10.1146/annurev.biophys.37.032807.125908

Rocha, A. G., Knight, S. A. B., Pandey, A., Yoon, H., Pain, J., Pain, D., et al. (2018). Cysteine desulfurase is regulated by phosphorylation of Nfs1 in yeast mitochondria. *Mitochondrion* 40, 29–41. doi: 10.1016/j.mito.2017.09.003

Roche, B., Aussel, L., Ezraty, B., Mandin, P., Py, B., and Barras, F. (2013). Iron/sulfur proteins biogenesis in prokaryotes: formation, regulation and diversity. *Biochim. Biophys. Acta* 1827, 455–469. doi: 10.1016/j.bbabio.2012.12.010

Roy, A., Solodovnikova, N., Nicholson, T., Antholine, W., and Walden, W. E. (2003). A novel eukaryotic factor for cytosolic Fe-S cluster assembly. *EMBO J.* 22, 4826–4835. doi: 10.1093/emboj/cdg455

Rudolf, J., Makrantoni, V., Ingledew, W. J., Stark, M. J., and White, M. F. (2006). The DNA repair helicases XPD and FancJ have essential iron-sulfur domains. *Mol. Cell* 23, 801–808.

Sanchez Garcia, J., Ciufo, L. F., Yang, X., Kearsey, S. E., and MacNeill, S. A. (2004). The C-terminal zinc finger of the catalytic subunit of DNA polymerase delta is responsible for direct interaction with the B-subunit. *Nucleic Acids Res.* 32, 3005–3016. doi: 10.1093/nar/gkh623

Sen, S., Igarashi, R., Smith, A., Johnson, M. K., Seefeldt, L. C., and Peters, J. W. (2004). A conformational mimic of the MgATP-bound "on state" of the nitrogenase iron protein. *Biochemistry* 43, 1787–1797. doi: 10.1021/bi0358465

Sharma, A. K., Pallesen, L. J., Spang, R. J., and Walden, W. E. (2010). Cytosolic iron-sulfur cluster assembly (CIA) system: factors, mechanism, and relevance to cellular iron regulation. *J. Biol. Chem.* 285, 26745–26751. doi: 10.1074/jbc.r110.122218

Sipos, K., Lange, H., Fekete, Z., Ullmann, P., Lill, R., and Kispal, G. (2002). Maturation of cytosolic iron-sulfur proteins requires glutathione. *J. Biol. Chem.* 277, 26944–26949. doi: 10.1074/jbc.m200677200

Skibbens, R. V. (2004). Chl1p, a DNA helicase-like protein in budding yeast, functions in sister-chromatid cohesion. *Genetics* 166, 33–42. doi: 10.1534/genetics.166.1.33

Song, D., and Lee, F. S. (2008). A role for IOP1 in mammalian cytosolic iron-sulfur protein biogenesis. *J. Biol. Chem.* 283, 9231–9238. doi: 10.1074/jbc.m708077200

Song, D., and Lee, F. S. (2011). Mouse knock-out of IOP1 protein reveals its essential role in mammalian cytosolic iron-sulfur protein biogenesis. *J. Biol. Chem.* 286, 15797–15805. doi: 10.1074/jbc.m110.201731

Srinivasan, V., Netz, D. J., Webert, H., Mascarenhas, J., Pierik, A. J., Michel, H., et al. (2007). Structure of the yeast WD40 domain protein Cia1, a component acting late in iron-sulfur protein biogenesis. *Structure* 15, 1246–1257. doi: 10.1016/j.str.2007.08.009

Stehling, O., Jeoung, J. H., Freibert, S. A., Paul, V. D., Banfer, S., Niggemeyer, B., et al. (2018). Function and crystal structure of the dimeric P-loop ATPase CFD1 coordinating an exposed [4Fe-4S] cluster for transfer to apoproteins. *Proc. Natl. Acad. Sci. U.S.A.* 115, E9085–E9094.

Stehling, O., Mascarenhas, J., Vashisht, A. A., Sheftel, A. D., Niggemeyer, B., Rosser, R., et al. (2013). Human CIA2A-FAM96A and CIA2B-FAM96B integrate iron homeostasis and maturation of different subsets of cytosolic-nuclear iron-sulfur proteins. *Cell Metab.* 18, 187–198. doi: 10.1016/j.cmet.2013.06.015

Stehling, O., Vashisht, A. A., Mascarenhas, J., Jonsson, Z. O., Sharma, T., Netz, D. J., et al. (2012). MMS19 assembles iron-sulfur proteins required for DNA metabolism and genomic integrity. *Science* 337, 195–199. doi: 10.1126/science.1219723

Suwa, Y., Gu, J., Baranovskiy, A. G., Babayeva, N. D., Pavlov, Y. I., and Tahirov, T. H. (2015). Crystal structure of the human pol alpha b subunit in complex with the C-terminal domain of the catalytic subunit. *J. Biol. Chem.* 290, 14328–14337.

Sviderskiy, V. O., Blumenberg, L., Gorodetsky, E., Karakousi, T. R., Hirsh, N., Alvarez, S. W., et al. (2020). Hyperactive CDK2 activity in basal-like breast cancer imposes a genome integrity liability that can be exploited by targeting DNA polymerase epsilon. *Mol. Cell* 80, 682–698.e7.

Takahashi, Y., and Tokumoto, U. (2002). A third bacterial system for the assembly of iron-sulfur clusters with homologs in archaea and plastids. *J. Biol. Chem.* 277, 28380–28383. doi: 10.1074/jbc.c200365200

Ter Beek, J., Parkash, V., Bylund, G. O., Osterman, P., Sauer-Eriksson, A. E., and Johansson, E. (2019). Structural evidence for an essential Fe-S cluster in the catalytic core domain of DNA polymerase. *Nucleic Acids Res.* 47, 5712–5722. doi: 10.1093/nar/gkz248

Thomas, D., Barbey, R., Henry, D., and Surdin-Kerjan, Y. (1992). Physiological analysis of mutants of *Saccharomyces cerevisiae* impaired in sulphate assimilation. *J. Gen. Microbiol.* 138, 2021–2028. doi: 10.1099/00221287-138-10-2021

Uzarska, M. A., Dutkiewicz, R., Freibert, S. A., Lill, R., and Muhlenhoff, U. (2013). The mitochondrial Hsp70 chaperone Ssq1 facilitates Fe/S cluster transfer from Isu1 to Grx5 by complex formation. *Mol. Biol. Cell* 24, 1830–1841. doi: 10.1091/mbc.e12-09-0644

Vaithiyalingam, S., Warren, E. M., Eichman, B. F., and Chazin, W. J. (2010). Insights into eukaryotic DNA priming from the structure and functional interactions of the 4Fe-4S cluster domain of human DNA primase. *Proc. Natl. Acad. Sci. U.S.A.* 107, 13684–13689. doi: 10.1073/pnas.1002009107

van der Lelij, P., Chrzanowska, K. H., Godthelp, B. C., Rooimans, M. A., Oostra, A. B., Stumm, M., et al. (2010). Warsaw breakage syndrome, a cohesinopathy associated with mutations in the XPD helicase family member DDX11/ChlR1. *Am. J. Hum. Genet.* 86, 262–266. doi: 10.1016/j.ajhg.2010.01.008

Van Vranken, J. G., Nowinski, S. M., Clowers, K. J., Jeong, M. Y., Ouyang, Y., Berg, J. A., et al. (2018). Is an Acetyl-CoA-dependent modification required for electron transport chain assembly. *Mol. Cell* 71, 567–580.e4.

van Wietmarschen, N., Moradian, A., Morin, G. B., Lansdorp, P. M., and Uringa, E. J. (2012). The mammalian proteins MMS19, MIP18, and ANT2 are involved in cytoplasmic iron-sulfur cluster protein assembly. *J. Biol. Chem.* 287, 43351–43358. doi: 10.1074/jbc.m112.431270

Veatch, J. R., McMurray, M. A., Nelson, Z. W., and Gottschling, D. E. (2009). Mitochondrial dysfunction leads to nuclear genome instability via an iron-sulfur cluster defect. *Cell* 137, 1247–1258. doi: 10.1016/j.cell.2009.04.014

Vernis, L., Facca, C., Delagoutte, E., Soler, N., Chanet, R., Guiard, B., et al. (2009). A newly identified essential complex, Dre2-Tah18, controls mitochondria integrity and cell death after oxidative stress in yeast. *PLoS One* 4:e4376. doi: 10.1371/journal.pone.0004376

Wallace, S. S. (2013). DNA glycosylases search for and remove oxidized DNA bases. *Environ. Mol. Mutagen.* 54, 691–704. doi: 10.1002/em.21820

Webert, H., Freibert, S. A., Gallo, A., Heidenreich, T., Linne, U., Amlacher, S., et al. (2014). Functional reconstitution of mitochondrial Fe/S cluster synthesis on Isu1 reveals the involvement of ferredoxin. *Nat. Commun.* 5:5013.

Weerapana, E., Wang, C., Simon, G. M., Richter, F., Khare, S., Dillon, M. B., et al. (2010). Quantitative reactivity profiling predicts functional cysteines in proteomes. *Nature* 468, 790–795.

Weiler, B. D., Bruck, M. C., Kothe, I., Bill, E., Lill, R., and Muhlenhoff, U. (2020). Mitochondrial [4Fe-4S] protein assembly involves reductive [2Fe-2S] cluster fusion on ISCA1-ISCA2 by electron flow from ferredoxin FDX2. *Proc. Natl. Acad. Sci. U.S.A.* 117, 20555–20565.

Weiner, B. E., Huang, H., Dattilo, B. M., Nilges, M. J., Fanning, E., and Chazin, W. J. (2007). An iron-sulfur cluster in the C-terminal domain of the p58 subunit of human DNA primase. *J. Biol. Chem.* 282, 33444–33451.

White, M. F. (2009). Structure, function and evolution of the XPD family of iron-sulfur-containing 5′–>3′ DNA helicases. *Biochem. Soc. Trans.* 37, 547–551.

White, M. F., and Dillingham, M. S. (2012). Iron-sulphur clusters in nucleic acid processing enzymes. *Curr. Opin. Struct. Biol.* 22, 94–100.

Wolski, S. C., Kuper, J., Hanzelmann, P., Truglio, J. J., Croteau, D. L., Van Houten, B., et al. (2008). Crystal structure of the FeS cluster-containing nucleotide excision repair helicase XPD. *PLoS Biol.* 6:e149. doi: 10.1371/journal.pbio.0060149

Wu, Y., and Brosh, R. M. Jr. (2009). FANCJ helicase operates in the Fanconi Anemia DNA repair pathway and the response to replicational stress. *Curr. Mol. Med.* 9, 470–482.

Wu, Y., and Brosh, R. M. Jr. (2012). DNA helicase and helicase-nuclease enzymes with a conserved iron-sulfur cluster. *Nucleic Acids Res.* 40, 4247–4260.

Wu, Y., Sommers, J. A., Khan, I., de Winter, J. P., and Brosh, R. M. Jr. (2012). Biochemical characterization of Warsaw breakage syndrome helicase. *J. Biol. Chem.* 287, 1007–1021.

Wu, Y., Sommers, J. A., Suhasini, A. N., Leonard, T., Deakyne, J. S., Mazin, A. V., et al. (2010). Fanconi anemia group J mutation abolishes its DNA repair function by uncoupling DNA translocation from helicase activity or disruption of protein-DNA complexes. *Blood* 116, 3780–3791.

Yeeles, J. T., Cammack, R., and Dillingham, M. S. (2009). An iron-sulfur cluster is essential for the binding of broken DNA by AddAB-type helicase-nucleases. *J. Biol. Chem.* 284, 7746–7755.

Yoon, T., and Cowan, J. A. (2003). Iron-sulfur cluster biosynthesis. Characterization of frataxin as an iron donor for assembly of [2Fe-2S] clusters in ISU-type proteins. *J. Am. Chem. Soc.* 125, 6078–6084.

Zerbe, L. K., and Kuchta, R. D. (2002). The p58 subunit of human DNA primase is important for primer initiation, elongation, and counting. *Biochemistry* 41, 4891–4900.

Zhang, Y., Lyver, E. R., Nakamaru-Ogiso, E., Yoon, H., Amutha, B., Lee, D. W., et al. (2008). Dre2, a conserved eukaryotic Fe/S cluster protein, functions in cytosolic Fe/S protein biogenesis. *Mol. Cell Biol.* 28, 5569–5582.

Conflict of Interest: The authors declare that the research was conducted in the absence of any commercial or financial relationships that could be construed as a potential conflict of interest.

Publisher's Note: All claims expressed in this article are solely those of the authors and do not necessarily represent those of their affiliated organizations, or those of the publisher, the editors and the reviewers. Any product that may be evaluated in this article, or claim that may be made by its manufacturer, is not guaranteed or endorsed by the publisher.

Advantages of publishing in Frontiers

OPEN ACCESS
Articles are free to read for greatest visibility and readership

FAST PUBLICATION
Around 90 days from submission to decision

HIGH QUALITY PEER-REVIEW
Rigorous, collaborative, and constructive peer-review

TRANSPARENT PEER-REVIEW
Editors and reviewers acknowledged by name on published articles

Frontiers
Avenue du Tribunal-Fédéral 34
1005 Lausanne | Switzerland

Visit us: www.frontiersin.org
Contact us: frontiersin.org/about/contact

REPRODUCIBILITY OF RESEARCH
Support open data and methods to enhance research reproducibility

DIGITAL PUBLISHING
Articles designed for optimal readership across devices

FOLLOW US
@frontiersin

IMPACT METRICS
Advanced article metrics track visibility across digital media

EXTENSIVE PROMOTION
Marketing and promotion of impactful research

LOOP RESEARCH NETWORK
Our network increases your article's readership